2022

Expanding the Applicability of Press-Brake-Formed Tub Girders Through the Extension of the Maximum Span Length and the Evaluation of Pier Continuity

Robert M. Tennant
West Virginia University, rmtennant@mix.wvu.edu

EXPANDING THE APPLICABILITY OF PRESS-BRAKE-FORMED TUB GIRDERS THROUGH THE EXTENSION OF THE MAXIMUM SPAN LENGTH AND THE EVALUATION OF PIER CONTINUITY

Robert M. Tennant

Dissertation submitted to the
Benjamin M. Statler College of Engineering and Mineral Resources
at
West Virginia University
in partial fulfillment of the requirements
for the degree of

Doctor of Philosophy
in
Civil and Environmental Engineering

Karl E. Barth, Ph.D., Chair
Gregory K. Michaelson, Ph.D.
Hung-Liang "Roger" Chen, Ph.D.
Udaya B. Halabe, Ph.D.
Edward M. Sabolsky, Ph.D.

Wadsworth Department of Civil and Environmental Engineering

Morgantown, West Virginia
2022

Keywords: steel bridge, press-brake-formed tub girders, experimental testing, link slab, finite element modeling

ABSTRACT

EXPANDING THE APPLICABILITY OF PRESS-BRAKE-FORMED TUB GIRDERS THROUGH THE EXTENSION OF THE MAXIMUM SPAN LENGTH AND THE EVALUATION OF PIER CONTINUITY

Robert M. Tennant

The Short Span Steel Bridge Alliance (SSSBA) is a group of bridge and buried soil steel structure industry leaders who provide educational information on the design and construction of short-span steel bridges in installations up to 140 feet in length. Within the SSSBA technical working group, a modular, shallow press-brake-formed tub girder (PBFTG) was developed to address the demand in the short-span steel bridge market for rapid infrastructure replacement solutions. PBFTGs consist of modular, shallow, trapezoidal boxes fabricated from cold-bent structural steel plate. A concrete deck, or other deck option, may be placed on the girder, and the modular unit can be shipped by truck to the bridge site.

PBFTGs perform exceptionally well in simply supported, right, straight bridges utilizing current American Association of State and Highway Transportation Officials Load Resistance and Factor Design Bridge Design Specifications' (AASHTO LRFD BDS) Live Load Distribution Factors (LLDFs). The specifications limit the use of PBFTGs outside of these scenarios, despite the expectation they would perform well in a variety of other situations. More research and data are necessary to validate the current limitations in the AASHTO LRFD BDS and increase the applicability of PBFTGs into continuous spans and skewed bridges.

The scope of this project was to expand the applicability and usability of the PBFTG system. This was performed in several stages. First, a complete understanding and background of PBFTGs, LLDFs, box-girder capacity determinations, link slabs, and the AASHTO LRFD BDS was provided. This understanding and background of the restrictions placed on PBFTGs provided insight when developing the methodologies to overcome these restrictions. Next, analytical modeling techniques were developed and refined utilizing complicated geometry and nonlinear finite element methods. These modeling techniques were benchmarked against numerous historical laboratory tests and live load field tests of in-service PBFTG bridges. Then, the analytical tools were employed in sensitivity and parametric studies on PBFTG bridge models, resulting in proposed simplified empirical LLDFs, which better predict live load distribution than those equations present in the AASHTO LRFD BDS. These tools were also used to assess the effect of bearing line skew on the capacity of PBFTGs. Finally, life cycle laboratory fatigue testing was performed on two PBFTGs joined by a full-scale link slab to assess the applicability of the joint in continuous PBFTG bridges. Results of this project demonstrate the use of PBFTGs can be expanded into continuous spans using link slabs and more accurate LLDFs may be used to increase the economic viability of the system in the short-span bridge market. In addition, the analytical tools developed during this study relating to the capacity of skewed PBFTGs will serve as the basis for future research in this field.

ACKNOWLEDGEMENTS

First, I want to offer my sincerest gratitude to my advisor Dr. Karl Barth for his guidance and support throughout my M.S. and Ph.D. studies. His encouragement throughout my six years of graduate school has been invaluable, and I could not imagine a better mentor and advisor at West Virginia University. Above all else, I am so thankful for the lessons he taught me academically, professionally, and personally.

I would like to extend my thanks to Drs. Gregory Michaelson, Roger Chen, Udaya Halabe, and Edward Sabolsky. Dr. Michaelson served as an integral mentor through the extensive programming performed during my doctoral studies, and I do not think this would have been possible without the countless phone calls, Zoom meetings, and emails shared. Dr. Chen has guided me through some of the toughest classes I have taken at West Virginia University, and I am grateful for the lessons learned and storied shared. Dr. Halabe has provided some of the most consistent academic support throughout my graduate experience, from advising me how to write my first real professional report in Senior Design to guiding me through some of the most intricate calculations in Earthquake and Wind Design. Dr. Sabolsky taught one of my first engineering courses, Statics, and I will never forget his excitement and enthusiasm for teaching. It is in no small part to Dr. Sabolsky I have pursued higher education to one day share my enthusiasm for teaching with students of my own.

This project would not have been possible without the support of the American Iron and Steel Institute and the West Virginia Division of Highways. Their financial support and willingness to take a chance on this exciting and groundbreaking technology was invaluable.

Next, I would like to thank the contributions of my fellow graduate students, Adam Roh and Brook Woldegabriel. Graduate school would have been significantly more difficult without their comradery and assistance at every phase of my studies. I am also thankful for the numerous undergraduate research assistants who have provided their physical and technical support to my laboratory and analytical testing. The experimental testing could not have been accomplished without the countless hours of labor and brain power provided by Jerry Nestor and Mark Skidmore. In addition, I could not have come this far without the graduate students who worked alongside me in the lab and basement of ESB over the last six years. We have shared many memories of long nights covered in hydraulic oil and concrete dust and discussed everything from hot wings to the struggles of graduate life.

Last, I would like to express my gratitude for my friends and family for their tireless support during graduate school. I would not have been able to do this without their constant encouragement and affirmations. Their support means the world to me. Finally, words cannot describe the appreciation for the countless sacrifices made by my wife Danielle Tennant. The amount of blood, sweat, and tears put into this work by her and her support throughout is unquantifiable.

TABLE OF CONTENTS

LIST OF TABLES

LIST OF FIGURES

CHAPTER 1: INTRODUCTION

1.1 Background / Overview

The Short Span Steel Bridge Alliance (SSSBA) is a group of bridge and buried soil steel structure industry leaders who provide educational information on the design and construction of short-span steel bridges in installations up to 140 feet in length. Within the SSSBA technical working group, a modular shallow press-brake-formed tub girder (PBFTG) was developed to address the demand in the short-span steel bridge market for rapid infrastructure replacement solutions. PBFTGs consist of modular, shallow, trapezoidal boxes fabricated from cold-bent structural steel plate, as seen in Figure 1.1. A concrete deck, or other deck option, may be placed on the girder, and the modular unit can be shipped by truck to the bridge site (SSSBA, 2022).

Figure 1.1: PBFTG after Cold Bending (SSSBA, 2021)

PBFTGs have proven economically and structurally competitive through multiple laboratory experiments and field demonstrations across the country. The American Association of State Highway and Transportation Officials (AASHTO) Innovation Initiative selected the PBFTG bridge system as a 2021 Focus Technology and has invested time and resources to encourage the adoption of the system across the nation. While this system is exceptionally efficient and economical, its applicability is limited by a lack of research in continuous spans and the AASHTO Load Resistance and Factor Bridge Design Specifications (LRFD BDS), hereafter referred to as the AASHTO LRFD BDS.

1.2 Project Scope & Objectives

The scope of this project is to explore the use of PBFTGs in a broader range of applications. Specifically, link slabs are explored with modular PBFTGs in continuous span scenarios, and extensive analytical modeling will be performed to assess the validity of the restrictions placed on box section flexural members as they relate to PBFTGs. These objectives will be achieved through the following:

- Reviewing literature relating to PBFTGs, link slab details, live load distribution, and the effect of compactness on the flexural capacity of sections.
- Developing analytical tools to assess the behavior and capacity of PBFTGs with varying dimensions and properties.
- Conducting behavioral and parametric studies to assess which parameters affect the computation of live load distribution factors for PBFTGs.
- Conducting behavioral studies to assess the effect of skew on the ultimate capacity of PBFTGs.
- Performing flexural testing on modular units transversely joined by a link slab.

1.3 Dissertation Organization

A brief overview of the organization of this dissertation is as follows:

- <u>Chapter 2</u>
    - This chapter summarizes previous research performed on cold-bent tub girder applications. Specific attention is given to research performed on PBFTGs in laboratory and field settings.

- Chapter 3
    - This chapter summarizes the development of current live load distribution factors found in the AASHTO LRFD BDS and the influence of global bridge parameters affecting live load distribution.
- Chapter 4
    - This chapter summarizes the determination of compactness of cross-sections and elements. Additionally, a brief review of the effects of skew on box-girders is provided.
- Chapter 5
    - This chapter summarizes previous laboratory, field, and analytical research performed on link slabs.
- Chapter 6
    - This chapter provides a comprehensive review of the AASHTO LRFD BDS relating to PBFTG bridges.
- Chapter 7
    - This chapter describes the analytical techniques developed using a commercial finite element software package. The analytical techniques were verified against previous experimental tests.
- Chapter 8
    - This chapter documents the behavioral studies performed on the PBFTG bridge system to determine the factors affecting live load distribution. These studies were used to develop live load distribution factors benchmarked against previous live load field tests.
- Chapter 9
    - This chapter documents the behavioral study performed on the PBFTG composite units to determine the effect of skew on the flexural capacity of the system.
- Chapter 10
    - This chapter discusses the research methods and results obtained from experimental testing. A detailed explanation of the experiment setup, loading, and results is provided.

- Chapter 11
    - This chapter provides a summary of the project and highlights key findings. Recommendations for future work and continued research to expand the applicability of the systems are also provided.
- Appendix A
    - This appendix documents the results of the live load distribution sensitivity study analysis.
- Appendix B
    - This appendix documents the results of the live load distribution parametric study analysis.
- Appendix C
    - This appendix documents the results of the compactness sensitivity analysis.
- Appendix D
    - This appendix documents the determination of the Fatigue I moment and cycle count used in the experimental testing.
- Appendix E
    - This appendix documents the experimental testing data.

CHAPTER 2: PRESS-BRAKE-FORMED TUB GIRDER LITERATURE REVIEW

2.1 INTRODUCTION

This chapter presents a discussion on the previous findings regarding PBFTGs. A review of literature pertaining to other forms of cold-bent tub girders is provided, with an emphasis on research on tub girders in negative bending regions and bracing requirements for typical welded tub girder sections. A comprehensive review of the research practicum undertook by researchers at West Virginia University (WVU) and Marshall University, relating to the design of PBFTGs and their implementation, is presented.

2.2 PREVIOUS APPLICATIONS OF COLD-BENT STEEL TUB GIRDERS

Prefabricated steel tub girder systems have been studied for decades but have recently been extensively used in the short-span bridge market. As accelerated bridge construction (ABC) has become more popular in bridge design and construction, PBFTGs have been shown to be economical and competitive in spans up to 60 feet. Several researchers and organizations have conducted studies on the use of systems employing various types of cold-bent steel tub girders.

2.2.1 Prefabricated press-formed steel T-box girder bridge system (Taly & Gangarao, 1979)

Taly and Gangarao (1979) proposed designs for several prefabricated superstructural systems for short-span highway bridges. One design consisted of a cold-formed steel T-box girder. The stem of the trapezoidal girder was cold formed from 3/8 inch thick A-36 steel plate shop welded to 3/8 inch thick steel top flanges (Figure 2.1). Proposed girder sections consisted of either 6 foot or 8 foot top flange widths with a total depth of 2.5 feet, 3 feet, or 3.5 feet, based on the total bridge width and span. A feasibility assessment demonstrated the system to be suitable in spans of up to 65 feet.

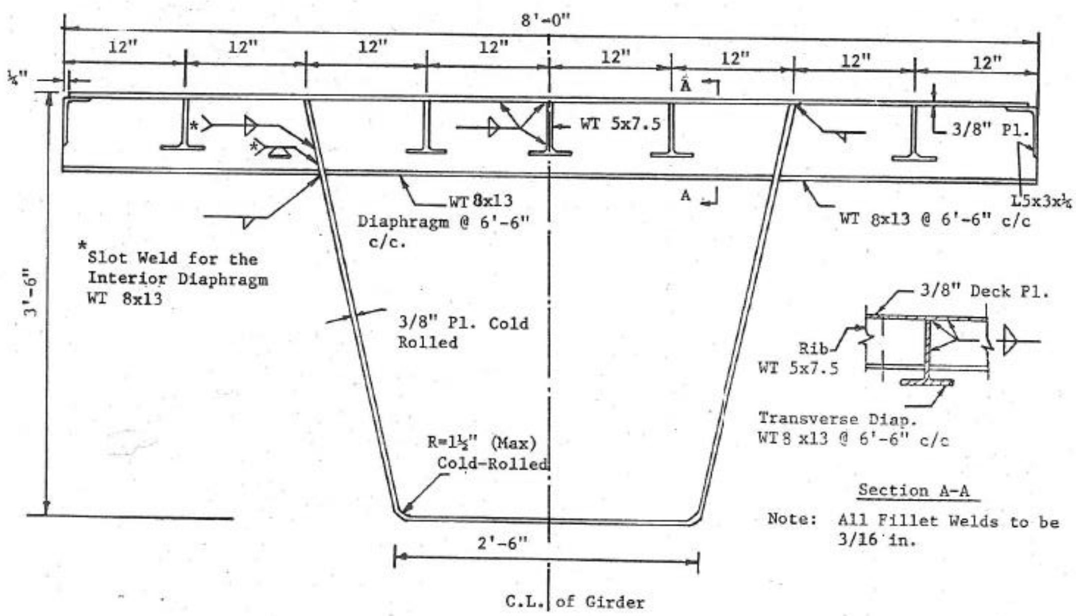

Figure 2.1: T-Box-Girder System, Typical Girder Section with 3/8 inch Steel Plate Deck (Taly & Gangarao, 1979)

Major advantages of this system include high strength-to-weight ratios and improved fabricability. The dead weight of the steel deck superstructure is significantly reduced compared with conventional concrete decks. Due to the closed section, a higher torsional stiffness is achieved, leading to lower live load distribution factors (LLDFs) and higher efficiency in horizontally curved structures. As the bridge system is nearly completely prefabricated, a better-quality product can be achieved. Improved quality is also achieved by the simplicity in the system, specifically the cold forming of the sections, as this reduces the amount of welding required.

A composite prefabricated cold-formed box-girder system was proposed as a modification to the all steel system. A 5 inch thick precast, prestressed concrete deck was to be utilized instead of a 3/8 inch thick steel plate (Figure 2.2). Composite action is developed through shear studs welded to the top flanges of the cold-bent section.

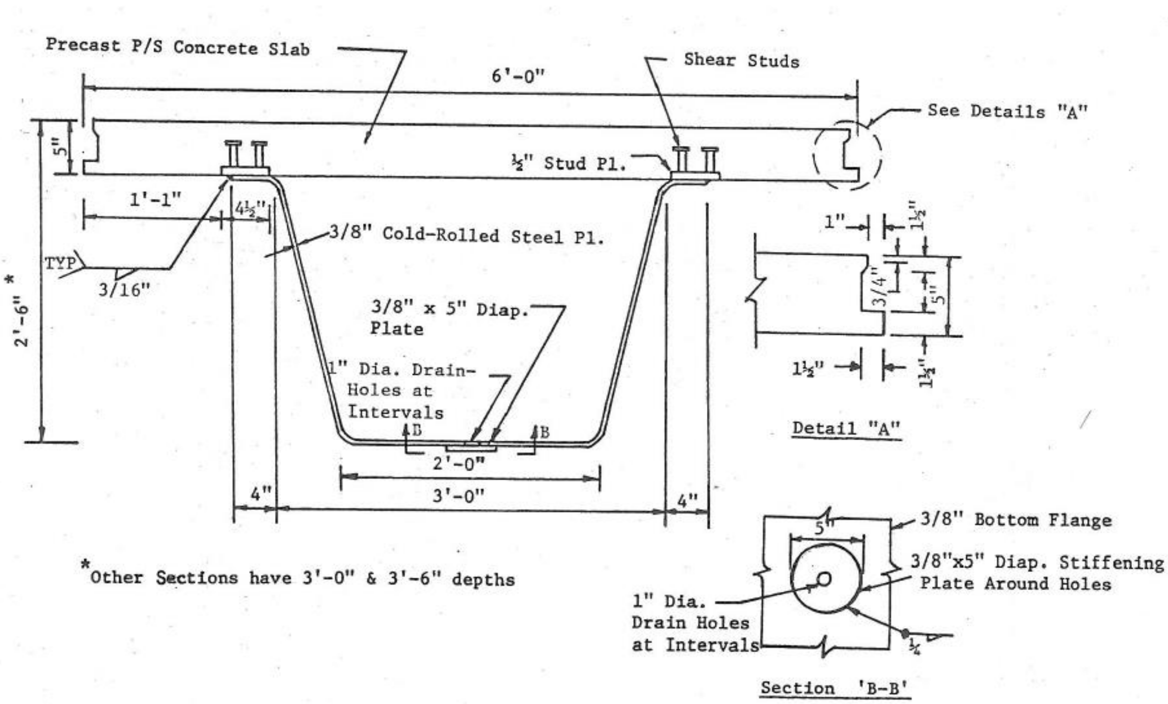

Figure 2.2: T-Box-Girder System, Typical Girder Section with 5 inch Precast, Prestressed Concrete Slab (Taly & Gangarao, 1979)

At the time, the AASHTO Standard Specifications did not provide design criteria for members using press-brake or composite box-girders. Therefore, the researchers evaluated their designs against the 1977 American Iron and Steel Institute specifications. The bends at the junction of the bottom flange and webs were found to provide inadequate crippling resistance over the bearings. To combat this, the designers provided a 5 inch by 1/2 inch stiffener along the bottom flange and a 3/8 inch thick steel plated diaphragm between the flanges and webs.

2.2.2 Composite girders with formed steel U-sections (Nakamura, 2002)

Nakamura (2002) proposed a continuous composite bridge system composed of cold-bent steel U-sections and a concrete deck. This bridge system, illustrated in Figure 2.3, acts compositely in the span centers where the positive bending moment is critical. As the top flange is composite with the concrete deck, buckling of the flange is restricted. However, at intermediate supports, where negative bending occurs, the bottom flange is vulnerable against buckling. To overcome this susceptibility, the U-Section was filled with concrete and the deck was prestressed utilizing prestressed steel bars. Typical prestressed concrete beams require extensive formwork for casting. However, the steel U-section works as much of the formwork itself, significantly reducing the time and cost associated with fabricating the formwork. While extra concrete in the negative bending regions increases the reaction forces at the intermediate supports, it does not vastly increase the bending moment as the concrete is filled only near the supports.

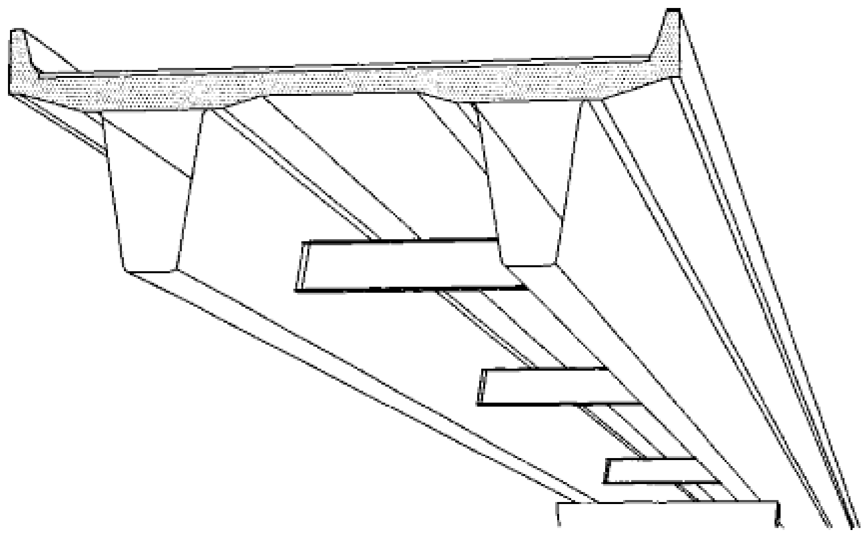

Figure 2.3: Composite Girders with Steel U-Section (Nakamura, 2002)

Nakamura conducted bending tests on three different cross-sections, one of which was the system in negative bending filled with concrete and prestressed. For this cross-section, the prestress forces initially kept the concrete slab in compression, but when the concrete slab entered tension, it quickly lost strength. The filled concrete performed well until the prestressed steel bars became fully plastic and the bottom flange buckled. The researcher found the calculated maximum load, from the Bernouli-Beam equation, in negative bending was 9% lower than the measured value, likely due to the confined nature of the filled concrete and the neglection of the tensile strength of the concrete slab.

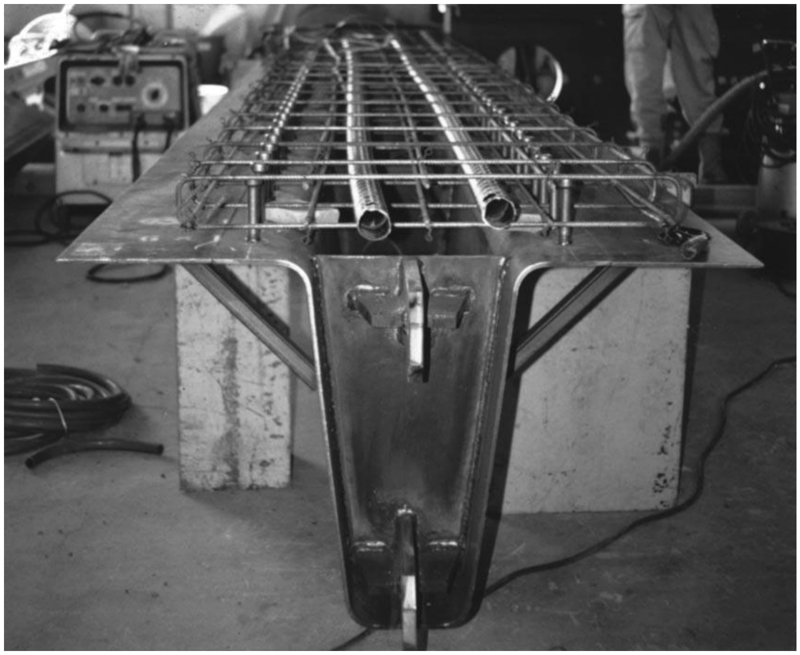

Figure 2.4: Negative Bending Test Specimen before Concrete Pour (Nakamura, 2002)

2.2.3 Texas Prefabricated Steel Tub-Girder System

The Texas Department of Transportation (TxDOT) explored shallow steel bridge tub girders for the FM 3267 bridge on I-35 (Chandar et al., 2010). One of the project goals was to provide a rapidly constructible and cost-efficient structure. Historically, larger steel tub girders were commonly used for horizontally curved bridge applications. Box-girders were used in this application due to their high torsional stiffness compared to wide flange sections. However, uses in straight girder applications had been limited due to economic efficiency and fabrication/handling issues.

For the FM 3267 bridge, one of the design challenges was to minimize the structural depth. The structural efficiency of trapezoidal girders allowed the designers to proportion the girders to meet the structural depth limitation. The bridge was constructed utilizing six rows of four 36 inch deep steel box-girders with a cast-in-place concrete deck poured in two stages joined by a longitudinal joint above one of the flanges (Figure 2.5). The girder sections were standardized, which saved design, fabrication, and erection costs.

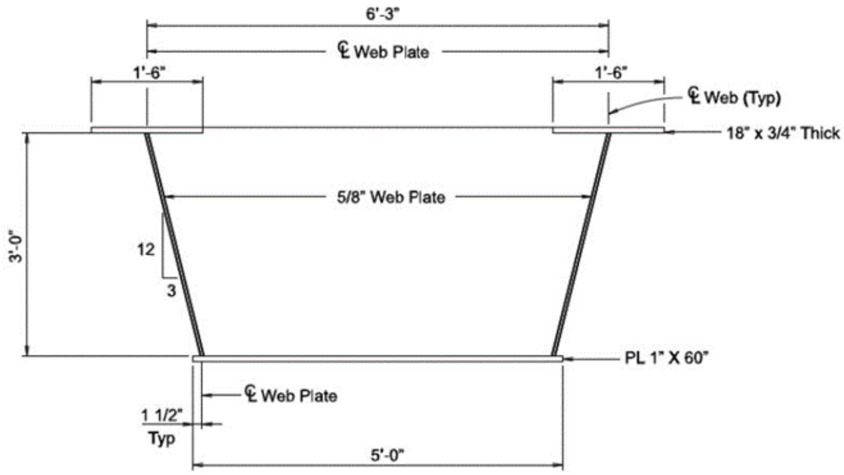

Figure 2.5: TxDOT Trapezoidal Box-Girder Cross-Section (Chandar et al., 2010)

Despite the structural advantages of the system and the use of ABC in the design, current practices for welded trapezoidal box-girders often include aspects which may lead to unnecessary fabrication costs and structural inefficiencies (Armijos-Moya et al., 2019). TxDOT sponsored research projects to increase the efficiency of steel tub girders by developing and modifying superstructure design details. Many detailing practices used for steel tub girders are based in traditional practices and require unnecessary bracing. Extensive amounts of internal bracing, both in the vertical plane and the longitudinal plane, were typically required as the noncomposite system does not have the high torsional resistance seen in the composite system (Figure 2.6).

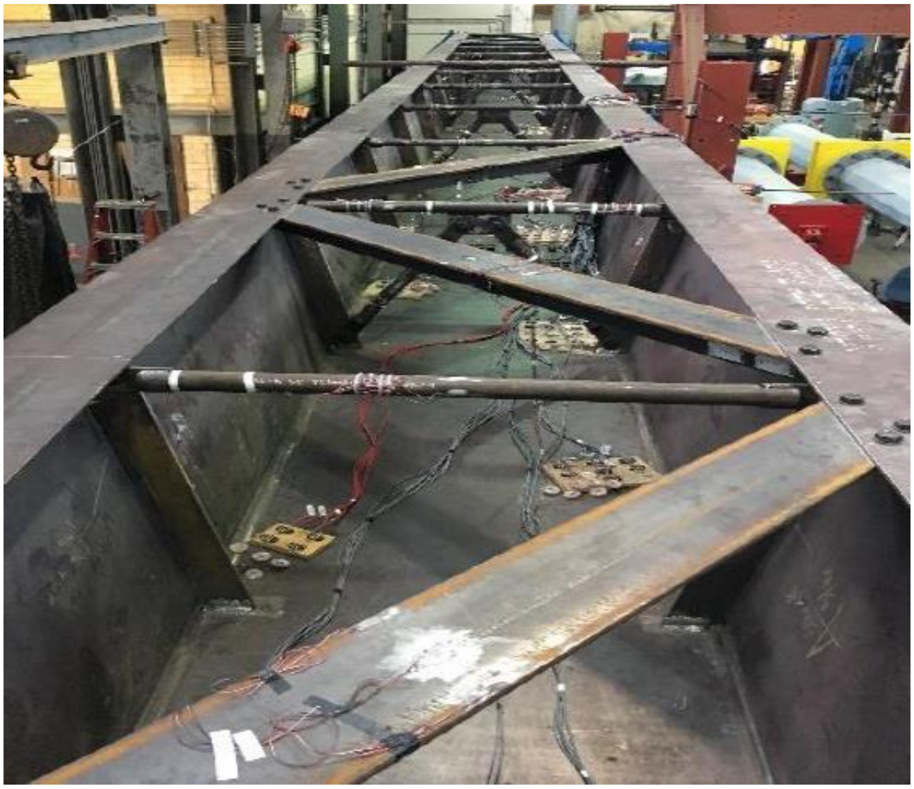

Figure 2.6: Top Lateral Bracing System (Armijos-Moya et al., 2019)

From parametric finite element analysis (FEA), researchers found removing 50% of the truss diagonals guarantees adequate torsional stiffness during construction of straight tub girder bridges. For straight tub girders, vertical K-frames could be placed at every third panel point with no loss to torsional stiffness. As found through experimental testing and FEA, offsetting the top flanges toward the inside of the tub girder allowed for simplified connections between top lateral truss elements and the top flanges of the girder. The researchers also investigated the use of shallower web slopes. The use of a lower web slope, such as 2.5:1, can increase the tributary width of the girder, potentially eliminating a girder line, but makes the section prone to global instability.

2.2.4 Con-Struct Pre-fabricated Steel Tub Girder System

The Con-Struct Prefabricated Bridge System was established in 2004 as an answer to the growing demand for ABC products (Valmont, 2022). The Con-Struct system is composed of hot-dip galvanized PBFTGs. The noncomposite PBFTGs are made composite with a concrete deck before being shipped to the bridge site (Figure 2.7). Once on site, the system is placed on the abutments and a longitudinal joint is poured between units. Designs of this system are valid up to 70 feet in length with skews up to 45° and girder spacings of 7 feet.

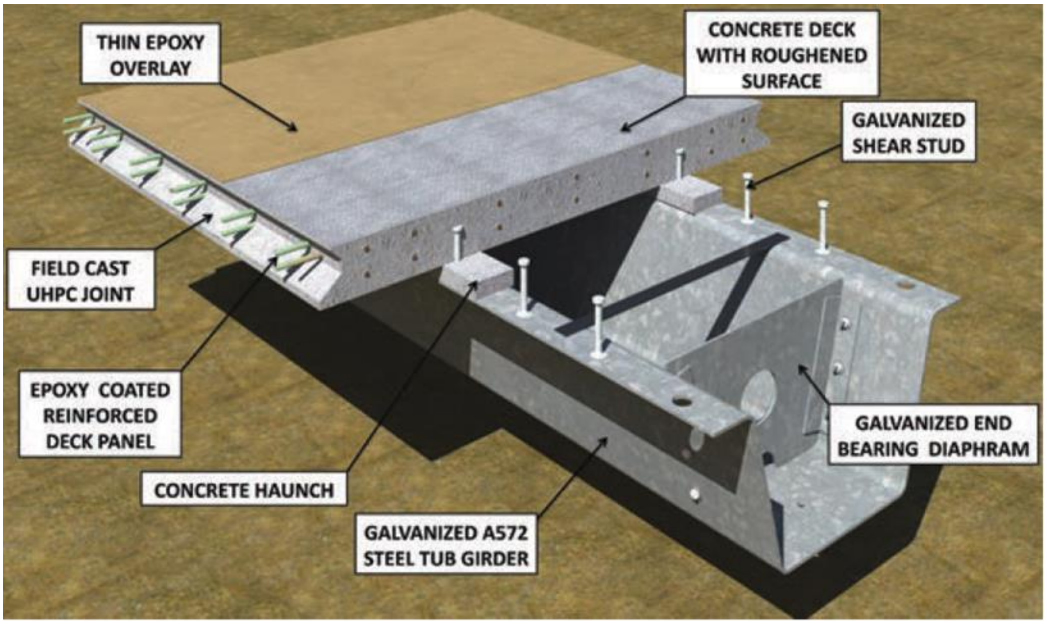

Figure 2.7: Standard Class Composite Bridge System (Valmont, 2022)

In 2017, the St. Clair County Road Commission replaced two severely deteriorated steel bridges with new PBFTG bridges. The two bridges consisted of a 25 foot span bridge with no skew and a 35 foot span bridge with a 45° skew. Each bridge consisted of hot-rolled W18 sections and a concrete deck for a total depth of approximately 2.5 feet. Due to the need for ABC, the existing abutments needed to be rehabilitated instead of replaced, requiring the new superstructure to match the existing superstructure's depth. The Con-Struct system was chosen for its light weight, low depth, and speed of construction. The composite modules were shipped to the bridge site, placed by crane and excavator, as seen in Figure 2.8, and a 6 inch wide high performance concrete deck joint was cast between the modules. The construction of both bridges was completed in 10 days.

Figure 2.8: Superstructure Placement of Composite Modules (SSSBA, 2021)

2.3 Previous Laboratory Testing of PBFTGs

The research practicum on the development and long-term performance of PBFTGs at WVU began in 2011. Researchers at WVU collaborated with the SSSBA to develop PBFTGs as an economical steel alternative in the short-span bridge market. This section details the experimental and analytical work performed at WVU in this area.

2.3.1 Development and Feasibility Assessment of Shallow Press-Brake-Formed Steel Tub Girders for Short-Span Bridge Applications (Michaelson, 2014)

The SSSBA developed a modular PBFTG, as seen in Figure 2.9, as an alternative to adjacent concrete box beams in short-span bridge installations up to 140 feet in length. The trapezoidal steel shape is fabricated from standard plate sizes and cold-bent using a large capacity press-brake. After the steel is bent into the desired shape, shear studs are welded to the top flange, and a reinforced concrete deck is compositely cast in a fabrication shop. Then, the composite PBFTG system can be shipped to the bridge site where the modular units will be joined with longitudinal closure pours.

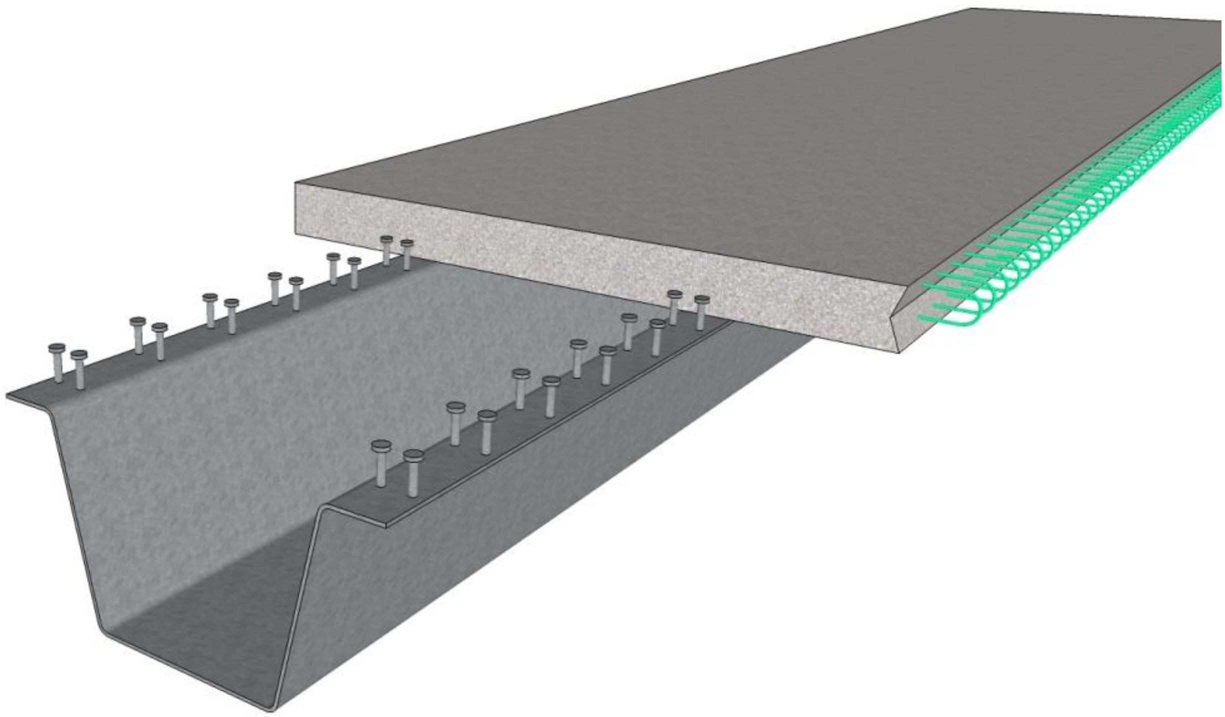

Figure 2.9: Modular Press-Brake-Formed Tub Girder (Michaelson, 2014)

Michaelson (2014) first developed a program to generate section properties of any configuration of PBFTG. Certain geometrical properties were held constant in the calculation: The slope of the webs were held at a constant 1:4 ratio, the inside bend radii of the bends were held to five times the thickness, the top flanges were kept at a constant 6 inches, the concrete deck dimensions were kept at 7.5 feet wide by 8 inches thick, the concrete's compressive strength was held at a constant 4 ksi, and the yield stress of the steel was held at 50 ksi. Three different standard plate thicknesses were considered: 7/16, 1/2, and 5/8 inch. Six different standard plate widths were evaluated: 60, 72, 84, 96, 108, and 120 inch. An optimum depth was chosen for each plate width corresponding to the maximum yield moment.

Following the design of the system, physical flexural testing was performed on two separate composite PBFTGs and two separate noncomposite PBFTGs. The dimensions of the steel specimens were uniform across all testing. Each specimen was constructed from 84 inch wide by 7/16 inch thick by 35 foot long plate. This plate was chosen because the composite PBFTGs formed from this plate were the largest the 330-kip servo-hydraulic actuator could test to ultimate failure. The deck thickness was shortened from 8 inches to 6 inches to ensure ultimate failure could be reached. Each girder was subjected to three-point bending.

The composite modules were loaded to failure at approximately 300 kip and a midspan vertical deflection of 3.1 inches. The result was crushing of the concrete deck and loss of composite action (Figure 2.10). The noncomposite girders were loaded until the girders exhibited excessive lateral deflection and twist under relatively small loads, 90 kip and 30 kip (Figure 2.11).

Figure 2.10: Typical Failure Mode for Composite Specimens (Michaelson, 2014)

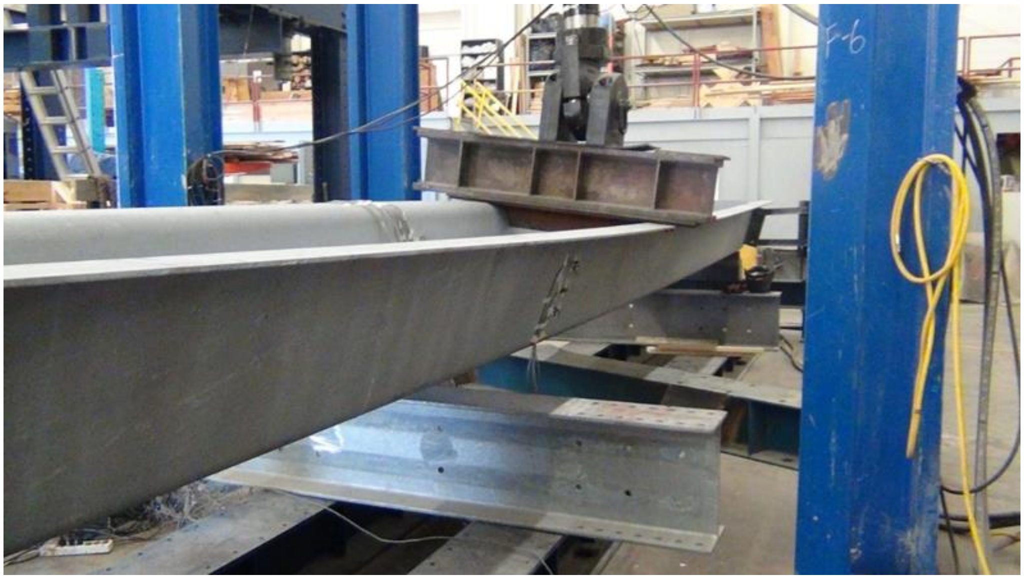

Figure 2.11: Typical Failure Mode for Noncomposite Specimens (Michaelson, 2014)

In addition to laboratory testing, Michaelson developed a three-dimensional nonlinear finite element modeling procedure to capture the behavior and ultimate capacity of composite and noncomposite PBFTGs. Michaelson showed the analysis accurately captured the behavior of the composite system through ultimate failure (Figure 2.12). This was used to assess the applicability of the AASHTO LRFD BDS for the system. The AASHTO LRFD BDS were found to be slightly conservative in computing the nominal capacity of the system and an improved expression was proposed. The noncomposite stability of the system was also assessed. The system was susceptible to lateral torsional buckling under low load levels. However, the installation of stay-in-place (SIP) metal formwork prior to girder erection was found to increase the torsional stiffness and reduce the severity of this issue.

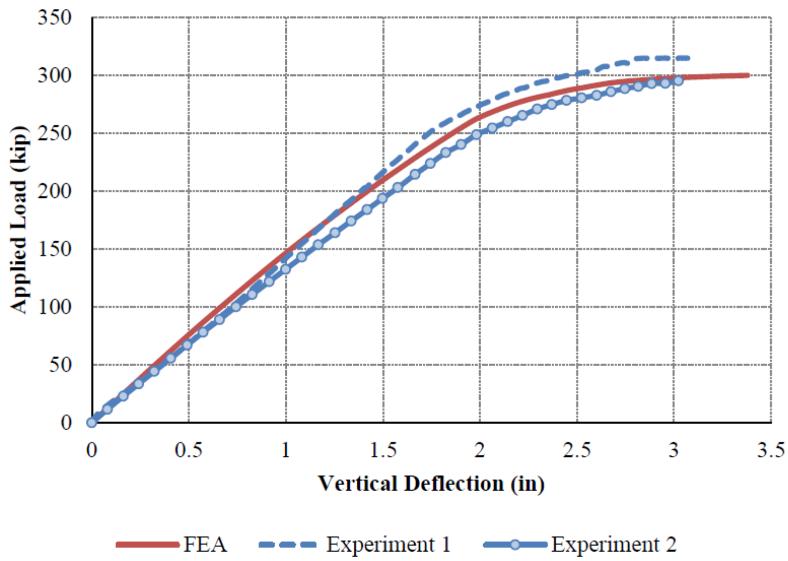

Figure 2.12: Comparison of Experimental and Analytical Results of the Composite Specimens (Michaelson, 2014)

Michaelson assessed the validity and competitiveness of the system in the short-span bridge market. A feasibility assessment was first performed to determine the maximum span length for each plate length and thickness at the Strength I limit state and Service II limit state and to check the live load deflection. A variety of plate widths and thicknesses were reduced to a handful of sections for mainstream use. The PBFTG system composed of 120 inch wide by 5/8 inch thick plate was the largest proposed system with an applicable span length of 80 feet. However, due to the current limit of large capacity press-brakes, a single PBFTG can only be fabricated up to 60 feet in length.

2.3.2 Experimental Evaluation of Noncomposite Shallow Press-Brake-Formed Steel Tub Girders (Kelly, 2014)

In conjunction with Michaelson, Kelly (2014) explored the stability and torsional behavior of noncomposite PBFTGs. The proposed PBFTG system consisted of a pre-cast concrete deck, but the option of a cast-in-place deck was explored. The critical stage of this construction method occurs while the concrete is being poured, as the noncomposite system must resist the construction loads. In this stage, the top flanges of the girder are in compression and are susceptible to torsional buckling. To assess this stage of construction, flexural testing was performed similarly to Michaelson (2014), with load applied through a WT section bolted to the top flange at girder midspan. Prior to testing, an initial twist was noticed in one of the specimens (Figure 2.13). Measurements taken at tenth points along the span measured the flange and web inclinations. Due to these initial imperfections, Kelly calculated the first-order lateral buckling capacity of PBFTG sections and found the critical load at mid-span was 92.3 kip.

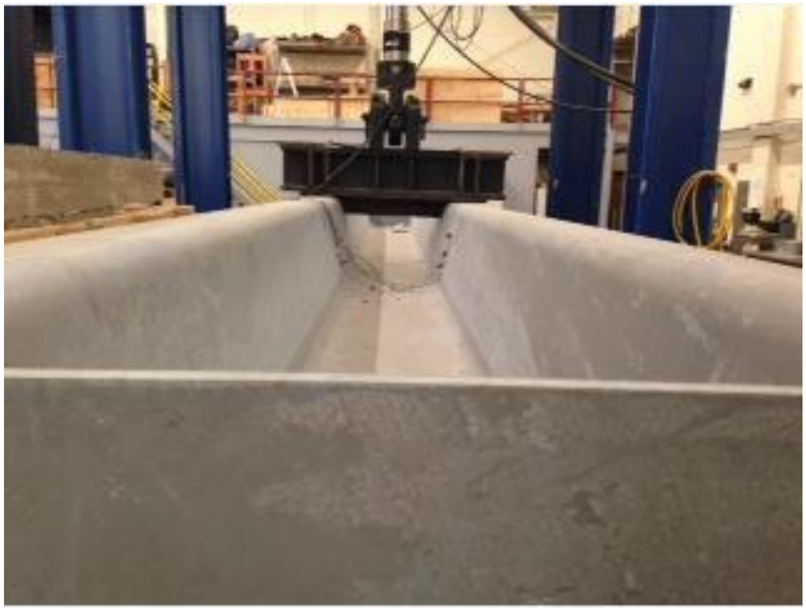

Figure 2.13: Initial Twist of Specimen #2 (Kelly, 2014)

The first experiment consisted of an uncoated specimen and the load deflection curve was linear up to a load of approximately 94 kip, corresponding to 2.25 inches of vertical deflection at midspan (Figure 2.14). At this point, the girder suddenly failed under lateral torsional buckling and the experiment was subsequently terminated due to large lateral deflections. The second experiment consisted of a galvanized specimen, and the flexural testing was similar to the first experiment, until it was terminated due to large lateral deflections under a load of approximately 33 kip. The loss of capacity was attributed to the second-order effects relating to the initial measured imperfections. The lateral torsional buckling failure mode is illustrated in Figure 2.15.

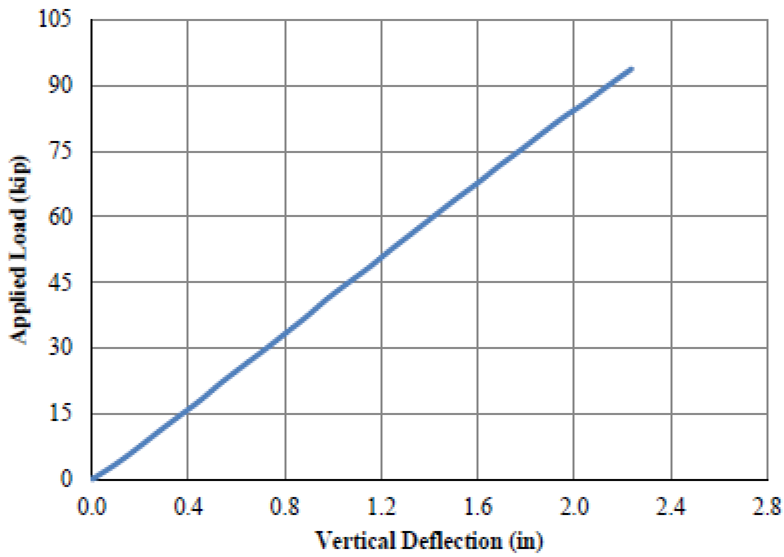

Figure 2.14: Load-Deflection Data from Experiment #1 (Kelly, 2014)

Figure 2.15: Lateral Torsional Buckling (Kelly, 2014)

Kelly (2014) developed modeling techniques to verify the noncomposite laboratory testing. Her focus on initial imperfections, specifically initial out-of-flatness of the web, initial tilt of the compression flange, and initial lateral sweep of the compression flange, were used to replicate the initial state of the PBFTGs. The results of the laboratory testing and FEA modeling showed the modeling techniques accurately captured the behavior of the system. The model also adequately captured the lateral torsional buckling failure mode similar to the experimental tests.

2.3.3 Evaluation of Modular Press-Brake-Formed Tub Girders with UHPC Joints (Kozhokin, 2016)

Kozhokin (2016) evaluated the performance of a longitudinal joint consisting of an ultra-high performance concrete (UHPC) pour between two modular PBFTGs. UHPC is a cementitious material containing Portland cement, silica fume, quartz flour, fine silica sand, high-range water reducer, water, and steel fibers. Testing the joint served two purposes: to prove the capability of the UHPC to transfer loads adequately between adjacent girders and to prove the applicability of PBFTGs as modular units.

UHPC can develop a connection over an extremely small amount of exposed rebar. The connection can be strengthened if bonded to a roughened concrete surface, opposed to a typical smoothed concrete edge. Two methods were proposed to obtain the desired roughened concrete edge. The first method involved the use of a retarder on the formwork and wire brushing the concrete. Two different retarders were used: one was used with 1/2 inch aggregate and smaller and the other was used with 3/4 inch aggregate and larger. The second method included 3/4 inch stone glued to the formwork to create voids in the concrete when the formwork was removed. The concrete used in this method was vibrated at different distances from the formwork to test the usability of the stone glued to the panel. The four connections were tested before performing large scale testing of the joint. The results of testing showed the use of retarder with larger aggregate and wire brushing provided the best shear key detail for bonding (Figure 2.16).

Figure 2.16: Concrete Surface after Wire-Brushing (Kozhokin, 2016)

The proposed joint detail was tested between two 35 foot long modular PBFTG units. Each modular unit consisted of a PBFTG formed from 84 inch wide by 7/16 inch thick plate with a pre-topped 6 inch thick concrete deck. After the deck concrete cured, the UHPC joint was poured, joining the two modular units (Figure 2.17). A 67.43 kip load was applied at midspan of one of the modular units over 2.7 million cycles to simulate infinite fatigue life. At a predetermined set of load cycles, a Service II load was applied statically, and strains were recorded in both the directly and indirectly loaded module to determine if the load was being adequately distributed.

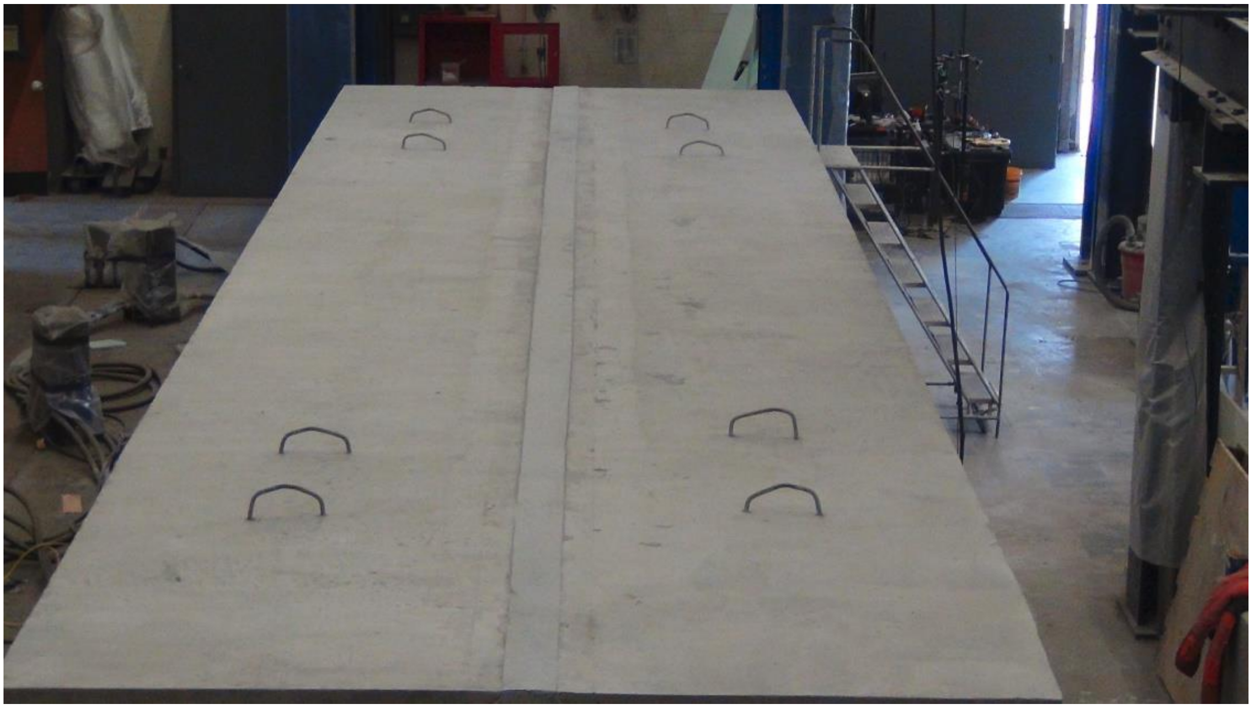

Figure 2.17: Concrete Deck with the UHPC Joint (Kozhokin, 2016)

After approximately 1.6 million fatigue cycles, the deck directly under the point of load application failed. Material testing of the deck concrete revealed the compressive strength of the concrete was only 3 ksi after 28 days, contributing to the punching shear failure of the concrete (Figure 2.18). As the UHPC joint was satisfactorily transferring load from one modular unit to the other, the load was moved to the undamaged girder, and a larger plate was used to apply load from the actuator to the deck. The UHPC joint continued transferring the load satisfactorily through the remainder of the fatigue testing. A minor difference was noted in the distribution factors and deflections from before and after the load was moved to the adjacent girder, but the UHPC joint was found to be an adequate joint material.

Figure 2.18: Concrete Deck Failure (Kozhokin, 2016)

2.3.4 Fatigue Performance of Uncoated and Galvanized Press-Brake-Formed Tub Girders (Tennant, 2018)

This study analyzed the fatigue performance of PBFTGs with and without a steel protective system. Concerns were raised about the hot-dip galvanization process regarding residual stresses present in the bends of the PBFTGs. Tennant (2018) examined the performance of two PBFTGs consisting of ASTM A709 steel: one uncoated and the other hot-dip galvanized. Each simply supported specimen was made composite with a 6 inch concrete deck and fatigue loaded simulating a 75-year design life in a rural environment. The PBFTGs were analyzed for rural loading due to the anticipated location of this type of short-span bridge. To avoid the localized concrete crushing found in Kozhokin (2016), a spreader beam and elastomeric bearing pads were utilized to distribute the load more adequately (Figure 2.19).

Figure 2.19: Galvanized Modular System (Tennant, 2018)

A Service II moment was induced into each PBFTG at a predetermined number of cycles to determine if the galvanization had a negative effect on the system. The strain and deflection of each PBFTG were recorded at each induction of the Service II moment. The concrete deck of the galvanized PBFTG was found to have a significantly lower compressive strength than that of the uncoated specimen, causing slightly higher deflections and strains. However, the study concluded the galvanization process did not negatively affect the performance of the composite system. Each system performed linearly throughout the fatigue life of the system, showing the heat of galvanization did not affect the residual stresses locked into the bends of PBFTGs.

2.4 PREVIOUS FIELD TESTING OF PBFTGS

As the economical and long-term feasibility of the system was confirmed by the experimental and analytical research performed at WVU, PBFTGs began to be used in the field. Multiple PBFTG bridges have been constructed and field tested by researchers from WVU and Marshall University across three states. This section describes the bridges constructed and methods used to analyze the performance of the structures under live loading. Specifically, the distribution of live load across the PBFTGs is discussed.

2.4.1 Field Performance of Press-Brake-Formed Tub Girder Superstructures (Gibbs, 2017)

Gibbs (2017) analyzed the performance of the first bridge designed, constructed, and opened to traffic using PBFTGs. The Amish Sawmill Bridge (Figure 2.20) in Buchanan County, Iowa consists of four galvanized PBFTGs made from 96 inch wide by 1/2 inch thick plate. The contractors chose to use a cast-in-place concrete deck. The goal of the research was to compare the results from a live load field test performed on site to analytical results obtained from finite element modeling.

Figure 2.20: New Amish Sawmill Bridge (Gibbs, 2017)

For the live load field test, researchers applied Bridge Diagnostics, Inc. strain gauges to the bottom flange of each PBFTG. Each girder was equipped with a minimum of three gauges at midspan for redundancy. Axle weights and distances of the loading truck were recorded to adequately model later using FEA. As the bridge was symmetric and not skewed, only five truck runs were necessary to complete the field test. One run was placed to maximize the load in an exterior girder and another run was placed to maximize the load in an interior girder. Two more loads were placed 12 feet away from either of the aforementioned runs to maximize the load in an interior or exterior girder from the two-lane loaded condition. The final truck was placed in the center of the bridge to determine if symmetrical results were produced.

LLDFs were calculated by dividing the strain in the girder in question by the sum of strain in all girders. LLDFs were also generated for two-lane loaded scenarios by superimposing strain values from two truck runs. The distribution factors matched closely, but the bottom flange strains generated by FEA were higher than those found from the field test. This discrepancy was attributed to differing boundary conditions. The Amish Sawmill Bridge utilized integral abutments, where the ends of each girder were encased in concrete, leading to much stiffer supports than traditional hinge-roller supports. However, integral abutments were not used in the finite element model as not enough information exists to adequately model this type of boundary condition. LLDFs from the experimental and analytical data were compared to LLDFs calculated according to the AASHTO LRFD BDS (Figure 2.21).

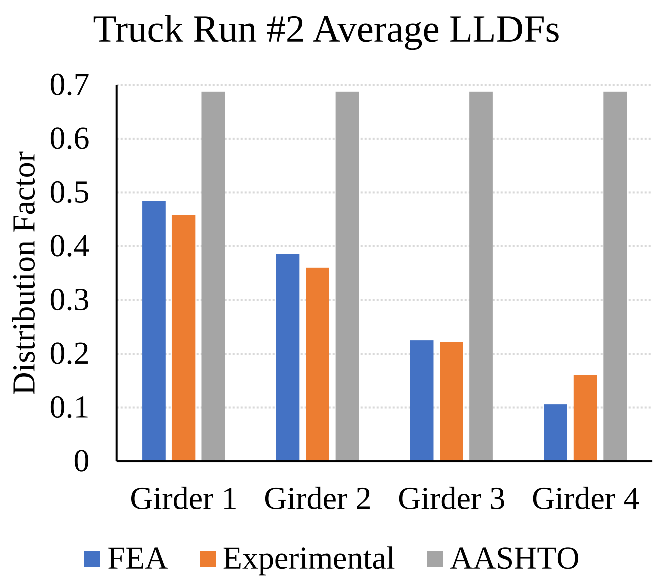

Figure 2.21: FEA vs. Experimental vs. AASHTO LLDFs for Truck Run 2 (Gibbs, 2017)

As seen in Figure 2.21, the analytical and experimental LLDFs are similar, while the AASHTO LRFD BDS provided significantly higher LLDFs for one-lane loaded scenarios. LLDFs for two-lane loaded scenarios for the experimental and analytical analysis showed less variation from the AASHTO LRFD BDS LLDFs but were still found to be conservative. The research proved PBFTGs can exhibit consistent performance and LLDFs provided by the AASHTO LRFD BDS can be used conservatively. Further research was proposed to provide less conservative distribution factor equations in the AASHTO LRFD BDS which more precisely simulate load distribution.

2.4.2 Field Performance and Rating Evaluation of Modular Press-Brake-Formed Steel Tub Girder with a Steel Sandwich Plate Deck (Underwood, 2019)

The Cannelville Road Bridge in Muskingum County, Ohio was the second bridge built utilizing PBFTGs and the first to be constructed using modular units. The superstructure was composed of four hot-dip galvanized PBFTGs constructed from 5/8 inch thick plate. The girders were both internally and externally braced every 6 feet. The girders were delivered to the construction site as two modular units consisting of two girders each, bolted to a sandwich plate steel (SPS®) deck. The use of the modular superstructure, as well as some other innovative ABC methods, allowed for expedient construction. Erection of the superstructure was completed in approximately 20 minutes, and the entire project from bridge demolition to opening of the new bridge was complete in 26 days.

Underwood (2019) worked with researchers from WVU and Marshall University to perform a live load field test on the Cannelville Road Bridge. The field test assessed the applicability of AASHTO LRFD BDS' LLDFs with regards to PBFTGs combined with an SPS® deck. Bridge Diagnostics, Inc. strain gauges were applied to the midspan of each girder in a manner similar to Gibbs (2017), and a tandem axle load truck was placed at predetermined grid points. The strain readings were not immediately recorded, allowing any vibrations to settle for a couple moments to negate any impact effects.

A finite element model of the bridge was developed to verify the results from the live load field test. Equivalent loads were applied to the structure to replicate the loads produced by the tandem axle load truck. The stresses were queried at each gauge location in the field and were compared. The stresses from the experimental and analytical tests were used to generate LLDFs and live load girder ratings. LLDFs were compared to equations present in the AASHTO LRFD BDS, and it was found, as in other tests, the AASHTO LRFD BDS tended to be overly conservative and underpredict the performance of PBFTGs (Figure 2.22).

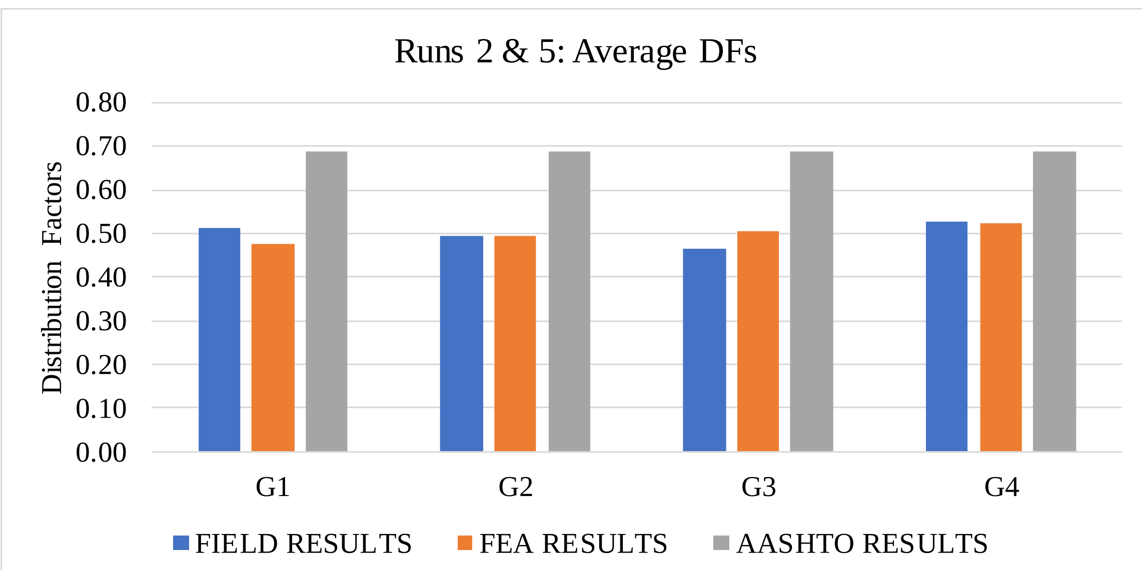

Figure 2.22: Field v. FEA v. AASHTO LLDFs (Underwood, 2019)

2.4.3 Field Evaluation of a Modular Press-Brake-Formed Steel Tub Girder in an Application that Includes Skew and Superelevation (Roh, 2020)

The Fourteen Mile Bridge in Lincoln County, West Virginia is a 58 foot long single span PBFTG bridge (Roh, 2020). The bridge has a skew angle of 10° and a superelevation of 8%. As this bridge has significant skew and superelevation, special attention was paid to detailing shear studs, end diaphragms, and mounting angles for interior formwork. Specifically, the use of sacrificial interior wooden formwork in conjunction with varying length shear studs was used to address the superelevation. Skew was addressed by cutting the plate at the ends of the girder and offsetting each girder from the previous (Figure 2.23). Once all five composite modules were completed, they were transported to the bridge site and placed onto the abutments by crane. After the five modules were placed, formwork was erected around the longitudinal joints for UHPC closure pours. No further exterior or interior bracing was required due to the high torsional stiffness of the composite PBFTG modules.

Figure 2.23: PBFTG with Completed Internal Formwork (Roh, 2020)

Generally following the methodology of Gibbs (2017) and Underwood (2019), Roh (2020) conducted live load field testing on the Fourteen Mile Bridge. Gauges were placed at quarter span to allow for ease of installation. Additional care was taken to ensure gauges were placed appropriately with regards to the skew present in each girder. As load placement was much harder to determine on site due to the superelevation and skew, the grid which the load would be applied was simplified to parallel lines at two-foot increments longitudinally and tenth points transversely. Linear interpolation would be used to generate the appropriate truck locations for worst case scenario one and two-lane loaded conditions.

Next, LLDFs from the live load field test, FEA, and empirical equations from the AASHTO LRFD BDS were compared. The strain readings from the three strain gauges on each bottom flange were averaged to account for torsion in the live load field test. Averaged girder strains and applicable multiple presence factors were used to generate LLDFs when the truck was at midspan. Midspan was chosen for comparison to the analytical model as the position would have the greatest effect on the girders. The results of the analytical modeling closely matched the results of the field testing, verifying the accuracy of both (Figure 2.24). As with previous research, Roh found the AASHTO LRFD BDS to be conservative when compared to analytical and experimental results.

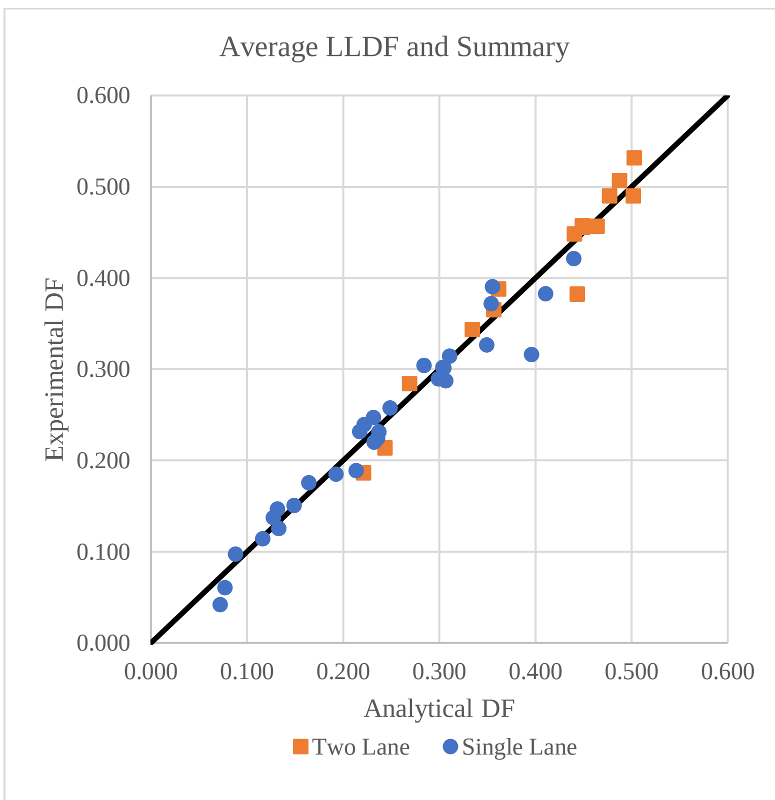

Figure 2.24: Comparison of Analytical and Experimental Results (Roh, 2020)

Additionally, Roh analytically investigated the effectiveness of bracing in noncomposite PBFTGs as a continuation of research performed by Kelly (2014). Instability issues can arise in the open shape of noncomposite PBFTGs, as they are susceptible to torsional effects. These torsional effects are insignificant in composite construction, and therefore are not accurately captured in the global FEA. Different assumptions with regards to initial imperfections, material modeling, and loading must be made. Geometric imperfections, specifically flange tilt and girder twist, were considered as they had the largest effect on the results found by Kelly (2014). Elastic-plastic constitutive laws were used to accurately capture the behavior of steel past the yield stress, as shown in Figure 2.25. Roh used the S4R element to model the noncomposite PBFTGs. The S4R is a 4-node general purpose shell element utilizing reduced integration with hourglass controls and is suitable for a wide range of applications The reduced integration used by the S4R elements can cause no strain at the integration points, so a small artificial stiffness associated with zero-energy deformation was introduced. Finally, the loading was applied using the modified Riks algorithm available in Abaqus/CAE to capture the complete nonlinear solution.

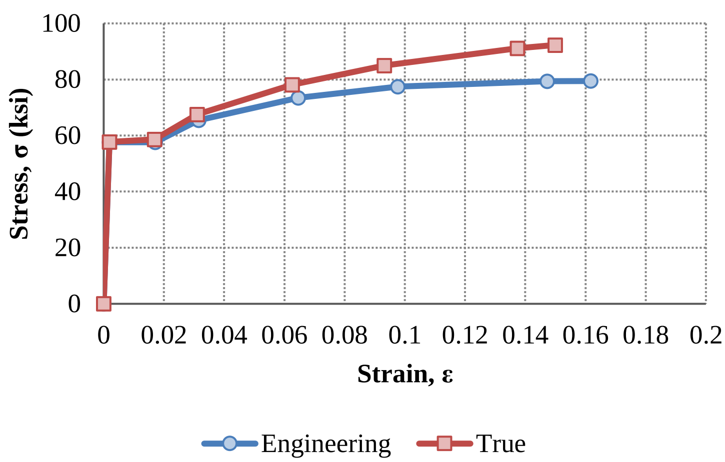

Figure 2.25: Multi-Linear Stress-Strain Curve (Roh, 2020)

A multitude of internal and external bracing scenarios were examined. L4x4x5/8 members were used as transverse and diagonal internal bracing elements between the top flanges. External bracing was modeled as transverse boundary conditions. Vertical and lateral deflections were compared from each internal and external bracing scenario to the results found from Kelly (2014). Results showed little effect of internal bracing or external bracing on vertical deflection. However, the addition of diagonal bracing had a large reduction on the lateral displacement of the PBFTG. The addition of external braces reduced the lateral deflection to zero, but this is due to the program forcing zero lateral deflection at the point of measurement.

2.5 Summary

Several researchers over many decades have explored the use of prefabricated bridge elements to increase the economy in ABC. Many researchers found iterations of PBFTGs to be competitive in the short-span bridge market. Extensive laboratory research at WVU has shown PBFTGs perform exceptionally well at the ultimate limit state and under fatigue loading conditions. This research has allowed for multiple PBFTGs in three states to be constructed and field tested to assess the live load distribution characteristics of the system. However, while the system has proven its efficiency and economy in simple bridge situations, the system has not yet been thoroughly explored in more complex scenarios, including continuous spans or skewed scenarios. The empirical equations found in the AASHTO LRFD BDS have been found to be conservatively applicable to PBFTG bridges; however, the current wording of the AASHTO LRFD BDS prohibits the use of the empirical equations provided.

CHAPTER 3: LIVE LOAD DISTRIBUTION FACTOR LITERATURE REVIEW

3.1 Introduction

This chapter details the historical development of LLDFs in bridge systems and discusses the influence of various parameters on the lateral distribution of load. The primary focus of much of the research performed on LLDFs has historically been on straight beam slab bridges, but special attention is given in this chapter to studies evaluating LLDFs for box sections.

3.2 Historical Development of Live Load Distribution Factors

LLDFs have been included in American bridge specifications since the first edition of the American Association of State Highway Officials Standard Specifications (AASHO, 1931). The current AASHTO Standard Specifications for Highway Bridges (AASHTO, 2002) include the original distribution factors with minor modifications. The first major change in the computation of the distribution of load occurred when AASHTO adopted the LRFD BDS in 1994.

3.2.1 AASHTO Standard Specifications

Although AASHTO Standard Specifications and current AASHTO LRFD BDS allow the use of more refined analysis for lateral distribution of load, the use of simplified methods is permitted and frequently used, when applicable. This simplified method involves the distribution of wheel load to adjacent longitudinal elements. This lateral distribution is used in conjunction with line girder analysis (LGA) to determine the maximum possible number of wheels the girders must resist. The simplified method of the lateral distribution of wheel load generally takes the following form:

$$g \leq \frac{S}{D} \qquad \text{Eq. 3.1}$$

Where:

g = distribution factor

S = beam spacing

D = parameter used in determination of load fraction of wheel load

This type of equation is dependent on the bridge type and is generally valid for bridges up to a certain beam spacing. Table 3.1 shows the distribution of wheel loads, organized based on floor type. In situations with a concrete floor supported by four or more steel stringers and beam spacing less than six feet, the fraction of the wheel load shall not be less than:

$$g \geq \frac{S}{5.5} \qquad \text{Eq. 3.2}$$

Where:

g = distribution factor

S = beam spacing

In situations where the concrete deck is supported by four or more steel stringers and beam spacing more than six feet, but less than fourteen feet, the minimum distribution factor is:

$$g \geq \frac{S}{4.0 + 0.25S} \qquad \text{Eq. 3.3}$$

Where:

g = distribution factor

S = beam spacing

Table 3.1: Distribution of Wheel Loads in Longitudinal Beams (AASHTO, 2002)

Kind of Floor	Bridge Designed for One Traffic Lane	Bridge Designed for Two or more Traffic Lanes
Timber:[a]		
Plank[b]	S/4.0	S13.75
Nail laminated[c] 4" thick or multiple layer[d] floors over 5" thick	S/4.5	S/4.0
Nail laminated[c] 6" or more thick	S15.0 If S exceeds 5' use footnote f.	S14.25 If S exceeds 6.5' use footnote f.
Glued laminated[e] Panels on glued laminated stringers		
4" thick	S14.5	S14.0
6" or more thick	S16.0 If S exceeds 6' use footnote f.	S/5.0 If S exceeds 7.5' use footnote f.
On steel stringers		
4" thick	S14.5	S/4.0
6" or more thick	S15.25 If S exceeds 5.5' use footnote f.	S/4.5 If S exceeds 7' use footnote f.
Concrete:		
On steel I-Beam stringers[g] and prestressed concrete girders	S/7.0 If S exceeds 10' use footnote f.	S15.5 If S exceeds 14' use footnote f.
On concrete T-Beams	S/6.5 If S exceeds 6' use foomote f.	S/6.0 If S exceeds 10' use footnote f.
On timber stringers	S/6.0 If S exceeds 6' use footnote f.	S/5.0 If S exceeds 10' use footnote f.
Concrete box girders[h]	S18.0 If S exceeds 12' use footnote f.	S/7.0 If S exceeds 16' use footnote f.
On steel box girders	See Article 10.39.2.	
On prestressed concrete spread box Beams	See Article 3.28.	
Steel grid:		
(Less than 4" thick)	S14.5	S/4.0
(4" or more)	S/6.0 If S exceeds 6' use footnote f.	S/5.0 If S exceeds 10.5' use foomote f.
Steel bridge Corrugated plank[i] (2" min. depth)	S15.5	S14.5

In situations where the beam spacing exceeds the values prescribed in Table 3.1 or the requirements in Equation 3.2 or Equation 3.3, the load on each stringer shall be the reaction of the wheel loads, assuming the flooring between the stringers acts as a simple beam. This method of lateral distribution of load is commonly known as lever rule, and a depiction is presented in Figure 3.1. It should be noted lever rule is still used in the current edition of the AASHTO LRFD BDS for certain loading scenarios.

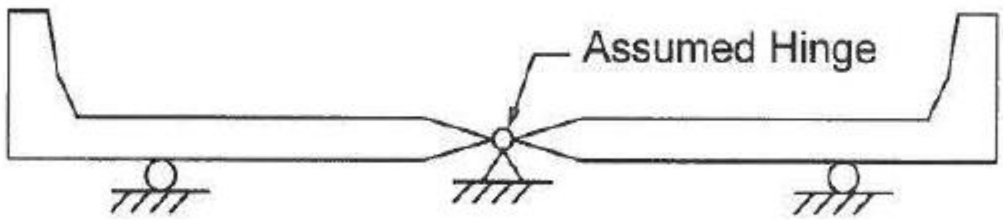

Figure 3.1: Notional Model for Applying Rule to Three-girder Bridges (AASHTO, 2020)

Slightly more complicated equations are used in AASHTO Standard Specifications for the determination of bending moment in steel box-girders. The current distribution factor in the AASHTO Standard Specifications for box-girder bridges was developed by Johnson and Mattock (1967):

$$W_L = 0.1 + 1.7R + \frac{0.85}{N_w} \qquad \text{Eq. 3.4}$$

In which:

$$\mathrm{R} = 0.5 \leq \frac{N_w}{Number\ of\ Box\ Girders} \leq 1.5 \qquad \text{Eq. 3.5}$$

$$N_w = \frac{W_c}{12}\ reduced\ to\ the\ nearest\ whole\ number \qquad \text{Eq. 3.6}$$

Where:

W_c = roadway width between curbs in feet, or barriers if curbs are not used

It should be noted that while the LLDF expressions in the AASHTO Standard Specifications, specifically the S/D equations, have been applied to a wide array of bridges, the bridges considered during the development of the LLDFs were exceptionally simple. Specifically, Equation 3.1 does not consider many prominent bridge factors, such as the type and size of the bridge deck, girder stiffness, or span length, resulting in substantially conservative distribution factors. Additionally, no consideration is given in Equation 3.1 to more complicated bridge structures, including skew, horizontal curves, or continuous spans.

In the 1980s, researchers determined the AASHTO Standard Specifications should be updated and modernized. Sanders (1984) synthesized the background of then current specification criteria, provided an overview of the research being performed, and performed an evaluation of design and load rating practices as they related to the supporting structure and deck system types. He concluded an extensive study of LLDFs for highway bridges was needed as improvements to the empirical equations for the sake of accuracy were made over time and have led to many inconsistencies. Additionally, some parameters, which had been thoroughly evaluated and determined to influence live load distribution, such as the number of loaded lanes and reduction of loading intensity with increased number of loaded lanes, are not incorporated into the AASHTO Standard Specifications. Finally, Sanders (1984) introduced a study which would become the basis for an updated and unified set of LLDFs to be included in the AASHTO LRFD BDS.

3.2.2 AASHTO LRFD Specifications

The first edition of the AASHTO LRFD BDS was published in 1994, and with the new bridge design specifications came new methods of distributing live load to the longitudinal bridge elements. To address the issues with the AASHTO Standard Specifications, The National Cooperative Highway Research Program (NCHRP) Project 12-26 was initiated to overhaul the previous provisions relating to live load distribution.

Zokaie et al. (1991) developed comprehensive specifications for the distribution of wheel loads on highway bridges in two phases. The first phase concentrated on beam and slab and box-girder bridges, and the second phase concentrated on slab, multi-box beam, and spread box beam bridges. For each general bridge type, three separate levels of analysis were proposed. Level One methods of analysis are the simplest and consist of equations distributing load laterally from the wheel lines. Level Two methods of analysis include graphical methods, nomographs, influence surfaces, and grillage analysis. Level Three methods are the most accurate and involve detailed modeling of the entire bridge superstructure, such as a complete FEA.

The basis of the LLDF equations used today were developed from a parametric study of 365 bridges across multiple states comprised of three different types of bridge superstructures: prestressed T-beams, concrete I-girders, and steel I-girders. The first step was to perform a sensitivity study to determine the effect of various parameters on the lateral distribution of live load in bridges. An average bridge was generated with the average properties of each type of bridge. To determine the effect of various bridge parameters, one parameter was varied at a time with respect to the average bridge.

In the sensitivity study performed by Zokaie et al., the following set of parameters were varied to determine their effect: girder spacing/number of girders, span length, girder stiffness, slab thickness, number of loaded lanes, deck overhang, skew, load configuration, support condition, and end diaphragms. After analyzing the sensitivity of these factors, the critical parameters for the most common type of bridge, beam and slab, were found to be girder spacing, span length, girder stiffness, and deck thickness. No revisions were proposed for bridges with a concrete deck on multiple steel box-girders. The equations presented in the AASHTO LRFD BDS are generally more complex than those found the in the AASHTO Standard Specifications but are also more accurate.

3.3 Evaluations of Current Live Load Distribution Factors

Research has been performed by multiple investigators throughout the development of the LLDFs used in modern bridges. Investigators have examined the accuracy the AASHTO Standard Specifications and the AASHTO LRFD BDS through analytical studies of finite element models and experimental studies of existing bridges. Although the topic of live load distribution has been analyzed since the inception of a standard specification for bridge design, this section will focus on and summarize the research performed in the last forty years.

3.3.1 Analytical Studies

Analytical studies conducted by various researchers have been used to evaluate LLDFs for moment and shear distribution in bridges. Many of the studies performed assess the LLDFs found in the AASHTO Standard Specifications and the AASHTO LRFD BDS. Research efforts have largely been focused on the accuracy of these specifications with respect to one or more specific parameters. Some studies have been performed to develop new and simplified equations to be used in conjunction with one-dimensional LGA. A summary of selected studies is presented herein.

Johnston and Mattock (1967) developed a computer program to assess the lateral distribution of load in simple span composite box-girder bridges without transverse diaphragms or internal stiffeners. The accuracy of the computer program was confirmed with quarter-scale experimental testing. The computer program was used to evaluate the behavior of 24 composite box-girder bridges with varying span lengths, number of lanes, and number of girders. As a result of the study, two equations were proposed for the transverse distribution of load to each box-girder. As stated in Section 3.2.1, the work performed in this study led to the current equation used in the AASHTO Standard Specification.

Wallace (1976) performed finite element analyses on 51 theoretical skewed concrete box-girder bridges using the program CELL to describe the behavior of the systems. The assessment focused on the effects of the width-to-span ratio, number of cells, skew angle, type of loading, and depth of box-girder members. Width-to-span, or aspect ratio, and skew angle were found to be the most significant factors affecting moment distribution, while span length and skew angle were found to be the most significant parameters affecting shear distribution for the exterior girder at the obtuse corner.

Hays et al. (1986) performed analysis using the computer program SALOD to evaluate lateral load distribution of simple span bridges in flexure. SALOD uses moment influence surfaces generated from the finite element system STRUDL for representative simple span bridges consisting of concrete girders, steel girders, T-beams, or flat slabs. The analytical study was verified by comparing it against field data recorded from eight bridges. A parametric study was performed to assess the effects of girder spacing and span length. The results of the study were then compared against the distribution factors calculated from the AASHTO Standard Specifications and the Ontario Bridge Design Code. The results of the study showed the effect of span length, which at the time was neglected by the design specifications, had a considerable impact. The researchers found the distribution factors from the AASHTO Standard Specifications were unconservative for span lengths up to 60 feet and girder spacings up to 6 feet. However, as span length and girder spacings increased, the AASTHO Standard Specifications became more conservative.

Khaleel and Itani (1990) performed FEA to determine the effects of skew on lateral load distribution for continuous skewed bridges. The researchers analyzed 112 continuous span bridges consisting of five pretensioned I-girders with spans between 80 and 120 feet and girder spacings between 6 and 9 feet. Skew angles between 0° and 60° were evaluated. The maximum moments found in the study were then compared to the AASHTO Standard Specifications, which did not account for the effects of skew. The researchers showed the AASHTO Standard Specifications distribution of wheel loads can underestimate the design moments by 6% in some instances and overestimate the design moments by 40% in others. The researchers proposed a skew reduction factor to be used in conjunction with the AASHTO Standard Specifications based on the span length, girder spacing, skew angle, and girder location.

Tarhini and Frederick (1992) performed analytical research specifically on the distribution of loads on concrete slab on steel I-girder bridges. To determine the effects of various parameters on the distribution of load, a typical bridge was selected, and one parameter was varied within practical ranges, while the others were held constant. The parameters considered were girder spacing, girder stiffness, presence of cross-bracing, concrete slab thickness, span length, single or continuous spans, and composite or noncomposite behavior. The distribution factor was calculated in this study by dividing the maximum moment in a girder found using FEA by the maximum moment in a girder found using LGA. An equation was developed for the live load distribution based on girder spacing and span length, as they were found to be the most influential. The researchers found this equation to be applicable to single or continuous span and composite or noncomposite bridges.

Ebeido and Kennedy (1996a and 1996b) performed parametric studies on over 600 prototype continuous skew composite bridges using FEA. The analytical modeling was verified against experimental tests on three continuous and six simple span, composite, concrete deck on steel beam bridges. Empirical equations were developed for main span moment, interior support moment, reaction, and shear distribution factors. Results from the study show increased skew decreases the main span and interior support moments while increasing the reactions and shear in the obtuse corner. Additionally, the influence of skew on shear and moment distribution factors significantly increases for skew angles above 30°.

Mabsout et al. (1997a, 1997b, and 1998) analytically explored the effects of various parameters on the distribution of wheel load and compared the results to the simplified equations found in the AASHTO LRFD BDS, AASHTO Standard Specifications, and previous experimental results. The researchers first explored the validity of four separate finite element modeling techniques on a simple span, two lane, composite steel I-girder bridge. Results from a parametric suite of girders with varying span length and girder spacing found each of the modeling techniques produced similar LLDFs, correlating well with the AASHTO LRFD BDS, but not with the AASHTO Standard Specifications. Following the verifications of the finite element modeling techniques, the researchers explored the effect of sidewalks, railings, and continuity on LLDFs. The researchers found when sidewalks and/or railings were constructed integrally with the bridge deck and properly reinforced, LLDFs of exterior girders increased. The researchers state the presence of sidewalks and/or railings can reduce LLDFs of interior girders by 5 to 30%. When considering continuous span bridges, the researchers also recommended the addition of a reduction factor for positive and negative moments of up to 5%.

Arockiasamy and Amer (1998) developed simplified equations for a multitude of varying bridge types based on analytical studies of numerous parameters. The analytical studies were based on finite element modeling using ANSYS 5.2 and were verified against field test data. The first phase of the research was to perform grillage analysis to study the effects of span length, bridge width, slab thickness, girder type, and number of lanes on moment and shear live load distribution. Generally, the researchers found LLDFs from the empirical equations found in the AASHTO LRFD BDS were slightly conservative compared to the calculated LLDFs from grillage analysis. The second phase of the research focused on the effects of skew and continuity on live load distribution. Similar to phase one, the influence of skew angle, girder spacing, span length, slab thickness, and number of lanes were studied in skewed slab-on-girder bridges. The authors explored skew angles between 0° and 60° and concluded the AASHTO LRFD BDS are accurate in reflecting the live load distribution in bridges, particularly for skew angles greater than 30°.

Additionally, the authors state the AASHTO LRFD BDS empirical equations overestimate the effect of slab thickness.

Mertz (2007) performed research to develop updated LLDFs for shear and moment. The goal of the research was to develop simplified LLDF equations with a larger range of applicability than those found in the AASHTO LRFD BDS. Three sources of data were used to develop a parametric suite of bridges: the NCHRP 12-26 bridge set, the Tennessee Technological University set, and a set of bridges from AASHTO Virtis/Opis used to compare rating procedures. Multiple simplified and rigorous analytical models were run on the suite of parametric bridges to generate LLDFs. LLDFs generated from this array of bridges was used to codify simplified moment and shear LLDFs across a wider range of applicability.

Yousif and Hindi (2007) compared LLDFs of simple span slab-on-girder concrete bridges calculated using the AASHTO LRFD BDS and several finite element linear elastic models. The researchers analyzed bridges across the full range of applicability specified by the AASHTO LRFD BDS regarding span length, slab thickness, girder spacing, and longitudinal stiffness. The deck was modeled as 4-node quadrilateral shell elements, and the beams were modeled as space frame elements. The vehicular live load plus the lane load, as specified in the AASHTO LRFD BDS, was placed longitudinally to generate the extreme force effect and placed transversely to investigate the one-lane, two-lanes, and three-lanes loaded scenario for each applicable girder. The researchers modeled a total of 886 bridges and concluded the AASHTO LRFD BDS empirical equations significantly overestimate LLDFs when compared to the analytical modeling, reaching a maximum of approximately 55%.

Michaelson (2010) developed new expressions for exterior girder LLDFs for concrete deck on steel beam bridges. Analytical modeling, benchmarked against experimental data, was used in a sensitivity study to determine the effect of key parameters on LLDFs for exterior girders. Following the results of the sensitivity study, parametric matrices of the most influential parameters were developed, and the results were compared to LLDFs from the empirical equations found in the AASHTO LRFD BDS. Finally, the results of the parametric matrices were used to develop empirical equations for exterior girder LLDFs for steel I-girder bridges. Michaelson found the key parameters for live load distribution were girder spacing, span length, deck overhang, and the number of beams in the cross-section.

Razzaq (2017) developed empirical equations for the assessment of LLDFs for composite skewed slab-on-steel I-girder bridges. A parametric study was performed on a composite bridge structure under dead and live loads for the ultimate, serviceability, and fatigue limit states. The researcher considered skew angle, girder stiffness, cross-frame layout, span length, girder spacing, number of girders, and number of design lanes in the determination of empirical equations for moment and shear LLDFs. The results of the study were compared to the equations presented in the Canadian Highway Bridge Design Code.

3.3.2 Experimental Studies

Many research efforts have been conducted to assess the validity of LLDF equations in existing bridge codes by performing experimental studies on in-service bridges. Researchers have devoted significant amounts of time and effort to determine LLDFs at varying loading stages, speeds, and locations.

Bakht and Jaegar (1992) performed an ultimate load test on a simply supported bridge consisting of a noncomposite concrete deck supported by six rolled steel wide flange shapes. A wooden frame was erected under midspan of the structure to allow for approximately 110 millimeters deflection to prevent the bridge from deflecting catastrophically. Uniaxial strain gauges were placed at midspan throughout the depth of each beam to measure the strain at each girder. The bridge was loaded by placing concrete blocks transversely in layers of 24 units at midspan to simulate one-lane loaded. The results of the study show: (1) the moment LLDFs improve when approaching the ultimate load; (2) any incidental composite action between the deck and the beams due to bond or friction completely breaks down approaching the ultimate load; and (3) the beams continue to carry load well past formation of first yield.

Stallings and Yoo (1993) performed a series of stationary and moving tests on three short-span, two lane, steel girder bridges. Tandem axle dump trucks were used to load the bridge under one and two-lane loaded scenarios. LLDFs were calculated from the single and two-lanes loaded stationary tests and impact factors were calculated from the results of the moving tests. Stallings and Yoo (1993) calculated LLDFs from the actual strains measured in the bottom flange as presented in Equation 3.7.

$$DF_i = \frac{n\varepsilon_i}{\sum_{j=1}^{k} \epsilon_j w_j} \qquad \text{Eq. 3.7}$$

Where:

DF_i = wheel load distribution factor for the *i*th girder

n = number of wheel lines of applied loading

ε_i = bottom flange strain of the *i*th girder

w_j = ratio of the section modulus of the *i*th girder to the section modulus of a typical interior girder

This equation can be simplified (Equation 3.8), assuming: the section modulus of an interior girder and an exterior girder are approximately the same; the number of wheel lines can be removed as it was a conversion factor between AASHTO Standard Specifications and AASHTO LRFD BDS; and the relationship between moment and strain is linear.

$$g_i = \frac{M_i}{\sum_{j=1}^{k} M_j} \qquad \text{Eq. 3.8}$$

Where:

g_i = LLDF for the *i*th girder

M_i = bending moment in the *i*th girder

k = number of girders

The researchers found LLDFs calculated using the AASHTO Standard Specifications S/D equations were consistently higher than LLDFs calculated from the experimental results. The researchers state the conservatism was attributed to inaccuracies in the assumptions made using the simplified analysis presented in the AASHTO Standard Specifications.

Fu et al. (1996) performed field testing of four existing I-girder bridges under real truck loading to evaluate parameters affecting live load distribution. LLDFs were calculated from measured strain data in addition to several empirical methods. Comparison of the live load field tests results to the AASHTO LRFD BDS empirical LLDFs of straight non-skewed bridges showed the AASHTO LRFD BDS' LLDFs to be anywhere from 7% to 42% conservative. Additionally, comparison between the live load field results of a skewed bridge to the AASHTO LRFD BDS' empirical LLDFs showed the AASHTO LRFD BDS' LLDF to be 13% unconservative.

Kim and Nowak (1997) performed live load field tests on two simply supported steel I-girder bridges to determine LLDFs and impact factors. Opposed to most other field tests, the recorded data was collected from daily traffic loads in addition to calibrated truck loads. The static strain of the daily traffic loads was measured after removing the dynamic impact component. The static strains in each girder were used to determine LLDFs following a methodology nearly identical to that used by Stallings and Yoo (1993). The strain data was further processed to obtain the mean and standard deviation of LLDFs under daily traffic. The researchers concluded the measured LLDFs were consistently lower than those found using the empirical equations found in the AASHTO LRFD BDS.

Cross et al. (2009) performed live load field tests on twelve bridges to determine the validity of shear LLDFs on typical interstate bridges. The bridges were specifically chosen to represent most interstate bridges in Illinois and to maintain a wide range of parameters. Each beam was instrumented on its web with strain gauge rosettes to measure shear stresses caused by loading vehicles. The load was run slowly across the bridge to model static loading in addition to dynamic tests at highway speeds. Analytical models were developed to verify the live load testing results. The researchers concluded AASHTO LRFD BDS shear live load distribution procedures closely approximate the actual shear live load distribution from analytical and field test results.

3.4 Influence of Parameters Affecting Live Load Distribution

Several previous researchers ((Newmark & Siess, 1942), (Zokaie et al., 1991), (Tarhini & Frederick, 1992), (Mabsout et al.,1997a and 1997b), (Arockiasamy & Amer, 1998), (Nowak et al., 2003), (Yousif & Hindi, 2007), (Li & Chen, 2011), (Razzaq, 2017), (White & Kamath, 2020)) have investigated the effect of numerous parameters on live load distribution in bridges. Two of the most comprehensive studies were conducted by Zokaie et al. (1991), as part of NCHRP 12-26, and Tarhini and Frederick (1992).

The contributions of Zokaie et al. (1991) were discussed in Section 3.2.2. Tarhini and Frederick (1992) focused their research on I-girder bridges with a concrete deck. Similar to the work performed for NCHRP 12-26, a typical bridge design was selected, and one parameter was varied at a time within practical limits. The parameters considered in the FEA included size and spacing of steel girders, presence of cross-bracing, concrete slab thickness, span length, single or continuous spans, and composite or noncomposite design. After performing FEA, girder spacing, span length and girder stiffness were determined to be the most significant parameters relating to live load distribution in slab on girder bridges. However, other parameters were investigated and were found to have a negligible effect, while some disagreement exists regarding the effects of others. This section will summarize the research performed on effects of many of those parameters.

3.4.1 Girder Spacing

Girder spacing has been considered the most influential factor affecting LLDFs since the early work developed for the AASHTO Standard Specifications. Newmark and Seiss (1942) originally developed LLDF empirical equations based on girder spacing, span length, and the ratio between girder and deck stiffnesses. However, later work by Newmark (1949) expressed LLDFs as linear functions of girder spacing only, removing the effects of span length and beam stiffness. This linear relationship is present in the most current AASHTO Standard Specifications with minimal changes since the adoption of the S/D factors.

However, many studies have shown the S/D factors used in the AASHTO Standard Specifications consistently produce overly conservative LLDFs. Studies performed as part of NCHRP 12-26 (Zokaie et al., 1991), and verified by Tarhini and Frederick (1992), demonstrate while the relationship between girder spacing and live load distribution is significant, it is not linear, but exponential. Many studies propose equations for beam slab bridges based on, at least in part, girder spacing. Khaloo and Mirzabozorg (2003) determined, while the effect of girder spacing is significant for the distribution of live load to exterior girders, the effects of girder spacing on the distribution of live load to interior girders is significantly less.

3.4.2 Span Length

Similarly to the effect of girder spacing, a nonlinear relationship between span length and LLDFs was determined by Zokaie et al. (1991) and verified by Tarhini and Frederick (1992). The relationship between span length and live load distribution was found to be more significant for moment in interior girders compared to shear in interior girders. Unlike girder spacing, span length was found to have an inverse effect, such that when span length increases, LLDFs decrease.

Bishara et. al. (1993) evaluated the distribution of live load in medium span length slab-on-girder bridges, with and without skew, to both interior and exterior girders. LLDFs were derived from FEA of 36 bridges. The results of this study showed span length had a slight effect on the distribution of live load to interior girders. However, span length was found to have a more significant effect on bridges with a smaller clear roadway width and with bridges with large skew angles. Khaloo and Mirzabozorg (2003) also determined span length has a small effect on LLDFs of interior girders, but exterior girder LLDFs increase more significantly with span length.

3.4.3 Girder Stiffness

The definition of girder stiffness has changed throughout the history of LLDFs. The first definition of relative stiffness comes from Newmark and Siess (1942), where the researchers compared the relative longitudinal stiffness of the girder to the relative transverse stiffness of the deck. This version of girder stiffness is expressed by the dimensionless parameter, H, as described by Equation 3.9:

$$H = \frac{E_b I_b}{aN} \qquad \text{Eq. 3.9}$$

In which:

$$N = \frac{EI}{1 - \mu^2} \qquad \text{Eq. 3.10}$$

Where:

H = a dimensionless coefficient which is a measure of the stiffness of the beam relative to that of the slab

E_b = modulus of elasticity of the material in a beam

I_b = moment of inertia of the cross-section of a beam

a = span of bridge, center to center of supports

N = measure of stiffness of an element of the slab

E = modulus of elasticity of the material in the slab

I = moment of inertia per unit width of the cross-section of the slab

μ = Poisson's ratio, generally taken as zero in the data given here

Initial results from Newmark and Siess (1942) showed this version of the stiffness parameter had a small, but significant, effect on the distribution of live load. Later results (Newmark, 1949) found the range of applicable values for any given bridge type is small enough the stiffness parameter, in this form, is negligible. Tarhini and Frederick (1992) concluded similar results in their studies, as the girder stiffness had a small, but negligible, effect on live load distribution. The researchers performed a parametric study on the variables in Equation 3.9, such as changing the moment of inertia of the girder or the thickness of the slab. The maximum difference in LLDFs in the study was approximately 5%, which the researchers considered insignificant.

Zokaie et al. (1991) defined girder stiffness in a different manner. The authors defined the longitudinal stiffness parameter, K_g, using Equation 3.11. The researchers confirmed an acceptable means of quantifying girder stiffness was by changing the moment of inertia, area, and eccentricity while maintaining a constant longitudinal stiffness parameter. The overall LLDF changed by approximately 1.5% with differing individual variables, confirming the longitudinal stiffness parameter is acceptable for quantifying the stiffness of the girder elements.

$$K_g = n\left(I + Ae_g^2\right) \qquad \text{Eq. 3.11}$$

In which:

$$n = \frac{E_B}{E_D} \qquad \text{Eq. 3.12}$$

Where:

K_g = longitudinal stiffness parameter

n = modular ratio between beam and deck

I = moment of inertia of beam

A = area of a stringer, beam, or component

e_g = distance between the centers of gravity of the basic beam and deck

E_B = modulus of elasticity of beam material

E_D = modulus of elasticity of the deck material

As the accepted definition of the longitudinal stiffness parameter changed, it was found to have a major impact on live load distribution. This increase in LLDF with increased girder stiffness typically occurs with longer bridges, as longer bridges require larger, more stiff longitudinal elements. Therefore, when these two elements are combined, they tend to negate each other. Later analysis performed by Arockiasamy and Amer (1998) demonstrated girder stiffness has a negligible impact on shear live load distribution. Additionally, the researchers found the AASHTO LRFD BDS overestimates the effect of girder stiffness on moment live load distribution. Additionally, Yousif and Hindi (2007) found AASHTO LRFD BDS' LLDFs in the intermediate applicable longitudinal stiffness range compared well to three-dimensional FEA but tended to deviate at the extreme range of the specified limitations.

3.4.4 Deck Thickness

The consequence of the effective thickness of the concrete deck has been a subject of debate in the research. It is undeniable the effective thickness of the concrete deck has a role in both the original and modern definitions of longitudinal stiffness of the girders or beams. Newmark and Siess (1942) state deck thickness affects live load distribution, as it has a direct influence on the relative stiffness. However, later studies performed by Zokaie et al. (1991) found varying the deck thickness between six and nine inches had less than a 10% impact on live load distribution. Studies performed by Tarhini and Frederick (1992) were in agreement and found deck thickness changes between 5.5 inches and 9.5 inches had a negligible impact on live load distribution.

Nonetheless, effective thickness of the deck is included in the AASHTO LRFD BDS' LLDFs for I-Girder beam and slab bridges.

3.4.5 Girder Location

Walker (1987) found the location of the girder, where the force effect is maximized, had an influence on live load distribution. The researchers calculated LLDFs using a two-dimensional grid model with plate elements. The analytical model was used to calculate 'D' constants to be used in the ASSHTO Standard Specification equations discussed in Section 3.2.1. These 'D' factors to be used in the S/D equations would be calibrated to produce the same LLDFs as the two-dimensional grid model.

Zokaie (2000), following the NCHRP Report 12-26, performed a study which concluded exterior girders are more sensitive to truck placement than interior girders. Due to this finding, lever rule is used to determine exterior girder one-lane loaded LLDFs, and a correction factor is applied to the interior girder LLDFs to determine the exterior girder two-lane loaded LLDFs.

3.4.6 Number of Girders

Zokaie et al. (1991) considered the number of girders in the cross-section of the bridge as a variable in determining LLDFs in their initial sensitivity study for beam and slab bridges. These studies assumed one or two-lanes loaded for all scenarios as they deemed the likelihood of three or more lanes loaded to be unlikely. Additionally, the small likelihood of three or more lanes loaded at one time, combined with the girder spacing required to have three loaded lanes affecting the distribution of live load to one girder, is exceptionally rare. The results of their sensitivity study show the effect of number of girders is very small, with a negligible increase in LLDFs from three to four girder cross-sections, and an even smaller increase from four to five or more girders.

3.4.7 Deck Overhang

Deck overhang was found to have a negligible effect on interior girder LLDFs but a linear effect on exterior girder LLDFs (Zokaie et al., 1991). This relationship was incorporated in the

AASHTO LRFD BDS in the form of a correction factor applied to interior girders to determine exterior girder LLDFs for two or more lanes loaded scenarios. Further research by Barr and Amin (2006) demonstrated deck overhang has a more significant effect on shear LLDFs for exterior girders than shear LLDFs for interior girders, mirroring the findings by Zokaie et al. (1991).

3.4.8 Skew

The skew angle of the bridge has been found to be one of the most significant factors affecting live load distribution. Increased skew angle decreases longitudinal stresses and strains in interior and exterior girders and increases transverse stresses and strains in the bridge deck when compared to bridges without skew (Newmark, 1948). Increased skew angle also increases the exterior girder shear LLDFs at the obtuse corner. Results have shown for bridges with a skew angle of 60° the maximum moment in interior and exterior girders is approximately 71% and 80% of those moments in a right bridge, respectively. The AASHTO LRFD BDS utilizes two correction factors, one decreasing moment LLDFs from those of a right bridge, and another increasing shear LLDFs in the obtuse corner from those of a right bridge.

3.5 SUMMARY

Current AASHTO LRFD BDS methodologies for static structural analysis for beam and slab bridges allow bridge engineers to consider longitudinal and transverse effects of live load separately, simplifying the analysis and design of the bridge. The current AASHTO LRFD BDS allow transverse distribution of live load to be calculated using simplified methods of analysis using LLDFs. While these factors are considerably more accurate than previous specifications, they have been shown to be overly conservative for a wide range of bridges. Specifically, through the major updates to live load distribution in the 1990s, minimal changes were made to the LLDFs used for box-girders.

A variety of research has been performed, both analytically and experimentally, on typical I-girder shaped beam and slab bridges, but very few researchers have considered box-shaped beam and slab bridges. Moving forward, more accurate and applicable LLDFs for PBFTG bridges can be developed by evaluating the parameters already shown to effect beam and slab bridges.

CHAPTER 4: COMPACTNESS AND SKEW LITERATURE REVIEW

4.1 INTRODUCTION

This chapter presents a review and evaluation of local and global compactness limits pertaining to PBFTGs. A brief synopsis of the history and basis for many of the limits used in the AASHTO LRFD BDS is provided. This understanding will be used to evaluate the applicability of the restrictions present in the AASHTO LRFD BDS as they relate to skewed PBFTGs.

4.2 STABILITY OF PLATES

All steel sections, whether rolled shapes, plate girders, or box-girders, are composed of plate elements. In flexural elements in negative bending, when the cross-section is broken down into its constitutive elements, the bottom flange is essentially a plate under compression. Consideration must not only be given to buckling of the entire cross-section, but also to local buckling of the plate elements making up the cross-section. Local buckling occurs when the element cannot resist additional load prior to the onset of yielding, reducing the efficiency of the cross-section. The general approach in this section follows that of Timoshenko & Woinowsky-Krieger (1959) and Timoshenko & Goodier (1961).

4.2.1 Elastic Local Buckling of Flat Plates

The buckling behavior of a plate simply supported along its edges is essential to understanding the local buckling behavior of plate assemblies (Ziemian, 2010). Ideally, the buckling stresses are derived from bifurcation of an initially perfect structure. However, in practice, the buckling response is continuous due to the presence of geometric imperfections and residual stresses. When the cross-section of a member consists of various connected elements, such as flanges and webs, a lower bound critical stress can be determined for each element assuming a simply supported boundary condition at each intersection and a free boundary condition for any other edge.

Bryan (1890) first presented the analysis of a rectangular plate simply supported along all edges subjected to a uniform compressive stress. The elastic critical stress of a plate is affected by the plate width-to-thickness ratio, restraint conditions along the longitudinal boundaries, and elastic material properties of the plate, namely the elastic modulus and Poisson's ratio. The theoretical elastic buckling stress can be expressed as:

$$F_{cr} = k\frac{\pi^2 E}{12(1-\nu^2)(b/t)^2} \qquad \text{Eq. 4.1}$$

In which:

$$k = \left[\frac{1}{m}\frac{a}{b} + m\frac{b}{a}\right]^2 \qquad \text{Eq. 4.2}$$

Where:

F_{cr} = elastic buckling stress

k = plate buckling coefficient

E = modulus of elasticity

ν = Poisson's ratio

b = transverse plate width

t = plate thickness

a = longitudinal plate length

m = number of half-sine waves that occur in the x-direction at buckling

Generally, plate compression elements can be separated into two categories: stiffened elements, those supported along two edges parallel to the direction of the compressive stress; and unstiffened elements, those supported along one edge and free on the other edge parallel to the direction of compressive stress (Ziemian, 2010). Examples of stiffened elements include I-shaped webs, bottom flanges of PBFTGs, or edges of hollow structural sections. Examples of unstiffened elements include I-shaped flanges, top flanges of noncomposite PBFTGs, or legs of an angle. Figure 4.1 shows the variation of the plate buckling coefficient with respect to the plate aspect ratio for most idealized edge conditions.

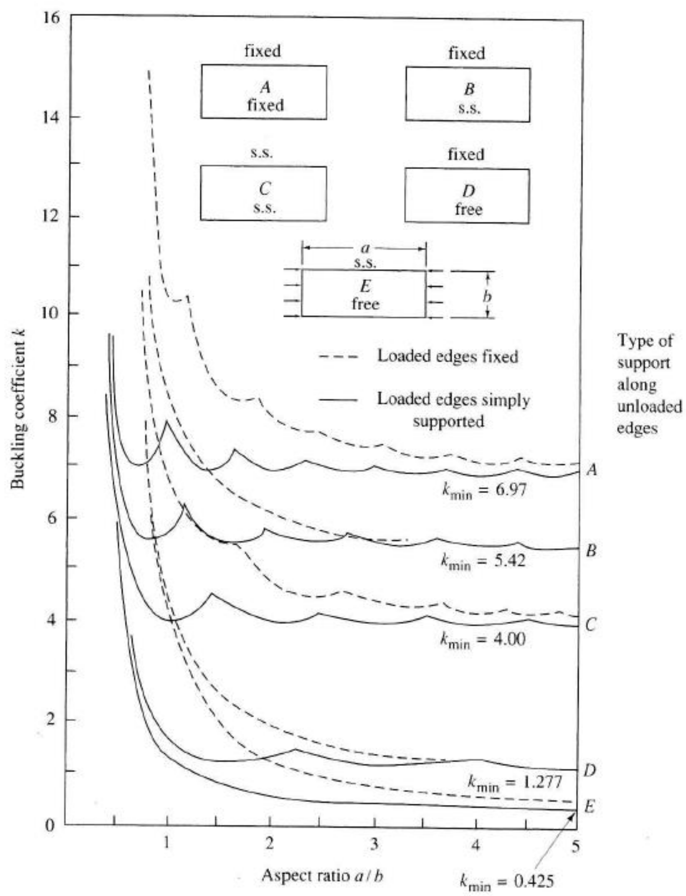

Figure 4.1: Elastic Buckling Coefficients for Compression in Flat Rectangular Plates (Ziemian, 2010)

Assuming ideal elastic-plastic material without geometric imperfections or residual stresses, the distribution of stress within the axially loaded plate remains uniform until the elastic buckling stress is reached. The load can be increased past this point, but the plate furthest from the side supports will begin to deflect out-of-plane, causing nonuniform stress distribution even though the loading is applied through rigid ends.

Figure 4.2 shows the plate strength under uniform edge compression consists of the sum of two components: the elastic or inelastic buckling stress represented by Equation 4.1 and the post-buckling strength. As seen in Figure 4.2, if the plate width-to-thickness ratio is very high, the post buckling strength becomes larger. Conversely, if the plate width-to-thickness is very low, not only does the post buckling strength drastically decrease, but the plate may have yielded and strain hardening may have already begun. In this case, the ratio of the elastic buckling stress to the yield stress becomes greater than one. For idealized plates, plates without residual stresses or geometric imperfections, three regions must be considered when determining strength: elastic buckling, yielding, and strain hardening.

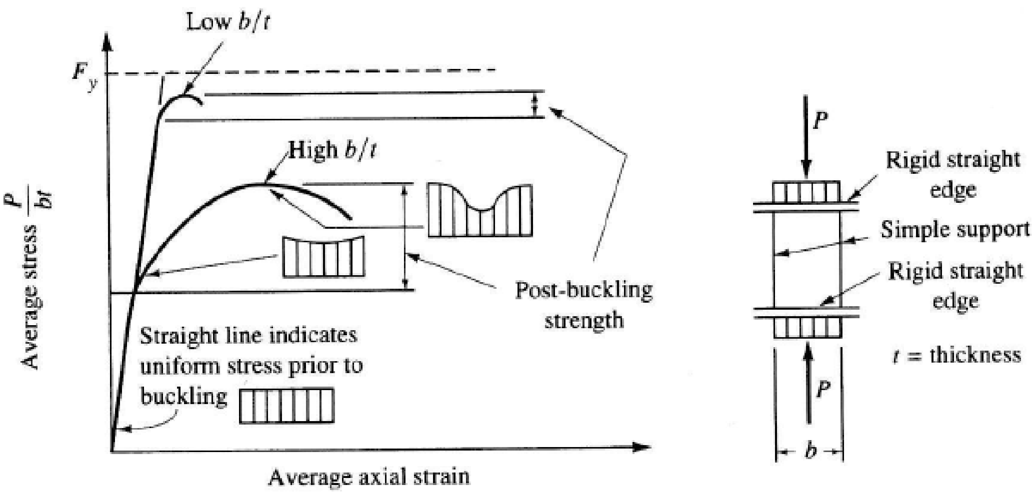

Figure 4.2: Behavior of Plate Under Edge Compression (Ziemian, 2010)

By redefining the ratio of the critical buckling stress to the yield stress, F_{cr}/F_y, as $1/\lambda^2$, and substituting into Equation 4.1, the slenderness ratio of plates, λ_c, becomes:

$$\lambda_c = \frac{b}{t}\sqrt{\frac{F_y 12(1-\nu^2)(b/t)^2}{\pi^2 Ek}} \qquad \text{Eq. 4.3}$$

Haaijer and Thurlimann (1957) discovered the most important factor determining the slenderness ratio needed to achieve the elastic critical buckling stress is whether the plate is supported along the edges parallel to loading. The researchers determined the type of restraint along the loaded edge has essentially no effect. As seen in Figure 4.3, curve (b) represents the case where one edge parallel to loading is supported, with a critical slenderness value of 0.46, and curve (c) represents the case where both edges parallel to loading are supported, with a critical slenderness value of 0.58. Figure 4.3 also shows a transition curve between strain hardening and the Euler Hyperbola due to initial residual stresses, reducing the actual resistance of the plate.

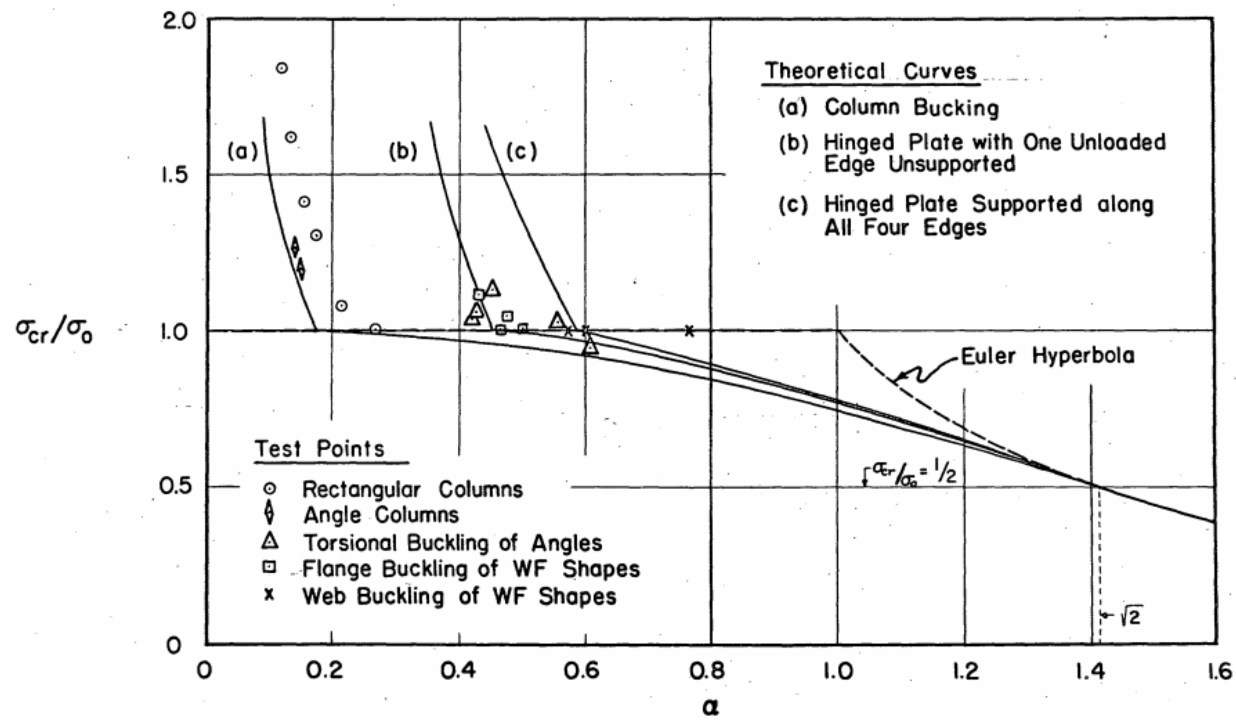

Figure 4.3: Buckling Curve Based on Slenderness Ratio (Haaijer & Thurlman, 1957)

When considering inelastic buckling, the generally accepted method is to extend the elastic critical buckling approximations already discussed to situations where material yielding has already occurred. Bleich & Ramsey (1952) provided a modification to the elastic critical buckling stress of a plate under uniform compressive stress by considering the tangent modulus. The researchers proposed Equations 4.4 and 4.5 when considering inelastic buckling:

$$F_{cr} = k\frac{\pi^2 E\sqrt{\eta}}{12(1-\nu^2)(b/t)^2} \qquad \text{Eq. 4.4}$$

In which:

$$\eta = \frac{E_t}{E} \qquad \text{Eq. 4.5}$$

Where:

$E_t =$ tangent modulus

4.2.2 AISC Width / Thickness Limitations

As discussed in Section 4.2.1: For low width-to-thickness values, strain hardening occurs without buckling; for medium width-to-thickness values, inelastic buckling occurs due to residual stresses and initial geometric imperfections; and for large width-to-thickness values, buckling occurs according to Equation 4.4. Plates with large width-to-thickness ratios have strengths exceeding the buckling strength, but these plates are conservatively limited to elastic buckling. To establish design requirements for members consisting of these elements, the desired performance must be ascertained.

A logical performance criterion of an element in compression would be to prevent local buckling of an element in the cross-section prior to achieving the full strength of the cross-section. In other words, the elastic buckling stress of the component should be greater than or equal to the elastic buckling stress of the cross-section. However, this would lead to acceptable width-to-thickness ratios dependent on the overall slenderness of the cross-section.

Current design limits assure the compression element reaches the yield stress without local buckling, even though the overall slenderness of the cross-section may prevent the element from reaching the yield stress. Table 4.1 provides the width-to-thickness ratio to prevent this local buckling prior to the yield stress, λ_r. By replacing the critical buckling stress with the yield stress in Equation 4.1, substituting known material properties of steel, and solving for the width-to-thickness ratio, Equation 4.1 becomes:

$$\frac{b}{t} \leq 162\sqrt{\frac{k}{F_y}} \qquad \text{Eq. 4.6}$$

The above equation assumes no residual stress is present in the cross-section. As residual stresses are present in all steel structural elements due to cold forming, plasma cutting, roll forming, and welding, a reduced slenderness ratio should be utilized to minimize the difference between idealized behavior and the assumed transition curve. An assumed reduction of 30% of the resistance is taken as a rational value, resulting in:

$$\frac{b}{t} \leq \left[(0.7)162 \sqrt{\frac{k}{F_y}} = 113 \sqrt{\frac{k}{F_y}} \right] \qquad \text{Eq. 4.7}$$

When the corresponding plate buckling coefficient, dependent on the boundary conditions parallel to the axis of loading of plate, are input into Equation 4.7, the limiting width-to-thickness values found in Table 4.1 are generated. Cross-sections with a governing width-to-thickness ratio greater than those provided in Table 4.1 are subject to local buckling limit states and associated capacity reductions found in the American Institute of Steel Construction (AISC) Steel Construction Manual (AISC, 2017) Section E7. Cross-sections where all elements have width-to-thickness ratios less than those provided in Table 4.1 are not subject to local buckling limit states.

Table 4.1: Width-to-Thickness Ratios for Elements Subject to Axial Compression (AISC, 2016)

	Case	Description of Element	Width-to-Thickness Ratio	Limiting Width-to-Thickness Ratio λ_r (nonslender/slender)	Examples
Unstiffened Elements	1	Flanges of rolled I-shaped sections, plates projecting from rolled I-shaped sections, outstanding legs of pairs of angles connected with continuous contact, flanges of channels, and flanges of tees	b/t	$0.56\sqrt{\frac{E}{F_y}}$	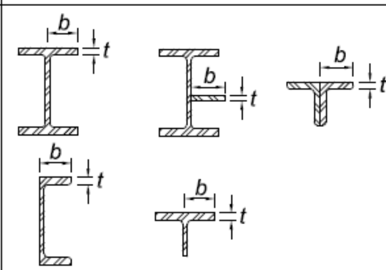
	2	Flanges of built-up I-shaped sections and plates or angle legs projecting from built-up I-shaped sections	b/t	$0.64\sqrt{\frac{k_c E}{F_y}}$ [a]	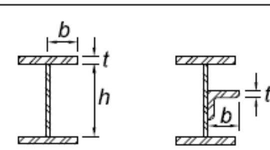
	3	Legs of single angles, legs of double angles with separators, and all other unstiffened elements	b/t	$0.45\sqrt{\frac{E}{F_y}}$	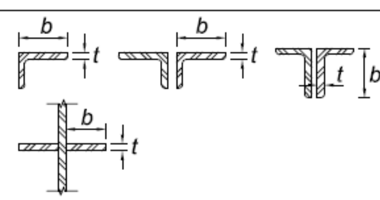
	4	Stems of tees	d/t	$0.75\sqrt{\frac{E}{F_y}}$	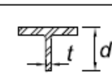

4.3 Categorization of Composite Box-Girder Bridges in the AASHTO LRFD BDS

AASHTO LRFD BDS Article 6.11.6.2.2, discussed in depth in Section 6.8.1 of this document, provides requirements on the nominal flexural resistance of box-girders. One of the requirements states the cross-section is part of a bridge satisfying the requirements of AASHTO LRFD BDS Article 6.11.2.3. AASHTO LRFD BDS Article 6.11.2.3 provides special restrictions on the use of LLDFs for multiple box sections. These restrictions, in addition to other cross-section and material restrictions, also form the basis for many other analysis and design simplifications. The first paragraph states:

> Cross-sections of straight sections for straight bridges consisting of two or more single-cell box sections, for which the live load flexural moment in each box is determined in accordance with the applicable provisions of Article 4.6.2.2.2b, shall satisfy the geometric restrictions specified herein. In addition, the bearing lines shall not be skewed (AASHTO, 2020).

The wording on the last sentence in this quote implies PBFTGs, which have any degree of bearing line skew, will not meet the requirements of AASHTO LRFD BDS Article 6.11.2.3, therefore not meeting the requirements of AASHTO LRFD BDS Article 6.11.6.2.3. Therefore, if the bridge contains skew, the capacity of PBFTGs is limited to the yield moment. The restrictions of AASHTO LRFD BDS Article 6.11.2.3 are based on the range of bridge characteristics conforming to the study performed by Johnston and Mattock (1967).

4.3.1 Johnston and Mattock

Johnston and Mattock (1967) developed a computer program to analyze steel trapezoidal girders made composite with a concrete deck with no internal or external stiffeners or bracing. The purpose of this computer program was to develop LLDFs for this type of structure. The thought at the time of the study was, due to the larger torsional stiffness of closed shape members compared to I-girders, a greater transverse distribution of load would be present with this form of construction. This increase in transverse load distribution would allow the engineer to design the structure to withstand less moment than an equivalent I-girder.

The analysis of this computer program is based on a folded plate structure consisting of adjoined thin plates rigidly connected along their edges. If the bridge is not skewed, the support diaphragms can effectively be neglected, as they can prevent displacement in their planes but can offer negligible resistance out of their plane. Similar to modern methods of three-dimensional FEA, the early computer program produces displacements and forces at each joint where coplanar plate elements are joined along their edges.

This computer program assumes isotropic linear elastic materials. It should be noted actual bridge structures will not meet these assumptions but should come close at the service level. In order to test the validity of the computer program and the structural and material assumptions, the researchers built a 1/4 scale model of an 80 foot long two lane bridge. The prototype bridge cross-section and the typical girder cross-section can be seen in Figures 4.4 and 4.5. The cross-section of the 1/4 scale model was made as close to 1/4 scale as reasonable given the limited plate thickness availability. The scale model concrete deck used reinforced mortar to simulate the prototype bridge. While the reinforcement size and spacing were reproduced to scale, the mortar had a compressive strength of 3.34 ksi, where the prototype was designed with a compressive strength of 4 ksi.

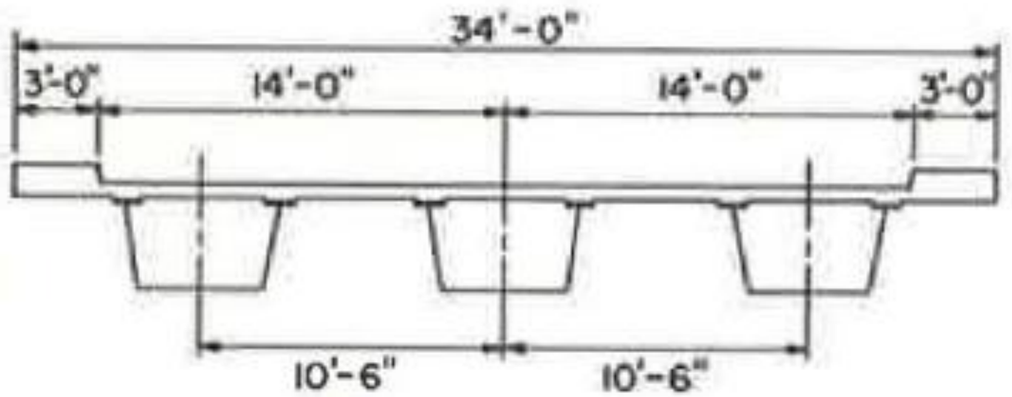

Figure 4.4: Bridge Cross-section (Johnston & Mattock, 1967)

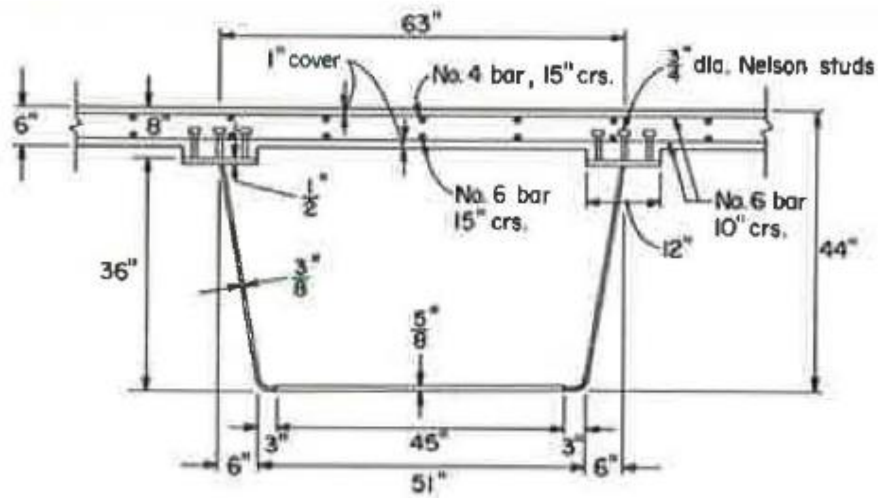

Figure 4.5: Girder Cross-section (Johnston & Mattock, 1967)

Two types of loading were conducted on the scaled bridge: influence line tests and truck loading tests. In the influence line test, the researchers individually placed a load at nine places at midspan and recorded girder deflections and bottom flange strains. The distribution of lateral load and deflection was calculated using the Stallings/Yoo methodology, discussed in Section 3.3.2. The analytical influence line testing results matched well with the experimental testing results.

The second type of loading, the truck loading, was performed by placing six concentrated loads concurrently to represent 1/4 scale HS-20 loading. These loads were created using a steel frame resting on the bridge with the scaled dimensions of the HS-20 truck, and a large concrete block with 1/4 of the design vehicle weight was placed on top of the steel frame. Figure 4.6 presents the 1/4 scale experimental truck loading at midspan. The truck was moved transversely in both design lanes of the bridge to produce the maximum desired force effect. The results of both loaded lanes were superimposed to generate two-lane loaded scenarios. The results from the experimental truck loading matched well with the analytical testing results, verifying the reliability of the computer program.

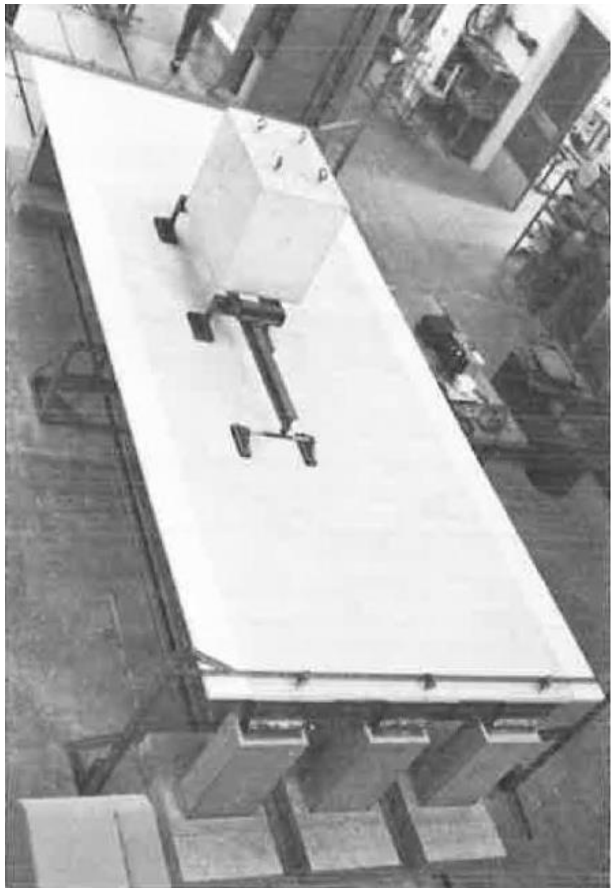

Figure 4.6: Truck Loading Test of the Model Bridge (Johnston & Mattock, 1967)

A matrix of 24 composite box-girder bridges was generated and analyzed using the folded plate theory computer program. The variables explored as part of the study included span length, number of loaded lanes, number of box-girders, width of lanes, and girder cross-section dimensions. The bridges analyzed in the study are provided in Figure 4.7 and Table 4.2.

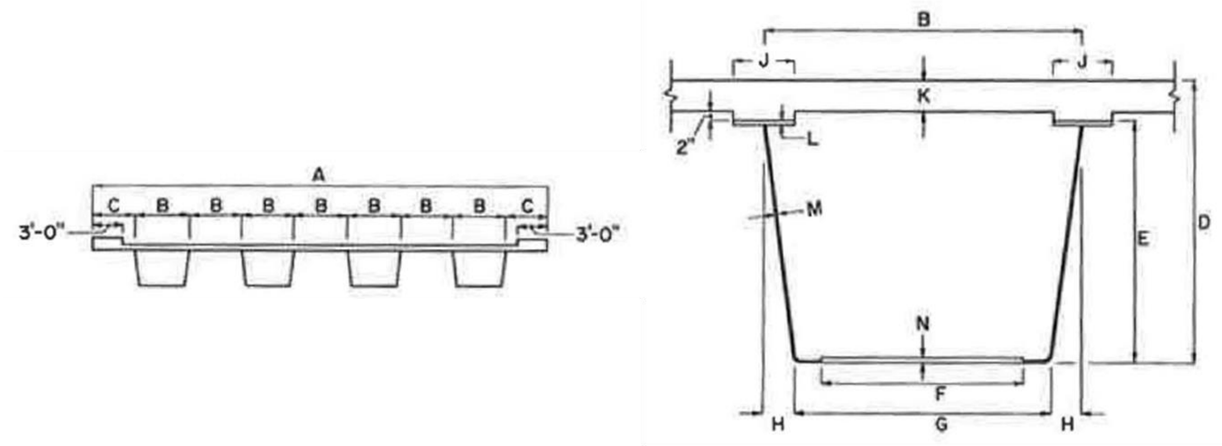

(a) ***(b)***

Figure 4.7: Typical Midspan Cross-sections for Bridges in the Analytical Study for the: (a) Bridge and (b) Girder (Johnston & Mattock, 1967)

Table 4.2: Dimension Summary for Bridges Considered in the Analytical Study (Johnston & Mattock, 1967)

Bridge No.	Span (ft)	No. of Lanes	No. of Girders	Dimension (See Fig. 9)[a]												
				A	B	C	D	E	F	G	H	J	K	L	M	N
50-1	50	2	2	34 ft 0 in.	96	60	29	20	76	88	4	12	7	$\frac{5}{8}$	$\frac{3}{8}$	$\frac{1}{2}$
50-2	50	2	3	34 ft 0 in.	63	$46\frac{1}{2}$	28	20	43	55	4	12	6	$\frac{1}{2}$	$\frac{3}{8}$	$\frac{1}{2}$
50-3	50	3	3	44 ft 6 in.	86	52	$28\frac{3}{4}$	20	60	78	4	12	$6\frac{3}{4}$	$\frac{9}{16}$	$\frac{3}{8}$	$\frac{1}{2}$
50-4	50	3	4	44 ft 6 in.	63	$46\frac{1}{2}$	28	20	43	55	4	12	6	$\frac{1}{2}$	$\frac{3}{8}$	$\frac{1}{2}$
50-5	50	4	4	55 ft 0 in.	80	50	$28\frac{1}{2}$	20	60	72	4	12	$6\frac{1}{2}$	$\frac{1}{2}$	$\frac{3}{8}$	$\frac{1}{2}$
50-6	50	4	5	55 ft 0 in.	63	$46\frac{1}{2}$	28	20	43	55	4	12	6	$\frac{1}{2}$	$\frac{3}{8}$	$\frac{1}{2}$
75-1	75	2	2	34 ft 0 in.	96	60	44	35	72	84	6	13	7	$\frac{3}{4}$	$\frac{7}{16}$	$\frac{5}{8}$
75-2	75	2	3	34 ft 0 in.	63	$46\frac{1}{2}$	43	35	39	51	6	12	6	$\frac{5}{8}$	$\frac{3}{8}$	$\frac{5}{8}$
75-3	75	3	3	44 ft 6 in.	86	52	$43\frac{3}{4}$	35	62	74	6	13	$6\frac{3}{4}$	$\frac{3}{4}$	$\frac{3}{8}$	$\frac{5}{8}$
75-4	75	3	4	44 ft 6 in.	63	$46\frac{1}{2}$	43	35	39	51	6	12	6	$\frac{5}{8}$	$\frac{3}{8}$	$\frac{5}{8}$
75-5	75	4	4	55 ft 0 in.	80	50	$43\frac{1}{2}$	35	56	68	6	12	$6\frac{1}{3}$	$\frac{3}{4}$	$\frac{3}{8}$	$\frac{5}{8}$
75-6	75	4	5	55 ft 0 in.	63	$46\frac{1}{2}$	43	35	39	51	6	12	6	$\frac{5}{8}$	$\frac{3}{8}$	$\frac{5}{8}$
100-1	100	2	2	34 ft 0 in.	96	60	58	49	72	84	6	14	7	1	$\frac{1}{2}$	$\frac{3}{4}$
100-2	100	2	3	34 ft 0 in.	63	$46\frac{1}{2}$	57	49	39	51	6	12	6	$\frac{3}{4}$	$\frac{7}{16}$	$\frac{3}{4}$
100-3	100	3	3	44 ft 6 in.	86	52	$57\frac{3}{4}$	49	62	74	6	13	$6\frac{3}{4}$	1	$\frac{7}{16}$	$\frac{3}{4}$
100-4	100	3	4	44 ft 6 in.	63	$46\frac{1}{2}$	57	49	39	51	6	12	6	$\frac{3}{4}$	$\frac{7}{16}$	$\frac{3}{4}$
100-5	100	4	4	55 ft 0 in.	80	50	$57\frac{1}{2}$	49	56	68	6	12	$6\frac{1}{3}$	1	$\frac{7}{16}$	$\frac{3}{4}$
100-6	100	4	5	55 ft 0 in.	63	$46\frac{1}{2}$	57	49	39	51	6	12	6	$\frac{3}{4}$	$\frac{7}{16}$	$\frac{3}{4}$
150-1	150	2	2	34 ft 0 in.	96	60	85	76	72	84	6	14	7	$1\frac{1}{2}$	$\frac{5}{8}$	1
150-2	150	2	3	34 ft 0 in.	63	$46\frac{1}{2}$	84	76	41	51	6	13	6	1	$\frac{1}{2}$	1
150-3	150	3	3	44 ft 6 in.	86	52	$84\frac{3}{4}$	76	58	70	8	13	$6\frac{3}{4}$	$1\frac{1}{2}$	$\frac{9}{16}$	1
150-4	150	3	4	44 ft 6 in.	63	$46\frac{1}{2}$	84	76	41	51	6	13	6	1	$\frac{1}{2}$	1
150-5	150	4	4	55 ft 0 in.	80	50	$84\frac{1}{2}$	76	52	64	8	12	$6\frac{1}{2}$	$1\frac{1}{2}$	$\frac{9}{16}$	1
150-6	150	4	5	55 ft 0 in.	63	$46\frac{1}{2}$	84	76	41	51	6	13	6	1	$\frac{1}{2}$	1

[a]Dimensions are given in inches except for A, the overall width of the bridge.

4.3.2 Compact Sections

Numerous AASHTO LRFD BDS Articles specify analysis and design simplifications based on the requirements for the use of simplified LLDF equations, and therefore conform to the dimensions analyzed by Johnston and Mattock (1967). If the simplified LLDF equations can be used, and box flanges are considered fully effective, key analysis simplifications can be made.

The first of these simplifications is distortion induced stresses in box cross-sections, due to torsion, may be neglected. These stresses include shear, warping, and plate bending stresses illustrated in Figure 4.8 (White, 2022). Further simplifications include the neglection of shear stresses due to St. Venant torsional shear in the design of box-girder webs and the shear connectors between the slab and the steel girder.

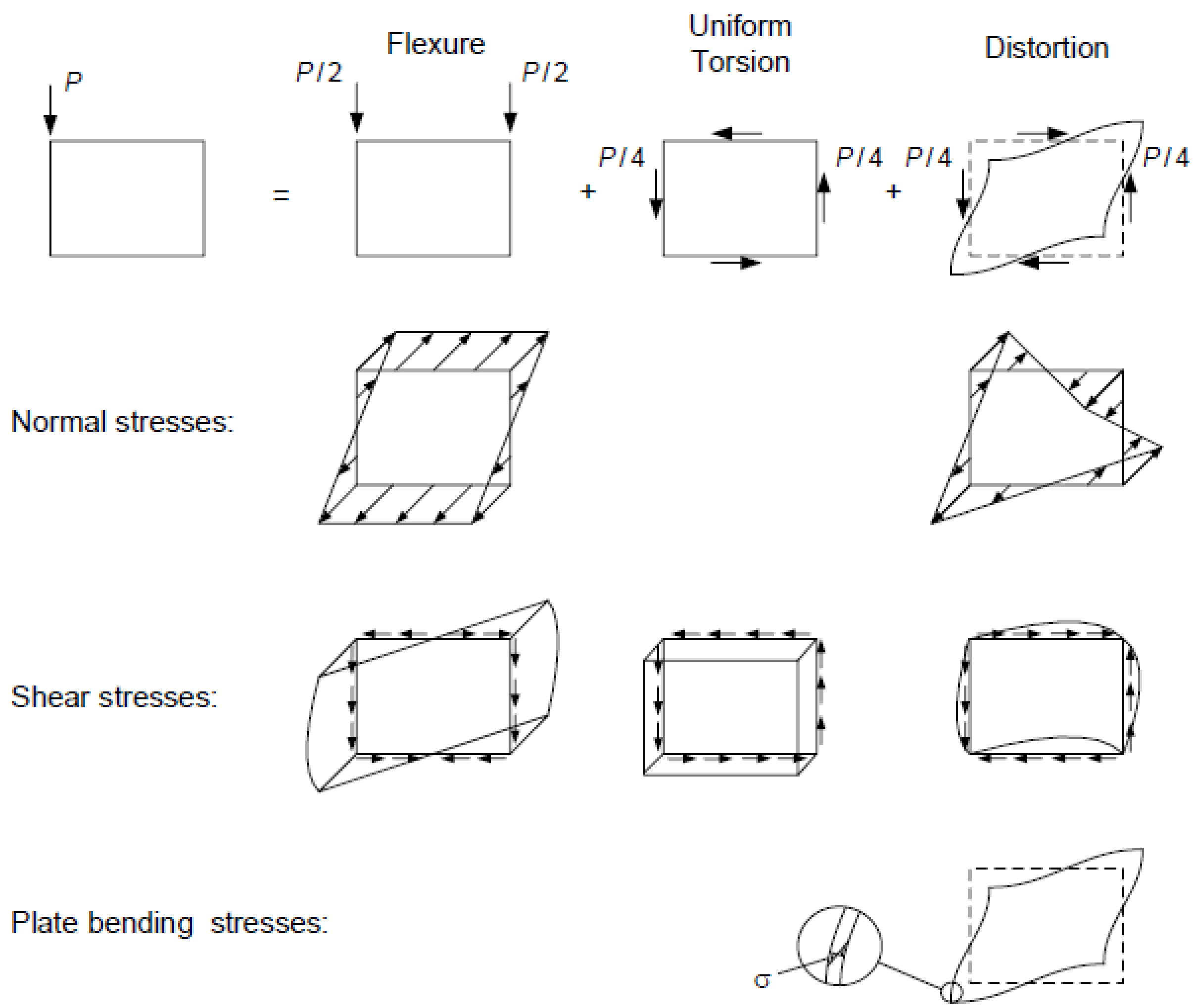

Figure 4.8: Stresses in a Single Box-Girder Subjected to an Eccentric Load (White, 2022)

Potentially the largest simplification the AASHTO LRFD BDS allows, when the previous restrictions are met, is that the section can be labeled compact. Compact sections are permitted to exceed the moment at first yield. The fully plastic cross-section models may be used as the basis for the member resistance calculations in composite compact sections in positive bending (White, 2022). The allowance of the fully plastic cross-section increases the nominal allowable moment on the section beyond the point of first yield.

4.3.3 Noncompact Sections

AASHTO LRFD BDS specify if any of the restrictions of AASHTO LRFD BDS Article 6.11.6.2.2-1, including if the cross-section does meet the requirements of AASHTO LRFD BDS Article 6.11.2.3, a more detailed analysis and design procedure for composite box-girder bridges is required. This requires a refined analysis, such as three-dimensional FEA, instead of one-dimensional LGA where simplified distribution factors may be used. Additionally, when designing the webs for shear and determining the number of top flange shear connectors, the design engineer must consider shear forces from both flexure and St. Venant torsion.

When a bridge does not meet the aforementioned requirements, the bridge is also labeled noncompact. Noncompact sections cannot exceed the moment at first yield. The ability of noncompact sections to develop a nominal flexural resistance greater than the moment at first yield in the presence of potentially significant St. Venant torsional shear and cross-sectional distortion stresses has not yet been demonstrated. For noncompact sections, the elastically computed stress, considering the effect of St. Venant torsional shear, in each flange due to the factored loads is compared to the yield stress modified by the appropriate flange reduction factor. Therefore, when a bridge consisting of longitudinal box-girders has any amount of support skew, not only is a more refined analysis required, but the nominal capacity of the system dramatically decreases.

4.4 Behavior of Skewed Steel Girder Bridges

Geometrically, a skewed bridge contains one or more bearing lines not orientated perpendicular to the longitudinal axis of the bridge. The effect of skew is largely dependent on the magnitude of skew, the skew index, and the layout of cross-frames, if present. For non-curved skewed I-girder bridges, the behavior of the system becomes increasingly three-dimensional with increased skew (White & Kamath, 2020).

The structural response of skewed bridges is influenced by the end bearing line and orientation of intermediate cross-frames. Skewed bearing lines cause the girders to twist to maintain continuity between the bearing stiffeners and the main longitudinal elements. The bearings are assumed to be laterally and longitudinally restrained for ease of analysis. As the girder bends under major axis rotation, the top flange longitudinally displaces relative to the bottom flange, as can be seen in Figure 4.9. However, as the girders are supported by skewed bearing lines with bearing stiffeners with relatively high in plane stiffness, the bearing stiffeners can only achieve the longitudinal displacement required by the girder major axis bending by rotating about an axis tangent to the bearing line. This rotation of the stiffener about its weak axis in turn causes a lateral displacement between the top flange and the bottom flange and a twist rotation of the main longitudinal elements. This twist finally induces girder torsional moments in the longitudinal members. Figure 4.10, adopted from White et al. (2012), demonstrates the girder end rotations of Girder G2 from Figure 4.9. Note these figures depict the reaction of I-girder members to skew required for compatibility with bearing cross-frames, but the same behavior occurs in box-girders with compatibility with bearing diaphragms.

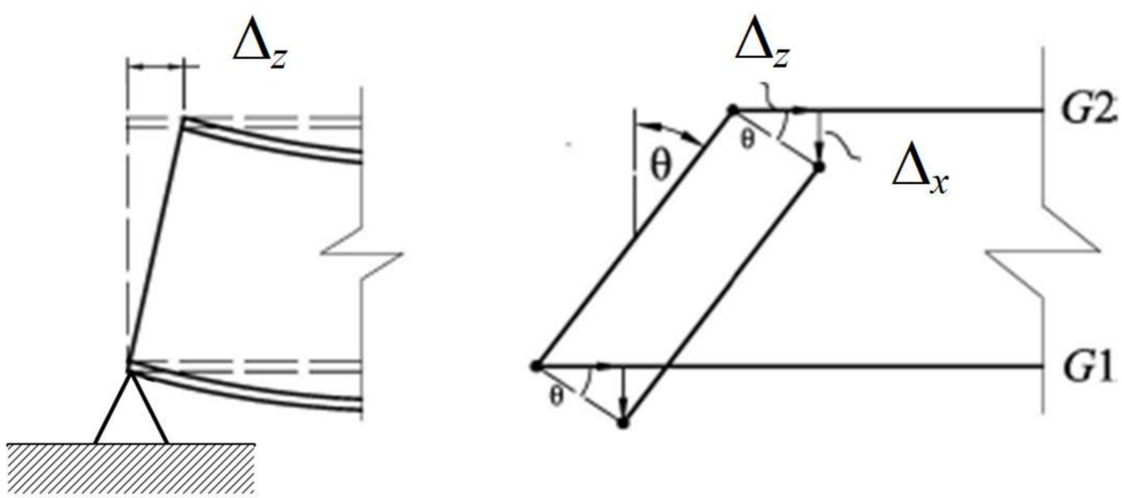

Figure 4.9: Relative Flange Displacement in a Skewed Bridge (Sanchez, 2011)

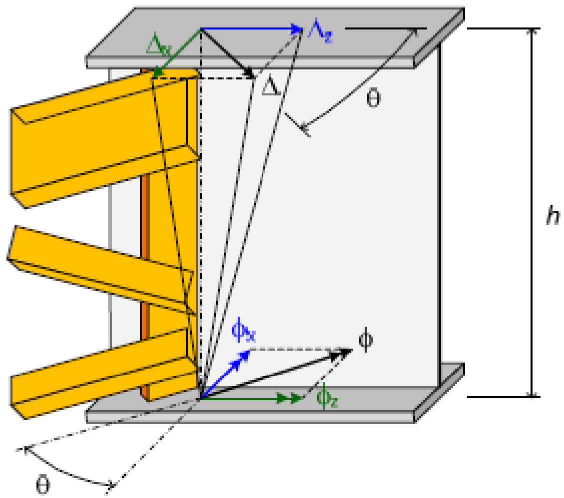

Figure 4.10: Girder Major Axis Bending and Twist Rotations Required for Compatibility at a Skewed Bearing Cross-Frame (White et al., 2012)

4.4.1 Torsional Stress Effects

Torsion induced in steel girders causes normal stresses and shear stresses throughout the girder cross-section. Typical I-girders and box-girders carry these stresses in different ways. As I-girders have low torsional stiffness, torsion is carried primarily through warping. This low torsional stiffness is a result of the open cross-sectional geometry resulting in low shear flow around the perimeter of the section. This shear flow can only generate small force couples, resulting in the ability of I-girders to carry torque via St. Venant torsion to be relatively low.

However, as box-shaped girders are closed sections, they have exceptionally high torsional stiffness. Closed cells are extremely efficient at carrying torsion by means of St. Venant torsional shear flow, because the shear flow around the circumference of the box has relatively large force couple distances (AASHTO, 2020). The final state of normal stress in box-girders is the sum of any axial stress, major axis bending stress, lateral bending stress, and warping normal stress. The final state of shear stress in box-girders is the sum of any vertical shear stress, horizontal shear stress, St. Venant torsional shear stress, and warping shear stress.

4.4.2 Torsional Deformation Effects

In addition to causing stresses in box shaped girders, torsion also causes deformations. Depending on the extent of the skew, span length, inclusion or exclusion of cross-frames, and type of deck casting used in PBFTGs, the deformations caused by skew can have a significant effect on the constructability of the bridge. This is not an issue with the preferred method of construction of PBFTG bridges as they are pre-topped with the concrete deck and do not have any external cross-frames between adjacent members. However, if a bridge is to be constructed using a traditional cast-in-place deck, the engineer and contractor constructing the bridge must be cognizant of the erection sequence and potential differential deflection between adjacent noncomposite PBFTGs.

4.5 Evaluation of Bottom Flange Compactness of Box-Girders

Due to the substantial structural efficiency provided by box-girders, many designers may specify thin and slender bottom flanges in large, welded plate girders, which are the closest comparison to PBFTGs. Specifying thin bottom flanges can result in problems during fabrication, transportation, erection, and the service life of the bridge. This is particularly true in regions of negative bending when the bottom flange is in compression. White et al. (2019) surveyed bridge owners and reviewed the literature and limited analytical studies to evaluate the behavior of bottom flange width and thicknesses. Discussed in this section are the findings and proposed limits for bottom flanges of box sections.

4.5.1 Bottom Flange Minimum Thickness Limits

A rational minimum thickness of any plate element is 2 inches. For typical welded plate girders, this is to limit welding distortions. This is not an issue with PBFTGs as the flanges and webs are cold-bent from one piece of sheet steel. However, this limit is still viable as it also limits out-of-plane deflections under the self-weight of the PBFTG. Many owners and designers prescribe larger minimum thicknesses. The TxDOT recommends a minimum flange thickness of 3/4 inch, with a preferred minimum thickness of 1 inch (TSQC, 2021). The Guidelines to Design for Constructability and Fabrication (AASHTO/NSBA Steel Bridge Collaboration, 2020) recommends a 3/4 inch minimum thickness due to welding considerations. As stated previously, these limits are due to welding considerations, so they may be neglected for PBFTGs. The minimum thickness of 1/2 inch for handling and erection reasons may be considered the minimum for typical PBFTGs. Additionally, these restrictions were intended to be utilized when designing box-sections with span lengths significantly longer than those where PBFTGs can be utilized.

4.5.2 Bottom Flange Slenderness Limits

Longitudinally unstiffened flanges are recommended to have a width-to-thickness ratio, or *b/t*, not exceeding 90. If the flange is longitudinally stiffened, a panel width-to-thickness ratio less than 90 is advised. Flanges exceeding these limits are prone to accidental axial compression, which may be experienced during transportation or erection, or exhibit noticeable oil canning or waviness due to welding residual stresses, which are not applicable to PBFTGs. It should be noted these limits are for flanges nominally designed for tension, but which may encounter accidental or unintended compressive loading. The researchers found the moments causing compression in the bottom flange have magnitudes comparable to those generated from the self-weight of the beam in simple span loading conditions.

4.5.3 Behavioral Considerations Correlated with Bottom Flange Limits

The combined limits specified in Section 4.5.1 and 4.5.2 limit the sagging of bottom flanges under their self-weight plus a transverse concentrated load of 0.3 kip. Bottom flange limits not meeting the limits specified can begin to generate undesirable effects. The following behavioral considerations can be approximately correlated with the prescribed width-to-thickness, *b/t*, ratios:

- *b/t* >100
    - Bridge fabricators, of welded box sections, will need to be especially cautious providing welds larger than those required for strength and/or minimum size requirements. The plate must also be adequately restrained during welding to ensure minimal distortion.
- *b/t*>130
    - Bottom flanges will begin to deflect out-of-plane under their self-weight with a small, concentrated transverse loads more than the maximum

deflection of 1/300 times the plate width. The researchers recommend when this limit is exceeded to introduce longitudinal stiffeners to the bottom flange.

- *b/t* > 210
  - Dynamic excitation of a flange exceeding this limit will begin to pose issues. These sections are susceptible to fatigue damage from the bottom flange breathing under cyclic tension. The initial allowable out-of-plane bow of the flange from geometric imperfections being cyclically straightened and released under live loading causes bending moments in the thin plate.

Note, the limits of box-section flanges subject to compression are significantly more stringent than those subject to tension. The AASHTO LRFD BDS effectively limits the width-to-thickness ratio for flanges subjected to compression to 24. The strength of box section flanges subjected to compression decreases relative to the yield strength as the width-to-thickness ratio increases. The ultimate strength of the plate is approximately $0.8F_y$ at b/t=40, $0.6F_y$ at b/t=60, and $0.4F_y$ at b/t=90.

4.6 Simplified Evaluation of the Effect of Skew on Box-Girders

Skew greatly complicates the behavior of steel girder bridges by introducing alternate load paths and causing greater interaction between the main girders and secondary framing members (Coletti et al., 2011). In most instances, the severity of these complications is negligible; however, in other cases, the complications can be more pronounced, including fit-up issues, distortion induced loading, and unaccounted torsional effects. Unfortunately, the line between negligible and severe effects is not clear or easy to define.

4.6.1 Rigid Diaphragm Behavior

The effects of skewed supports on the behavior of girders can be evaluated by considering the girder major axis bending rotations and the transverse and longitudinal constraint provided by the support diaphragms. The support diaphragms are assumed effectively rigid in their own planes but are free to rotate with respect to the support lines. The interaction of the girder major axis bending with the restraint of displacement along the support line from the diaphragm causes the girders to twist along the major axis. This twist causes the top flanges of the box-girder to displace laterally with respect to the bottom flange. The twist between the skewed supports causes a torsional moment throughout the span.

Only one type of diaphragm is present in PBFTGs: the internal bearing diaphragm. These diaphragms are present at the ends of the girder and are welded along their sides to the bottom flange and the webs of PBFTGs. The bearing diaphragm aids in the transfer of load between the concrete deck and the bearing and prevents cross-section distortion. Most box-girder bridge diaphragms are solid-plate components with relatively thin thicknesses compared to their depth. Therefore, they are typically very stiff components able to resist loads acting on the plane of the diaphragm with small deformations when compared to their weak axis deformations.

Three-dimensional FEA performed by Chong (2012) displayed bearing diaphragm thickness has a small effect on the overall torsion due to skew. Chong performed analysis on two straight skewed and horizontally curved bridges and found the discrepancy between the maximum torque in the box-girders with a diaphragm thickness of 5/16 inch and 2 inch was only 0.2%.

4.6.2 Skew Induced Torque

In non-skewed bridges, as the main longitudinal members deflect vertically, the longitudinal member rotates about the support bearing. Compatibly, the diaphragms, acting as rigid plates, rotate about the bearing lines with the longitudinal members. In skewed bridges, as the main longitudinal members deflect vertically and attempt to rotate about their support bearing, the diaphragm, acting as a rigid plate in its own plane, forces the girder to twist to maintain compatibility (Figure 4.11). The bearing diaphragms can be idealized as rigid components in their own plane and offer no resistance out of their plane. By assuming the plate is rigid in its own plane and is rigidly connected to the box-girders, the box-girders have two components of force when a load is applied vertically: one corresponding to the major axis bending rotation of the girders and one corresponding to the twist rotation of the girders, as seen in Figure 4.12 (Chong, 2021).

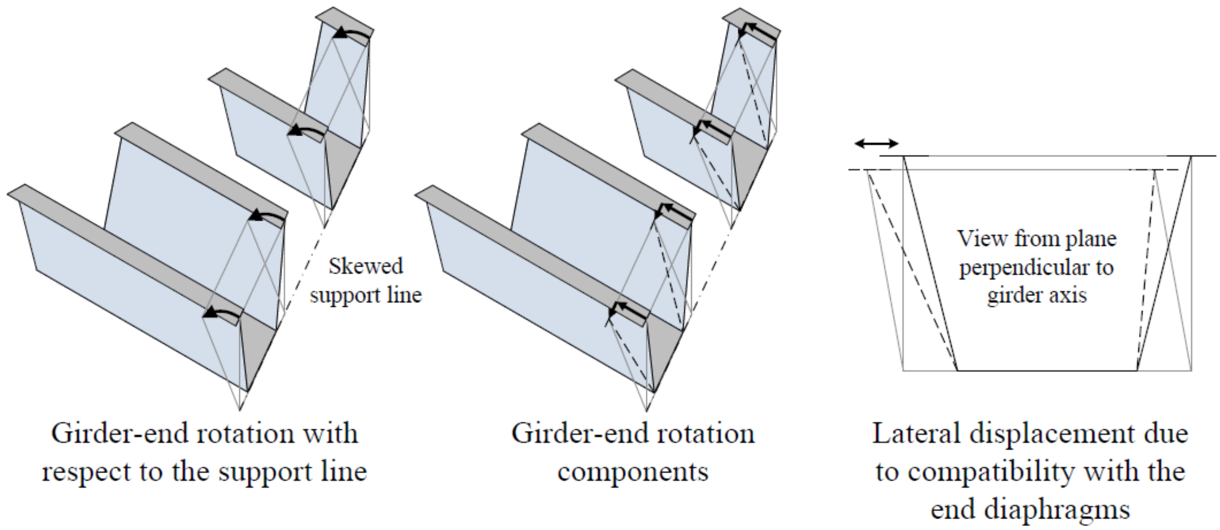

Figure 4.11: Lateral Displacements due to Rotation About the Line of the Support (Chong, 2012)

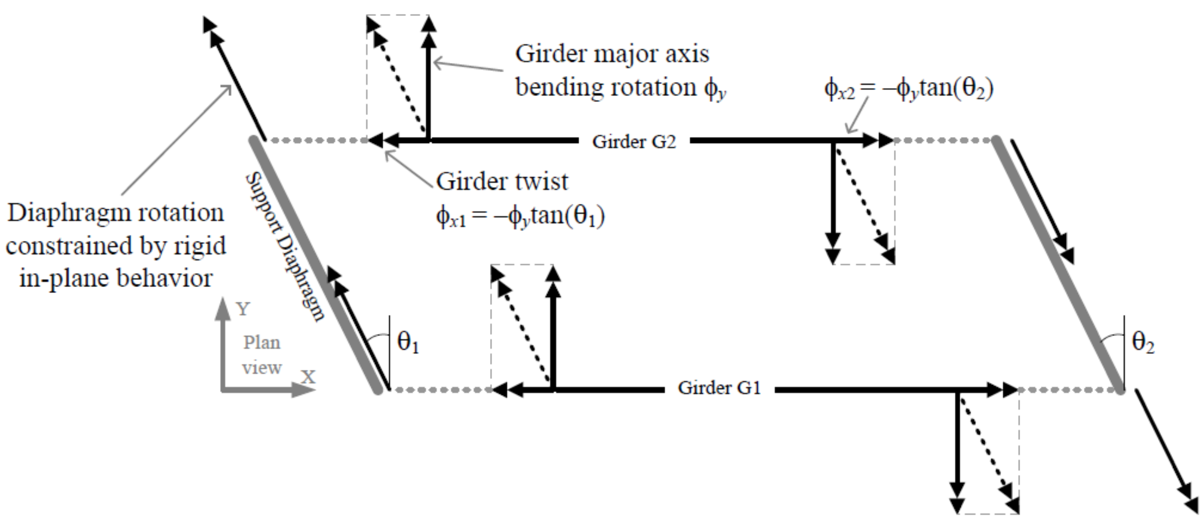

Figure 4.12: Rigid Diaphragm Rotation Mechanism at a Skewed Support (Chong, 2012)

The girder twist at the supports can be mathematically approximated in terms of the major axis bending rotation and the support skew angle. From the girder twist, the girder torques along the span can be calculated by multiplying the twist by the girder torsional stiffness and summing the results from the effects of the twist at both supports. This produces a constant torsional moment due to skewed supports represented by Equation 4.8:

$$T_S = -\frac{GJ}{L}\left(\phi_{y1}\tan\theta_1 + \phi_{y2}\tan\theta_2\right) \qquad \text{Eq. 4.8}$$

4.7 Summary

This chapter presented a review of the local buckling of flat plates and their effect on the capacity of sections built from them. A brief synopsis of the specifications governing the limits on the width-to-thickness ratio values of plates making up cross-sections of longitudinal elements was provided. The categorization of box-girder sections and basis for the categorization was included to give context related to distinction between compact and noncompact sections as defined in the AASHTO LRFD BDS. Using the synopsis of the local and global compactness limits, a discussion of the force effects affecting PBFTGs and an evaluation of the bottom flange compactness limits of box-girders was provided.

CHAPTER 5: LINK SLAB LITERATURE REVIEW

5.1 Introduction

Link slabs are a transverse deck level connection at piers between the decks of two adjacent spans, providing a jointless bridge without continuity. The deck is made continuous across the pier, but the supporting beams or girders are not connected. In addition -to simpler designs consisting of simple spans instead of continuous spans, link slabs can allow for prefabricated bridge elements to be implemented, further reducing the total cost of the bridge.

Approximately one third of state Department of Transportations have experience with link slab applications. Of those states, two thirds have performed research or implemented the link slab system in the field, and one third have provided design provisions or official details. North Carolina, Michigan, Virginia, and New York have been identified as significant users.

5.2 Previous Laboratory Testing on Link Slabs

Link slabs have been explored as a potential design solution as a replacement for expansion joints. Many previous research efforts have shown link slabs have the potential to be economical and reduce degradation associated with expansion joints. As PBFTGs have grown in popularity in recent years, the potential of this innovative system in continuous spans must be evaluated. The purpose of this section is to discuss previous research findings as they relate to laboratory testing of link slabs.

5.2.1 Instantaneous and Time-Dependent Response and Strength of Jointless Bridge Beams (Gastal, 1986)

Gastal (1986) explored the elimination of structural joints by casting a fully continuous deck over simply supported girders. The researcher developed an FEA model to capture the elastic and inelastic response of jointless bridge decks. The model consisted of isoperimetric beam elements representing the girders and a deck with uniaxial spring elements located at the centroid of the deck representing the link slab. The model was verified against a suite of analytical and experimental data on simply supported and continuous beams.

Gastal applied his solution to two separate design problems. Various loadings, support conditions, continuity, and construction schemes were analyzed on a two-span bridge with steel girders and a four-span bridge with prestressed concrete girders. As no experimental data was collected, the analytical methods were benchmarked against several previous experimental tests of simply supported beams.

Based on the study, Gastal concluded the behavior of jointless deck-continuous beams was significantly influenced by the support conditions of the girders. Five support conditions were analyzed by changing the conditions at the end of each girder between hinged (H) supports and roller (R) supports. Four of the arrangements, HRHR, HRRH, HRRR, and RRRR, behaved similarly to a non-continuous beam, but with slightly smaller vertical deflections and significantly less ductility. The fifth arrangement, RHHR, behaved similarly to fully continuous beams. As with the first four arrangements, the maximum capacity is controlled by yielding in the reinforcing steel, but the ultimate capacity was significantly higher than that of a non-continuous beam.

5.2.2 Behavior and Design of Link Slabs (Caner & Zia, 1998)

Caner and Zia (1998) conducted a testing program on two jointless bridge decks, one on a continuous reinforced concrete deck cast on two simple-span steel beams and the other on a similar deck cast on two simple-span precast reinforced concrete beams. The steel specimen consisted of two 20.5 foot long simply-supported W12x26 steel beams with a 2 inch gap between the adjacent ends, as seen in Figure 5.1. The 24 inch wide by 4 inch thick concrete deck was made composite to the beam with shear connectors welded to the top of the steel beam over most of the two spans. The concrete deck was debonded from each steel beam equivalent to 5% of each adjacent bridge span to reduce the stiffness and stress in the link slab. The material and geometrical properties of each bridge is provided in Table 5.1.

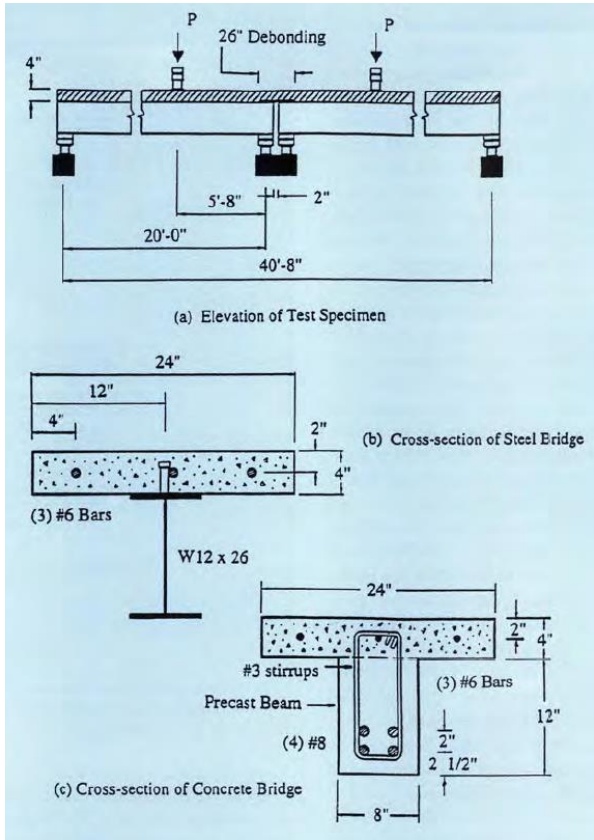

Figure 5.1: Details of Test Specimens (Caner & Zia, 1998)

Table 5.1: Material and Geometrical Properties of Steel and Concrete Bridges (Caner & Zia, 1998)

Properties	Steel bridge	Concrete bridge
Compressive strength of concrete deck	4200 psi	5670 psi
Compressive strength of girder	—	4580 psi
Girder yield strength	52,000 psi	—
Girder modulus of elasticity	30,500,000 psi	—
Girder reinforcement	—	(4) #8
Girder reinforcement yield strength	—	62,000 psi
Girder reinforcement modulus of elasticity	—	29,550,000 psi
Girder cross-sectional area (gross)	7.65 sq in.	96 sq in.
Girder moment of inertia (gross)	204 in.^{4}	1152 in.^{4}
Deck width	24 in.	24 in.
Deck thickness	4 in.	4 in.
Link slab reinforcement	(3) #6	(3) #6
Link slab reinforcement yield strength	63,600 psi	72,400 psi
Link slab reinforcement modulus of elasticity	28,500,000 psi	30,300,000 psi

The steel bridge setup was tested with four of the support conditions used by Gastal (1986): HRHR, HRRH, RRRR, and RHHR. The goal of the testing was to observe if any differences could be observed from the differing boundary conditions. Testing was performed to a maximum of 40% of the estimated ultimate load capacity to observe the behavior of the elastic range using the same specimen for each support condition. Incremental loads, strains, deflections, and crack growth were recorded.

In the elastic range of the testing, all four test cases behaved similarly, and the load-deflection behavior was nearly identical in both spans. The deflections measured compared closely to the predicted deflections from Gastal (1986) and El-Safty (1984) when neglecting the link slab and treating the bridge as two simply supported spans. This indicates the behavior of a steel bridge with a link slab is similar to a simply supported bridge. Under the first increment of loading, a crack developed in the top face of the link slab which did not extend to the bottom face. This showed the link slab was in bending and behaved like a beam instead of a tension member.

Under ultimate loading, the load deflection remained linear until the tensile flange of the steel beams began to yield. Following yielding of the steel sections, the tensile bars in the link slab began to yield. The final failure of the link slab occurred when crushing of the compression concrete at the bottom of the link slab was observed.

5.2.3 Durable Link Slabs for Jointless Bridge Decks Based on Strain-hardening Cementitious Composites (Li et al., 2003)

Due to the unique structural demand on link slabs, Li et al. (2003) explored the use of Engineered Cementitious Composite (ECC), a high-performance cementitious composite with high tensile strain capacity, high tensile strength, and excellent post-crack strain hardening properties. Specifically, the high ductility of ECC provides small crack width in the unique loading seen by link slabs.

The researchers proposed a modification to the link slab proposed by Caner and Zia (1998), which included an additional transition zone outside the standard link slab where the concrete is poured with the link slab, but shear studs are provided. The original link slab detail included termination of the debond zone and additional reinforcement spliced to the existing reinforcement at the deck slab/link slab interface. The abrupt termination imposed a high stress concentration and ultimately made the interface the weakest part of the link slab detail. The proposed detail, shown in Figure 5.2, included a transition zone of 2.5% of each adjacent span, in addition to a conventional debonded zone of 5%. The addition of shear connectors in this transition zone allowed the development of composite action over a region instead of at the interface, reducing the stress concentration.

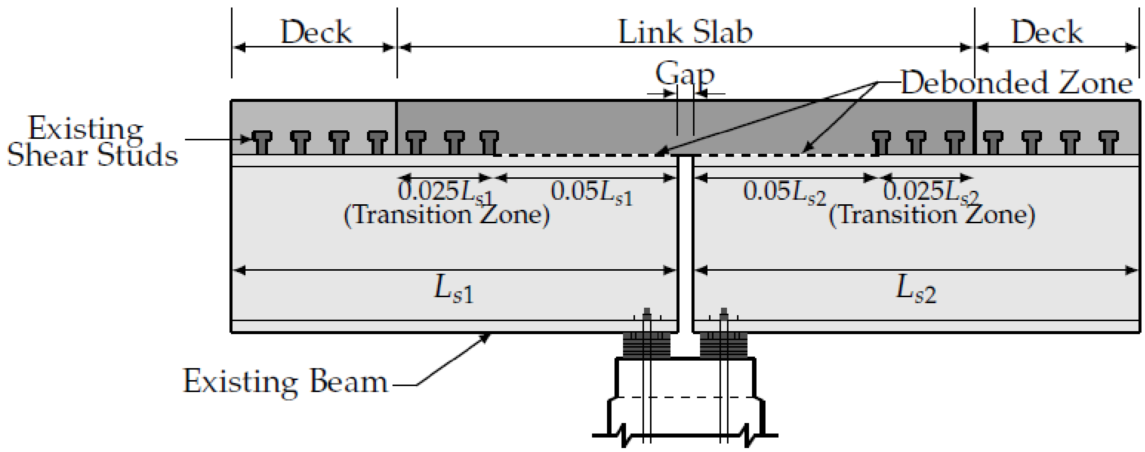

Figure 5.2: Improved Link Slab Configuration (Li et al, 2003)

The researchers performed monotonic and cyclic fatigue testing on three full-scale specimens utilizing the improved link slab design detail (Figure 5.2) and ECC. The specimens represented link slabs found between two identical 80 foot spans (Figure 5.3). Specimen LS-1 represented the new conventional link slab construction, where the link slab was cast with the adjacent spans' concrete decks. Specimen LS-2 was prepared by removing the concrete link slab from specimen LS-1 and replacing it with an ECC link slab. This specimen represented a retrofit to an existing concrete link slab where the reinforcement remains. Specimen LS-3 was prepared by removing the ECC from Specimen LS-2 and cutting the existing reinforcement 20 inches from link slab/deck slab interface and pouring a new ECC link slab with smaller reinforcement. Specimen LS-3 was prepared to investigate the role of reinforcement ratio on the fatigue performance of ECC link slabs.

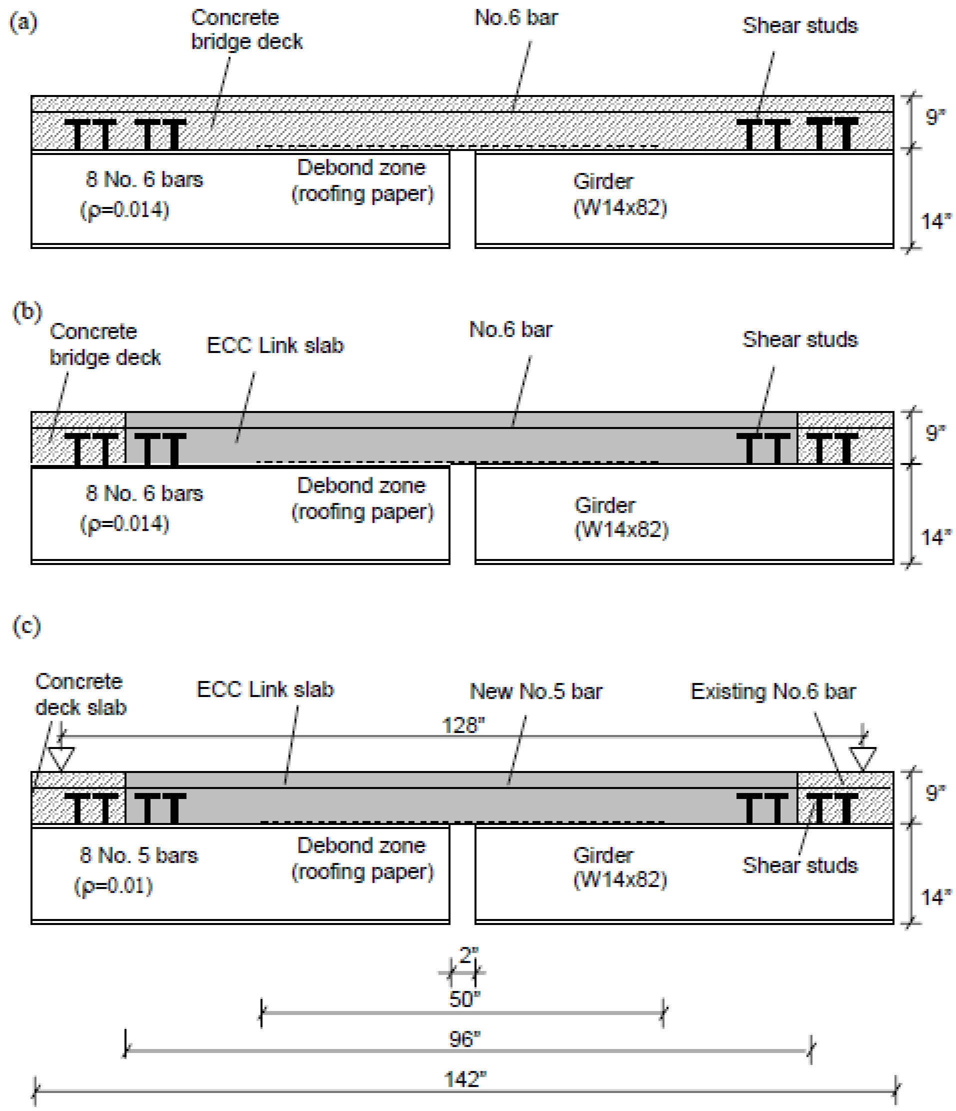

Figure 5.3: Geometry of Link Slab Specimens (Li et al, 2003)

The physical testing of the link slab was conducted on the inverted specimens with simply supported conditions at the inflection points. This reduced the total size of the experiment as two complete spans were not necessary. The specimens were statically loaded until the stress in the rebar reached 40% of its yield strength. In subsequent cyclic loading, the static loading was chosen as the mean load with the maximum load corresponding to a maximum link slab rotation when the allowable midspan deflection reaches L/800. The cyclic loading was carried out to 100,000 cycles.

The researchers concluded that ECC was a suitable material in link slabs. The smaller size of rebar required in a link slab utilizing ECC allowed for a link slab with lower flexural stiffness. This, coupled with the high ductility inherent with ECC, provided highly beneficial properties for link slabs. The improved transition zone detail eliminated the cracking previously found at the link slab/concrete deck interface, further reducing the amount of cracking found in link slabs.

5.2.4 High Skew Link Slab Bridge System with Deck Sliding Over Backwall or Backwall Sliding Over Abutments (Aktan & Attanayake, 2011)

A detailed analysis of skewed link slabs and calculation of the associated moment and force envelopes at the link slab section directly over the pier centerline was performed by Aktan & Attanayake (2011). Finite element modeling was performed on a suite of bridges with consistent span length, width, and girder type while varying the support conditions and degree of skew from 0° to 45°. The results of the finite element modeling were used to develop design recommendations for bridges with high degrees of skew.

The study determined the moment generated in a link slab under temperature gradient loads was not dependent on span length. It was also observed the moment developed in a link slab under live loads decreases with span length. This indicates the system behaves more like two independent simple spans with increased span length. Further, the researchers found the minimum amount of reinforcement required by the AASHTO LRFD BDS to be adequate for most skewed link slabs with either the HRRR or RRHR boundary conditions. Additional reinforcement in the bottom layer may be required to resist large tensile stresses which can develop near the boundaries of the debonded region.

5.2.5 Utilization of Ultra-High Performance Concrete in New York (Royce, 2016)

Royce (2016) presented multiple case studies on the utilization of prefabricated bridge elements and systems with field cast UHPC joints. The researcher discussed the achievement of ABC, but had concern with the durability of the structures, specifically the performance of joints between prefabricated elements. He discussed each case study with respect to the UHPC joints and the lessons learned from each. The researcher found the following to be beneficial in the utilization of link slabs: tight leak-free formwork due to the highly flowable nature of UHPC, exposed aggregate finish on the concrete slab/joint surface to improve bonding, use of epoxy coated or stainless steel rebar to avoid macro corrosion, and application of heat for several hours during curing to increase the strength gain. Ultimately, when construction speed is needed, precast components with UHPC joints provide good value.

In addition, Royce (2016) included a section specifically on UHPC link slabs. The New York State Department of Transportation uses a detail, like Figure 5.5, to eliminate transverse deck joints whenever feasible. Girder rotations at link slabs are accommodated by micro cracking within the UHPC link slab, as the UHPC can develop ultimate tensile strains up to 0.007. No visible cracks were reported on the link slabs in the studies, but proper design was crucial as there are several factors which influence the performance of the link slab. He also noted poor design of the link slab may cause failure of not only the link slab, but may cause structural damage to other bridge components.

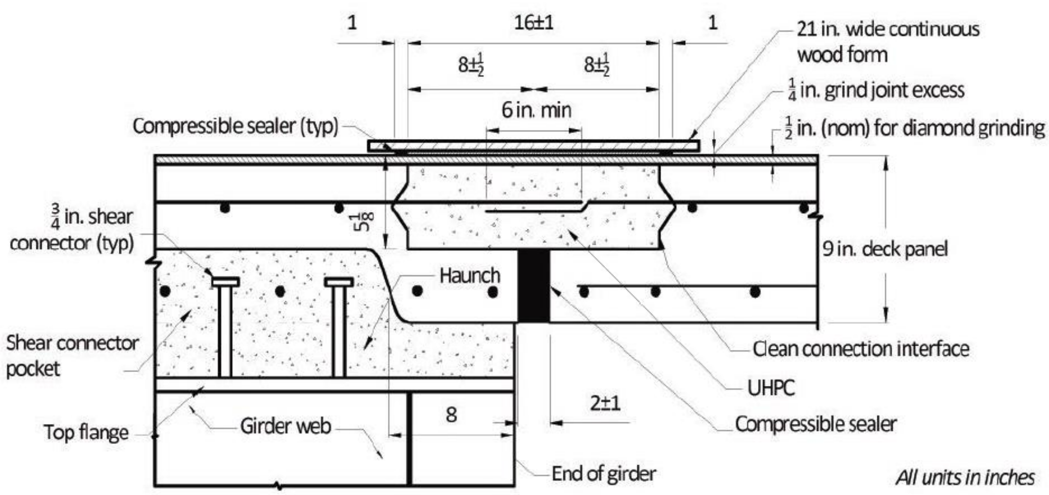

Figure 5.4: Typical UHPC Link Slab Connection Detail (Graybeal, 2014)

5.2.6 Evaluation of High-Performance Fiber-Reinforced Concrete for Bridge Deck Connections, Closure Pours, and Joints (Hoomes et al., 2017)

The researchers evaluated the mechanical properties and performance of fiber-reinforced concrete and other cementitious composites in controlling cracking for bridge deck closure pours, such as link slabs (Hoomes et al., 2017). The high-performance fiber reinforced concretes evaluated include: ECC, hybrid fiber-reinforce concrete with steel and synthetic fibers, hybrid fiber-reinforce concrete with only synthetic fibers, and UHPC. A multitude of fresh and hardened material tests were performed, and the results were compared against Virginia Department of Transportation Class A4 concrete, typical for bridge decks. The researchers concluded mixtures which underwent deflection hardening exhibited a series of fine cracks, instead of fewer large cracks. These small cracks reduced the amount of damaging material which penetrated the bridge deck. The researchers also concluded that UHPC attained the highest stress capacity, but the material did not undergo strain hardening, as seen in Figure 5.4, which may have been in part due to settling of the steel fibers to the bottom of the forms.

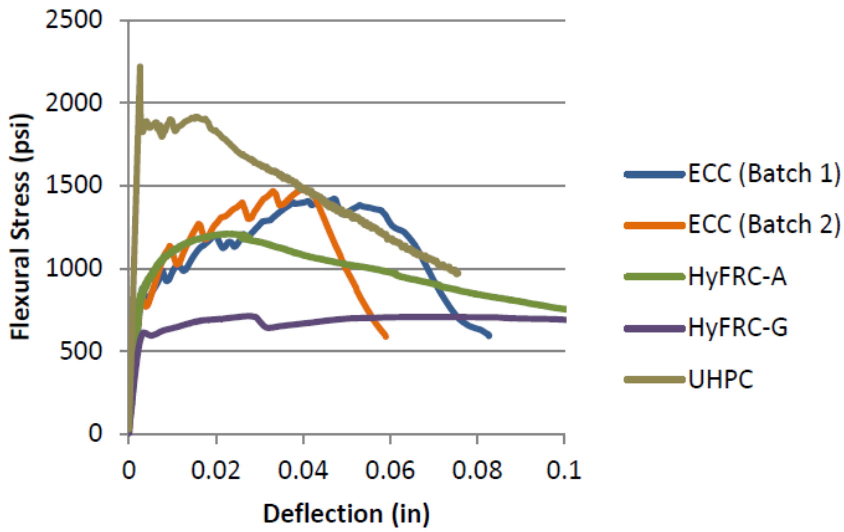

Figure 5.5: Flexural Performance of High-Performance Fiber-Reinforced Concrete Systems (Hoomes et al., 2017)

5.3 PREVIOUS FIELD TESTING OF LINK SLABS

Following the successful laboratory testing of link slabs, field testing could take place to demonstrate full-scale link slabs subjected to actual live loading. Most link slabs have been used for rehabilitation purposes. Currently most link slabs in the United States are designed using the methodology proposed by Caner and Zia (1998). The purpose of this section is to discuss the methodology of testing and the results of previous live load field testing.

5.3.1 Behavior, Analysis, and Design of an Instrumented Link Slab Bridge (Wing & Kowalsky, 2005)

Wing and Kowalsky (2005) performed research to assess the long-term performance of jointless link slabs. The North Carolina Department of Transportation rehabilitated an existing bridge and installed the first link slabs in the state, which were monitored over the course of a year. The original bridge included three interior expansion joints but after rehabilitation, only the center expansion joint remained with the other two being replaced with link slabs. The primary focus of the research was to determine if the bridge design assumptions were valid, specifically if link slab bridge girders can be assumed to be simply supported for dead and live load.

The bridge was instrumented to monitor seasonal and service level loading by measuring temperature, strain, and deflections. Following a year of monitoring, including a controlled live load field test, the link slab performed well under traffic and thermal induced loads. While the thermal loads induced a higher rotation than traffic loading, both demands were much smaller than the assumed design rotational demand. As a result, it is acceptable, although conservative, to design the girders for simply supported spans. Additionally, while cracking in the link slab was found to exceed the design criteria, it did not reduce the serviceability of the bridge. It was determined the cracking in the link slab was due to a saw cut forcing all the deformation to occur in one crack. The researchers suggested a larger crack limit to be developed in conjunction to saw cuts in link slabs. Finally, a design approach based on rotation demand and crack control criteria of the bridge was proposed to size the reinforcement in the link slab.

5.3.2 Field Demonstration of Durable Link Slabs for Jointless Bridge Decks based on Strain-hardening Cementitious Composites (Li et al., 2005)

Li et al. (2005) performed a field demonstration of the improved design detail proposed by Li et al. (2003). The link slab was designed by utilizing a set of design guidelines produced by the Michigan Department of Transportation incorporating ECC. Large scale test mixes were poured to provide insight into the mixing of large quantities of ECC material in conventional concrete mixers. These tests showed large scale mixing of ECC is possible, and the ECC maintains its fresh material properties up to one hour. During the preparation of the link slab construction, several raw material substitutions were made addressing the availability of some raw materials. As in the previous large-scale mixes, the final demonstration mix provided by the supplier met all the requirements set by the researchers.

Following the first phase of the partial width construction, several shrinkage cracks developed in the link slab. The cracks tended to form around the reinforcing bars and propagated radially outward. The additional cracking was attributed to higher water-to-cement ratios due to excessive washing of the concrete trucks. Changes were made to the mix design for the second half of the partial width construction, and a significant reduction in cracking occurred.

A full-scale live load field test was performed to assess the validity of the design approach proposed by Li et al. (2003). The parameters of interest included the surface strains of the link slab and the end span rotations. A strong correlation was found between girder rotations and strain measured on the link slab surface. The compatibility between the strain predicted from the measured girder rotation and the strain transducers in the link slab validate the design methodology.

5.4 SUMMARY

Several researchers over multiple decades have researched the economic potential of transverse link slabs in continuous span bridges. Many researchers found this technology to be a valid replacement of traditional expansion joints. However, while many researchers concluded the system is effective in removing these joints, many of these systems are limited by complex concrete materials, which would increase the total cost of the system. In addition, link slabs have not been explored in conjunction with PBFTGs. Therefore, modular PBFTGs joined by transverse link slabs would present a competitive solution in the short-span continuous bridge market.

CHAPTER 6: OVERVIEW OF CURRENT AASHTO SPECIFICATIONS RELATING TO PBFTGS

6.1 Introduction

The AASHTO LRFD BDS employ the LRFD methodology, utilizing probability-based factors to achieve a specific probability of failure. AASHTO LRFD BDS Section 6 covers the design of steel structures, where AASHTO LRFD BDS Article 6.11 specifically relates to the flexure of steel tub sections. While some of sections of the AASHTO LRFD BDS do not directly apply, or are not accurate, in the analysis and capacity of PBFTGs, a review of the current governing provisions is necessary to understand the philosophy of the AASHTO LRFD BDS. This understanding will be used to propose modifications to the provisions, increasing the applicability of PBFTGs in the short-span steel bridge market.

6.2 Loads and Load Combinations

AASHTO LRFD BDS Sections 1 and 3 discuss the various aspects of loads, and Section 4 discusses the combinations of loads for which the designer must consider. This section will discuss and review the various applicable loads and limit state load combinations to avoid any non-governing load combinations.

6.2.1 Structural Loads

Bridge loads are divided into two main categories: permanent loads and transient loads. Permanent loads are assumed to be either constant upon completion of construction or varying over a long-time interval and consist of dead load and earth loads. Transient loads can vary over a short time interval relative to the lifetime of the structure and consist of vehicular load and environmental loads, such as snow, wind, or seismic. For the purposes of this review, only dead loads and live loads will be reviewed, as they are the chief components of the Strength I, Service II, and Fatigue I and II load combinations (see Section 6.2.2).

Dead loads include the weight of all components of the structure, including appurtenances, utilities, wearing surface, and future overlays. The AASHTO LRFD BDS provides traditional unit weights to calculate the total dead load, as seen in Table 6.1.

Table 6.1: Unit Weights (AASHTO, 2020)

Material		Unit Weight (kcf)
Aluminum Alloys		0.175
Bituminous Wearing Surfaces		0.140
Cast Iron		0.450
Cinder Filling		0.060
Compacted Sand, Silt, or Clay		0.120
Concrete	Lightweight	0.110 to 0.135
	Normal Weight with $f'_c \leq 5.0$ ksi	0.145
	Normal Weight with $5.0 < f'_c \leq 15.0$ ksi	$0.140 + 0.001 f'_c$
Loose Sand, Silt, or Gravel		0.100
Soft Clay		0.100
Rolled Gravel, Macadam, or Ballast		0.140
Steel		0.490
Stone Masonry		0.170
Wood	Hard	0.060
	Soft	0.050
Water	Fresh	0.0624
	Salt	0.0640
Item		Weight per Unit Length (klf)
Transit Rails, Ties, and Fastening per Track		0.200

Dead loads can be broken down into the dead load of structural components and nonstructural attachments (DC) and the dead load of wearing surfaces and utilities (DW). Structural component dead loads can be further broken down into noncomposite dead loads (DC_1) and composite dead loads (DC_2). DC_1 loads are resisted by the noncomposite section before the concrete deck is composite with the girders and include the girder self-weight, the wet concrete deck, concrete haunches, overhang tapers, stay-in-place metal formwork, shear studs, and cross-frames. DC_2 loads are resisted by the composite section after the concrete deck and steel girder become composite and include the weight of the traffic barriers, pedestrian railing, and sidewalks. DW loads are also resisted by the composite section but are differentiated from other dead loads because they are slightly more variable than the dead loads discussed earlier.

Vehicular live load (LL) on the roadway of bridges is designated as the HL-93. The live load model, consisting of either a design truck or tandem, applied concurrently with a design lane load, was developed to represent typical truck loading to produce shears and moments permitted on highways. The design lane consists of a 0.64 klf distributed load present on spans maximizing the force effect in consideration. The weights and spacings of axles for the design truck are shown in Figure 6.1. The distance between the two 32-kip axles is varied between 14 feet and 30 feet to produce the maximum force effect in consideration. The design tandem consists of two 25-kip axles spaced at a constant 4 feet. Only those areas or parts of areas positively contributing to the extreme force effect should be loaded. The loaded area should be determined by the points were the influence surface meets the centerline of the design lane.

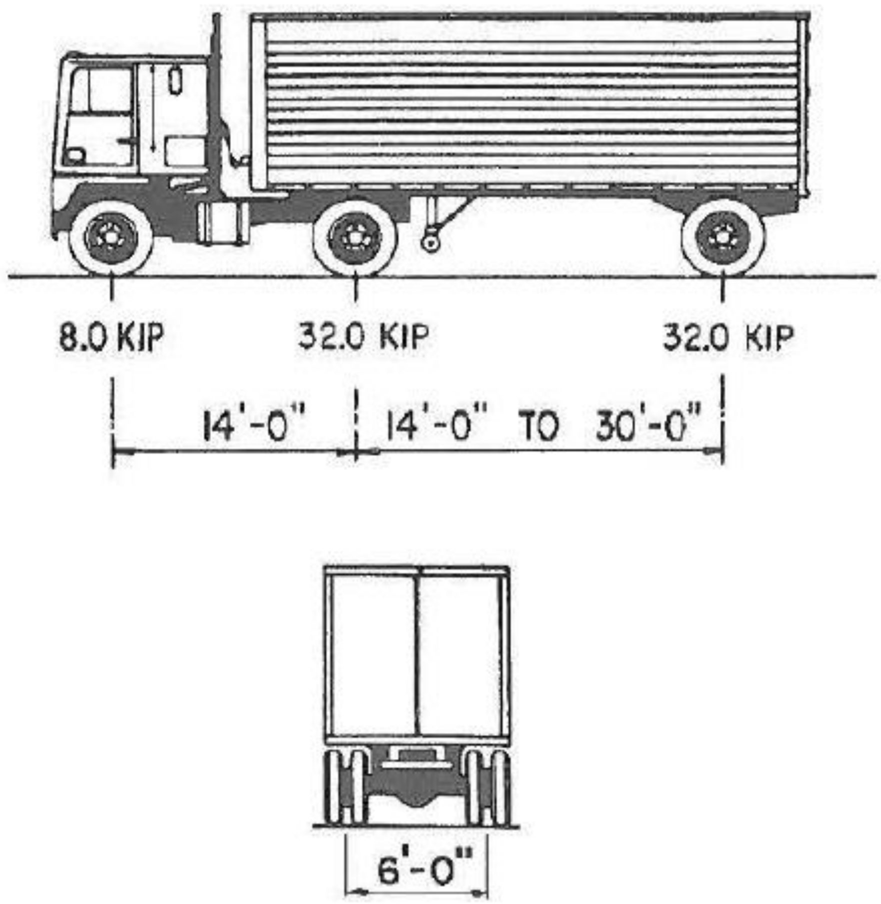

Figure 6.1: Characteristics of the Design Truck (AASHTO, 2020)

Multiple presence factors are employed to account for the probability of multiple vehicles concurrent in adjacent lanes. As noted in the AASHTO LRFD BDS commentary, the multiple presence factors are included in the approximate equations for live load distribution, but when performing graphical analysis such as lever rule or Special Analysis, the designer should consider these factors. It should also be noted multiple presence factors are not to be used when assessing fatigue, as one design truck is used regardless of the number of possible lanes loaded. The multiple presence factors are listed in Table 6.2.

Table 6.2: Multiple Presence Factors (AASHTO, 2020)

Number of Loaded Lanes	Multiple Presence Factors, m
1	1.20
2	1.00
3	0.85
>3	0.65

The dynamic load allowance (IM) accounts for dynamic effects caused primarily by hammering effects from the wheel assembly interacting with riding surface discontinuities, such as deck joints, cracks, or potholes, and the response of the bridge due to long undulations in the roadway pavement from the resonant excitation because of loading. This effect is accounted for by modifying the static wheel loads from the design truck and design tandem. The dynamic load allowance increases the static loads for most components and limit states by 33%. For the fatigue limit state, the live load is increased by 15%, and for deck joints at all limit states, the live load is increased by 75%.

6.2.2 Load Combinations

LRFD is a scheme of designing structures where both the resistance and load effects are statistically modified. The AASHTO LRFD BDS employs several resistance and load factors to account for various types of uncertainties (Galambos, 1981). Each component and connection in any given structure designed using the AASHTO LRFD BDS must satisfy the following equation:

$$\sum \eta_i \gamma_i Q_i \leq \phi R_n = R_r \qquad \text{Eq. 6.1}$$

Where:

γ_i = load factor: a statically based multiplier applied to force effects

ϕ = resistance factor: a statistically based multiplier applied to nominal resistance

η_i = load modifier: a factor relating to ductility, redundancy, and operational classification

Q_i = force effect

R_n = nominal resistance

R_r = factored resistance

Ductility, redundancy, and operational classification are included in the η_i factor to encourage enhanced ductility and redundancy and provide additional reliability for more important bridges. As of the 9th Edition of the AASHTO LRFD BDS (2020), modifications for the ductility and redundancy factors have not been implemented.

Service limit states account for restrictions of excessive stress, deformation, and crack width under service level loads. These load combinations are experience based and cannot always be derived from strength or statistical calculations, unlike other limit states. The service limit states are listed as follows:

- Service I: load combination relating the normal operational use of the bridge with a 55 mph wind
- Service II: load combination intended to control yielding steel structures and slip of slip critical connections due to vehicular load
- Service III: load combination for longitudinal analysis relating to tension in prestressed concrete
- Service IV: load combination relating to tension in prestressed concrete columns

Fatigue limit states account for restrictions of stress range caused by a single design truck occurring over an expected number of cycles. These limit states are intended to limit crack growth under repetitive loads to prevent fracture during the design life of the bridge. The fatigue limit states are listed as follows:

- Fatigue I: load combination related to infinite-induced fatigue life
- Fatigue II: load combination related to finite-induced fatigue life

Strength limit states ensure the local and global strength and stability of members resists the statistically significant load combination the bridge is expected to experience in its life. The stability or yielding of each structural element is considered, and if any element resistance has been exceeded, the bridge resistance has been exceeded. Excessive distress and structural damage may occur under the strength limit states provided below, but overall structural integrity is expected to be maintained:

- Strength I: load combination for normal vehicular use without wind
- Strength II: load combination for the use of owner-specified special design vehicles, evaluation permit vehicles, or both without wind
- Strength III: load combination for design wind speeds
- Strength IV: load combination for high dead to live load force effects
- Strength V: load combination for normal vehicular use with a wind speed of 80 mph

Extreme event limit states ensure the structural survival of the bridge. Such extreme events include earthquakes, floods, vehicle collisions, or ice floes. These loading situations are considered unique occurrences with severe operational impact whose return period may be significantly larger than the design life of the bridge. The extreme event limit states are listed as follows:

- Extreme Event I: load combination for earthquake
- Extreme Event II: load combination for ice load, collisions by vessels and vehicles, flooding, and other hydraulic events

6.3 Structural Analysis and Evaluation

AASHTO LRFD BDS Article 4.6.2.2.1 provides criteria which must be met to utilize the provided LLDFs for moment and shear in one-dimensional LGA. While performing LGA, correct distribution of the live load to individual girders is paramount to establish the total moment and shear on interior and exterior girders. There are several restrictions on the use of multiple steel box-girders in LGA, and bridges not meeting these restrictions must be analyzed using more refined methods of analysis. These restrictions will be discussed in depth in Section 6.4. For bridges constructed of multiple steel box-girders topped with a concrete deck, only one equation is used for determining LLDFs, regardless of the number of lanes loaded. The applicable expression is listed as Equation 6.2 and is valid for moment and shear in interior or exterior beams. The range of applicability of Equation 6.2 is provided by Equation 6.3. Multiple presence factors are already incorporated into the expression for the calculation of distribution factors by approximate means.

$$0.05 + 0.85\frac{N_L}{N_b} + \frac{0.425}{N_L} \qquad \text{Eq. 6.2}$$

$$0.5 \leq \frac{N_L}{N_b} < 1.5 \qquad \text{Eq. 6.3}$$

Where:

N_L = number of design lanes as specified in AASHTO LRFD BDS Article 3.6.1.1.1

N_b = number of girders

6.4 Cross-Section Proportion Limits

Equations 6.4 and 6.5 provide practical upper limits on the slenderness of webs without or with longitudinal stiffeners, respectfully. These equations are valid for minimum yield strengths of the web up to 100 ksi and further allow web-bend buckling to be disregarded in the design of composite sections in positive flexure. The webs of box sections must meet the following proportion limits:

Webs without longitudinal stiffeners:

$$\frac{D}{t_w} \leq 150 \qquad \text{Eq. 6.4}$$

Webs with longitudinal stiffeners:

$$\frac{D}{t_w} \leq 300 \qquad \text{Eq. 6.5}$$

Where:

D = depth of the web plate measured along the slope

t_w = web thickness

Equations 6.6 through 6.8 apply to the top flanges of tub sections. Equation 6.6 provides a lower limit of flange thickness to ensure the flange will not excessively distort when welded to the web. Equation 6.7 provides a lower limit on flange width to ensure adequate strength and moment rotation characteristics. Equation 6.8 ensures the flanges provide adequate restraint against web shear buckling and the boundary conditions in the web-flange juncture used in buckling formulations are sufficiently accurate. It should be noted that all PBFTGs do not meet Equation 6.8, as the flange thickness and the web thickness are the same as they are formed from the same plate. However, this is not an issue, as the intended purpose of system is to ship the units pre-topped with the concrete deck, providing adequate rigidity to the top flange.

$$\frac{b_f}{t_f} \leq 12.0 \qquad \text{Eq. 6.6}$$

$$b_f \geq D/6 \qquad \text{Eq. 6.7}$$

$$t_f \geq 1.1t_w \qquad \text{Eq. 6.8}$$

Where:

b_f = full width of the widest top flange width within the section under consideration

t_f = flange thickness

D = depth of the web plate measured along the slope

t_w = web thickness

Cross-sections of bridges consisting of two or more box sections must meet additional specifications to utilize the LLDFs mentioned previously. First, the bearing lines must not be skewed. Second, the distance center-to-center of flanges of adjacent boxes, *a*, shall be between 80 to 120% of the distance center-to-center of the flanges of each adjacent box, *w*, as illustrated in Figure 6.2. Third, the inclination of the web plates to a plane normal to the bottom flange shall not exceed a 1 to 4 slope. Lastly, the cantilever overhang of the concrete deck shall not be greater than

60% of the distance center-to-center of flanges of adjacent boxes, *a*. If these restrictions are met, not only are the LLDFs in the AASHTO LRFD BDS applicable, but the shear due to St. Venant torsion and secondary distortional stresses may be neglected.

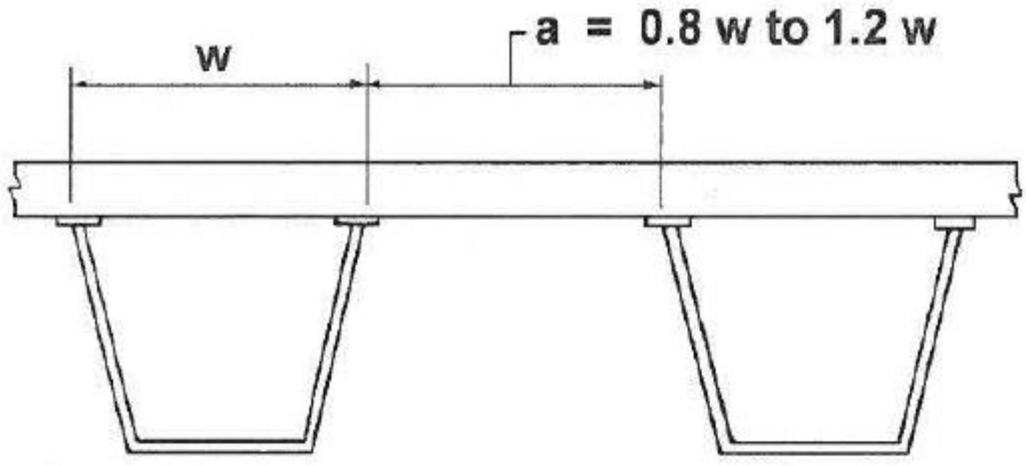

Figure 6.2: Center-to-Center Flange Distance (AASHTO, 2020)

6.5 DESIGN FOR CONSTRUCTABILITY

Issues such as deflection, strength of steel, and stability during critical stages of construction is addressed using AASHTO LRFD BDS Article 6.11.3. Nominal yielding or reliance on post-buckling resistance is not permitted for main load-carrying members during critical stages of construction. AASHTO LRFD BDS Article 6.11.3 references AASHTO LRFD BDS Article 6.10.3 significantly but provides some key differences. Unlike plate girders, where different flange thickness may be used throughout the bridge span, tub girders must maintain constant cross-section geometry. Internal or external diaphragms or cross-frames ensure deformations of the cross-section is controlled.

For tub girders in flexure, Equations 6.9 through 6.11 must be satisfied. Although these equations apply to flanges of I-sections, they may also be applied to top flanges of tub sections where struts between the tub girder flanges may be considered brace points. The AASHTO LRFD BDS distinguishes between discretely and continually braced flanges, as flange lateral bending need not be considered if the flange is continuously braced. It should be noted that for sections with compact or noncompact webs, Equation 6.10 need not be checked.

For discretely braced flanges in compression:

$$f_{bu} + f_l < \phi_f R_h F_{yc}$$ Eq. 6.9

$$f_{bu} + \frac{1}{3} f_l \leq \phi_f F_{nc}$$ Eq. 6.10

$$f_{bu} \leq \phi_f F_{crw}$$ Eq. 6.11

For discretely braced flanges in tension:

$$f_{bu} + f_l < \phi_f R_h F_{yt}$$ Eq. 6.12

For continuously braced flanges in tension or compression:

$$f_{bu} < \phi_f R_h F_{yt}$$ Eq. 6.13

In addition to the above requirements specified in AASHTO LRFD BDS Article 6.10.3, the following requirements are specified in AASHTO LRFD BDS Article 6.11.3 for noncomposite box flanges during critical stages of construction:

$$f_{bu} \leq \phi_f F_{nc}$$ Eq. 6.14

$$f_{bu} \leq \phi_f F_{crw}$$ Eq. 6.15

$$f_{bu} < \phi_f R_h F_{yf} \Delta$$ Eq. 6.16

In which:

$$\Delta = \sqrt{1 - 3\left(\frac{f_v}{F_{yf}}\right)^2}$$ Eq. 6.17

$$f_v = \frac{T}{2A_O t_f}$$ Eq. 6.18

Where:

ϕ_f = resistance factor for flexure

f_{bu} = flange stress calculated without consideration of flange lateral bending

f_l = flange lateral bending stress

F_{crw} = nominal bend-buckling resistance for webs

F_{nc} = nominal flexural resistance of box flanges in compression

R_h = hybrid girder factor

F_{yc} = specified minimum yield strength of the compression flange

F_{yt} = specified minimum yield strength of the tension flange

F_{yf} = specified minimum yield strength of the flange under consideration

Δ = reduction factor for the maximum stress in a box flange

f_v = St. Venant torsional shear stress in the flange to the factored loads at the section under consideration

A_o = enclosed area with the box section

T = internal torque due to the factored loads

Webs shall satisfy the following shear requirements during critical stages of construction:

$$V_u \leq \phi_v V_{cr} \quad \text{Eq. 6.19}$$

$$V_{ui} = \frac{V_u}{\cos\theta} \quad \text{Eq. 6.20}$$

Where:

ϕ_v = resistance factor for shear

V_u = vertical shear due to the factored loads on one inclined web of a box section

V_{cr} = shear-buckling resistance

V_{ui} = shear due to the factored loads along one inclined web of a box section

θ = the angle of inclination of the web plate to the vertical

6.6 Design for Serviceability

Service limit states ensure the durability and serviceability of the bridge and its components under normal traffic loading, traditionally termed service loads (Mertz, 2022a). Two of the serviceability limit states provided in the AASHTO LRFD BDS are applicable to steel bridges.

The first limit state is intended to limit elastic deformations, while the second is intended to limit permanent deformations.

The Service I limit state load combination is an optional limit state in the AASHTO LRFD BDS; however, most states require live load deflection control. It is intended to control human perception of deflection, but bridge frequency or period would be a better measure to control intended perceived deflections. Dynamic analysis could address this, but non-seismic bridge design does not typically include dynamic analysis. AASHTO LRFD BDS Article 2.5.2.6 lists suggested limits for elastic live load deflections for steel structures (Figure 6.3).

- Vehicular load, general Span/800,
- Vehicular and pedestrian loads Span/1,000,
- Vehicular load on cantilever arms...... Span/300, and
- Vehicular and pedestrian loads on cantilever arms Span/375.

Figure 6.3: Live Load Deflection Limits (AASHTO, 2020)

The Service II limit state ensures permanent deformation caused by localized yielding does not impair the rideability of the structure. The degree of composite action between the concrete deck and the steel girder determines which sections the Service II loads are applied. Upon investigation of the limit states and their load combinations, Service II limit states could only govern if the section is compact. Note, while I-girders may redistribute negative moment at interior pier sections, box sections may not utilize moment redistribution. The following equations must be satisfied to prevent objectionable permanent deformations under severe traffic loading. It should be noted AASHTO LRFD BDS Article 6.11.4 states the provisions of AASHTO LRFD BDS Article 6.10.4 shall apply with some modifications. Therefore, some equations, such as Equations 6.21 and 6.22, from AASHTO LRFD BDS Article 6.10.4 have modifications.

For the top steel flange of composite sections:

$$f_f < 0.95 R_h F_{yf} \qquad \text{Eq. 6.21}$$

For the bottom steel flange of composite sections:

$$f_f < 0.95 R_h F_{yf} \qquad \text{Eq. 6.22}$$

Where:

f_f = flange stress at the section under consideration due to the Service II loads calculated with consideration of flange lateral bending

F_{yf} = specified minimum yield strength of the flange under consideration

R_h = hybrid girder factor

Web bend buckling should be considered for all sections except for composite sections in positive flexure where the web satisfies the requirement of AASHTO LRFD BDS Article 6.10.2.1.1. For sections not meeting those requirements, the following restriction is provided to ensure the web has sufficient capacity to resist web bend buckling:

$$f_c \leq F_{crw} \qquad \text{Eq. 6.23}$$

Where:

f_c = compression-flange stress at the section under consideration due to the Service II loads calculated without consideration of flange lateral bending

F_{crw} = nominal bend-buckling resistance for webs

6.7 DESIGN FOR FATIGUE

Fatigue in metals is the process of initiation and growth of cracks under the action of repetitive tensile loads (Mertz, 2022(b)). Fatigue cracks can develop at stress levels significantly lower than those associated with cracking under static loading conditions. In the design of elements subject to fatigue, consideration of the total number of cycles and the element type are key. The

AASHTO LRFD BDS addresses two types of fatigue: load induced fatigue and distortion induced fatigue, discussed in AASHTO LRFD BDS Articles 6.6.1.2 and 6.6.1.3, respectively.

For load induced fatigue, only the live load plus impact needs to be considered when determining the stress range in the short-term composite section. Residual stresses need not be considered, and regions where the unfactored dead load produces compressive stress higher than the live load tensile stress also need not be considered. Connection and fabrication details are arranged by detail category where differing fatigue details can withstand differing fatigue threshold ranges as discussed in AASHTO LRFD BDS Table 6.6.1.2.3-1.

For load-induced fatigue considerations, each detail must satisfy:

$$\gamma(\Delta f) \leq (\Delta F)_n \qquad \text{Eq. 6.24}$$

Where:

γ = load factor specified in ASSHTO LRFD BDS Table 3.4.1-1 for the fatigue load combination

(Δf) = force effect, live load stress range due to the passage of the fatigue load

$(\Delta F)_n$ = nominal fatigue resistance

For the Fatigue I load combination and infinite life:

$$(\Delta F)_n = (\Delta F)_{TH} \qquad \text{Eq. 6.25}$$

Where:

$(\Delta F)_{TH}$ = constant amplitude fatigue threshold taken from AASHTO LRFD Table 6.6.1.2.5-3

For the Fatigue II load combination and finite life

$$(\Delta F)_n = \left(\frac{A}{N}\right)^{\frac{1}{3}} \qquad \text{Eq. 6.26}$$

In which:

$$N = (365)(75)n(ADTT)_{SL} \quad \text{Eq. 6.27}$$

Where:

A = detail category constant

N = number of fatigue cycles over the design life of the structure

n = number of stress range cycles per truck passage

$(ADTT)_{SL}$ = single lane *ADTT*

Distortion-induced fatigue is caused by secondary out-of-plane stresses not normally quantified in typical analysis and design of bridges. Rigid load paths must be provided to adequately transfer the forces from transverse bracing members from the web of the longitudinal element to the flanges (Mertz, 2022(b)). Load paths are established by bolting or welding connecting diaphragms, internal or external diaphragms, and floor beams or stringers to the compression and tension flanges.

Unstable crack growth, or fracture, occurs when the effects of total stress and flaw size exceed a critical value, commonly referred to as the fracture toughness (Mertz, 2022(b)). AASHTO LRFD BDS Article 6.6.2 defines the required fracture toughness based on the Charpy V-Notch impact test. All primary members and components subject to a net tensile stress under the Strength I load combination require Charpy V-Notch testing. Each member or component must be able to absorb a specified amount of energy depending on the steel grade and the applicable minimum temperature zone.

6.8 DESIGN FOR STRENGTH

The strength limit state ensures adequate strength and stability of the bridge against statistically predicted moments and shears over the entire life of the bridge. The AASHTO LRFD BDS typically provides strength limit state functions based on moments or shears, but in limited circumstances, such as noncompact girders, the strength limit states are defined by stress. This is mostly due to the application of loads to different sections. AASHTO LRFD BDS Article 6.11.6

describes the strength limit state for box-girders and directs the user to the appropriate articles for the design of box-girders in positive and negative flexure.

6.8.1 General Requirements

Sections which meet the requirements of AASHTO LRFD BDS Article 6.11.6.2.2 qualify as compact and are permitted to exceed the moment at first yield according to the provisions of AASHTO LRFD BDS Article 6.10.7. The following are the required limits:

- The section is not horizontally curved.
- The section is straight, without skew.
- The specified minimum yield strength of the flanges and web do not exceed 70 ksi.
- The web satisfies the cross-section proportion limit in AASHTO LRFD BDS Article 6.11.2.1.2.
- The section meets the special restrictions on the use of LLDFs discussed in AASHTO LRFD BDS Article 6.11.2.3.
- The box flange is fully effective as specified in AASHTO LRFD BDS Article 6.11.1.1.
- The section satisfies the following web slenderness limit:

$$\frac{2D_{cp}}{t_w} \leq 3.76\sqrt{\frac{E}{F_{yc}}} \qquad \text{Eq. 6.28}$$

Where:

D_{cp} = depth of the web in compression at the plastic moment

t_w = web thickness

E = modulus of elasticity of steel

F_{yc} = specified minimum yield strength of the compression flange

Compact sections shall satisfy the requirements specified in AASHTO LRFD BDS Article 6.11.7.1. Sections which do not meet the requirements listed above are labeled noncompact and must meet the requirements specified in AASHTO LRFD BDS Article 6.11.7.2. The ability of such sections to develop a nominal flexural resistance greater than the moment at first yield in the presence of potentially significant St. Venant torsional shear and cross-sectional distortion stresses has not been demonstrated (AASHTO, 2020).

Compact and noncompact sections shall satisfy the ductility requirement as follows:

$$D_p \leq 0.42 D_t \quad \text{Eq. 6.29}$$

Where:

D_p = distance from the top of the concrete deck to the neutral axis of the composite section at the plastic moment

D_t = total depth of the composite section

6.8.2 Flexural Resistance of Composite Sections

For compact sections, the section shall meet the following provisions:

$$M_u \leq \phi_f M_n \quad \text{Eq. 6.30}$$

Where:

ϕ_f = resistance factor for flexure

M_n = nominal flexural resistance of the section

M_u = bending moment about the major axis of the cross-section due to the factored loads at the section under consideration

If $D_p \leq 0.1\ D_t$, then:

$$M_n \leq M_p \quad \text{Eq. 6.31}$$

Otherwise:

$$M_n = M_p \left(1.07 - 0.7 \frac{D_p}{D_t}\right) \quad \text{Eq. 6.32}$$

Where:

D_p = distance from the top of the concrete deck to the neutral axis of composite section at the plastic moment

D_t = total depth of the composite section

M_n = nominal flexural resistance of a section

M_p = plastic moment of composite section

In a continuous span, the nominal flexural resistance is limited by:

$$M_n \leq 1.3 R_h M_y \qquad \text{Eq. 6.33}$$

Where:

M_n = nominal flexural resistance of a section

R_h = hybrid girder factor determined as specified in Article 6.10.1.10.1

M_y = yield moment

For noncompact sections, the section shall meet the following provisions:

At the strength limit state, compression flanges shall satisfy:

$$f_{bu} \leq \phi_f F_{nc} \qquad \text{Eq. 6.34}$$

Where:

ϕ_f = resistance factor for flexure

f_{bu} = flange stress calculated without consideration of flange lateral bending or longitudinal warping

F_{nc} = nominal flexural resistance of box flanges in compression

The nominal flexural resistance of the compression flange of closed-box sections shall be taken as:

$$F_{nc} = R_b R_h F_{yc} \Delta \qquad \text{Eq. 6.35}$$

In which:

$$\Delta = \sqrt{1 - 3\left(\frac{f_v}{F_{yf}}\right)^2} \quad \text{Eq. 6.36}$$

$$f_v = \frac{T}{2A_O t_f} \quad \text{Eq. 6.37}$$

Where:

F_{nc} = nominal flexural resistance of box flanges in compression

R_b = web load shedding factor

R_h = hybrid girder factor

F_{yc} = specified minimum yield strength of the compression flange

Δ = reduction factor for the maximum stress in a box flange

f_v = St. Venant torsional shear stress in the flange to the factored loads at the section under consideration

A_o = enclosed area with the box section

T = internal torque due to the factored loads

At the strength limit state, tension flanges shall satisfy:

$$f_{bu} \leq \phi_f F_{nt} \quad \text{Eq. 6.38}$$

Where:

ϕ_f = resistance factor for flexure

f_{bu} = flange stress calculated without consideration of flange lateral bending or longitudinal warping

F_{nt} = nominal flexural resistance of box flanges in tension

The nominal flexural resistance of the tension flange of closed-box sections shall be taken as:

$$F_{nt} = R_h F_{yt} \Delta \quad \text{Eq. 6.39}$$

In which:

$$\Delta = \sqrt{1 - 3\left(\frac{f_v}{F_{yf}}\right)^2} \quad \text{Eq. 6.40}$$

$$f_v = \frac{T}{2A_O t_f} \quad \text{Eq. 6.41}$$

Where:

F_{nt} = nominal flexural resistance of box flanges in tension

R_h = hybrid girder factor

F_{yt} = specified minimum yield strength of the tension flange

Δ = reduction factor for the maximum stress in a box flange

f_v = St. Venant torsional shear stress in the flange to the factored loads at the section under consideration

A_o = enclosed area with the box section

T = internal torque due to the factored loads

6.8.3 Flexural Resistance of Noncomposite Sections

The following provisions are applied to noncomposite sections:

At the strength limit state, compression flanges shall satisfy:

$$f_{bu} \leq \phi_f F_{nc} \quad \text{Eq. 6.42}$$

Where:

ϕ_f = resistance factor for flexure

f_{bu} = flange stress calculated without consideration of flange lateral bending or longitudinal warping

F_{nc} = nominal flexural resistance of box flanges in compression

The nominal flexural resistance of unstiffened compression flanges shall be taken as:

$$F_{nc} = F_{cb}\sqrt{1 - \left(\frac{f_v}{\phi_v F_{cr}}\right)^2} \qquad \text{Eq. 6.43}$$

In which:

If $\lambda_f \leq \lambda_p$, then:

$$F_{cb} = R_b R_h F_{yc} \Delta \qquad \text{Eq. 6.44}$$

If $\lambda_p < \lambda_f \leq \lambda_r$, then:

$$F_{cb} = R_b R_h F_{yc}\left[\Delta - \left(\Delta - \frac{\Delta - 0.3}{R_h}\right)\left(\frac{\lambda_f - \lambda_p}{\lambda_r - \lambda_p}\right)\right] \qquad \text{Eq. 6.45}$$

If $\lambda_f > \lambda_r$, then:

$$F_{cb} = \frac{0.9 E R_b k}{\lambda_f^2} \qquad \text{Eq. 6.46}$$

If $\lambda_f \leq 1.12\sqrt{\frac{Ek_s}{F_{yc}}}$, then:

$$F_{cv} = 0.58 F_{yc} \qquad \text{Eq. 6.47}$$

If $1.12\sqrt{\frac{Ek_s}{F_{yc}}} \leq \lambda_f \leq 1.40\sqrt{\frac{Ek_s}{F_{yc}}}$, then:

$$F_{cv} = \frac{0.65\sqrt{Ek_s}}{\lambda_f} \qquad \text{Eq. 6.48}$$

If $\lambda_f > 1.40\sqrt{\frac{Ek_s}{F_{yc}}}$, then:

$$F_{cv} = \frac{0.9Ek_s}{\lambda_f^2} \qquad \text{Eq. 6.49}$$

$$\lambda_f = \frac{b_{fc}}{t_{fc}} \qquad \text{Eq. 6.50}$$

$$\lambda_p = 0.57\sqrt{\frac{Ek}{F_{yc}\Delta}} \qquad \text{Eq. 6.51}$$

$$\lambda_r = 0.95\sqrt{\frac{Ek}{F_{yr}}} \qquad \text{Eq. 6.52}$$

$$\Delta = \sqrt{1 - 3\left(\frac{f_v}{F_{yc}}\right)^2} \qquad \text{Eq. 6.53}$$

$$f_v = \frac{T}{2A_O t_c} \qquad \text{Eq. 6.54}$$

$$F_{yr} = (\Delta - 0.3)F_{yc} \qquad \text{Eq. 6.55}$$

Where:

ϕ_v = resistance factor for shear

F_{cb} = nominal axial compression buckling resistance of the flange under compression alone

F_{cv} = nominal shear buckling resistance of the flange

λ_f = slenderness ratio of the compression flange

λ_p = limiting flange slenderness where the elastic buckling stress equals $R_bF_{yc}\Delta$

λ_r = limiting flange slenderness where the elastic buckling stress equals R_bF_{yr}

Δ = reduction factor for the maximum stress in a box flange

f_v = St. Venant torsional shear stress in the flange to the factored loads at the section under consideration

A_o = enclosed area with the box section

T = internal torque due to the factored loads

F_{yr} = smaller of the compression flange stress at the onset of nominal yield, with consideration or residual stress effects, or the specified minimum yield strength of the web

k = plate-buckling coefficient for uniform normal stress = 4

k_s = compression-flange width between webs

b_{fc} = limiting flange slenderness where the elastic buckling stress equals R_bF_{yr}

t_{fc} = compression flange thickness

R_b = web load-shedding factor

R_h = hybrid girder factor

E = modulus of elasticity of steel

The nominal flexural resistance of stiffened compression flanges is determined in the same manner as unstiffened flanges with the following modifications:

- W shall be substituted for b_{fc}
- The plate buckling coefficient for uniform stress, k, shall be taken as:
    - If n = 1, then:

$$k = \left(\frac{8I_s}{wt_{fc}^3}\right)^{\frac{1}{3}} \qquad \text{Eq. 6.56}$$

    - If n = 3, then:

$$k = \left(\frac{0.894I_s}{wt_{fc}^3}\right)^{\frac{1}{3}} \qquad \text{Eq. 6.57}$$

$$1.0 \leq k \leq 4.0$$

- The plate buckling coefficient for shear stress, k_s, shall be taken as:

$$k_s = \frac{5.34 + 2.84\left(\frac{I_s}{wt_{fc}^3}\right)^{\frac{1}{3}}}{(n+1)^2} \leq 5.34 \qquad \text{Eq. 6.58}$$

Where:

I_s = moment of inertia of a single longitudinal flange stiffener about an axis parallel to the flange and taken at the base of the stiffener

n = number of equally spaced longitudinal flange stiffeners

w = larger of the width of the flange between longitudinal flange stiffeners or the distance from a web to the nearest longitudinal flange stiffener

t_{fc} = thickness of the compression flanges

At the strength limit state, tension flanges shall satisfy:

$$f_{bu} \leq \phi_f F_{nt} \qquad \text{Eq. 6.59}$$

Where:

ϕ_f = resistance factor for flexure

f_{bu} = flange stress calculated without consideration of flange lateral bending or longitudinal warping

F_{nt} = nominal flexural resistance of box flanges in tension

The nominal flexural resistance of tension flanges of tub sections shall be taken as:

$$F_{nt} = R_h F_{yt} \qquad \text{Eq. 6.60}$$

Where:

R_h = hybrid girder factor

F_{yt} = specified minimum yield strength of the tension flange

6.8.4 Shear Resistance

At the strength limit state, each of the inclined webs will be designed for a shear due to the factored loads specified below:

$$V_u \leq \phi_v V_n \qquad \text{Eq. 6.61}$$

$$V_{ui} = \frac{V_u}{\cos\theta} \qquad \text{Eq. 6.62}$$

Where:

V_{ui} = vertical shear due to the factored loads on the inclined web

V_u = vertical shear due to the factored loads one inclined web

θ = the angle of inclination of the web plate to the vertical

ϕ_v = resistance factor for shear

V_n = nominal shear resistance for unstiffened or stiffened webs

The nominal shear resistance of unstiffened webs shall be taken as:

$$V_n = V_{cr} = CV_p \qquad \text{Eq. 6.63}$$

In which:

$$V_p = 0.58F_{yw}Dt_w \qquad \text{Eq. 6.64}$$

Where:

V_n = nominal shear resistance

V_{cr} = shear-buckling resistance

C = ratio of the shear-buckling resistance to the shear yield strength

V_p = plastic shear force

F_{yw} = specified minimum yield strength of the web

D = depth of the web

t_w = thickness of the web

Stiffened interior web panels of nonhybrid and hybrid members satisfying Equation 6.65 can develop post buckling shear resistance due to tension field action:

$$\frac{2Dt_w}{\left(b_{fc}t_{fc} + b_{ft}t_{ft}\right)} \leq 2.5 \qquad \text{Eq. 6.65}$$

If Equation 6.65 is satisfied, the nominal shear resistance of a stiffened interior web panel shall be taken as:

$$V_n = V_p\left[C + \frac{0.87(1-C)}{\sqrt{1+\left(\frac{d_o}{D}\right)^2}}\right] \qquad \text{Eq. 6.66}$$

If Equation 6.65 is not satisfied, the nominal shear resistance of a stiffened interior web panel shall be taken as:

$$V_n = V_p\left[C + \frac{0.87(1-C)}{\sqrt{1+\left(\frac{d_o}{D}\right)^2} + \frac{d_o}{D}}\right] \qquad \text{Eq. 6.67}$$

In which:

$$V_p = 0.58F_{yw}Dt_w \qquad \text{Eq. 6.68}$$

Where:

V_n = nominal shear resistance

C = ratio of the shear-buckling resistance to the shear yield strength

V_p = plastic shear force

F_{yw} = specified minimum yield strength of the web

d_o = transverse stiffener spacing

D = depth of the web

t_w = thickness of the web

The ratio, *C*, shall be determined as specified below:

- If $\frac{D}{t_w} \leq 1.12\sqrt{\frac{Ek}{F_{yw}}}$, then:

$$C = 1.0 \qquad \text{Eq. 6.69}$$

- If $1.12\sqrt{\frac{Ek}{F_{yw}}} \leq \frac{D}{t_w} \leq 1.40\sqrt{\frac{Ek}{F_{yw}}}$, then:

$$C = \frac{1.12}{\frac{D}{t_w}}\sqrt{\frac{Ek}{F_{yw}}} \qquad \text{Eq. 6.70}$$

- If $\frac{D}{t_w} > 1.40\sqrt{\frac{Ek}{F_{yw}}}$, then:

$$C = \frac{1.12}{\left(\frac{D}{t_w}\right)^2}\left(\frac{Ek}{F_{yw}}\right) \qquad \text{Eq. 6.71}$$

In which:

$$k = 5 + \frac{5}{\left(\frac{d_o}{D}\right)^2} \qquad \text{Eq. 6.72}$$

Where:

D = depth of the web

t_w = thickness of the web

E = modulus of elasticity of steel

k = shear buckling coefficient

F_{yw} = specified minimum yield strength of the web

C = ratio of the shear-buckling resistance to the shear yield strength

d_o = transverse stiffener spacing

The nominal shear resistance of a stiffened end panel shall be taken as:

$$V_n = V_{cr} = CV_p \quad \text{Eq. 6.73}$$

In which:

$$V_p = 0.58F_{yw}Dt_w \quad \text{Eq. 6.74}$$

Where:

V_n = nominal shear resistance

C = ratio of the shear-buckling resistance to the shear yield strength

V_p = plastic shear force

F_{yw} = specified minimum yield strength of the web

d_o = transverse stiffener spacing

D = depth of the web

t_w = thickness of the web

6.9 AASHTO REFERENCES

Table 6.3 details a summary of the equations, figures, and tables referenced in this chapter, along with their respective AASHTO LRFD BDS equation reference and page numbers.

Table 6.3: AASHTO LRFD BDS References (AASHTO, 2020)

Chapter 6	AASHTO LRFD BDS 9th Edition Reference	AASHTO LRFD BDS 9th Edition Page Number
Table 6.1	Table 3.5.1-1	3-21
Figure 6.1	Figure 3.6.1.2.2-1	3-25
Table 6.2	Table 3.6.1.1.2-1	3-23
Equation 6.1	Equation 1.3.2.1-1	1-3
Equation 6.2	Table 4.6.2.2.2b-1	4-38
Equation 6.3	Table 4.6.2.2.2b-1	4-38
Equation 6.4	Equation 6.11.2.1.2-1	6-222
Equation 6.5	Equation 6.11.2.1.3-1	6-222
Equation 6.6	Equation 6.11.2.2-1	6-222
Equation 6.7	Equation 6.11.2.2-2	6-222
Equation 6.8	Equation 6.11.2.2-3	6-222
Figure 6.2	Figure 6.11.2.3-1	6-223
Equation 6.9	Equation 6.10.3.2.1-1	6-160
Equation 6.10	Equation 6.10.3.2.1-2	6-160
Equation 6.11	Equation 6.10.3.2.1-3	6-160
Equation 6.12	Equation 6.10.3.2.2-1	6-162
Equation 6.13	Equation 6.10.3.2.3-1	6-162
Equation 6.14	Equation 6.11.3.2-1	6-224
Equation 6.15	Equation 6.11.3.2-2	6-224
Equation 6.16	Equation 6.11.3.2-3	6-224
Equation 6.17	Equation 6.11.3.2-4	6-224
Equation 6.18	Equation 6.11.3.2-5	6-225
Equation 6.19	Equation 6.10.3.3-1	6-163
Equation 6.20	Equation 6.11.9-1	6-238
Figure 6.3	Article 2.5.2.6.2	2-12
Equation 6.21	Equation 6.10.4.2.2-1	6-168
Equation 6.22	Equation 6.10.4.2.2-2	6-168
Equation 6.23	Equation 6.10.4.2.2-4	6-169
Equation 6.24	Equation 6.6.1.2.2-1	6-40
Equation 6.25	Equation 6.6.1.2.5-1	6-56
Equation 6.26	Equation 6.6.1.2.5-2	6-57
Equation 6.27	Equation 6.6.1.2.5-3	6-57
Equation 6.28	Equation 6.11.6.2.2-1	6-230
Equation 6.29	Equation 6.10.7.3-1	6-182
Equation 6.30	Equation 6.11.7.1.1-1	6-231

Table 6.3: AASHTO LRFD BDS References (cont'd) (AASHTO, 2020)

Chapter 6	AASHTO LRFD BDS 9th Edition Reference	AASHTO LRFD BDS 9th Edition Page Number
Equation 6.31	Equation 6.10.7.1.2-1	6-179
Equation 6.32	Equation 6.10.7.1.2-2	6-179
Equation 6.33	Equation 6.10.7.1.2-3	6-179
Equation 6.34	Equation 6.11.7.2.1-1	6-231
Equation 6.35	Equation 6.11.7.2.2-2	6-232
Equation 6.36	Equation 6.11.7.2.2-3	6-232
Equation 6.37	Equation 6.11.7.2.2-4	6-232
Equation 6.38	Equation 6.11.7.2.1-2	6-232
Equation 6.39	Equation 6.11.7.2.2-5	6-233
Equation 6.40	Equaiton 6.11.7.2.2-6	6-233
Equation 6.41	Equation 6.11.7.2.2-7	6-233
Equation 6.42	Equation 6.11.8.1.1-1	6-233
Equation 6.43	Equation 6.11.8.2.2-1	6-235
Equation 6.44	Equation 6.11.8.2.2-2	6-235
Equation 6.45	Equation 6.11.8.2.2-3	6-235
Equation 6.46	Equaiton 6.11.8.2.2-4	6-235
Equation 6.47	Equation 6.11.8.2.2-5	6-235
Equation 6.48	Equation 6.11.8.2.2-6	6-236
Equation 6.49	Equation 6.11.8.2.2-7	6-236
Equation 6.50	Equation 6.11.8.2.2-8	6-236
Equation 6.51	Equation 6.11.8.2.2-9	6-236
Equation 6.52	Equation 6.11.8.2.2-10	6-236
Equation 6.53	Equation 6.11.8.2.2-11	6-236
Equation 6.54	Equation 6.11.8.2.2-12	6-236
Equation 6.55	Equation 6.11.8.2.2-13	6-236
Equation 6.56	Equation 6.11.8.2.3-1	6-237
Equation 6.57	Equation 6.11.8.2.3-2	6-237
Equation 6.58	Equation 6.11.8.2.3-3	6-237
Equation 6.59	Equation 6.11.8.1.2-4	6-234
Equation 6.60	Equation 6.11.8.3-1	6-238
Equation 6.61	Equation 6.10.9.1-1	6-193
Equation 6.62	Equation 6.11.9-1	6-238
Equation 6.63	Equation 6.10.9.2-1	6-194
Equation 6.64	Equation 6.10.9.2-2	6-194
Equation 6.65	Equation 6.10.9.3.2-1	6-195

Table 6.3: AASHTO LRFD BDS References (cont'd) (AASHTO, 2020)

Chapter 6	AASHTO LRFD BDS 9th Edition Reference	AASHTO LRFD BDS 9th Edition Page Number
Equation 6.66	Equation 6.10.9.3.2-2	6-195
Equation 6.67	Equation 6.10.9.3.2-8	6-196
Equation 6.68	Equation 6.10.9.3.2-3	6-195
Equation 6.69	Equation 6.10.9.3.2-4	6-195
Equation 6.70	Equation 6.10.9.3.2-5	6-196
Equation 6.71	Equation 6.10.9.3.2-6	6-196
Equation 6.72	Equation 6.10.9.3.2-7	6-196
Equation 6.73	Equation 6.10.9.3.3-1	6-196
Equation 6.74	Equation 6.10.9.3.3-2	6-196

6.10 Summary

This chapter summarized the applicable articles and equations from the AASHTO LRFD BDS related to PBFTGs. As PBFTGs are a relatively new type of system, specifications directly relating to them in the AASHTO LRFD BDS do not exist. The system was designed using the applicable articles found in AASHTO LRFD BDS Article 6.11 as they relate to large, welded box-girders. However, several sections are not applicable to the design of most PBFTG bridges. For example, as written, the LLDFs found in AASHTO LRFD BDS Article 4.6.2.2 are not directly applicable to PBFTGs, as they inherently violate special restrictions on the use of LLDFs for multiple box sections found in AASHTO LRFD BDS Article 6.11.2.3. Additionally, the limit of skew on the compactness, and therefore ultimate capacity of PBFTGs, greatly reduces the applicability of PBFTGs in skewed bridge configurations. Based on the findings of this chapter, a more refined analysis was performed on PBFTGs with the focus of improving the AASHTO LRFD BDS relating to PBFTGs.

CHAPTER 7: FINITE ELEMENT MODELING TECHNIQUES

7.1 INTRODUCTION

This chapter details the analytical modeling techniques developed to assess the capacity of PBFTG systems. FEA was performed utilizing the commercial finite element software suite Abaqus/CAE (Dassault Systèmes, 2020). An input file was generated by writing a routine in MATLAB (Mathworks, 2021) and was ran using Abaqus/CAE in the command window. A three-dimensional nonlinear finite element modeling procedure was developed to determine the ultimate capacity of skewed PBFTGs. A second technique, based on the first, was used to model linear PBFTG bridges to assess live load distribution characteristics of PBFTG bridges.

7.2 ELEMENT SELECTION

Abaqus/CAE provides the user with a vast amount of element types to discretize the three-dimensional model. Therefore, an investigation into the suitability of the appropriate element type is warranted. As shown by several previous researchers (Barth, 1996; Yang, 2004; Roberts, 2005: Righman, 2005), S4R elements are sufficiently accurate to model the behavior of plate girders.

7.2.1 Element Naming Convention

Each element utilized in Abaqus/CAE has a unique name which conveys the key attributes of the element. The element name contains five identifiers, if applicable, which describe the family, degrees of freedom, number of nodes, formulation, and integration. The first letter of the element name describes the general type, or family of element. For example, 'S' represents a shell element or 'C' represents a continuum, or solid, element. Directly related to the element family are the degrees of freedom. In a stress/displacement analysis, the degrees of freedom are translations at each node. Typically, all degrees of freedom are considered for an element and not specified in the name. However, if a degree of freedom is restrained, the degree of freedom restrained follows the family, and is in turn followed by a 'D', i.e., 'C3D8.' In this example, an 8-node continuum element is restrained in the third degree of freedom, or the translation in direction 3. Typically, the number of nodes in an element is clearly identified in the name, such as the ‘8’ for 8-node in the previous example. An element’s formulation describes the mathematical theory defining the element’s behavior. Unless specified with an ‘H’ at the end of the element name, the element is assumed to use the standard element family formulation. Abaqus/CAE uses numerical techniques to integrate quantities over the element. Gaussian quadrature is used for most elements, where the material response is evaluated at each integration point. Some elements can use reduced integration and are signified by using an ‘R’ at the end of the element name.

7.2.2 General-Purpose Shell Elements

Analytical research performed on PBFTGs (Michaelson, 2014; Kelly, 2014; Gibbs, 2017; Underwood, 2019; Roh, 2020) demonstrates the S4R element most accurately predicts the actual behavior of PBFTGs. The S4R element is a 4-node general purpose shell element utilizing reduced integration with hourglass controls and is suitable for a wide range of applications. While the S4R is robust enough to be used in thick and thin shelled problems, its use in this study is limited to thin shell behavior. Thin shell problems assume the transverse shear deformation may be neglected (Dassault Systèmes, 2020). Figure 7.1 demonstrates the difference between thin shells and thick shells where (a) illustrates material lines remain normal throughout deformation in thin wall elements and (b) illustrates material lines do not necessarily remain normal to the surface in thick wall elements. Kirchhoff shell theory is utilized in this study, that is, plane sections remain normal to the midsection and transverse shear strains are assumed to be zero.

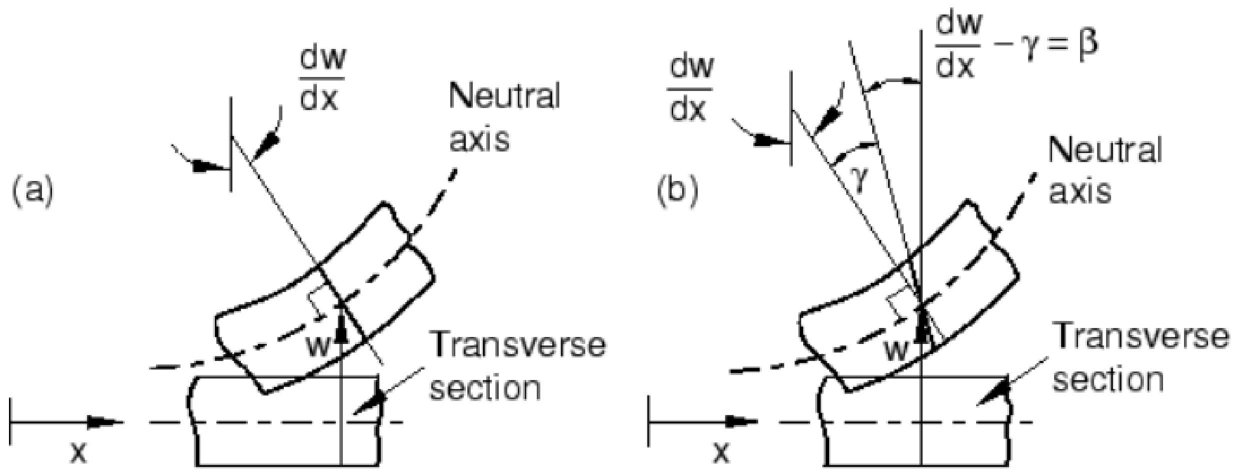

Figure 7.1: Behavior of Transverse Shell Sections in (a) Thin Shells and (b) Thick Shells (Dassault Systèmes, 2020)

S4R elements employ reduced integration where the elements use one fewer Gauss integration point in each direction, or a total of one in the case of 4-noded elements, to determine the element stiffness matrix. There are two main advantages of reduced integration over full integration. First, the strains and stresses are calculated at locations known to provide optimal accuracy. Second, the use of fewer integration points decreases the size of the model and associated computation time. However, the mass matrix and force matrix are still integrated exactly, even though the stiffness matrix is reduced. Displacements are then calculated at each node and linear interpolation is used to determine the displacements at other locations within the element using:

$$u = \sum f_i u_i \qquad \text{Eq. 7.1}$$

In which:

$$f_i = \frac{1}{4}(1 + \xi_0)(1 + \eta_0) \qquad \text{Eq. 7.2}$$

$$\xi_0 = \xi_i \xi \qquad \text{Eq. 7.3}$$

$$\eta_0 = \eta_i \eta \qquad \text{Eq. 7.4}$$

Where:

u_i = displacement at node i

f_i = shape function at node i

ξ_0 = local coordinate shape factor variable

η_0 = local coordinate shape factor variable

ξ_i = nodal local coordinate as specified in Figure 7.2

η_i = nodal local coordinate as specified in Figure 7.2

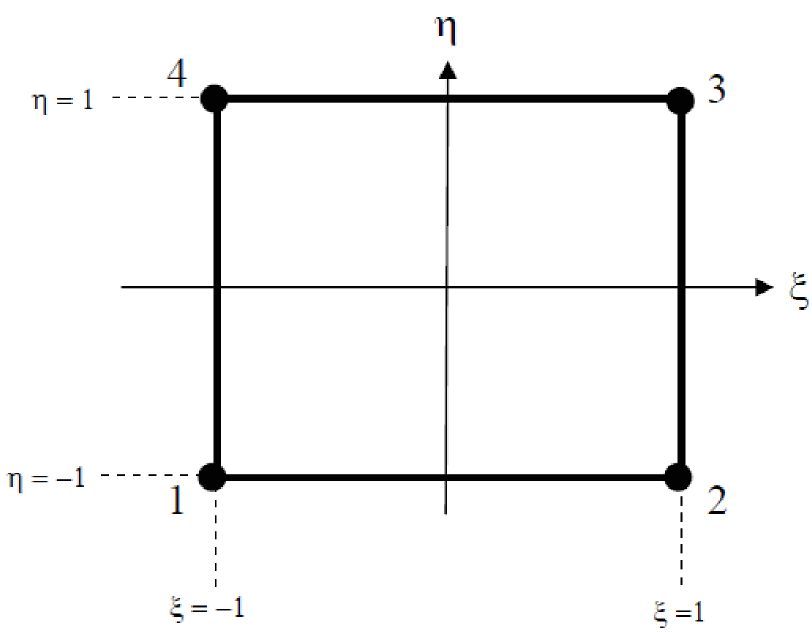

Figure 7.2: Element Natural Coordinate System (Dassault Systèmes, 2020)

The main disadvantage of reduced integration is that deformation modes causing no strain at the integration points may be omitted. These zero-energy modes can propagate through the system causing inaccuracies in a phenomenon known as hourglassing. Hourglassing is an issue which can arise in FEA when the number of integration points is reduced where only the linearly varying part of the incremental displacement field is considered for strain calculation and the rest of the notal displacement field is neglected. Neglecting the effect of these other nodes can lead to mesh distortion. To prevent this problem, a small artificial stiffness associated with zero-energy deformation is added using the '*SECTION CONTROLS' command in the Abaqus input file.

7.2.3 General Purpose Continuum Elements

Through these research efforts, more accurate deck modeling was needed in nonlinear skewed scenarios. As the degree of skew increased, while using shell elements, the ultimate capacity of the system increased, but the model would terminate at a significantly lower corresponding deflection. The C3D8R element was found, as part of this research effort, to represent the behavior of the deck more accurately in skewed scenarios. The C3D8R element is an 8-node general purpose brick element utilizing reduced integration with hourglass controls suitable for complex nonlinear analysis involving contact, plasticity, and large deformations. Some of the shortcomings of this type of element including lack of stiffness in bending and less accurate results away from the integration point, or the middle of the element. This type of element is also prone to hourglassing, as discussed previously, so hourglass controls are also utilized in conjunction with this element.

7.3 MATERIAL MODELING

An elastic-plastic constitutive law, including strain hardening effects, is used in the single-girder modeling portion of this work. This constitutive law is used when the loading in the system approaches the ultimate capacity of the specimen. When the system is under service level loading, such as the bridge system modeling, the steel and concrete are expected to behave elastically.

7.3.1 Structural Steel

Structural steel was modeled using an elastic-plastic constitutive law including strain hardening effects. Specifically, the '*PLASTIC' command was used to model the post yield behavior of the steel used in the ultimate capacity determination. An elastic-plastic constitutive model featuring standard von Mises surfaces, an associated plastic flow rule, and isotropic flow hardening has been found suitable to represent rate dependent behavior of a metal subjected to a relatively monotonic loading where creep effects are non-critical (Barth, 1996; Yang, 2004; Righman, 2005; Michaelson 2014).

A multilinear stress-strain relationship developed by Galindez (2009) was used to develop the stress-strain relationship used in the steel material modeling. The linear approximation is derived from the equations listed in Table 7.1. As the PBFTGs used during the experimental testing are the same specimens Michaelson (2014) utilized in his research, the same structural material properties were used in these efforts (Table 7.2). In Figure 7.3, the engineering stress-strain model used in Roh's (2020) modeling efforts is presented. The engineering stress-strain model was then converted to the true stress-strain model required for input into Abaqus/CAE.

Table 7.1: Expressions for Computing Steel Stress-Strain Behavior (Galindez, 2009)

Point	Strain	Stress
1	$\varepsilon_1 = \frac{\sigma_y}{E}$	$\sigma_1 = \sigma_y$
2	$\varepsilon_2 = \varepsilon_{st}$	$\sigma_2 = \sigma_y$
3	$\varepsilon_3 = \frac{1}{10}(\varepsilon_u - \varepsilon_{st}) + \varepsilon_{st}$	$\sigma_3 = \frac{E_{st}}{10}(\varepsilon_u - \varepsilon_{st}) + \sigma_y$
4	$\varepsilon_4 = \frac{2}{7}(\varepsilon_6 - \varepsilon_3) + \varepsilon_3$	$\sigma_4 = \frac{4}{7}(\sigma_6 - \sigma_3) + \sigma_3$
5	$\varepsilon_5 = \frac{2}{7}(\varepsilon_6 - \varepsilon_3) + \varepsilon_4$	$\sigma_5 = \frac{2}{7}(\sigma_6 - \sigma_3) + \sigma_4$
6	$\varepsilon_6 = \varepsilon_u - \frac{1}{10}(\varepsilon_u - \varepsilon_{st})$	$\sigma_6 = \left(\frac{\sigma_y}{\sigma_{0.2\%}}\right)\sigma_u - \frac{100}{E_{st}}(\varepsilon_u - \varepsilon_{st})$
7	$\varepsilon_7 = \varepsilon_u$	$\sigma_7 = \left(\frac{\sigma_y}{\sigma_{0.2\%}}\right)\sigma_u$

Table 7.2: Average Steel Plate Properties (Michaelson, 2014)

Property	Average Value
Modulus of Elasticity, E (ksi)	29559
Static Yield Stress, σ_y (ksi)	60.962
Offset Yield Stress, $\sigma_{0.2\%}$ (ksi)	63.05
Strain at the Onset on Strain Hardening, ε_{st} (%)	1.7883
Strain Hardening Modulus, E_{st} (ksi)	1033.5
Tensile Stress, σ_u (ksi)	84.382
Strain at the Tensile Stress, ε_u (%)	13.165

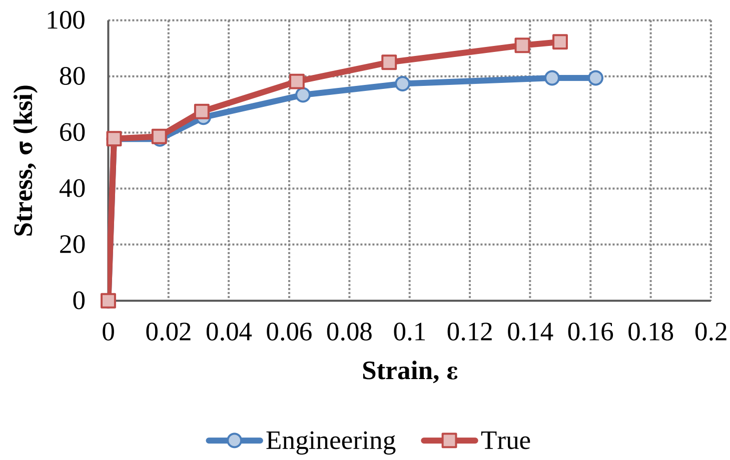

Figure 7.3: Multi-Linear Stress-Strain Curve (Roh, 2020)

7.3.2 Reinforced Concrete

A damaged plasticity concrete model is used in this study to model reinforced concrete elements. The damaged plasticity model provides the capability to model concrete and other quasi-brittle materials. While this model can be used for plain concrete, it is primarily intended for the analysis of reinforced concrete structures. The damaged plasticity model uses isotropic damaged plasticity concepts in combination with isotropic tensile and compressive plasticity to represent the inelastic behavior of concrete (Dassault Systèmes, 2020). Specifically, the concrete in the composite deck of the PBFTG specimens and link slabs is modeled using the '*CONCRETE COMPRESSION HARDENING' and '*CONCRETE TENSION STIFFENING' commands in the Abaqus input file. The '*CONCRETE COMPRESSION HARDENING' option defines the compression damage properties, and the '*CONCRETE TENSION STIFFENING' option defines the cracking and post cracking properties of the concrete damaged plasticity material model. Note, when using these options, once a crack appears in the model, it remains for rest of the calculation.

The concrete material model used in this study, when considering nonlinearity in its response, assumes the uniaxial tensile and compressive response is characterized by damaged plasticity (Figures 7.4 and 7.5). Figure 7.4 shows the compressive model of concrete with a compressive strength of 4 ksi and a modulus of elasticity of 3,640 ksi. Figure 7.5 shows the tensile model of concrete with a rupture strength of 0.522 ksi. Tension stiffening is utilized in the damaged plasticity model to approximate the reinforcement interaction with concrete in a simple manner.

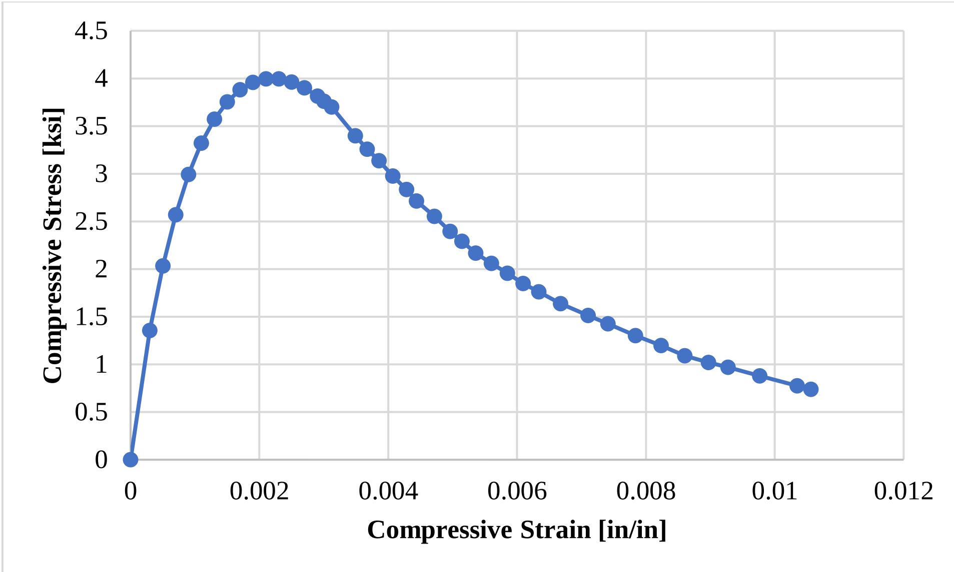

Figure 7.4: Stress-Strain Curve for Reinforced Concrete (Compressive Region)

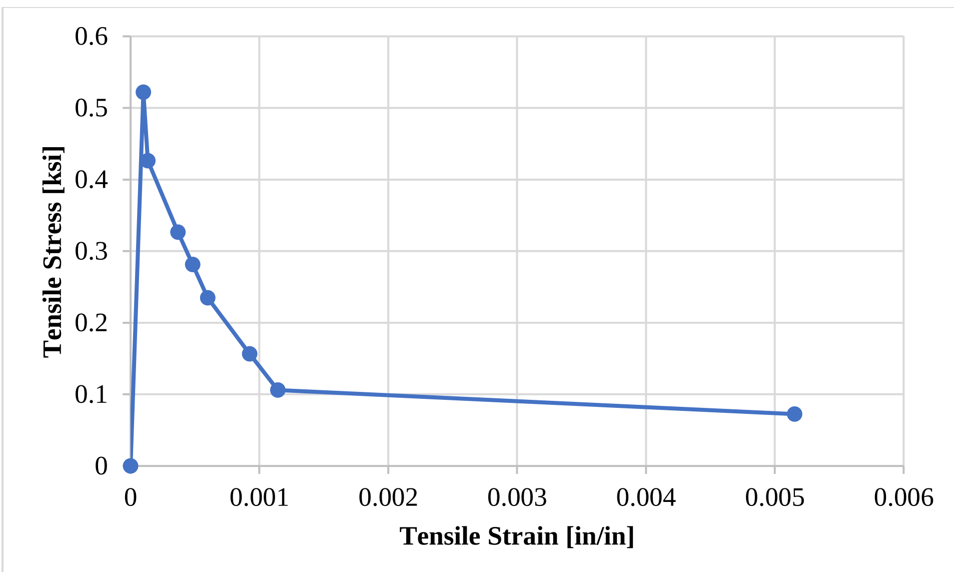

Figure 7.5: Stress-Strain Curve for Reinforce Concrete (Tension Region)

The modeling of concrete elements included considerations for the steel reinforcement within the deck. Specifically, the reinforcement is considered using the '*REBAR' option in the Abaqus input file and represents a smeared layer of reinforcement at user specified locations within the concrete deck. The material model for the steel reinforcement is similar to the model used for structural steel, with the following differences: a modulus of elasticity of 29,000 ksi, instead of 29,599 ksi, and a yield stress of 60 ksi, instead of 50 ksi.

7.4 Additional Modeling Considerations

Composite steel girders undergoing flexure predominately experience failure due to yielding of steel elements in tension or loss of stiffness of concrete components due to excessive compressive stress or cracking (Michaelson, 2014). In composite PBFTGs, the plastic neutral axis is in or near the top flange, and the top flange is continuously laterally supported by the concrete deck. However, in noncomposite steel girders, these conditions are not true, and girders can be susceptible to lateral torsional buckling, local flange buckling, and/or local web buckling. Therefore, initial geometric imperfections and residual stresses can have an impact on the noncomposite behavior of steel flexural elements. While the focus of these efforts is on composite behavior, attention must be paid to initial imperfections to ensure adequate modeling.

7.4.1 Geometric Imperfections

The nonlinear response due to initial imperfections present throughout the steel girder has a measurable impact on the girder's response to flexural loading and its susceptibility to buckling modes when the compression flange(s) are not restrained. A more refined response is necessary to model the effect of the imperfections than conventional bifurcation provides. Introducing geometric imperfections to the ideal cross-section ensures a degree of buckling occurs before the critical load in the ideal system is reached. Therefore, the introduction of these imperfections is a critical step in modeling the behavior of steel members.

In welded plate girders, initial geometric imperfections are typically generated during the welding process and/or occur due to initial plate out-of-flatness present in all plate steel. Three types of geometric imperfections are considered in these efforts to capture these characteristics: initial out of flatness of web panel(s), initial tilt of compression flange(s), and initial sweep of the compression flange(s). These imperfections are illustrated in Figure 7.6.

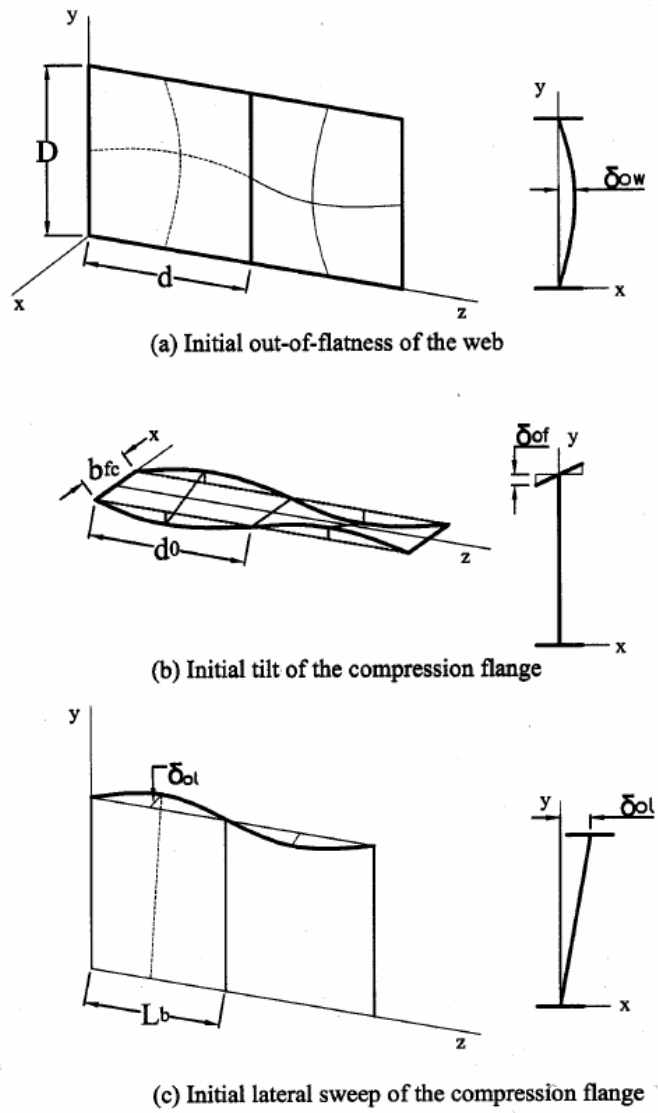

Figure 7.6: Initial Geometric Imperfections (Yang, 2004)

The values prescribed for these three types of imperfections are based on maximum allowable tolerances specified by the American Welding Society (AWS) and engineering judgement (Righman, 2005). AWS specifies a different tolerance for initial web out-of-flatness based on if the web is transversely stiffened. For girders with one-sided transverse stiffeners, the maximum allowable initial out-of-flatness of the web, δ_{ow}, as seen in Figure 7.6a, is to be taken as $d/67$, where d is the minimum panel dimension, either the depth of the web, D, or the distance between stiffeners, d_0. Alternatively, for girders without stiffeners, the maximum allowable initial out-of-flatness of the web is taken as $d/150$. In the analytical modeling performed for part of this doctoral research, the maximum allowable initial out-of-flatness of the web shall be taken as $d/100$, which represents a midpoint between the above requirements. This distortion is applied to the web as a sine wave in both the vertical and longitudinal directions of the web with maximum values located at the mid-height of the web and the midpoint between stiffeners. Furthermore, the longitudinal direction of distortion alternates between adjacent web panels.

AWS specifies the maximum allowable initial tilt of the compression flanges, δ_{of}, as seen in Figure 7.6b, is to be taken as the greater of 0.25 inches or $b_f/100$, where b_f is the flange width. However, while performing relevant verification studies, it is unlikely the distortion of the flanges would be this severe for the relatively short panel lengths utilized in these girders. In the analytical modeling performed for part of this doctoral research, the maximum allowable initial tilt of the compression flange is taken to be the lesser value of $b_{fc}/150$ or $0.3d_0/150 = d_0/500$. This results in values slightly smaller than those permitted by AWS for girders with long panel lengths (i.e., b_{fc} $<0.3d_0$), while resulting in values significantly smaller than permitted by AWS for short panel lengths. This distortion is applied linearly along the width of the flange with maximum distortion occurring at the flange edges and as a sine wave longitudinally along the flange. Furthermore, the longitudinal direction of distortion alternates between adjacent panels separated by stiffeners.

AWS specifies the maximum allowable sweep of the compression flange, δ_{oL}, as seen in Figure 7.6c, is to be taken as $L_b/960$, where L_b is the distance between lateral bracing. In the analytical modeling performed for part of this doctoral research, the allowable sweep of the compression flange is taken as $L_b/1500$, as specified by Yang (2004) and Righman (2005). This distortion is applied linearly along the vertical axis of the member starting at unity at the tension flange-web junction and reaching its maximum at the compression flange-web junction. This distortion is applied as a sine wave longitudinally along the girder. As with other imperfections, the longitudinal direction of the distortion alternates between panels separated by stiffeners. Note, the sweep of compression flange and the tilt of the compression flange should be prescribed in the same direction in each web panel to ensure the effects of these imperfections are cumulative.

7.4.2 Residual Stresses

The longitudinal residual stresses in welded plate girders are primarily caused by flame cutting the plates to the dimension required and welding between the flanges and the web. The tensile residual stresses are typically equal to the yield stress of the steel in a small area, termed the heat affect zone, while a smaller, near constant self-equilibrating compression stress is developed within the remainder of the plate. The residual stress pattern may be idealized by assuming that, when the section is free of external forces, the residual stresses over the cross-section must satisfy equilibrium.

In these efforts, residual stresses are modeled by specifying initial stress conditions prior to applying external loads. The magnitude and direction of initial residual stresses are applied depending on the location of the element. For verification studies relating to plate girders, Figure 7.7 demonstrates the residual stress pattern used. When initial stresses are provided, the initial stress state may not be in exact equilibrium for the finite element matrix. Therefore, an initial step, prior to loading, must be provided to allow Abaqus/CAE to achieve equilibrium. Specifically, the dead load is applied using the '*STATIC' option before exterior loading, ensuring equilibrium is achieved once residual stresses have been included.

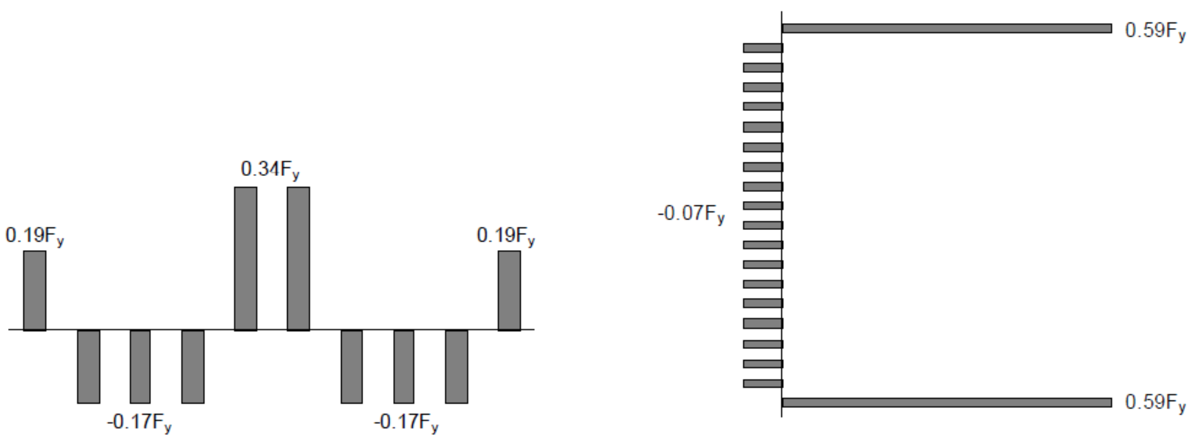

(a) Residual Stress Pattern for Flanges (b) Residual Stress Pattern for Webs

Figure 7.7: Residual Stress Pattern (Righman, 2005)

7.5 Solution Algorithm

To capture the behavior of specimens post-yielding and post-buckling, an unstable collapse and post-buckling analysis procedure were needed in these studies, specifically for the ultimate capacity determinations. A modified Riks algorithm available in Abaqus/CAE was chosen to be used in these studies, as it is one of the most versatile and efficient methods capable of obtaining a complete nonlinear solution (Figure 7.8). The Riks method was initially developed by Riks (1979) and improved by several researchers, such as Crisfield (1983), Ramm (1981), and Powell and Simons (1981). The modified Riks method allows for the ability to pass the elastic limit point and trace the unloading portion of the nonlinear equilibrium path, allowing for the solution to be obtained regardless of whether the response is stable or unstable. In addition, this method provides efficient usage of computational resources during the nonlinear solution process.

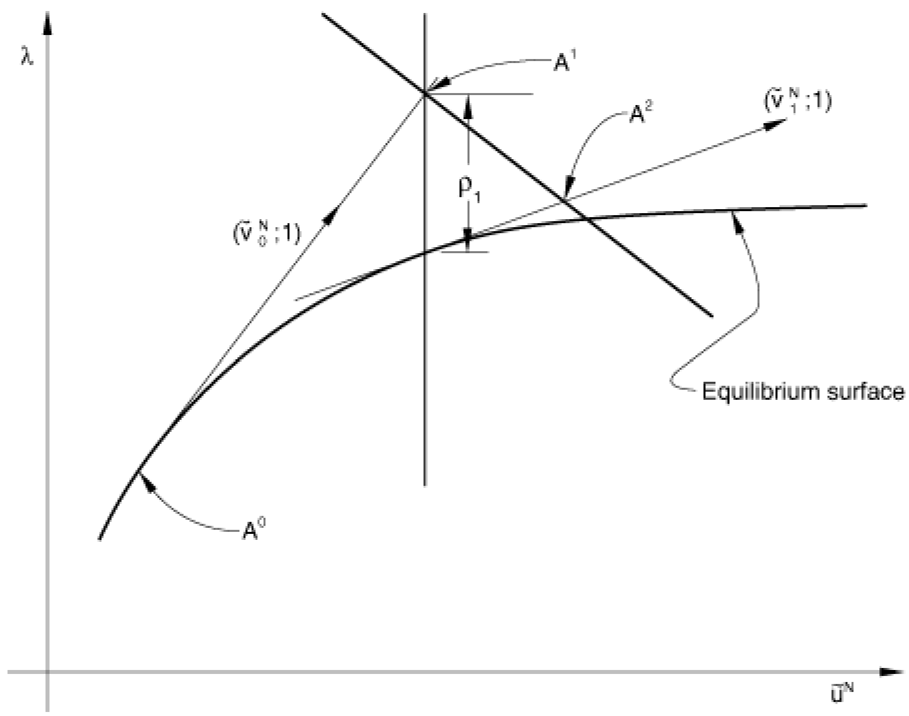

Figure 7.8: Modified Riks Algorithm (Dassault Systèmes, 2020)

The modified Riks method uses the magnitude of the load as an additional unknown and solves simultaneously for loads and displacements assuming the loading is proportional, i.e., load magnitudes vary with a single scalar parameter, and the response is reasonably smooth, i.e., sudden bifurcations do not occur. As solution progress is independent of the load increment, Abaqus/CAE uses the distance along the static equilibrium path in the load-displacement space, or arc length, to control the increment size. This value is initially set by the user and is later modified by Abaqus/CAE based on the convergence rate of the solution. Development of the solution requires traveling this path as far as required. The basic algorithm specifies a finite radius of convergence. The increment size is limited by moving a given distance along the line tangent to the previous solution and searching for equilibrium in the plane passing through the point obtained that is orthogonal to the same tangent line. In summary, the modified Riks method can be viewed as the discovery of a single equilibrium path defined by the space of displacements, rotations, and the loading parameter.

Another important change in the solution algorithm was the number of Gauss integration points through the depth of the concrete slab. This value was increased from 5 points (the default Abaqus/CAE value) to 7 points. A linear search technique was used by changing the load level during integration. These changes are well established and better capture the crushing and cracking of the concrete and improve the speed of convergence (Barth & Wu, 2006).

7.6 Boundary Conditions and Multiple-Point Constraints

Boundary conditions on all models in the studies presented herein represent 'hinge-roller' conditions, which limit vertical and longitudinal displacement. The girder(s) are restrained vertically at all nodes of the bottom flange at each support location. The girders(s) are restrained longitudinally at the center node of the bottom flange at one end of each girder. The girder(s) are restrained transversely at the center of one of the webs at each support location.

In the finite element modeling, the composite action between the reinforced concrete deck and the steel girder was ensured by using beam-type multi-point constraints (MPCs). These constraints provide a rigid beam between two nodes to constrain the displacement and rotation at the first node to the displacement and rotation at the second node, corresponding to the presence of a rigid beam between the two nodes (Dassault Systèmes, 2020). To create the MPC elements, the mesh of the concrete slab was generated to have nodes vertically above the nodes in the middle of the top flange. Specifically, the '*MPC' option was used to rigidly connect the nodes in the center of the top flange, at the web-flange conjunction, to the node directly above junction in the concrete deck.

An image of one of the finite element models in the sensitivity study described in Chapter 8 is shown in Figure 7.9. Figure 7.9 displays the boundary conditions in orange and the mesh discretization. For the purpose of clarity, the MPC labels have been removed from the display, but connections can be seen between the concrete deck and the top flanges of the PBFTGs.

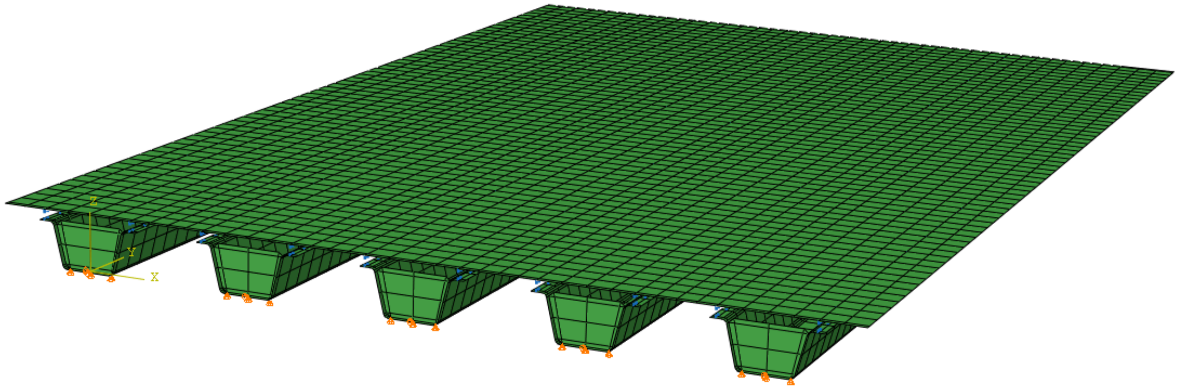

Figure 7.9: Abaqus/CAE Screen Capture of a Sensitivity Bridge Model

7.7 Application of Load

Once the PBFTGs were modeled in Abaqus/CAE, the models were loaded with the AASHTO LRFD BDS design truck, as discussed in Section 6.2.1, to determine the behavior of the single girder or bridge system. This section will provide a description of the methodology behind the truck placement on the bridge models and the methodology of applying either the concentrated truck loads to the bridges or the distributed load to the single girder system.

7.7.1 Placement of the AASHTO LRFD BDS Truck Loading

As part of these research efforts, a simple live load generator encompassing the Design Truck and Design Tandem, as described in the AASHTO LRFD BDS Article 3.6.1.2, for simple span bridges was developed. The design vehicular loading is placed on bridges to produce the maximum force effect to be investigated. However, the AASHTO LRFD BDS outline specific rules regarding the placement of live loads on bridges. These rules, as they relate to simple span bridges can be summarized as follows:

- AASHTO LRFD BDS Article 3.6.1.1.1
    - Unless specified otherwise, the width of the design lanes should be taken as 12 feet. The number of design lanes is determined by taking the integer part of the ratio *w*/12, where *w* is the clear roadway width in feet between curbs, barriers, or both.

    - Roadway widths from 20 to 24 feet shall have two design lanes, each equal to one-half the roadway width.
- AASHTO LRFD BDS Article 3.6.1.3.1
    - Both the design lanes and the 10 foot loaded width in each lane shall be positioned to produce extreme force effects.
    - The design truck or tandem shall be positioned transversely, such that the center of any wheel load is no closer than 2 feet from the edge of the design lane.

For exterior girders, the vehicular live loads were placed laterally, as close to the edge of the bridge as possible. For one-lane-loaded scenarios, this meant placing the design vehicular live load 2 feet from the edge of the barrier. For two-lanes-loaded scenarios, if a second design lane was available, the 10 foot loaded width was placed as close to the exterior girder as possible, resulting in a lateral spacing between wheel lines of adjacent vehicular live loads of 6 feet. For interior girders, a wheel line of the vehicular live load was placed over the girder being analyzed, or as close as possible given the aforementioned rules. For two-lanes-loaded scenarios, the placement of the 10 foot loaded portion within the 12 foot design lane resulted in a lateral spacing between wheel lines of adjacent vehicular live loads between 4 and 6 feet.

Kassimalli (2015) specifies the longitudinal placement of the design vehicular live load as:

> In a simply supported beam subjected to a series of moving concentrated loads, the maximum bending moment develops under a load when the midspan of the beam is located halfway between the load and the resultant of all loads on the beam.

7.7.2 Finite Element Model Loading

Once the loading location was determined, the point loads were linearly distributed to the neighboring nodes. A schematic of this loading is shown in Figure 7.10, and Equations 7.1 through 7.4 describe the loading. According to AASHTO LRFD BDS Article 4.6.3.3.1, nodal loads shall be statically equivalent to the actual loads being applied. It can be shown the equations corresponding to Figure 7.10, once summed, will equal the applied point load.

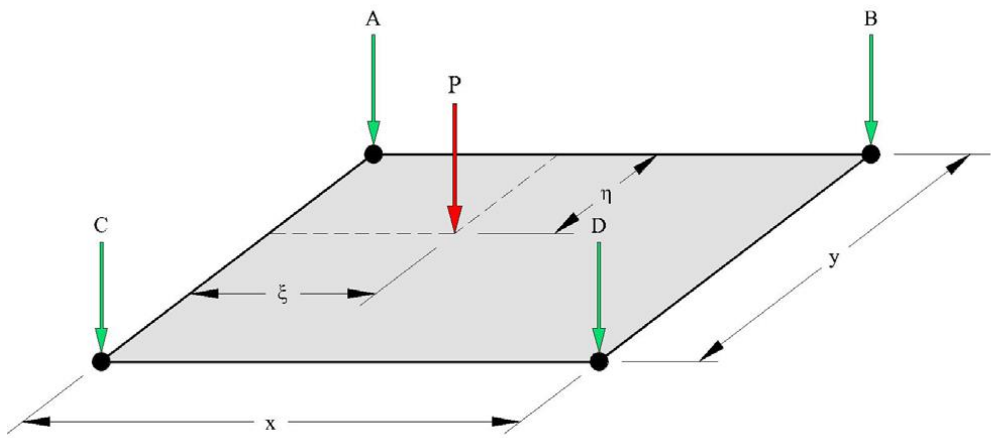

Figure 7.10: Schematic of Nodal Distribution of Point Loads

$$A = P\left(1 - \frac{\xi}{x}\right)\left(1 - \frac{\eta}{y}\right) \quad \text{Eq. 7.1}$$

$$B = P\left(\frac{\xi}{x}\right)\left(1 - \frac{\eta}{y}\right) \quad \text{Eq. 7.2}$$

$$C = P\left(1 - \frac{\xi}{x}\right)\left(\frac{\eta}{y}\right) \quad \text{Eq. 7.3}$$

$$D = P\left(\frac{\xi}{x}\right)\left(\frac{\eta}{y}\right) \quad \text{Eq. 7.4}$$

7.8 Verification of Finite Element Modeling

To assess the validity and accuracy of these modeling techniques, experimental data from previous laboratory experiments were employed as benchmarks. Discussed in this section are the laboratory and live load field tests used and the results from those experiments compared against the analytical results of these tools.

7.8.1 Benchmark Analysis #1: Schilling & Morcos (1988)

Schilling and Morcos (1988) performed experimental testing on three plate girders to determine moment-rotation curves for noncompact plate girders with improved rotation characteristics. These girders, denoted ‘S’ for shallow, ‘M’ for medium depth, and ‘D’ for deep, were tested in three-point bending with simply supported conditions at the ends and a concentrated load at midspan, approximating the negative moment region over the pier in continuous-span bridges. Specimen D was chosen for verification purposes as the web slenderness value is more representative of the web slenderness found in PBFTGs. Figure 7.11 shows the plate dimensions and locations of two-sided bearing stiffeners and one-sided transverse stiffeners.

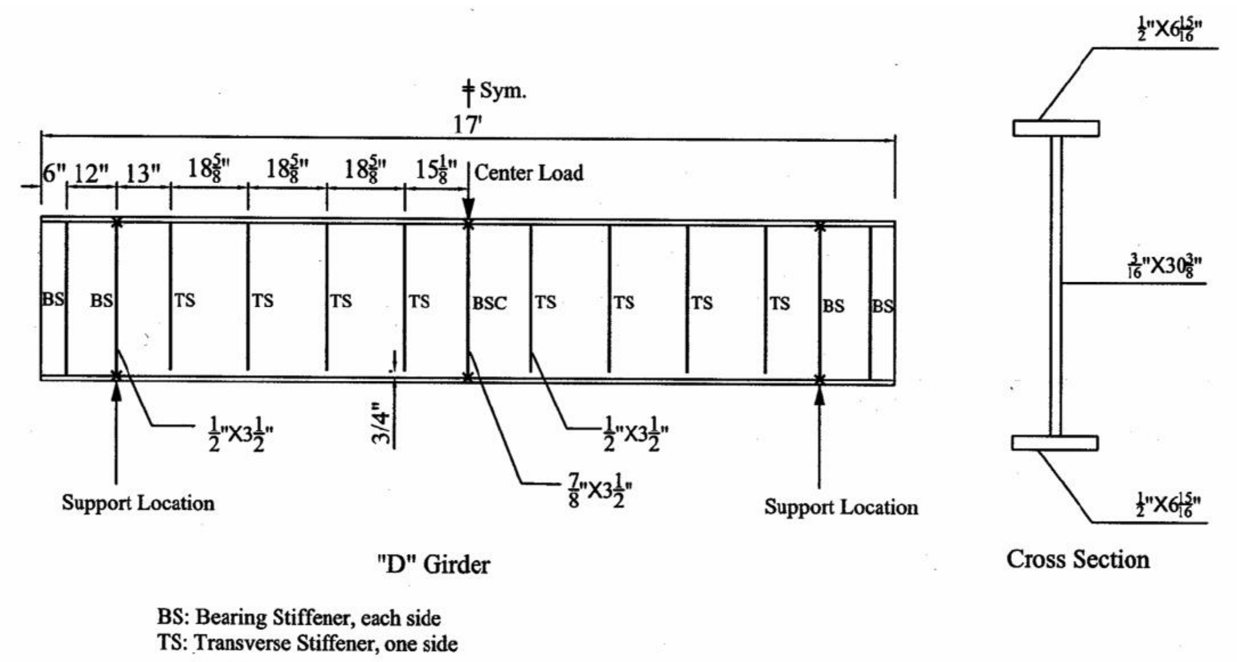

Figure 7.11: Specimen D Dimensions (Schilling & Morcos, 1988)

The appropriate mesh density was found to be crucial as relatively large elements will result in unrealistically low predicted strengths due to stress concentration effects, while relatively small elements will result in an overestimation of the energy dissipation capacity (Righman, 2005). Yang (2004) evaluated the ideal mesh density of the plate girders represented in this study. Coarser meshes of the steel, such as four elements across the width of the flanges and six elements in the depth of the web, overestimate the strength of the girder, while finer meshes, such as ten elements across the width of the flanges and twenty elements in the depth of the web, can yield results with differences of 0.3%. Thus, this finer mesh density was chosen for this verification.

The shape of longitudinal elements was made as close to square as possible. With the mesh density of the cross-section discussed above, it is not possible to achieve perfectly square longitudinal elements for both the web and the flanges. It is prudent to have the longitudinal elements in both the web and flanges to have the same longitudinal length so these elements can share coincident nodes at the web-flange junction. To overcome this shortcoming, an approximate longitudinal element length is provided to minimize the aspect ratio for all elements. This aspect ratio was found to be approximately 1.4 for all elements.

An input file was generated using the aforementioned modeling techniques to model Specimen D, and FEA was performed using Abaqus/CAE. The load-deflection curve from experimental testing was plotted against the analytical modeling (Figure 7.12). As shown, the modeling techniques described previously capture the nonlinear behavior of this experimental test.

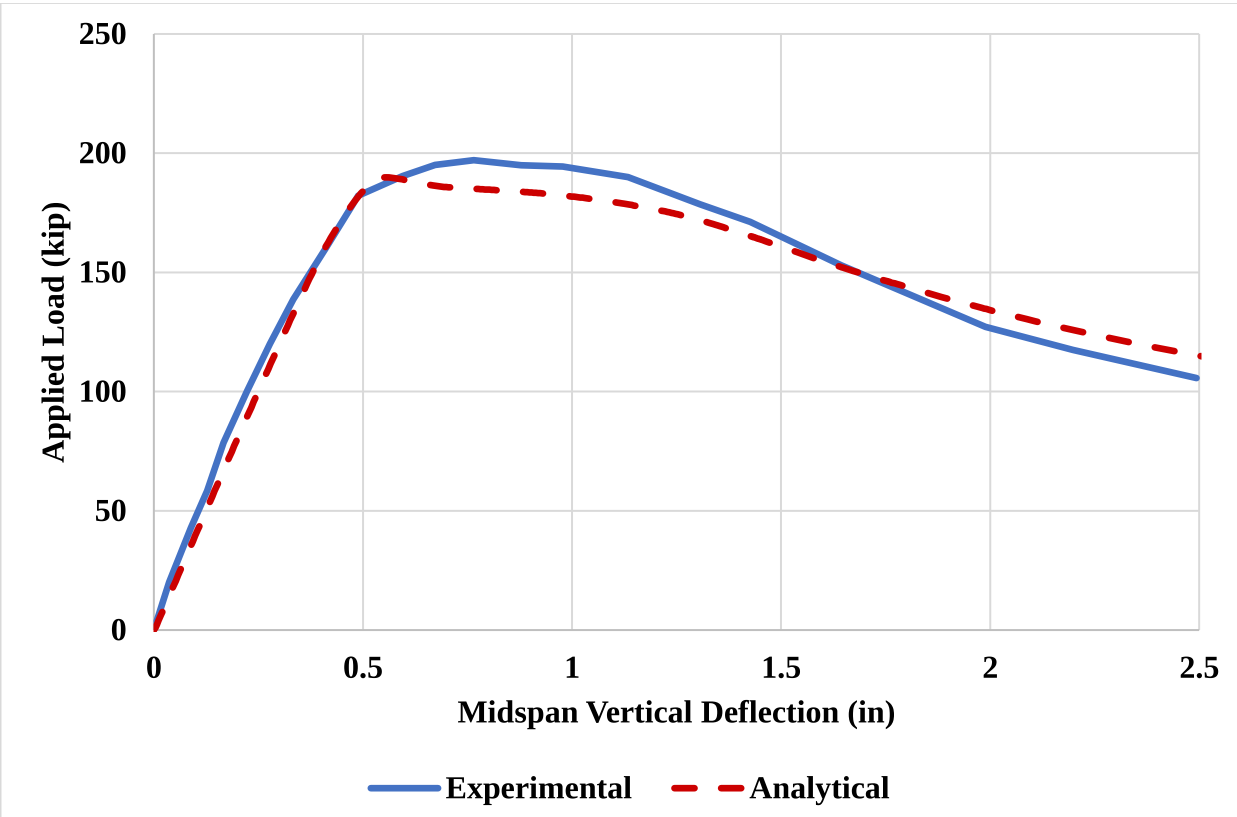

Figure 7.12: Comparison of the Schilling and Morcos (1988) Specimen D Experimental and Analytical Results

7.8.2 Benchmark Analysis #2: Lay et al. (1964)

Lay et al. (1964) performed experimental testing on multiple steel elements to obtain rational plastic design procedures for high strength steels. Part of the testing program included calculation of the full plastic moment where beams were subjected to concentrated loads at the ends of the members and supported at third points. The 'HT-29' test was chosen for a benchmark to model nonlinear material modeling and geometric imperfections as Lay et al. (1964) presented this test as the sample of all beam tests performed as part of their research. Figure 7.13 details the experimental test setup of the 'HT-29' test.

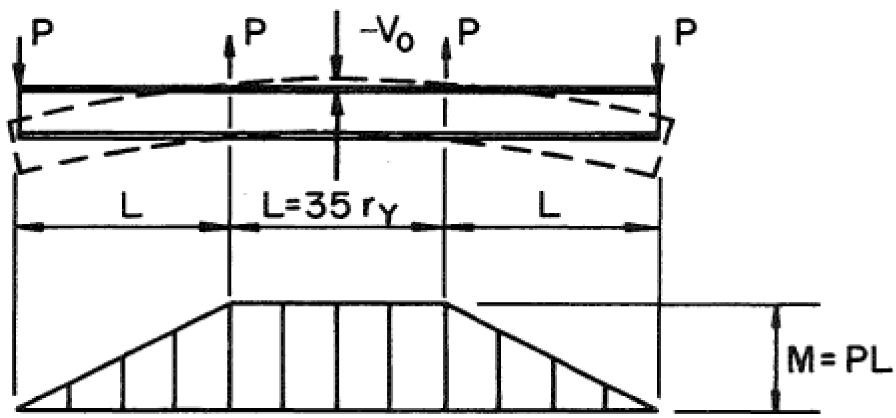

Figure 7.13: 'HT-29' Test Schematic (Lay et al., 1964)

An input file was generated using the aforementioned modeling techniques, including the target mesh density discussed in Section 7.6, to model the 'HT-29' test, and FEA was performed using Abaqus/CAE. The load-deflection curve from experimental testing was plotted against the analytical modeling (Figure 7.14). As shown, the modeling techniques described previously capture the nonlinear behavior of this experimental test.

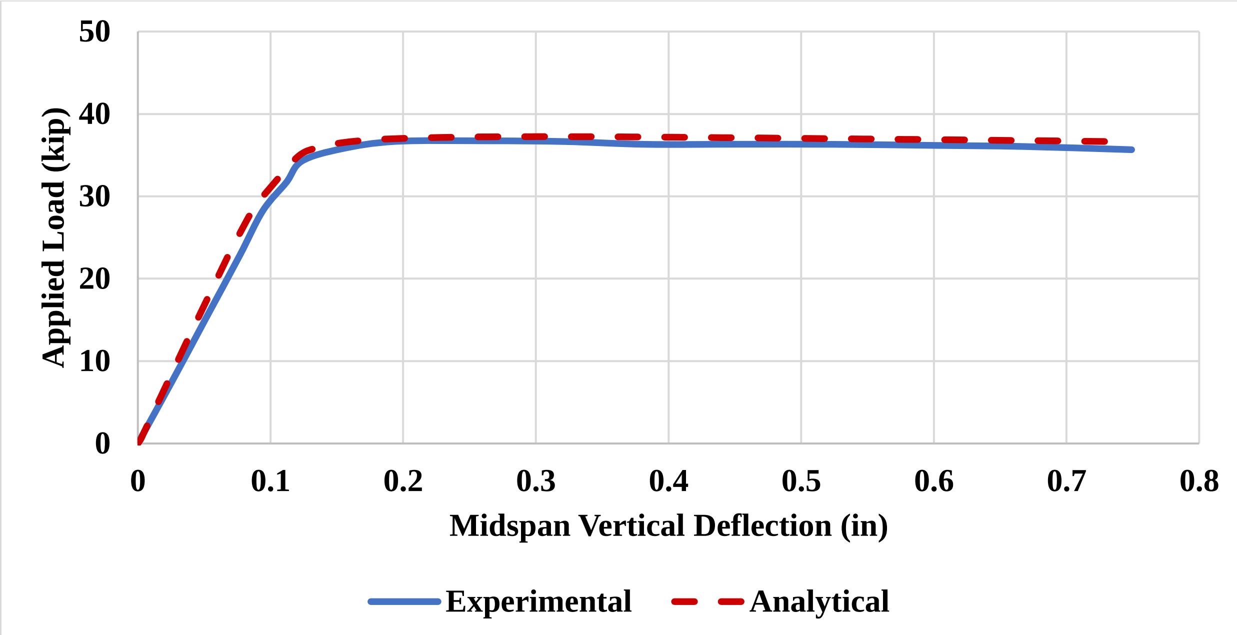

Figure 7.14: Comparison of the Lay et al. (1964) 'HT-29' Experimental and Analytical Results

7.8.3 Benchmark Analysis #3: Roberts (2005)

Roberts (2004) performed experimental testing on three composite girders to develop a more complete understanding of the ductility of composite positive bending sections and develop a less conservative ultimate strength equation for compact composite sections in positive bending. 'Specimen R1,' which will be used in this verification study, consisted of a W24x55 A572 Grade 50 rolled shape with a 42 inch wide by 7 inch thick reinforced concrete deck. The concrete deck had two layers of reinforcement, and full composite action was developed using 7/8 inch diameter head shear studs spaced 9 inches along the length of the girder. Figure 7.15 details the experimental test setup of the Specimen R1 test.

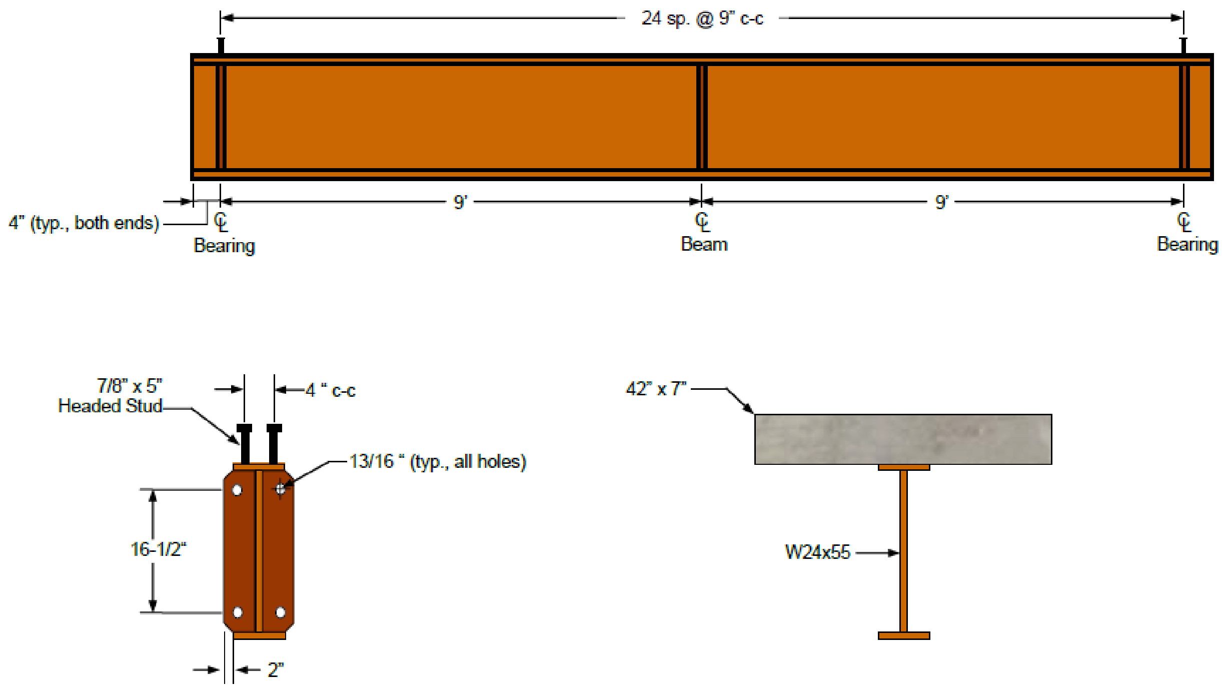

Figure 7.15: Geometry of Specimen R1 (Roberts, 2005)

An input file was generated using the aforementioned modeling techniques, including the target mesh density discussed in Section 7.6, to model the Specimen R1 test, and FEA was performed using Abaqus/CAE. The load-deflection curve from experimental testing was plotted against the analytical modeling performed by Roberts (2005) and the analytical modeling performed in these studies (Figure 7.16). As shown, the modeling techniques described previously capture the nonlinear behavior of this experimental test and match the modeling techniques adopted from Roberts (2005).

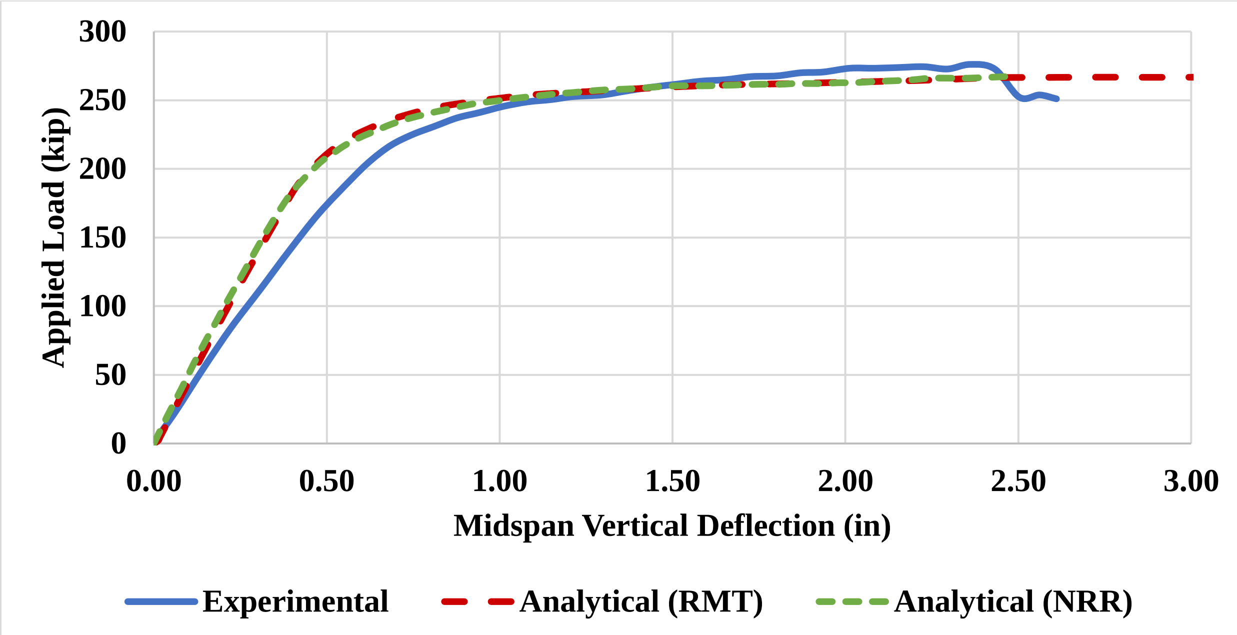

Figure 7.16: Comparison of the Roberts (2005) 'R1' Experimental and Analytical Results

7.8.4 Benchmark Analysis #4: Michaelson (2014)

As described in Section 2.3.1, Michaelson (2014) performed experimental testing on PBFTGs to develop and refine the system for use in the short-span bridge market. An 84 inch wide by 7/16 inch thick plate was formed into a PBFTG, and a 60 inch wide by 6 inch thick reinforced concrete deck was compositely cast, creating a modular unit. Destructive flexural testing was performed on the composite specimen, and analytical procedures were developed to verify the capacity of the proposed system. Figures 7.17 and 7.18 show the cross-section of a PBFTG without and with the concrete deck, respectively.

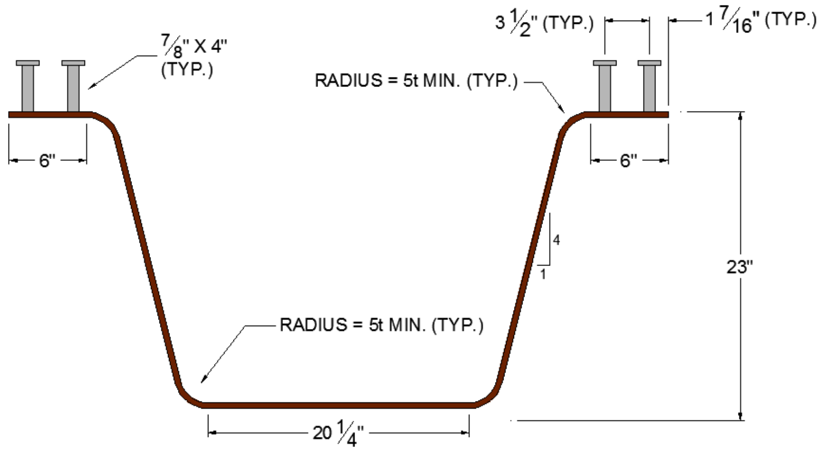

Figure 7.17: Testing Specimen Dimensions (Michaelson, 2014)

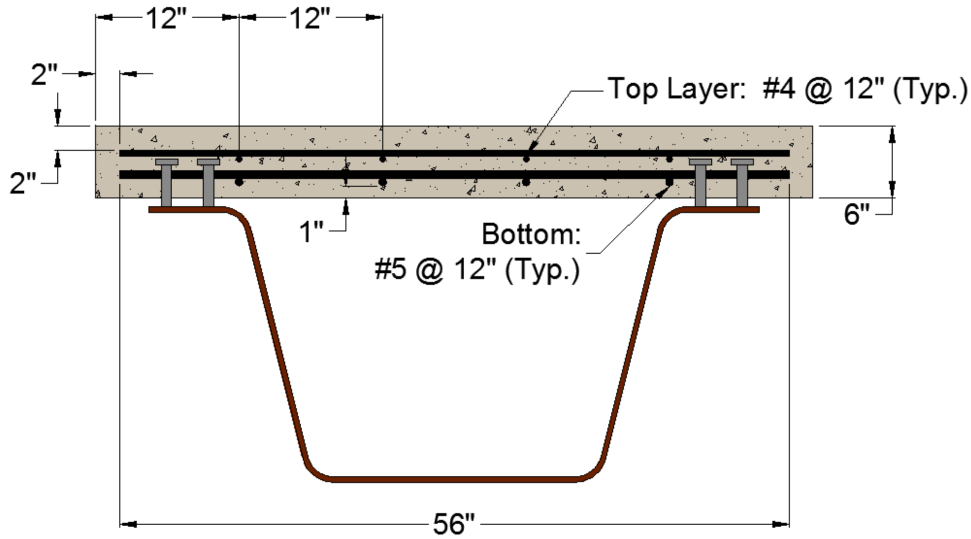

Figure 7.18: Deck Reinforcement for Composite Sections (Michaelson, 2014)

An input file was generated using the aforementioned modeling techniques, including the target mesh density and the use of multi-point constraints discussed in Section 7.6, to model the composite experiments performed by Michaelson (2014), and FEA was performed using Abaqus/CAE. The load-deflection curve from experimental testing was plotted against the analytical modeling performed by Michaelson (2014) and the analytical modeling performed in these studies (Figure 7.19). As shown, the modeling techniques described previously capture the behavior of non-skewed PBFTGs.

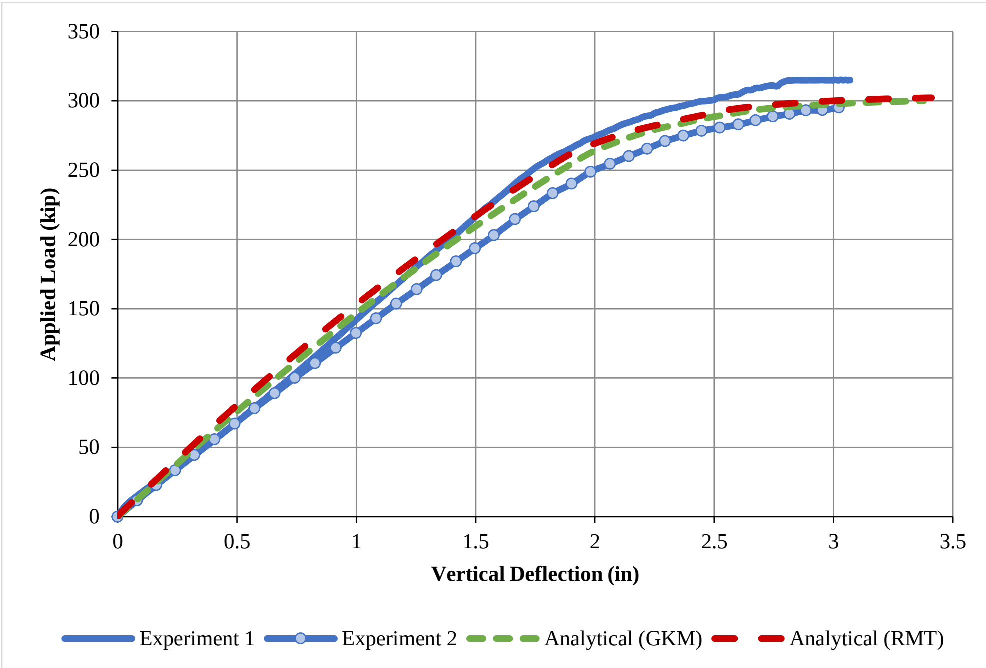

Figure 7.19: Comparison of the Michaelson (2014) Composite Experimental and Analytical Results

7.8.5 Benchmark Analyses #5: Amish Sawmill Bridge

To verify the validity of the finite element modeling techniques regarding bridge systems, physical load data from three field tests were compared to the analytical results of finite element models of the bridges using the modeling techniques described previously. As described in Section 2.4.1, Gibbs (2017) performed a live load field test on the Amish Sawmill Bridge in Buchanan County, Iowa. The bridge consisted of four PBFTGs fabricated from 96 inch wide by 1/2 inch thick plate with a girder spacing of 7.5 feet, as seen in Figure 7.20. A loading truck was placed at points, both transversely and longitudinally, along the bridge, and strains were recorded.

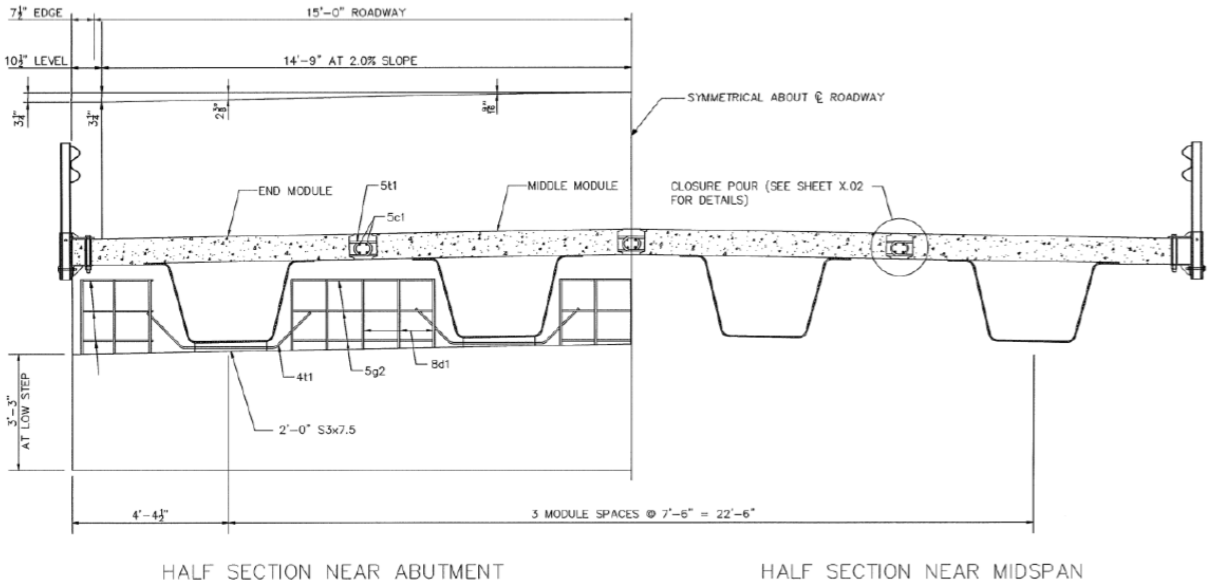

Figure 7.20: Cross-section of the Amish Sawmill Bridge (Gibbs, 2017)

An input file was generated using the modeling techniques described previously, except for the nonlinear analysis. As the loading of bridge was representative of actual vehicular traffic, the magnitude of the loading would never approach the loading and material nonlinearity seen in the previous laboratory experiments. A comparison of the field recorded data and the analytical modeling to verify the accuracy of the modeling techniques of this study is shown in Table 7.3. Specifically, from the field test, the truck run maximizing the load in the first interior girder is shown. The strains, and therefore LLDFs, of Girder 2 at midspan were reported as these values directly compared with the field test data. As shown, the analytical model very accurately predicted LLDFs. The largest absolute difference in values was only 0.024, equivalent to 8.86% difference.

Table 7.3: Amish Sawmill Bridge Analytical Model Verification

Girder 2, Truck Run 2, LLDF Comparisons					
Longitudinal Truck Placement		Field Test LLDF	Analytical LLDF	Absolute Difference	Absolute Percent
x (ft)	x/L				
0	0	---	---	---	---
5.2	0.1	0.282	0.299	0.017	5.88%
10.4	0.2	0.312	0.303	0.009	3.02%
15.6	0.3	0.300	0.303	0.003	1.06%
20.8	0.4	0.302	0.306	0.004	1.24%
26	0.5	0.332	0.312	0.020	5.99%
31.2	0.6	0.328	0.314	0.014	4.24%
36.4	0.7	0.303	0.309	0.006	1.89%
41.6	0.8	0.275	0.299	0.024	8.65%
46.8	0.9	0.269	0.293	0.024	8.86%
52	1	---	---	---	---
Average		**0.300**	**0.304**	**0.013**	**4.54%**
Maximum (in magnitude)		**0.332**	**0.314**	**0.024**	**8.86%**
Minimum (in magnitude)		**0.269**	**0.293**	**0.003**	**1.06%**

7.8.6 Benchmark Analyses #6: Fourteen Mile Bridge

As discussed in Section 2.4.3, Roh (2020) performed a live load field test on the Fourteen Mile Bridge in Lincoln County, West Virginia. The bridge consisted of five PBFTGs fabricated from 96 inch wide by 1/2 inch thick plate with a girder spacing of 7 feet and a span length of 58 feet. This bridge has unique characteristics, such as a skew of 10° and a superelevation of 8%, as seen in Figure 7.21. The loading truck, while chosen to model the HL-93 Design Load, did not exactly match, so axle weights and dimensions were recorded for use in the field test and the analytical model. The Stallings/Yoo Method was chosen to calculate the distribution factors in the analytical model, as this methodology was used in the live load field test.

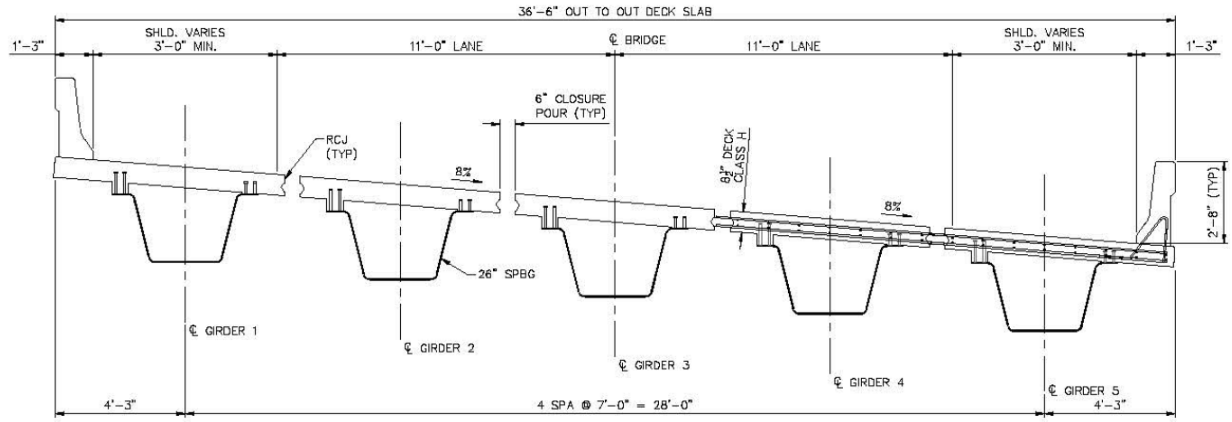

Figure 7.21: Cross-section of the Fourteen Mile Bridge (Roh, 2020)

Following a methodology identical to that used for the Amish Sawmill bridge, an input file was generated and analyzed using Abaqus/CAE. The results were exported, and post-processing was completed to determine LLDFs for an exterior, the first interior girder, and the center girder. A comparison of the field recorded data and the analytical data is shown in Table 7.4. Specifically, from the field test, the truck run maximizing the load in an exterior girder is shown. The strains, and therefore LLDFs, of Girder 1 at quarter span were reported as these values directly compared with the field test data. As the values were recorded at quarter span, instead of midspan, where the strains produced by the loading vehicle would be the highest, smaller strains were recorded. It should be noted that, while percent differences have been reported, they can be somewhat deceptive as differences of a fraction can represent somewhat large percentage differences. When comparing LLDFs computed at midspan, the analytical model only overestimates by 0.046 on a bridge with significant layout complications. This slight overestimation is within the allowable error discussed in AASHTO LRFD BDS Article C4.6.2.2.1.

Table 7.4: Fourteen Mile Bridge Analytical Model Verification

Girder 1, Truck Run 1, LLDF Comparisons					
Longitudinal Truck Placement		Field Test LLDF	Analytical LLDF	Absolute Difference	Absolute Percent
x (ft)	x/L				
0	0	---	---	---	---
5.8	0.1	---	---	---	---
11.6	0.2	0.456	0.347	0.109	23.91%
17.4	0.3	0.403	0.382	0.021	5.27%
23.2	0.4	0.406	0.427	0.021	5.28%
29	0.5	0.421	0.467	0.046	10.84%
34.8	0.6	0.420	0.491	0.071	16.81%
40.6	0.7	0.453	0.527	0.074	16.29%
46.4	0.8	0.499	0.578	0.079	15.89%
52.2	0.9	0.567	0.613	0.046	8.14%
58	1	---	---	---	---
Average		**0.453**	**0.479**	**0.058**	**12.80%**
Maximum (in magnitude)		**0.567**	**0.613**	**0.109**	**23.91%**
Minimum (in magnitude)		**0.403**	**0.347**	**0.021**	**5.27%**

7.8.7 Benchmark Analyses #7: Flat Run Bridge

A third live load field test was performed concurrently with these research efforts. The test was performed on the Flat Run Bridge in Marion County, West Virginia. The bridge consisted of four PBFTGs fabricated from 96 inch wide by 1/2 inch thick plate with a girder spacing of 8 feet and a span length of 56 feet. The Flat Run Bridge did not have any skew or superelevation, as seen in Figure 7.22. Similar to the Fourteen Mile Bridge live load field test, the loading truck was chosen to model the HL-93 Design Load, but as the axle weights and dimensions did not exactly match, the weights and dimensions were recorded for use in the field determined LLDFs and the analytical modeling. This difference in loading should correspond to similar LLDFs, as the actual truck was chosen to produce similar force effects. Additionally, the AASHTO LRFD BDS Design Truck is the loading used in the studies determining empirical LLDFs.

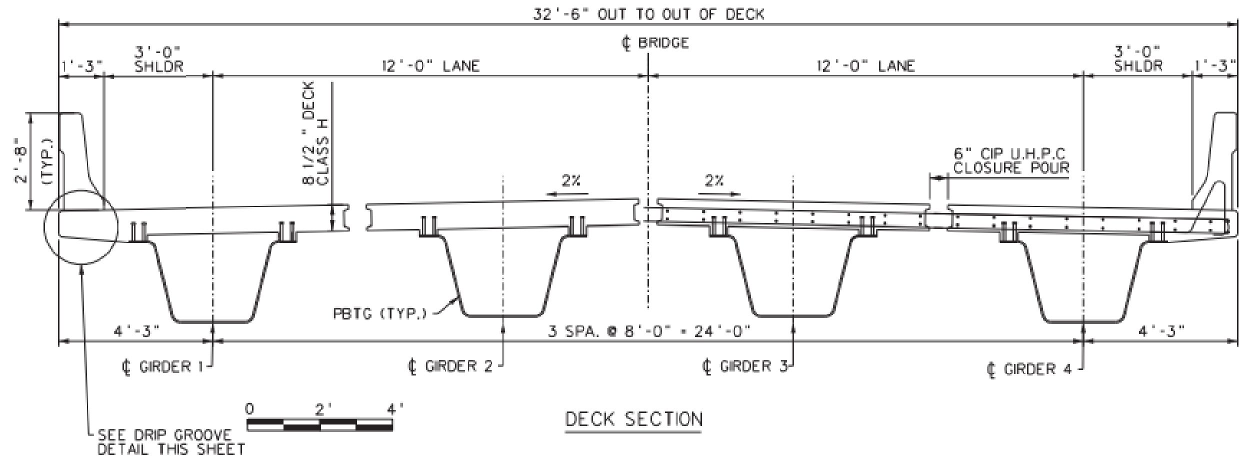

Figure 7.22: Cross-section of the Flat Run Bridge

A distinct difference for this analysis was the use of the Tarhini/Frederick method in addition to the Stallings/Yoo method of calculating LLDFs. The Stallings/Yoo calculation of LLDFs was performed as part of the field study, while the Tarhini/Frederick calculation of LLDFs was performed as part of this research. A comparison of the field recorded data and the analytical modeling maximizing load in Girder 1 with one lane loaded is shown in Table 7.5. As shown, the differences in both LLDF methodologies with the live load field test are negligible, verifying the validity of the analytical modeling techniques in determining LLDFs for PBFTG bridges.

Table 7.5: Flat Run Bridge Analytical Model Verification

	Field Calculated	Stallings/ Yoo	Tarhini/ Frederick	Field Calculated vs Stallings/Yoo		Field Calculated vs Tarhini/Frederick	
				Absolute Difference	Absolulte Percent	Absolute Difference	Absolulte Percent
Girder 1	0.51	0.47	0.53	0.04	7.84%	0.02	3.92%
Girder 2	0.37	0.34	0.36	0.03	8.11%	0.01	2.70%
Girder 3	0.2	0.23	0.19	0.03	15.00%	0.01	5.00%
Girder 4	0.12	0.16	0.13	0.04	33.33%	0.01	8.33%

7.9 SUMMARY

This chapter detailed an explanation of the analytical modeling techniques used for assessing PBFTGs. The accuracy of these models has been benchmarked against previous experimental investigations. The results of these benchmarks show the analytical tools accurately capture the behavior of noncomposite and composite plate girder testing and capture the behavior of non-skewed PBFTGs. This chapter has shown the extensive verification of the tools used in this research from the behavior of plates acting under point loads to behavior of PBFTGs past yielding of the steel to global behavior of PBFTGs in bridge system applications. These tools will be used in the following chapters to develop LLDFs utilizing PBFTGs and the ultimate capacity of compact PBFTGs.

CHAPTER 8: DEVELOPMENT OF LLDFS FOR PBFTG BRIDGES

8.1 INTRODUCTION

The following chapter presents the research performed to develop LLDFs for PBFTG bridges. First, a matrix of bridges was generated and analyzed using a commercial finite element software to determine the sensitivity of commonly used parameters in the distribution of live load to longitudinal elements. Next, a modified matrix was generated based on the assessment of the key parameters most affecting on the distribution of live load in PBFTG bridges. LLDFs generated from the parametric matrix of over 50,000 hypothetical PBFTG bridges were used to generate simplified equations to be used in conjunction with LGA. Finally, the simplified equations were verified against experimental and analytical results from three in-service PBFTG bridges.

8.2 SENSITIVITY STUDY

The following section describes a matrix of bridges analyzed using Abaqus/CAE to determine the sensitivity of certain parameters on the live load distribution characteristics in PBFTG bridges. Specifically, this section will discuss the bridges modeled with their respective constant and varied parameters. The results of the sensitivity study are discussed, highlighting the influence of the varied parameters and the comparisons between the analytically derived LLDFs and the empirical equations presented in the AASHTO LRFD BDS.

8.2.1 Typical Bridge Cross-Sections

A crucial component in the development of simplified methods for live load distribution is the range of applicability. To ensure common values of various parameters were considered, four common bridges were used as the basis for the matrix of bridges to be analyzed in the sensitivity study. The four standard bridges are described in Table 8.1, and a cross-section of a typical bridge is shown in Figure 8.1.

Table 8.1: Standard Bridge Dimensions

Bridge Number	Plate Size (in)	Span Length (ft)	Number of Girders	Girder Spacing (ft)	Deck Thickness (in)	Overhang Width (ft)
1	72 x 1/2	30	3	6	8	2.22
2	84 x 1/2	40	4	8	8	2.11
3	96 x 1/2	60	5	8	8	1.8
4	120 x 5/8	80	6	10	8	1.29

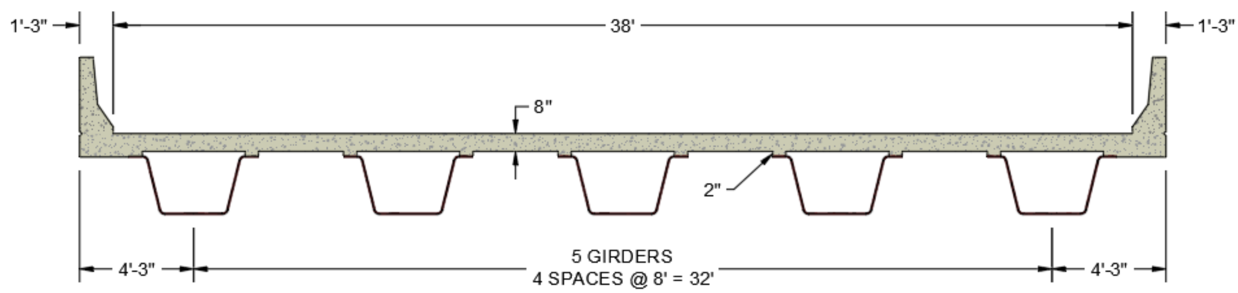

Figure 8.1: Sensitivity Bridge Cross-Section

8.2.2 Constant Parameters

The following parameters remained constant in the sensitivity matrix:

- The distance between the top of the top flange and the bottom of the deck was held at a constant 2 inches.
- The width of the barrier was held at a constant 15 inches.
- Normal weight reinforced concrete was used throughout. In accordance with AASHTO LRFD BDS Table 3.5.1-1, this equates to a unit weight of 0.150 kcf. Also, in accordance with the same table, the unit weight of steel was taken to be 0.490 kcf.
- The following material properties were also employed:
    - For reinforced concrete, which was taken to have a compressive strength of 4 ksi, according to the provisions of AASHTO LRFD BDS Section 5.4.2.4, the modulus of elasticity of concrete was determined to be 3,640 ksi. Also, according to AASHTO LRFD BDS Section 5.4.2.5, Poisson’s ratio was taken to be 0.2.

    - For steel, which was taken to have a yield strength of 50 ksi, according to the provisions of AASHTO LRFD BDS Section 6.4.1, the modulus of elasticity of steel was taken to be 29,000 ksi. Also, Poisson's ratio was taken to be 0.3.
- The boundary conditions were kept simply supported.
- Finally, the same style and thickness of bearing stiffeners were used for all girders.

8.2.3 Varied Parameters

The following parameters were varied in the sensitivity matrix and investigated to determine their respective effect on the live load distribution in PBFTG bridges:

- Thirteen possible span lengths: 20 feet to 80 feet in 5 feet increments
- Four possible number of girders in the cross-section: 3, 4, 5, and 6 girders
- Four possible individual PBFTG cross-sections consisting of different plate sizes: 72 inch by 0.5 inch, 84 inch by 0.5 inch, 96 inch by 0.5 inch, and 120 inch by 0.625 inch
- Seven possible girder spacings: 4 feet to 16 feet in 2 feet increments
- Seven possible deck thicknesses: 8 inches to 9.5 inches in 0.25 inch increments
- Five overhang ratios: 0.2 × Girder Spacing to 0.4 × Girder Spacing in 0.05 increments
- One or two-lanes loaded
- Load placement to maximize moment in an interior or exterior girder

8.3 RESULTS OF SENSITIVITY STUDY

As the tabulated results of the sensitivity study are too large to be included in this chapter, a comprehensive summary of the results has been provided in Appendix A. Appendix A summarizes the effect of each varied parameter in tabular and graphical form. The general trends of the sensitivity study results will be discussed herein, specifically the effect of the parameters on the distribution of live load in a multitude of loading scenarios.

8.3.1 Comparison with AASHTO LRFD BDS LLDFs

Generally, as shown in many previous studies, such as the ones discussed in Chapter 3, the LLDFs obtained from the analytical modeling were generally lower than those calculated using the methods found in the AASHTO LRFD BDS. A comparison between LLDFs calculated from the analytical model and LLDFs calculated using empirical methods from the AASHTO LRFD BDS is shown in Figure 8.2. It should be noted the AASHTO LRFD BDS I-Girder methodology is dependent on the lever rule methodology, and any restrictions for the use of LLDFs per the AASHTO LRFD BDS have been neglected to compare results.

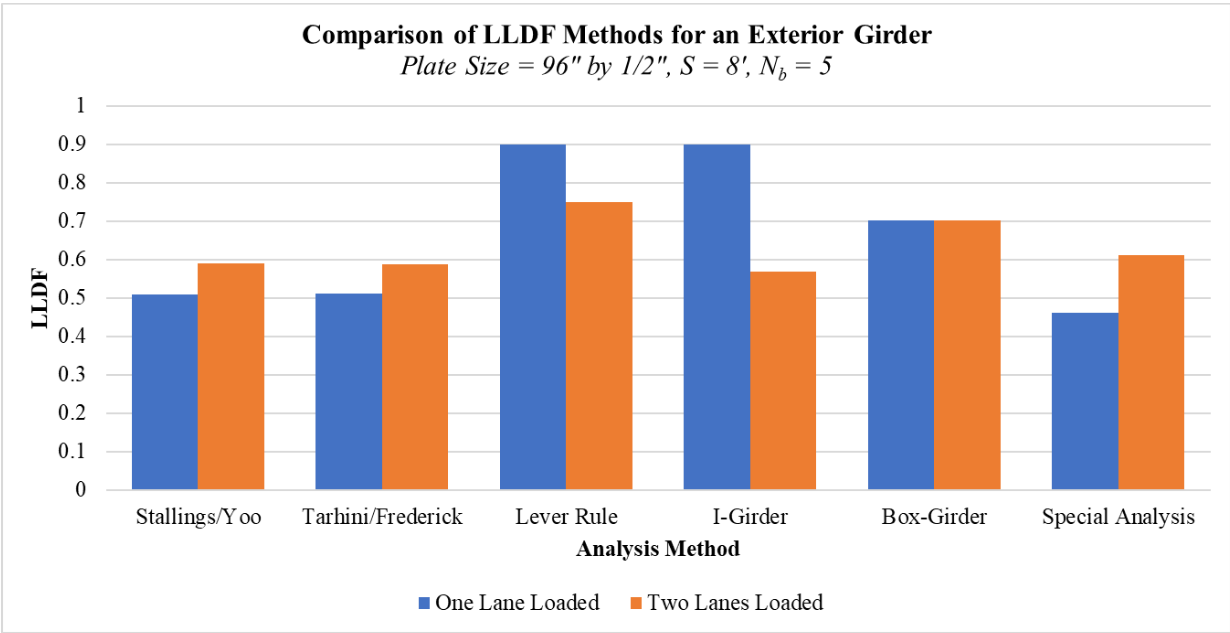

Figure 8.2: Comparison of Analytical and Empirical LLDF Methods

For the sensitivity matrix, the one-lane loaded LLDFs for exterior girders, averaged from the Stallings/Yoo and the Tarhini/Frederick analytical methods, are 34% lower compared to the lever rule and 22% lower compared to the box-girder simplified LLDFs. For the two-lane loaded LLDFs for exterior girders, the averaged analytical LLDFs are 7% higher than the I-girder simplified LLDFs and 11% lower than the box-girder simplified LLDFs. A similar pattern was found for the interior girder LLDFs.

8.3.2 Influence of Span Length

The influence of span length on LLDFs on Standard Bridge 3, as described in Section 8.2.1, is shown in Figure 8.3. Figure 8.3 has been divided into four components for clarity, each component representing the girder being maximized and the number of lanes loaded. Each set of vertical bars represents a different live load distribution method, and each different color bar represents a bridge with a different span length, in feet, as shown in the legend. Additionally, the methodology of Special Analysis is discussed in Section 8.7.1 and can only be performed on exterior girders, so values are only shown in Figure 8.3c and 8.3d.

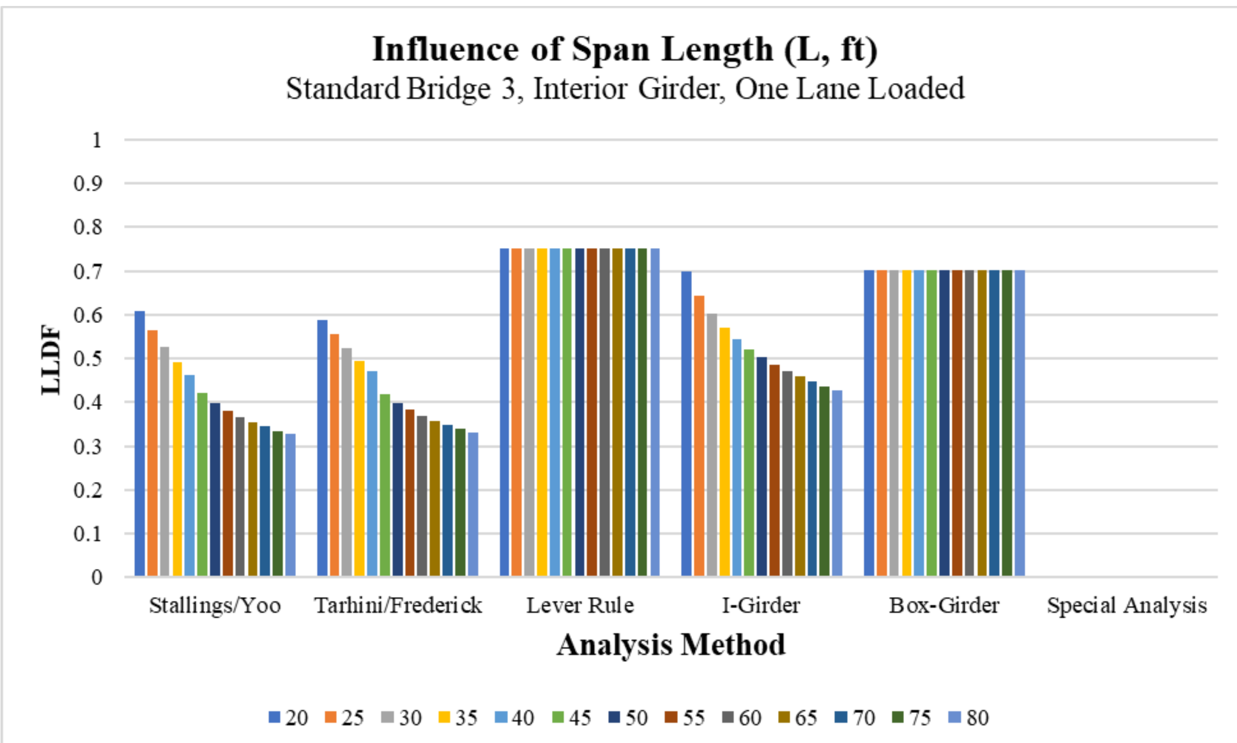

(a)

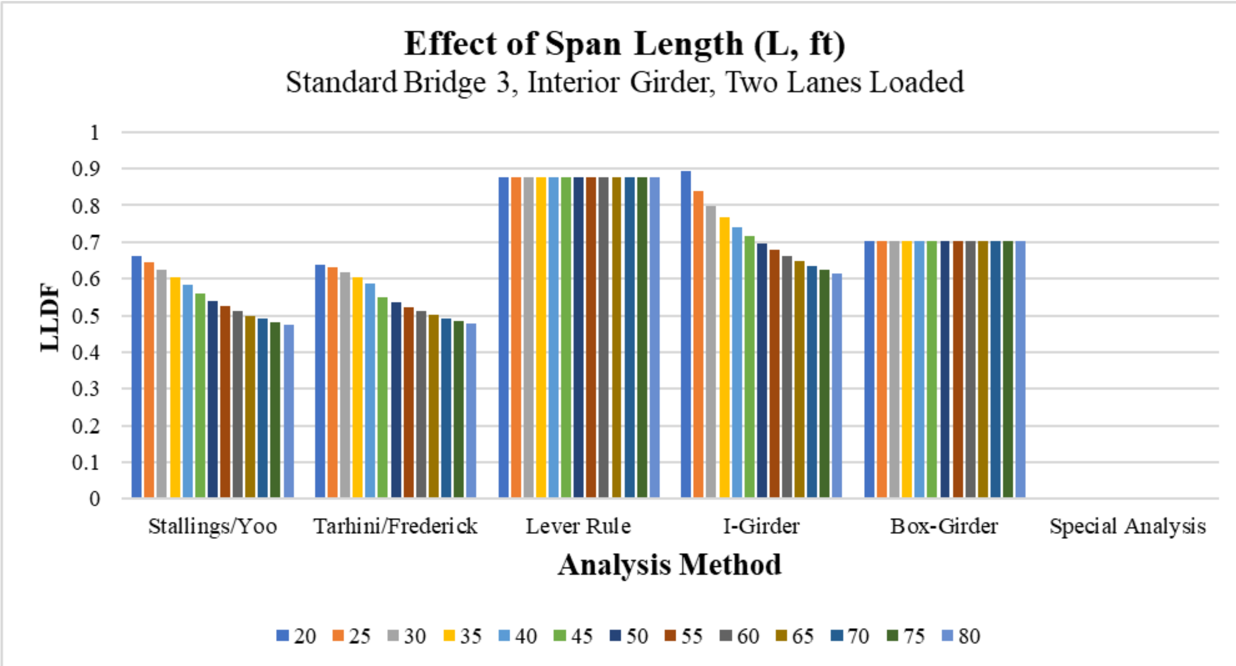
Effect of Span Length (L, ft)
Standard Bridge 3, Interior Girder, Two Lanes Loaded
LLDF
1
0.9
0.8
0.7
0.6
0.5
0.4
0.3
0.2
0.1
0
Stallings/Yoo
Tarhini/Frederick
Lever Rule
I-Girder
Box-Girder
Special Analysis
Analysis Method
20
25
30
35
40
45
50
55
60
65
70
75
80

(b)

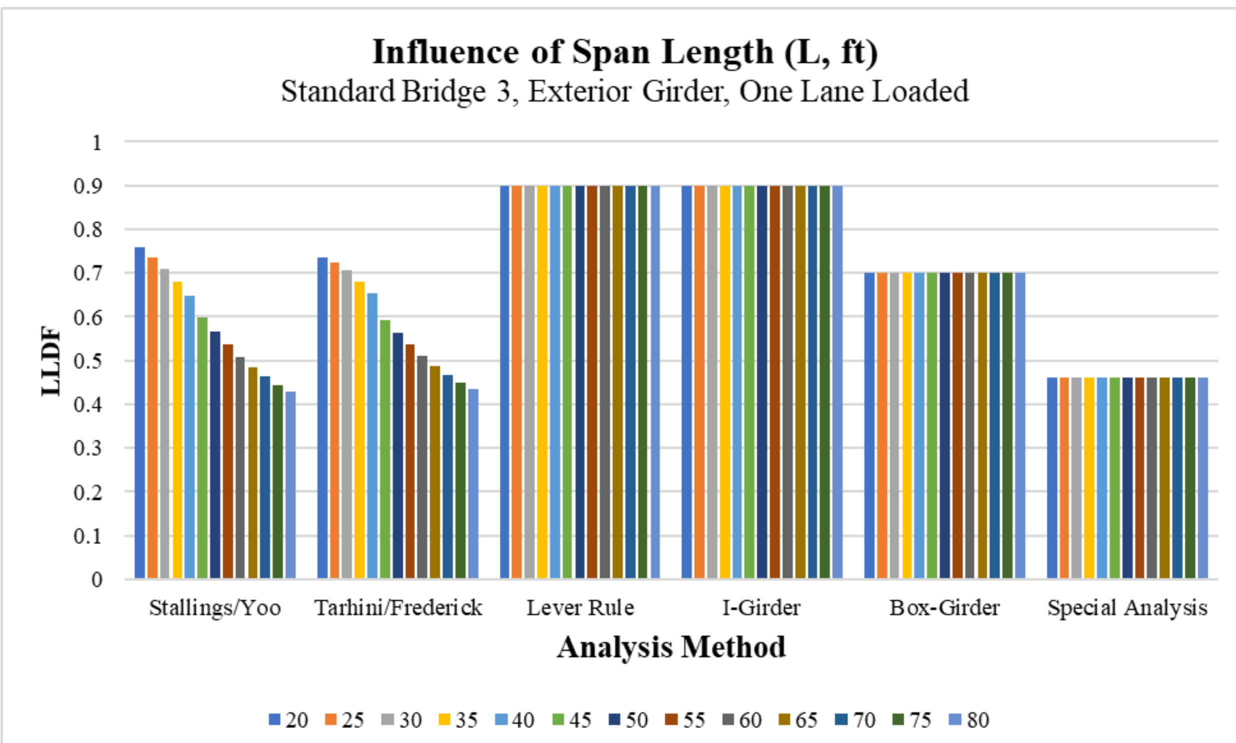
Influence of Span Length (L, ft)
Standard Bridge 3, Exterior Girder, One Lane Loaded
LLDF
1
0.9
0.8
0.7
0.6
0.5
0.4
0.3
0.2
0.1
0
Stallings/Yoo
Tarhini/Frederick
Lever Rule
I-Girder
Box-Girder
Special Analysis
Analysis Method
20
25
30
35
40
45
50
55
60
65
70
75
80

(c)

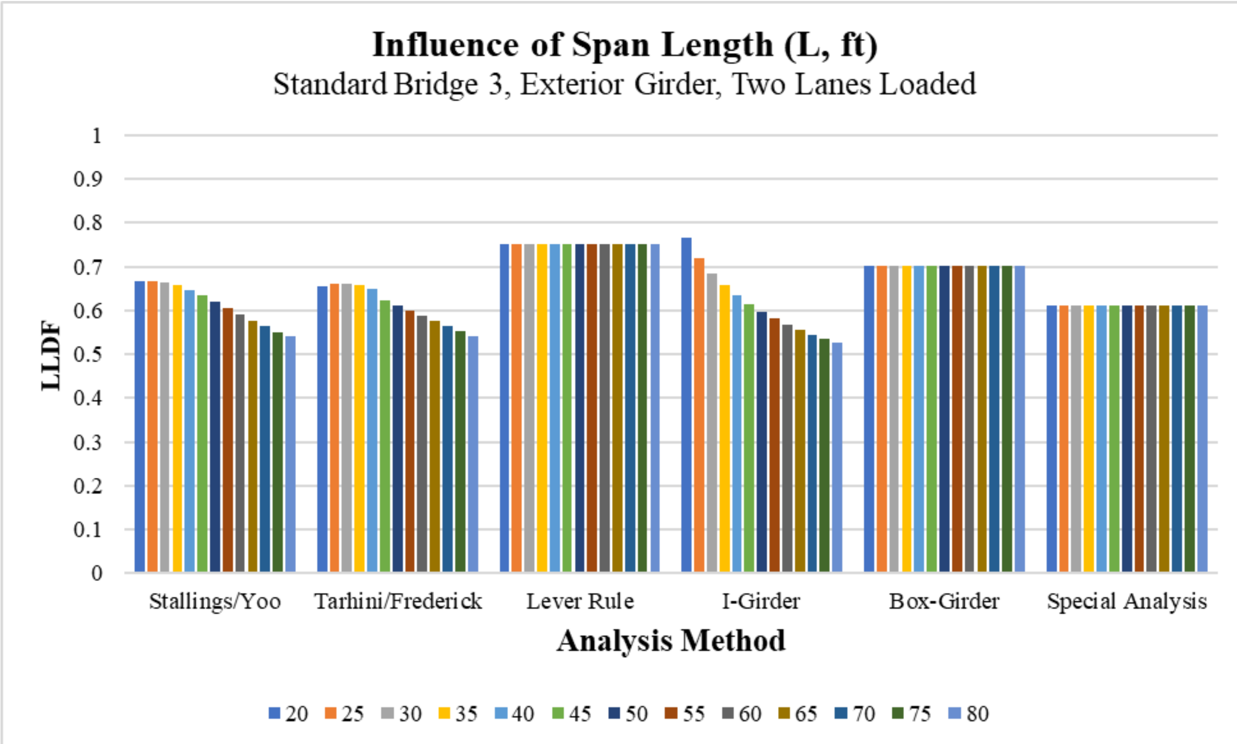

(d)

Figure 8.3: Comparison of the Inlfuence of Span Length on Standard Bridge 3 on an: (a) Interior Girder One-Lane Loaded, (b) Interior Girder Two-Lanes Loaded, (c) Exterior Girder One-Lane Loaded, (d) Exterior Girder Two-Lanes Loaded

From these graphs, it was concluded span length has a significant impact on PBFTG LLDFs. Span length will be considered in the parametric study. Another interesting conclusion from this data is that span length seems to have a more significant impact on one-lane loaded LLDFs. Of the potential simplified distribution methods provided by the AASHTO LRFD BDS, the I-Girder methodology most accurately reflects the trend of LLDFs with respect to span length.

8.3.3 Influence of Number of Beams

The influence of the number of beams in the cross-section on LLDFs on Standard Bridge 4, as described in Section 8.2.1, is shown in Figure 8.4. Figure 8.4 has been divided into four components for clarity, each component representing the girder being maximized and the number of lanes loaded. Each set of vertical bars represents a different live load distribution method, and each different color bar represents a bridge with a different number of beams, as shown in the legend. Additionally, the methodology of Special Analysis is discussed in Section 8.7.1 and can only be performed on exterior girders, so values are only shown in Figure 8.4c and 8.4d.

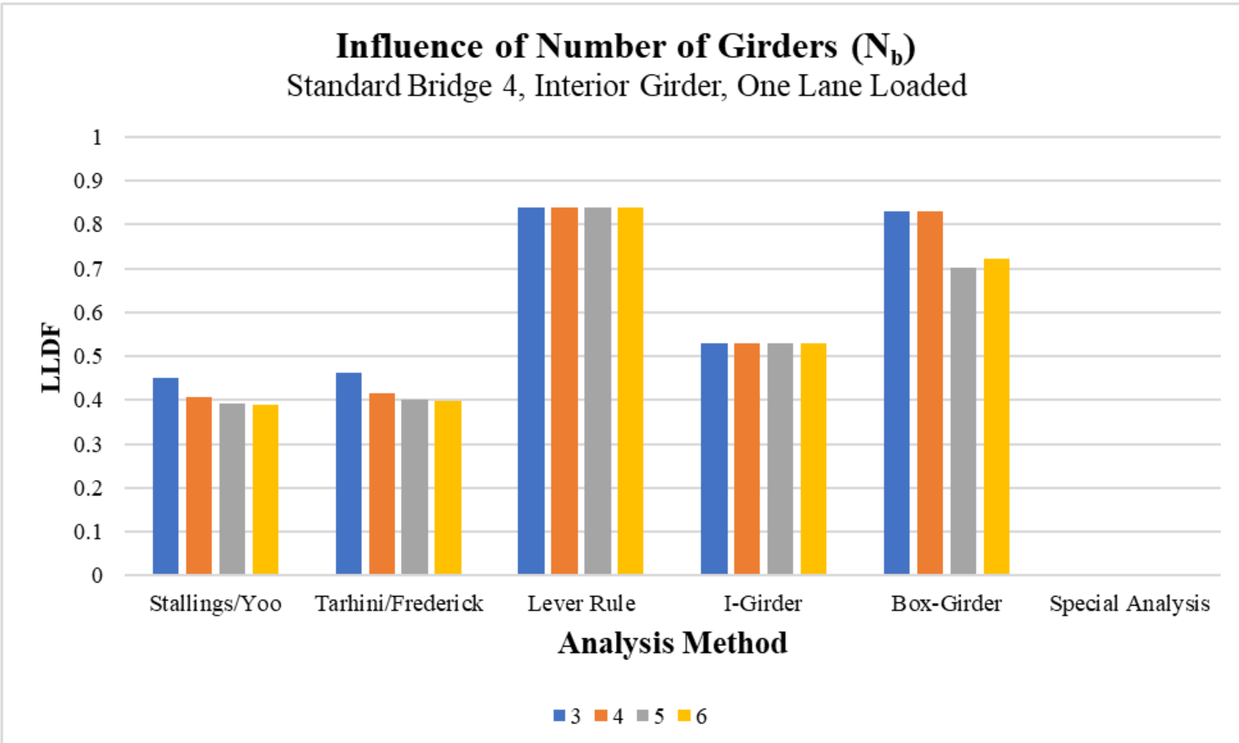

(a)

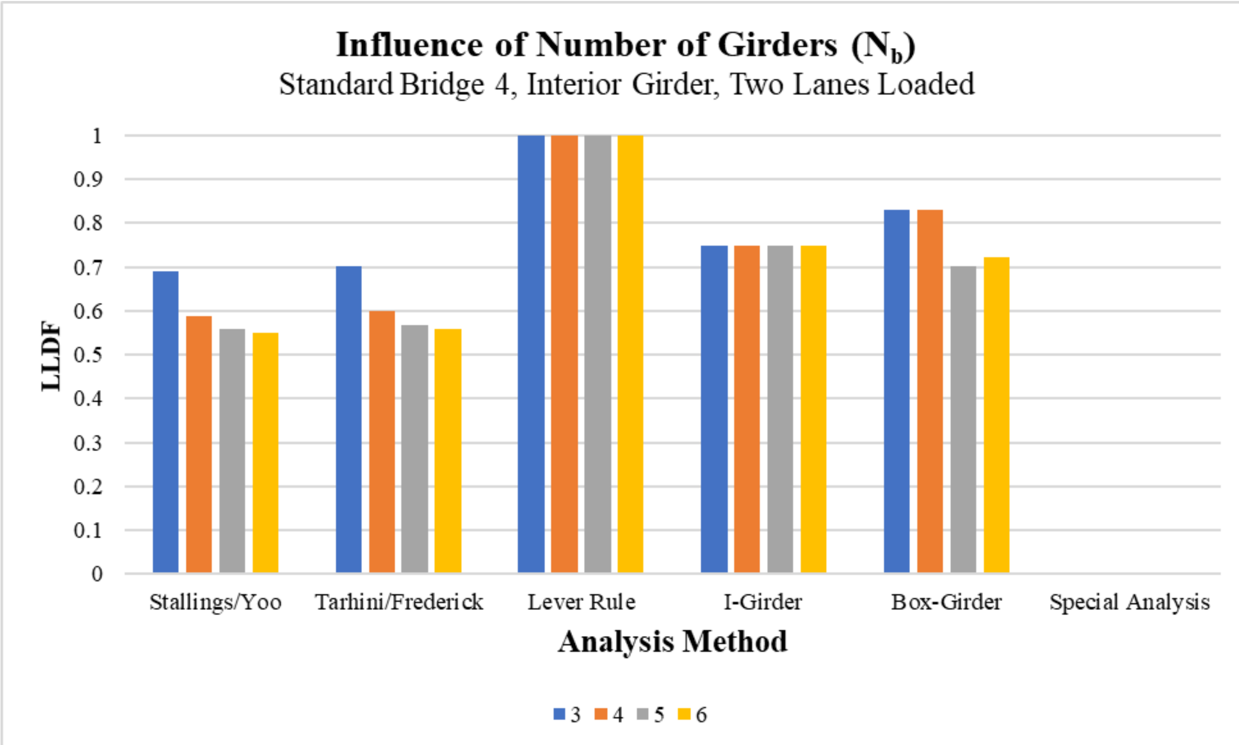
Influence of Number of Girders (N_b)
Standard Bridge 4, Interior Girder, Two Lanes Loaded
LLDF
1
0.9
0.8
0.7
0.6
0.5
0.4
0.3
0.2
0.1
0
Stallings/Yoo
Tarhini/Frederick
Lever Rule
I-Girder
Box-Girder
Special Analysis
Analysis Method
3
4
5
6

(b)

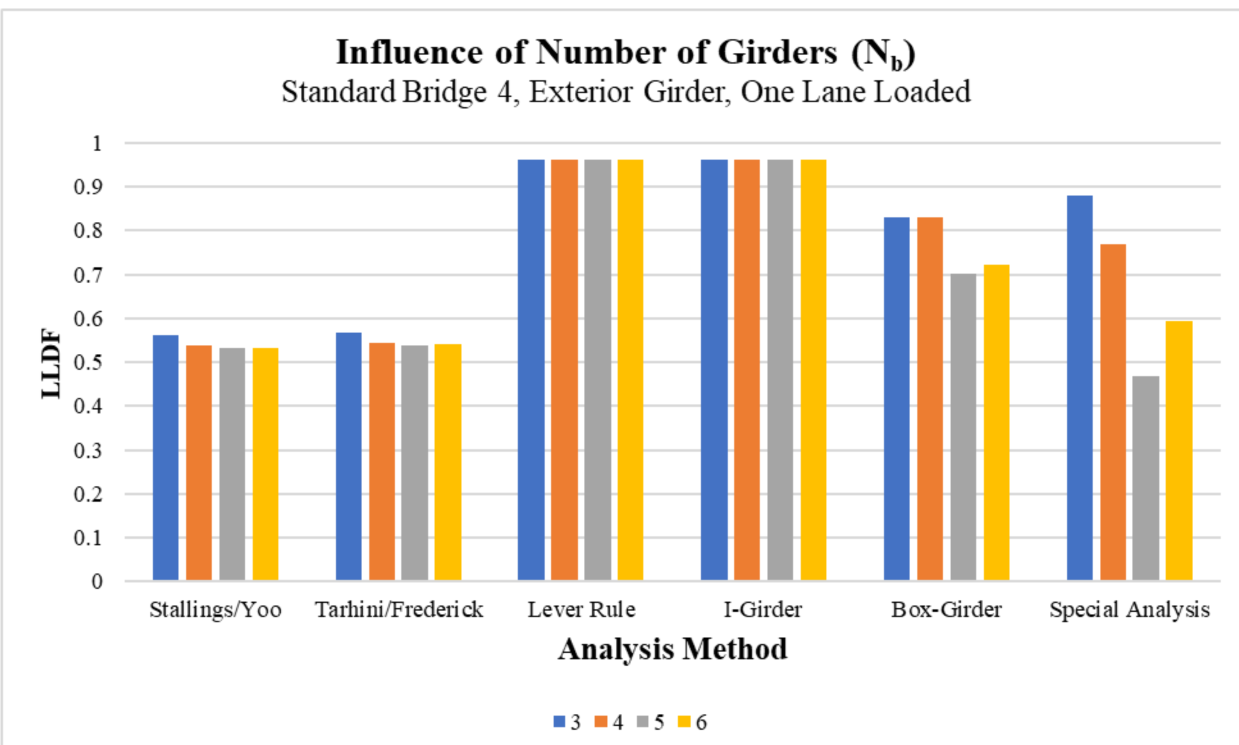
Influence of Number of Girders (N_b)
Standard Bridge 4, Exterior Girder, One Lane Loaded
LLDF
1
0.9
0.8
0.7
0.6
0.5
0.4
0.3
0.2
0.1
0
Stallings/Yoo
Tarhini/Frederick
Lever Rule
I-Girder
Box-Girder
Special Analysis
Analysis Method
3
4
5
6

(c)

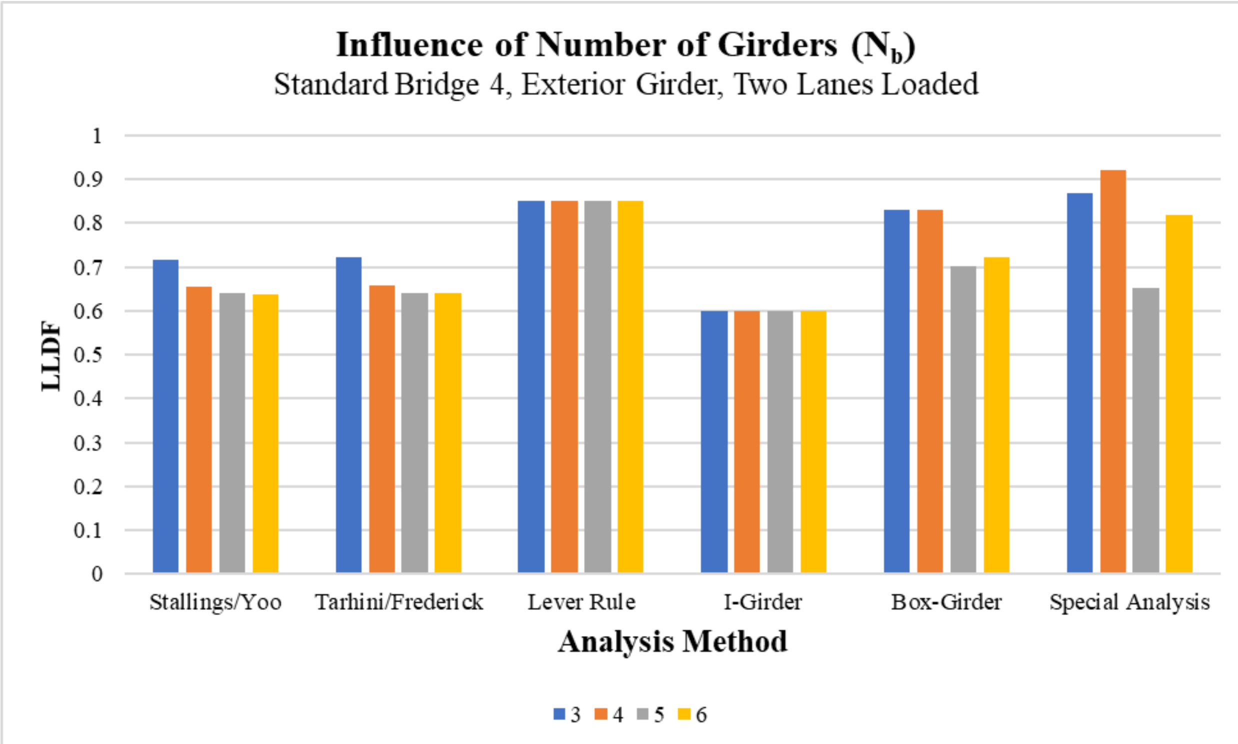

(d)

Figure 8.4: Comparison of the Effect of Number of Girders on Standard Bridge 4 on an: (a) Interior Girder One-Lane Loaded, (b) Interior Girder Two-Lanes Loaded, (c) Exterior Girder One-Lane Loaded, (d) Exterior Girder Two-Lanes Loaded

The number of beams in the cross-section has a small effect on PBFTG LLDFs. The number of beams will be considered in the parametric study to determine if the trend of increased number of beams corresponds to decreased effect on PBFTG live load distribution. Similar to the effect of span length, the I-Girder methodology accurately reflects the trend of LLDFs with respect to the number of beams in the cross-section. An interesting difference between the comparisons of span length and number of beams using the I-Girder methodology is the I-Girder methodology underestimates LLDFs when varying number of girders, where the same methodology overestimates LLDFs when varying span length.

8.3.4 Influence of PBFTG Size

The influence of the size of PBFTGs on LLDFs on Standard Bridge 4, as described in Section 8.2.1, is shown in Figure 8.5. Figure 8.5 has been divided into four components for clarity, each component representing the girder being maximized and the number of lanes loaded. Each set of vertical bars represents a different live load distribution method, and each different color bar represents a bridge with a different PBFTG utilized, as shown in the legend. Additionally, the methodology of Special Analysis is discussed in Section 8.7.1 and can only be performed on exterior girders, so values are only shown in Figure 8.5c and 8.5d.

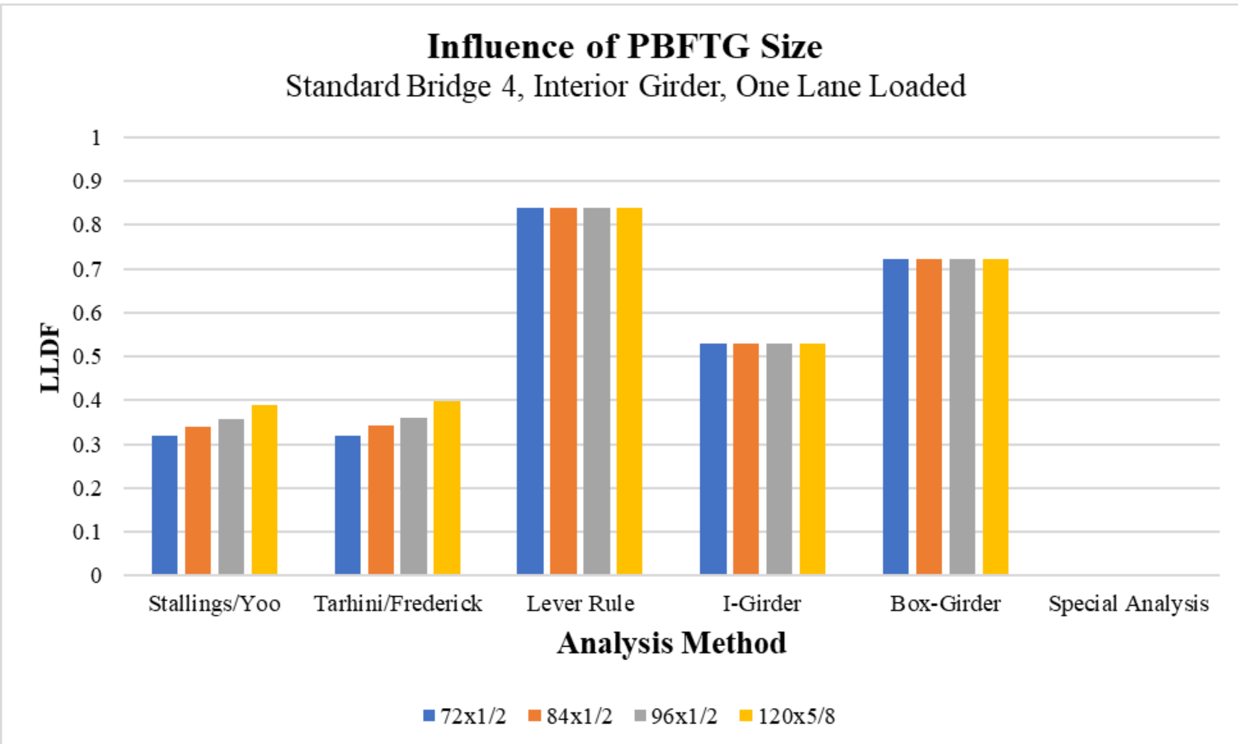

(a)

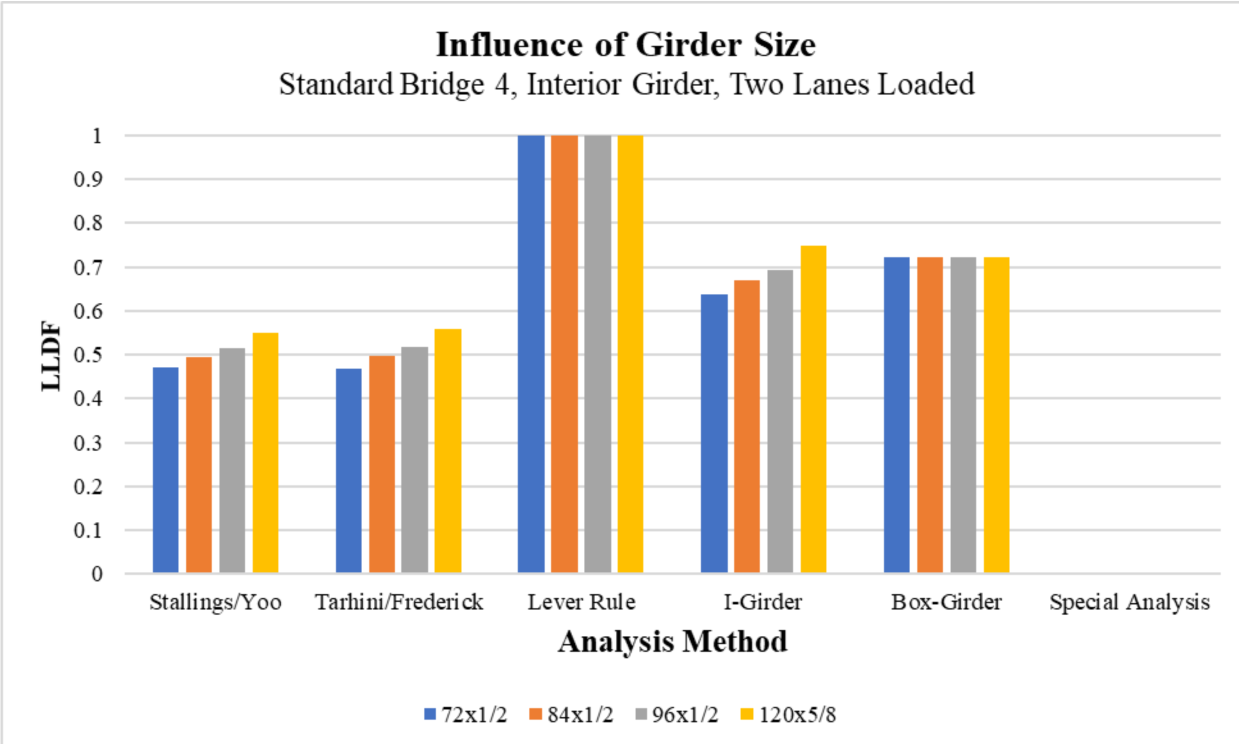

Influence of Girder Size
Standard Bridge 4, Interior Girder, Two Lanes Loaded
LLDF
1
0.9
0.8
0.7
0.6
0.5
0.4
0.3
0.2
0.1
0
Stallings/Yoo
Tarhini/Frederick
Lever Rule
I-Girder
Box-Girder
Special Analysis
Analysis Method
72x1/2
84x1/2
96x1/2
120x5/8

(b)

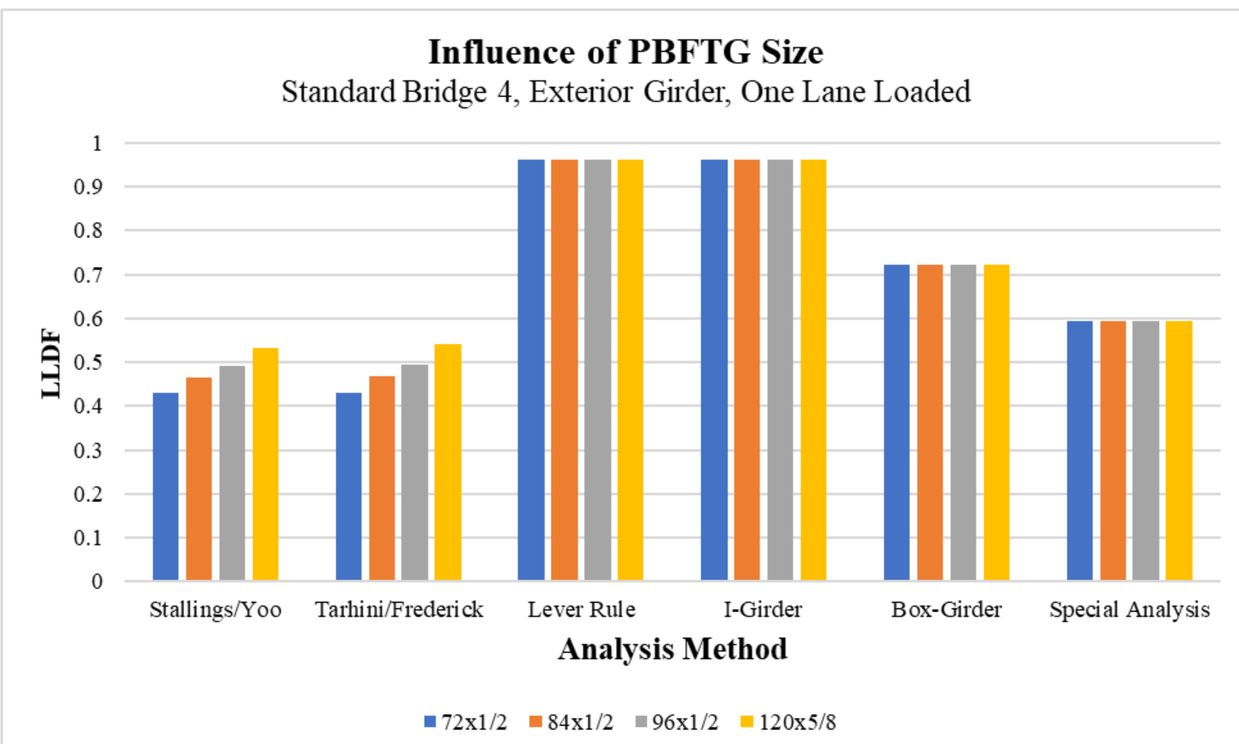

Influence of PBFTG Size
Standard Bridge 4, Exterior Girder, One Lane Loaded
LLDF
1
0.9
0.8
0.7
0.6
0.5
0.4
0.3
0.2
0.1
0
Stallings/Yoo
Tarhini/Frederick
Lever Rule
I-Girder
Box-Girder
Special Analysis
Analysis Method
72x1/2
84x1/2
96x1/2
120x5/8

(c)

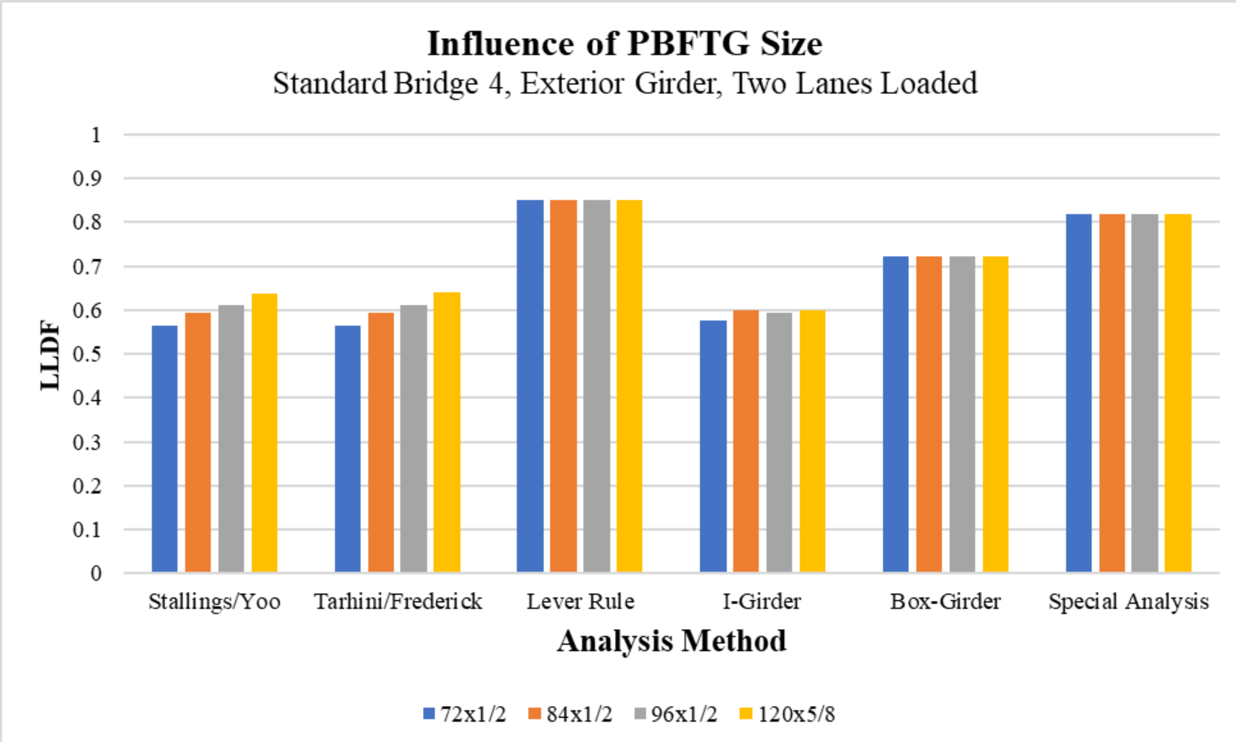

(d)

Figure 8.5: Comparison of the Influence of Girder Size on Standard Bridge 4 on an: (a) Interior Girder One-Lane Loaded, (b) Interior Girder Two-Lanes Loaded, (c) Exterior Girder One-Lane Loaded, (d) Exterior Girder Two-Lanes Loaded

The PBFTG size directly correlates to the longitudinal stiffness of the girder. As shown in Figure 8.5, the PBFTG size, and by correlation, the longitudinal stiffness does have a minor impact on live load distribution. However, for exterior girders, this evaluation is somewhat difficult to justify based on this data, as the overhang ratio is dependent on the PBFTG size. As the size of the PBFTGs increase, not only does the longitudinal stiffness parameter increase, but the width of the PBFTGs increase. This increase in width causes the exterior wheel line to move further away from the center of the bridge, causing higher exterior girder LLDFs. This difficulty is further addressed in the assessment of overhang ratio later in the sensitivity study and in the parametric study.

8.3.5 Influence of Girder Spacing

The influence of girder spacing on LLDFs on Standard Bridge 1, as described in Section 8.2.1, is shown in Figure 8.6. Figure 8.6 has been divided into four components for clarity, each component representing the girder being maximized and the number of lanes loaded. Each set of vertical bars represents a different live load distribution method, and each different color bar represents a bridge with a different girder spacing, in feet, as shown in the legend. Additionally, the methodology of Special Analysis is discussed in Section 8.7.1 and can only be performed on exterior girders, so values are only shown in Figure 8.6c and 8.6d.

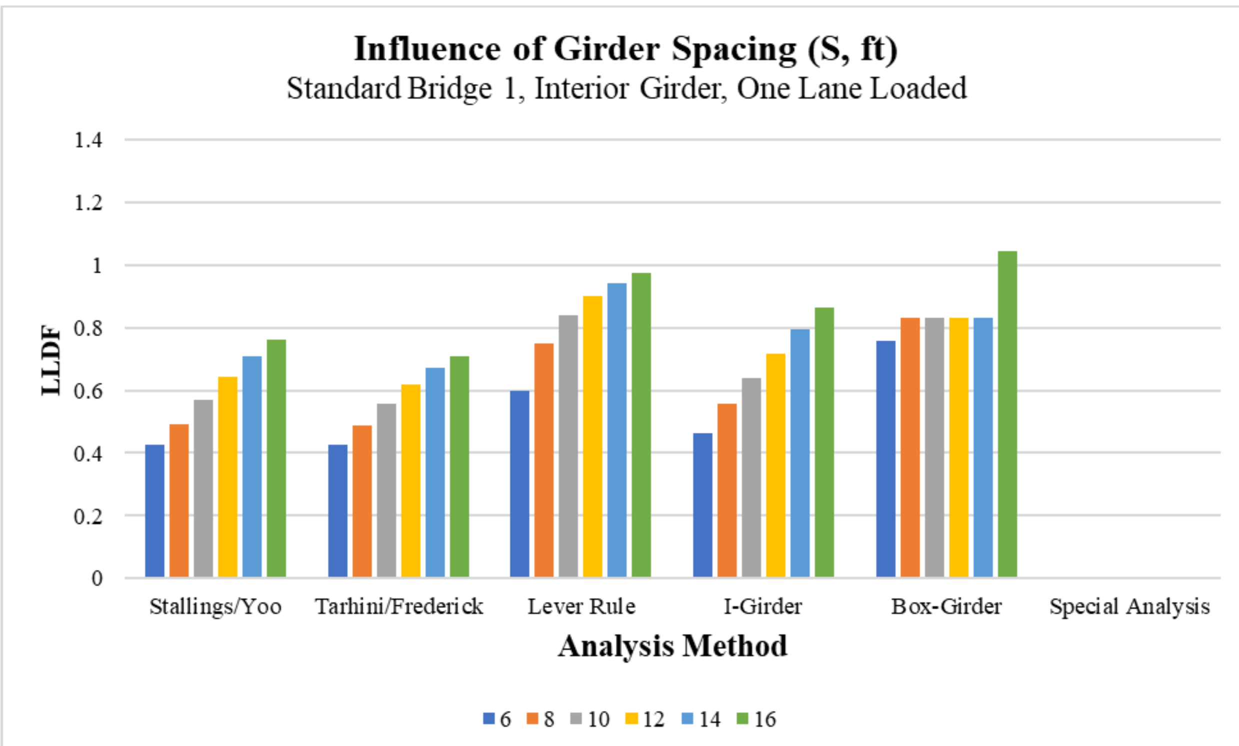

(a)

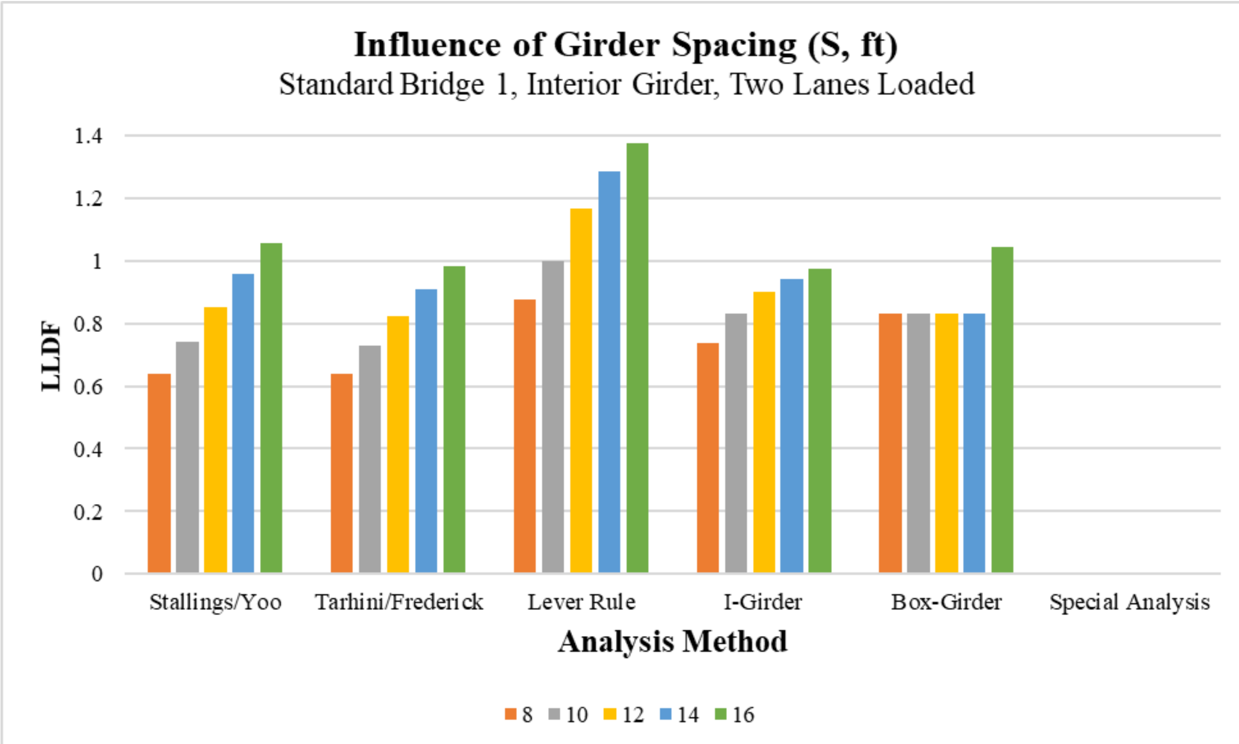

Influence of Girder Spacing (S, ft)
Standard Bridge 1, Interior Girder, Two Lanes Loaded
1.4
1.2
1
0.8
0.6
0.4
0.2
0
LLDF
Stallings/Yoo
Tarhini/Frederick
Lever Rule
I-Girder
Box-Girder
Special Analysis
Analysis Method
8
10
12
14
16

(b)

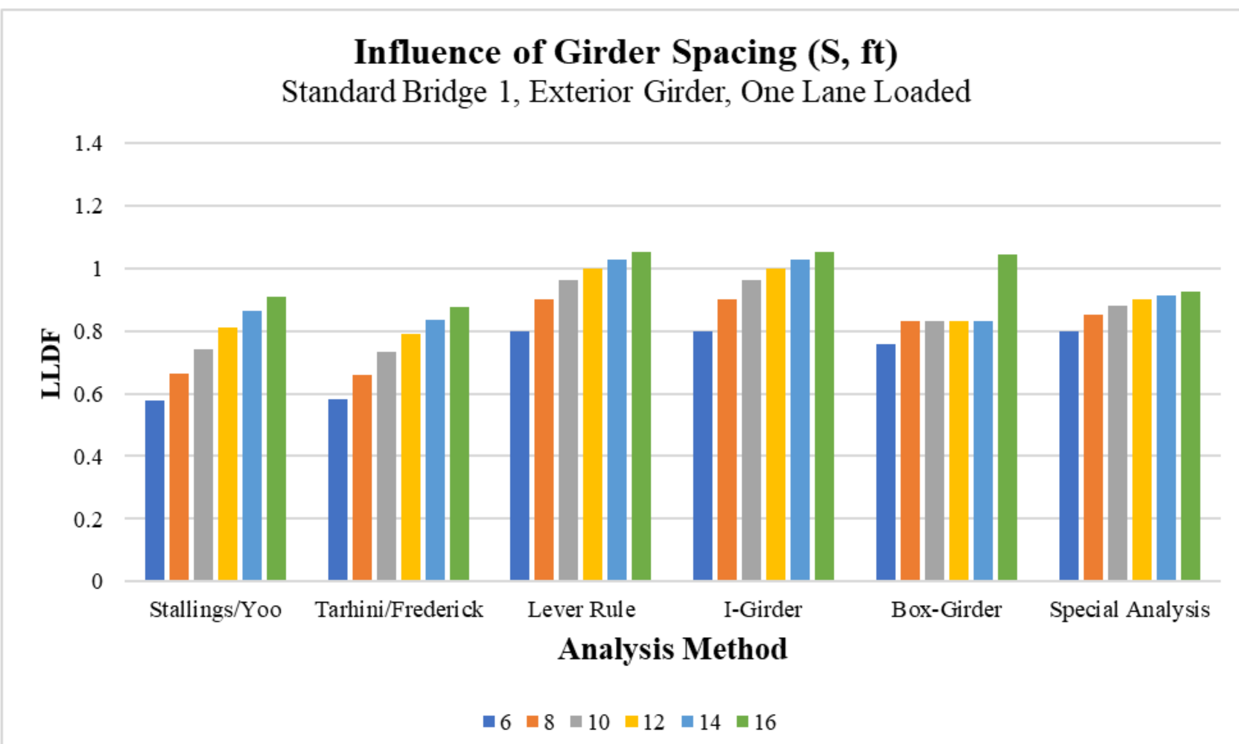

Influence of Girder Spacing (S, ft)
Standard Bridge 1, Exterior Girder, One Lane Loaded
1.4
1.2
1
0.8
0.6
0.4
0.2
0
LLDF
Stallings/Yoo
Tarhini/Frederick
Lever Rule
I-Girder
Box-Girder
Special Analysis
Analysis Method
6
8
10
12
14
16

(c)

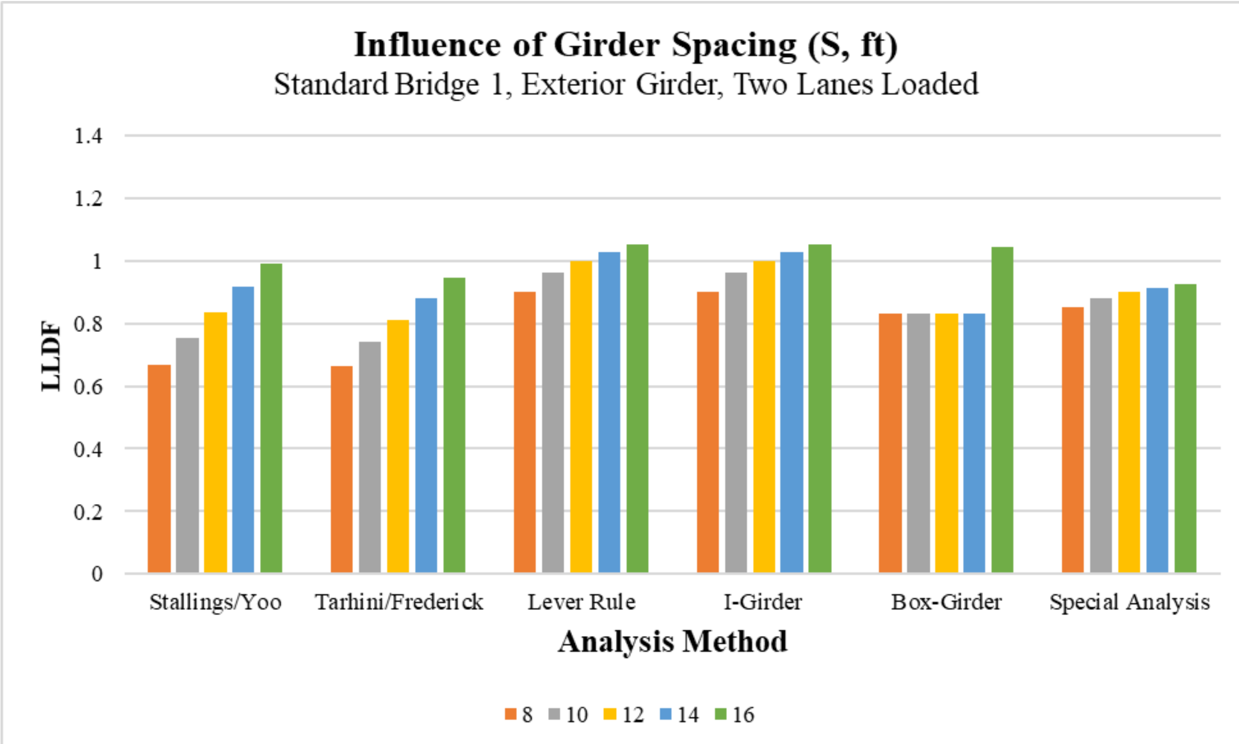

(d)

Figure 8.6: Comparison of the Influence of Girder Spacing on Standard Bridge 1 on an: (a) Interior Girder One-Lane Loaded, (b) Interior Girder Two-Lanes Loaded, (c) Exterior Girder One-Lane Loaded, (d) Exterior Girder Two-Lanes Loaded

As anticipated, girder spacing has a significant effect on live load distribution in all cases. Girder spacing will be considered in the parametric study. Note, Figures 8.6b and 8.6d do not have girder spacings of 6 feet, as bridges with a girder spacing of 6 feet cannot be loaded with two design lanes due to the clear roadway width being below the allowable minimum of 20 feet for two design lanes. Additionally, the scale for the LLDFs was modified from a maximum of 1.0 to 1.4 to accommodate large LLDFs calculated in this study. In addition, not every bridge cross-section will utilize the entire breadth of possible girder spacings. For example, it would be a rather unique bridge to utilize PBFTGs bent out of 72 inch wide by 1/2 inch thick plate with a girder spacing of 16 feet. This will be considered when developing the parametric study.

8.3.6 Influence of Deck Thickness

The influence of deck thickness on LLDFs on Standard Bridge 2, as described in Section 8.2.1, is shown in Figure 8.7. Figure 8.7 has been divided into four components for clarity, each component representing the girder being maximized and the number of lanes loaded. Each set of vertical bars represents a different live load distribution method, and each different color bar represents a bridge with a different deck thickness, in inches, as shown in the legend. Additionally, the methodology of Special Analysis is discussed in Section 8.7.1 and can only be performed on exterior girders, so values are only shown in Figure 8.7c and 8.7d.

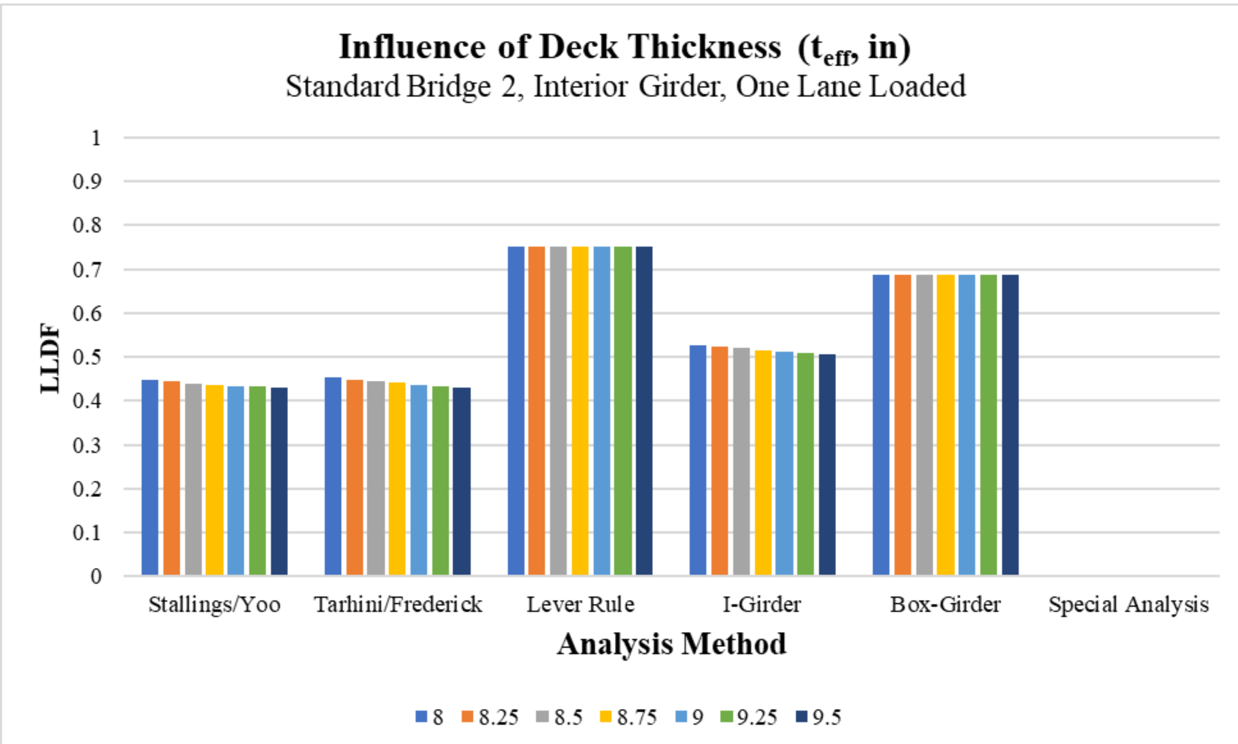

(a)

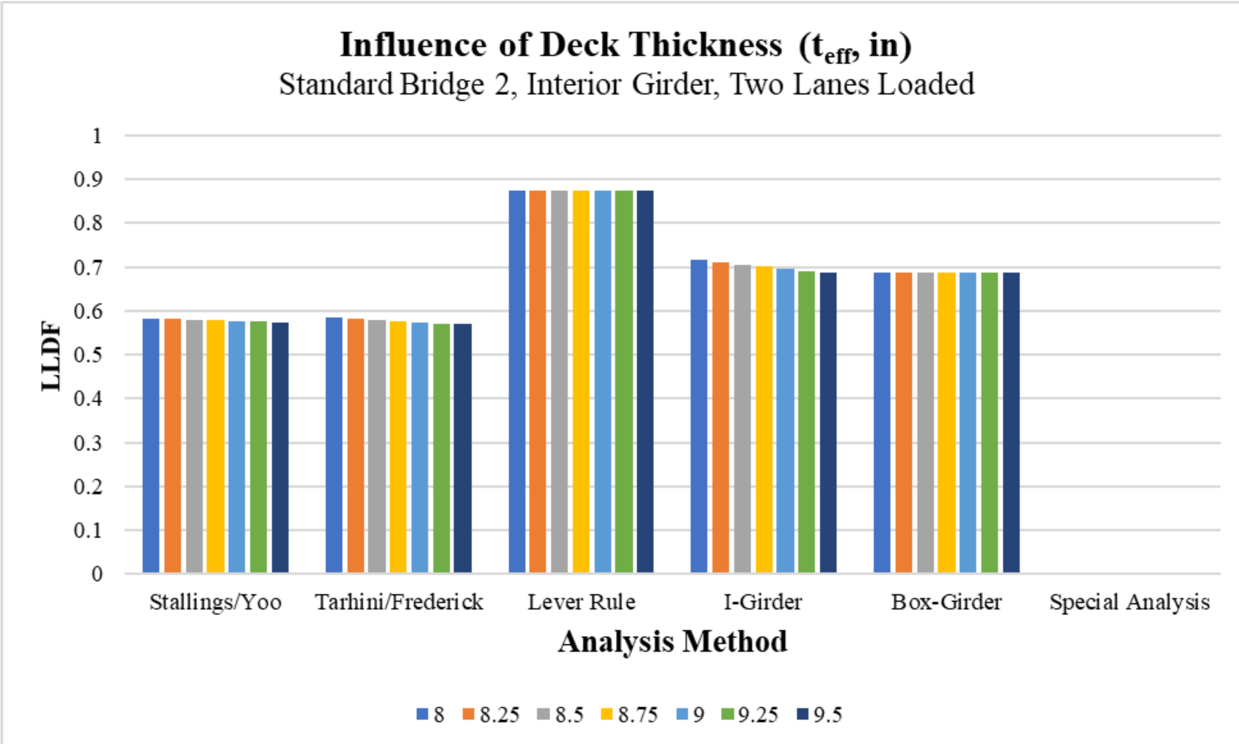

Influence of Deck Thickness (t_{eff}, in)
Standard Bridge 2, Interior Girder, Two Lanes Loaded
LLDF
1
0.9
0.8
0.7
0.6
0.5
0.4
0.3
0.2
0.1
0
Stallings/Yoo
Tarhini/Frederick
Lever Rule
I-Girder
Box-Girder
Special Analysis
Analysis Method
8
8.25
8.5
8.75
9
9.25
9.5

(b)

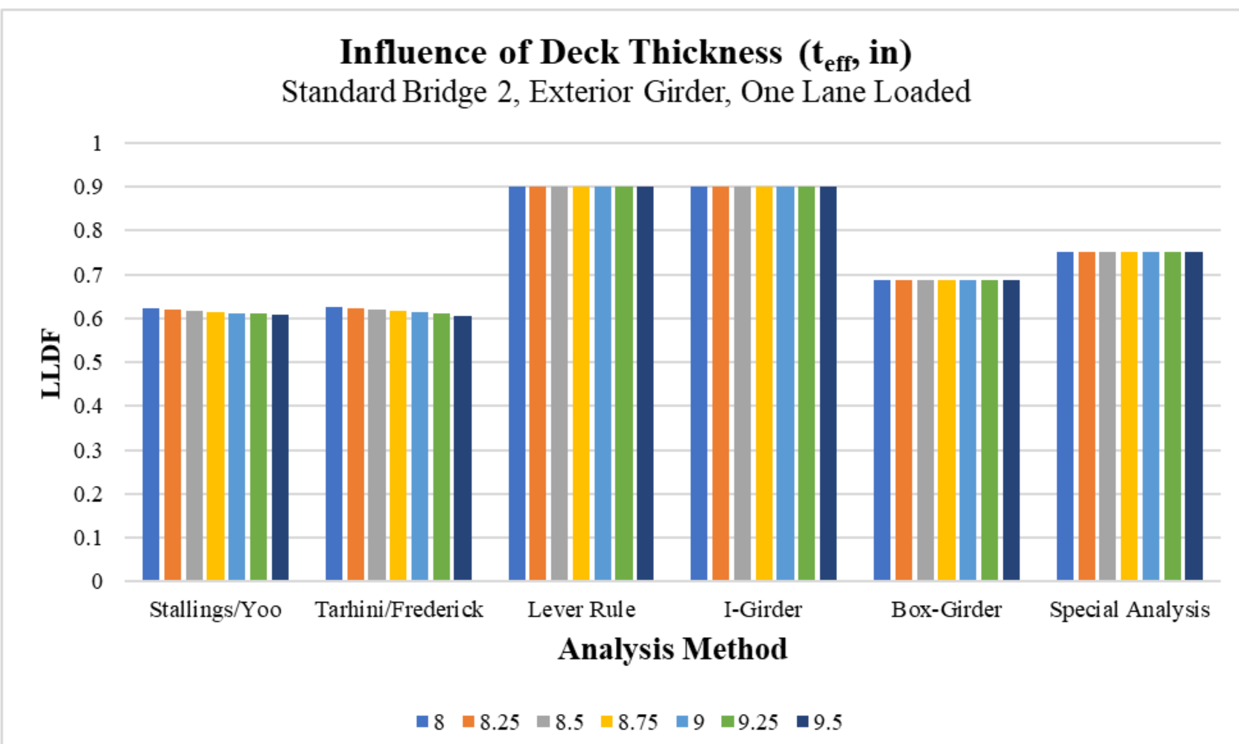

Influence of Deck Thickness (t_{eff}, in)
Standard Bridge 2, Exterior Girder, One Lane Loaded
LLDF
1
0.9
0.8
0.7
0.6
0.5
0.4
0.3
0.2
0.1
0
Stallings/Yoo
Tarhini/Frederick
Lever Rule
I-Girder
Box-Girder
Special Analysis
Analysis Method
8
8.25
8.5
8.75
9
9.25
9.5

(c)

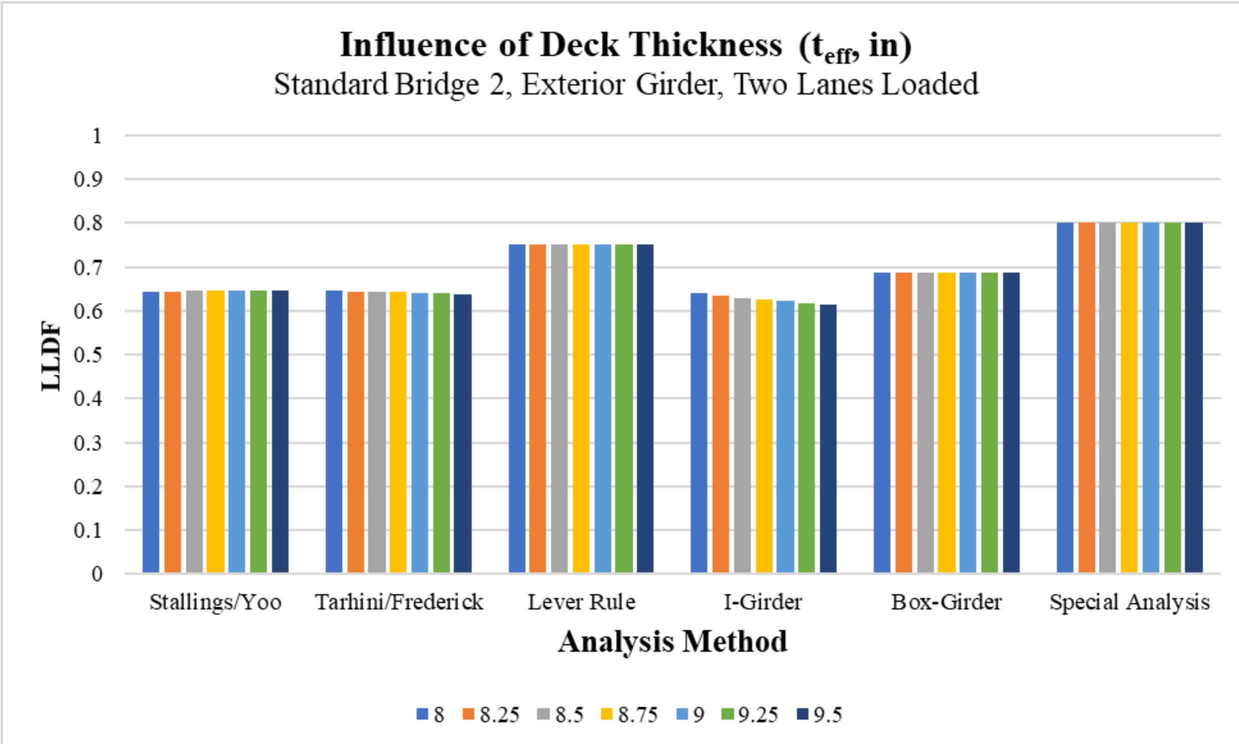

(d)

Figure 8.7: Comparison of the Influence of Deck Thickness on Standard Bridge 3 on an: (a) Interior Girder One-Lane Loaded, (b) Interior Girder Two-Lanes Loaded, (c) Exterior Girder One-Lane Loaded, (d) Exterior Girder Two-Lanes Loaded

The thickness of the deck has a negligible effect on LLDFs in PBFTG. As seen in Figure 8.7, all distribution methods agree, which cannot be stated for the other factors in the sensitivity matrix. However, deck thickness is a variable in the longitudinal stiffness parameter, which was not directly assessed in this study.

8.3.7 Influence of Overhang Ratio

The influence of overhang ratio on LLDFs on Standard Bridge 4, as described in Section 8.2.1, is shown in Figure 8.8. Figure 8.8 has been divided into four components for clarity, each component representing the girder being maximized and the number of lanes loaded. Each set of vertical bars represents a different live load distribution method, and each different color bar represents a bridge with a different overhang ratio, as shown in the legend. Additionally, the methodology of Special Analysis is discussed in Section 8.7.1 and can only be performed on exterior girders, so values are only shown in Figure 8.8c and 8.8d.

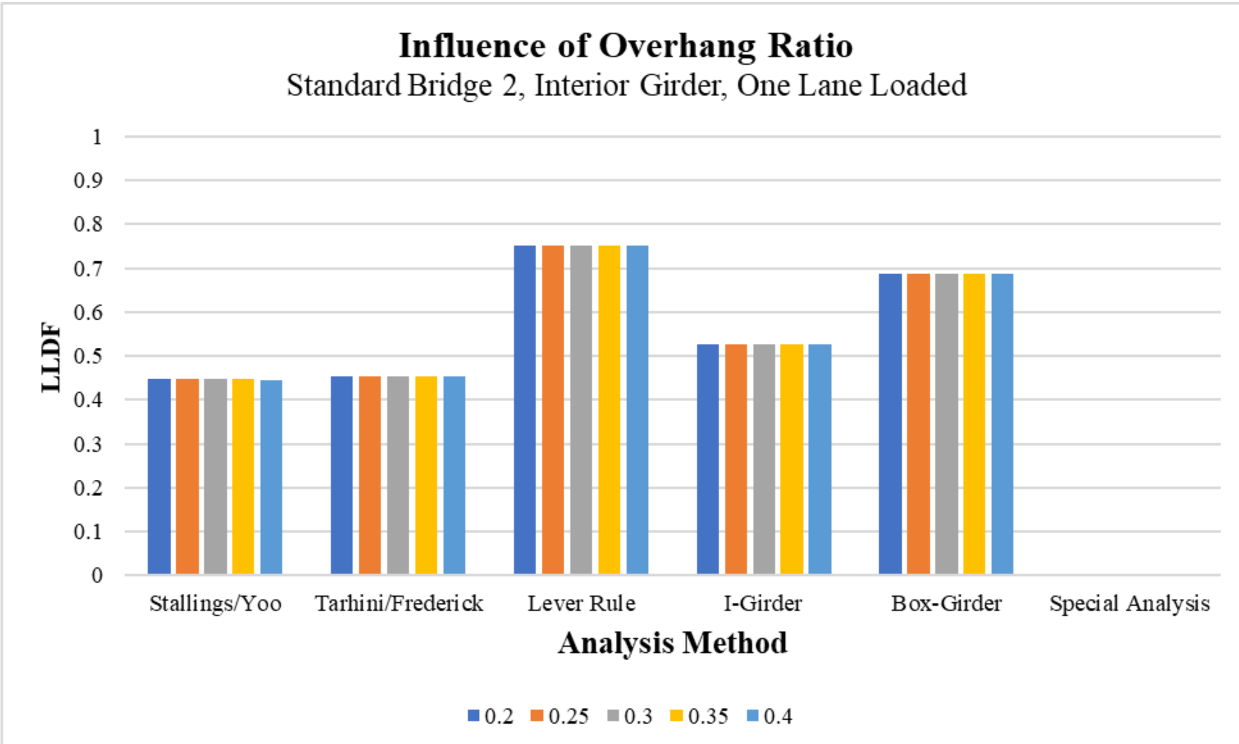

(a)

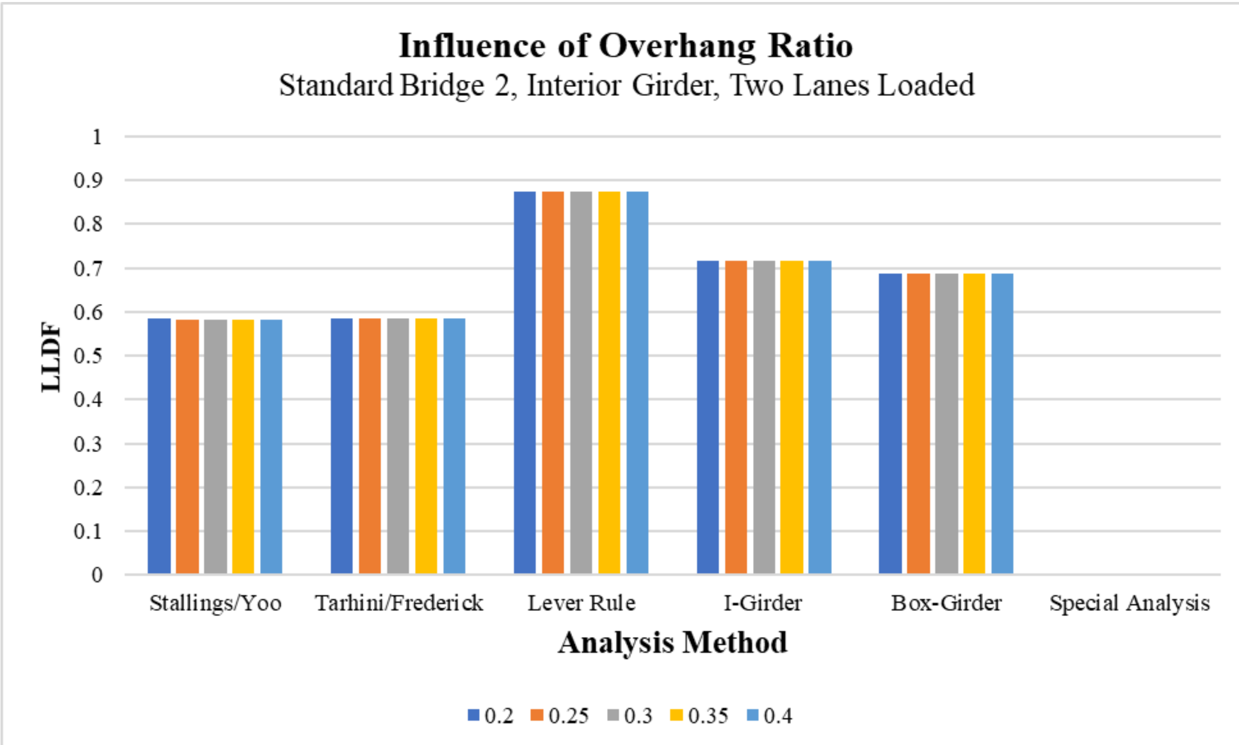
Influence of Overhang Ratio
Standard Bridge 2, Interior Girder, Two Lanes Loaded
LLDF
1
0.9
0.8
0.7
0.6
0.5
0.4
0.3
0.2
0.1
0
Stallings/Yoo
Tarhini/Frederick
Lever Rule
I-Girder
Box-Girder
Special Analysis
Analysis Method
0.2
0.25
0.3
0.35
0.4

(b)

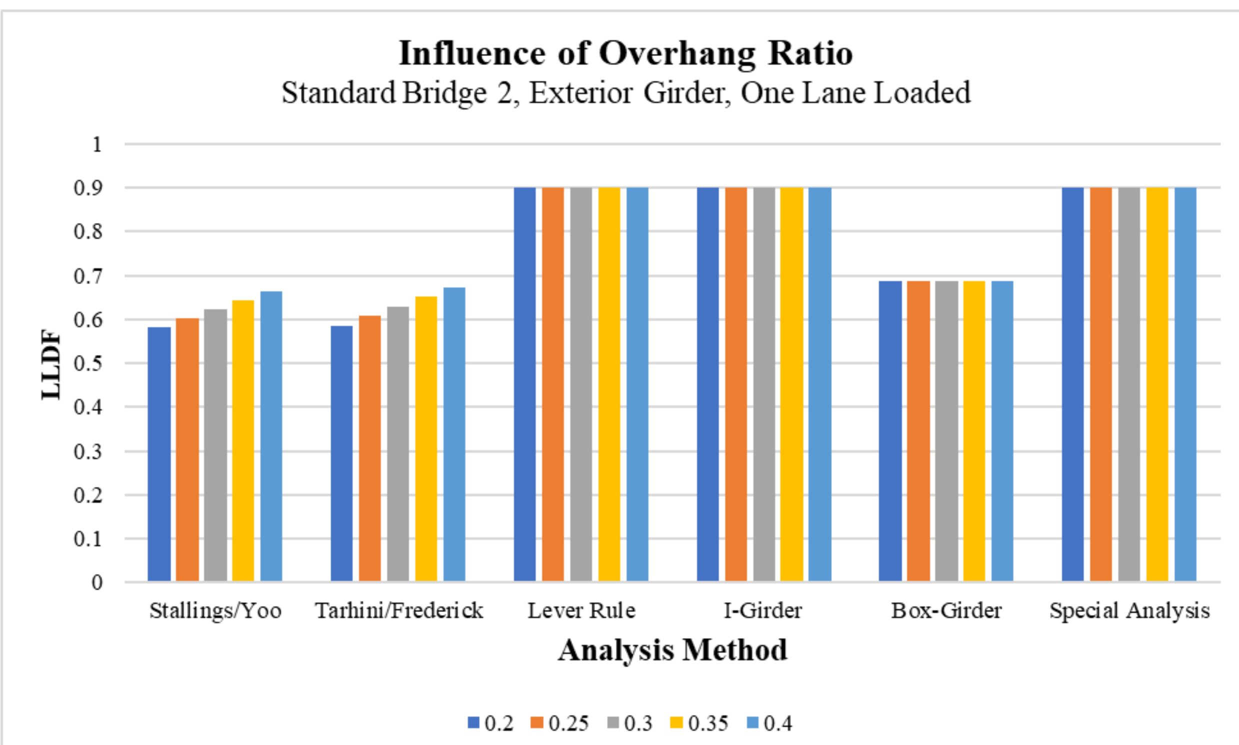
Influence of Overhang Ratio
Standard Bridge 2, Exterior Girder, One Lane Loaded
LLDF
1
0.9
0.8
0.7
0.6
0.5
0.4
0.3
0.2
0.1
0
Stallings/Yoo
Tarhini/Frederick
Lever Rule
I-Girder
Box-Girder
Special Analysis
Analysis Method
0.2
0.25
0.3
0.35
0.4

(c)

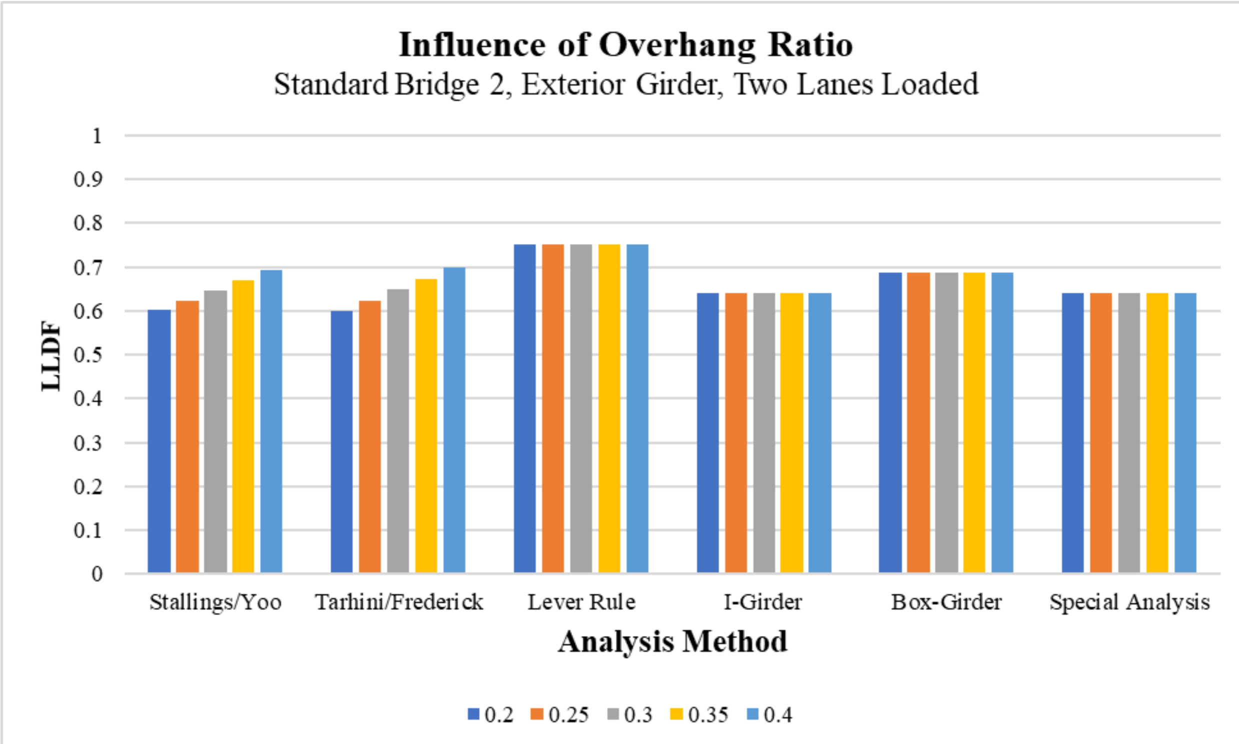

(d)

Figure 8.8: Comparison of the Influence of Overhang Ratio on Standard Bridge 3 on an: (a) Interior Girder One-Lane Loaded, (b) Interior Girder Two-Lanes Loaded, (c) Exterior Girder One-Lane Loaded, (d) Exterior Girder Two-Lanes Loaded

Overhang ratio is defined as the ratio of the girder spacing to the distance measured from the center of the top exterior flange to the edge of the deck. As the placement of the truck, relative to the center of the girders, is also dependent on the width of the PBFTG, similar to girder size, it is difficult to evaluate the effect of this parameter solely. Additionally, this parameter is dependent on the girder spacing for any given bridge. As can be seen from Figure 8.8, the overhang ratio has a negligible effect on interior girder LLDFs but an obvious effect on exterior girder LLDFs. Due to this effect on exterior girder LLDFs, the overhang will continue to be considered in the parametric study, but the approach will be slightly different.

8.4 Parametric Study

The following section describes an updated matrix of bridges analyzed using Abaqus/CAE to determine the effect of key parameters on the live load distribution characteristics in PBFTG bridges. This matrix was developed based on the assessment of the results of the sensitivity matrix to further investigate the parameters found to have the most significant impact on PBFTG live load distribution. This section will additionally discuss the modified constant and varied parameters and their respective limits. The new matrix of bridges consisted of 50,312 bridges to assess the effects of a more focused set of key parameters more accurately on PBFTG LLDFs. These bridges utilize the same constant parameters discussed in Section 8.2.2.

8.4.1 Typical Bridge Cross-Sections

To visually ascertain the effect of the parameters used in this study, a generic cross-section was developed for comparison. The generic cross-section was developed with standard parameters to ensure the comparison was not skewed to one extreme end of the data set. The generic cross-section consists of six PBFTGs constructed from 96 inch wide by 1/2 inch thick plate spaced at seven feet apart on center with a span length of 60 feet. The distance from the center of the exterior flange to the edge of the parapet is twelve inches and effective deck thickness is nine inches.

8.4.2 Varied Parameters

As discussed in Section 8.3, while the sensitivity study allowed for global analysis of key factors, a more detailed assessment of a refined range of variation of key variables is necessary. Based on the results of the sensitivity study, some modifications on the definitions and bounds of certain parameters were made. As PBFTGs are intended to be prefabricated bridge elements, required to be able to be fabricated in a shop and transported to the bridge site, the maximum modular width, and therefore girder spacing, was reduced from 16 feet to 9 feet. Additionally, the minimum girder spacing was increased to 5 feet, as none of the bridges in the sensitivity study were able to utilize 4 foot girder spacings.

The deck thickness variations were increased from 0.25 inch increments to 0.5 increments due to the lack of sensitivity to the variable. However, the deck thickness remained as a variable to allow for the exploration of the longitudinal stiffness parameter. Additionally, to mirror the methodology already in place in the AASHTO LRFD BDS, the effect of width of overhang was modified from the overhang ratio to the d_e term, as defined in the AASHTO LRFD BDS.

The number of PBFTG sizes was reduced from four to three to decrease the number of parametric variations without losing the total variety of PBFTG sizes available. The sizes remaining in the study are the ones proposed by Michaelson (2014). Additionally, as not all PBFTG size combinations are appropriate for the entire range of applicability for the PBFTG system, span ranges were provided for each PBFTG size encompassing their individual applicable span ranges.

Using the aforementioned modifications, the following parameters were varied in the parametric matrix to determine their respective effect on live load distribution in PBFTG bridges:

- Three possible individual PBFTG cross-sections consisting of different plate sizes with corresponding span lengths
    - 72 inch by 0.5 inch with span lengths from 20 feet to 50 feet in 5 feet increments
    - 96 inch by 0.5 inch with span lengths from 40 feet to 80 feet in 5 feet increments
    - 120 inch by 0.625 inch with span lengths from 50 feet to 100 feet in 5 feet increments
- Six possible number of girders in the cross-section: 3, 4, 5, 6, 7, and 8 girders
- Five possible girder spacings: 5 feet to 9 feet in 1 foot increments
- Four possible deck thicknesses: 8 inch to 9.5 inch in 1/2 inch increments
- Five possible distances from the centerline of the exterior flange to the edge of parapet: 0 inch to 24 inch in 6 inch increments
- One or two-lanes loaded
- Load placement to maximize moment in an interior or exterior girder

8.5 Results of Parametric Study

As the tabulated results of the parametric study are too large to be included in this chapter, a comprehensive summary of the results has been provided in Appendix B. Appendix B summarizes the effect of the varied parameter in graphical form. The general trends of the parametric study results will be discussed herein, specifically the effect of the parameters on the distribution of live load in a multitude of loading scenarios.

8.5.1 Influence of Span Length

Figure 8.9 presents the comparison of different girder spacings used in the parametric study. Each curve in the figure represents one of the four loading scenarios of the typical bridge. Figure 8.9 has been divided into two components for clarity, each component representing a different analytical technique to determine LLDFs.

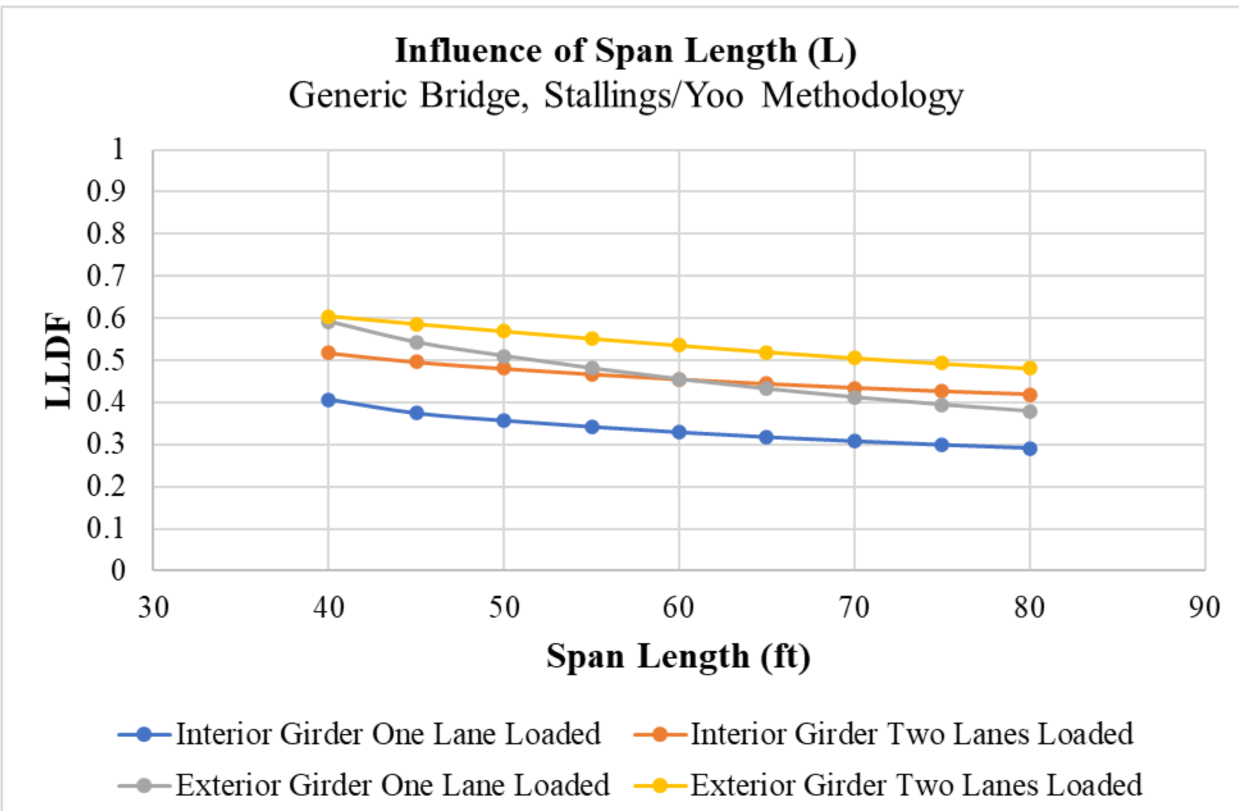

(a)

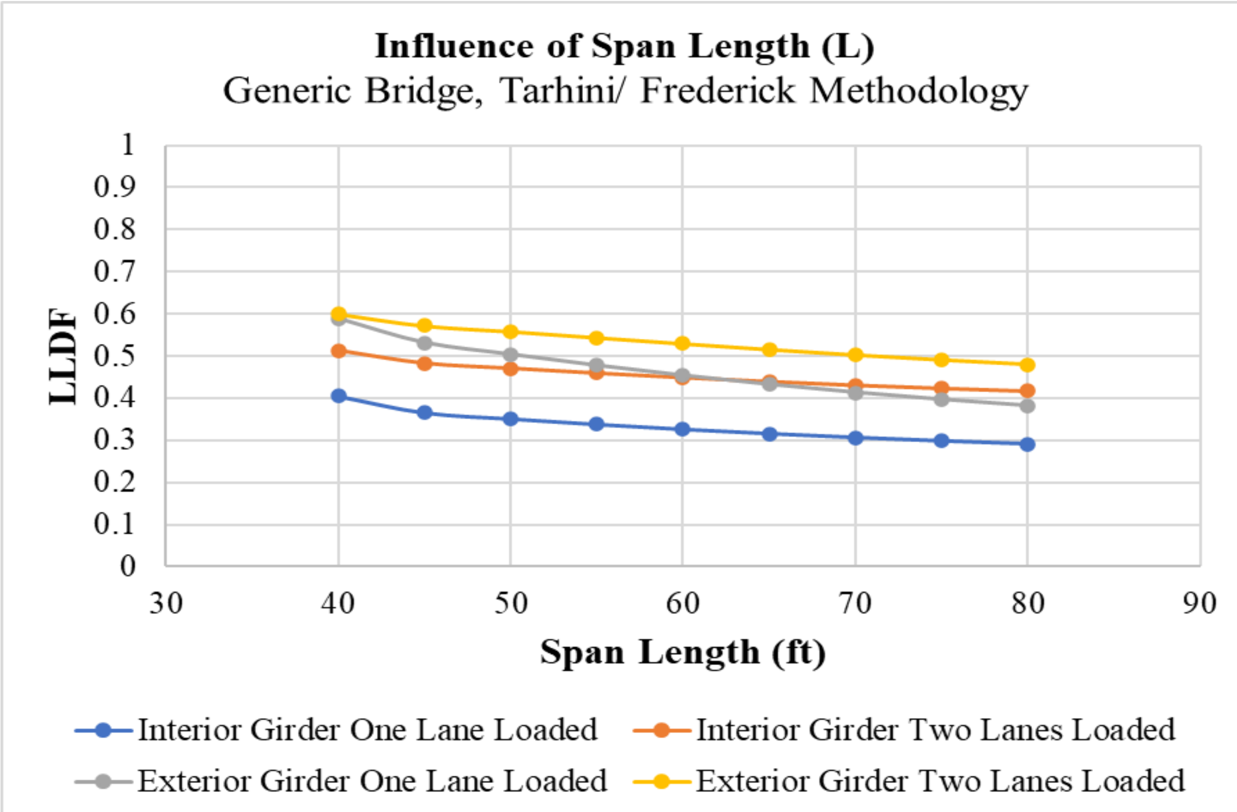

(b)

Figure 8.9: Comparison of the Influence of Span Length using the: (a) Stallings/Yoo Method, (b) Tarhini/Frederick Method

As expected, span length had the same effect in the parametric study as it did in the sensitivity study. A slight difference can be seen in the magnitude of the effect of span length in the applicable range of the girder. The effect appears to be of a slightly more linear nature than found in the sensitivity study. This more linear relationship can be attributed to the larger span ranges where this beam would be utilized and removing the smaller spans were the nonlinearity would be more pronounced. Some amount of nonlinearity does exist, as seen most pronounced in the shorter span ranges when utilizing one-lane loaded scenarios.

8.5.2 Influence of Number of Beams

Figure 8.10 presents the comparison of different numbers of beams used in the parametric study. Each curve in the figure represents one of the four loading scenarios of the typical bridge. Figure 8.10 has been divided into two components for clarity, each component representing a different analytical technique to determine LLDFs.

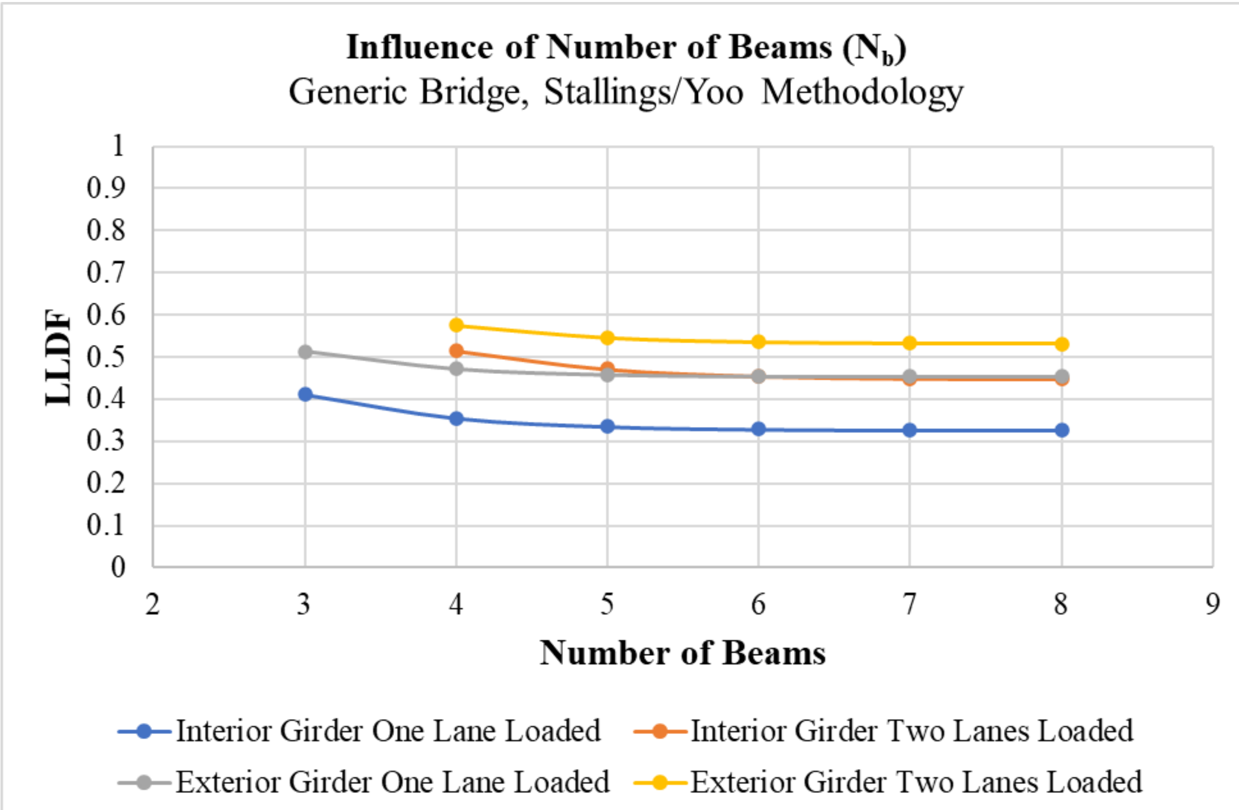

(a)

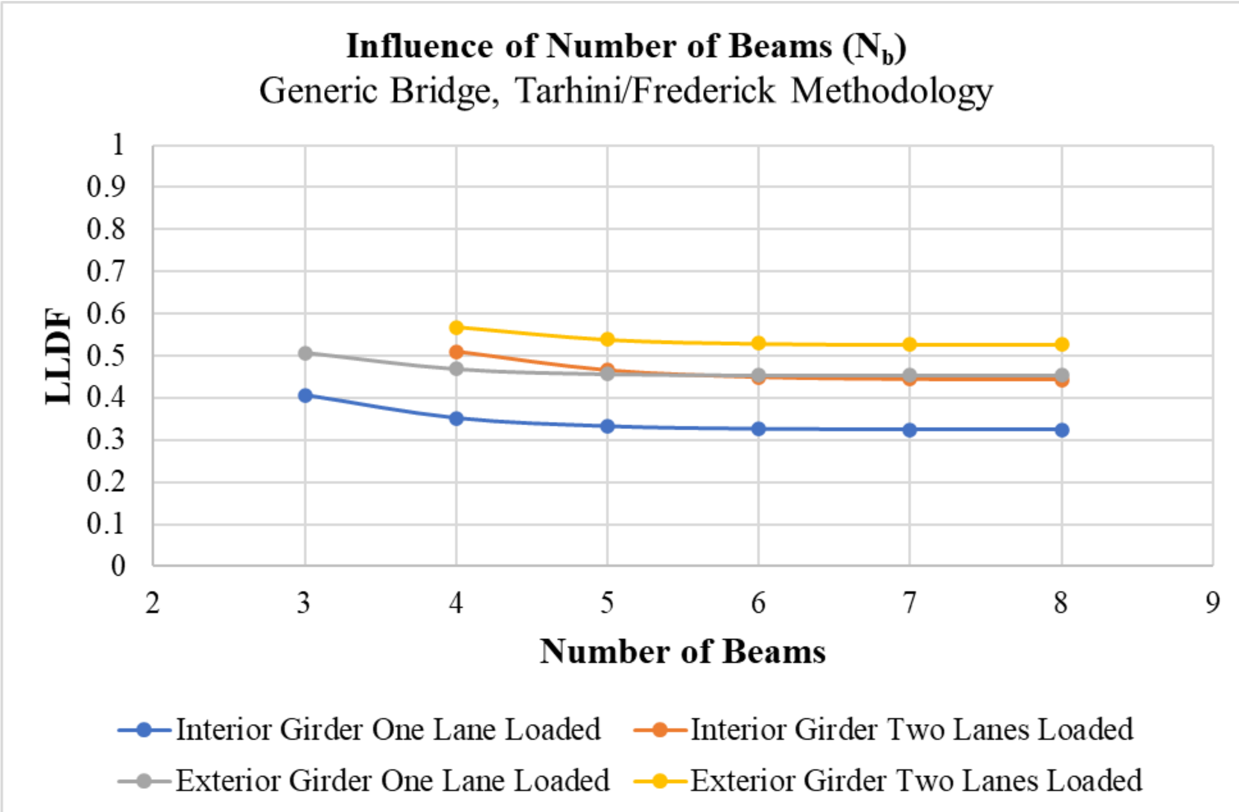

(b)

Figure 8.10: Comparison of the Influence of Number of Beams using the: (a) Stallings/Yoo Method, (b) Tarhini/Frederick Method

As expected, the number of beams had a similar effect in the parametric study as it did in the sensitivity study. The effect of increased number of beams becomes negligible for all types of loading after the bridge contains five beams in the cross-section. The number of beams has a more significant effect for smaller numbers of beams, but it is unlikely typical bridges utilizing PBFTGs will consist of such few main longitudinal members.

8.5.3 Influence of PBFTG Size

Figure 8.11 presents the comparison of different PBFTG sizes used in the parametric study. Each curve in the figure represents one of the four loading scenarios of the typical bridge. Figure 8.11 has been divided into two components for clarity, each component representing a different analytical technique to determine LLDFs. Note, for this generic cross-section, the smallest PBFTG size, the 72 inch by 1/2 inch PBFTG, is not applicable for the generic cross-section.

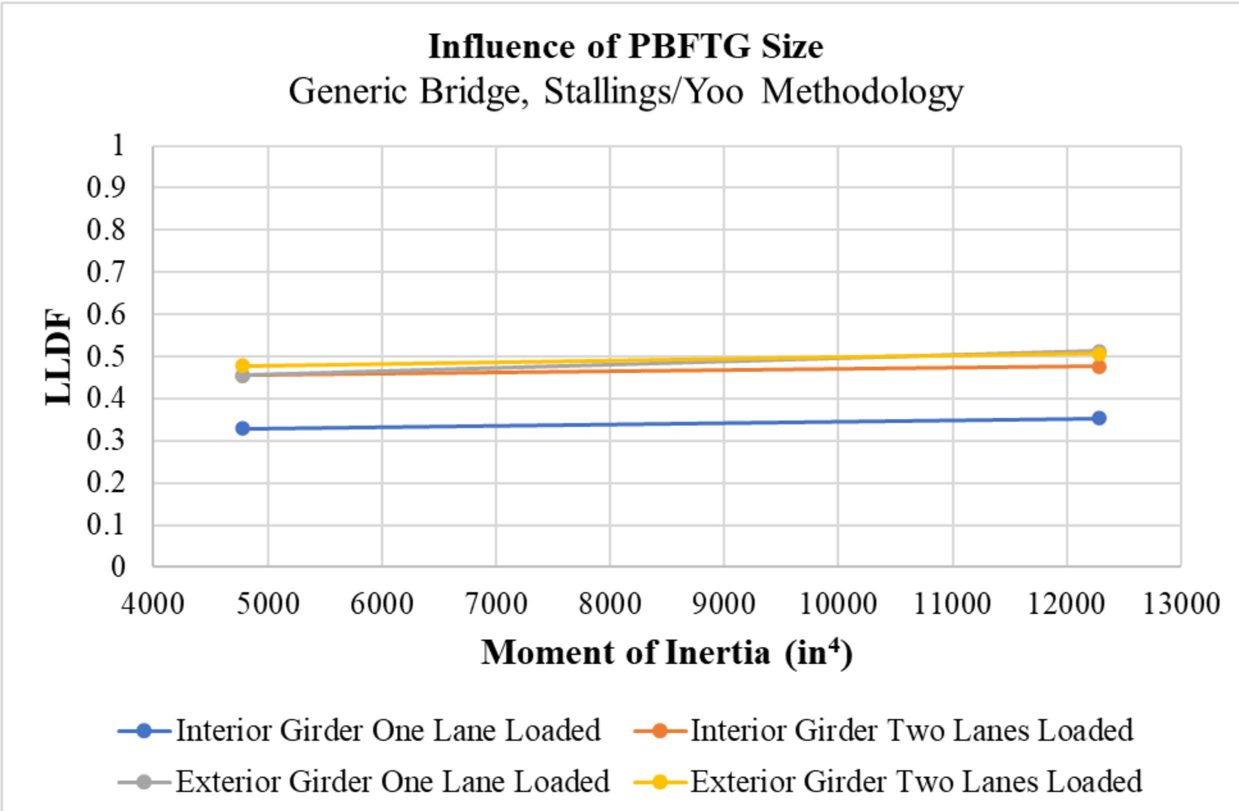

(a)

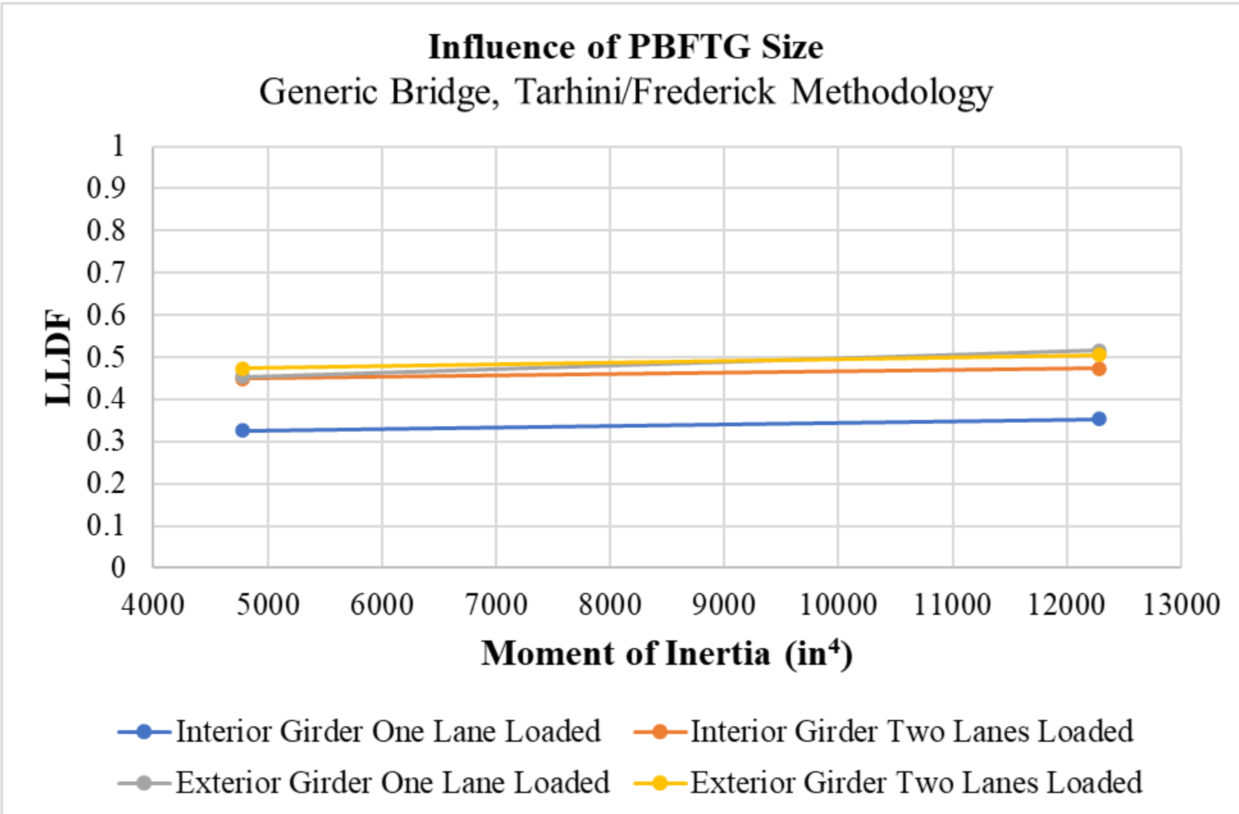

(b)

Figure 8.11: Comparison of the Influence of Girder Size using the: (a) Stallings/Yoo Method, (b) Tarhini/Frederick Method

While the size, and therefore moment of inertia, of PBFTGs does have a slight effect on live load distribution, it is important to remember what these bridges represent. The 96 inch wide by 1/2 inch thick plate is the basis for the bridge used in this comparison. The larger PBFTG, while usable in this instance, would represent an exceptionally conservative design. However, this evaluation may be somewhat difficult to make on its own, as a longitudinal stiffness parameter considering the concrete deck on composite specimens may be a more accurate representation of stiffness when it comes to live load distribution. However, the longitudinal stiffness parameter can be difficult to isolate as it is dependent on girder size, deck thickness, and span length.

8.5.4 Influence of Girder Spacing

Figure 8.12 presents the comparison of different girder spacings used in the parametric study. Each curve in the figure represents one of the four loading scenarios of the typical bridge. Figure 8.12 has been divided into two components for clarity, each component representing a different analytical technique to determine LLDFs.

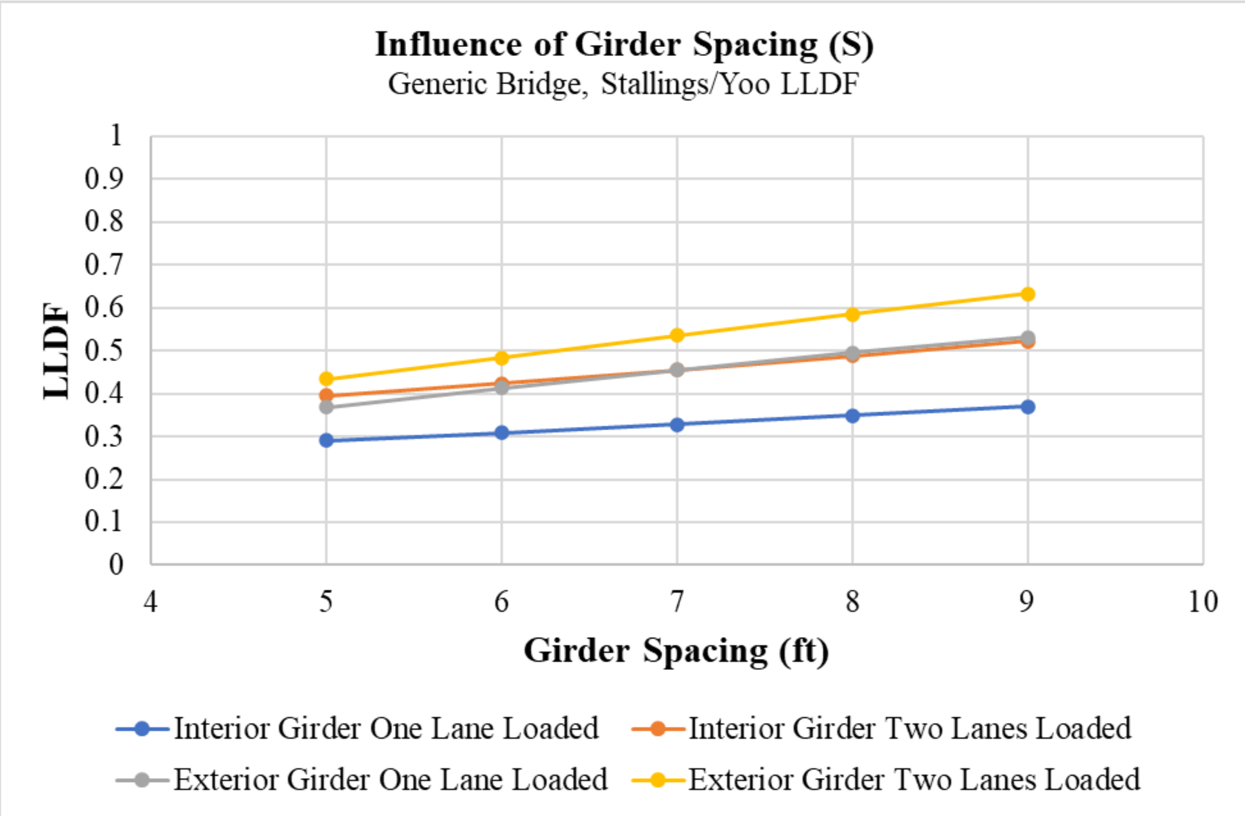

(a)

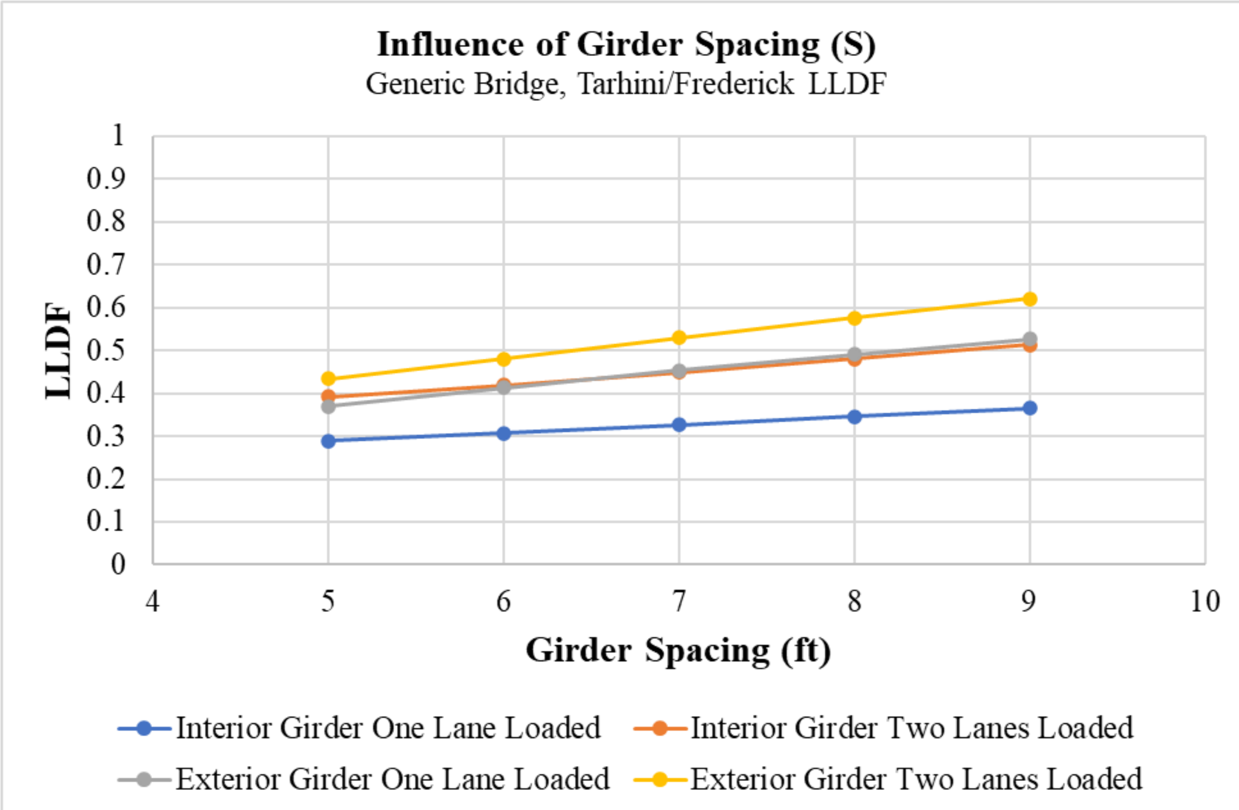

(b)

Figure 8.12: Comparison of the Influence of Girder Spacing using the: (a) Stallings/Yoo Method, (b) Tarhini/Frederick Method

As expected, girder spacing has a similar effect on live load distribution in the parametric study as the sensitivity study. The influence of girder spacing has been verified by numerous other researchers, as noted in Section 3.4.1. Similar to the work performed by Zokaie et al. (1991), this study found girder spacing and span length may be better defined together as an aspect ratio instead of separate parameters.

8.5.5 Influence of Deck Thickness

Figure 8.13 presents the comparison of different deck thicknesses used in the parametric study. Each curve in the figure represents one of the four loading scenarios of the typical bridge.

Figure 8.13 has been divided into two components for clarity, each component representing a different analytical technique to determine LLDFs.

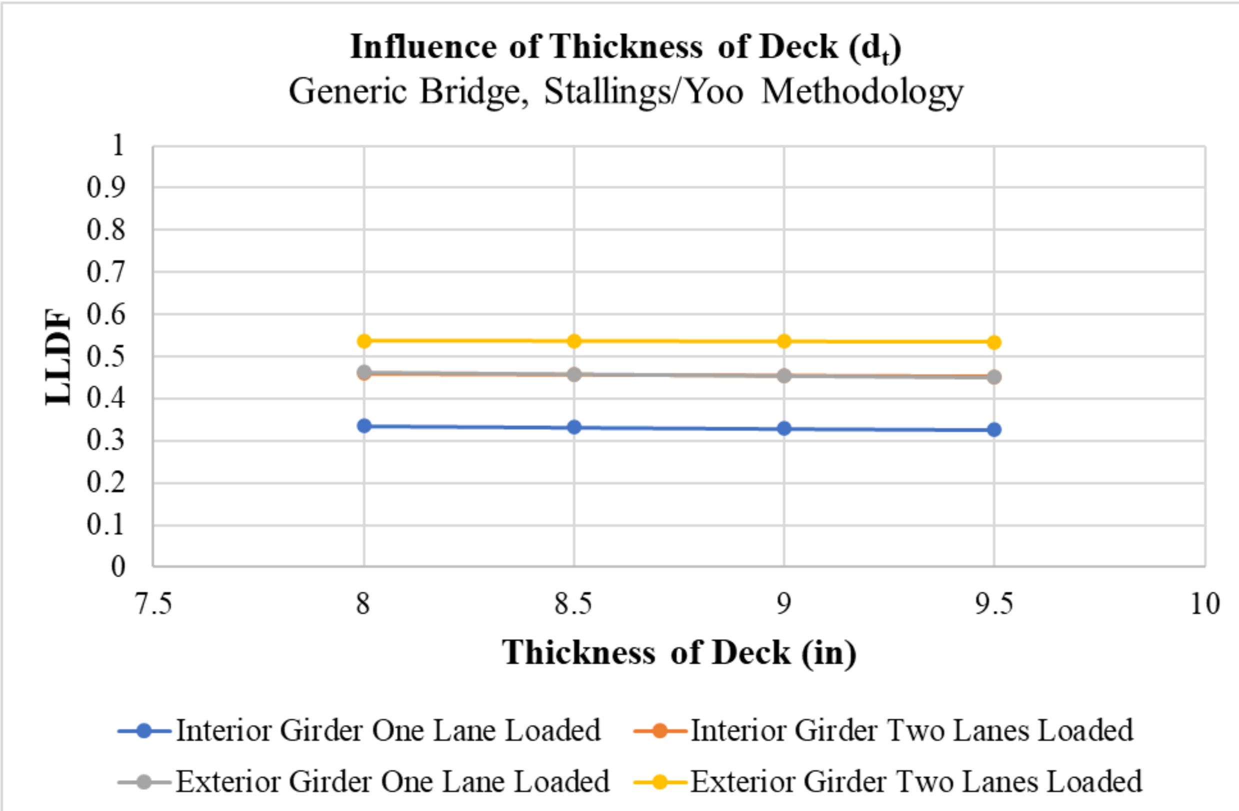

(a)

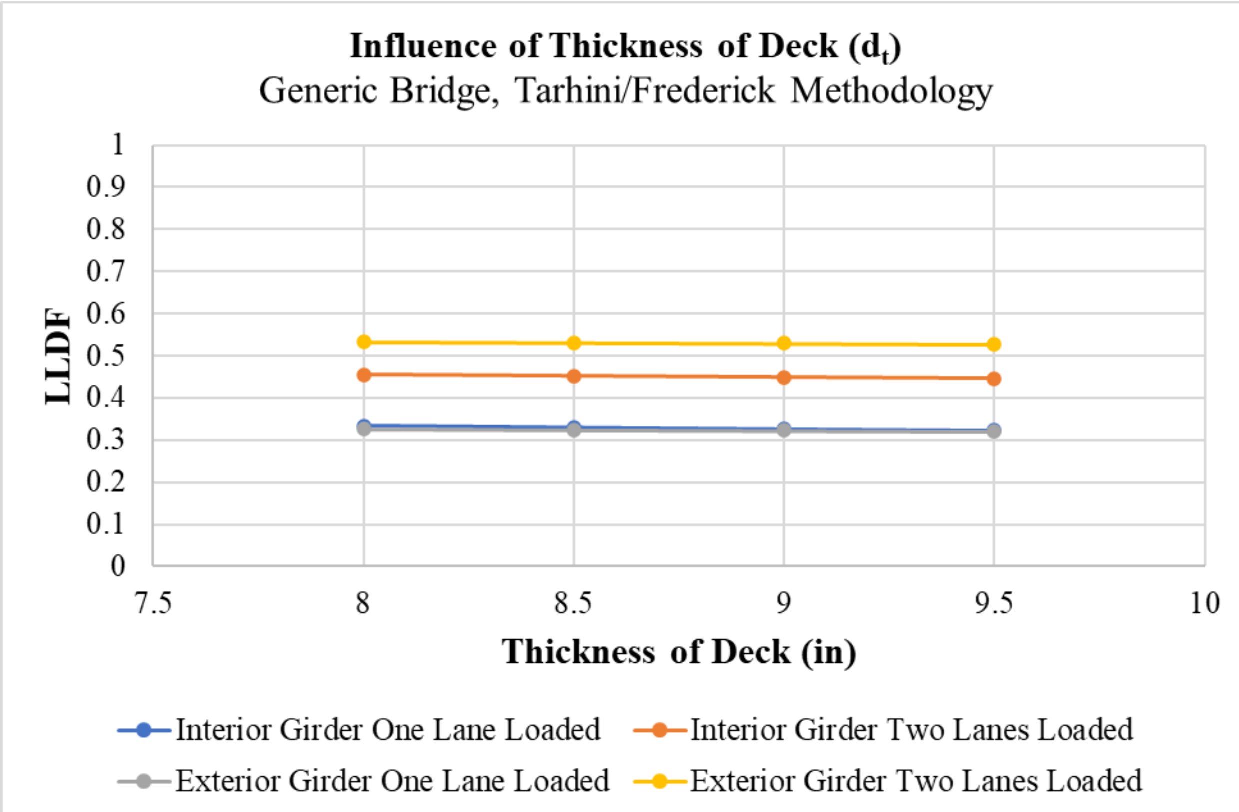

(b)

Figure 8.13: Comparison of the Influence of Thickness of Deck using the: (a) Stallings/Yoo Method, (b) Tarhini/Frederick Method

As expected, deck thickness, on its own, has a negligible effect on the distribution of live load. As stated in Section 8.3.6, as deck thickness is a variable in the longitudinal stiffness, it was deemed appropriate to consider it as a variable when developing LLDFs.

8.5.6 Influence of Edge Distance

Figure 8.14 presents the comparison of different edge distances used in the parametric study. Each curve in the figure represents one of the four loading scenarios of the typical bridge. Figure 8.14 has been divided into two components for clarity, each component representing a different analytical technique to determine LLDFs.

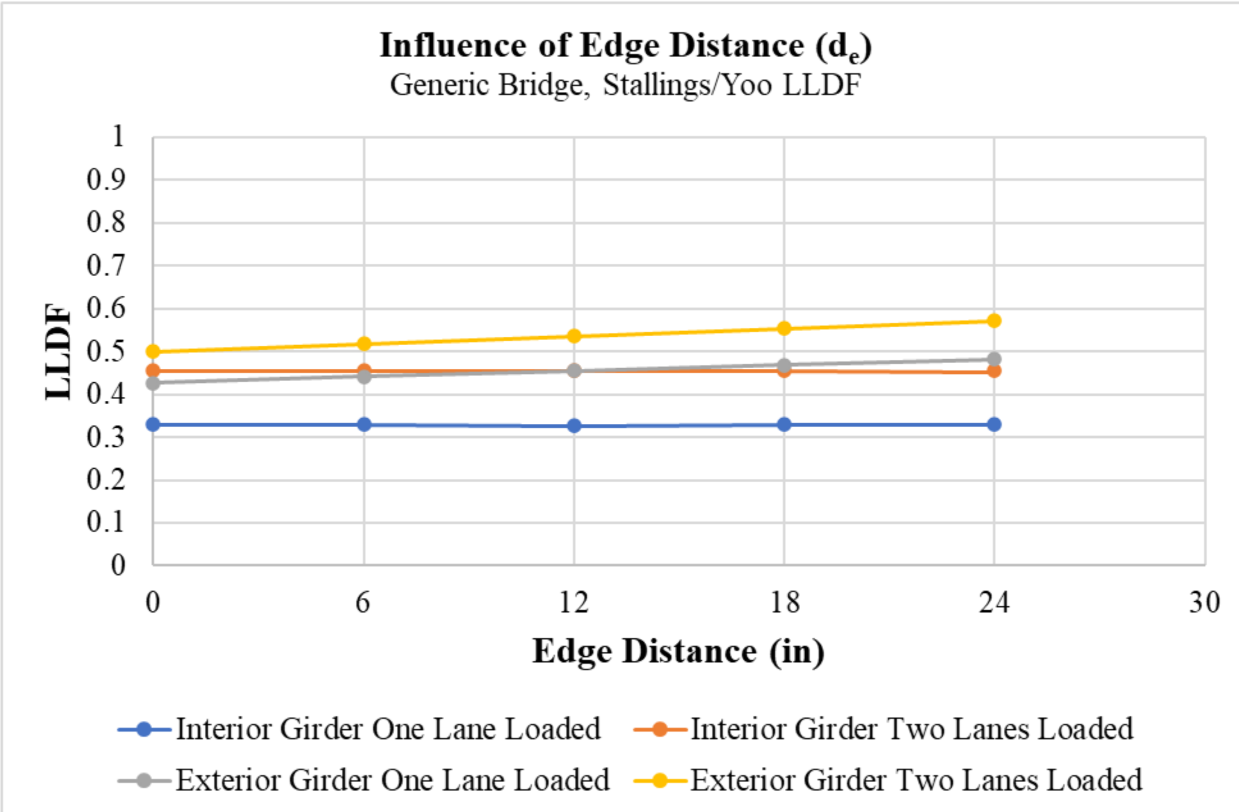
Influence of Edge Distance (d_e)
Generic Bridge, Stallings/Yoo LLDF
LLDF
1
0.9
0.8
0.7
0.6
0.5
0.4
0.3
0.2
0.1
0
0
6
12
18
24
30
Edge Distance (in)
Interior Girder One Lane Loaded
Interior Girder Two Lanes Loaded
Exterior Girder One Lane Loaded
Exterior Girder Two Lanes Loaded

(a)

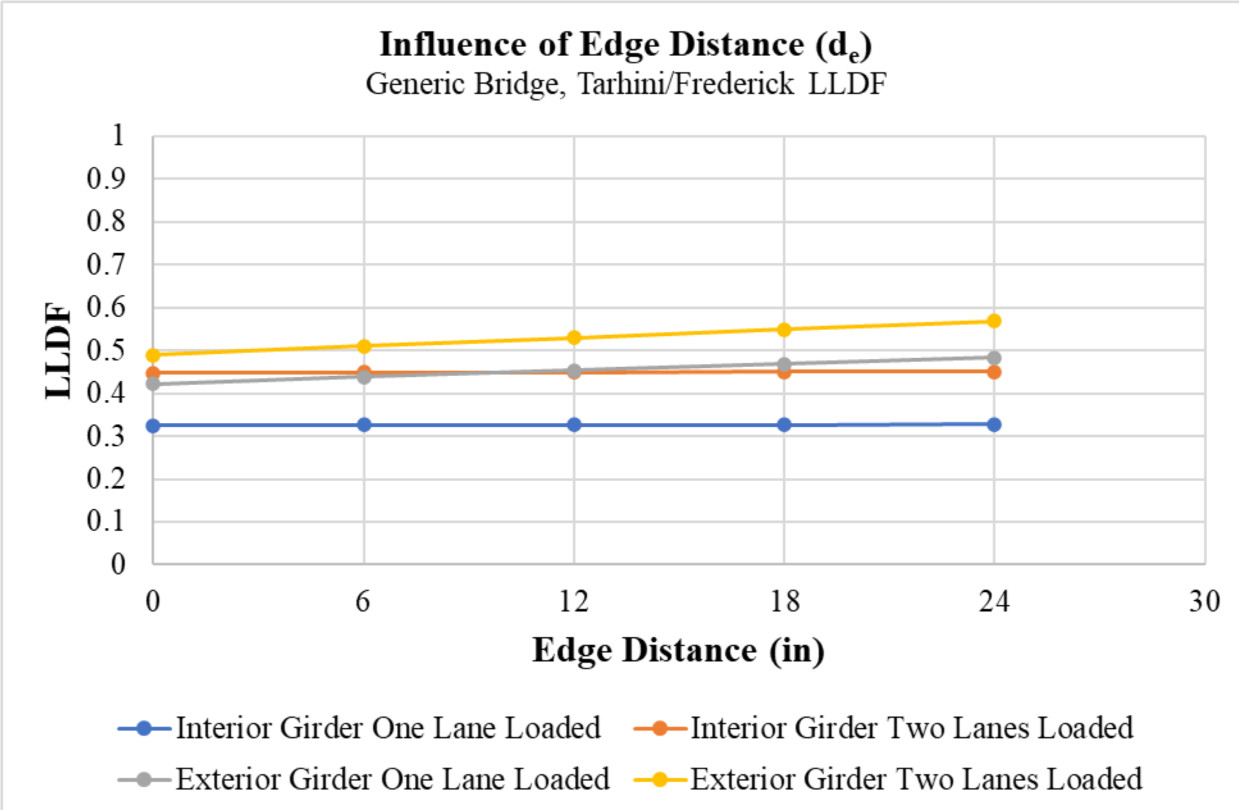

(b)

Figure 8.14: Comparison of the Influence of Edge Distance using the: (a) Stallings/Yoo Method, (b) Tarhini/Frederick Method

As expected, the influence of edge distance is negligible for interior girders but significant for exterior girders. The purpose of the change from overhang ratio to edge distance was to isolate the effect of the parameter. Seen in this manner, the effect of edge distance has a linear relationship with LLDFs of exterior girders. This correlates with the findings of Zokaie et al. (1991) as discussed in Section 3.4.7.

8.6 Development of PBFTG LLDFs

The following section describes the methodology used to develop empirical equations for interior and exterior girder, one or two-lanes loaded, LLDFs for PBFTG bridges. Specifically, a Multiple Linear Regression (MLR) relationship was used to relate the results from the parametric study with the factors found to have the most prominent effect on live load distribution. MLR modeling was used to develop simplified empirical equations for PBFTG LLDFs. MLR is a statistical linear relationship between the dependent variable, the LLDF, and multiple independent variables, the bridge and girder parameters. Finally, the proposed equations and their correlation with the analytically determined LLDFs is presented.

8.6.1 Analytical Computation Technique

The first step to utilizing MLR is to determine which live load distribution methodology will be used to generate LLDFs. The Stallings/Yoo methodology calculates LLDFs for each girder in the cross-section by dividing the maximum bending strain of the girder in question by the sum of the maximum bending strains in every girder in the cross-section. The Tarhini/Frederick methodology calculates LLDFs for each girder by dividing the maximum bending strain calculated using three-dimensional FEA by the maximum bending strain calculated using LGA. The Tarhini/Frederick methodology was chosen due to lack of dependence on the strains and stresses of other girders and its use of LGA similar to methodologies found in the AASHTO LRFD BDS.

8.6.2 Methodology

As previously stated, MLR represents a linear relationship between a dependent variable, such as the Tarhini/Frederick LLDF, and multiple independent variables, such as key bridge parameters. To apply MLR, a model representing the relationship between the dependent and independent variables must be defined. This linear model is expressed in Equation 8.1:

$$y_i = c_0 + c_1 x_{i1} + c_2 x_{i2} + \cdots + c_k x_{ik} \qquad \text{Eq. 8.1}$$

Where:

y = dependent variable

x = independent variable

c = constant coefficients

i = number of samples

k = number of independent variables

For equations with more than one independent variable, the curve fitting process becomes more difficult. To overcome this difficulty, matrices are used to define the regression model and the subsequent analysis. As the relationship between the LLDF and key bridge parameters is not necessarily linear, and the use of the proposed equation in the AASHTO LRFD BDS is desirable, a model for the LLDF resembling those equations already in the AASHTO LRFD BDS was adopted as a working model. This model assumption was verified, as the parameters present in the AASHTO LRFD BDS for I-girder LLDFs were also the parameters found to have the most significant impact on PBFTG LLDFs. Therefore, the format for interior I-girder LLDFs form the basis of the equation as expressed in Equation 8.2.

$$g = c_0(x_1)^{c_1}(x_2)^{c_2}(x_3)^{c_3} \qquad \text{Eq. 8.2}$$

As the MLR is applied to a linear model, opposed to the power model shown by Equation 8.2, the natural logarithm was applied to both sides of the equation as demonstrated by Equation 8.3 and simplified into Equation 8.4.

$$\ln(g) = \ln(c_0(x_1)^{c_1}(x_2)^{c_2}(x_3)^{c_3}) \qquad \text{Eq. 8.3}$$

$$\ln(g) = \ln(c_0) + c_1\ln(x_1) + c_2\ln(x_2) + c_3\ln(x_3) \qquad \text{Eq. 8.4}$$

When applying Equation 8.4 for *k* number of bridges, the linear equation can be formulated in matrix format, as seen in Equation 8.5.

$$\begin{bmatrix} y_1 \\ y_2 \\ \vdots \\ y_k \end{bmatrix} = \begin{bmatrix} x_{11} & x_{12} & x_{13} \\ x_{21} & x_{22} & x_{23} \\ \vdots & \vdots & \vdots \\ x_{k1} & x_{k2} & x_{k3} \end{bmatrix} \begin{bmatrix} c_1 \\ c_2 \\ c_3 \end{bmatrix} \qquad \text{Eq. 8.5}$$

The matrices used in Equation 8.5 can be simplified into Equation 8.6:

$$\boldsymbol{Y} = \boldsymbol{XC} \qquad \text{Eq. 8.6}$$

After generating the above matrices, MLR was employed using the least square approximation procedure from Strang (2016). Strang states the solution to Equation 8.6 is expressed as Equation 8.7:

$$\boldsymbol{C} = (\boldsymbol{X}^{\boldsymbol{T}}\boldsymbol{X})^{-\boldsymbol{1}}\boldsymbol{X}^{\boldsymbol{T}}\boldsymbol{Y} \qquad \text{Eq. 8.7}$$

Following the determination of the coefficients to the above equations, the coefficients were rounded to the number of significant figures found in the AASHTO LRFD BDS simplified equations. Another constant was added to the determined equations to shift the confidence interval to where nearly 100% of LLDFs generated using the proposed equations would result in conservative designs.

8.6.3 Proposed Equations

Using the key parameters found to have the most significant impact in the parametric study, including girder spacing, longitudinal stiffness, thickness of slab, and edge distance, the simplest combination of these variables producing the most accurate equations was determined. The accuracy of these equations was measured using the coefficient of multiple determination, or R^2, which is a numerical index reflecting the variation of the dependent variable with respect to two or more independent variables. Low values indicate the dependent variable is relatively unrelated to the independent variables, where high values corelate to high degrees of relation.

After analyzing the results of multiple combinations of parameters, Equations 8.8 through 8.11 were proposed to calculate LLDFs for PBFTG bridges.

For interior girders with one-lane loaded:

$$g = 0.08 + \left(\frac{S}{384}\right)^{0.1}\left(\frac{S}{L}\right)^{0.3}\left(\frac{K_g}{12.0Lt_s}\right)^{0.1} \qquad \text{Eq. 8.8}$$

For interior girders with two-lanes loaded:

$$g = 0.13 + \left(\frac{S}{27}\right)^{0.3} \left(\frac{S}{L}\right)^{0.2} \left(\frac{K_g}{12.0Lt_s}\right)^{0.1} \quad \text{Eq. 8.9}$$

For exterior girders with one-lane loaded:

$$g = 0.09 + \left(1.07 + \frac{d_e}{11.3}\right) g_{int} \quad \text{Eq. 8.10}$$

For exterior girders with two-lanes loaded:

$$g = 0.08 + \left(0.86 + \frac{d_e}{13.3}\right) g_{int} \quad \text{Eq. 8.11}$$

Where:

g = LLDF for corresponding girder and number of loaded lanes

S = girder spacing

L = span length

K_g = longitudinal stiffness parameter

t_s = slab thickness

d_e = edge distance

g_{int} = LLDF for the interior girder for the corresponding number of loaded lanes

These equations exhibit good correlation between the key parameters identified in the parametric study and the proposed simplified LLDF equations. For Equation 8.8, the resulting R^2 value was 0.915; for Equation 8.9, the resulting R^2 value was 0.801; for Equation 8.10, the resulting R^2 value was 0.921; and for Equation 8.11, the resulting R^2 value was 0.838. These R^2 values indicate these equations are fairly accurate in determining PBFTG LLDFs.

8.7 Comparison of Proposed Equations with AASHTO LRFD BDS Simplified Equations

In this section, comparisons are made between the proposed LLDF equations for PBFTG bridges with existing methodologies present in the AASHTO LRFD BDS. For this purpose, each of the proposed LLDFs, dependent on the girder being maximized and the number of loaded lanes, will be compared against lever rule, Special Analysis, if applicable, the LLDF for I-girders, and the LLDF for box-shaped girders. The details about each moment LLDF equation and their comparison to the proposed LLDF equation will be presented in the following subsections.

8.7.1 Applicable AASHTO LRFD BDS Live Load Distribution Methods

The lever rule methodology for calculating LLDFs involves summing moments about one girder line to find the reaction at another girder line, assuming the supported components are hinged at an interior support. The provisions of AASHTO LRFD BDS Article 3.6.1.1.1, regarding placement of the design lanes and the wheel lines within those lanes, should be followed when utilizing lever rule. It is important to include the applicable multiple presence factor to the LLDF calculated using lever rule when considering the strength and service limit states.

While not directly applicable to most PBFTG bridges, another LLDF methodology regularly used for exterior girder LLDFs from the AASHTO LRFD BDS is Special Analysis. Special Analysis is discussed in AASHTO LRFD BDS Article C4.6.2.2.2d and is used for steel bridge cross-sections with cross-frames or diaphragms. The LLDF for exterior girders is not to be taken as less than that which would be obtained by assuming the cross-section deflects and rotates as a rigid cross-section (Grubb et al., 2020). This methodology is included in the AASHTO LRFD BDS because it was found the simplified LLDF equations for moment were determined without consideration of cross-frames and are generally unconservative for exterior girders. Exterior girder LLDFs can be calculated by using Equation 8.12. As with lever rule, the provisions of AASHTO LRFD BDS Article 3.6.1.1.1 and the applicable multiple presence factors should be utilized.

$$R = \frac{N_L}{N_b} + \frac{X_{ext}\sum_1^{N_L} e}{\sum_1^{N_b} x^2} \qquad \text{Eq. 8.12}$$

Where:

R = reaction on exterior beam in terms of lanes

N_L = number of loaded lanes under consideration

e = eccentricity of a design truck or a design lane load from the center of gravity of the pattern of girders

x = horizontal distance from the center of gravity of the pattern of girder to each girder

X_{ext} = horizontal distance from the center of gravity of the pattern of girders to the exterior girder

N_b = number of beams or girders

As discussed in Chapter 3, more complex LLDF equations were developed in the 1980s and 1990s to more accurately represent live load distribution compared to the previous S/D equations found in the AASHTO Standard Specifications. LLDFs found in the AASHTO LRFD BDS were modified from the research performed by Zokaie et al. (1991) to consider the multiple presence factor. Another difference between LLDFs in the AASHTO LRFD BDS and the AASHTO Standard Specification is that the modern LLDFs are now expressed in units of lanes rather than wheel lines.

The LLDF equation for bending moment in interior beams or girders with a concrete deck made composite with a steel beam with one design lane loaded is expressed by Equation 8.13, as found in AASHTO LRFD BDS Table 4.6.2.2.2b-1. However, to use this equation, a multitude of requirements must be met, which all bridges analyzed in the parametric study met. Another important note is that the I-girder equation is being compared against the proposed equation because the format of the I-girder equation is similar to the proposed equations. Additionally, when the cross-section consists of three longitudinal elements, the designer should use the lesser value of Equation 8.13 or lever rule.

$$g_{IG\ OLL} = 0.06 + \left(\frac{S}{14}\right)^{0.4} \left(\frac{S}{L}\right)^{0.3} \left(\frac{K_g}{12.0Lt_s^3}\right)^{0.1} \qquad \text{Eq. 8.13}$$

Where:

$g_{IG\ OLL}$ = LLDF for an interior girder with one-lane loaded

S = spacing of beams or webs

L = span length of beam

K_g = longitudinal stiffness parameter

t_s = depth of concrete slab

The LLDF equation for bending moment in interior beams or girders with a concrete deck made composite with a steel beam with two or more design lanes loaded is expressed by Equation 8.14, as found in AASHTO LRFD BDS Table 4.6.2.2.2b-1. Additionally, when the cross-section consists of three longitudinal elements, the designer should use the lesser value of Equation 8.14 or lever rule.

$$g_{IG\ 2LL} = 0.075 + \left(\frac{S}{9.5}\right)^{0.6} \left(\frac{S}{L}\right)^{0.2} \left(\frac{K_g}{12.0Lt_s^3}\right)^{0.1} \qquad \text{Eq. 8.14}$$

Where:

$g_{IG\ 2LL}$ = LLDF for an interior girder with two-lanes loaded

S = spacing of beams or webs

L = span length of beam

K_g = longitudinal stiffness parameter

t_s = depth of concrete slab

The LLDF equation for bending moment in exterior beams or girders with a concrete deck made composite with a steel beam with one design lane loaded is expressed using lever rule for bridge cross-sections containing three or more longitudinal elements. The LLDF equation for bending moment in exterior beams or girders with a concrete deck made composite with a steel beam with two or more design lanes loaded is expressed by Equation 8.15, which is a modified version of the equation found in AASHTO LRFD BDS Table 4.6.2.2.2d-1. It should be noted the LLDF for two or more lanes loaded is dependent on the LLDF for the same bridge but for the interior girder. The overhang distance in Equation 8.15 shall be taken as positive if the exterior web is inside the interior face of the parapet and negative if the exterior web is outside the interior face of the parapet. Additionally, when the cross-section consists of three longitudinal elements, the designer should use the lesser value of Equation 8.15 or lever rule.

$$g_{EG\ 2LL} = \left(0.77 + \frac{d_e}{9.1}\right) g_{IG\ 2LL} \qquad \text{Eq. 8.15}$$

Where:

$g_{EG\ 2LL}$ = LLDF for an exterior girder with two-lanes loaded

d_e = horizontal distance from the centerline of the exterior web or exterior beam at deck level to the interior edge of curb or traffic barrier

$g_{IG\ OLL}$ = LLDF for an interior girder with two-lanes loaded

The LLDF equation for bending moment in all beams or girders with a concrete deck made composite with multiple steel box-girders, regardless of the number of loaded lanes, is expressed by Equation 8.16, as found in AASHTO LRFD BDS Table 4.6.2.2.2b-1. Note, not all bridges in the parametric study meet the range of applicability as expressed in Equation 8.17. Additionally, not all bridges in the parametric study meet the special restrictions on the use of LLDFs discussed in AASHTO LRFD BDS Article 6.11.2.3. All bridges in the parametric study were assumed to meet the restrictions to allow comparisons against the proposed equations. If the restrictions specified in the AASTHO LRFD BDS are not met, the designer must utilize a more refined analysis.

$$0.05 + 0.85\frac{N_L}{N_b} + \frac{0.425}{N_L} \qquad \text{Eq. 8.16}$$

$$0.5 \leq \frac{N_L}{N_b} < 1.5 \qquad \text{Eq. 8.17}$$

Where:

N_L = number of design lanes as specified in AASHTO LRFD BDS Article 3.6.1.1.1

N_b = number of girders

8.7.2 Interior Girder One-Lane Loaded LLDFs

The comparisons of the equations and methodologies found in the AASHTO LRFD BDS for LLDFs for interior girder one-lane loaded scenarios is presented in Figure 8.15 and Table 8.2. The comparison revealed the proposed moment LLDF equation more accurately predicts LLDFs than those of any other LLDF methodology or equation present in the AASHTO LRFD BDS. These comparisons serve to verify the applicability of the equation for use in PBFTG bridges.

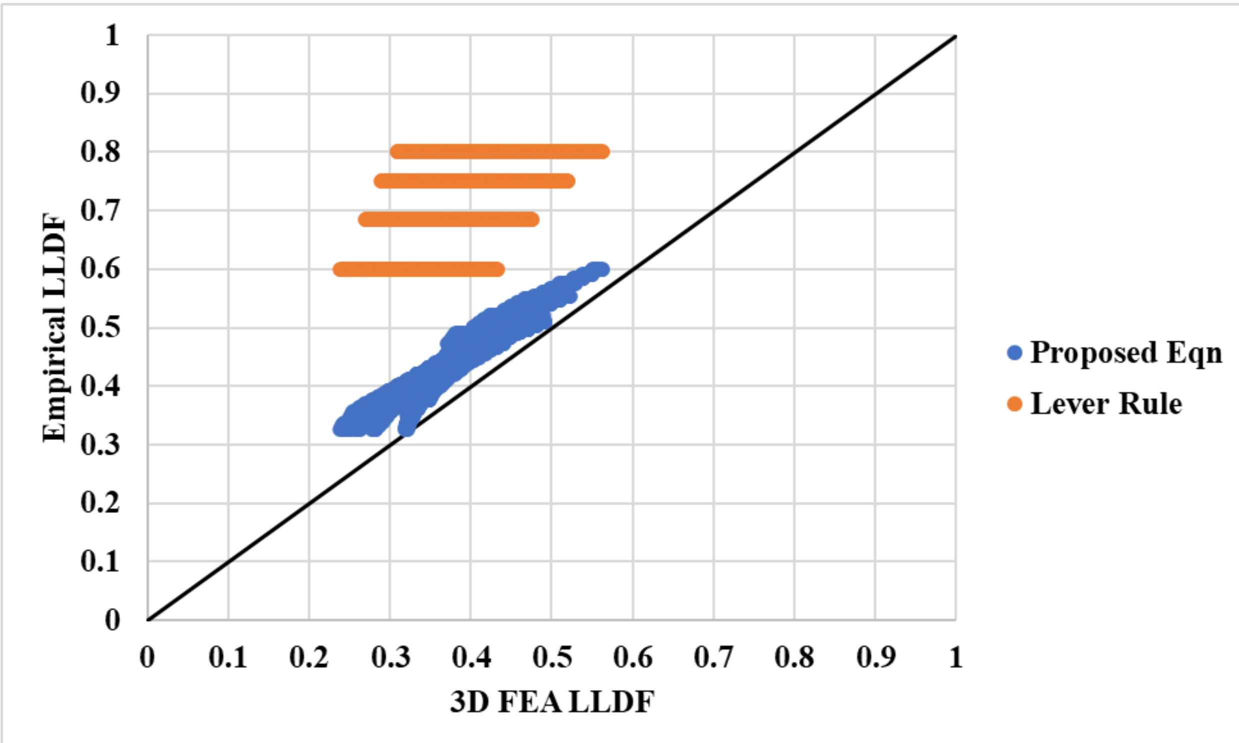

(a)

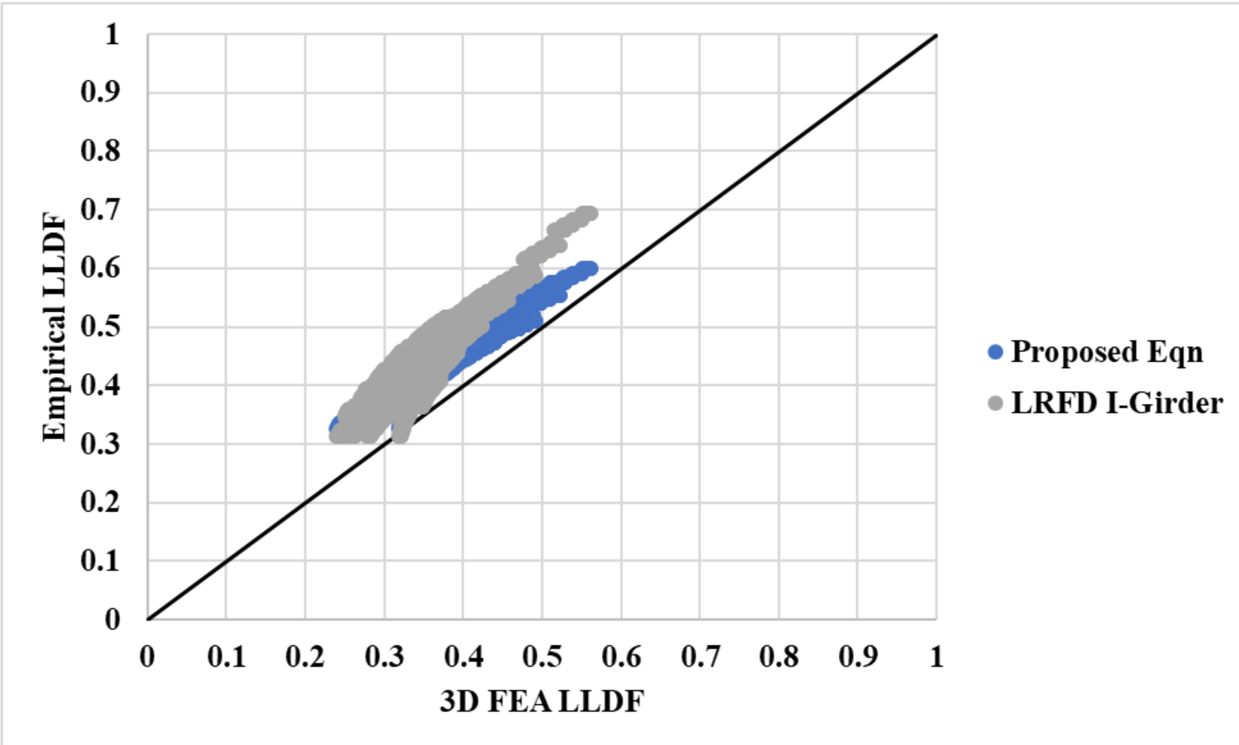

1
0.9
0.8
0.7
0.6
0.5
0.4
0.3
0.2
0.1
0
Empirical LLDF
0
0.1
0.2
0.3
0.4
0.5
0.6
0.7
0.8
0.9
1
3D FEA LLDF
Proposed Eqn
LRFD I-Girder

(b)

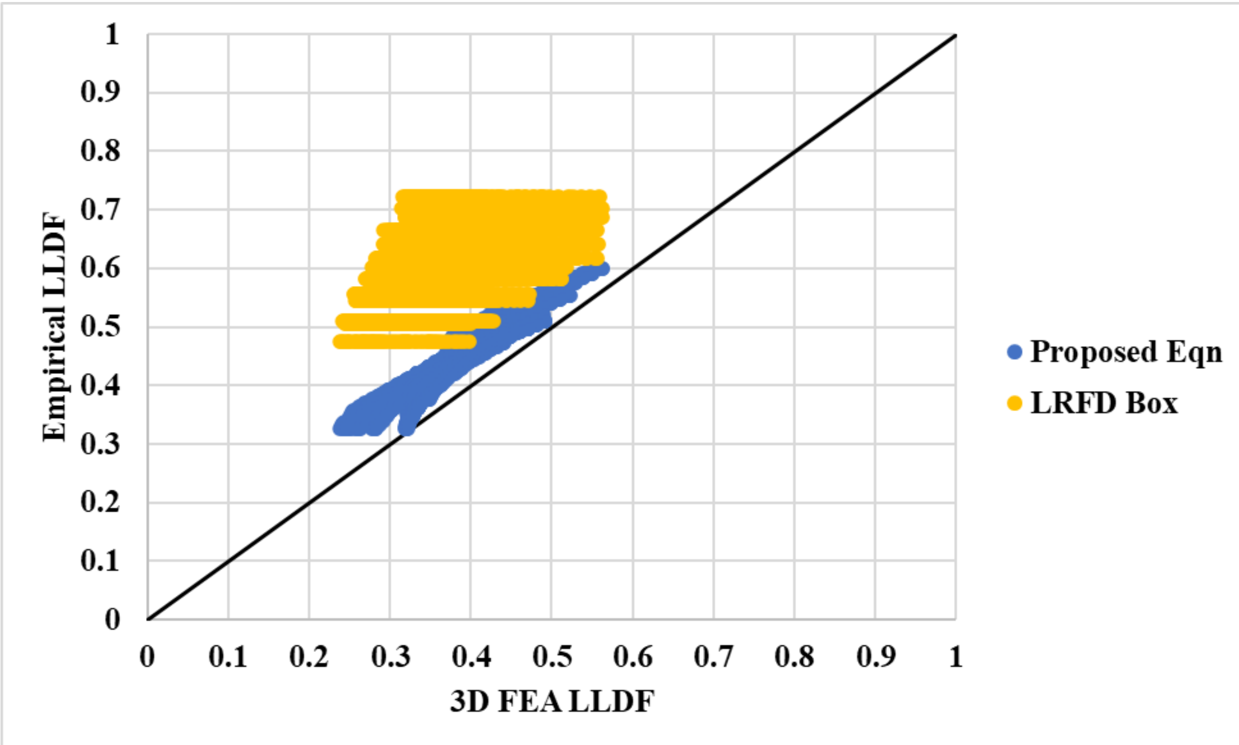

(c)

Figure 8.15: Correlation Between Proposed LLDF Equation for Interior Girders with One-Lane Loaded with: (a) Lever Rule, (b) I-Girder Equation, and (c) Box-Girder Equation

Table 8.2: Interior Girder One-Lane Loaded Statistical Analysis

Interior Girder One Lane Loaded				
LLDF Methodology	Proposed Eq.	Lever Rule	I-Girder Eq.	Box-Girder Eq.
Max Overestimation	0.11	0.49	0.15	0.41
Min Overestimation/Max Underestimation(*)	0.00	0.17	0.01*	0.06
Average	0.07	0.34	0.09	0.26
Standard Deviation	0.016	0.070	0.027	0.062

8.7.3 Interior Girder Two-Lanes Loaded LLDFs

The comparisons of the equations and methodologies found in the AASHTO LRFD BDS for LLDFs for interior girder two-lanes loaded scenarios is presented in Figure 8.16 and Table 8.3. The comparison revealed the proposed moment LLDF equation more accurately predicts LLDFs than those of any other LLDF methodology or equation present in the AASHTO LRFD BDS. These comparisons serve to verify the applicability of the equation for use in PBFTG bridges.

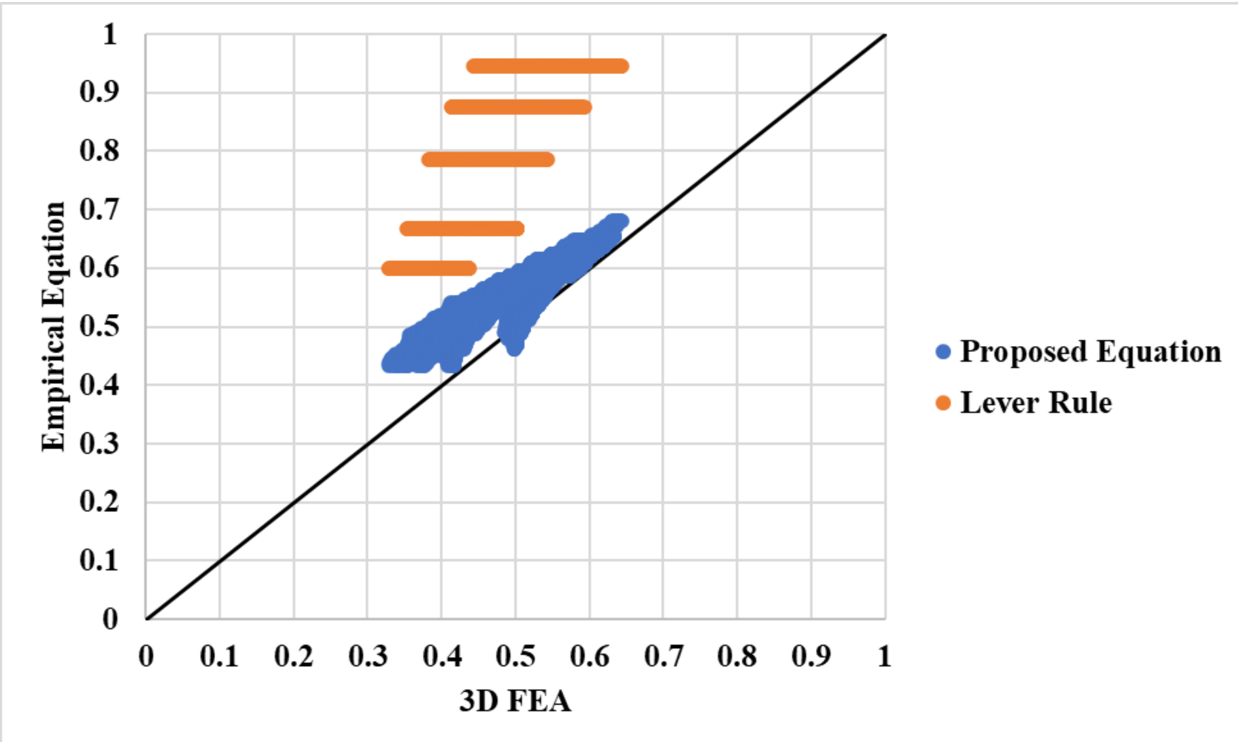

(a)

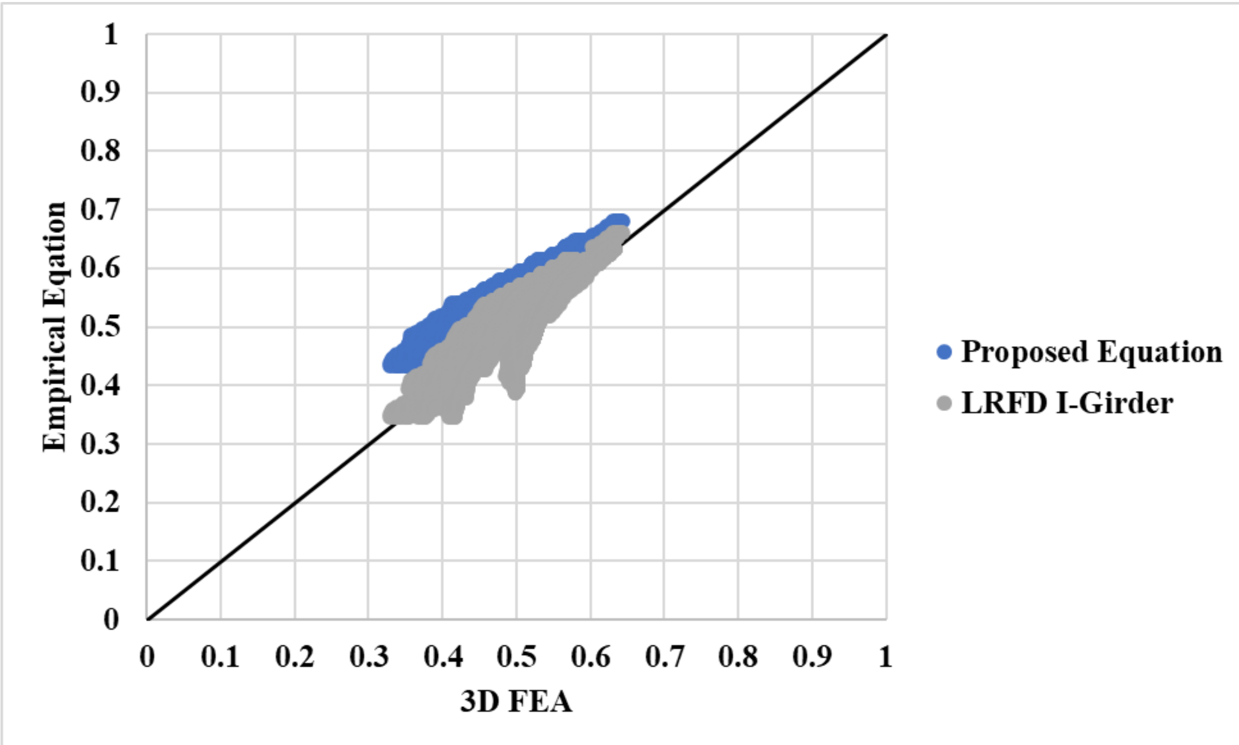

1
0.9
0.8
0.7
0.6
0.5
0.4
0.3
0.2
0.1
0
Empirical Eqation
0
0.1
0.2
0.3
0.4
0.5
0.6
0.7
0.8
0.9
1
3D FEA
Proposed Equation
LRFD I-Girder

(b)

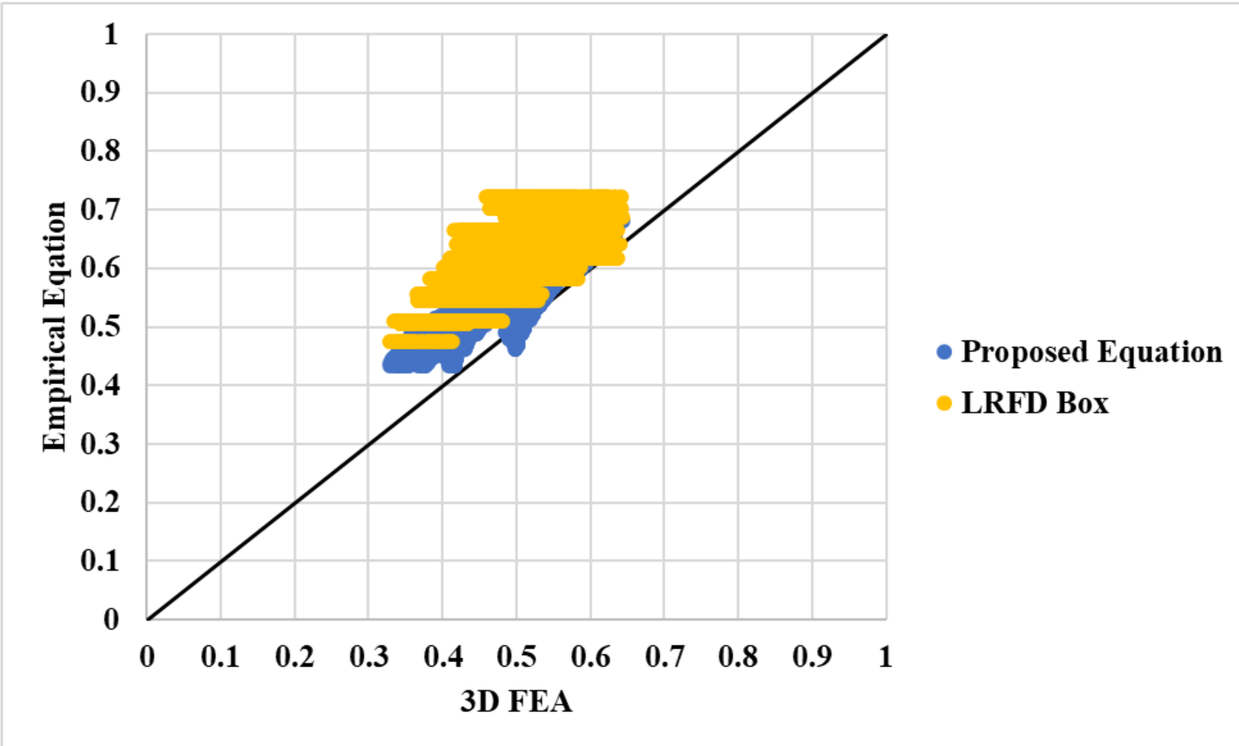

(c)

Figure 8.16: Correlation Between Proposed LLDF Equation for Interior Girders with Two-Lanes Loaded with: (a) Lever Rule, (b) I-Girder Equation, and (c) Box-Girder Equation

Table 8.3: Interior Girder Two-Lanes Loaded Statistical Analysis

Interior Girder Two Lanes Loaded				
LLDF Methodology	Proposed Eq.	Lever Rule	I-Girder Eq.	Box-Girder Eq.
Max Overestimation	0.13	0.50	0.08	0.26
Min Overestimation/Max Underestimation(*)	0.04*	0.16	0.11*	0.02
Average	0.07	0.32	0.01	0.13
Standard Deviation	0.028	0.084	0.030	0.043

8.7.4 Exterior Girder One-Lane Loaded LLDFs

The comparisons of the equations and methodologies found in the AASHTO LRFD BDS for LLDFs for exterior girder one-lane loaded scenarios is presented in Figure 8.17 and Table 8.4. The comparison revealed the proposed moment LLDF equation more accurately predicts LLDFs than those of any other LLDF methodology or equation present in the AASHTO LRFD BDS. These comparisons serve to verify the applicability of the equation for use in PBFTG bridges.

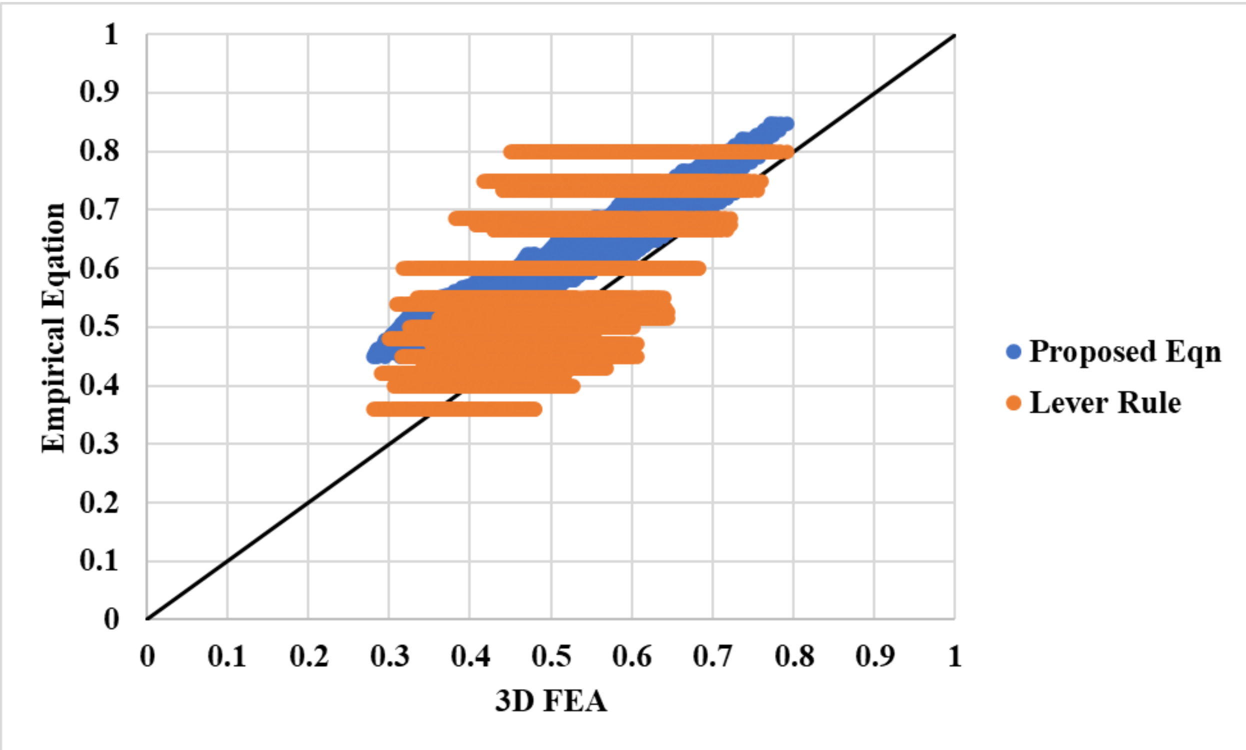

(a)

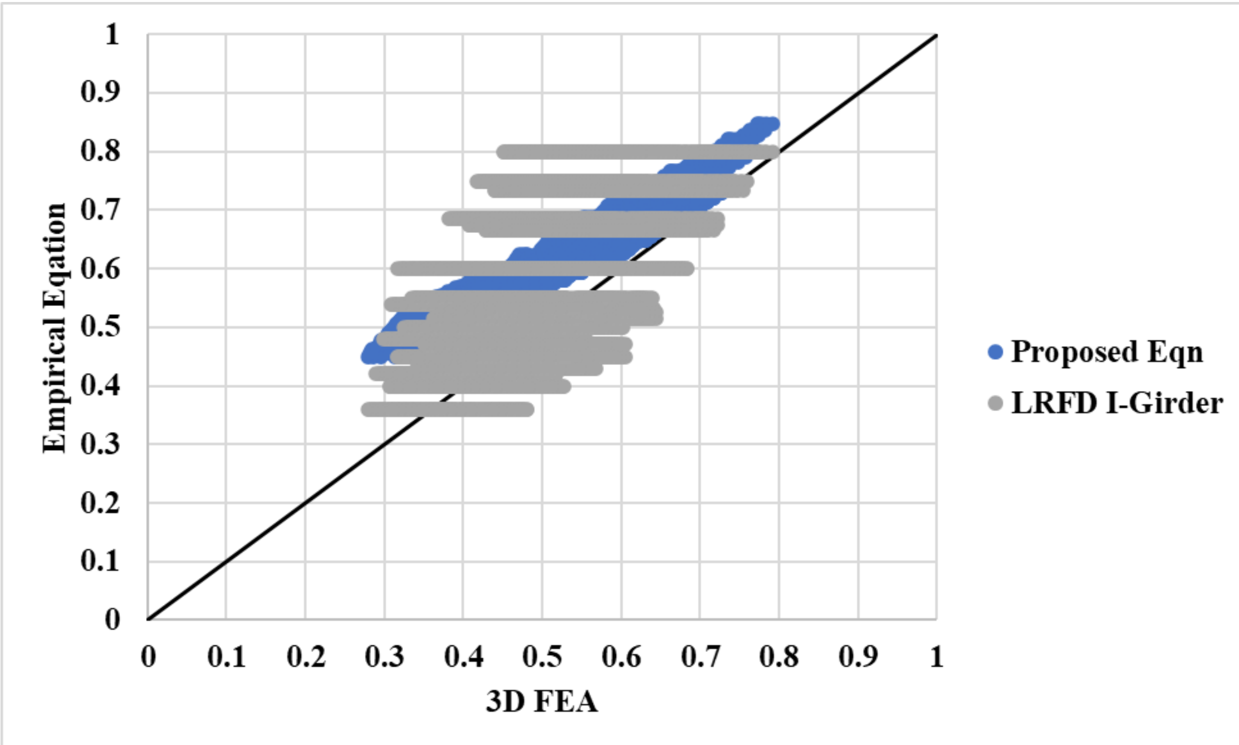
1
0.9
0.8
0.7
0.6
0.5
0.4
0.3
0.2
0.1
0
Empirical Eqation
0
0.1
0.2
0.3
0.4
0.5
0.6
0.7
0.8
0.9
1
3D FEA
Proposed Eqn
LRFD I-Girder

(b)

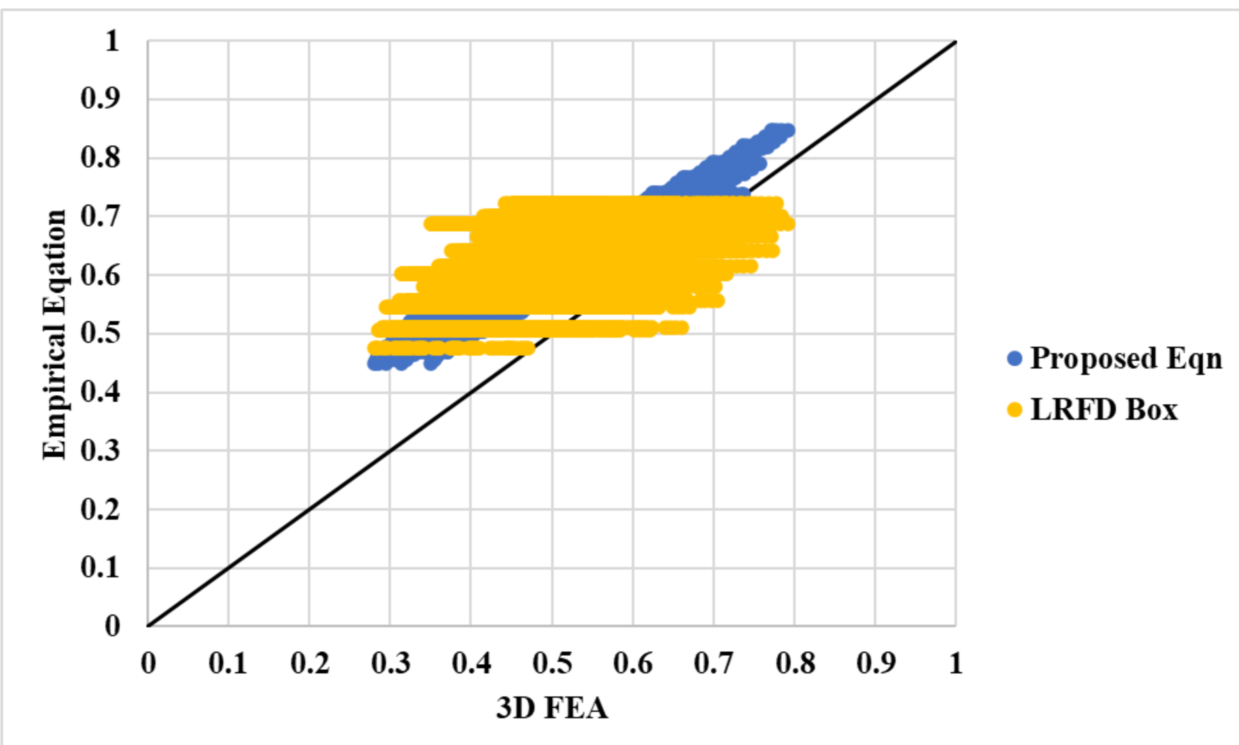
1
0.9
0.8
0.7
0.6
0.5
0.4
0.3
0.2
0.1
0
Empirical Eqation
0
0.1
0.2
0.3
0.4
0.5
0.6
0.7
0.8
0.9
1
3D FEA
Proposed Eqn
LRFD Box

(c)

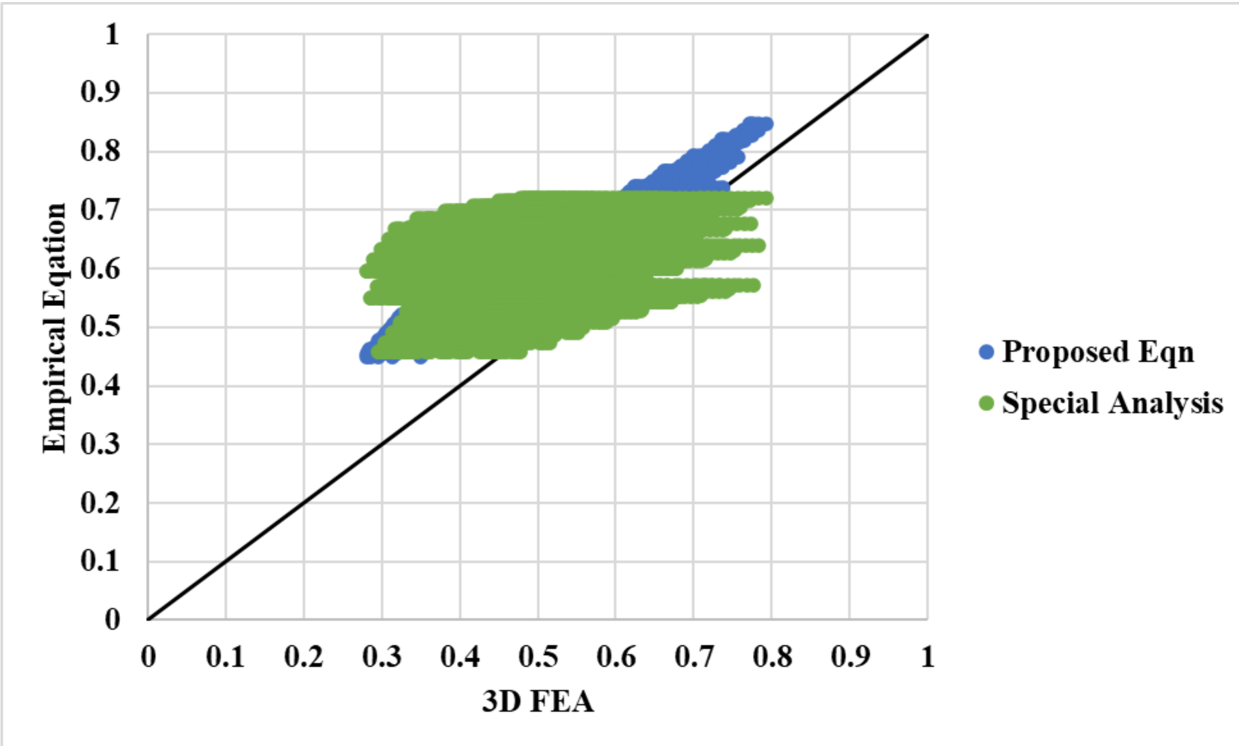

(d)

Figure 8.17: Correlation Between Proposed LLDF Equation for Exterior Girders with One-Lane Loaded with: (a) Lever Rule, (b) I-Girder Equation, (c) Box-Girder Equation, and (d) Special Analysis

Table 8.4: Exterior Girder One-Lane Loaded Statistical Analysis

Exterior Girder One Lane Loaded					
LLDF Methodology	Proposed Eq.	Lever Rule	I-Girder Eq.	Box-Girder Eq.	Special Analysis
Max Overestimation	0.20	0.35	0.35	0.34	0.35
Min Overestimation/Max Underestimation(*)	0.00	0.16*	0.16*	0.15*	0.21*
Average	0.10	0.08	0.08	0.13	0.13
Standard Deviation	0.033	0.099	0.099	0.085	0.089

8.7.5 Exterior Girder Two-Lanes Loaded LLDFs

The comparisons of the equations and methodologies found in the AASHTO LRFD BDS for LLDFs for exterior girder two-lanes loaded scenarios is presented in Figure 8.18 and Table 8.5. The comparison revealed the proposed moment LLDF equation more accurately predicts LLDFs than those of any other LLDF methodology or equation present in the AASHTO LRFD BDS. These comparisons serve to verify the applicability of the equation for use in PBFTG bridges.

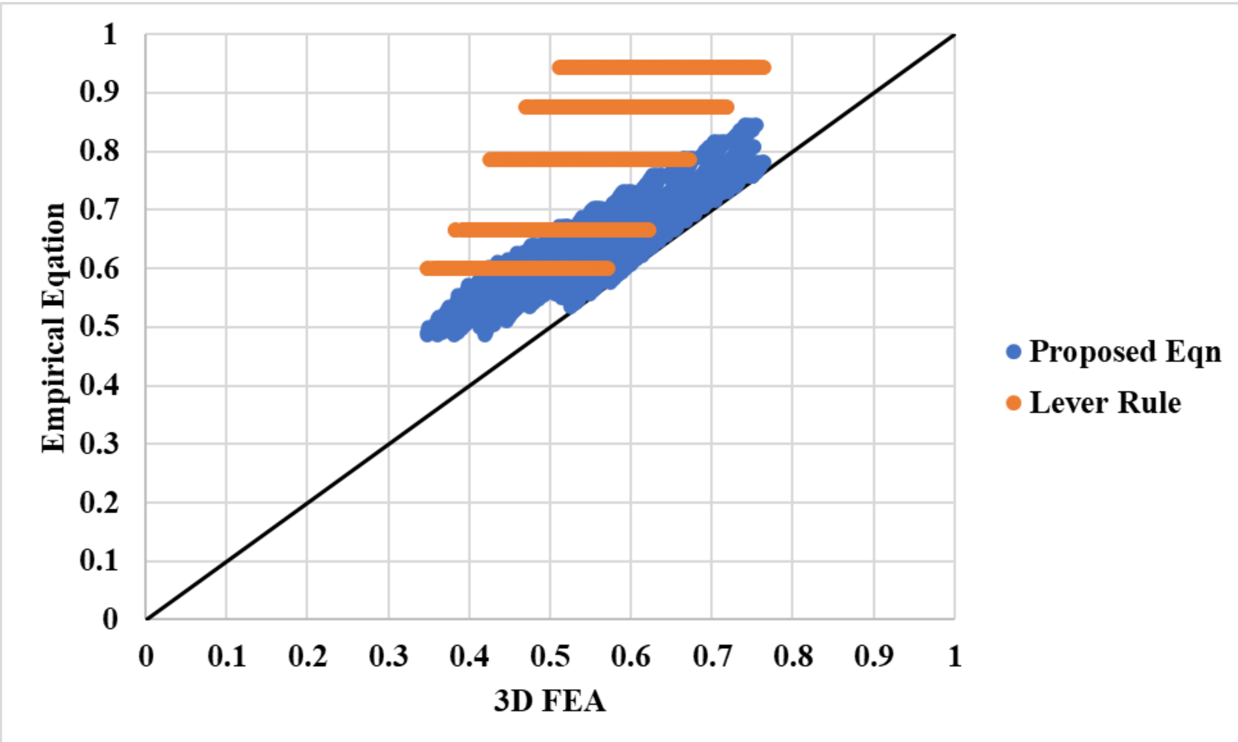

(a)

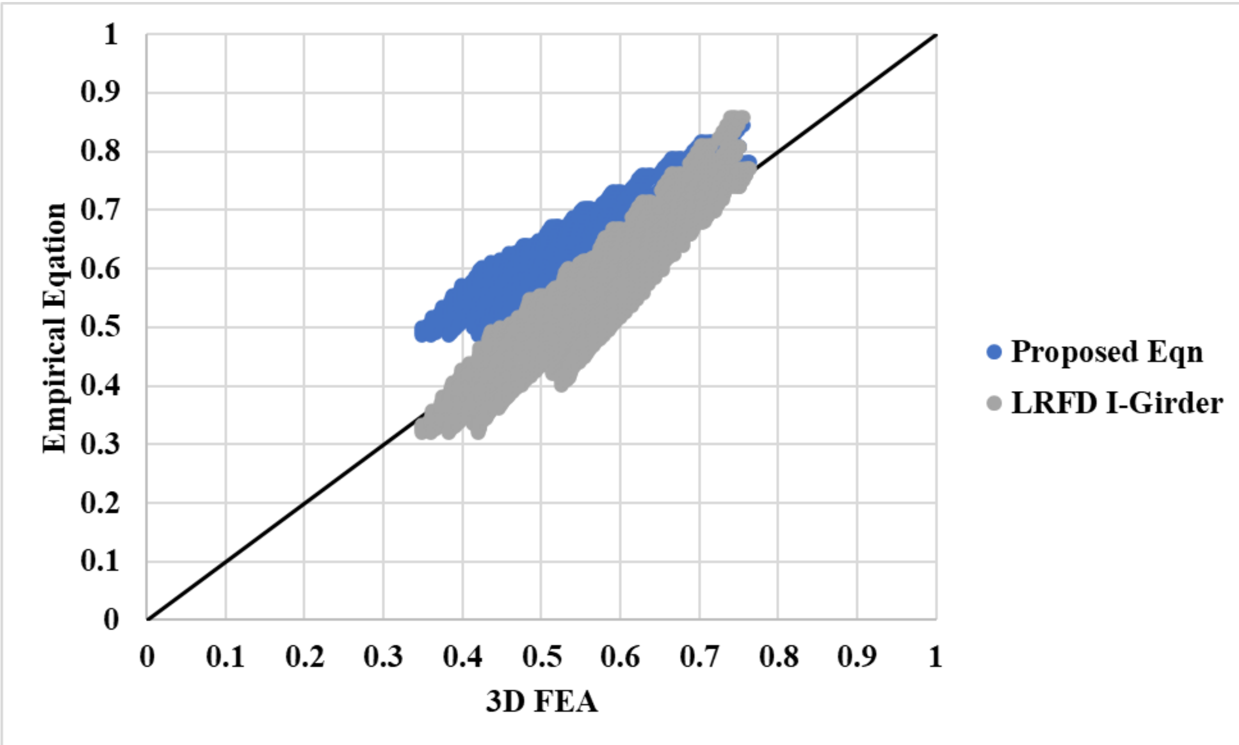

1
0.9
0.8
0.7
0.6
0.5
0.4
0.3
0.2
0.1
0
Empirical Eqation
0
0.1
0.2
0.3
0.4
0.5
0.6
0.7
0.8
0.9
1
3D FEA
Proposed Eqn
LRFD I-Girder

(b)

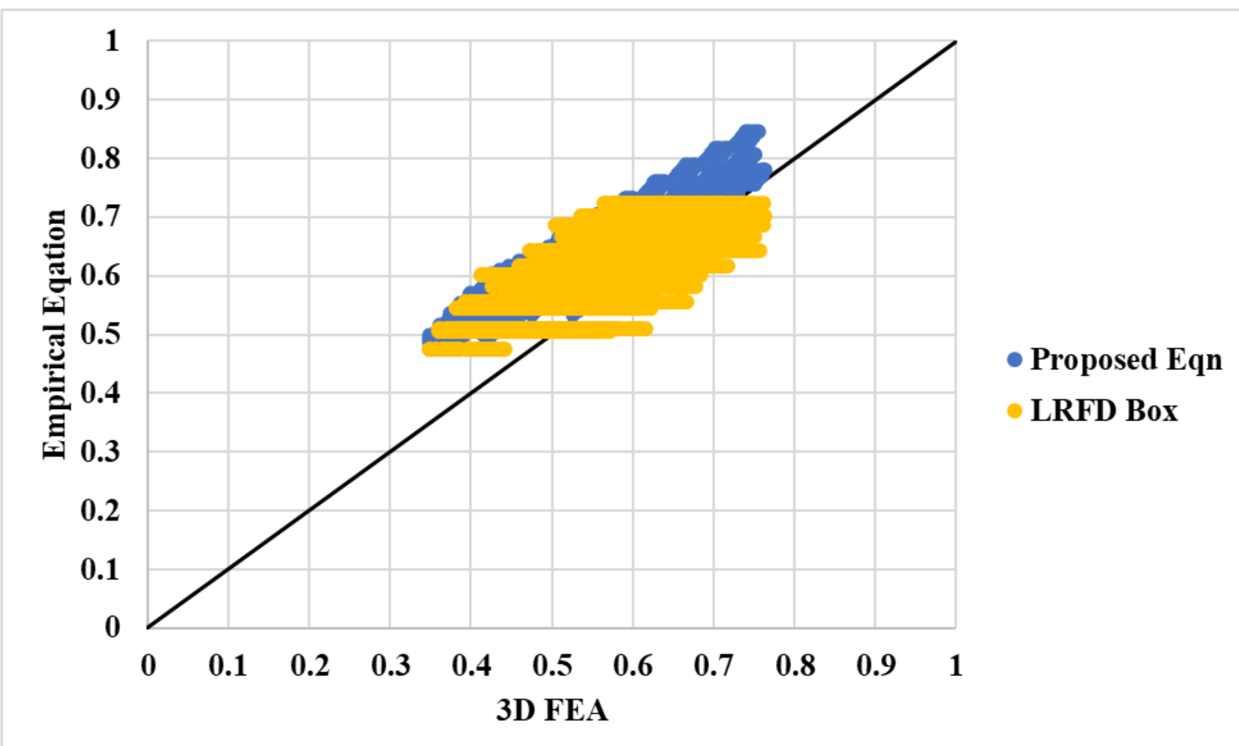

1
0.9
0.8
0.7
0.6
0.5
0.4
0.3
0.2
0.1
0
Empirical Eqation
0
0.1
0.2
0.3
0.4
0.5
0.6
0.7
0.8
0.9
1
3D FEA
Proposed Eqn
LRFD Box

(c)

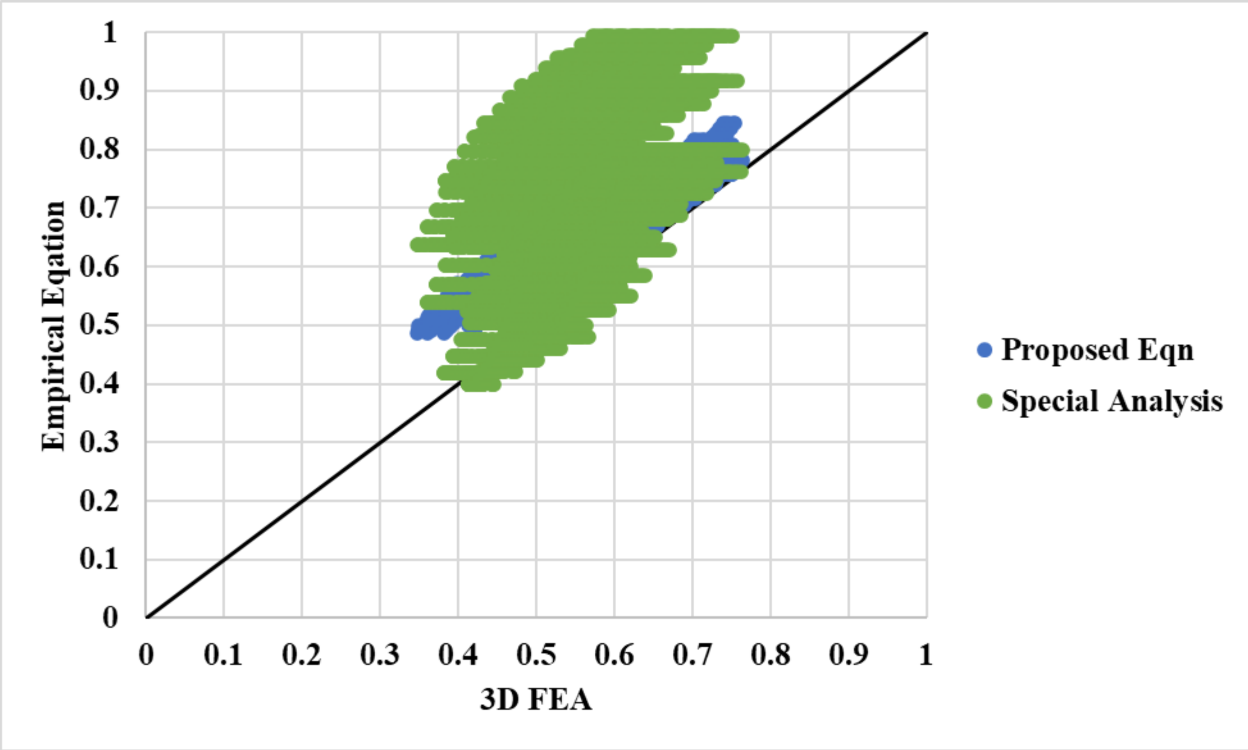

(d)

Figure 8.18: Correlation Between Proposed LLDF Equation for Exterior Girders with Two-Lanes Loaded with: (a) Lever Rule, (b) I-Girder Equation, (c) Box-Girder Equation, and (d) Special Analysis

Table 8.5: Exterior Girder Two-Lanes Loaded Statistical Analysis

Exterior Girder Two Lanes Loaed					
LLDF Methodology	Proposed Eq.	Lever Rule	I-Girder Eq.	Box-Girder Eq.	Special Analysis
Max Overestimation	0.18	0.10	0.12	0.19	0.43
Min Overestimation/Max Underestimation(*)	0.00	0.22*	0.12*	0.12*	0.09*
Average	0.08	-0.08	0.02	0.06	0.16
Standard Deviation	0.033	0.061	0.031	0.055	0.122

8.8 Verification with In-Service PBFTG Bridges

To verify the applicability and accuracy of the proposed equation, LLDFs were computed for three in-service PBFTG bridges. The results of the live load field tests performed on each bridge were compared against the analytically derived results and the proposed equation. An important note for each comparison is the live load field test utilized an actual truck with its own unique axle spacings and wheel loads to determine LLDFs, where the analytical model, and therefore the proposed equations, are derived assuming the HL-93 axle spacings and wheel loads.

8.8.1 The Amish Sawmill Bridge

The Amish Sawmill Bridge live load field test and previous analytical studies, performed by Gibbs (2017) were discussed in Section 2.4.1. In Section 7.8.5, the finite element modeling techniques used throughout this study were verified against the live load field test and analytical modeling performed by Gibbs (2017) utilizing the Stallings/Yoo live load distribution methodology and the truck model used in the live load field test. Presented in Figure 8.19 is the comparison of LLDFs obtained experimentally, analytically, and with the proposed simplified equation. As seen in Figure 8.19, the results from all three methodologies closely correlate. The largest difference occurs in the interior girder one-lane loaded scenario where the proposed simplified equation underestimated the experimental LLDF by 5%, but the two-lane loaded distribution factor would govern regardless.

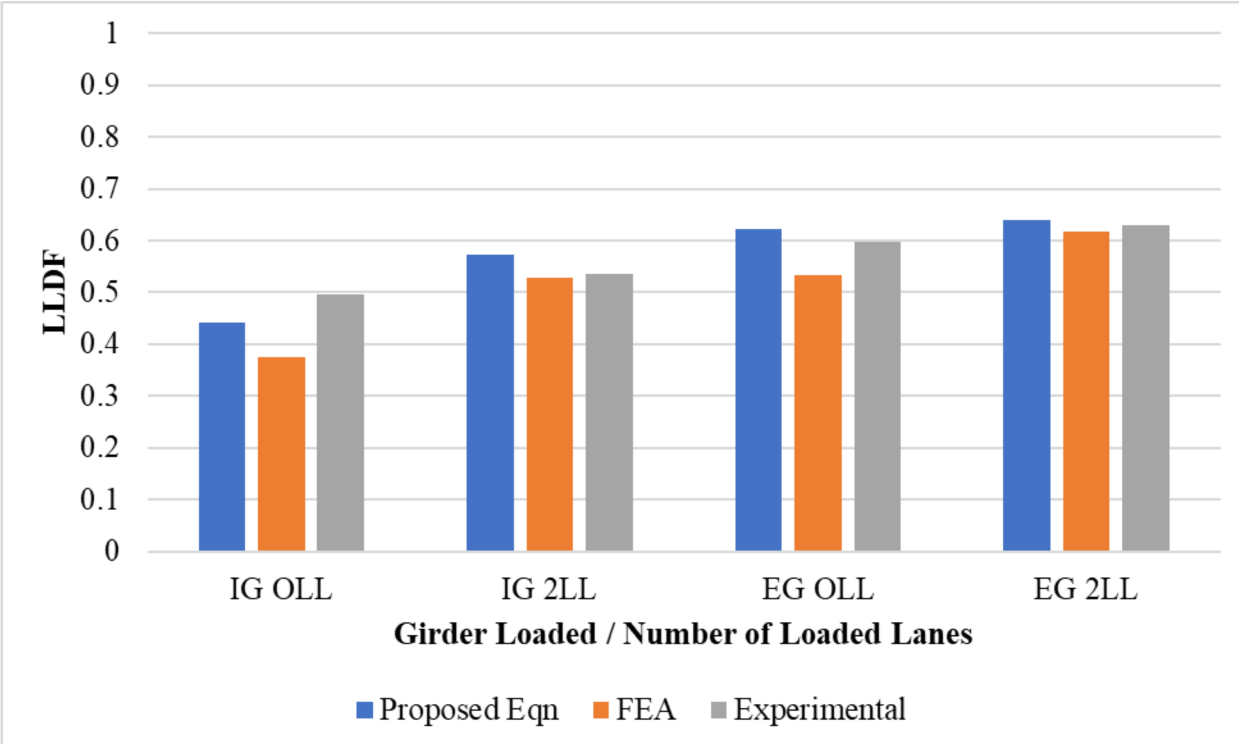

Figure 8.19: Comparison of LLDF Methodologies for the Amish Sawmill Bridge

8.8.2 The Fourteen Mile Bridge

The Fourteen Mile Bridge live load field test and previous analytical studies, performed by Roh (2020) were discussed in Section 2.4.3. In Section 7.8.6, the finite element modeling techniques used throughout this study were verified against the live load field test and analytical modeling performed by Roh (2020) utilizing the Stallings/Yoo live load distribution methodology and the truck model used in the live load field test. Presented in Figure 8.20 is the comparison of LLDFs obtained experimentally, analytically, and with the proposed simplified equation. As seen in Figure 8.20, the results from all three methodologies closely correlate. The largest difference occurs in the exterior girder one-lane loaded scenario where the proposed simplified equation overestimated the experimental LLDF by 15%, but the two-lane loaded distribution factor would govern regardless. Note, the Fourteen Mile Bridge is skewed approximately 10°. The proposed equations do not consider the effect of skew for moment LLDFs. The addition of a skew correction factor to reduce moment LLDF could account for the discrepancy, but it was not investigated in this study.

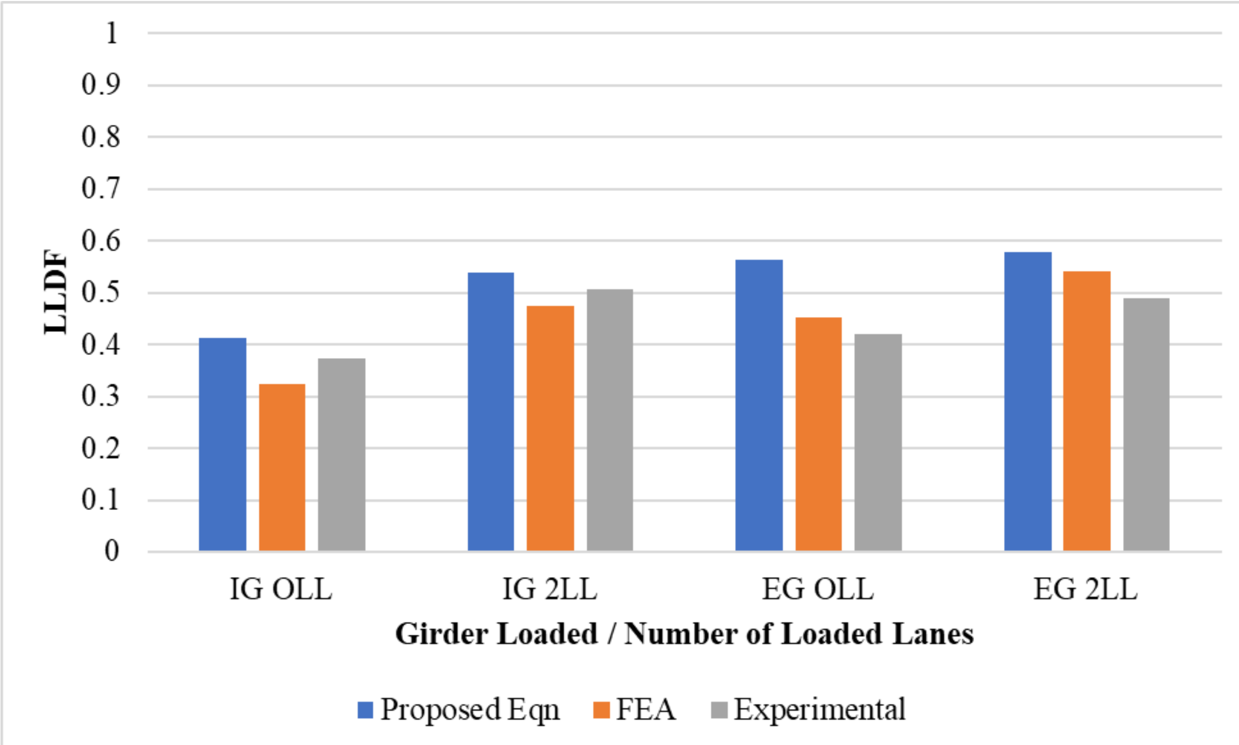

Figure 8.20: Comparison of LLDF Methodologies for the Fourteen Mile Bridge

8.8.3 The Flat Run Bridge

In Section 7.8.7, the finite element modeling techniques used throughout the Flat Run Bridge study were verified against the live load field test and analytical modeling performed as part of a study utilizing the Stallings/Yoo live load distribution methodology and the truck model used in the live load field test. Presented in Figure 8.21 is the comparison of LLDFs obtained experimentally, analytically, and with the proposed simplified equation. As seen in Figure 8.21, the results from all three methodologies closely correlate. The largest difference occurs in the exterior girder one-lane loaded scenario where the proposed simplified equation overestimated the experimental LLDF by 9%, but the two-lane loaded distribution factor would govern regardless.

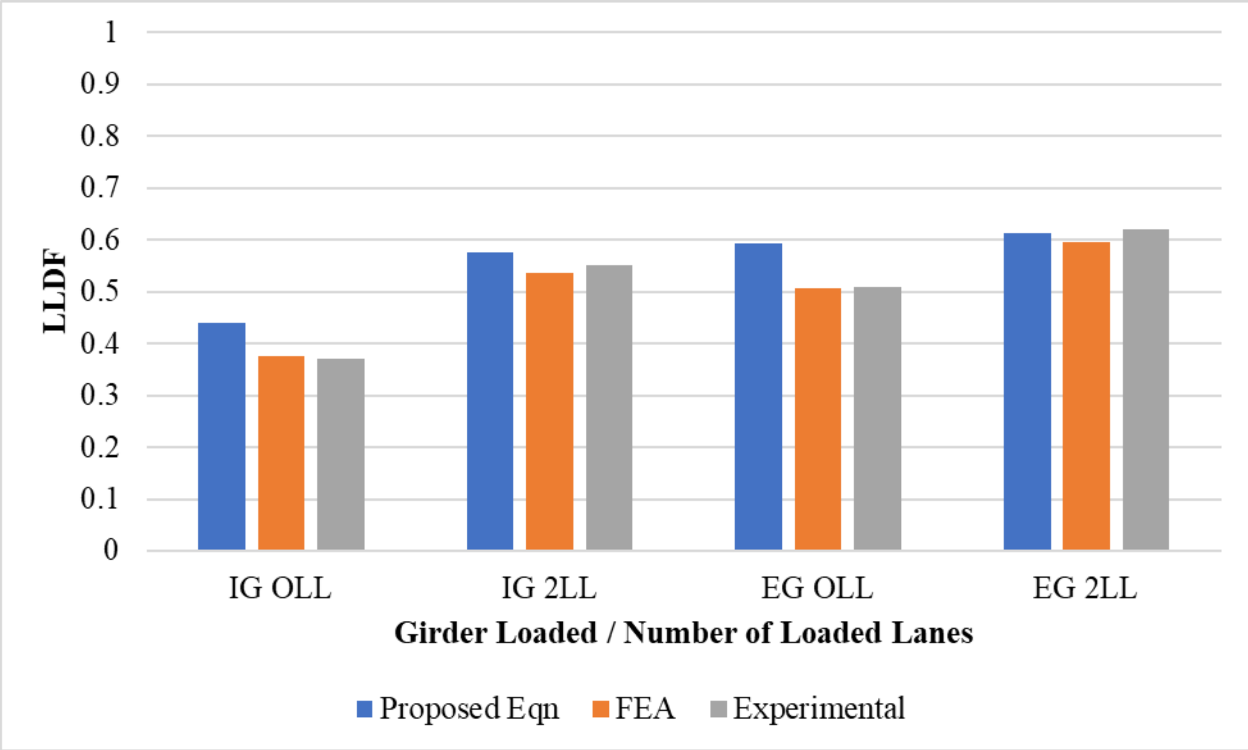

Figure 8.21: Comparison of LLDF Methodologies for the Flat Run Bridge

8.9 SUMMARY

The preceding chapter summarized the methodology and results of the study used to determine LLDFs for PBFTG bridges. First, a matrix of bridges was analyzed using a commercial finite element software package to determine the sensitivity of certain parameters on the influence of live load distribution in PBFTG bridges. From the results of the sensitivity matrix, a more refined parametric matrix was generated and analyzed to study the effect of the key parameters pertaining to PBFTG bridge LLDFs. The goal of this parametric matrix was to encapsulate the parameters deemed to have a significant impact on live load distribution and to ensure the parameters used were within reasonable limits to simulate potential real bridges. LLDFs of the parametric study were then used to generate simplified equations to be used with LGA for PBFTG bridges. Finally, the proposed equations were verified against the analytical and live load field test results of three in-service PBFTG bridges.

CHAPTER 9: ASSESSMENT OF SKEW ON THE FLEXURAL RESISTANCE OF PBFTGS BEHAVIORAL STUDY

9.1 Introduction

The purpose of this chapter is to assess the behavior of skewed PBFTG bridges. The goal of this study is to determine the applicability of the AASHTO LRFD BDS as they relate to the capacity of skewed PBFTG bridges. Specifically, previous composite laboratory testing was analytically skewed to determine if the ultimate capacity of the system was affected by the degree of support skew.

9.2 Importance of Study

As discussed in Section 4.3.3, per AASHTO LRFD Article 6.11.6, any box-girder section not meeting the requirements of AASHTO LRFD BDS Article 6.11.2.3 is considered noncompact for the nominal capacity of the section. AASHTO LRFD BDS Article 6.11.2.3 discusses the restrictions required to be met to use the LLDFs specified in AASHTO LRFD BDS Article 4.6.2.2. One of the restrictions is the limitation of bearing line skew; specifically, it states "bearing lines shall not be skewed." In other words, if a box-girder bridge has bearing lines skewed 1°, the nominal capacity of the section is limited to the yield moment, and a more rigorous analysis must be used to determine the loads resisted by the structure.

9.3 Refinement of the Analytical Model

The laboratory experimental tests performed by Michaelson (2014) served as a basis for the determination of the effect of skew on PBFTGs. The analytical tools discussed in Chapter 7 were applied to the PBFTGs described in Michaelson's (2014) physical laboratory experiment as discussed in Section 2.3.1. Key differences between the verification study and the behavioral study, regarding skew, are material modeling definitions and the use of a different type of element in the concrete deck.

9.3.1 Original Experimental Test

A brief description of the experimental test performed by Michaelson (2014) is provided herein, with a more detailed description of the entire scope of work provided in Section 2.3.1. Destructive flexural testing was performed on two composite PBFTG specimens. Each specimen was formed from 84 inch wide by 7/16 inch thick by 35 foot long plate. The 6 inch thick by 60 inch wide reinforced concrete deck was made composite with the PBFTG with four rows of the 7/8 inch diameter by 4 inch long shear stud connecters with a pitch of 12 inches. 3/4 inch bearing stiffeners were placed 3 inches from the ends of the PBFTG, resulting in a clear span length of 34.5 feet.

The girders were subjected to three-point bending and loaded at midspan with a 330-kip servo-hydraulic actuator. The load-deflection graph of the composite specimens was recreated in Figure 9.1. As seen in Figure 9.1, eventually the load no longer increased with increased deflection, as a plastic hinge formed in the specimens at approximately 300 kip and 3 inches of deflection.

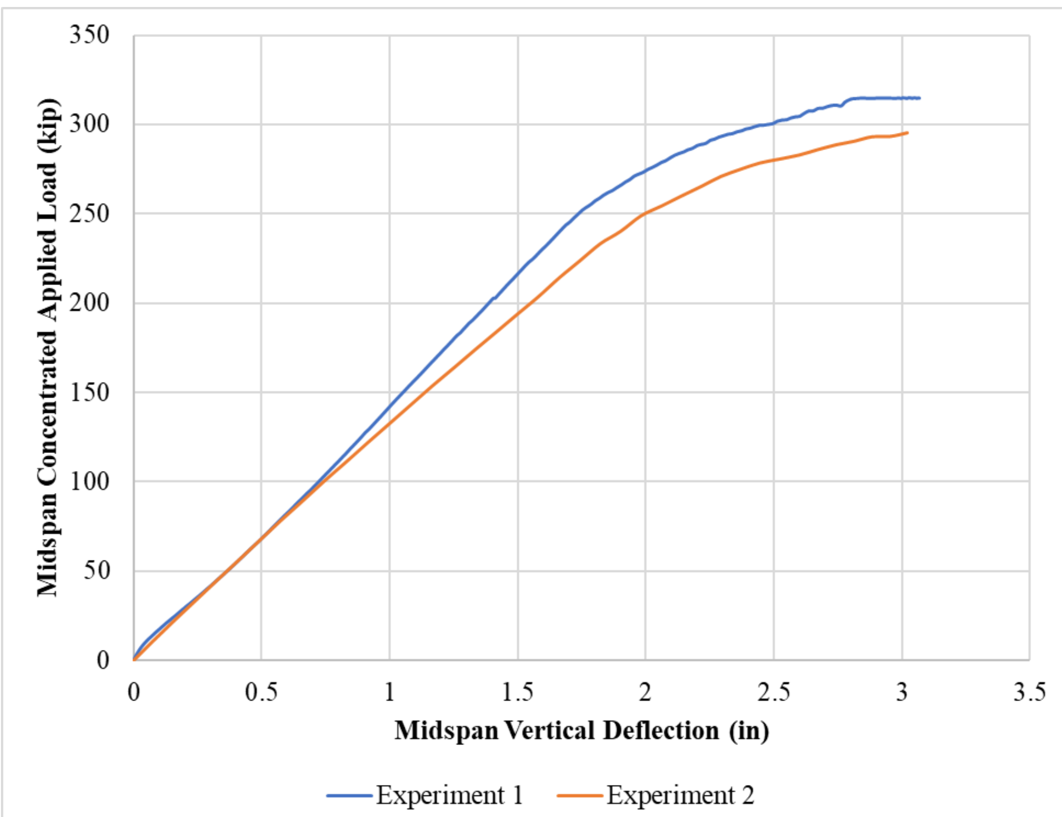

Figure 9.1: Load-Deflection Data from Flexural Testing of Composite Specimens (Michaelson, 2014)

9.3.2 Modifications to the Analytical Model

In the verification study, shell elements were used to model the concrete deck. When bearing skew was applied to the analytical model, the model would prematurely fail at loads close to yielding of the steel and cracking of the concrete. Shell elements were thought to not be able to adequately model this concrete cracking behavior, as a crack in the bottom face of the shell element would immediately propagate through the entire thickness of the deck, which is not accurate. To address this issue, continuum elements were used in place of shell elements in the concrete deck. As the concrete deck could now have multiple elements throughout the deck thickness, a crack could propagate through some of the deck elements and not cause failure. Figure 9.2 presents an image of the cross-section of the composite PBFTG with multiple continuum elements through the thickness of the deck.

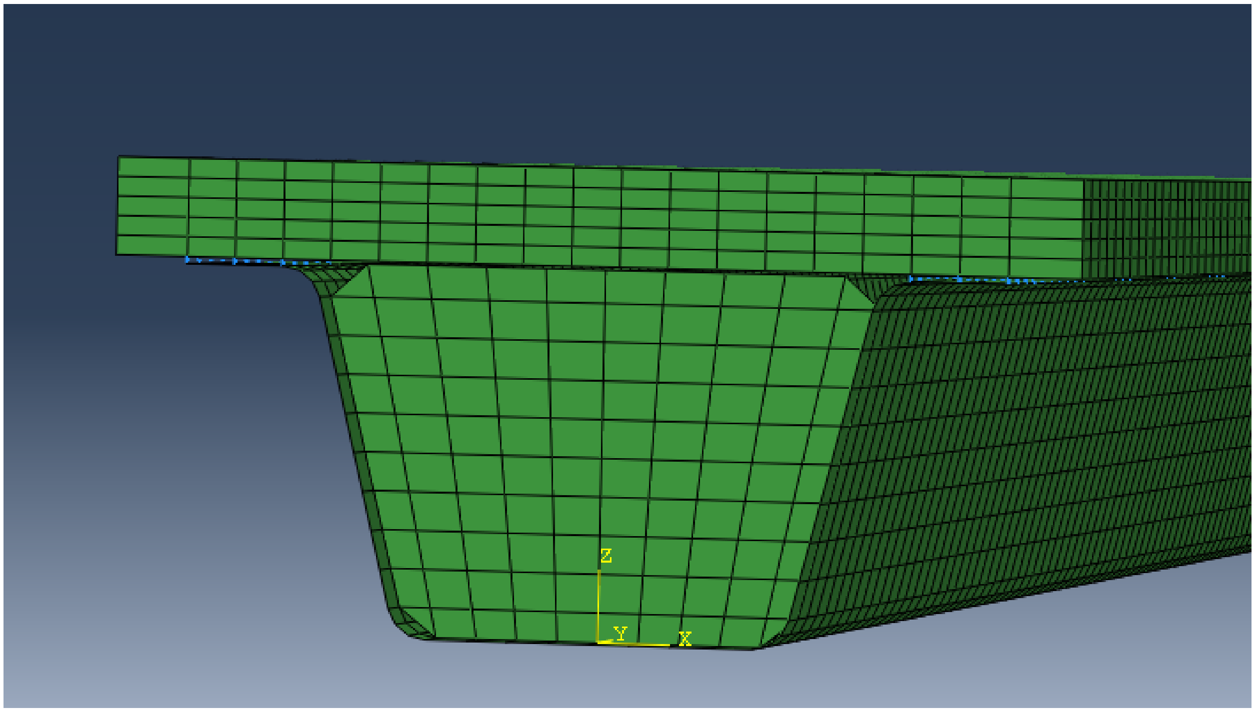

Figure 9.2: Cross-Section of PBFTG with Continuum Elements in the Deck

The addition of continuum elements did not solve all issues with the concrete material model. In all previous studies, the smeared crack material model provided accurate modeling of PBFTG systems. However, even with the use of continuum elements, the analytical model would still prematurely fail before significant loading could be applied. Consistent error messages would arise stating the results were diverging with skew angles as low as 5°. It was noticed the models would fail when the bottom face of the concrete deck directly under the load would reach the tensile rupture stress of the concrete.

To overcome this shortcoming of the material model, a damaged plasticity concrete model, as discussed in Section 7.3.2, was utilized. This material model would allow a significant reduction of the tensile capacity of the concrete without fully losing the element. When using this adjusted material model, the finite element model would behave nearly identically to the proven smeared crack model but would run out following the same general response as the 0° skewed models for longer during the analysis.

9.4 Assessment of Composite Unit Capacity

The restrictions discussed in AASHTO LRFD BDS Article 6.11.2.3 are based on the research performed by Johnston and Mattock (1967) on the specific cross-sections analyzed in their study. Additionally, the commentary of Article 6.11.2.3 states the reason the supports shall not be skewed is because additional torsional effects occur in the box section and the lateral distribution of load is affected. No other steel section has the capacity of the section limited by the restrictions placed on live load analysis. Additionally, if the proposed equations presented in Chapter 8 are to be utilized, the restrictions of AASHTO LRFD BDS Article 6.11.2.3 would not be applicable. Therefore, the validity of the requirements of the article, specifically those relating to bearing skew, were explored. If these restrictions can be neglected, or removed entirely, the applicable range of PBFTGs can be greatly expanded, not only through skewed scenarios, but also when PBFTGs do not meet the spacing restrictions explored by Johnston and Mattock (1967).

9.4.1 AASHTO LRFD BDS Requirements for Sections in Positive Flexure

AASHTO LRFD BDS Article 6.11.6.2.2, as discussed in Section 6.8.1, presents the requirements for a composite box-girder section to qualify as a compact section. First, the specified minimum yield strengths of the flanges and the web do not exceed 70 ksi. This requirement is easily met by choosing standard mill plate with the required material properties. Secondly, the web slenderness ratio shall not exceed 150. If the designers utilize one of the standardized PBFTG sections suggested by Michaelson (2014), such as the ones used in this study, this requirement will be met. The third requirement states the section must be part of a bridge that satisfies the requirements of AASHTO LRFD BDS Article 6.11.2.3. These research efforts are meant to explore the validity of this requirement. Further discussion of this article can be found in Sections 6.4 and 4.3.1. The fourth requirement is that the box flange is fully effective, as specified in AASHTO LRFD Article 6.11.1.1. Box flanges in simple spans are considered fully effective in resisting flexure if the width of flange does not exceed one-fifth of the span length. This is not an issue in this study as the smallest bridges analyzed were 20 feet long and the largest bottom flange width is less than 3 feet wide. The final requirement is the section must satisfy the web slenderness limit specified in Equation 9.1.

$$\frac{2D_{cp}}{t_w} \leq 3.76\sqrt{\frac{E}{F_{yc}}} \qquad \text{Eq. 9.1}$$

Where:

D_{cp} = depth of the web in compression at the plastic moment

t_w = web thickness

E = modulus of elasticity of steel

F_{yc} = specified minimum yield strength of the compression flange

This limit was thoroughly evaluated by Michaelson (2014) in a study with 450 composite PBFTG modules with varying PBFTG sizes and deck widths. The study showed the plastic neutral axis was typically located in the concrete deck or the top flange resulting in a D_{cp} value of zero. Only 22 out of the 450 cases evaluated resulted in a nonzero value of D_{cp}, leading to web slenderness values in the plastic range significantly lower than the limit presented in Equation 9.1.

9.4.2 AASHTO LRFD BDS Flexural Resistance of Compact Sections

From the previous section and the assumptions made about the special limitations on the use of LLDFs from AASHTO LRFD BDS Article 6.11.2.3, the specimen analyzed was considered compact. If a composite box-girder qualifies as compact, the nominal flexural resistance of the section is determined using Equation 9.2 or Equation 9.3:

If $D_p \leq 0.1\, D_t$, then:

$$M_n \leq M_p \qquad \text{Eq. 9.2}$$

Otherwise:

$$M_n = M_p\left(1.07 - 0.7\frac{D_p}{D_t}\right) \qquad \text{Eq. 9.3}$$

Where:

D_p = distance from the top of the concrete deck to the neutral axis of composite section at the plastic moment

D_t = total depth of the composite section

M_n = nominal flexural resistance of a section

M_p = plastic moment of composite section

The yield moment of the composite section in positive flexure is calculated following a procedure specified in AASHTO LRFD BDS Section D6.2. Symbolically, the procedure is shown by solving Equations 9.4 and 9.5. Additionally, the yield moment of the section shall be taken as the lesser value calculated for the compression flange or the tension flange.

Solve for M_{AD} from the equation:

$$F_{yf} = \frac{M_{D1}}{S_{NC}} + \frac{M_{D2}}{S_{LT}} + \frac{M_{AD}}{S_{ST}} \qquad \text{Eq. 9.4}$$

Then calculate:

$$M_y = M_{D1} + M_{D2} + M_{AD} \qquad \text{Eq. 9.5}$$

Where:

F_{yf} = yield strength of the flange under consideration

M_{D1} = moment due to the noncomposite dead loads

M_{D2} = moment due to the composite dead loads

M_{AD} = moment due to the additional applied loads

S_{NC} = noncomposite elastic section modulus

S_{ST} = short-term elastic section modulus

S_{LT} = long-term elastic section modulus

M_y = yield moment

As the concrete deck was shored during construction and no additional composite dead loads were applied during testing, Equations 9.4 and 9.5 can be combined and simplified to form Equation 9.6.

$$M_y = \min\,(F_{yc}S_{fc}, F_{yt}S_{ft}) \qquad \text{Eq. 9.6}$$

Where:

M_y = yield moment

F_{yc} = yield strength of the compression flange

F_{yc} = yield strength of the compression flange

S_{fc} = short-term composite compression flange elastic section modulus

S_{ft} = short-term composite tension flange elastic section modulus

Solving Equation 9.6 provides a yield moment of 1768 kip-feet for the experimental composite PBFTG.

The plastic moment of the composite PBFTG was calculated following the procedure outlined in ASSHTO LRFD BDS Article D6.1. The plastic moment was calculated as the moment of the plastic forces about the plastic neutral axis. This was accomplished by first calculating the element forces and using them to determine whether the plastic neutral axis was in the webs, top bends, top flanges, or the concrete deck. Second, the location of the plastic neutral axis was determined by the equilibrium of forces from the first step by ensuring no net axial force existed in the section. Finally, the plastic moment was calculated by summing the plastic forces of each section about the plastic neutral axis. Conservatively, the forces in the longitudinal rebar were neglected in these calculations. For the experimental composite PBFTG, the plastic moment, M_p, was determined to be 2256 kip-feet, and the distance from the top of the concrete deck to the neutral axis of composite section at the plastic moment, D_p, was determined to be 4.90 inches. By solving Equations 9.2 and 9.3, with the values of M_p and D_p calculated previously, the nominal flexural moment of the experimental composite PBFTG system is 1993 kip-feet.

9.5 Behavioral Study

Utilizing the analytical procedures discussed in Chapter 7, with the modifications discussed in Section 9.3.2, a series of analytical models were generated to evaluate behavior of composite PBFTGs with varying degrees of skew. The first step in the behavioral study was to verify analytical modeling techniques against experimental results. As shown in Figure 9.3, the modeling techniques efficiently capture the nonlinear behavior of the experimental composite PBFTG.

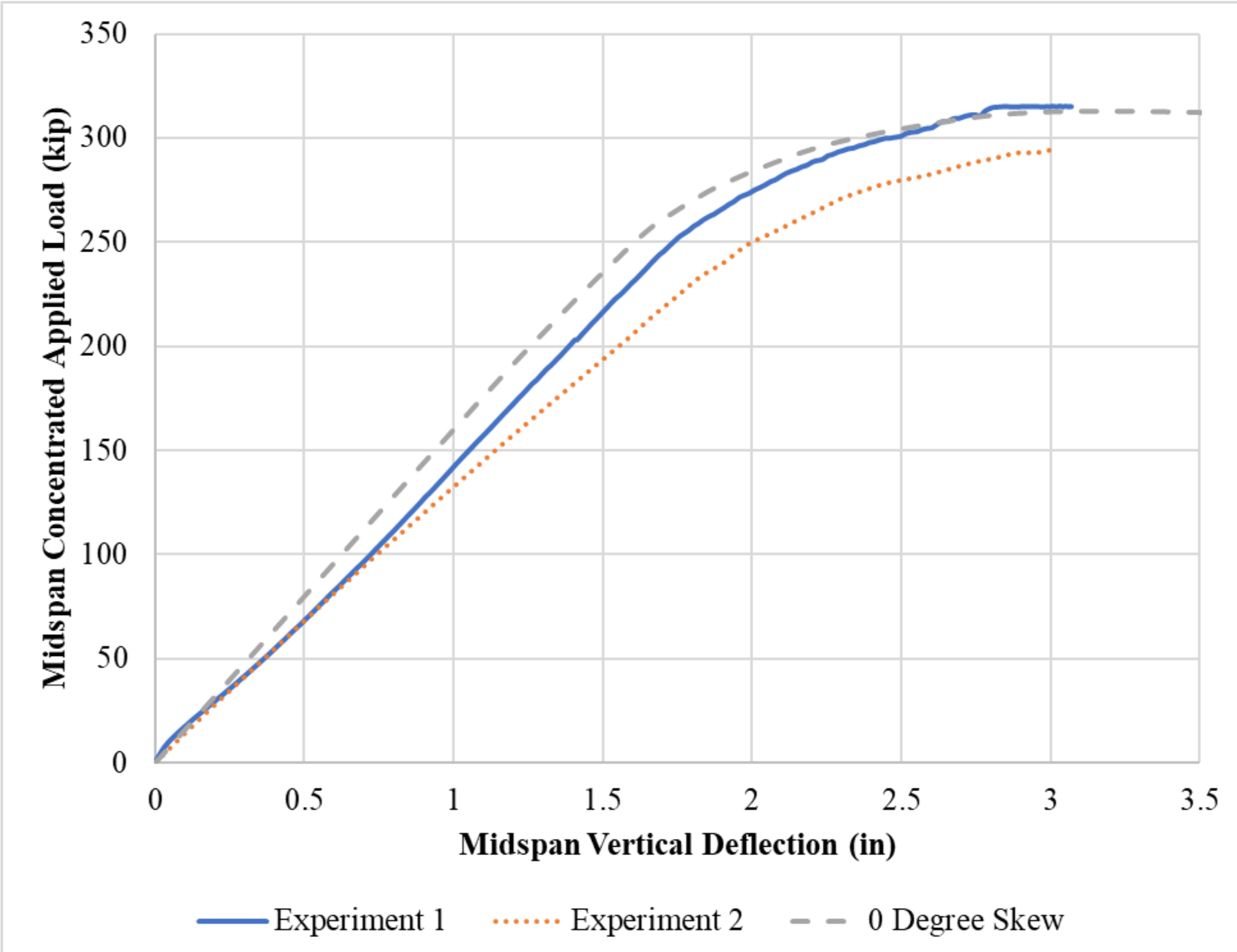

Figure 9.2: Verification of Improved Modeling Techniques Against Experimental Laboratory Results

Following the verification of the modeling techniques of a specimen without skew, the bearing skew was varied from 0° to 45° in 5° increments. The load was applied perpendicular to the longitudinal axis of the PBFTG and distributed equally across the width of the concrete deck. Additionally, to represent the effect of the spreader beam placed under the 330-kip servo-hydraulic actuator, the load is distributed longitudinally over the width of the spreader beam flange, or approximately 12 inches.

9.6 PRELIMINARY RESULTS

Figures 9.3 and 9.4 present the load/midspan deflection results of the behavioral study. As seen in Figure 9.3, the load/deflection history of the iterations with bearing line skew under 20° follows the same curve. While the load-deflection plots for PBFTGs with bearing skews under 20° follows the same shape as the 0° bearing line skew test, the stiffness of the system seems to increase, based on the longitudinal strains recorded from the model. However, as the degree of bearing skew increases beyond 20°, the analytical model terminates before the load-deflection curve can plateau in a manner similar to the low bearing skew girders. This abrupt termination in the analysis of the higher bearing line skews is presented in Figure 9.4.

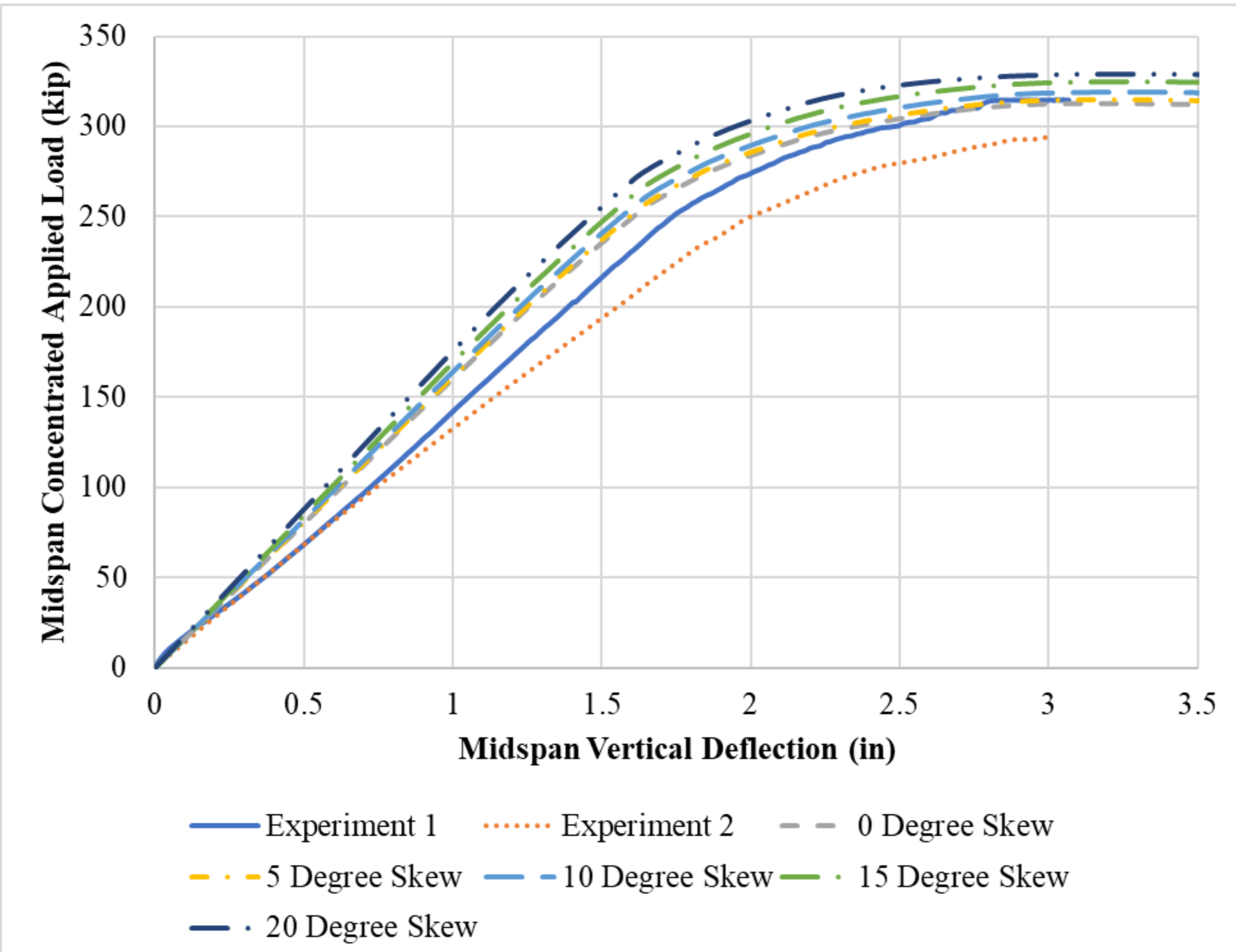

Figure 9.3: Load vs. Deflection Plots for Bearing Line Skews up to 20°

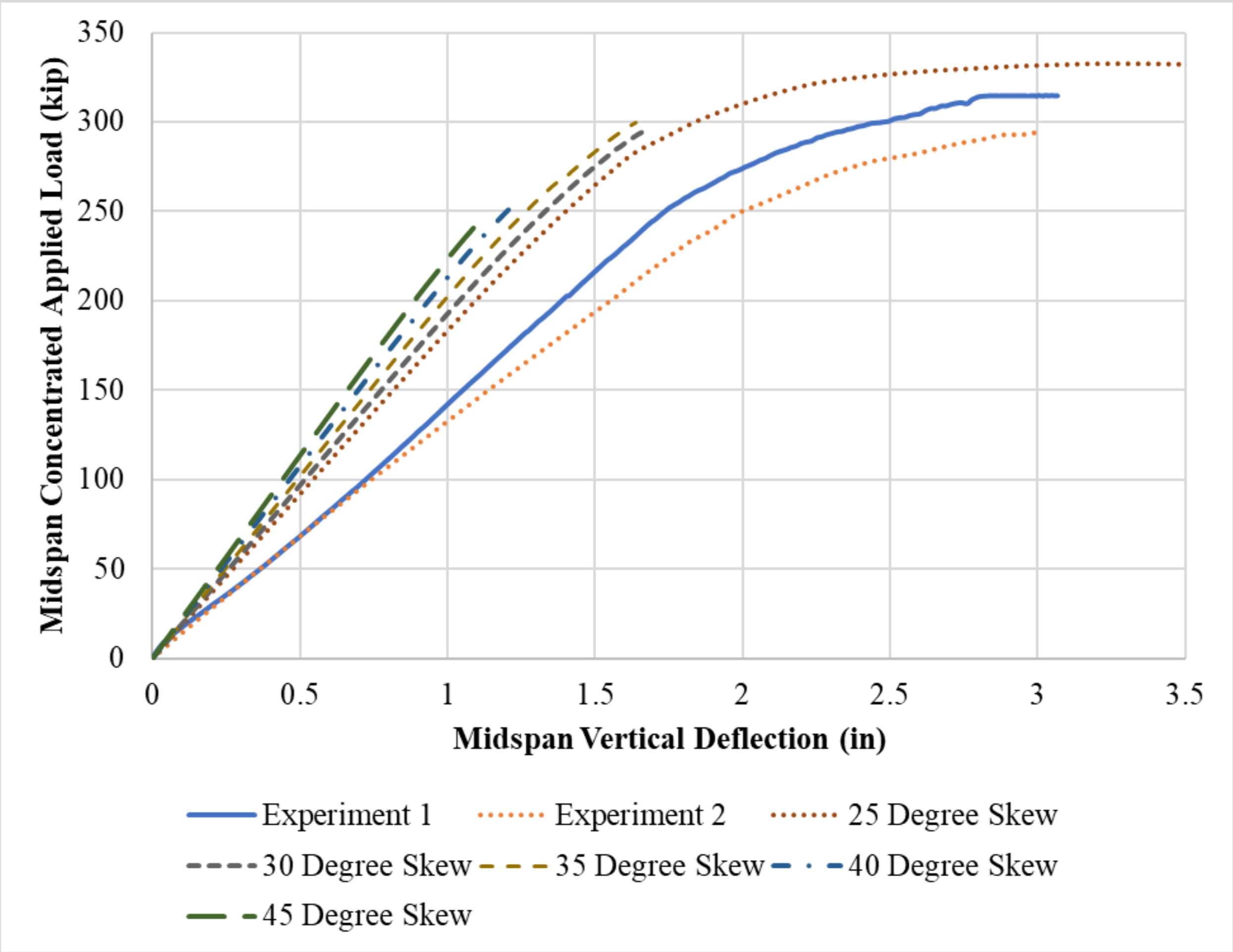

Figure 9.4: Load vs. Deflection Plots for Bearing Line Skews above 20°

To compare the results of the sensitivity study against the nominal flexural resistance calculations presented in the AASHTO LRFD BDS, the yield moment, plastic moment, and nominal flexural resistance from Equation 9.3, rewritten as point loads, are presented in Figure 9.5. These comparisons show the experimental PBFTG has capacity even above the nominal plastic moment load.

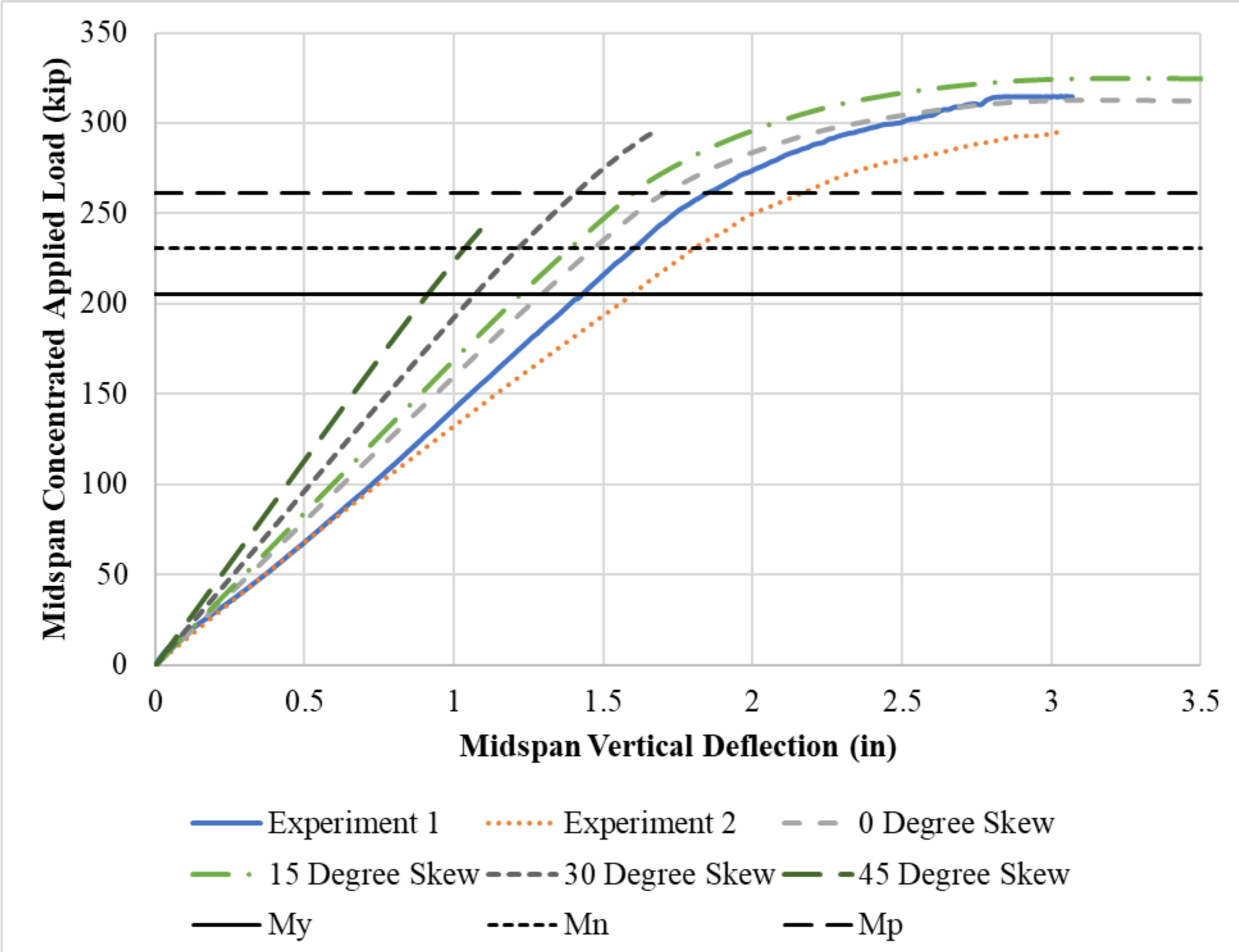

Figure 9.5: Comparison of Load vs. Deflection Plots Against Point Loads Inducing Design Moments

9.7 Summary

This chapter served to assess the behavior of skewed PBFTGs. The goal of this study was to determine the applicability of the restrictions present in AASHTO LRFD BDS Article 6.11.2.3 on the capacity of skewed PBFTGs. AASHTO LRFD BDS Article 6.11.2.3 was deemed to not be applicable to the capacity of PBFTGs up to bearing line skews of 20°. The nominal capacity calculations for the PBFTG analyzed, assuming the restrictions of AASHTO LRFD BDS Article 6.11.2.3 could be ignored, are still applicable in bearing line skews of up to 45°.

CHAPTER 10: EXPERIMENTAL TESTING OF A LINK SLAB BETWEEN PBFTGS

10.1 INTRODUCTION

This chapter contains an overview of the physical experimental testing completed to assess the performance of the proposed link slab detail in conjunction with PBFTGs. A brief description of the specimen tested is provided herein, along with an instrumentation plan, a description of equipment used, and the results of the testing effort.

10.2 OVERVIEW OF TESTING PROGRAM

To verify the performance of the link slab detail in conjunction with PBFTGs, physical flexural testing was conducted at the Major Units Lab at WVU. Fatigue testing conducted on two composite PBFTGs joined with a link slab with a load at approximately midspan of each PBFTG is shown in Figures 10.1 and 10.2.

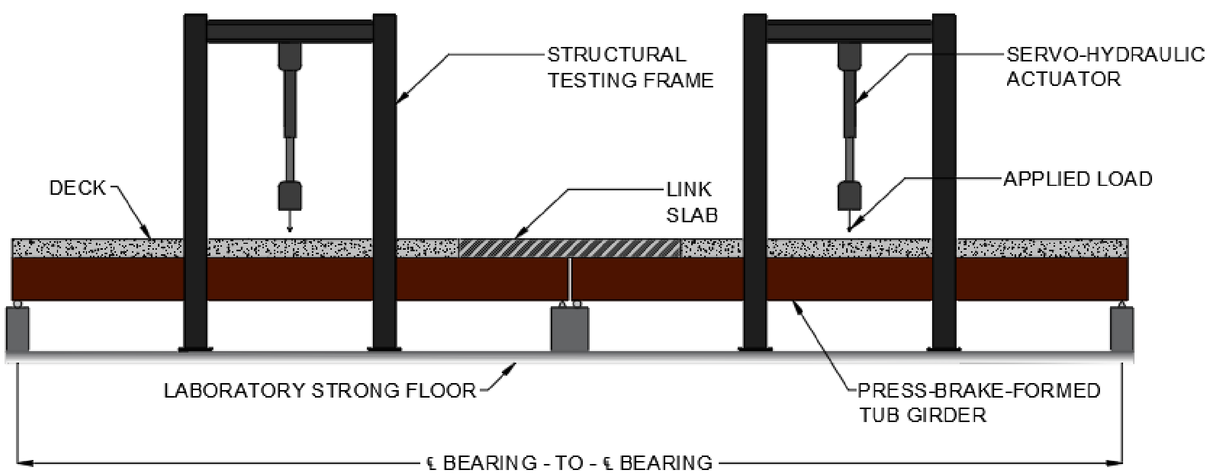

Figure 10.1: Test Setup Schematic

Figure 10.2: Isometric View of Test Setup

Each of the girders were supported under each bearing stiffener by a 2 inch round diameter bar. One support for each girder was welded to the plate beneath the roller, simulating a pinned boundary condition (Figure 10.3), and the other support was placed in a small groove allowing displacement in the longitudinal axis, simulating a roller boundary condition (Figure 10.4). The 2 inch diameter bars were supported by 6 inch by 24 inch by 2 inch steel plates. The exterior plates were each supported by a 12 inch by 24 inch by 3 inch steel plate, and the interior plates were supported by a single 24 inch by 24 inch by 3 inch plate. Each 3 inch plate rested on two 6 inch by 6 inch by 24 inch long hollow structural sections filled with high strength concrete. Four 1 inch diameter threaded rods connect the hollow structural sections to the vertical structural support system (Figure 10.5). Lateral bracing, consisting of equal leg angles, located at the exterior supports, prevented unintentional transverse motion. 1/2 inch thick steel plates welded immediately adjacent to the bearing stiffeners of each PBFTG operated as connection plates for the lateral bracing system. Figure 10.6 demonstrates the setup of the lateral force resisting system.

Figure 10.3: View of a Pinned Boundary Condition

Figure 10.4: View of a Roller Boundary Condition

Figure 10.5: Plan View of the Vertical Force Resisting System

Figure 10.6: Cross-Section View of the Lateral Force Resisting System

10.3 Specimen Descriptions

Michaelson (2014) proposed standardized cross-section geometry for standard mill plate widths and thicknesses. The PBFTGs in this study were fabricated from 84 inch by 7/16 inch by 300 inch plate and were bent to have a 23 inch depth with 6 inch wide top flanges, as seen in Figure 10.7. Each girder was fabricated by placing the flat plate in a large capacity press-brake and cold-bent with the inside bend radius equal to five time the thickness of the plate. Table 10.1 presents the noncomposite section properties of PBFTGs formed from 84 inch wide by 7/16 inch thick plate. 3/4 inch thick bearing stiffeners were welded 3 inches from the end of each specimen to prevent premature bearing failure during testing (Figure 10.8). Both specimens consist of HPS-50 steel. One specimen remained uncoated while the other was hot-dip galvanized prior to any further fabrication. Research has shown the hot-dip galvanization process does not affect the fatigue performance of PBFTGs (Tennant, 2018).

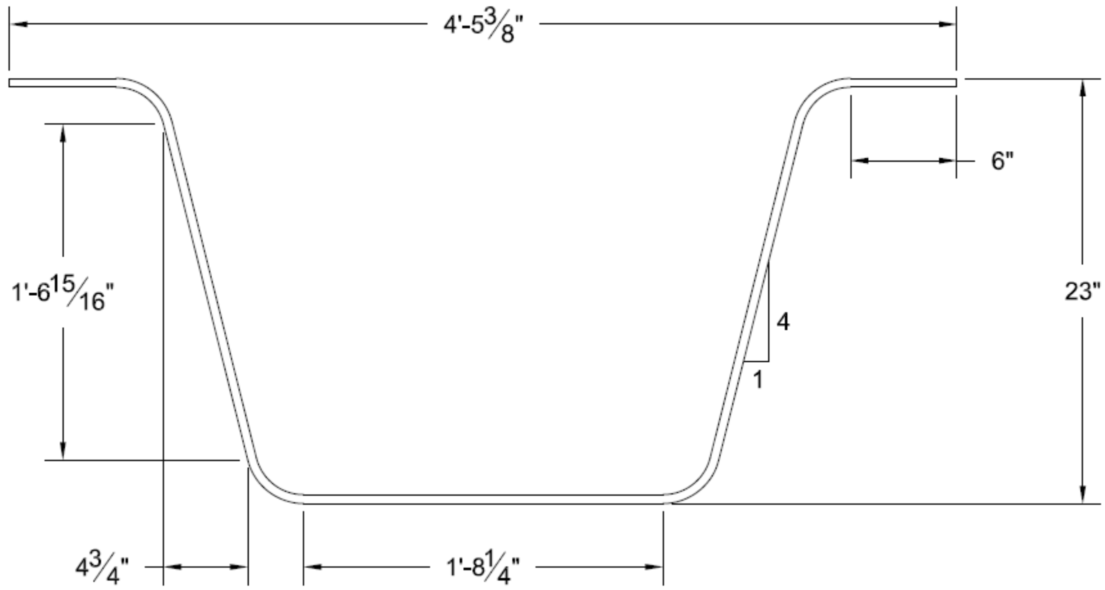

Figure 10.7: 84 inch by 7/16 inch PBFTG Cross-section

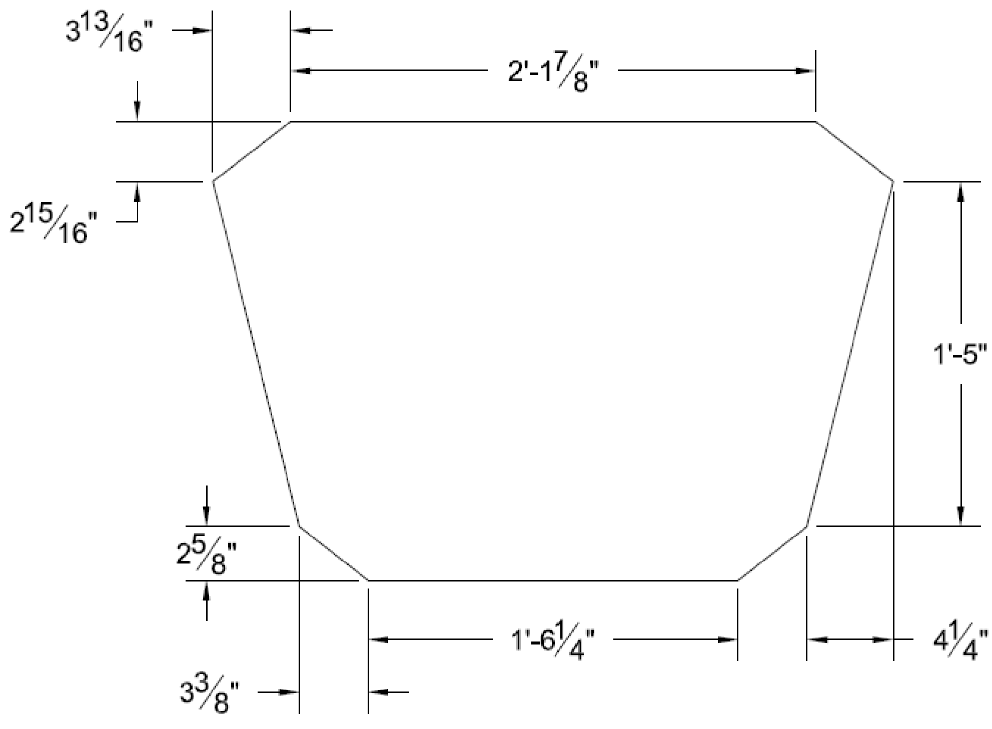

Figure 10.8: Bearing Diaphragm Cross-section

Table 10.1: Noncomposite PBFTG Section Properties

Property	Value
E (ksi)	29,000
G (ksi)	11,154
A (in^2)	36.75
I_x (in^4)	2893
I_y (in^4)	8050
I_{open} (in^4)	2.345
I_{closed} (in^4)	69,000
I_w (in^6)	140,000
β_x (in)	-19.7

10.4 Test Specimen Assembly

Following the welding of the end bearing diaphragm to the cold-bent plate, the specimens could be constructed with additional design details. To prepare the composite units, various design details surrounding the concrete deck were constructed. This section will describe the construction of the composite units from the installation of the stay-in-place formwork through the casting of the link slab.

10.4.1 SIP Metal Formwork

Stay-in-place (SIP) metal formwork was utilized between the top flanges of each specimen (Figure 10.9). 2 inch deep pans were utilized on the uncoated specimen and 3 in deep pans were utilized on the galvanized specimen. The SIP metal formwork ran from the exterior support of each girder longitudinally until approximately 9 inches from the interior support. This allowed for a purely unbonded region to develop between the concrete and the girders at the interior support region. 7/8 inch by 6 inch shear studs were shot through the SIP formwork, in the strong position of the bottom flute, to achieve composite action between the concrete deck and the steel specimens. 21 rows of studs, 4 studs in each row, were placed longitudinally along the girders. The first row of studs was placed directly above the bearing diaphragm, and subsequent rows were spaced 12 inches apart. The final four bottom flutes were left without shear studs to develop the transition zone of the link slab. These final flutes were plug welded to connect the formwork to the girder without the use of studs in the transition zone.

Figure 10.9: Isometric view of the SIP Formwork and Shear Studs

10.4.2 Exterior Formwork

Most of the exterior formwork was reused from previous testing performed by Michaelson (2014), Kozhokin (2016), and Tennant (2018), as the cross-section and specimen height were the same (Figure 10.10). However, as the concrete deck was designed thicker to simulate the dimensions of a full-scale link slab, the wooden forms used against the concrete were replaced with 2 inch by 12 inch lumber cut to produce a total deck thickness of 10 inches. The forms allowed for a total deck width of 60 inches with overhangs on either side of the exterior of either flange measuring approximately 3 inches. The exterior formwork was braced against the structural testing frames and large concrete blocks, acting as dead-man anchors, as seen in Figure 10.11. A temporary transverse board was placed at the deck-link slab interface.

Figure 10.10: Isometric View of Vertical Deck Supports

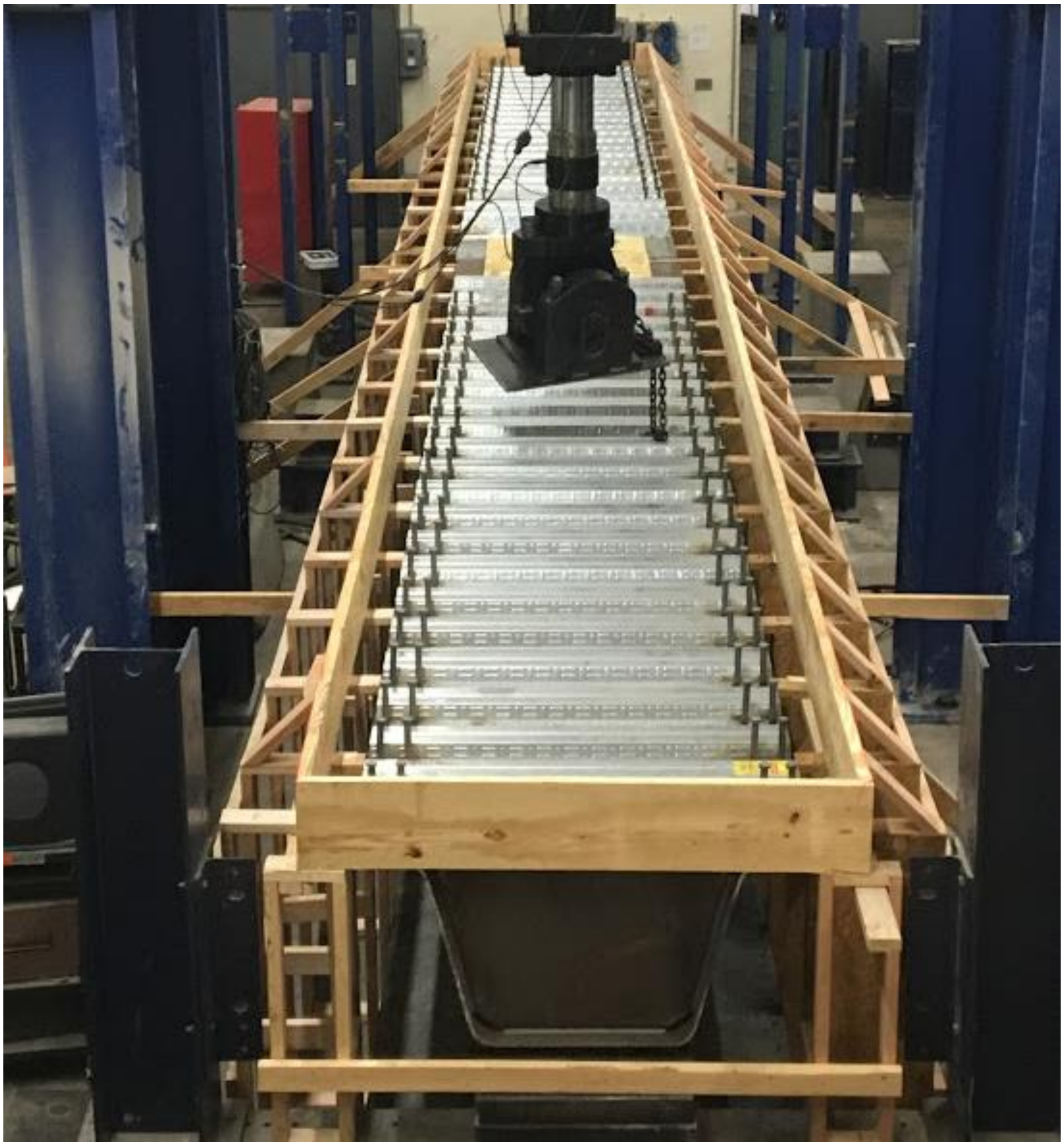

Figure 10.11: Isometric View of Complete Exterior Deck Forms

10.4.3 Main Span Reinforcement

The concrete decks of the main spans were designed following the empirical deck design method described in AASHTO LRFD BDS Article 9.7.2. The bottom longitudinal reinforcement consisted of #5 rebar spaced at 12 inches on center with an edge distance of 2 inches. 1 inch of clear cover was provided between the top of the 3 inch deep SIP metal deck and the bottom of the bottom mat of rebar, equating to 2 inches of clear cover between the 2 inch deep SIP metal deck and the bottom mat of rebar. The bottom layer of transverse reinforcement was placed directly above the bottom layer of longitudinal reinforcement and consisted of #5 rebar spaced 12 inches on center, which coincided with the placement of the shear studs. The top layer of longitudinal reinforcement consisted of #4 rebar with the same spacing as the bottom layer of longitudinal reinforcement. The top layer of transverse reinforcement consisted of #4 rebar placed directly above the top mat of longitudinal reinforcement with the same spacing as the bottom mat. With this layout, 2 3/8 inches of top cover was provided. The deck reinforcement can be seen in Figures 10.12 and 10.13.

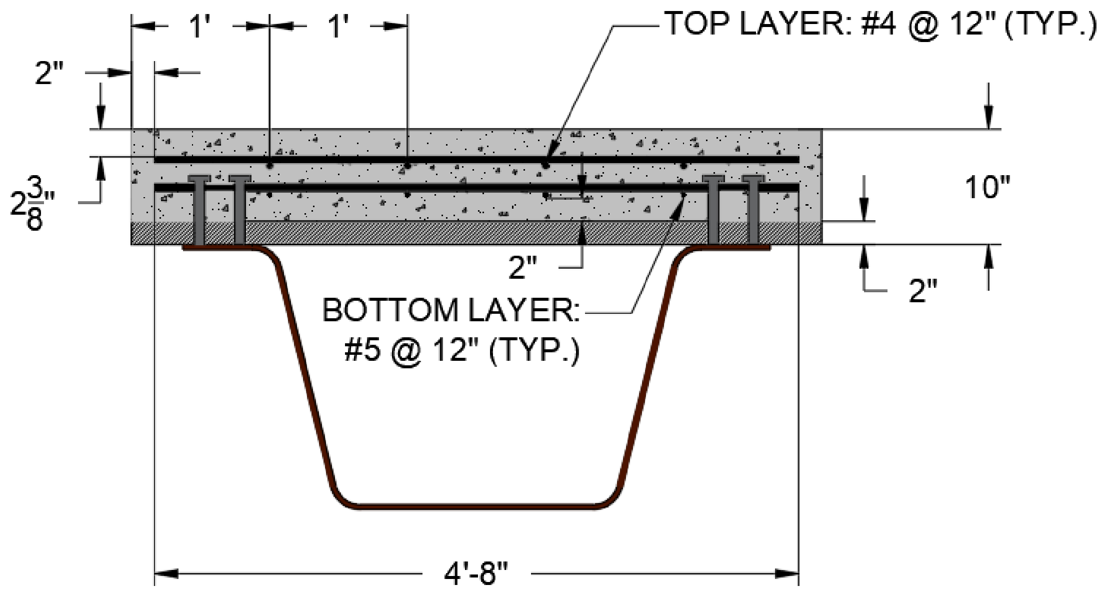

Figure 10.12: Cross-section View of Concrete Deck Reinforcement

Figure 10.13: Placement of Concrete Deck Reinforcement

10.4.4 Main Span Concrete Pour

On the day of the concrete pour, the wooden formwork was heavily coated with form release to allow for easy removal without significant damage to the concrete deck. As seen in Figure 10.13, any gaps in the wooden formwork were filled with foam. The upper flutes of the SIP metal formwork were also filled with foam so the concrete would not flow through the flutes into the tub section. Once the concrete arrived on site, four 6 inch diameter cylinders were poured for material testing. The concrete was placed into the forms utilizing a 1 yard concrete bucket attached to an overhead ten ton crane, as seen in Figure 10.14. After each successive concrete pour for both specimens, the concrete was vibrated to minimize air pockets and honey combing.

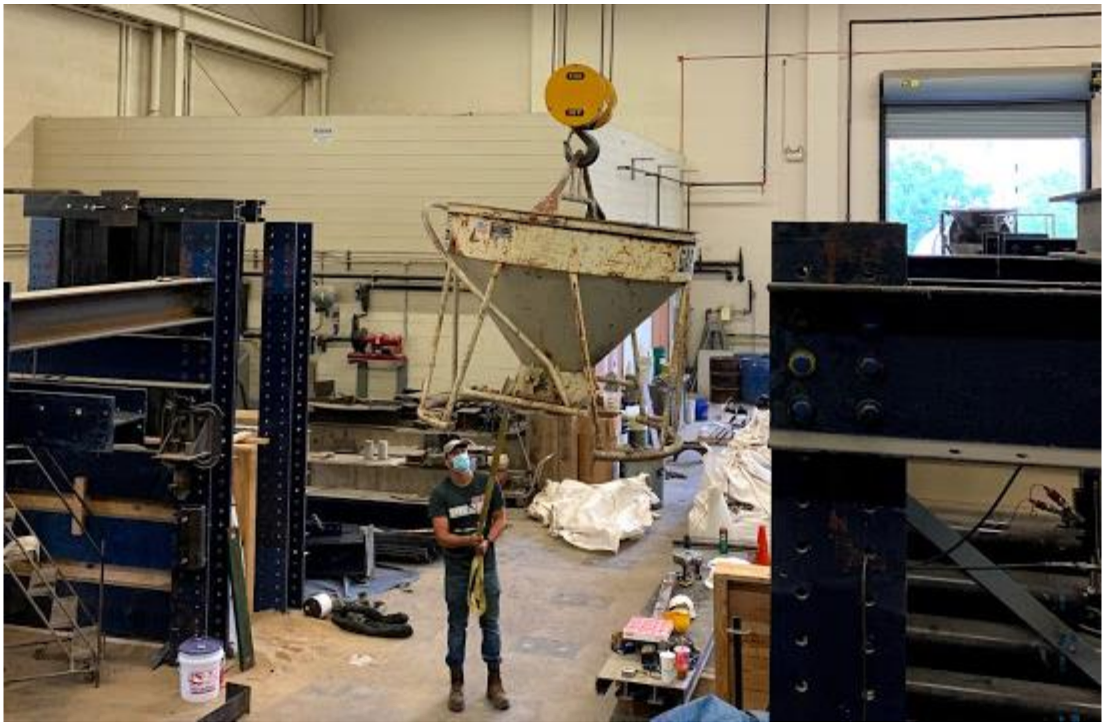

Figure 10.14: Concrete Bucket Transporting 1 Yard of Concrete

The concrete pour for the two main slab specimens was completed in approximately two hours and can be seen in Figure 10.15. Burlap was placed over the curing concrete to control surface cracking during hydration. The burlap was rehydrated every day for two weeks following the pour to ensure the concrete surface remained moist. After one week of curing, the forms around the main slab specimens were removed with minimal localized damage where the forms were pried away from the deck.

Figure 10.15: Finished Main Span Concrete Decks

10.4.5 Link Slab Construction

A combination of the methodologies provided by Caner and Zia (1998) and Li et al. (2003) produced the size and layout of the link slab reinforcement. As the use of the link slab does not behave similarly to two simple spans or continuous spans, the calculation of the moment at the link slab is not easily calculated. To calculate the required reinforcement area in the link slab, the rotation at the center of the link slab was the limiting parameter chosen. Another key difference in the construction of the link slab was the need to debond the concrete deck from the underlying steel girders. This was achieved by placing plywood over the open ends of the tubs not covered by the SIP metal formwork and covering the entire bottom face of the link slab with standard roofing paper. The roofing paper allowed movement of the link slab independently from the underlying girders. The corrugation of the SIP formwork with the roofing paper allowed for the transition zone to develop between the flat link slab and the main deck (Figure 10.16).

Figure 10.16: Isometric View of Transition Zone

The same bottom mat of reinforcement used in each main span was also used for the bottom mat of the link slab reinforcement: #5 rebar spaced 12 inches on center. The required area of steel in the top mat of rebar for the link slab was found to be 1.073 inches per 12 inches of link slab width. #10 rebar spaced 12 inches on center would have been the optimum rebar size, but due to lack of availability, two #7 rebar tied together were chosen to replace a single #10 rebar. To develop the rebar in the link slab with the rebar protruding from the main spans, the link slab rebar was overlapped and tied together with the main span rebar over 5 feet. A similar development of the lower longitudinal rebar can be seen in Figure 10.17. #4 rebar was used as transverse reinforcement in the top mat.

Figure 10.17: Completed Link Slab Reinforcement

A similar procedure to the main span concrete pour was used during the link slab concrete pour. The forms were prepared similarly, with foam filling any cracks and form release spread on the outer formwork. Four test cylinders were poured for material testing. Concrete was transported using a 1 yard concrete bucket from the mixer truck to the link slab, where it was poured and vibrated to remove any air pockets. The link slab was finished with special attention paid to the link slab-main span interface to ensure a smooth joint. The finished link slab can be seen in Figure 10.18. After the pour, it cured under wet burlap for 14 days, then dry cured for the recommended further 14 days.

Figure 10.18: Poured Link Slab

10.5 Instrumentation

Data was collected throughout link slab testing, including continuous load and deflection monitoring and periodical static testing. Data included strain gauges to obtain the moment at various cross-sections in the specimens and vertical deflections at the points of loading. This section will describe the instruments, layout, and installation used throughout the testing.

10.5.1 Instruments

Foil-resistor uniaxial strain gauges were employed throughout testing. Strain was recorded at four different cross-sections on the main span specimens and on the rebar placed in the link slab. The strain gauges were connected to a Micro-Measurements Model 5100 Scanner utilizing StrainSmart software to record strain and displacement data (Micro-Measurements, 2010). Two different hydraulic actuators applied load to the system. An MTS Model 243.70T 330-kip servo-hydraulic actuator applied load to the uncoated specimen and an MTS Model 243.40 110-kip servo-hydraulic actuator applied load to the galvanized specimen. Each of the servo-hydraulic actuators are equipped with instruments to measure the deflection at the point of loading and the magnitude of loading.

10.5.2 Layout and Installation of Girder Strain Gauges

Four separate cross-sections were chosen between the two PBFTGs to record strains, as seen in Figure 10.19. Nine strain gauges were located at each cross-section to capture the tensile strains in the steel girder. Three strain gauges were placed on each of the webs and the bottom flange. As seen in Figure 10.20, the first strain gauge on each face was located at the center of the face, and the other two strain gauges were spaced six inches away from the first in both directions along the cross-section. The strain gauges placed near midspan of each PBFTG were offset 46 inches, or two times the steel girder depth, away from the point of load application to avoid strain concentration effects.

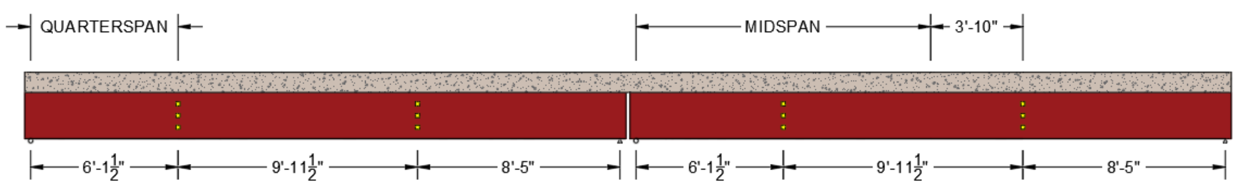

Figure 10.19: Strain Gauge Longitudinal Layout

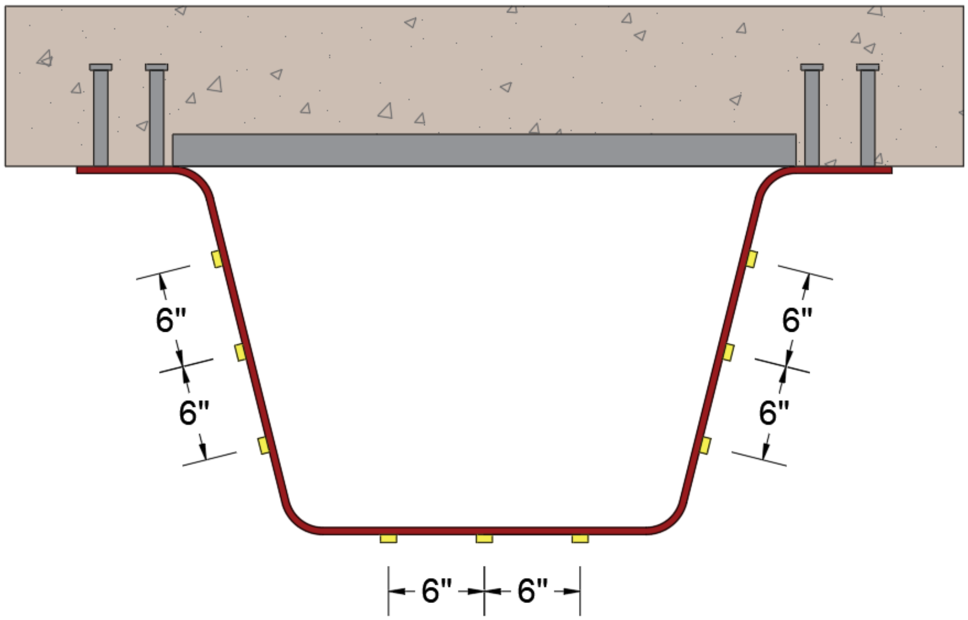

Figure 10.20: Strain Gauge Cross-Section Layout

10.5.3 Layout and Installation of Link Slab Gauges

Eight uniaxial strain gauges were placed on the underside of the top mat of longitudinal reinforcement in the link slab. Two strain gauges were placed on each of the longitudinal lines of rebar for redundancy. The first cross-section of rebar was placed directly in the center of the link slab and the second cross-section was placed two feet toward the uncoated specimen. As these strain gauges were to be exposed to the concrete of the link slab, additional protection in the form of Micro-Measurements M-Coat JA-3 Polysulfide Coating and plastic sheathing was provided. The polysulfide coating can be seen on the link slab rebar in Figure 10.21.

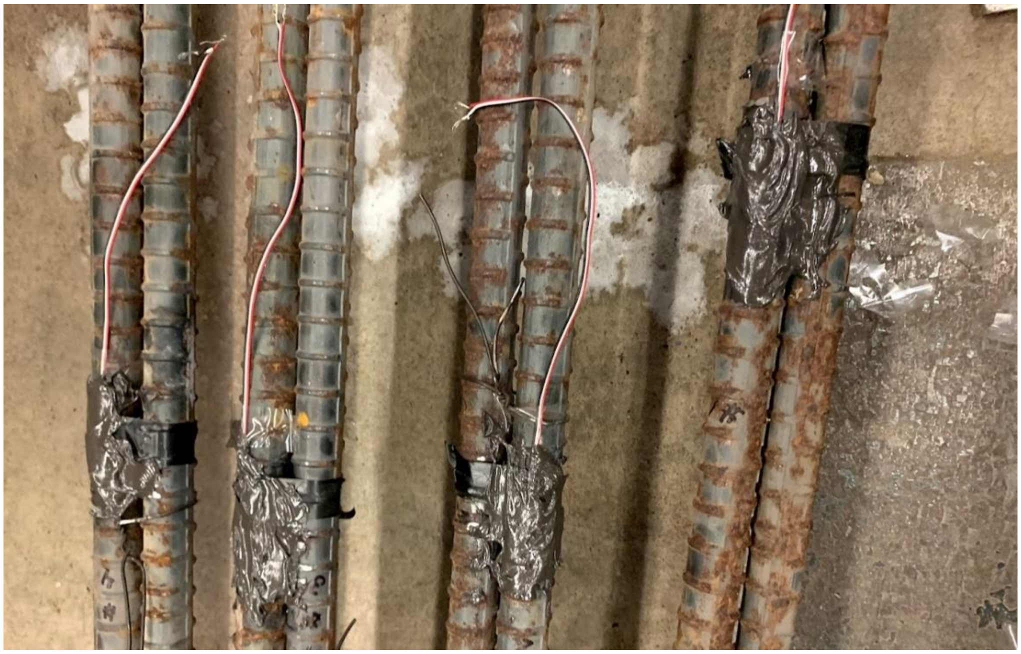

Figure 10.19: Polysulfide Coating on Link Slab Reinforcement

10.6 Material Testing

The steel and concrete used in this research were tested to obtain material properties for use in the data reduction of the composite specimens. Steel tensile coupons were taken from appropriate locations during the fabrication of the noncomposite specimens and were tested by Turner-Fairbank's Highway Research Center. As the noncomposite specimens were previously used in nondestructive testing performed by Michaelson (2014), further discussion of the material testing can be found in his dissertation. The coupon test results from Turner-Fairbanks tensile testing can be seen in Figure 10.22.

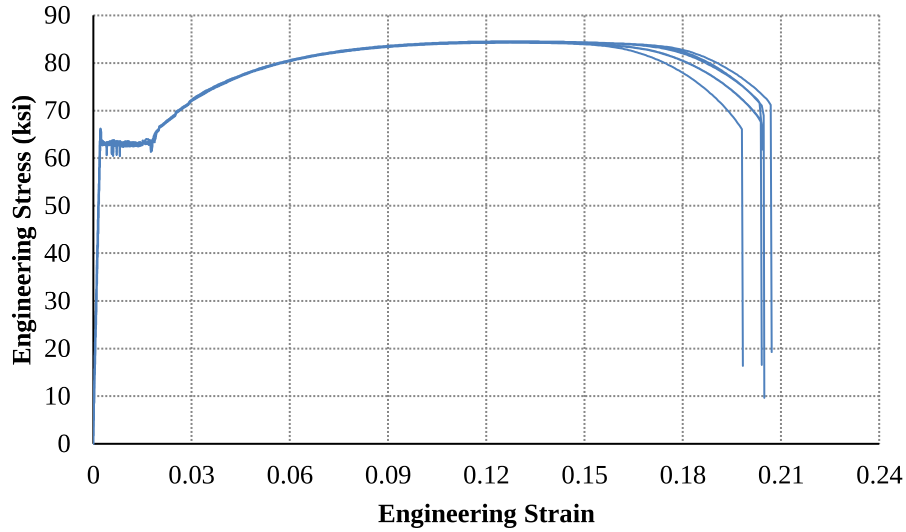

Figure 10.20: Results from Tensile Testing of Steel Coupons (Michaelson, 2014)

For this research, four concrete cylinders were cast during the main span and link slab concrete pours. Cylinders were tested 28 days after casting to obtain the in-place compressive strength of the composite specimens and the link slab. The mean of the compressive strengths was recorded to obtain the compressive strength used in the mechanistic models. The average compressive strength of the main span specimens was found to be 3.86 ksi, and the average compressive strength of the link slab was found to be 3.74 ksi.

10.7 Load Configuration

Load was applied at midspan of the composite uncoated specimen by an MTS 330-kip servo-hydraulic actuator mounted to a large, steel structural frame bolted to the floor of the Major Unit's Laboratory, as seen in Figure 10.23. An MTS 110-kip servo-hydraulic actuator applied load to the galvanized specimen in a manner similar to the load application on the uncoated specimen. Large spreader beams were used to distribute the load from the heads of the actuators to the composite specimens to avoid localized concrete crushing due to concentrated load effects. Elastomeric bearing pads, which consist of alternating layers of steel strips and neoprene in industrial grade rubber, were placed between the steel spreader beams and the concrete deck to further aid in the transfer of load in the system.

Figure 10.21: Isometric View of the PBFTG Specimens Placed Within the Structural Frames

10.8 Cyclic Loading Magnitude and Frequency Determination

The loading sequence was used to simulate a 75-year design life of the system. The Fatigue I limit state reflects the fatigue and fracture load combination relating to infinite load-induced fatigue life and reflects load levels found to be representative of the maximum stress range of the truck population for infinite fatigue life design. The loads required to induce the Fatigue I moment in the main span specimens were calculated prior to testing. Equation 10.1 demonstrates the load factors used in this testing, which were previously defined in Section 6.2.2.

$$Fatigue\ I = 1.75(LL + IM) \quad \text{Eq. 10.1}$$

Where:

Fatigue I = force effect from the Fatigue I load combination

LL = force effect from vehicular live load

IM = force effect from vehicular dynamic load allowance

The servo-hydraulic actuators applied a load of 87.5 kip simultaneously on both specimens to induce the Fatigue I moment in the composite specimens. Procedures describing the calculation of this load are described in Appendix D.

The AASHTO LRFD BDS were used to determine the number of cycles the system must sustain over the course of its design life. The following assumptions were made to determine the number of required fatigue cycles:

1. The average daily traffic was 850 vehicles
2. The bridge was located in a non-interstate rural environment
3. The bridge had a design life of 75 years
4. The bridge had two lanes available to trucks

The average daily truck traffic (ADTT) can be determined by multiplying the average daily traffic (ADT) by the fraction of trucks in the traffic. AASHTO LRFD BDS Table C3.6.1.4.2-1 may be used in lieu of site-specific traffic data. Assuming the bridge was located in a non-interstate rural environment, the fraction of trucks in traffic may be assumed to 15% of the ADT. The single-lane ADTT is for the traffic lane in which most truck traffic crosses the bridge. AASHTO LRFD BDS Table 3.6.1.4.2-1 is used to determine the fraction of truck traffic in a single lane, *p*. Assuming the bridge had two lanes available to trucks, the fraction of trucks in a single lane is taken as 85% of the ADTT. The number of fatigue cycles, assuming a 75-year design life, was determined as follows:

Number of Cycles = 850 (ADT) × 0.15 (fraction of trucks in traffic) × 0.85 (*p*) × 365 (days/year) × 75 (years) = 2,966,766 Cycles

10.9 Testing Procedure

Static testing was performed prior to fatigue loading. Five strain gauge readings were recorded prior to loading to obtain zero readings. The load was increased in stroke control in 8.75 kip intervals until ultimately reaching the Fatigue I loading. After each step in the incremental loading was reached, the load was allowed to sit on the specimens for five minutes allowing the system to settle into a constant loading state and settle any vibration effects, removing any impact on the system. After the five-minute delay, five strain readings were recorded and the process was repeated until the Fatigue I loading was reached. After the Fatigue I loading was reached, the load was removed and allowed to settle for ten minutes before the process was repeated and the readings at each load level were averaged. The static testing occurred at different numbers of cycles based on the behavior of the specimens. After any long-term stoppage of the system, which will be described in later sections, static testing occurred after 100,000 cycles. When testing was somewhat continuous, static testing occurred after 200,000 cycles. The static testing occurred at the following number of cycles: 1e5; 2e5; 3e5; 4e5; 6e5; 7e5; 8e5; 9e5; 1e6; 1.2e6; 1.3e6; 1.4e6; 1.5e6; 1.7e6; 1.9e6; 2.1e6; 2.3e6; 2.5e6. A thorough investigation of the link slab, transition zone, slab/girder interface, and bottom flange bend regions was performed after each static test.

10.10 Loss of Composite Action in the Galvanized Specimen

After 300,000 fatigue cycles, composite action was lost in the galvanized specimen. Under the application of fatigue loading, a separation between the SIP metal formwork and the top flange of the PBFTG could be observed longitudinally between the point of loading and the link slab. Improper welding of the shear studs through the SIP metal formwork through the galvanization at the top flange is assumed to be a large contributing factor in the loss of composite action.

To regain composite action in the system, a methodology evaluated by Kreitman et. al. (2016) was used to install new shear connectors in the region where the pre-installed shear connectors had failed. Kreitman et. al considered many different methods of strengthening bridge systems with post-installed shear connectors and ultimately decided to pursue the use of adhesive anchors, as shown in Figure 10.24.

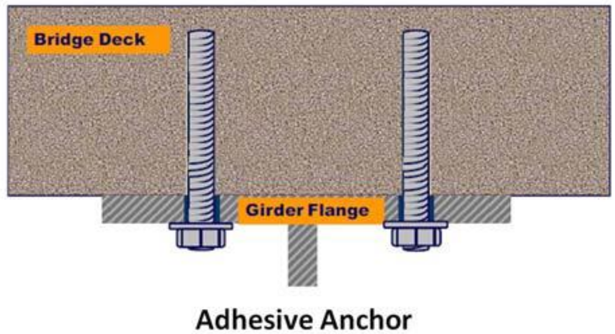

Figure 10.22: Post-Installed Shear Connectors

The adhesive anchor shear connectors were composed of 12 inch long by 7/8 inch diameter ASTM A193 B7 Zinc fully threaded rods. A two-part adhesive, Hilti HIT-HY 200-R, was used in conjunction with the threaded rods. The connectors were installed using the following procedure:

1. For placement of the 7/8 inch rods, measurements were marked longitudinally and transversely on each top flange. Longitudinally, the locations occurred every 12 inches on center, beginning directly under the load application and running into the link slab transition zone. This measurement was determined to ensure rods were placed in the bottom flute of the SIP formwork three inches from the failed shear studs. Transversely, at every longitudinal measure mark, two marks were made: The exterior line was 1.5 inches from the edge of the flange and the interior line was 5 inches from the edge of the flange, coinciding with the locations of the failed shear studs.
2. At the intersections of the longitudinal and transverse lines, a punch and hammer were used to create a starter hole for drilling.
3. Using a portable drill with a magnetic base, drilling through the flange began where starter holes were punched. Drilling was performed using a small drill bit to begin each hole and increasing in steps until a 1 1/16 inch diameter hole was drilled through the flange (Figure 10.25).
4. Through the hole in the flange, a 1 inch diameter concrete bit was used to drill 8 inches into the concrete deck (Figure 10.26).

5. The finished hole in the flange was cleaned with a wire brush attachment and compressed air, as specified by the adhesive installation procedures of the HIT-HY 200 Hybrid Adhesive Anchoring System.
6. Before beginning the threaded rod installation process, all threaded rods were prepared with two washers and a heavy hex nut, as the adhesive provided limited work time.
7. Using the Hilti HDM Manual Adhesive Dispenser, the adhesive was injected into the hole from the top down to avoid air bubbles. Each hole was approximately 2/3 filled with adhesive (Figure 10.27).
8. The threaded rod was inserted into the hole using a twisting motion, so the adhesive filled the threads (Figure 10.28).
9. Washers were then pressed against the girder and the nut was tightened by hand.
10. The rod was held in place until the adhesive could hold the rods in the flange without external support.
11. The adhesive was allowed to cure the recommended time from the manufacturer.
12. After the adhesive cured, the nuts were tightened to the torque specified by the manufacturer (Figure 10.29).

Figure 10.23: Drilling Through the PBFTG Top Flange

Figure 10.24: Concrete Drilling with Wet and Dry Shop Vacuum to Control Dust

Figure 10.25: Hilti HIT-HY 200-R Adhesive Injection

Figure 10.26: Insertion of Threaded Rods with a Twisting Motion

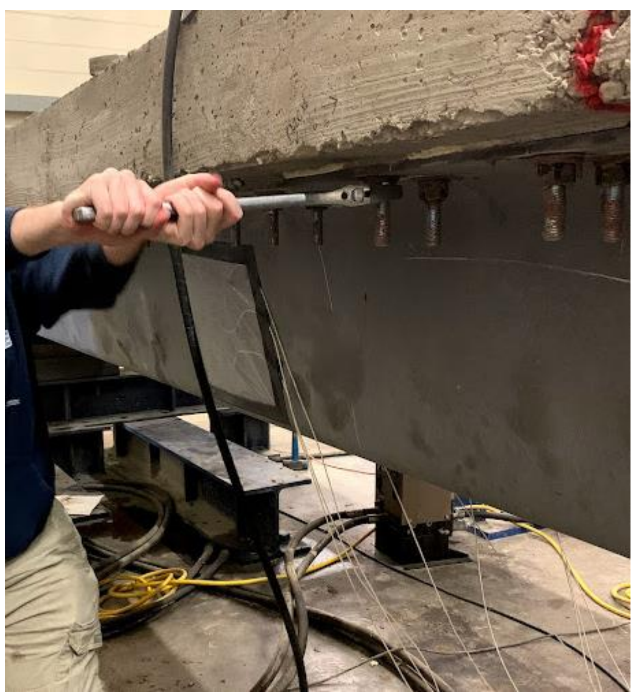

Figure 10.27: Tightening of Nut

10.11 LOSS OF COMPOSITE ACTION IN THE UNCOATED SPECIMEN

After 1,400,000 fatigue cycles, composite action was lost in the uncoated specimen. Due to user error, the concrete at the point of loading needed to be replaced. Longitudinally, 54 inches on either side of the load application point, the concrete deck was removed. The concrete deck was removed by scoring the concrete with a 14 inch diameter concrete saw and jack hammering the weakened layers, as seen in Figures 10.30 and 10.31.

Figure 10.28: Concrete Deck Scoring

Figure 10.29: Concrete Deck Removal

Care was taken to not damage the longitudinal rebar to ensure proper load transfer through the new concrete deck. Following a method similar to that discussed in Section 10.10, holes were drilled through the top flange of the uncoated specimen and threaded rods were inserted to restore composite action in the damaged portion of the deck. As the concrete was removed, a nut and washer were placed on the top of the top flange to anchor the threaded rod to the top flange.

As only a portion of the concrete deck was removed and composite action restored, the applied load was recalculated to obtain the same link slab rotation. After the concrete had cured for 28 days, a static test was performed to determine the load needed to cause the same deflection at the point of loading. Static testing was performed on the link slab specimens at small intervals of load to determine the load required to reach the same midspan deflections produced pre-concrete deck failure. The loads were increased in 5 kip increments until a load of 70 kip was reached, corresponding to the desired midspan deflection.

10.12 RESULTS

This section describes the results obtained during fatigue testing and the methods used to analyze the collected data. The procedure used to calculate the induced stresses and moments by the applied loading is included herein. In addition, this section includes testing summaries and comparison of the experimental versus back calculated loading at each static test time interval. The deflections of each girder throughout the fatigue life are also provided.

10.12.1 Gauge Configuration

The stresses throughout the system were obtained from the recorded strain data using a method developed by Helwig and Fan (2000). Longitudinal stresses in thin wall members can be calculated by considering axial forces and bending moments while neglecting warping stresses. The longitudinal stresses induced by axial forces and bending moments are assumed to be linearly distributed across the cross-section. Using this method, only three stress readings from non-collinear points are needed to determine the distribution of stresses in the cross-section. The stress distribution of the cross-section can be expressed by Equation 10.2:

$$f(x, y) = a + bx + cy \qquad \text{Eq. 10.2}$$

Where:

f = longitudinal Stress (ksi)

a, b, c = constants

x, y = coordinate system on the cross-section of the member (in)

The strain gauge locations in terms of the transverse and vertical directions, x- and y-, respectively, are shown in Table 10.2 where the x-datum is the center of the bottom flange and the y-datum is the noncomposite section centroid.

Table 10.2: x-, y- Coordinates of Strain Gauges

Gauge Coordinates		
Gauges	From Datum	
	x (in)	y (in)
G01, G10, G19, G28	-16.06	6.87
G02, G11, G20, G29	-14.61	1.05
G03, G12, G21, G30	-13.15	-4.77
G04, G13, G22, G31	-6.00	-10.39
G05, G14, G23, G32	0.00	-10.39
G06, G15, G24, G33	6.00	-10.39
G07, G16, G25, G34	13.15	-4.77
G08, G17, G26, G35	14.61	1.05
G09, G18, G27, G36	16.06	6.87

10.12.2 Gauge Data Selection

After the system was statically loaded twice, following the methodology described in Section 10.9, the strain data was collected and sorted to only include consistent results. Typically, a gauge presenting irregularly on any given static test would continue to behave irregularly on following static tests. For the data used for further reduction, once a gauge recorded inconsistent results, it was not included in any further stress calculations. The data inclusion matrices for each girder can be seen in Tables 10.3 and 10.4 where '0' denotes data which was kept and '1' indicates data which was discarded due to inconsistency.

Table 10.3: Gauge Inclusion Matrix for the Galvanized Specimen

Gauge	Cycle Count																					
	Base Test	100,000	200,000	300,000	GG LoCA Base Test	400,000	500,000	600,000	700,000	800,000	900,000	1,000,000	1,200,000	UG LoCA Base Test	1,300,000	1,400,000	1,500,000	1,700,000	1,900,000	2,100,000	2,300,000	2,500,000
G01	0	0	0	0	0	1	1	1	1	1	1	1	1	1	1	1	1	1	1	1	1	1
G02	0	0	0	0	0	0	0	0	0	0	0	0	0	1	1	1	1	1	1	1	1	1
G03	0	0	0	0	0	0	0	0	0	0	1	1	1	1	1	1	1	1	1	1	1	1
G04	0	0	0	0	0	0	0	0	0	0	0	0	0	0	0	0	0	0	0	0	0	0
G05	1	1	1	1	1	1	1	1	1	1	1	1	1	1	1	1	1	1	1	1	1	1
G06	0	0	0	0	0	0	0	0	0	0	0	0	0	1	1	1	1	1	1	1	1	1
G07	0	0	0	0	0	0	0	0	0	0	0	0	0	1	1	1	1	1	1	1	1	1
G08	0	0	0	0	0	0	0	0	0	0	0	0	0	0	0	0	0	0	0	0	0	0
G09	0	0	0	0	0	0	0	0	0	0	0	0	0	0	0	0	0	0	0	0	0	0
G10	0	0	0	0	0	0	0	0	0	0	0	0	0	0	1	1	1	1	1	1	1	1
G11	0	0	1	1	1	1	1	1	1	1	1	1	1	1	1	1	1	1	1	1	1	1
G12	0	0	0	0	0	0	0	0	0	0	0	0	0	1	1	1	1	1	1	1	1	1
G13	0	0	0	0	0	0	0	0	0	0	0	0	0	0	0	0	0	0	1	1	1	1
G14	0	0	0	0	1	1	1	1	1	1	1	1	1	1	1	1	1	1	1	1	1	1
G15	0	0	0	0	0	0	1	1	1	1	1	1	1	1	1	1	1	1	1	1	1	1
G16	0	0	0	0	0	0	0	0	0	0	0	0	0	0	0	0	0	0	0	0	0	0
G17	0	0	0	0	0	0	0	0	0	0	0	0	0	0	0	0	0	0	0	0	0	0
G18	0	0	0	0	0	0	0	0	0	0	0	0	0	0	0	0	0	0	0	0	0	0

Table 10.4: Gauge Inclusion Matrix for the Uncoated Specimen

Gauge	Cycle Count																					
	Base Test	100,000	200,000	300,000	GG LoCA Base Test	400,000	500,000	600,000	700,000	800,000	900,000	1,000,000	1,200,000	UG LoCA Base Test	1,300,000	1,400,000	1,500,000	1,700,000	1,900,000	2,100,000	2,300,000	2,500,000
G19	0	0	0	1	1	1	1	1	1	1	1	1	1	1	1	1	1	1	1	1	1	1
G20	0	0	0	0	0	0	1	1	1	1	1	1	1	1	1	1	1	1	1	1	1	1
G21	0	0	0	0	0	0	0	0	0	0	0	0	0	0	0	0	0	0	0	0	0	0
G22	0	0	0	0	0	0	0	0	0	0	0	0	0	1	1	1	1	1	1	1	1	1
G23	0	0	0	1	1	1	1	1	1	1	1	1	1	1	1	1	1	1	1	1	1	1
G24	0	0	0	0	1	1	1	1	1	1	1	1	1	1	1	1	1	1	1	1	1	1
G25	0	0	0	0	0	0	0	0	0	0	0	0	0	0	0	0	0	0	0	0	0	0
G26	0	0	0	0	0	0	0	0	0	0	0	0	0	0	0	0	0	0	0	0	0	0
G27	0	0	0	0	0	0	0	0	0	0	0	0	0	1	1	1	1	1	1	1	1	1
G28	0	0	0	0	0	0	0	0	0	0	0	0	0	0	0	0	0	0	0	0	0	0
G29	1	1	1	1	1	1	1	1	1	1	1	1	1	1	1	1	1	1	1	1	1	1
G30	0	0	0	0	1	1	1	1	1	1	1	1	1	1	1	1	1	1	1	1	1	1
G31	0	0	0	0	0	0	0	0	0	0	0	0	0	1	1	1	1	1	1	1	1	1
G32	0	0	0	0	0	0	0	0	0	0	0	0	0	0	0	0	0	0	0	0	0	0
G33	0	0	0	0	0	0	0	0	0	0	0	0	0	0	0	0	0	0	0	0	0	0
G34	0	0	0	0	0	0	0	1	1	1	1	1	1	1	1	1	1	1	1	1	1	1
G35	0	0	0	0	0	0	0	0	0	0	0	0	0	0	0	0	0	0	0	0	0	0
G36	0	0	0	0	0	0	0	0	0	0	0	0	0	0	0	0	0	0	0	0	0	0

10.12.3 Linear Regression

A three-dimensional linear regression algorithm, based on least square regression, was employed to further reduce errors from physical strain measurements. The regression model is a statistical toll which does not rely on physical assumptions. To determine the constants, *b* and *c*, in Equation 10.2, the following set of linear equations are to be solved:

$$\begin{bmatrix} L_{11} & L_{12} \\ L_{21} & L_{22} \end{bmatrix} \begin{Bmatrix} b \\ c \end{Bmatrix} = \begin{Bmatrix} L_{10} \\ L_{20} \end{Bmatrix} \quad \text{Eq. 10.3}$$

$$L_{11} = \sum_{i=1}^{n} (x_i - \bar{x})^2 \quad \text{Eq. 10.4}$$

$$L_{22} = \sum_{i=1}^{n} (y_i - \bar{y})^2 \quad \text{Eq. 10.5}$$

$$L_{12} = L_{21} = \sum_{i=1}^{n} (x_i - \bar{x})(y_i - \bar{y}) \quad \text{Eq. 10.6}$$

$$L_{10} = \sum_{i=1}^{n} (x_i - \bar{x})\left(f_i - \bar{f}\right) \quad \text{Eq. 10.7}$$

$$L_{20} = \sum_{i=1}^{n} (y_i - \bar{y})\left(f_i - \bar{f}\right) \quad \text{Eq. 10.8}$$

$$\bar{x} = \frac{1}{n}\sum_{i=1}^{n} x_i \quad \text{Eq. 10.9}$$

$$\bar{y} = \frac{1}{n}\sum_{i=1}^{n} y_i \quad \text{Eq. 10.10}$$

$$\bar{f} = \frac{1}{n}\sum_{i=1}^{n} f_i \quad \text{Eq. 10.11}$$

$$a = \bar{f} - b\bar{x} - c\bar{y} \quad \text{Eq. 10.12}$$

Where:

f_i = longitudinal stress at the i^{th} gauge (ksi)

x_i = transverse coordinate at the i^{th} gauge (in)

y_i = vertical coordinate at the i^{th} gauge (in)

10.12.4 Calculation of Induced Moment

The induced moment is calculated following a procedure developed by Imhoff (1998), where the load carrying mechanism is broken into three parts. The first part is the steel girder bending about its own neutral axis, M_L. The second part is the concrete deck bending about its own neutral axis, M_U. The final component is a moment couple induced by the composite action between the steel girder and the concrete deck, Na. Equations 10.13 through 10.16 were used to determine the total moment at each cross-section instrumented (Bertoldi, 2009). The concrete and steel properties are summarized in Section 10.6.

$$M_L = (\sigma_O - \sigma_{CG})S_{steel} \qquad \text{Eq. 10.13}$$

$$M_u = \left(\frac{E_{conc}I_{conc}}{E_{steel}I_{steel}}\right)M_L \qquad \text{Eq. 10.14}$$

$$Na = \sigma_{CG}A_{steel}\left(d_{steel} - y_{steel} + t_{haunch} + \frac{t_{conc}}{2}\right) \qquad \text{Eq. 10.15}$$

$$M_T = M_L + M_u + Na \qquad \text{Eq. 10.16}$$

Where:

S_{steel} = section modulus of the noncomposite PBFTG (in^3)

E_{conc} = modulus of elasticity of the concrete deck (ksi)

I_{conc} = moment of inertia of the concrete deck about its *x*-axis (in^4)

E_{steel} = modulus of elasticity of the PBFTG (ksi)

I_{steel} = moment of inertia of the PBFTG about its *x*-axis (in^4)

A_{steel} = cross-sectional area of the PBFTG (in^2)

d_{steel} = depth of the PBFTG (in)

y_{steel} = noncomposite depth of neutral axis (in)

t_{haunch} = haunch thickness (in)

t_{conc} = concrete deck thickness (in)

As two of the gauge locations were offset *2d* (46 inches) away from midspan during testing, the moments calculated at those locations were adjusted to calculate the moments at midspan. It is assumed each PBFTG is simply supported to calculate the moments at midspan and the quarter-span, where gauges were located. The moment calculations for each cross-section use a span length of 24.5 feet. These values were used to back calculate the load required to induce the calculated moment. Some deviation is shown between the applied load and the back calculated load due to the assumed simply supported conditions and assumption of full composite action between the PBFTG and the concrete deck throughout testing. The percent error values and the R^2 values for each cross-section at each static loading between the applied loads and the back calculated loads of 87 kip and 70 kip are shown in Tables 10.5 through 10.8. The small R^2 values and erratic error values are due to the loss of gauges through testing, as seen in Table 10.3. When there are no longer three non-colinear gauges, the reduction methodology is no longer valid and produces nonrealistic results.

Table 10.5: Least Squares and Percent Error for the Galvanized Specimen at Midspan

Cycle Count	Least Square, R^2	Percent Error, %
Base Test	1.0000	-7.57%
0,100,000	0.9989	-11.07%
0,200,000	0.9997	-10.91%
0,300,000	0.9998	-11.32%
GG LoCA Base Test	0.9999	-12.97%
0,400,000	0.9997	-12.93%
0,500,000	0.9991	-13.34%
0,600,000	0.9995	-13.09%
0,700,000	0.9995	-13.45%
0,800,000	0.9998	-14.75%
0,900,000	0.9993	-11.67%
1,000,000	0.9996	-14.93%
1,200,000	0.9995	-16.00%
UG LoCA Base Test	0.9999	-37.78%
1,300,000	0.9995	-29.68%
1,400,000	0.9995	-33.98%
1,500,000	0.9994	-34.06%
1,700,000	0.9981	-25.98%
1,900,000	0.9995	-34.73%
2,100,000	0.9995	-34.07%
2,300,000	0.9995	-33.83%
2,500,000	0.9989	-34.54%

Table 10.6: Least Squares and Percent Error for the Galvanized Specimen at Quarter Span

Cycle Count	Least Square, R^2	Percent Error, %
Base Test	0.9993	9.98%
0,100,000	0.9931	16.55%
0,200,000	0.9971	8.25%
0,300,000	0.9976	9.40%
GG LoCA Base Test	0.9995	9.45%
0,400,000	0.9986	10.35%
0,500,000	0.9927	21.09%
0,600,000	0.9975	17.38%
0,700,000	0.9971	18.73%
0,800,000	0.9995	17.13%
0,900,000	0.9975	16.89%
1,000,000	0.9979	18.86%
1,200,000	0.9972	16.56%
UG LoCA Base Test	0.9997	2.28%
1,300,000	0.9963	15.42%
1,400,000	0.9972	11.07%
1,500,000	0.9974	10.05%
1,700,000	0.9951	10.68%
1,900,000	0.3926	-729.20%
2,100,000	0.0004	47.68%
2,300,000	0.1123	125.81%
2,500,000	0.5336	-725.54%

Table 10.7: Least Squares and Percent Error for the Uncoated Specimen at Midspan

Cycle Count	Least Square, R^2	Percent Error, %
Base Test	1.0000	-3.13%
0,100,000	0.9994	-1.70%
0,200,000	0.9993	-3.15%
0,300,000	0.9996	0.31%
GG LoCA Base Test	1.0000	0.53%
0,400,000	0.9998	0.80%
0,500,000	0.9991	3.33%
0,600,000	0.9994	4.11%
0,700,000	0.9995	2.98%
0,800,000	0.9999	3.13%
0,900,000	0.9994	1.96%
1,000,000	0.9995	3.05%
1,200,000	0.9996	3.58%
UG LoCA Base Test	0.9999	19.31%
1,300,000	0.9921	21.38%
1,400,000	0.9990	17.48%
1,500,000	0.9988	15.70%
1,700,000	0.9973	13.82%
1,900,000	0.9986	14.42%
2,100,000	0.9983	14.75%
2,300,000	0.9984	14.70%
2,500,000	0.9969	29.72%

Table 10.8: Least Squares and Percent Error for the Uncoated Specimen at Quarter Span

Cycle Count	Least Square, R^2	Percent Error, %
Base Test	0.9999	4.36%
0,100,000	0.9963	5.45%
0,200,000	0.9993	3.62%
0,300,000	0.9993	4.40%
GG LoCA Base Test	0.9992	-0.27%
0,400,000	0.9996	0.80%
0,500,000	0.9978	9.28%
0,600,000	0.9988	7.60%
0,700,000	0.9992	7.04%
0,800,000	0.9997	6.57%
0,900,000	0.9991	7.16%
1,000,000	0.9993	6.44%
1,200,000	0.9994	7.30%
UG LoCA Base Test	0.9999	18.70%
1,300,000	0.9994	31.80%
1,400,000	0.9992	23.34%
1,500,000	0.9993	22.89%
1,700,000	0.9942	23.37%
1,900,000	0.9995	20.92%
2,100,000	0.9992	21.80%
2,300,000	0.9994	23.49%
2,500,000	0.9884	21.11%

Figures 10.32 and 10.33 summarize the comparisons between the loads applied to the girders at each static test and the back calculated loads computed from the strain data and three-dimensional linear regression. Select static tests have been removed due to recording errors. As shown, the girders' and link slab's behavior remained constant throughout the 75-year design life. A slight discrepancy is shown in Figure 10.32 where the back calculated vertical load is higher than the applied load. This is attributed to the rigidity retained in the galvanized specimen when composite action was lost in the uncoated specimen, and the loads were adjusted accordingly. Data for each static load test can found in Appendix E.

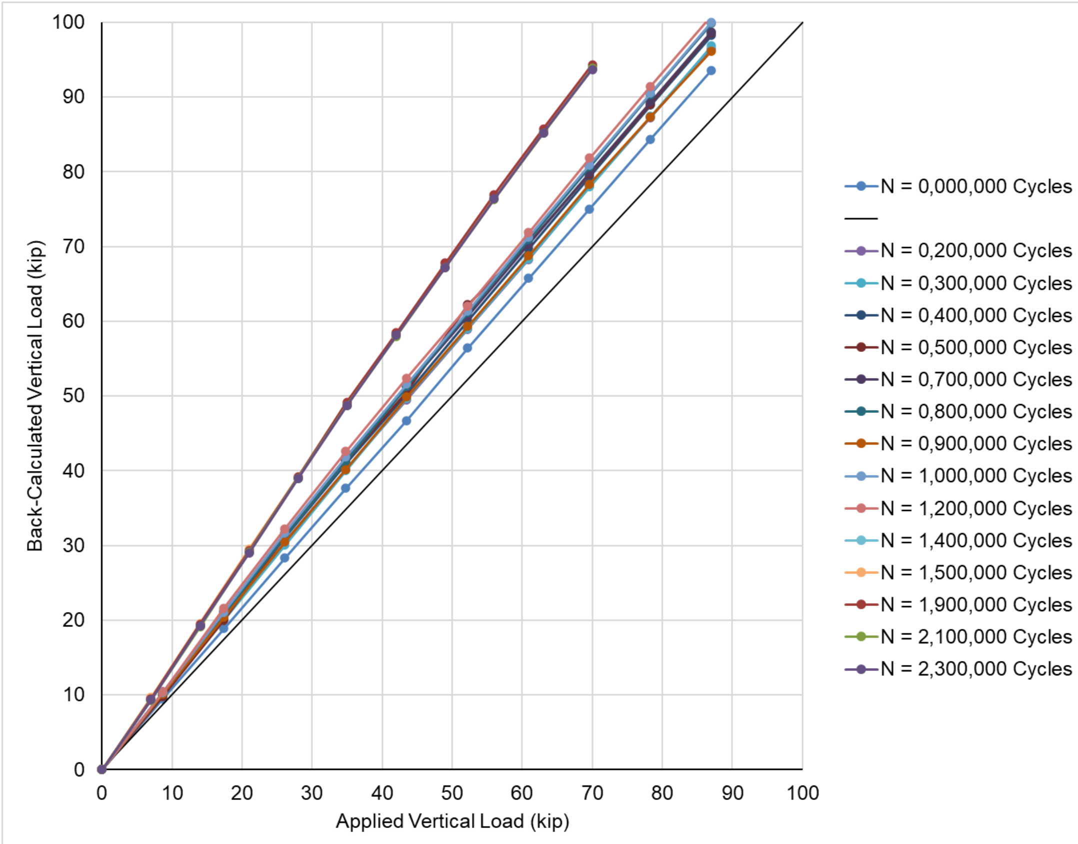

Figure 10.30: Correlation of the Applied Load to the Back Calculated Load of the Galvanized Specimen

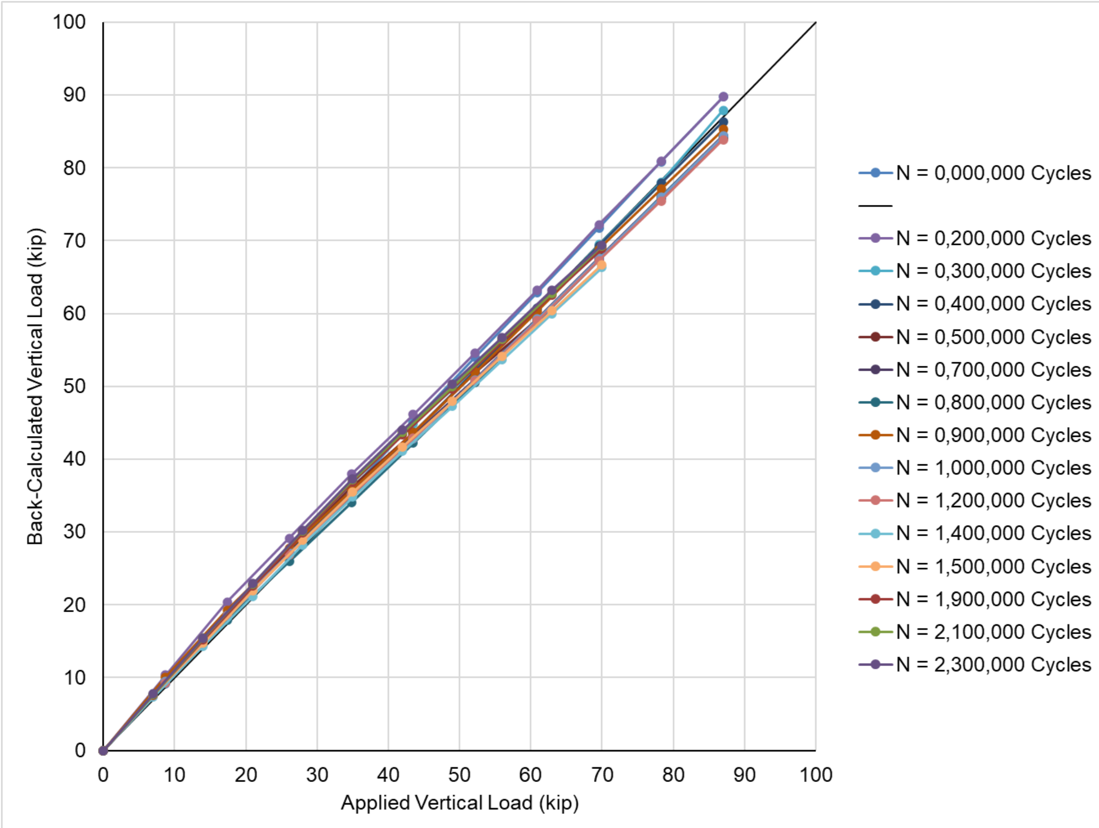

Figure 10.31: Correlation of the Applied Load to the Back Calculated Load of the Uncoated Specimen

Figure 10.34 presents the midspan deflections recorded throughout the cyclic loading of both specimens. As shown in Figure 10.34, the deflections remained consistent throughout the design life of the PBFTGs. This further shows the link slab continued to act as a stable structural element, even after composite action was lost in both PBFTGs at different times.

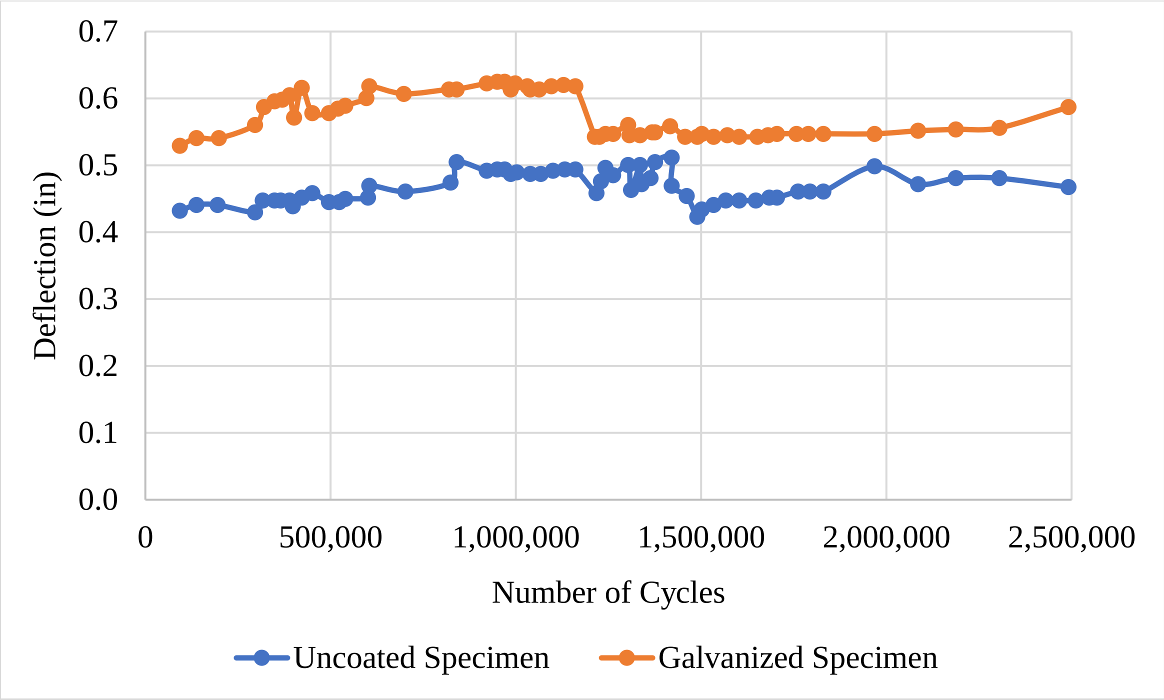

Figure 10.32: Midspan Deflection of Each Specimen Throughout Testing

10.13 SUMMARY

This chapter described the physical flexural testing performed on a full-scale link slab constructed between two PBFTGs. The simply supported PBFTGs were formed from 300 inch long by 84 inch wide by 1/2 inch thick HPS-50 steel. Each specimen was cold-bent before delivery to the Major Units Lab where a concrete deck was cast on each specimen separately. After the specimens were fully composite, a link slab was poured longitudinally between the PBFTGs. Cyclic loading was applied to simulate a 75-year design life in a rural environment and static testing was performed throughout testing to monitor any change in the link slab behavior. Strain and deflection data were recorded at each static testing and linear regression was used to transform the strain at each given cross-section to the moment at each location. The consistent behavior shown, in both the strain and deflection data, demonstrates link slabs can adequately transfer load throughout the design life of PBFTGs.

CHAPTER 11: CONCLUDING REMARKS

11.1 PROJECT SUMMARY

The scope of this project was to demonstrate PBFTGs can be utilized in a broader range of applications in the short-span bridge market. This was achieved by performing the following tasks:

- Reviewing literature relating to PBFTGs, live load distribution, the effect of compactness on the flexural capacity of sections, and link slab details.
    - PBFTGs have been utilized successfully in multiple experimental and in-service bridge scenarios. However, multiple researchers have shown PBFTGs can be utilized more efficiently in terms of ultimate capacity and applicable LLDFs.
    - Live load distribution has been extensively evaluated for bridges containing I-girder longitudinal elements but not box-girder longitudinal elements. The current restrictions on LLDFs for box-girders, and therefore PBFTGs, are based on a limited scope of analytical tests from the 1960s.
    - Compactness, as it relates to the capacity of PBFTGs, is based on the same limited set of analytical studies from the 1960s. Studies have not shown the current restrictions to be scientifically derived. Instead, these limits were established because the complicated behavior of PBFTGs was not understood.
    - Link slabs have been utilized successfully as a transverse bridge detail for nearly two decades, eliminating undesirable joints. However, link slabs have not been evaluated with PBFTGs and could become a competitive solution to the buckling issue of the slender bottom flange over pier regions.
- Developing analytical tools to assess the behavior and capacity of PBFTGs with varying dimensions and properties.
    - Analytical modeling techniques were developed and refined to determine the behavior of modular PBFTGs loaded to ultimate capacity and PBFTG bridges under service level loads.
    - These tools are sophisticated, as they can be used with complex bridge and girder geometry as well as linear or non-linear material properties.

   - Loading can be applied to the model in a multitude of different ways, including linearly perpendicular to the longitudinal elements, linearly along the skew of the bridge/girder, HL-93 design truck and tandem loading, or user input vehicular loading.
   - These tools have been thoroughly benchmarked against numerous experimental and field tests, including seminal noncomposite plate girder experiments, composite plate girders experiments, destructive flexural testing of PBFTGs, and multiple in-service live load field tests of PBFTGs.
- Conducting sensitivity and parametric studies to assess which parameters affect the computation of LLDFs for PBFTGs.
   - A sensitivity study was developed to determine the effects of key bridge and girder parameters on live load distribution in PBFTG bridges.
   - The results of the sensitivity study were used to generate a matrix of over 50,000 PBFTG bridges with different combinations of the parameters found to have the greatest effect on live load distribution.
   - MLR was used on the results of the parametric study to determine simplified equations to be used with LGA.
   - Based on comparisons with the parametric study and three in-service PBFTG bridges, the proposed equations prove more accurate than current simplified methodologies presented in the AASHTO LRFD BDS.
- Conducting behavioral studies to assess the effect of skew on the ultimate capacity of PBFTGs.
   - An analytical model was generated, based on and verified against the results of a previous ultimate capacity PBFTG experimental test.
   - The bearing skew was increased in 5° increments up to 45° and loaded past the ultimate theoretical strength.
   - Preliminary results from the study show bearing skew does not influence the ultimate capacity of PBFTGs.
- Performing flexural testing on modular PBFTGs transversely joined by a link slab.
   - A full-scale link slab was constructed between two PBFTG specimens.

- The link slab was fatigue loaded simulating the 75-year design of the specimens in a rural non-interstate environment.
- Deflection data was recorded throughout the fatigue testing, and strain data was recorded periodically throughout the design life of the link slab during static testing.
- Results showed the link slab behaved linearly throughout its design life and can adequately serve as a transverse bridge detail over piers of continuous PBFTG bridges.

This project has expanded the potential market for the innovative PBFTG system into multiple span arrangements, increasing the system's versatility. This new work will help continue to promote the commercial advancement of this technology.

11.2 Recommendations for Continued Research

The author recommends the following tasks for future work and/or expansions to this project:

- As more PBFTG bridges are built in the field, additional live load field testing is recommended to verify the validity of the proposed LLDF equations.
- Investigate additional parameters to determine the effect on live load distribution in PBFTG bridges. These parameters may include skew, presence of sidewalks/barriers for stiffness, continuity/support conditions, and superelevation.
- Perform sensitivity and parametric studies to determine the effects of key bridge and girder parameters on shear live load distribution in PBFTG bridges.
- Perform experimental testing to confirm the analytical result that skew does not have an impact on the capacity of PBFTGs.
- Investigate the behavior of bearing stiffeners in PBFTGs. During the behavioral study to assess the effect of skew, it was noticed the bearing stiffener stresses significantly increased with increased degree of skew.
- Perform feasibility studies to determine the maximum applicable ranges of the standardized PBFTG sections using the proposed simplified equations.

- Practices for bolted and welded splices should be assessed for PBFTGs utilized in longer spans.
- Perform live load field testing on a continuous span PBFTG bridge with a link slab over an interior pier.
- Perform destructive flexural testing on a link slab between PBFTGs.

REFERENCES

AASHTO/NSBA Steel Bridge Collaboration. (2020). Guidelines to Design for Constructability and Fabrication (Report No. NSBAGDC-4). Washington, DC: American Association of State Highway and Transportation Officials.

Aktan, H., & Attanayake, U. (2011). *High skew link slab bridge system with deck sliding over backwall or backwall sliding over abutments* (Report No. RC-1563). Lansing, MI: Michigan Department of Transportation.

American Association of State Highway and Transportation Officials. (2020). AASHTO LRFD Bridge Design Specifications, Ninth Edition. Washington, DC.

American Association of State Highway Officials. (1931). AASHO Standard Specifications for Highway Bridges, First Edition. Washington, DC.

American Institute of Steel Construction. (2017). *Steel Construction Manual* (15th ed). Chicago, IL.

Armijos-Moya, S., Wang, Y., Helwig, T. A., Clayton, P. M., Engelhardt, M. D., & Williamson, E. B. (2019). *Improved tub girder details: Final report* (Report No. FHWA/TX-19/0-6862-1). Austin, TX: Texas Department of Transportation.

Arockiasamy, M., & Amer, A. (1998). Load distribution on highway bridges based on field test data: Phase III (Report No. WPI 0510668). Tallahassee, Florida: Florida Department of Transportation.

Bakht, B., & Jeager, L. G. (1992). Ultimate load test of slab-on-girder bridge. *Journal of Structural Engineering*, *118*(6), 1608-1624.

Barr, P. J., & Amin, MD. N. (2006). Shear live-load distribution factors for I-girder bridges. *Journal of Bridge Engineering*, *11*(2), 197-204. doi: 10.1061/(ASCE)1084-0702(2006)11:2(197)

Barth, K. E. (1996). Moment-rotation characteristics for inelastic design of steel bridge beams and girders (Doctoral dissertation, Purdue University).

Barth, K. E., & Wu, H. (2006). Efficient nonlinear finite element modeling of slab on steel stringer bridges. Finite Elements in Analysis and Design 42(14), 10.

Bertoldi, A. G. (2009). A strength and serviceability assessment of high performance steel Bridge 10462 (Master's thesis, West Virginia University). Available from ProQuest.

Bishara, A. G., Liu, M. C., & El-Ali, N. D. (1993) Wheel load distribution on simply supported skew I-beam composite bridges. *Journal of Structural Engineering, 119*(2), 399-419.

Bleich, F., & Ramsey, L. B. (1952). *Buckling strength of metal structures*. New York, NY: McGraw-Hill Book Company.

Bryan, G. H. (1890). On the stability of a plane plate under thrusts in its own plane, with applications to the "buckling" of the sides of a ship. *Cambridge Philosophical Society, 6*, 54-67.

Caner, A., & Zia, P. (1998). Behavior and design of link slabs for jointless bridge decks. Journal of the Precast/Prestressed Concrete Institute, 68-80.

Chandar, G., Hyzak, M. D., & Wolf, L. M. (2010). Rapid, economical bridge replacement. *Modern Steel Construction*.

Chong, J. M. J. (2012) *Construction engineering of steel tub-girder bridge systems for skew effects* (Doctoral dissertation, Georgia Institute of Technology). Available from ProQuest.

Coletti, D., Chavel, B., & Gatti, W. J. (2011). Challenges of skew in bridges with steel girders. Transportation Research Record: Journal of the Transportation Research Board, 2251, 47-56. doi: 10.3141/2251-05

Crisfield, M. A. (1983). An arc-length method including line searches and accelerations. International Journal for Numerical Methods in Engineering, 19, 1269-1289.

Cross, B., Vaughn, B., Panahshahi, N., Petermeier, D., Siow, Y. S., & Domagalski, T. (2009). Analytical and experimental investigation of bridge girder shear distribution factors. *Journal of Bridge Engineering, 14*(3), 154-163. doi: 10.1061/(ASCE)1084-0702(2009)14:3(154)

Dassault Systèmes. (2020). Abaqus/CAE Version 6.20. Dassault Systèmes Simulia Corp., Providence, RI.

Ebeido, T., & Kennedy, J. B. (1996). Girder moments in continuous skew composite bridges. Journal of Bridge Engineering, 1(1), 37-45.

Ebeido, T., & Kennedy, J. B. (1996). Shear and reaction distributions in continuous skew composite bridges. Journal of Bridge Engineering, 1(4), 155-165.

El-Safty, A. K. (1984). Analysis of jointless bridge decks with partially debonded simple span beams (Doctoral dissertation, North Carolina State University).

Fu, C. C., Elhelbawey, M., Sahin, M. A., & Schelling, D. R. (1996). Lateral distribution factor from bridge field testing. *Journal of Structural Engineering, 122*(9), 1106-1109.

Galambos, T. V. (1981). Load and resistance factor design. *American Institute of Steel Construction Engineering Journal*, 74-82.

Galindez, N. Y. (2009). Levels of lateral flange bending in straight, skewed and curved steel I-girder bridges during deck placement (Doctoral dissertation, West Virginia University). Available from ProQuest.

Gastal, F. P. S. L. (1986). Instantaneous and time-dependent response and strength of jointless bridge beams (Doctoral dissertation, North Carolina State University).

Gibbs, C. L. (2017). Field performance assessment of press-brake-formed steel tub girder superstructures (Master's thesis, West Virginia University). Available from ProQuest.

Graybeal, B. (2014). *Design and construction of field-cast UHPC connections* (Report No: FHWA-HRT-14-084). Washington, DC: US Department of Transportation Federal Highway Administration.

Grubb, M., Coletti, D., Nelson, A., & Ream, A. (2020). *NSBA Guide to Navigating Routine Steel Bridge Design*. Chicago, IL: American Institute of Steel Construction.

Haaijer, G., & Thurlimann, B. (1957). *On inelastic buckling in steel* (Fritz Laboratory Report No. 205E.9). Retrieved from Lehigh University, Department of Civil Engineering.

Hayes, C. O., Jr., Sessions, L. M., & Berry, A. J. (1986). Further studies on lateral load distribution using a finite element method. *Transportation Research Record, 1072*, 6-14.

Helwig, T. A., & Fan, Z. (2000). Field and computational studies of steel trapezoidal box girder bridges (Report No. 1395-3). Austin, Texas: Texas Department of Transportation.

Hoomes, L. C., Ozyildirim, H. C., & Brown, M. C. (2017). *Evaluation of high-performance fiber-reinforced concrete for bridge deck connections, closure pours, and joints* (Report No. FHWA/VTRC 17-R15). Richmond, VA: Virginia Department of Transportation and US Department of Transportation Federal Highway Administration.

Imhoff, C. M. (1998). Testing and modeling of Bridge R-289 (Master's thesis, University of Missouri). Available from University of Missouri.

Johnston, S. B., & Mattock, A. H. (1967). Lateral distribution of load in composite box girder bridges. Highway Research Record: Bridges and Structures, 167, 25-33.

Kassimali, A. (2015). *Structural Analysis* (5th ed). Stamford, CT: Cengage Learning.

Kelly, L. T. (2014). Experimental evaluation of non-composite shallow press-brake-formed steel tub girders (Master's thesis, West Virginia University). Available from ProQuest.

Khaleel, M. A., & Itani, R. Y. (1990). Live-load moments for continuous skew bridges. *Journal of Structural Engineering, 116*(9), 2361-2373.

Khaloo, A. R., & Mirzabozorg, H. (2003). Load distribution factors in simply supported skew bridges. *Journal of Bridge Engineering, 8*(4), 241-244. doi: 10.1061/(ASCE)1084-0702(2003)8:4(241)

Kim, S., & Nowak, A. S. (1997). Load distribution and impact factors for I-girder bridges. *Journal of Bridge Engineering, 2* (3), 97-104.

Kozhokin, P. (2016). Evaluation of modular press-brake-formed tub girders with UHPC joints (Master's thesis, West Virginia University). Available from ProQuest.

Kreitman, K., Azad, A. R.G., Patel, H., Engelhardt, M. D., Helwig, T. A., Williamson, E. B., & Klingner, R. (2016). *Strengthening existing continuous non-composite steel girder bridges using post-installed shear connectors* (Report No. FHWA/TX-16/0-6719-1). Austin, TX: Texas Department of Transportation.

Lay, M. G., Adams, P. F., & Galambos, T. V. (1964). Experiments on high strength steel members (Report No. 297.8). Bethlehem, Pennsylvania: Fritz Engineering Laboratory, Lehigh University.

Li, J., & Chen, G. (2011). Method to computer live-load distribution in bridge girders. *Practice Periodical on Structural Design and Construction, 16*(4), 191-198. doi: 10.1061/(ASCE)SC.1943-5576.0000091

Li, V. C., Fischer, G., Kim, Y., Lepech, M., Qian, S., Weimann, M., & Wang, S. (2003). Durable link slabs for jointless bridge decks based on strain-hardening cementitious composites (Report No: RC-1438). Lansing, Michigan: Michigan Department of Transportation.

Li, V. C., Lepech, M., & Li, M. (2005). *Field demonstration of durable link slabs for jointless bridge decks based on strain-hardening cementitious composites* (Report No. RC-1471). Lansing, MI: Michigan Department of Transportation.

Mabsout, M. E., Tarhini, K. M., Frederick, G. R., & Kesserwan, A. (1998) Effect of continuity on wheel load distribution in steel girder bridges. Journal of Bridge Engineering, 3(3), 103-110.

Mabsout, M. E., Tarhini, K. M., Frederick, G. R., & Kobrosly, M. (1997). Influence of sidewalks and railings on wheel load distribution in steel girder bridges. Journal of Structural Engineering, 2(3), 88-96.

Mabsout, M. E., Tarhini, K. M., Frederick, G. R., & Tayar, C. (1997). Finite-element analysis of steel girder highway bridges. Journal of Structural Engineering, 2(3), 83-87.

The Mathworks, Inc. (2021). MATLAB. Natick, MA, The Mathworks, Inc.

Mertz, D. (2007). *Simplified live load distribution factor equations* (NCHRP Report No. 592). Washington, DC: The National Academies Press.

Mertz, D. (2022). Chapter 10: Limit states. *Steel Bridge Design Handbook* (pp. 1-14). Chicago, IL: American Institute of Steel Construction.

Mertz, D. (2022). Chapter 12: Design for failure. *Steel Bridge Design Handbook* (pp. 1-36). Chicago, IL: American Institute of Steel Construction.

Michaelson, G. K. (2010). Live load distribution factors for exterior girders in steel I-girder bridges (Master's thesis, West Virginia University). Available from ProQuest.

Michaelson, G. K. (2014). Development and feasibility assessment of shallow press-brake-formed steel tub girders for short-span bridge applications (Doctoral dissertation, West Virginia University). Available from ProQuest.

Micro-Measurements, Inc. (2010). StrainSmart [Data Collection]. Raleigh, North Carolina: Micro-Measurements, Inc.

Nakamura, S. (2002). Bending behavior of composite girders with cold formed steel U section. ASCE Journal of Structural Engineering, 128(9), 1169-1176. doi: 10.1061-(ASCE)0733-9455(2002)128:9(1169)

Newmark, N. M. (1949). Design of I-beam bridges. Transportation ASC, 114, 997-1022.

Newmark, N. M., & Siess, C. P. (1942). Moments in I-beam bridges. University of Illinois Bulletin, 39(44), 1-154.

Newmark, N. M., Siess, C. P., & Peckman, W. M. (1948). Studies of slab and beam highway bridges Part II: Tests of simple-span skew I-beam bridges. University of Illinois Bulletin, 45(31), 1-70.

Nowak, A. S., Eom, J., & Ferrand, D. (2003). Verification of girder distribution factors for continuous steel girder bridges (Report No. RC-1429). Lansing, Michigan: Michigan Department of Transportation.

Powell, G., & Simons, J. (1981). Improved iteration strategy for nonlinear structures. International Journal for Numerical Methods in Engineering, 17(10), 1455-1467.

Ramm, E. (1981) Strategies for tracing the nonlinear response near limit points. In E. Wunderlich, E. Stein, & K. J. Bathe (Eds), Nonlinear Finite Element Analysis in Structural Mechanics (pp. 63-89). Berlin: Springer-Verlag.

Razzaq, M. K. (2017). Load distribution factors for skewed composite steel I-girder bridges (Doctoral dissertation, University of Windsor). Available from ProQuest.

Righman, J. (2005). Rotation compatibility approach to moment redistribution for design and rating of steel I-girders (Doctoral dissertation, West Virginia University). Available from ProQuest.

Riks, E. (1979). An incremental approach to the solution of snapping and buckling problems. International Journal of Solids and Structures, 15, 529-551.

Roberts, N. (2005). Evaluation of the ductility of composite steel I-girders in positive bending (Master's thesis, West Virginia University). Available from ProQuest.

Roh, A. D. (2020). Field evaluation of a modular press-brake-formed steel tub girder in an application that includes skew and superelevation (Master's thesis, West Virginia University). Available from ProQuest.

Royce, M. (2016, July 18-20). Utilization of ultra-high performance concrete (UHPC) in New York. In B. Graybeal, S. Sritharan, & K. Wille (Chairs), *International Interactive Symposium on Ultra-High Performance Concrete* [Symposium]. Des Moines, IA.

Sanchez, T. A. S. (2011). Influence of bracing systems on the behavior of curved and skewed steel I-girder bridges during construction (Doctoral dissertation, Georgia Institute of Technology). Available from ProQuest.

Sanders, W. W. (1984). Distribution of wheel loads on highway bridges. National Cooperative Highway Research Program Synthesis of Highway Practice, 111, 1-22.

Schilling, C. G. & Morcos, S. S. (1988). Moment-rotation tests of steel girders with ultracompact flanges. Project 188 Autostress Design of Highway Bridges. American Iron and Steel Institute.

Short Span Steel Bridge Alliance. (2020). *Steel press-brake formed tub girder system selected for 2021 AASHTO Innovation Initiative focus technology*. SSSBA, Washington, DC.

Stallings, J. M., & Yoo, C. H. (1993). Tests and ratings of short-span steel bridges. *Journal of Structural Engineering, 119*(7), 2150-2168.

Strang, G. (2016). *Introduction to linear algebra* (5th ed). Wellesley, MA: Cambridge Press.

Taly, N. B., & Gangarao, H. V. S. (1976). Development and design of standardized short span bridge superstructural. (Report No. FHWA-WV-76-5).

Tarhini, K. M., & Frederick, G. R. (1992). Wheel load distribution in I-girder highway bridges. Journal of Structural Engineering, 118(5), 1285-1294.

Tennant, R. M. (2018). Fatigue performance of uncoated and galvanized composite press-brake-formed tub girders (Master's thesis, West Virginia University). Available from ProQuest.

Texas Steel Quality Council. (2021). *Preferred practices for steel bridge design, fabrication, and erection*. Austin, TX: Texas Department of Transportation.

Timoshenko, S., & Goodier, J. N. (1961). *Theory of elasticity*. New York, NY: McGraw-Hill Book Company.

Timoshenko, S., & Woinowsky-Krieger, S. (1959). *Theory of plates and shells* (2nd ed). New York, NY: McGraw-Hill Book Company.

Underwood, N. M. H. (2019). Field performance and rating evaluation of a modular press-brake-formed steel tub girder with a steel sandwich plate deck (Master's thesis, West Virginia University). Available from ProQuest.

Valmont Structures. (2022). *Product details*. https://bridge.constructbridge.com/ProductDetails

Walker, W. H. (1987). Lateral load distribution in multi-girder bridges. *Engineering Journal, 24*(1), 21-28.

Wallace, M. R. (1976). Studies of skewed concrete box-girder bridges. Committee on Concrete Bridges, 50-55.

White, D. (2022). Chapter 4: Strength behavior and design of steel. *Steel Bridge Design Handbook* (pp. 1-291). Chicago, IL: American Institute of Steel Construction.

White, D. W., & Kamath. A. (2020). Straight steel I-girder bridges with skew index approaching 0.3 (Report No. FDOT BE535). Tallahassee, Florida: Florida Department of Transportation.

White, D. W., Coletti, D., Chavel, B. W., Sanchez, A., Ozgur, G., Chong, J. M. J.,…Kowatch, G. T. (2012). *Guidelines for analysis methods and construction engineering of curved and skewed steel girder bridges* (NCHRP Report No. 725). Washington, DC: The National Academies Press. doi: 10.17226/22729

White, D. W., Grubb, M., King, C., & Slein, R. (2019). *Proposed AASHTO guidelines for bottom flange limits of steel box girders*.

Wing, K. M., & Kowalsky, M. J. (2005). Behavior, analysis, and design of an instrumented link slab bridge. *Journal of Bridge Engineering, 10*(3), 331-344. doi: 10.1061/(ASCE)1084-0702(2005)10:3(331)

Yang, L. (2004). Evaluation of moment redistribution for hybrid HPS 70W bridge girders (Master's thesis, West Virginia University). Available from ProQuest.

Yousif, Z., & Hindi, R. (2007). AASHTO-LRFD live load distribution for beam-and-slab bridges: Limitations and applicability. Journal of Bridge Engineering, 12(6), 765-773. doi: 10.1061/(ASCE)1084-0702(2007)12:6(765)

Ziemian, R. D. (2010). *Guide to stability design criteria for metal structures*. Hoboken, NJ: John Wiley & Sons, Inc.

Zokaie, T. (2000). AASHTO-LRFD live load distribution specifications. *Journal of Bridge Engineering*, 131-138.

Zokaie, T., Osterkamp, T. A., & Imbsen, R. A. (1991). Distribution of wheel loads on highway bridges. National Cooperative Highway Research Program Transportation Research Board National Research Council, 12-26/1, 1-710.

APPENDIX A: LLDF SENSITIVITY MATRIX RESULTS

The following appendix lists in graphical form the comparison of LLDFs calculated from the finite element models of the typical bridges analyzed during the sensitivity study discussed in Section 8.2. For the reader's convenience, this data has been organized such that each graph is focused on the influence of a single parameter on the distribution of moment to a single girder for each live load distribution methodology. Note, some graphs are not available as the typical bridge may not be applicable in certain situations. These situations will be labeled 'No Data Available' in place of the typical graph. Additionally, not every parameter will be present in every graph, as some parameters are not feasible with every standard bridge. The graphs were generated using MATLAB (Mathworks, 2021).

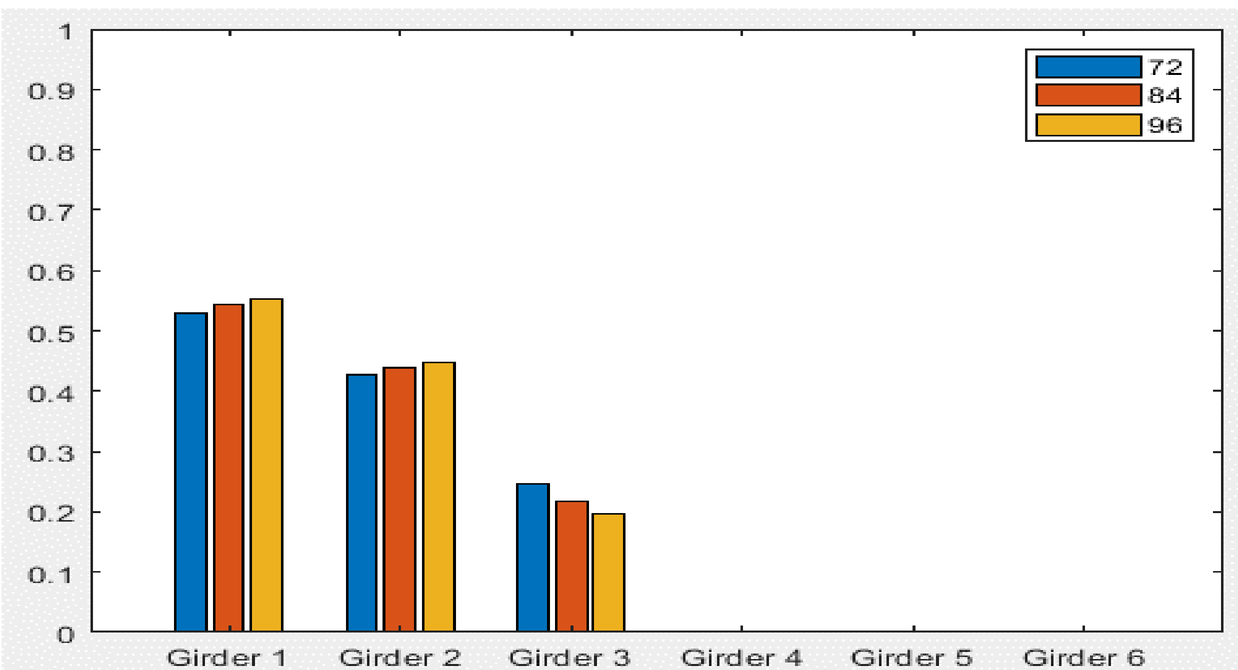

Typical Bridge #1, Stallings/Yoo Methodology, IG OLL, Variable = PBFTG Size

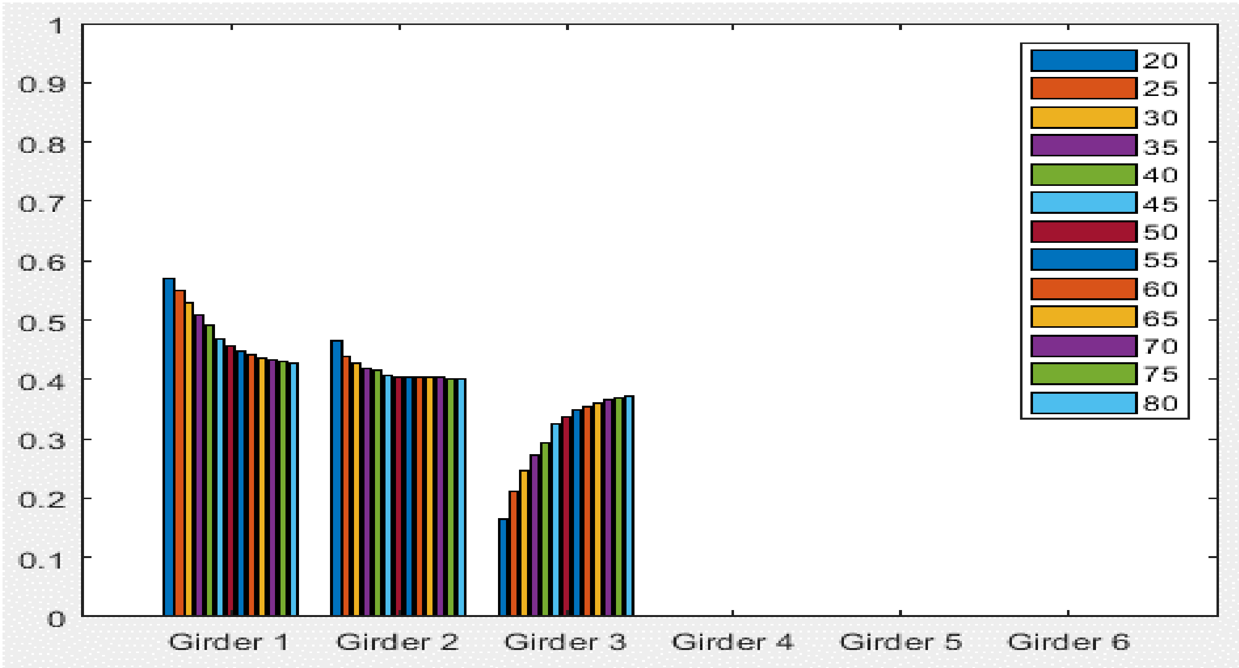

Typical Bridge #1, Stallings/Yoo Methodology, IG OLL, Variable = Span Length (ft)

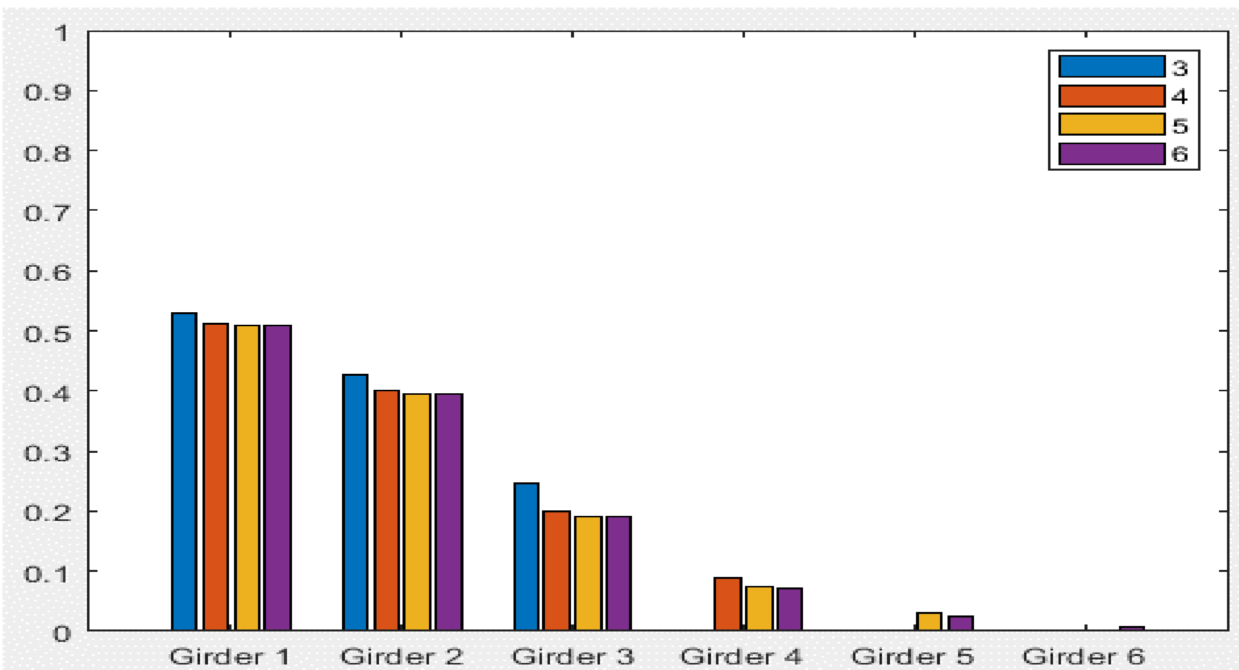

Typical Bridge #1, Stallings/Yoo Methodology, IG OLL, Variable = Number of Girders

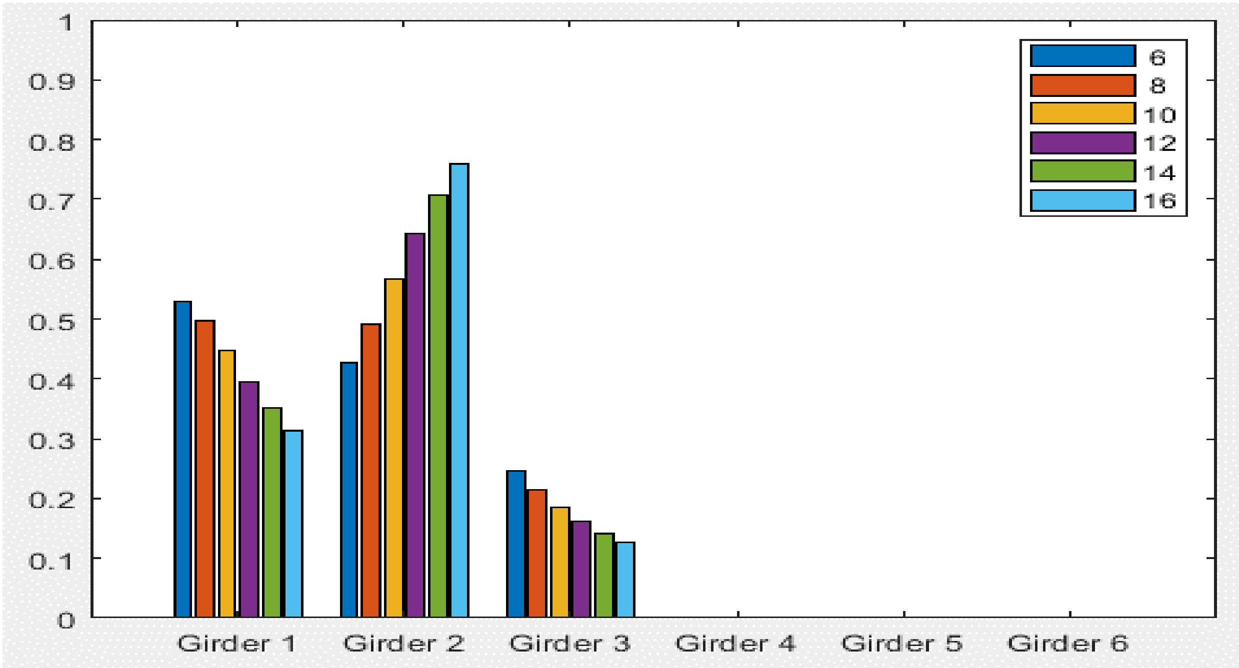

Typical Bridge #1, Stallings/Yoo Methodology, IG OLL, Variable = Girder Spacing (ft)

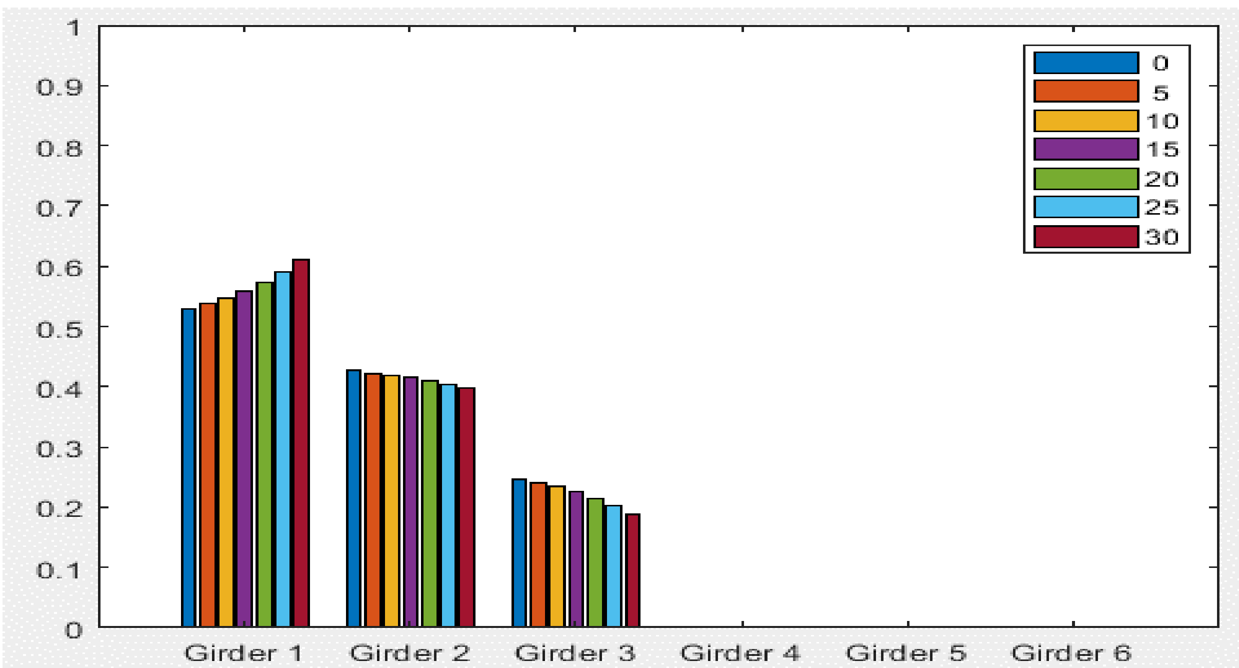

Typical Bridge #1, Stallings/Yoo Methodology, IG OLL, Variable = Degree of Skew (deg)

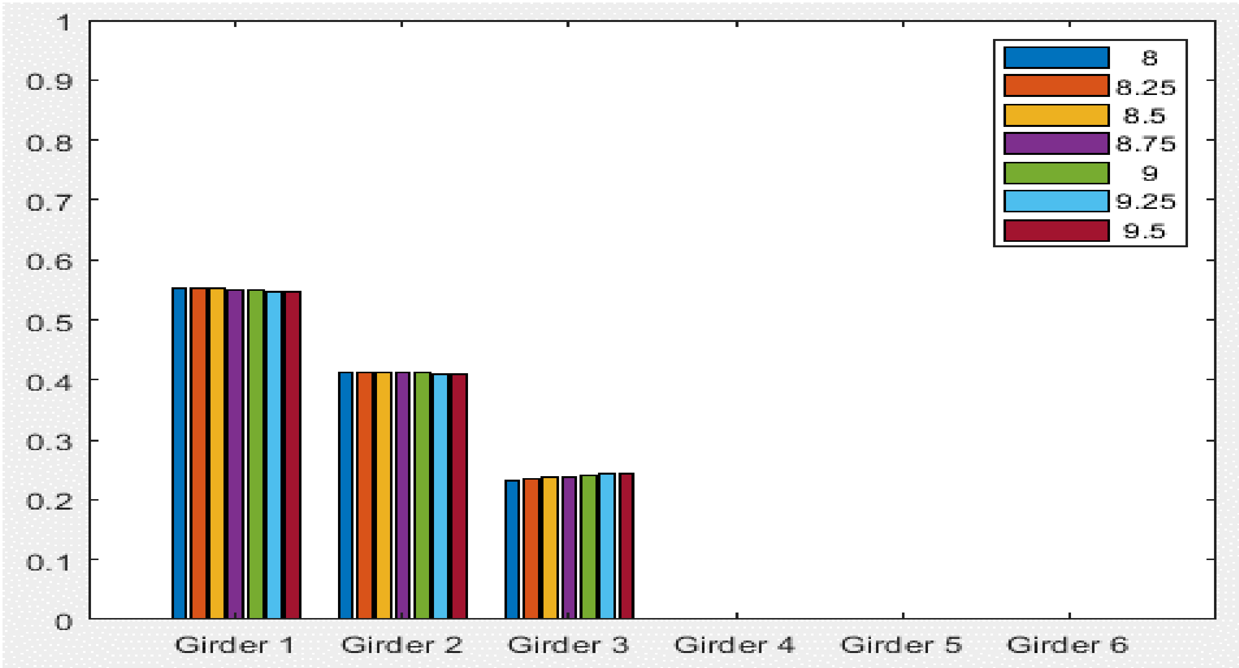

Typical Bridge #1, Stallings/Yoo Methodology, IG OLL, Variable = Deck Thickness (in)

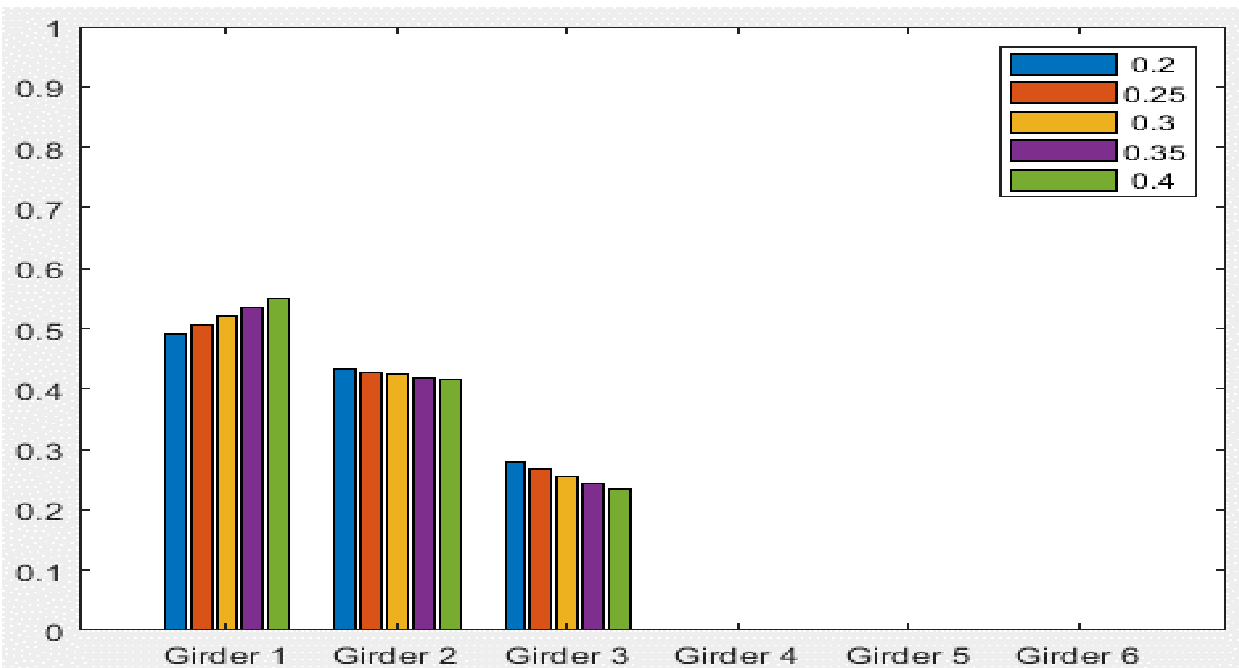

Typical Bridge #1, Stallings/Yoo Methodology, IG OLL, Variable = Overhang Ratio

NO DATA AVAILABLE

Typical Bridge #1, Stallings/Yoo Methodology, IG 2LL, Variable = PBFTG Size

NO DATA AVAILABLE

Typical Bridge #1, Stallings/Yoo Methodology, IG 2LL, Variable = Span Length (ft)

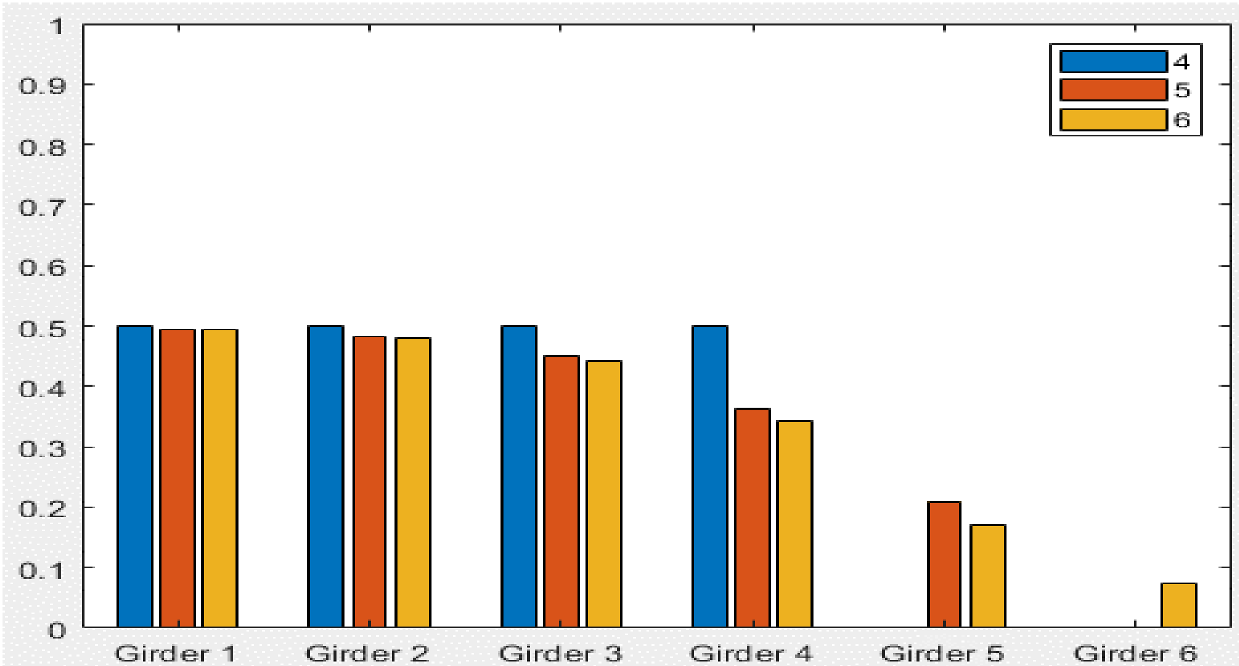

Typical Bridge #1, Stallings/Yoo Methodology, IG 2LL, Variable = Number of Girders

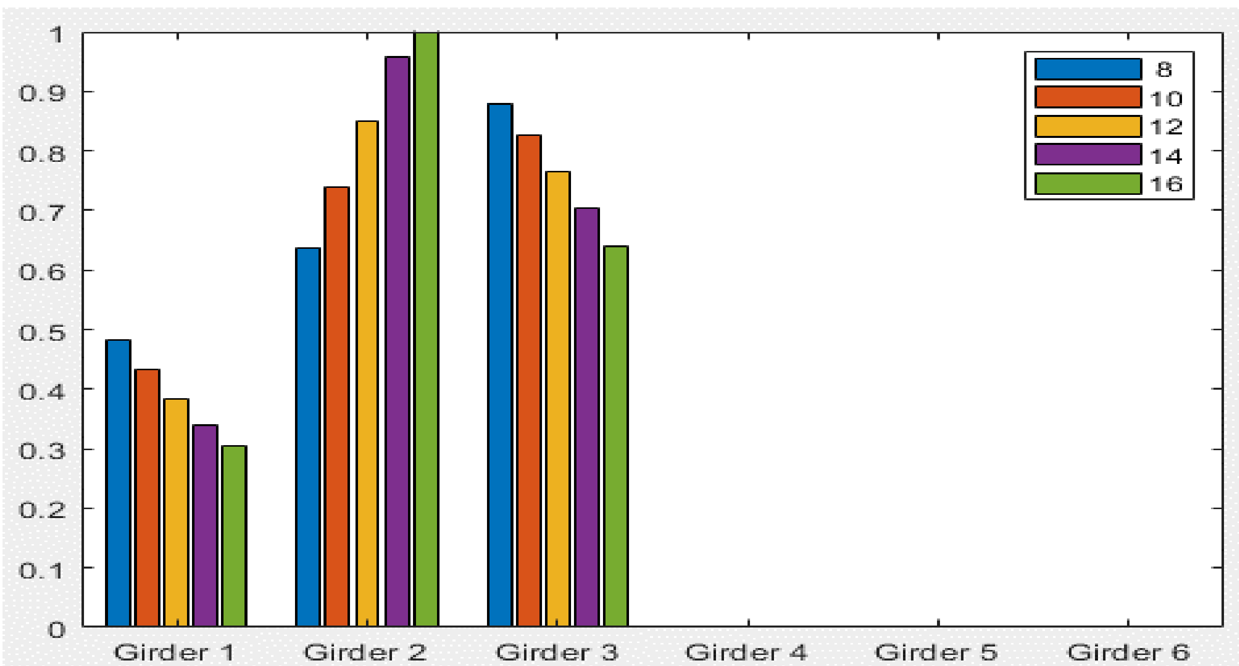

Typical Bridge #1, Stallings/Yoo Methodology, IG 2LL, Variable = Girder Spacing (ft)

NO DATA AVAILABLE

Typical Bridge #1, Stallings/Yoo Methodology, IG 2LL, Variable = Degree of Skew (deg)

NO DATA AVAILABLE

Typical Bridge #1, Stallings/Yoo Methodology, IG 2LL, Variable = Deck Thickness (in)

NO DATA AVAILABLE

Typical Bridge #1, Stallings/Yoo Methodology, IG 2LL, Variable = Overhang Ratio

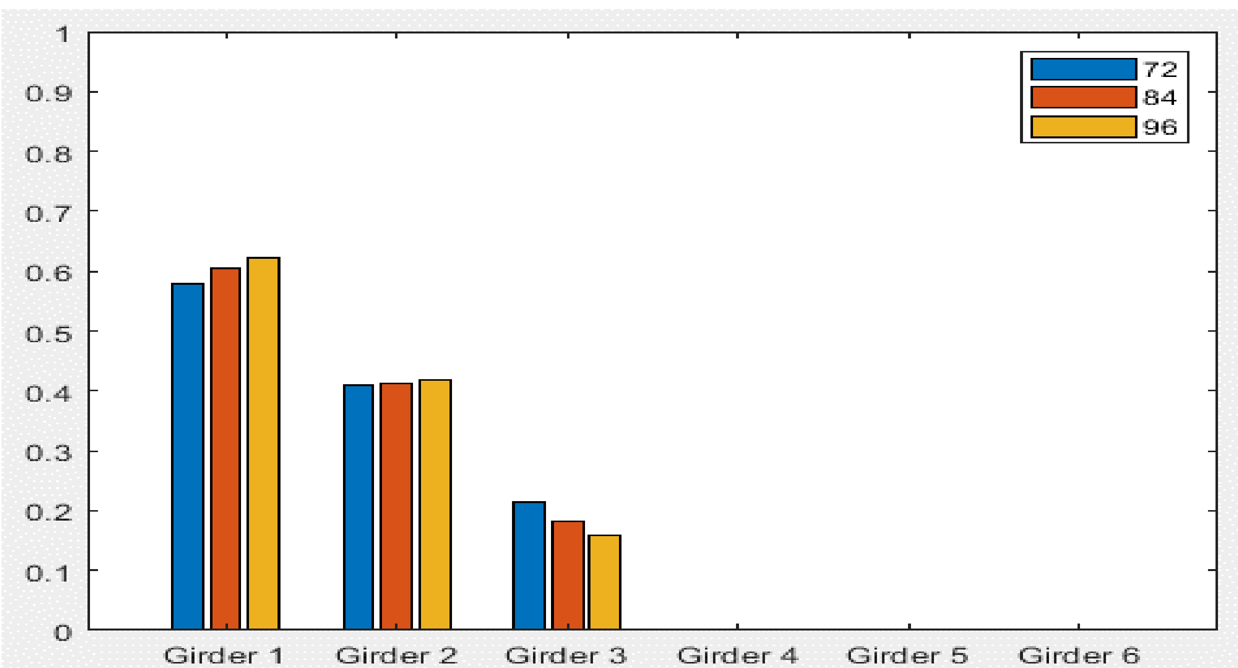

Typical Bridge #1, Stallings/Yoo Methodology, EG OLL, Variable = PBFTG Size

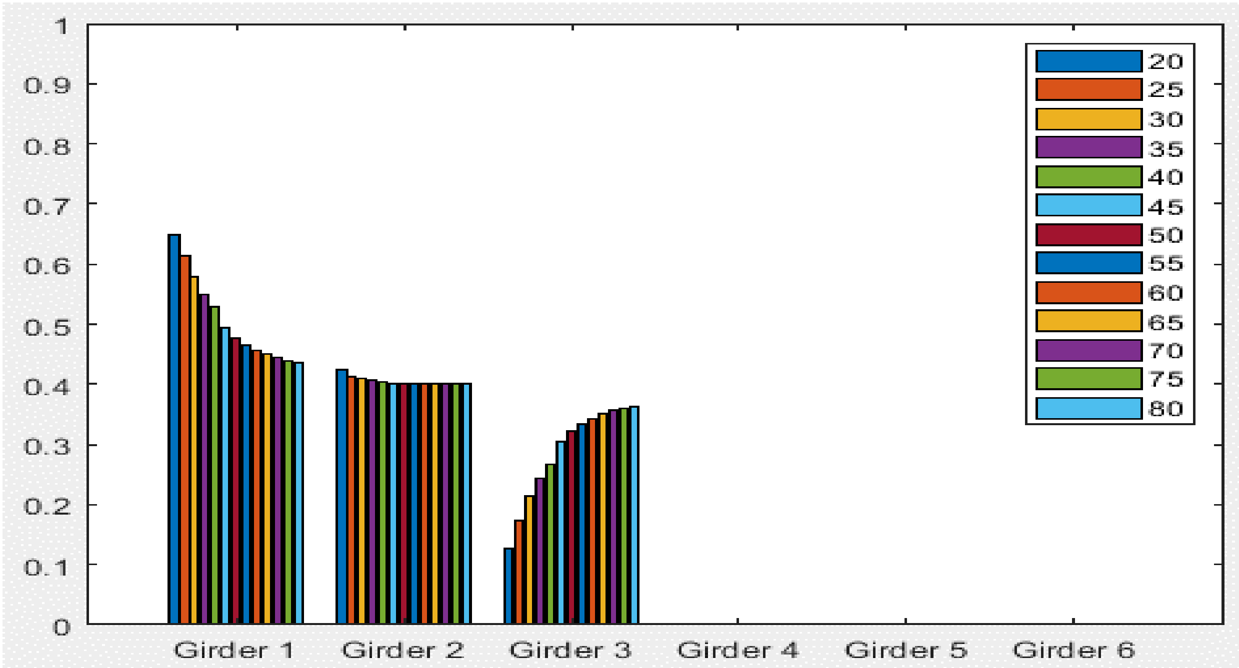

Typical Bridge #1, Stallings/Yoo Methodology, EG OLL, Variable = Span Length (ft)

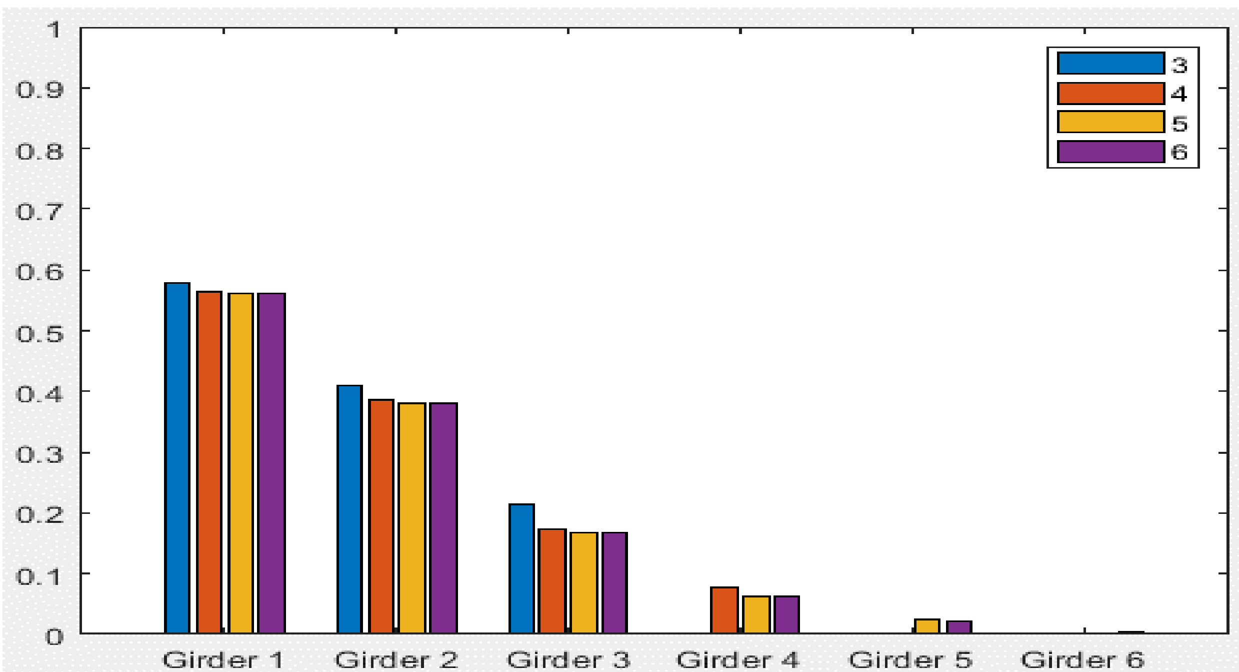

Typical Bridge #1, Stallings/Yoo Methodology, EG OLL, Variable = Number of Girders

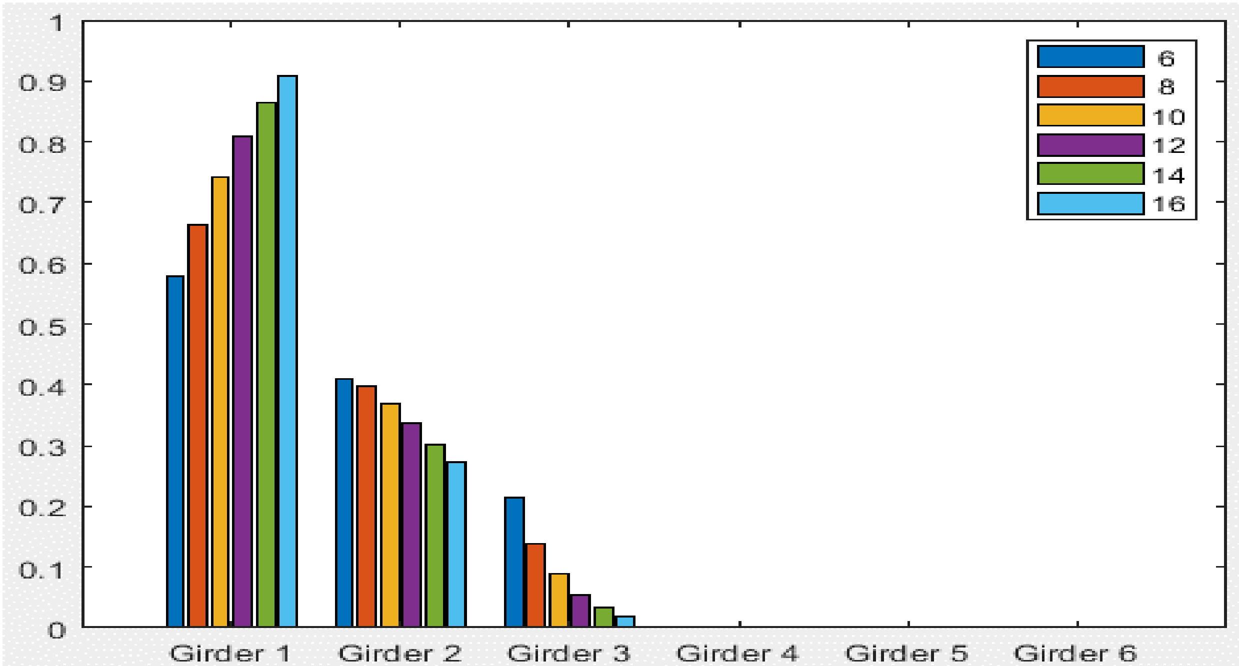

Typical Bridge #1, Stallings/Yoo Methodology, EG OLL, Variable = Girder Spacing (ft)

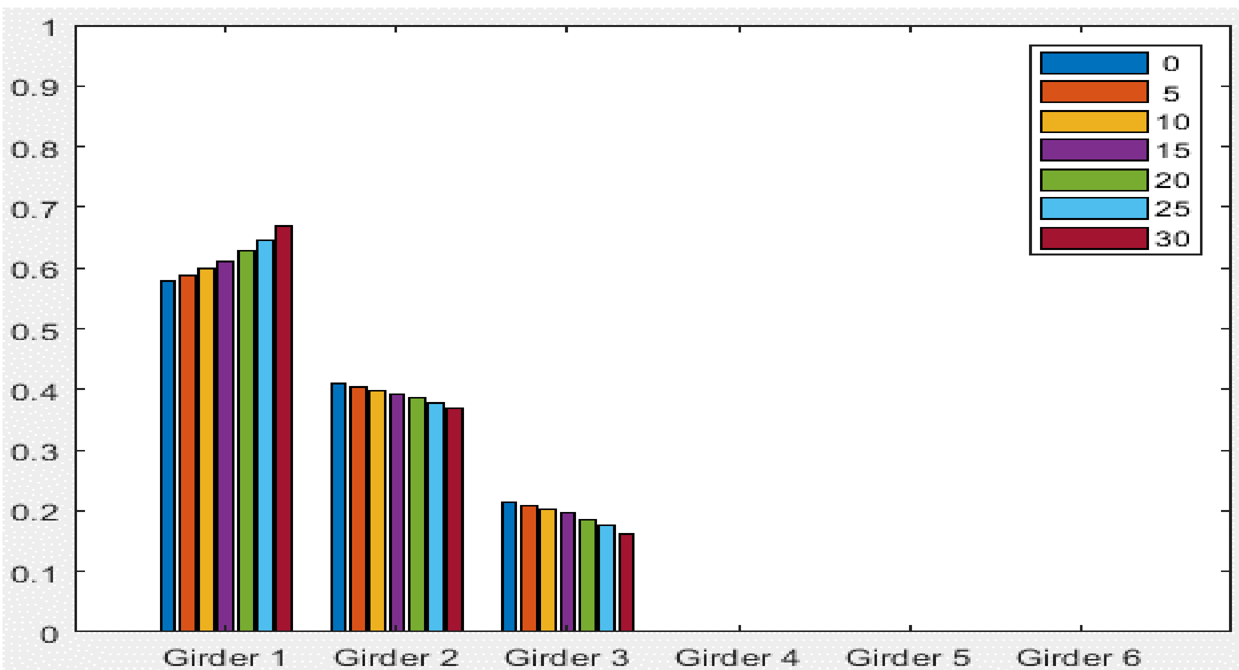

Typical Bridge #1, Stallings/Yoo Methodology, EG OLL, Variable = Degree of Skew (deg)

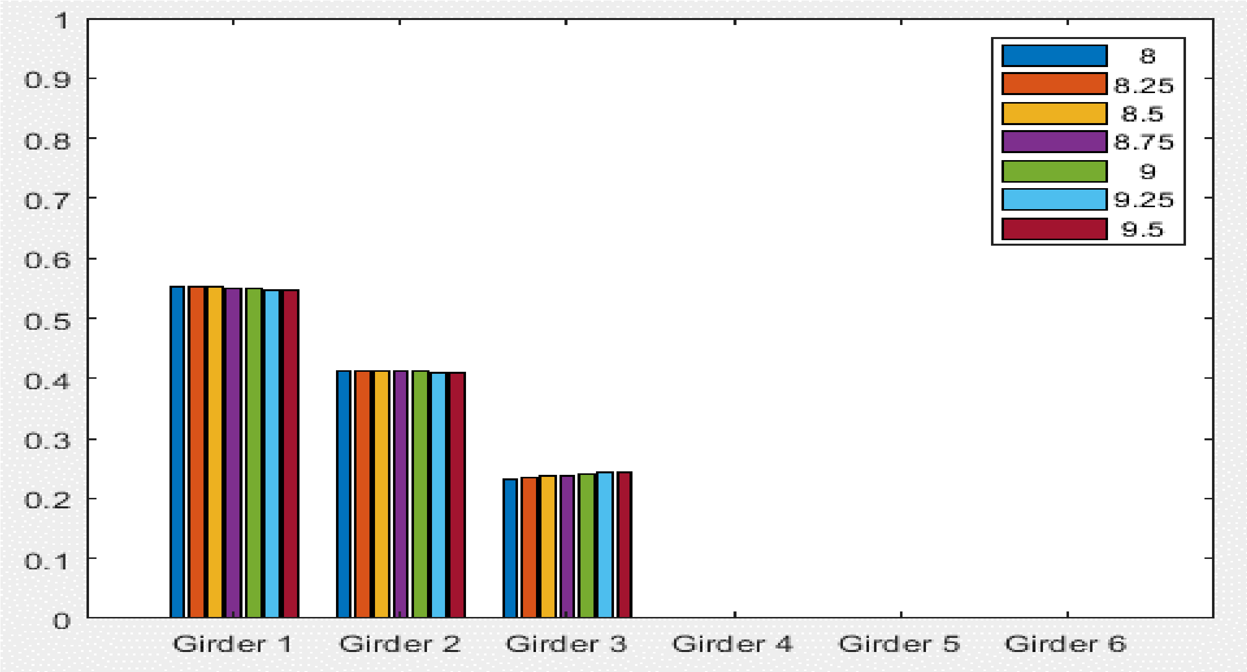

Typical Bridge #1, Stallings/Yoo Methodology, EG OLL, Variable = Deck Thickness (in)

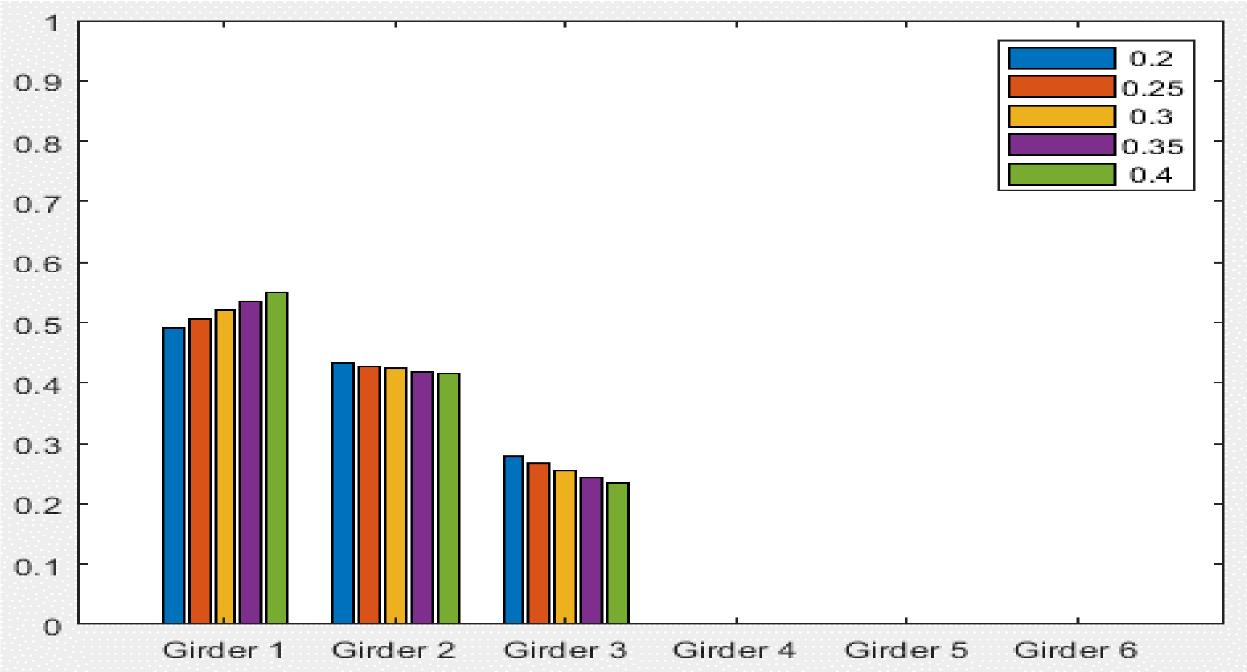

Typical Bridge #1, Stallings/Yoo Methodology, EG OLL, Variable = Overhang Ratio

NO DATA AVAILABLE

Typical Bridge #1, Stallings/Yoo Methodology, EG 2LL, Variable = PBFTG Size

NO DATA AVAILABLE

Typical Bridge #1, Stallings/Yoo Methodology, EG 2LL, Variable = Span Length (ft)

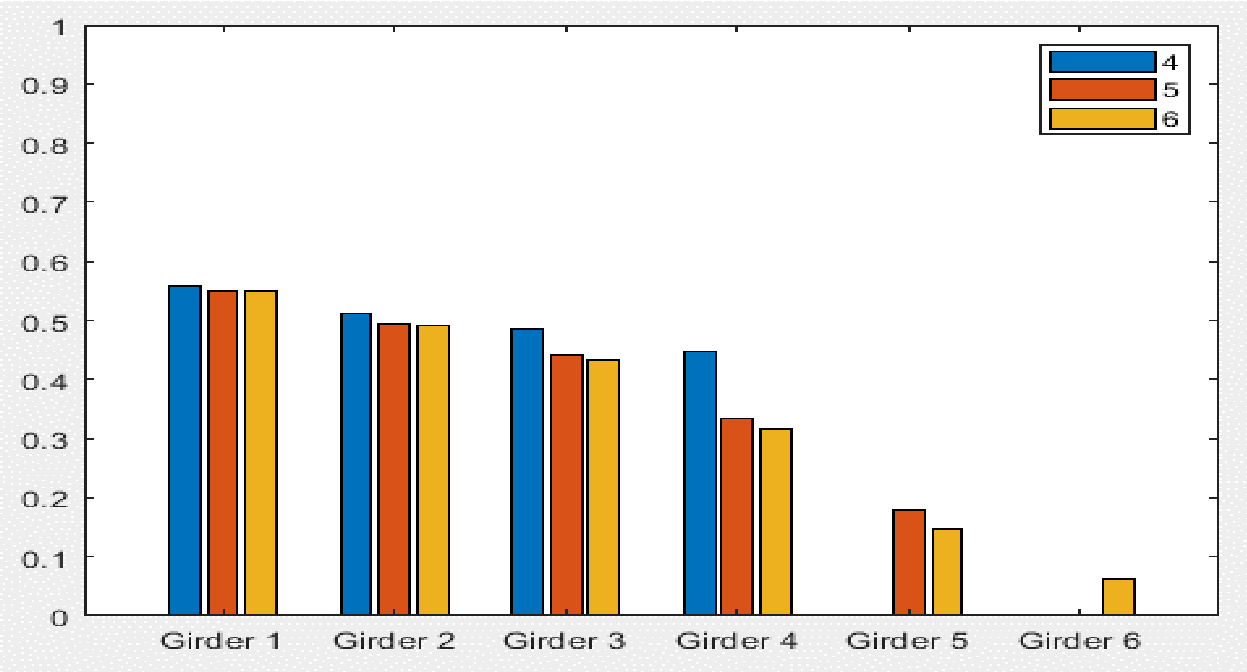

Typical Bridge #1, Stallings/Yoo Methodology, EG 2LL, Variable = Number of Girders

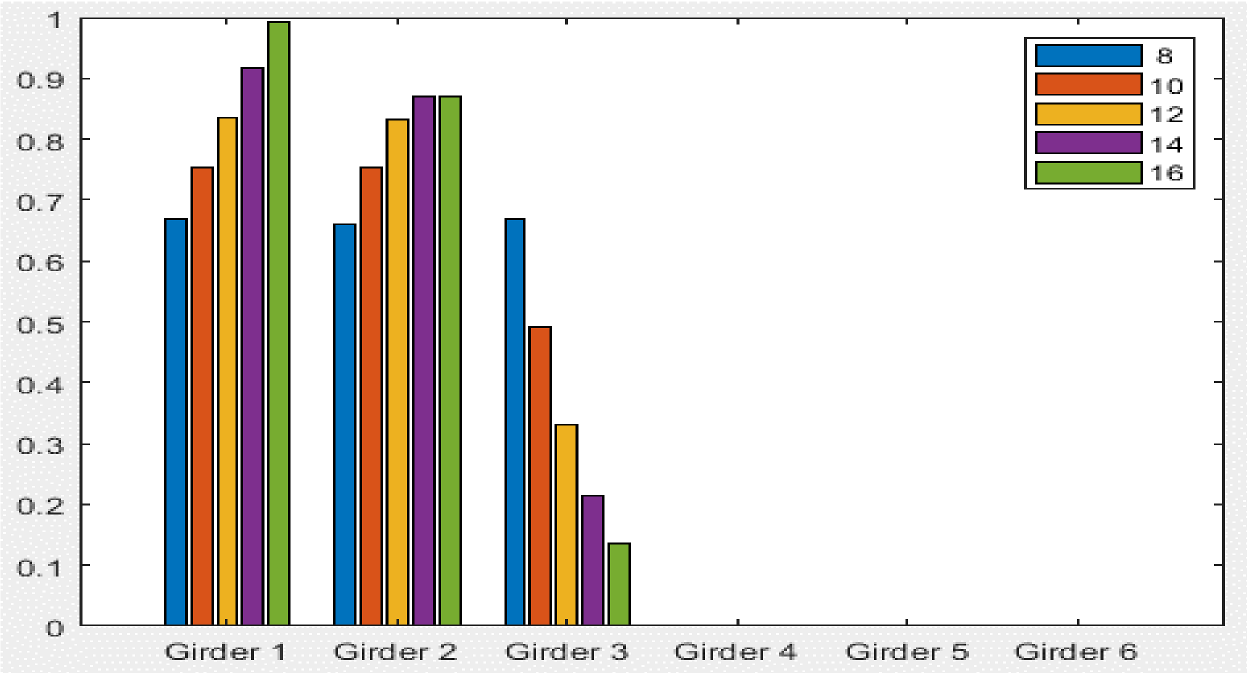

Typical Bridge #1, Stallings/Yoo Methodology, EG 2LL, Variable = Girder Spacing (ft)

NO DATA AVAILABLE

Typical Bridge #1, Stallings/Yoo Methodology, EG 2LL, Variable = Degree of Skew (deg)

NO DATA AVAILABLE

Typical Bridge #1, Stallings/Yoo Methodology, EG 2LL, Variable = Deck Thickness (in)

NO DATA AVAILABLE

Typical Bridge #1, Stallings/Yoo Methodology, EG 2LL, Variable = Overhang Ratio

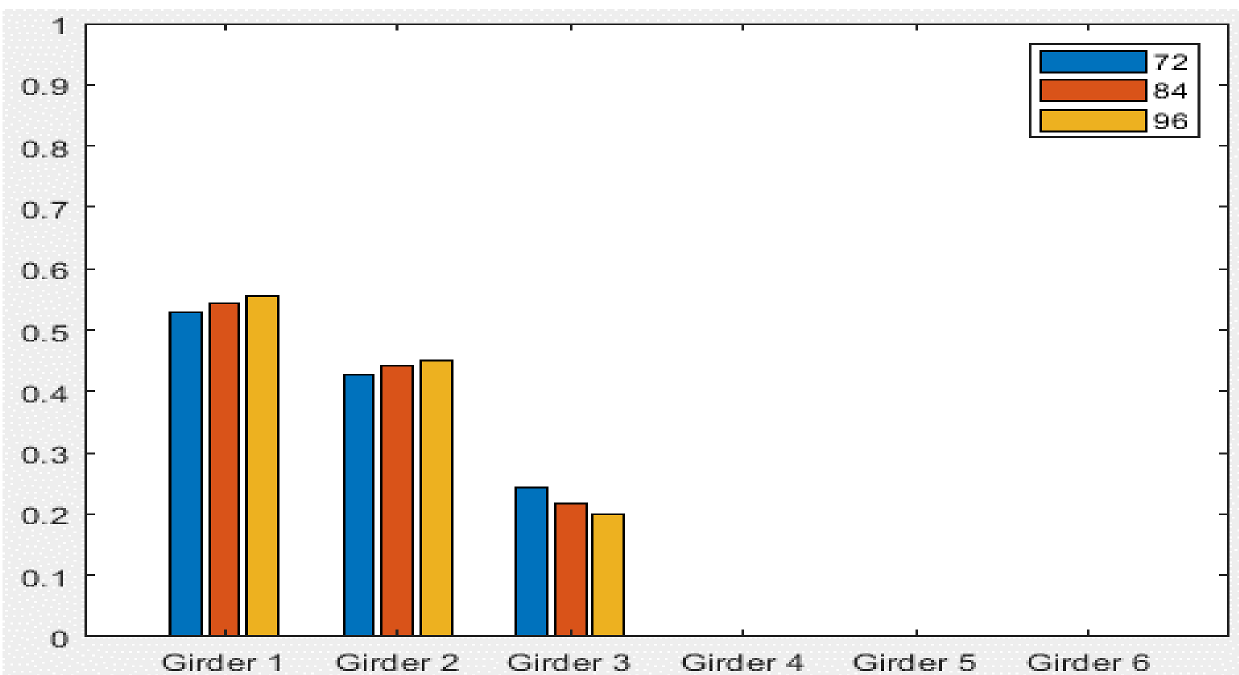

Typical Bridge #1, Tarhini/Frederick Methodology, IG OLL, Variable = PBFTG Size

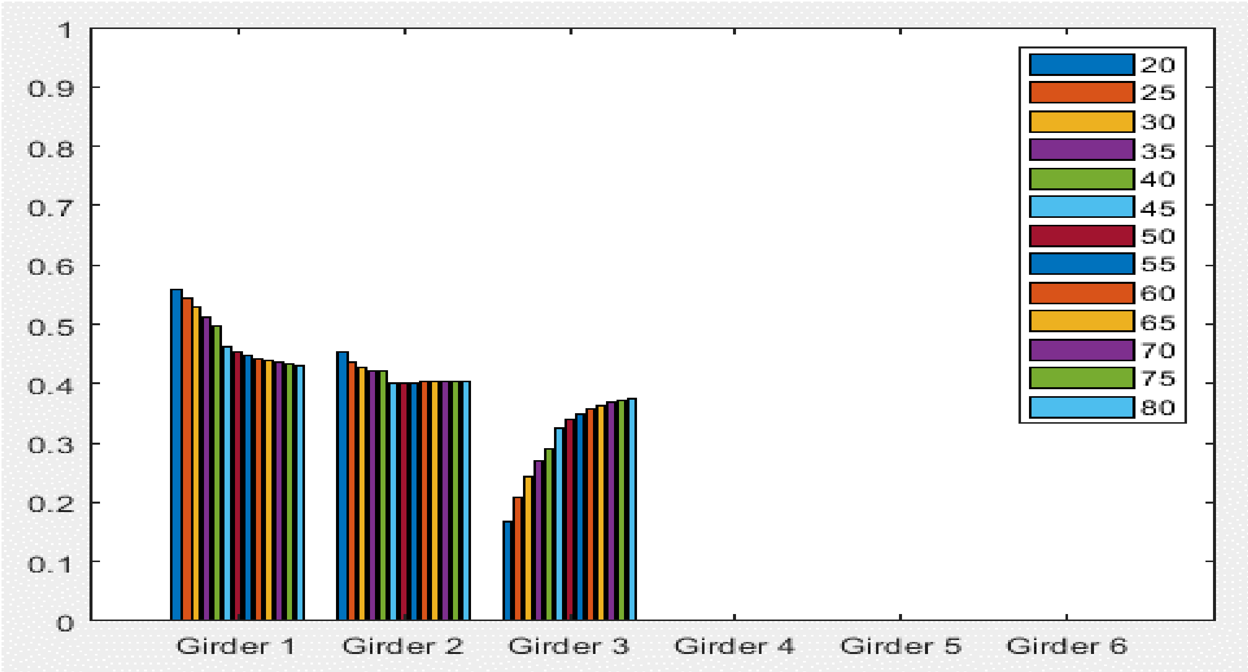

Typical Bridge #1, Tarhini/Frederick Methodology, IG OLL, Variable = Span Length (ft)

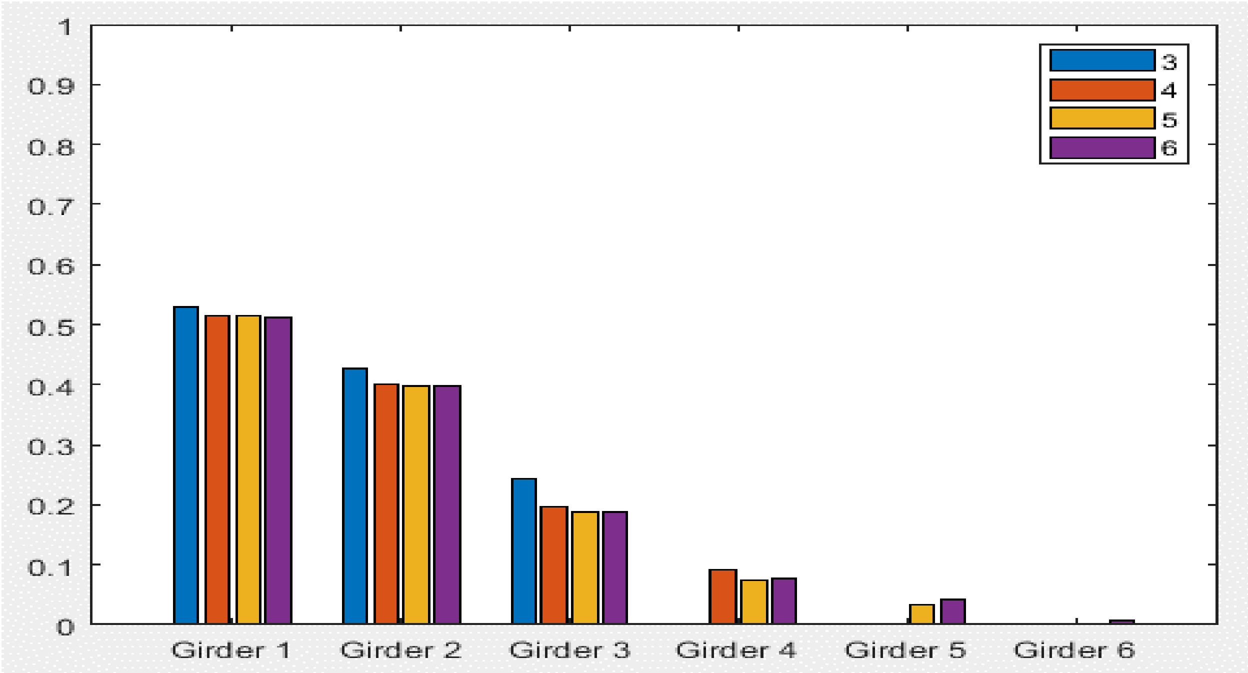

Typical Bridge #1, Tarhini/Frederick Methodology, IG OLL, Variable = Number of Girders

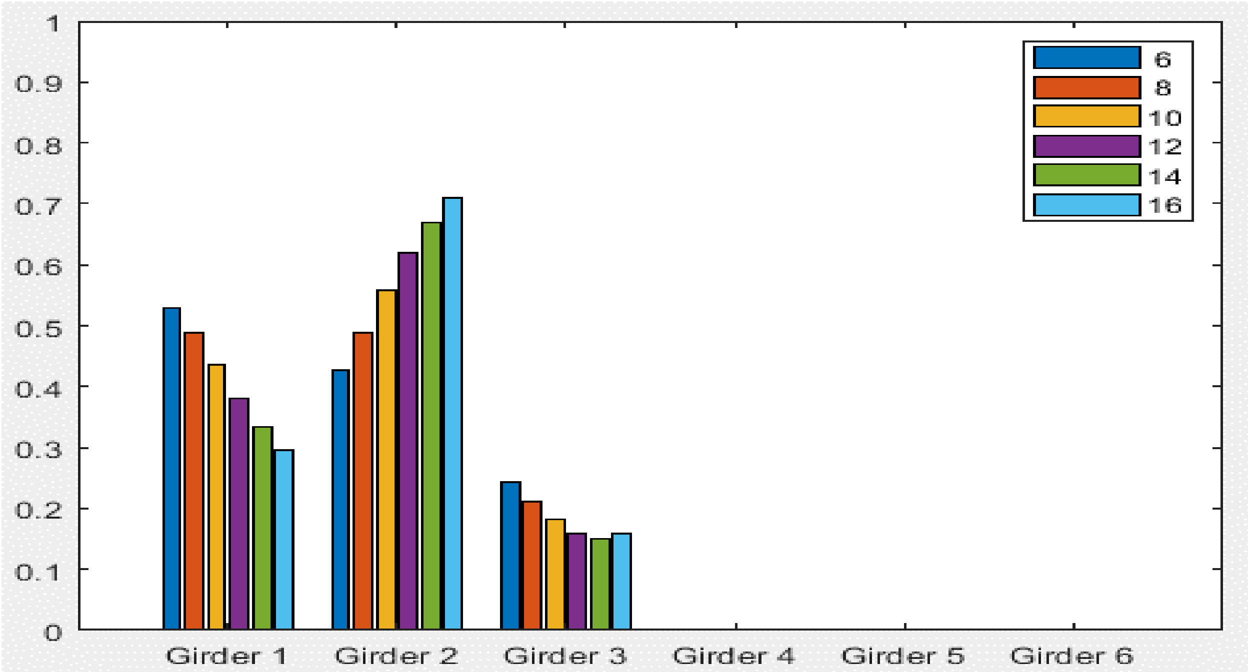

Typical Bridge #1, Tarhini/Frederick Methodology, IG OLL, Variable = Girder Spacing (ft)

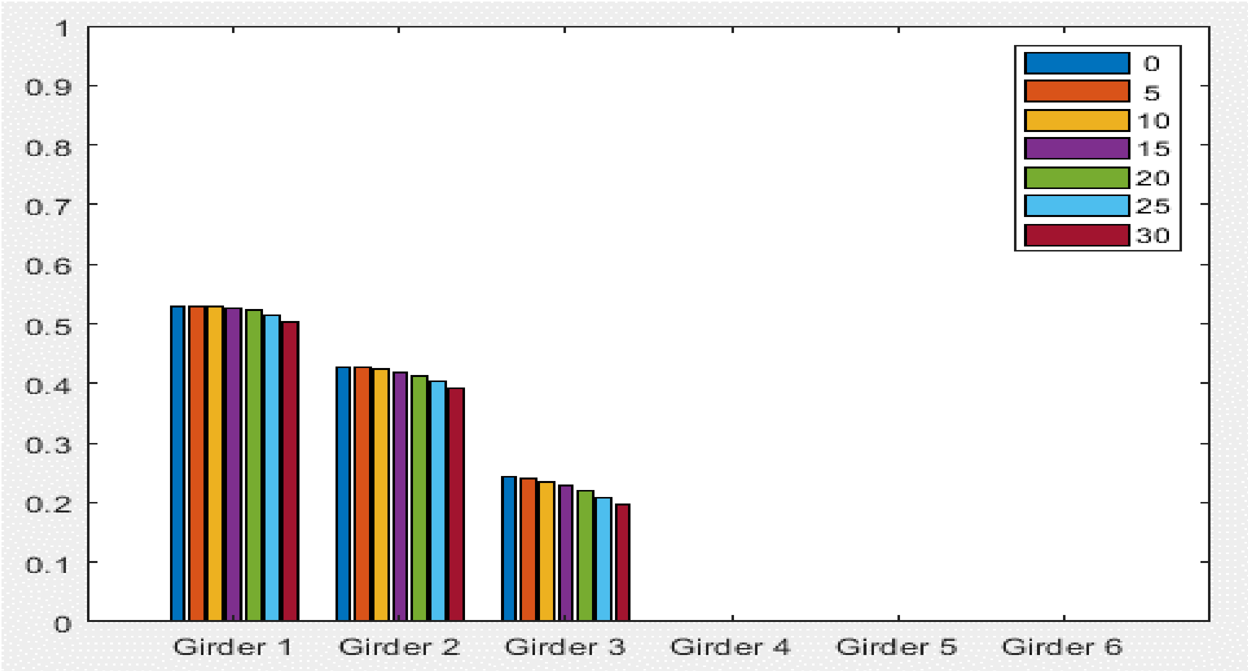

Typical Bridge #1, Tarhini/Frederick Methodology, IG OLL, Variable = Degree of Skew (deg)

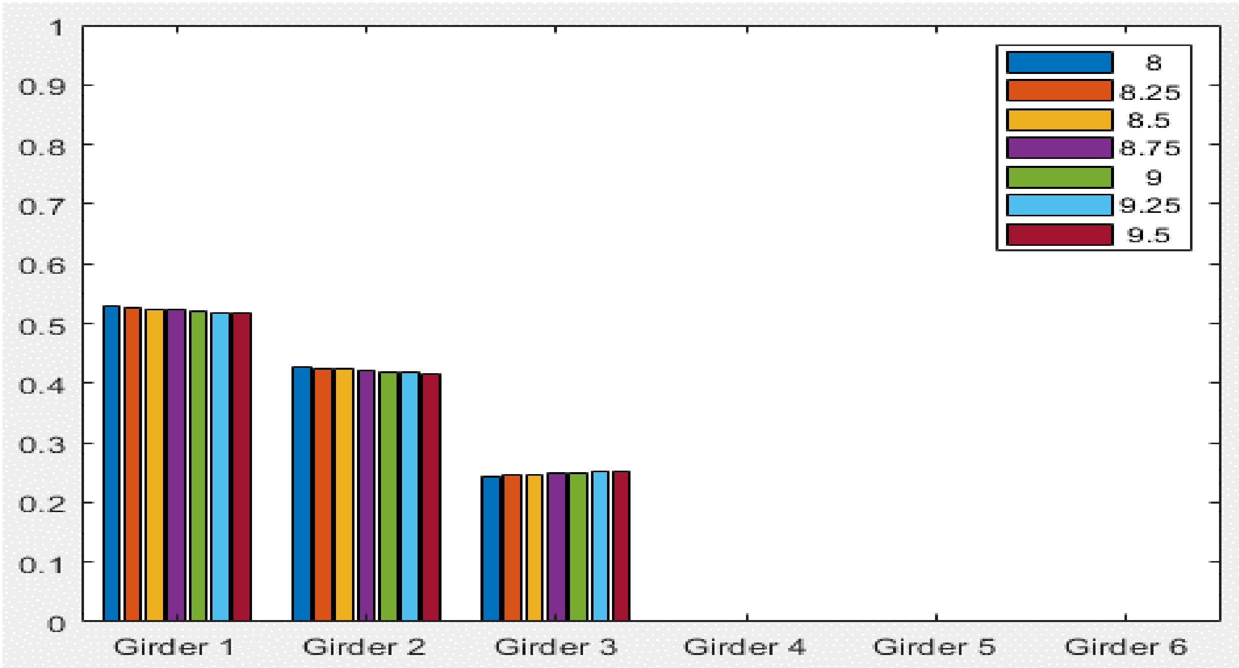

Typical Bridge #1, Tarhini/Frederick Methodology, IG OLL, Variable = Deck Thickness (in)

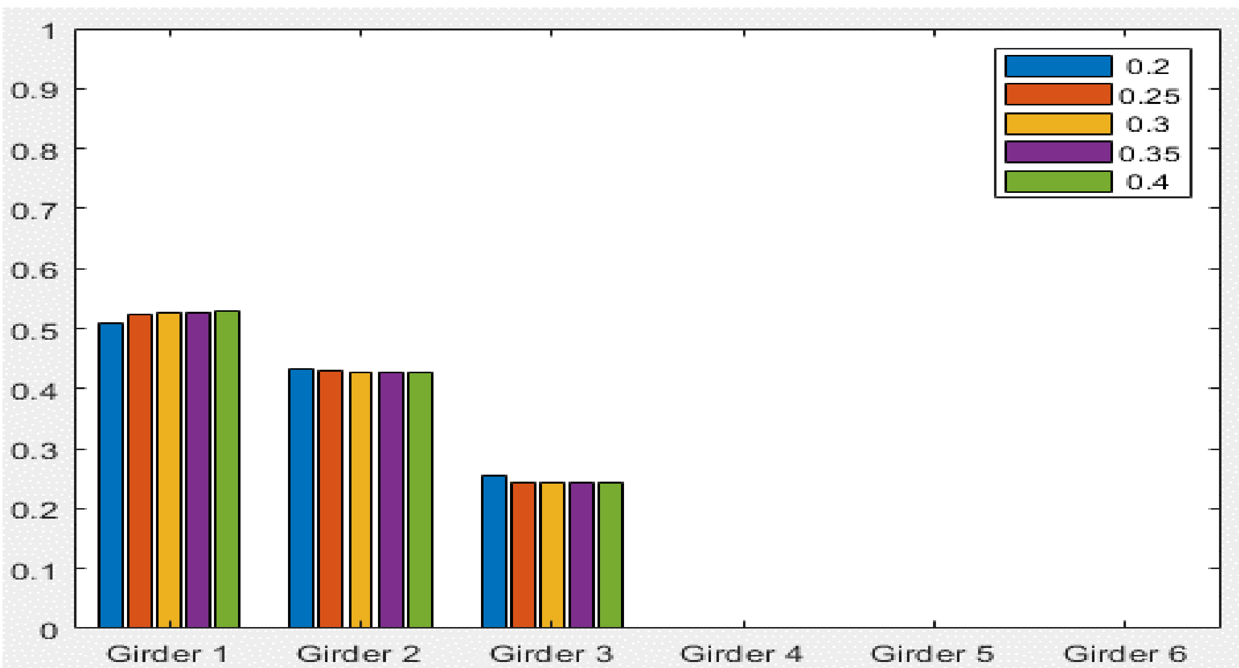

Typical Bridge #1, Tarhini/Frederick Methodology, IG OLL, Variable = Overhang Ratio

NO DATA AVAILABLE

Typical Bridge #1, Tarhini/Frederick Methodology, IG 2LL, Variable = PBFTG Size

NO DATA AVAILABLE

Typical Bridge #1, Tarhini/Frederick Methodology, IG 2LL, Variable = Span Length (ft)

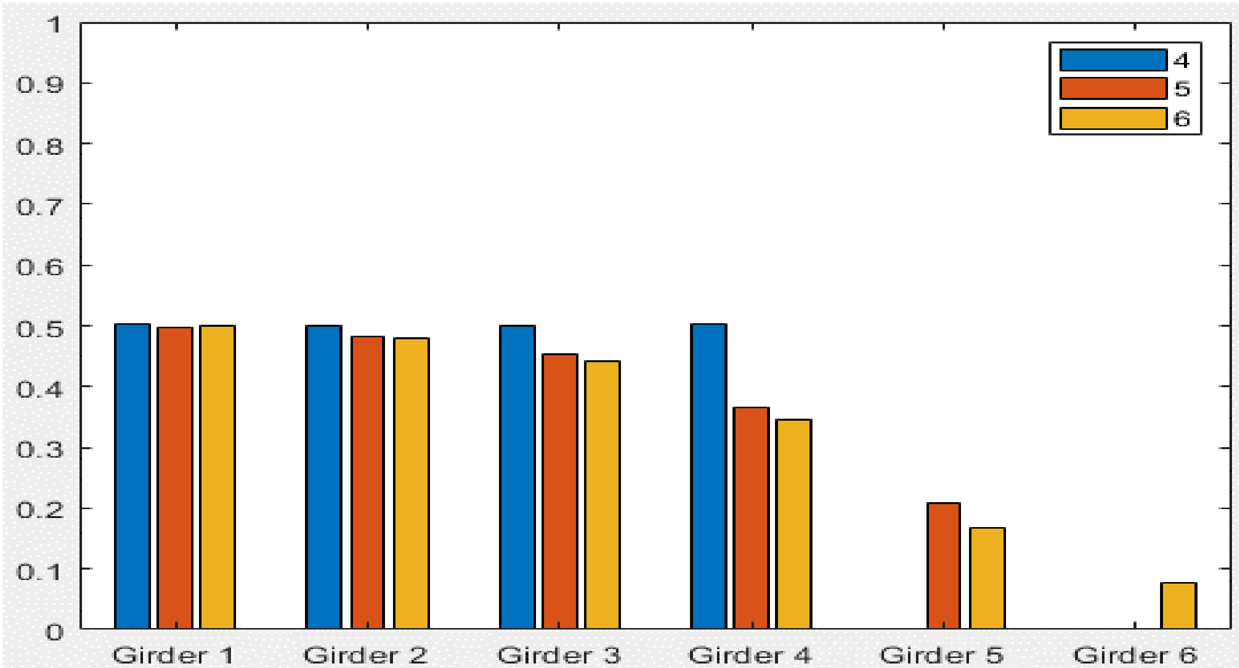

Typical Bridge #1, Tarhini/Frederick Methodology, IG 2LL, Variable = Number of Girders

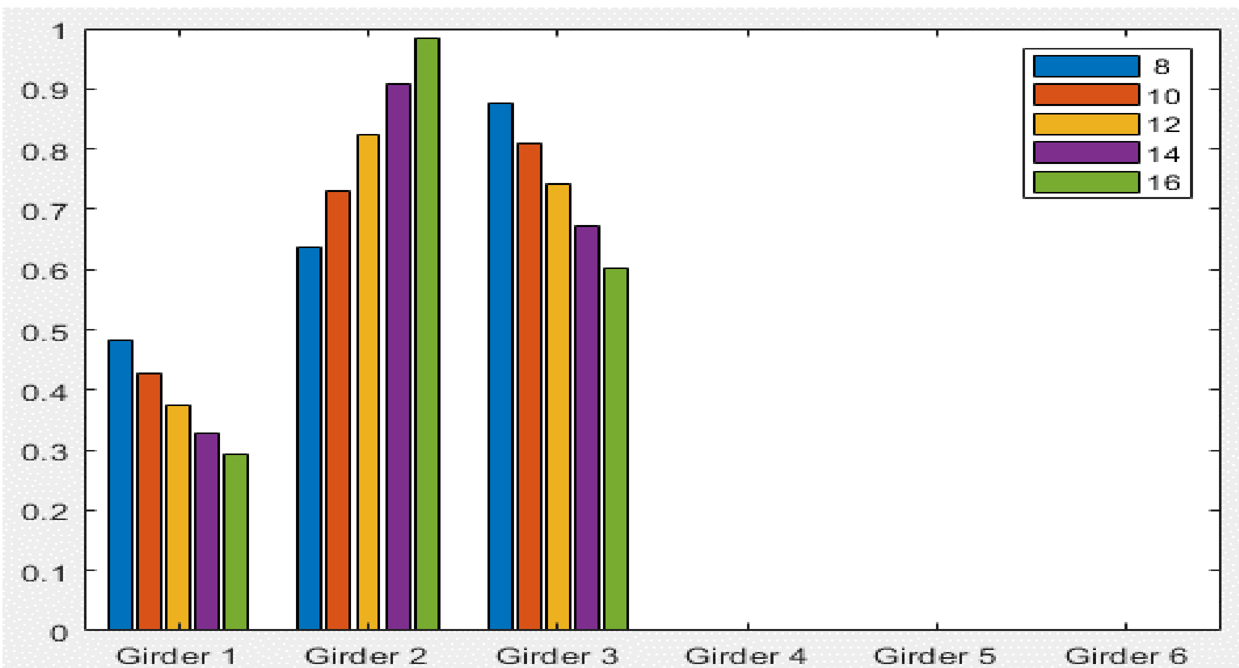

Typical Bridge #1, Tarhini/Frederick Methodology, IG 2LL, Variable = Girder Spacing (ft)

NO DATA AVAILABLE

Typical Bridge #1, Tarhini/Frederick Methodology, IG 2LL, Variable = Degree of Skew (deg)

NO DATA AVAILABLE

Typical Bridge #1, Tarhini/Frederick Methodology, IG 2LL, Variable = Deck Thickness (in)

NO DATA AVAILABLE

Typical Bridge #1, Tarhini/Frederick Methodology, IG 2LL, Variable = Overhang Ratio

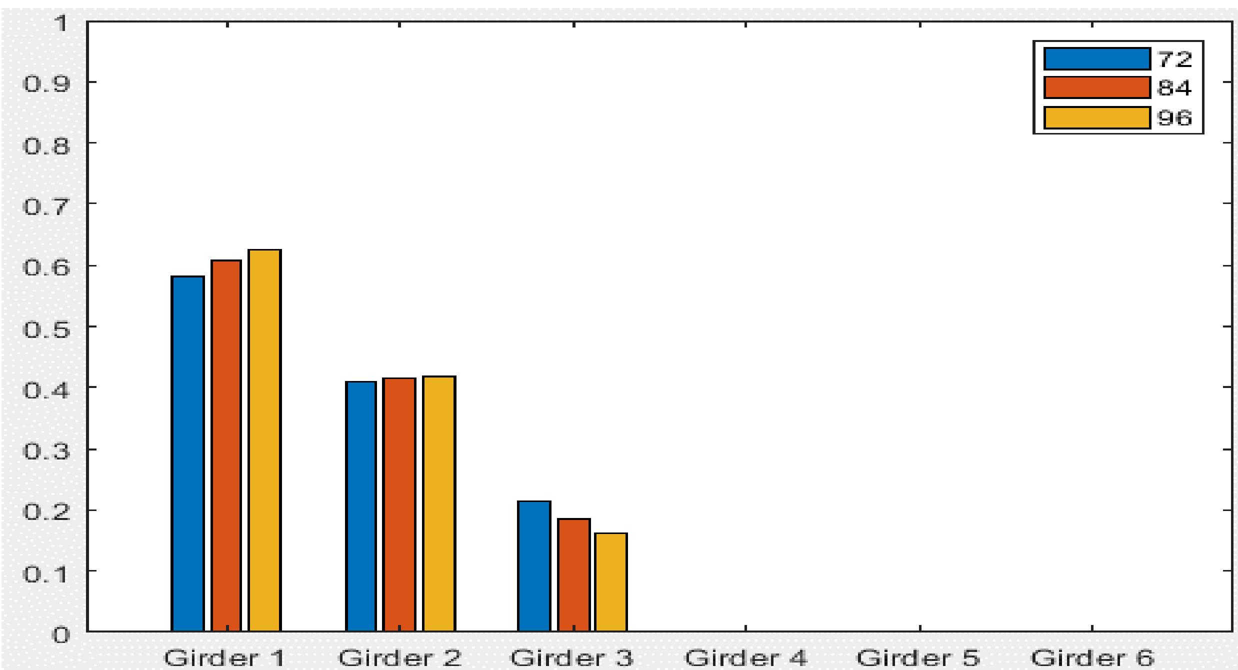

Typical Bridge #1, Tarhini/Frederick Methodology, EG OLL, Variable = PBFTG Size

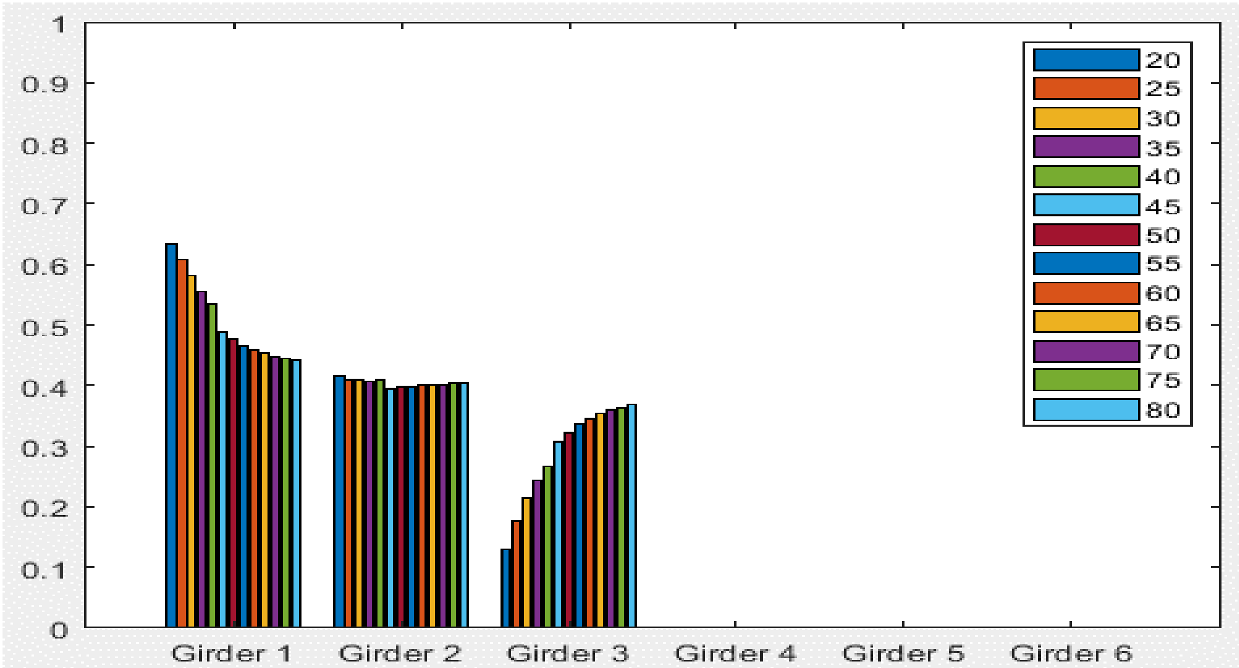

Typical Bridge #1, Tarhini/Frederick Methodology, EG OLL, Variable = Span Length (ft)

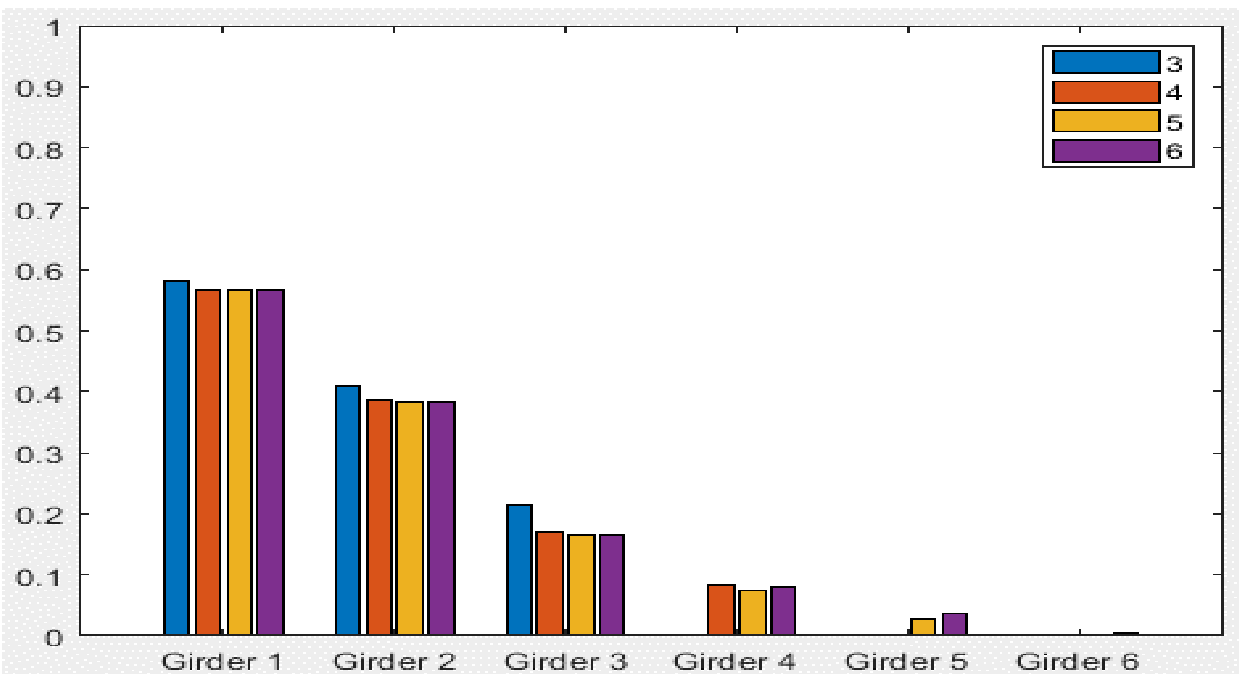

Typical Bridge #1, Tarhini/Frederick Methodology, EG OLL, Variable = Number of Girders

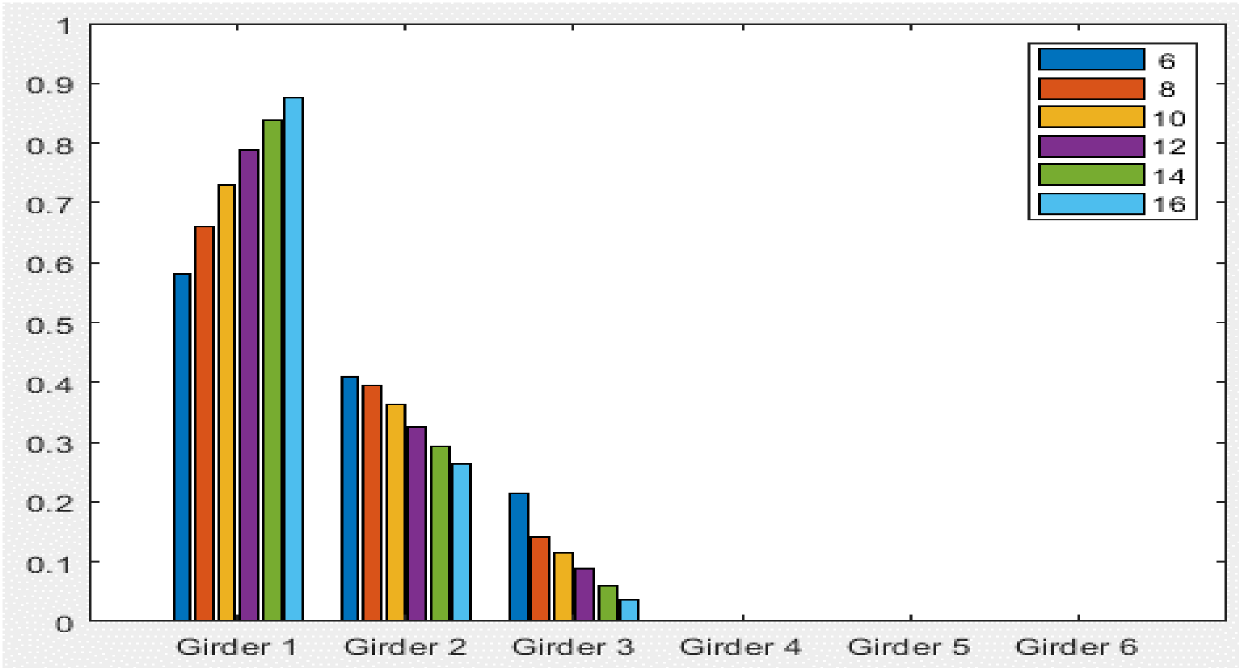

Typical Bridge #1, Tarhini/Frederick Methodology, EG OLL, Variable = Girder Spacing (ft)

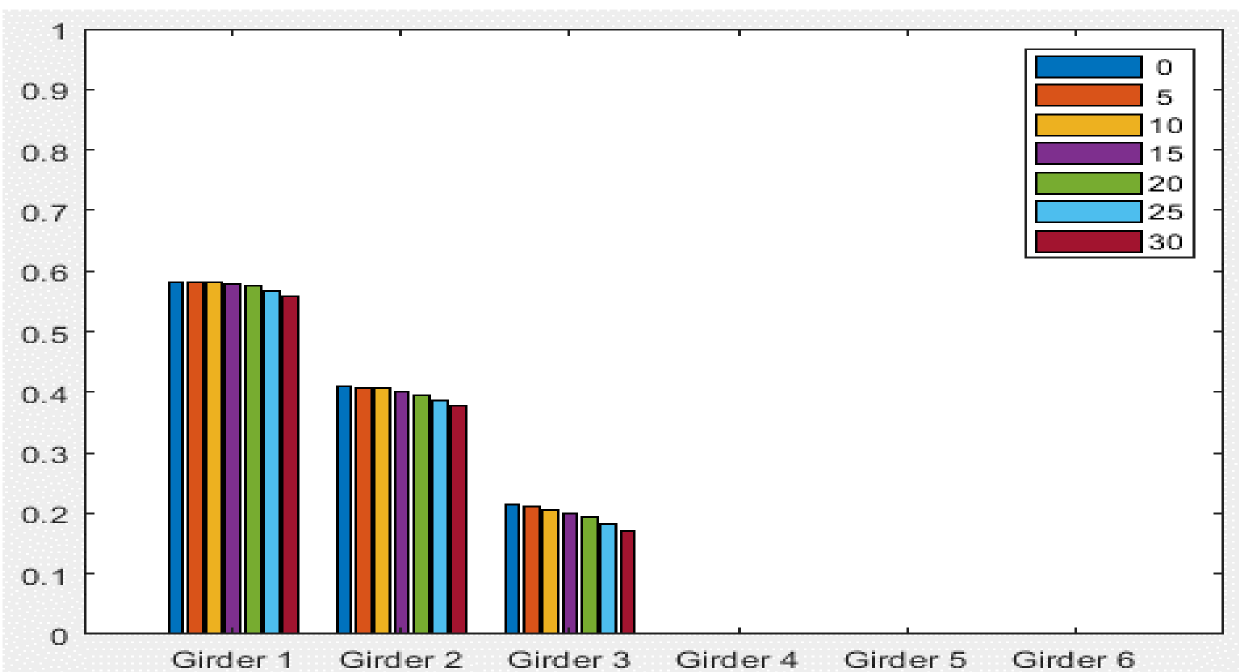

Typical Bridge #1, Tarhini/Frederick Methodology, EG OLL, Variable = Degree of Skew (deg)

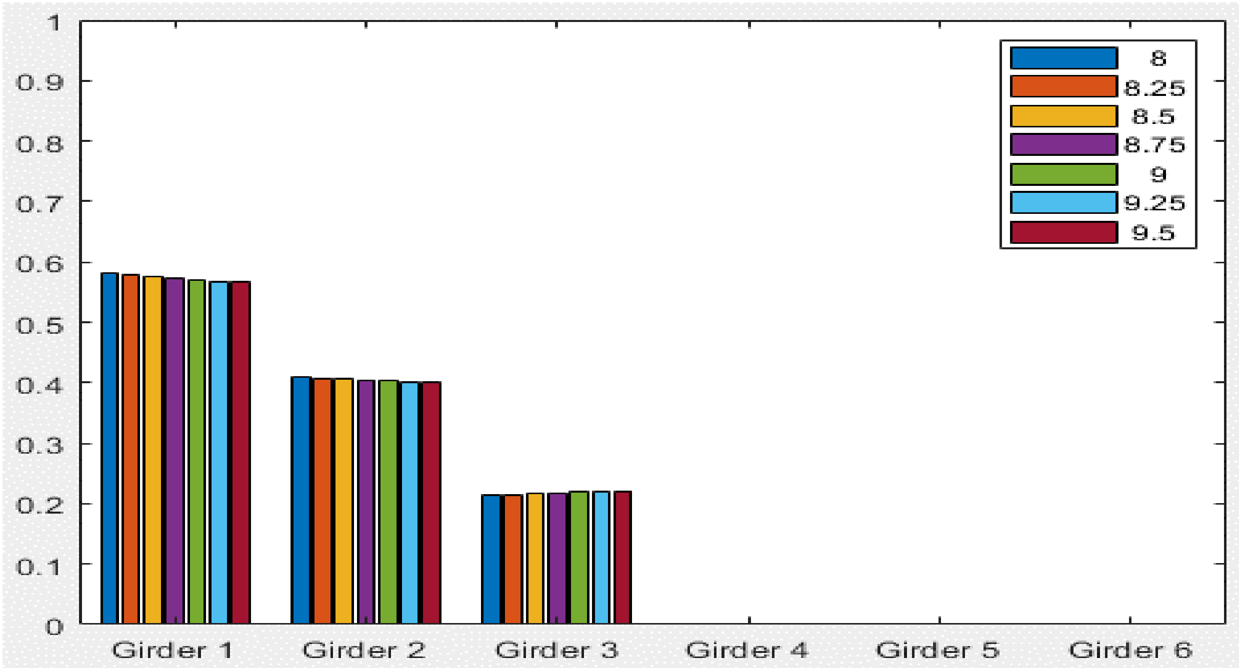

Typical Bridge #1, Tarhini/Frederick Methodology, EG OLL, Variable = Deck Thickness (in)

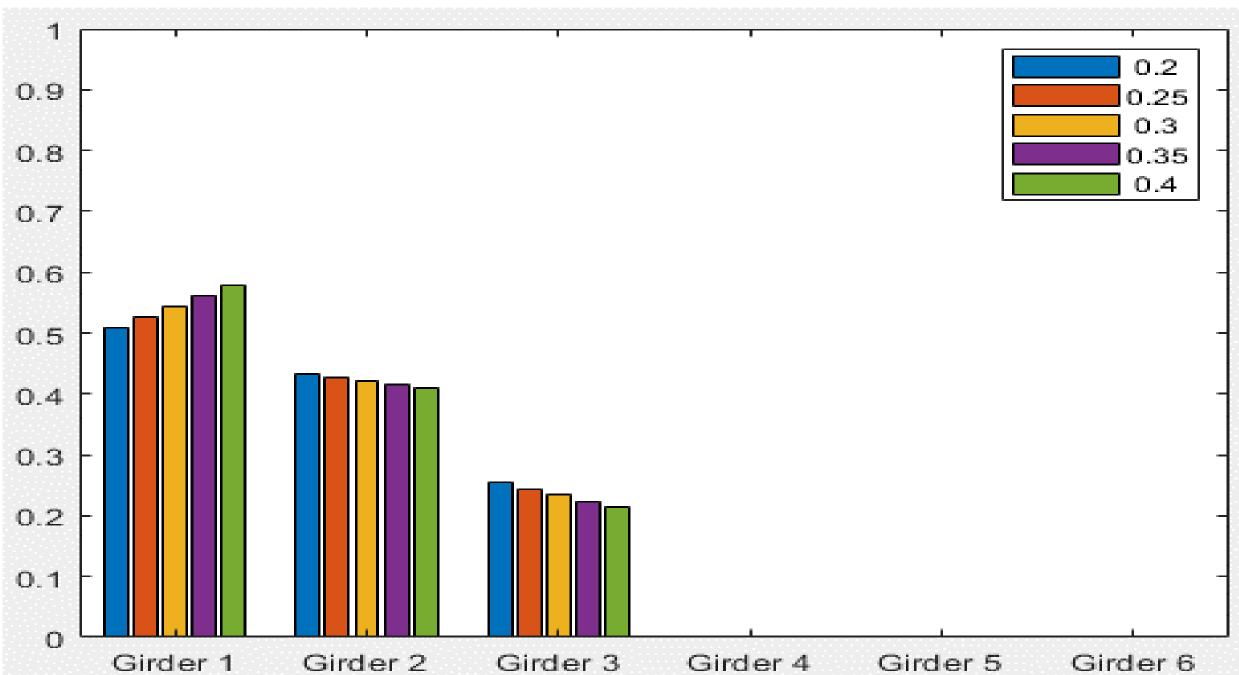

Typical Bridge #1, Tarhini/Frederick Methodology, EG OLL, Variable = Overhang Ratio

NO DATA AVAILABLE

Typical Bridge #1, Tarhini/Frederick Methodology, EG 2LL, Variable = PBFTG Size

NO DATA AVAILABLE

Typical Bridge #1, Tarhini/Frederick Methodology, EG 2LL, Variable = Span Length (ft)

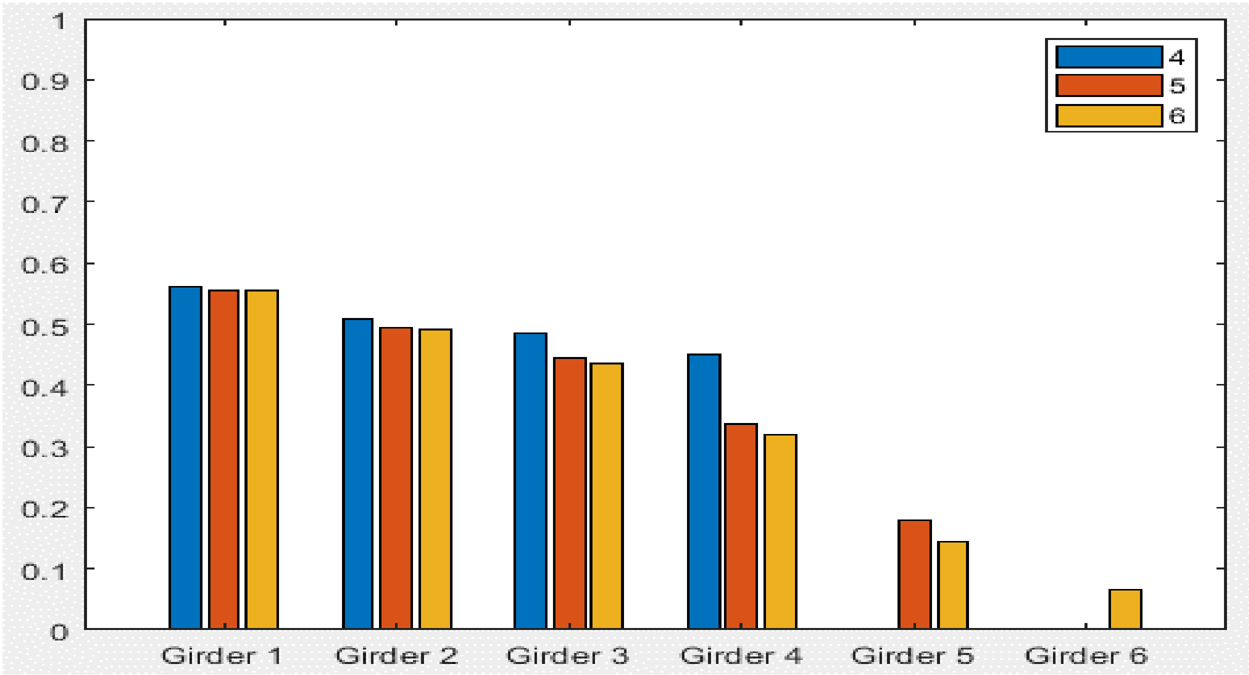

Typical Bridge #1, Tarhini/Frederick Methodology, EG 2LL, Variable = Number of Girders

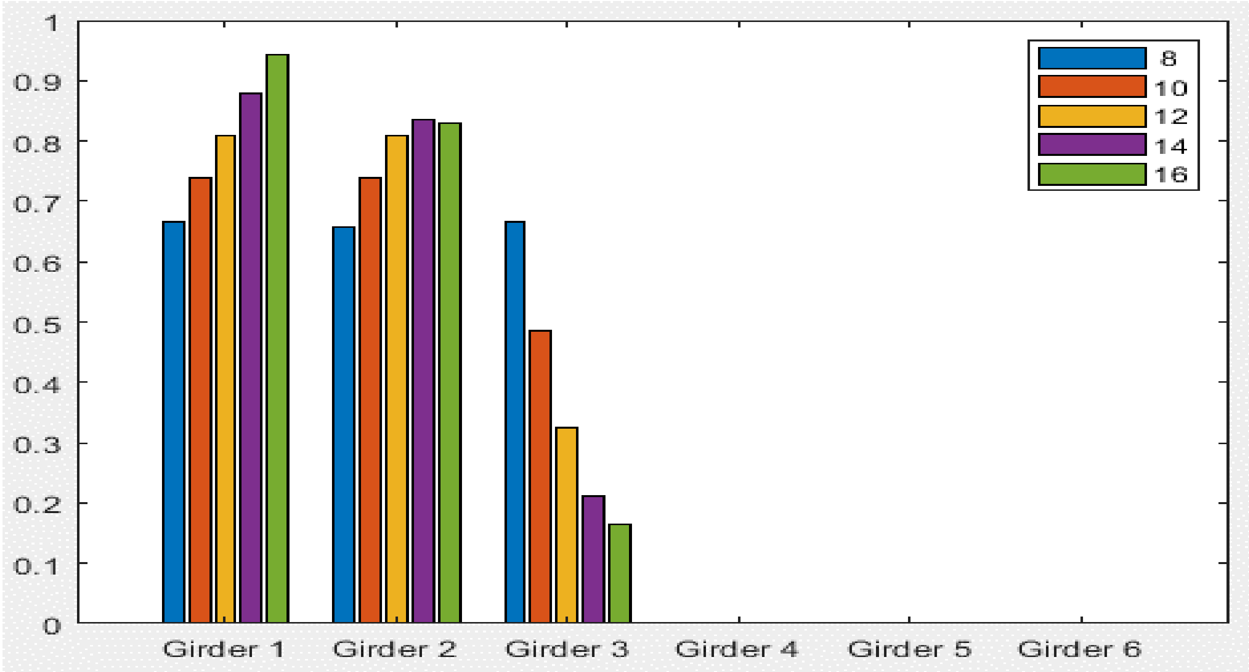

Typical Bridge #1, Tarhini/Frederick Methodology, EG 2LL, Variable = Girder Spacing (ft)

NO DATA AVAILABLE

Typical Bridge #1, Tarhini/Frederick Methodology, EG 2LL, Variable = Degree of Skew (deg)

NO DATA AVAILABLE

Typical Bridge #1, Tarhini/Frederick Methodology, EG 2LL, Variable = Deck Thickness (in)

NO DATA AVAILABLE

Typical Bridge #1, Tarhini/Frederick Methodology, EG 2LL, Variable = Overhang Ratio

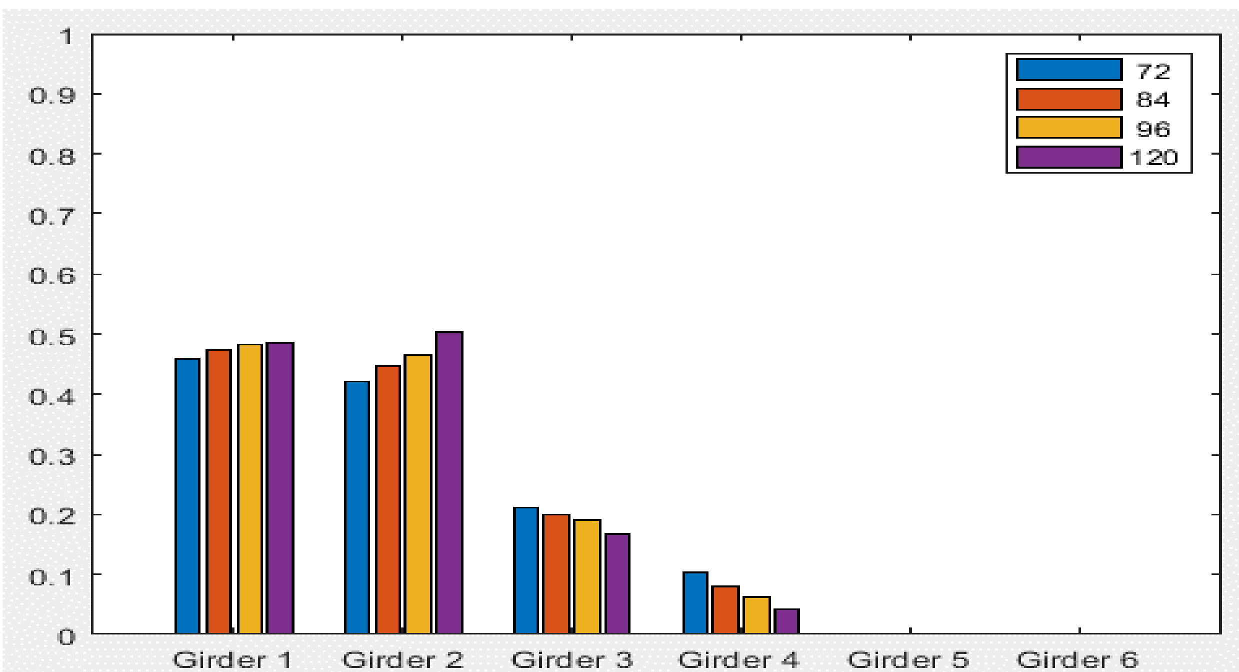

Typical Bridge #2, Stallings/Yoo Methodology, IG OLL, Variable = PBFTG Size

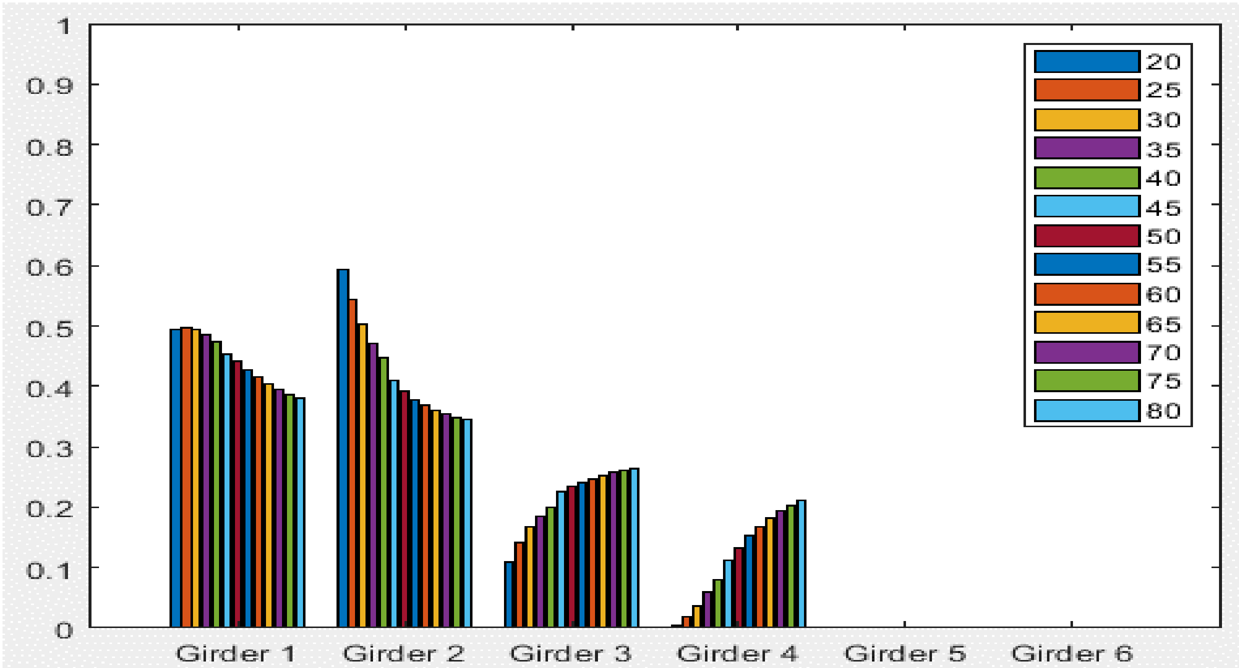

Typical Bridge #2, Stallings/Yoo Methodology, IG OLL, Variable = Span Length (ft)

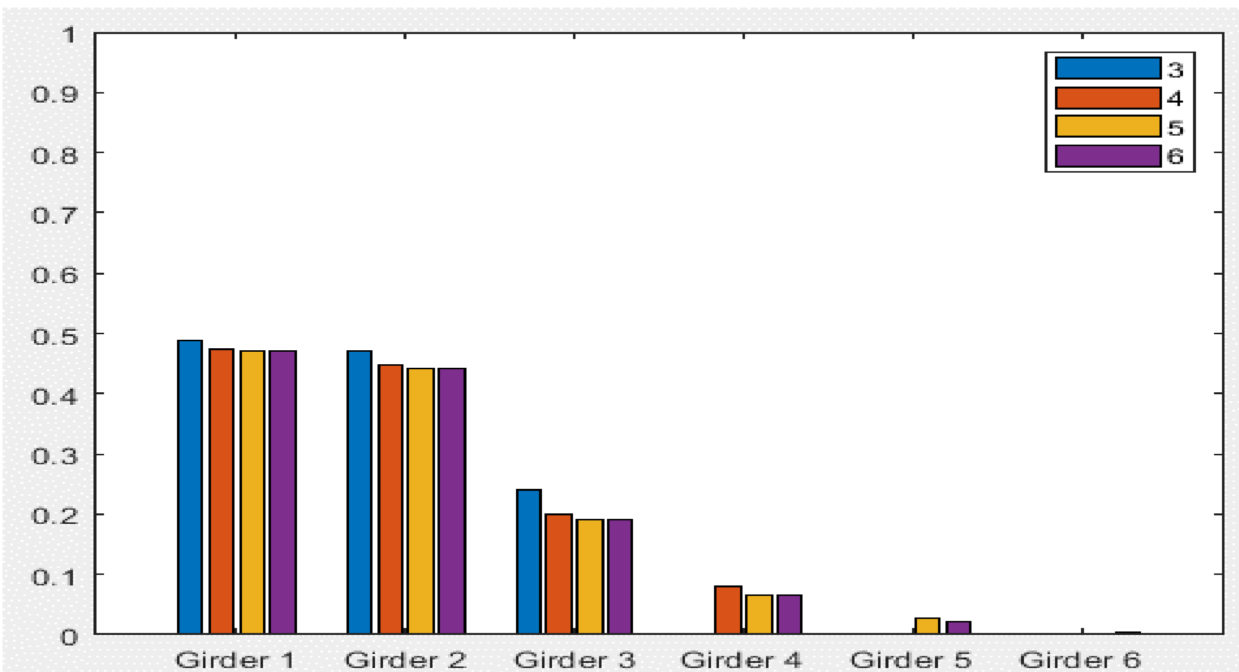

Typical Bridge #2, Stallings/Yoo Methodology, IG OLL, Variable = Number of Girders

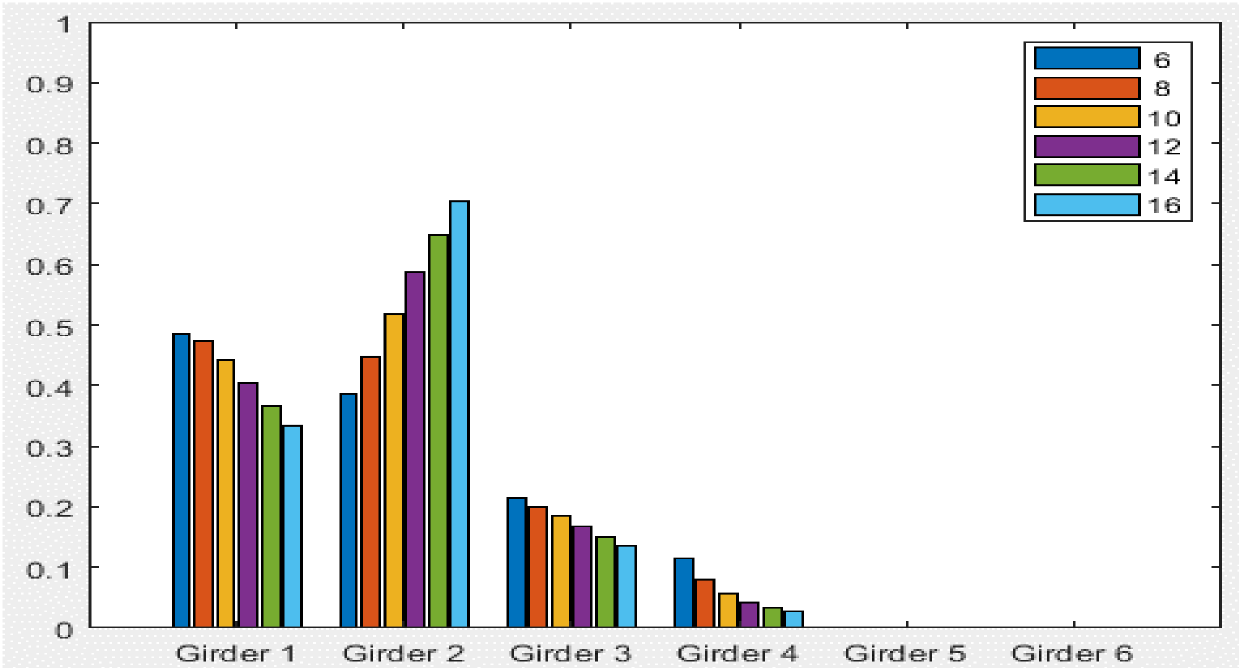

Typical Bridge #2, Stallings/Yoo Methodology, IG OLL, Variable = Girder Spacing (ft)

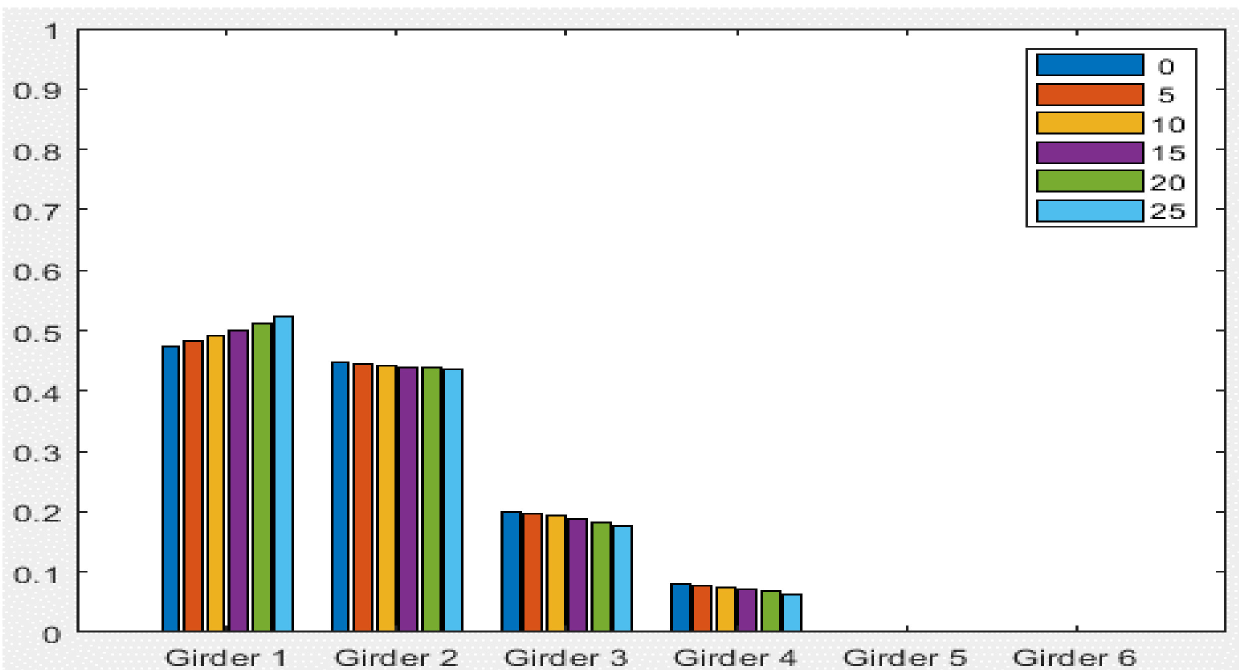

Typical Bridge #2, Stallings/Yoo Methodology, IG OLL, Variable = Degree of Skew (deg)

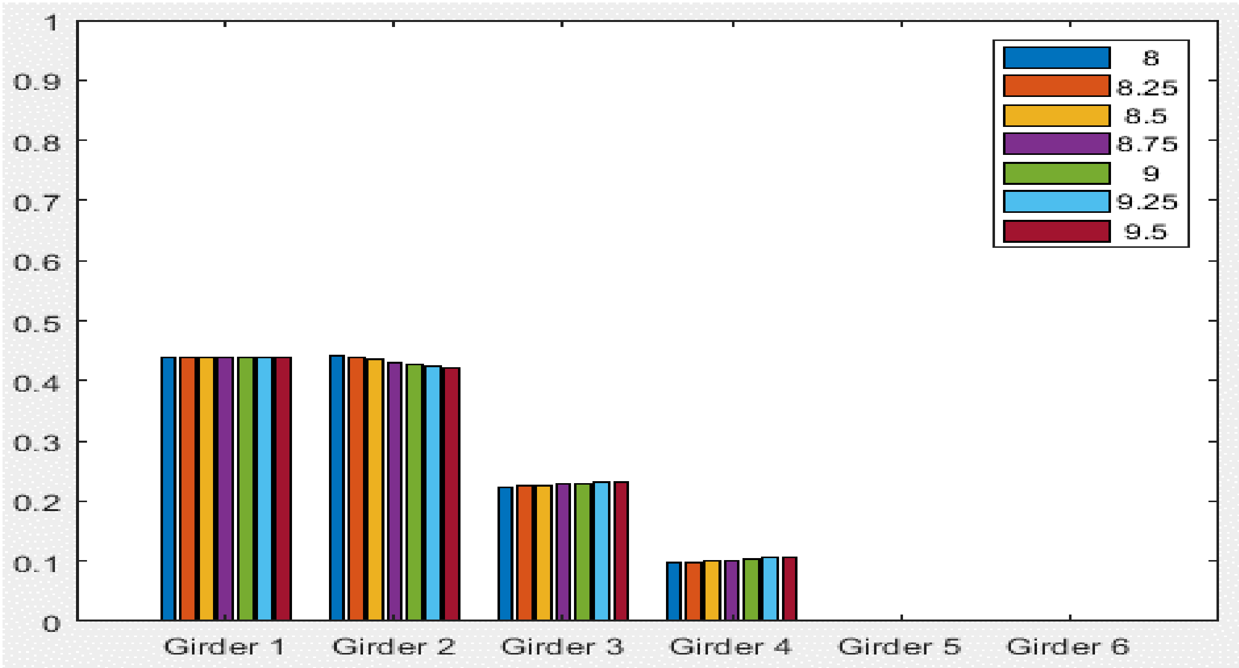

Typical Bridge #2, Stallings/Yoo Methodology, IG OLL, Variable = Deck Thickness (in)

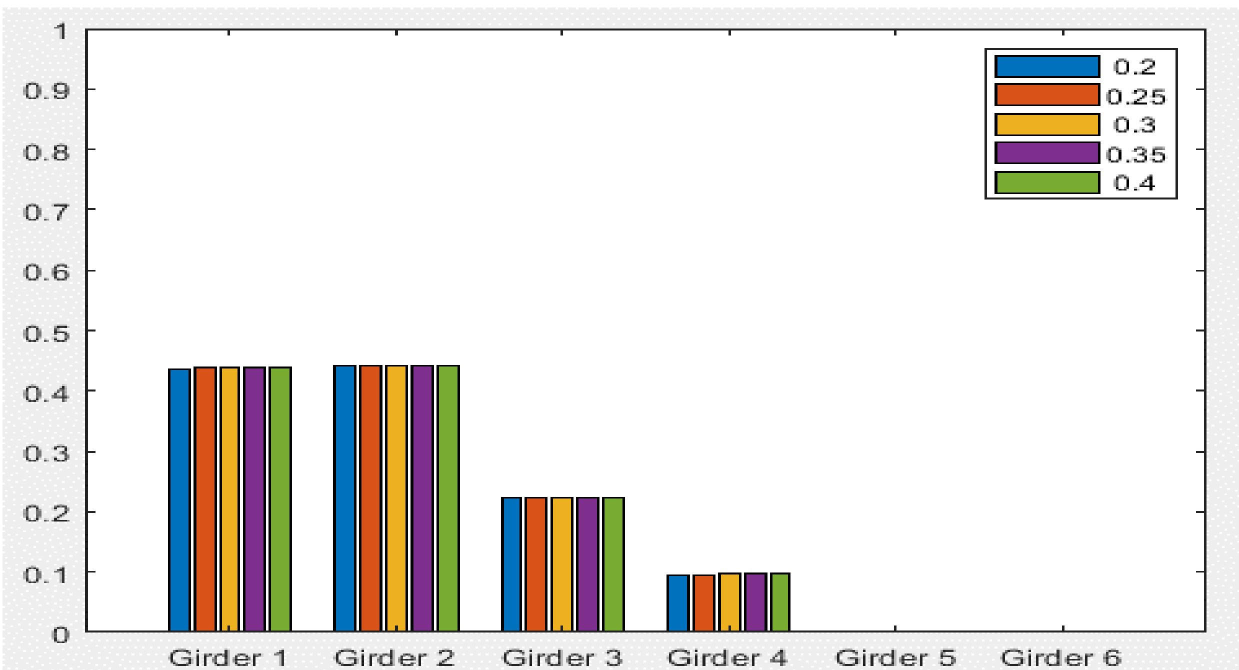

Typical Bridge #2, Stallings/Yoo Methodology, IG OLL, Variable = Overhang Ratio

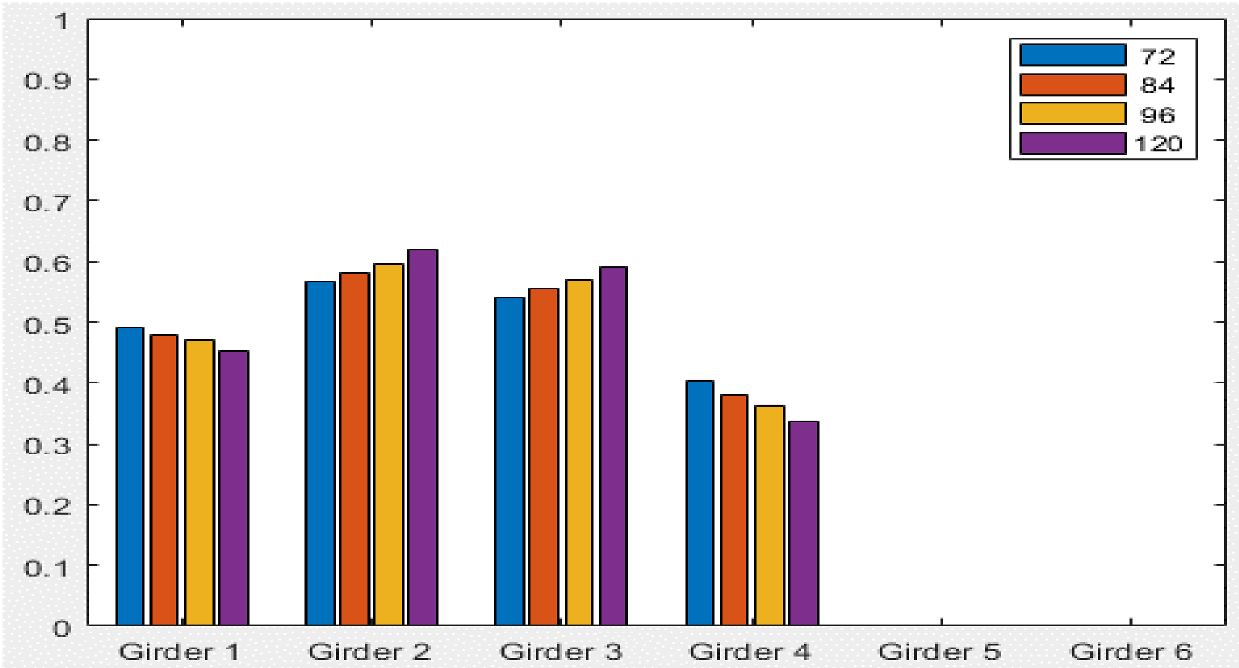

Typical Bridge #2, Stallings/Yoo Methodology, IG 2LL, Variable = PBFTG Size

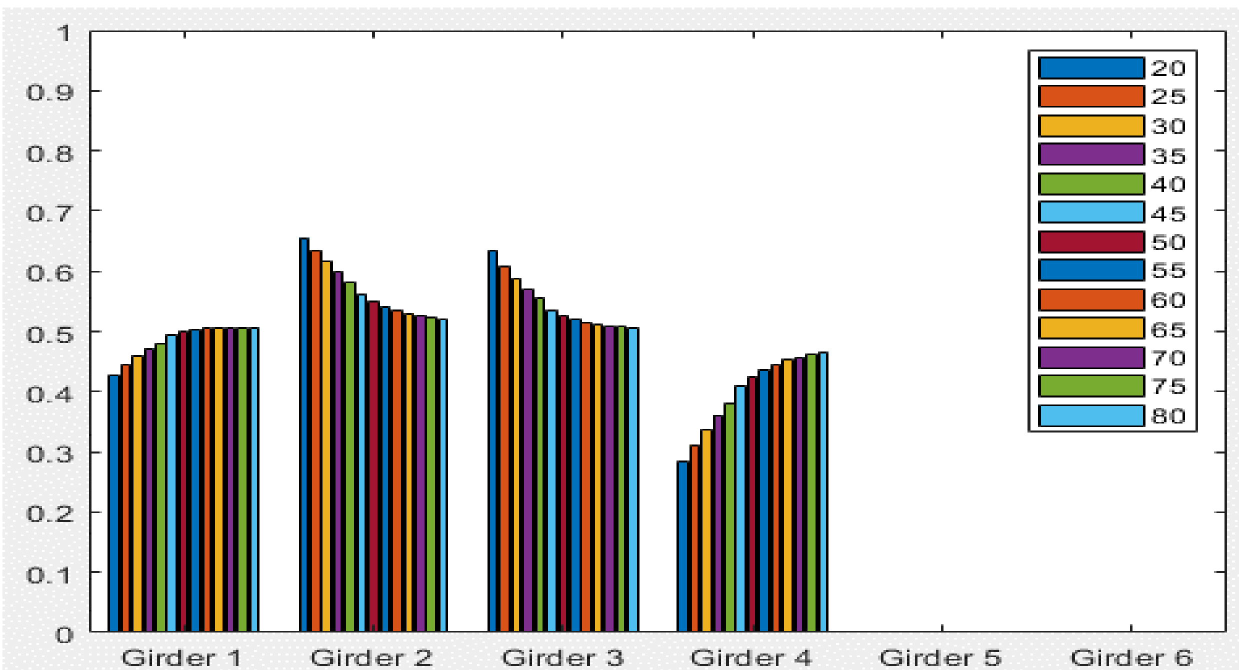

Typical Bridge #2, Stallings/Yoo Methodology, IG 2LL, Variable = Span Length (ft)

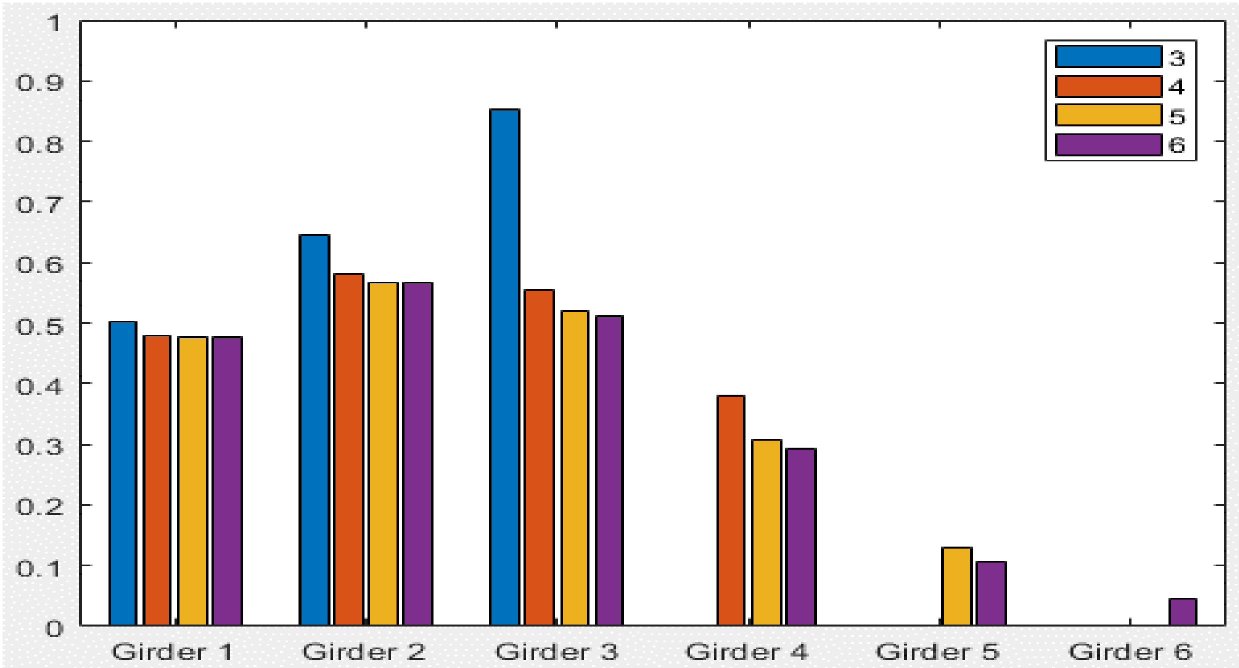

Typical Bridge #2, Stallings/Yoo Methodology, IG 2LL, Variable = Number of Girders

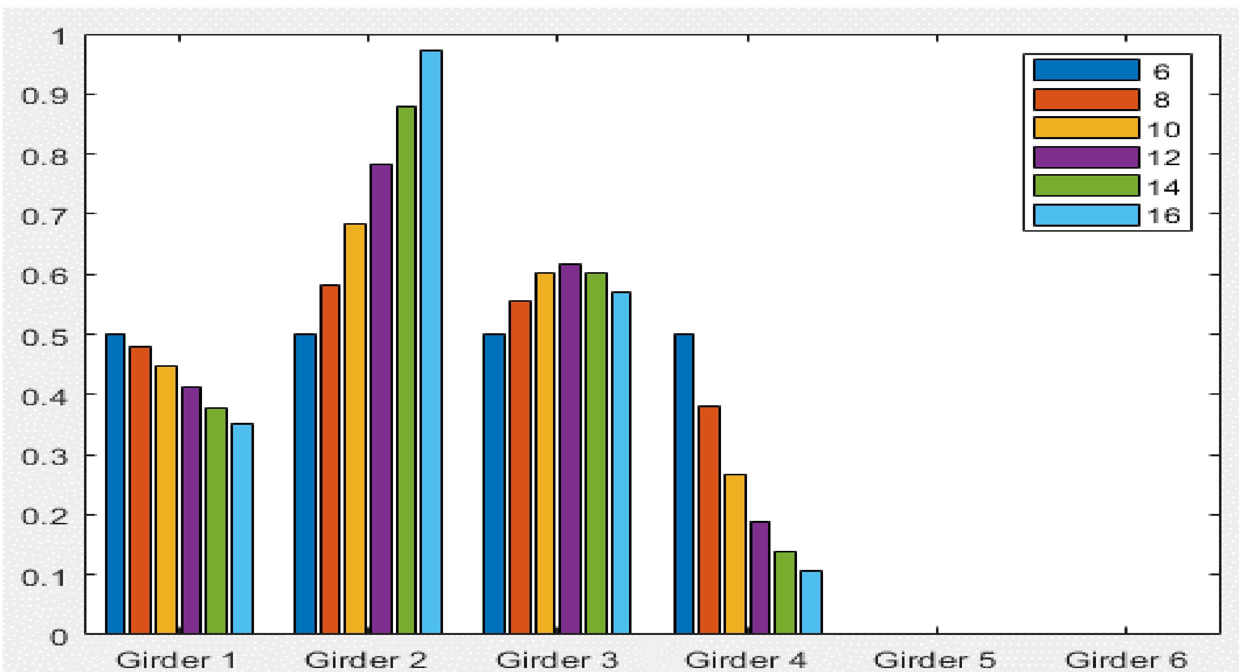

Typical Bridge #2, Stallings/Yoo Methodology, IG 2LL, Variable = Girder Spacing (ft)

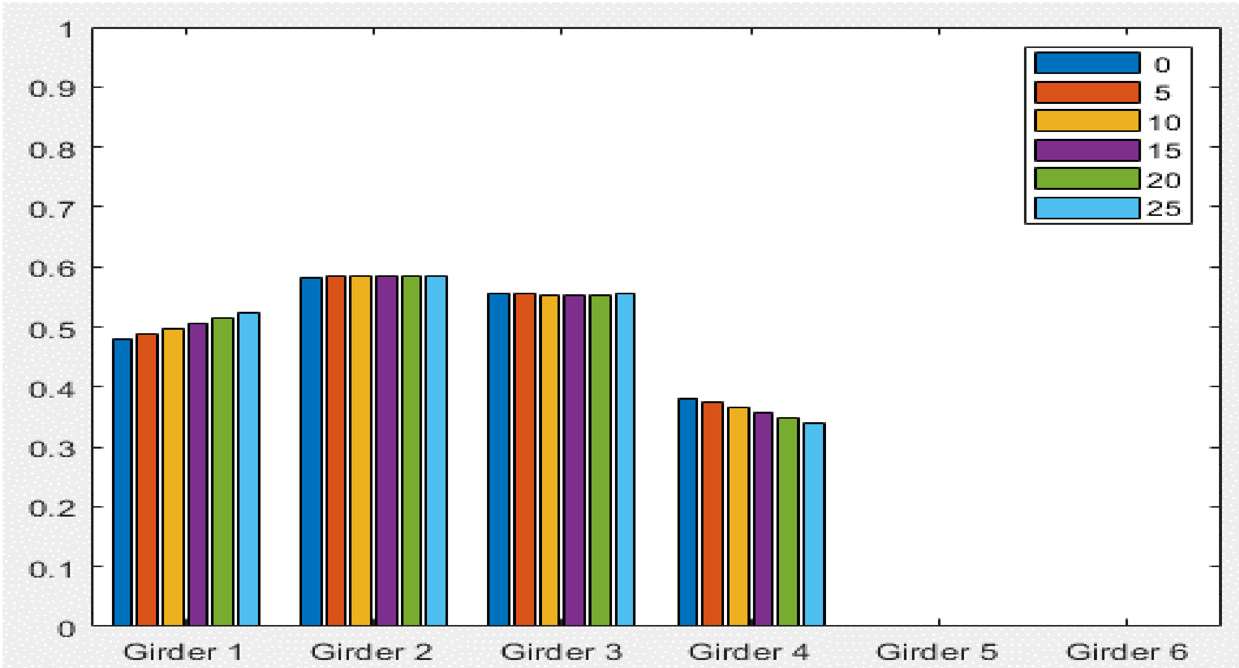

Typical Bridge #2, Stallings/Yoo Methodology, IG 2LL, Variable = Degree of Skew (deg)

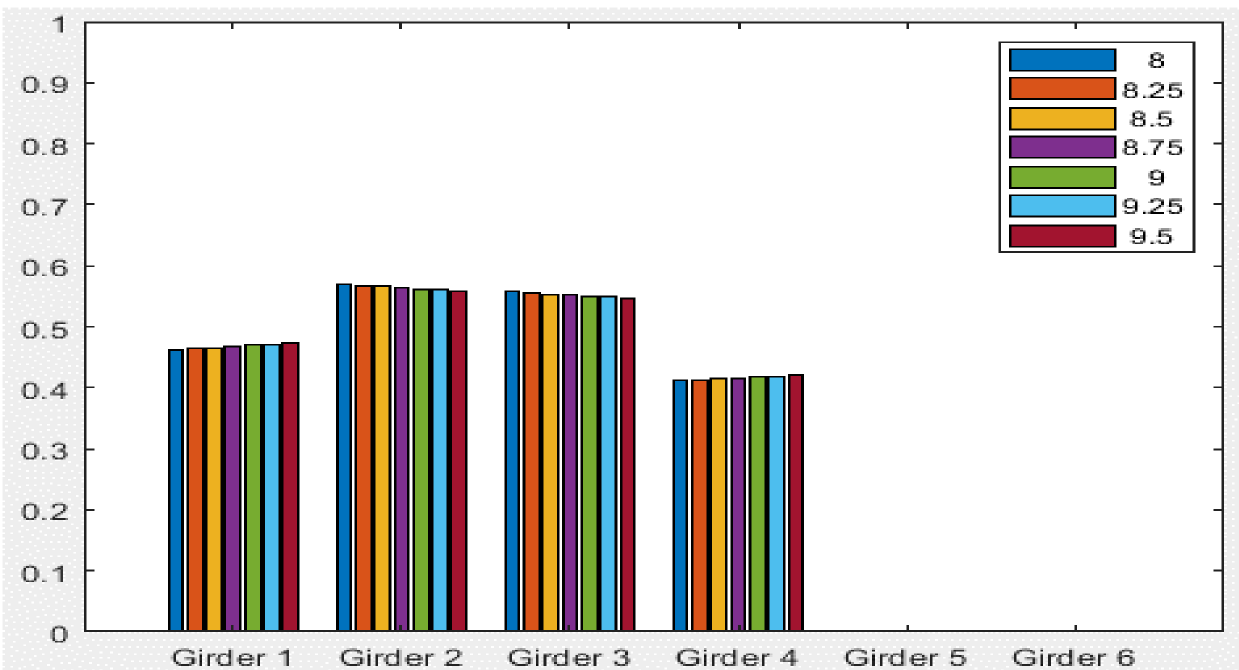

Typical Bridge #2, Stallings/Yoo Methodology, IG 2LL, Variable = Deck Thickness (in)

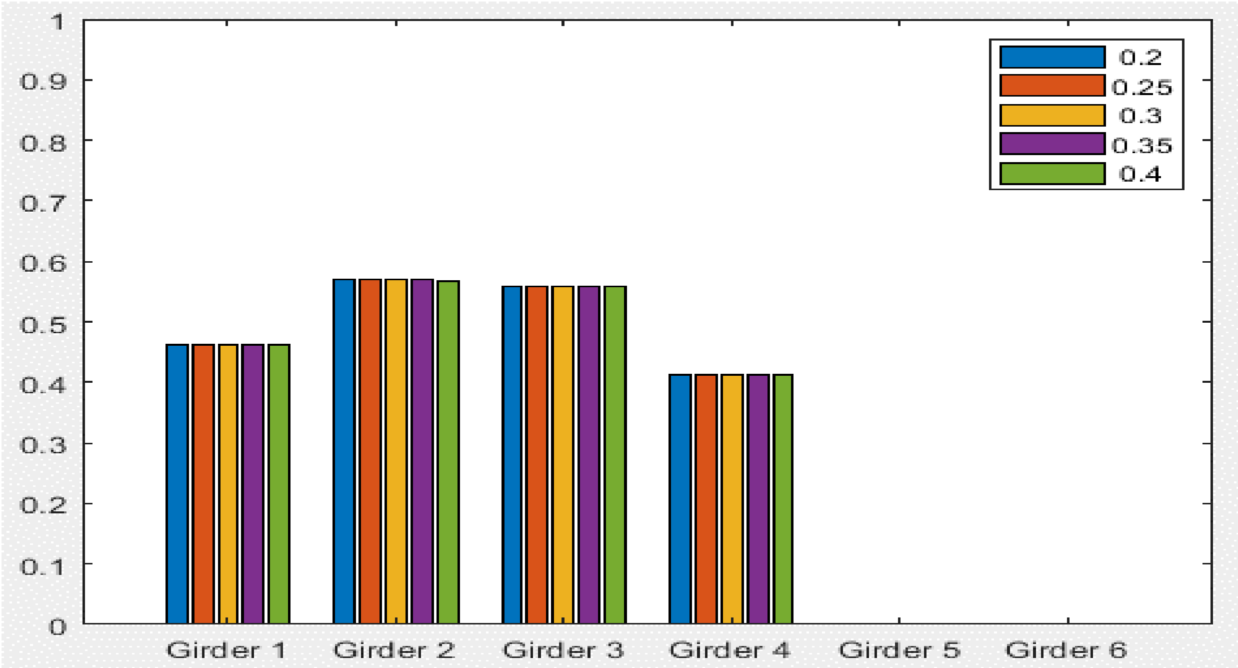

Typical Bridge #2, Stallings/Yoo Methodology, IG 2LL, Variable = Overhang Ratio

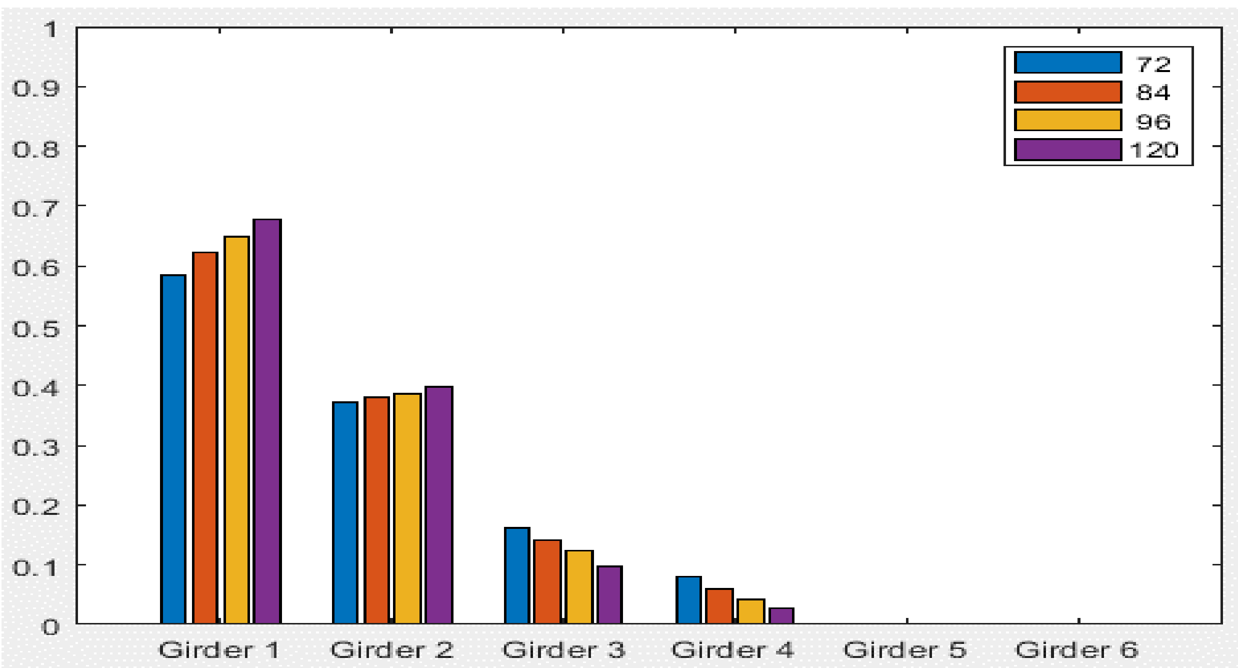

Typical Bridge #2, Stallings/Yoo Methodology, EG OLL, Variable = PBFTG Size

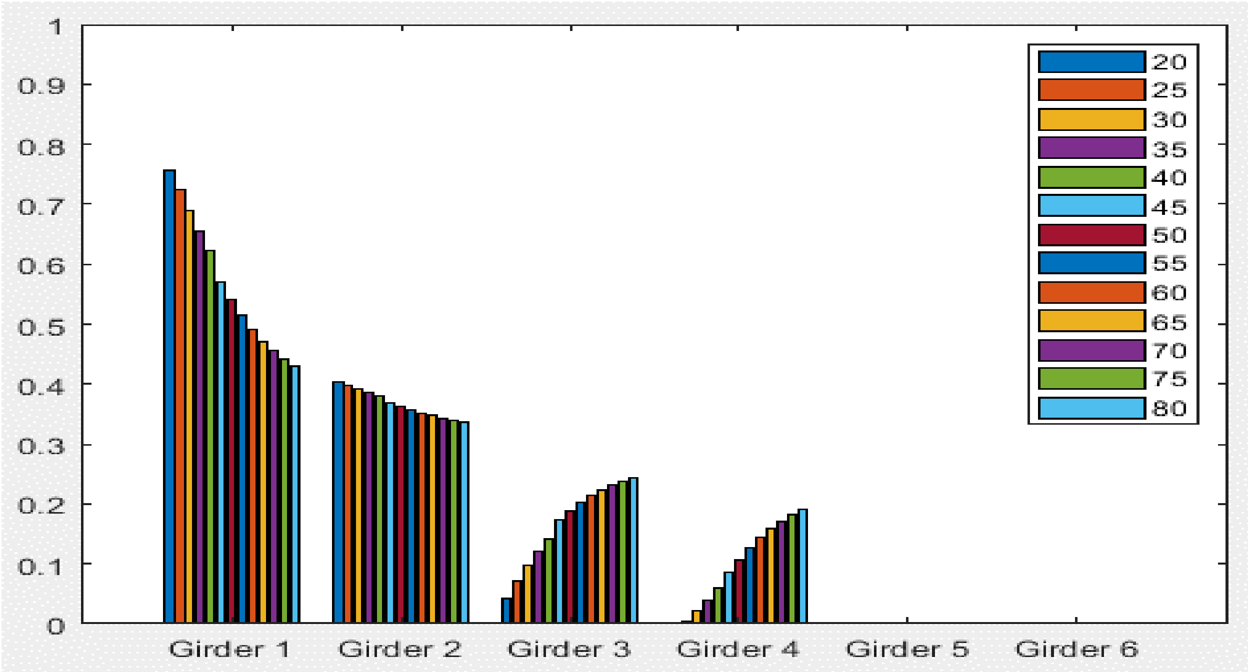

Typical Bridge #2, Stallings/Yoo Methodology, EG OLL, Variable = Span Length (ft)

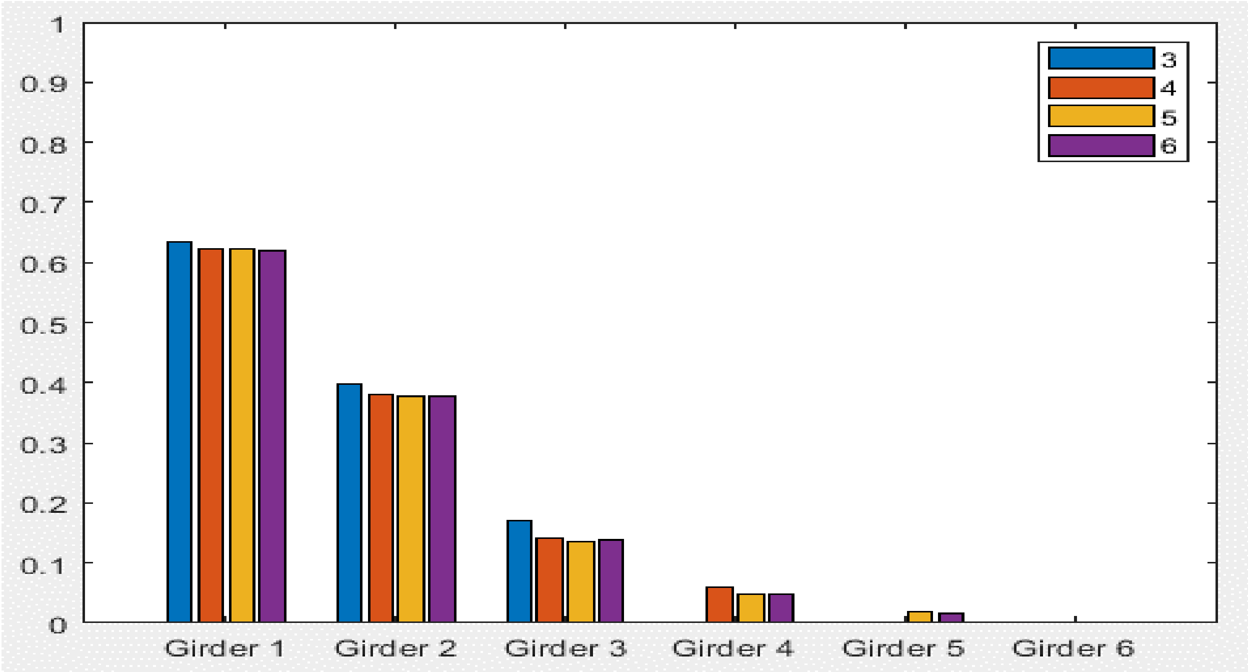

Typical Bridge #2, Stallings/Yoo Methodology, EG OLL, Variable = Number of Girders

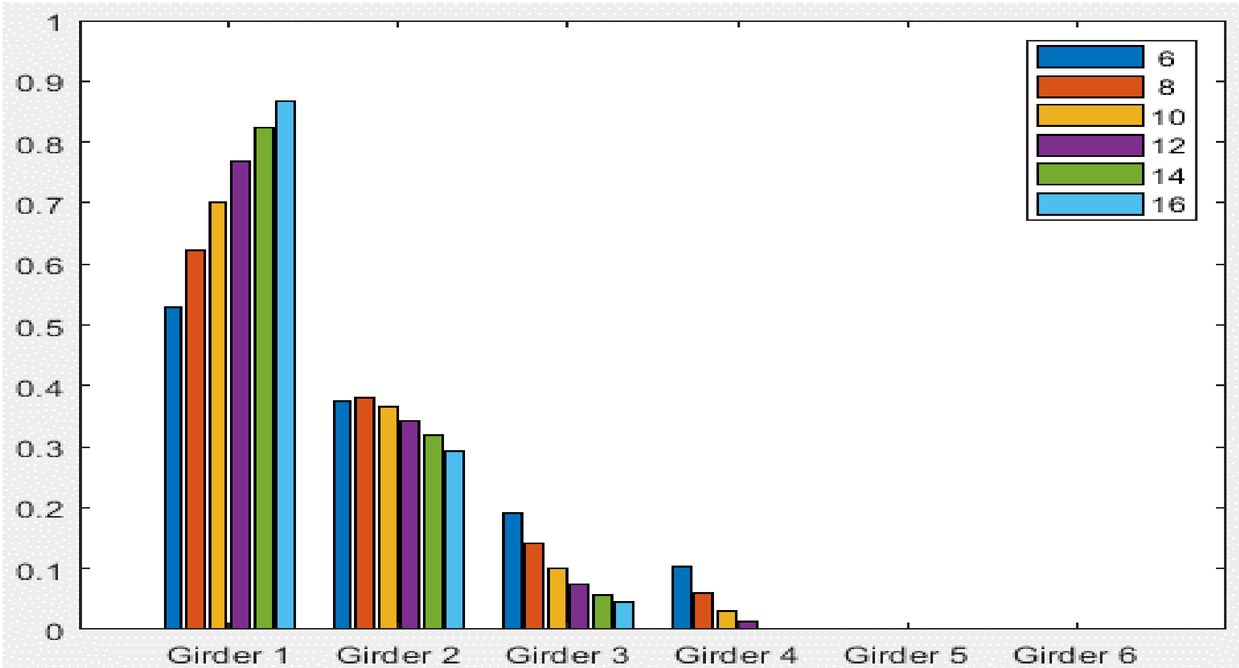

Typical Bridge #2, Stallings/Yoo Methodology, EG OLL, Variable = Girder Spacing (ft)

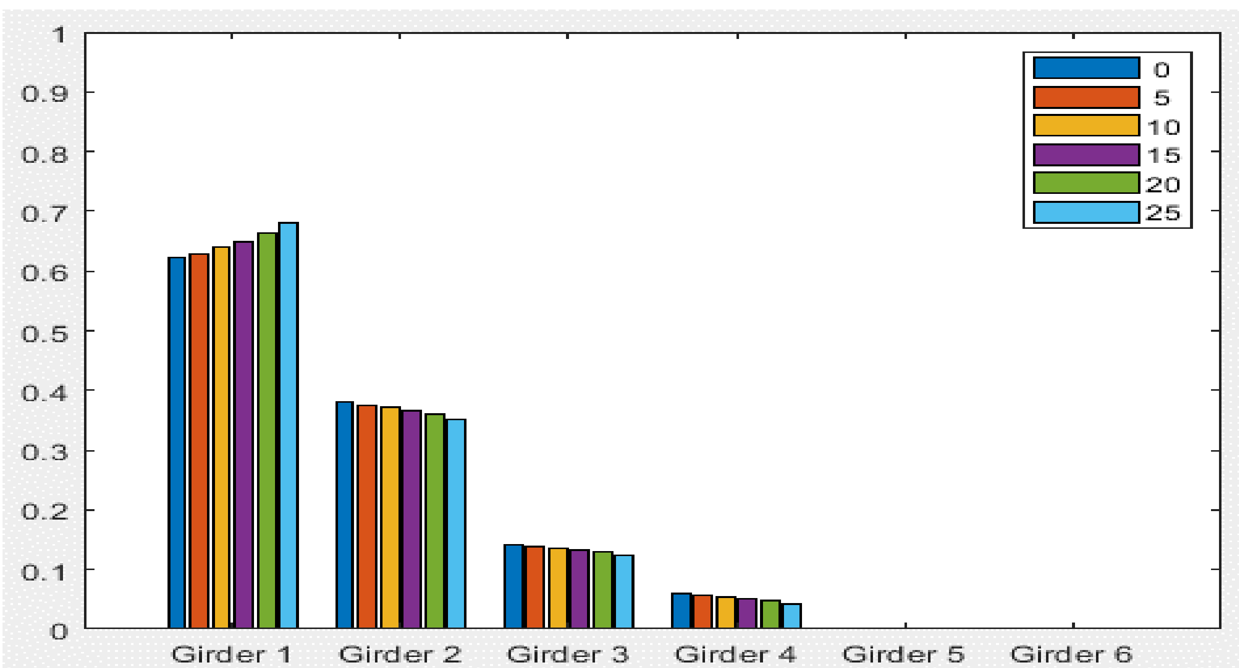

Typical Bridge #2, Stallings/Yoo Methodology, EG OLL, Variable = Degree of Skew (deg)

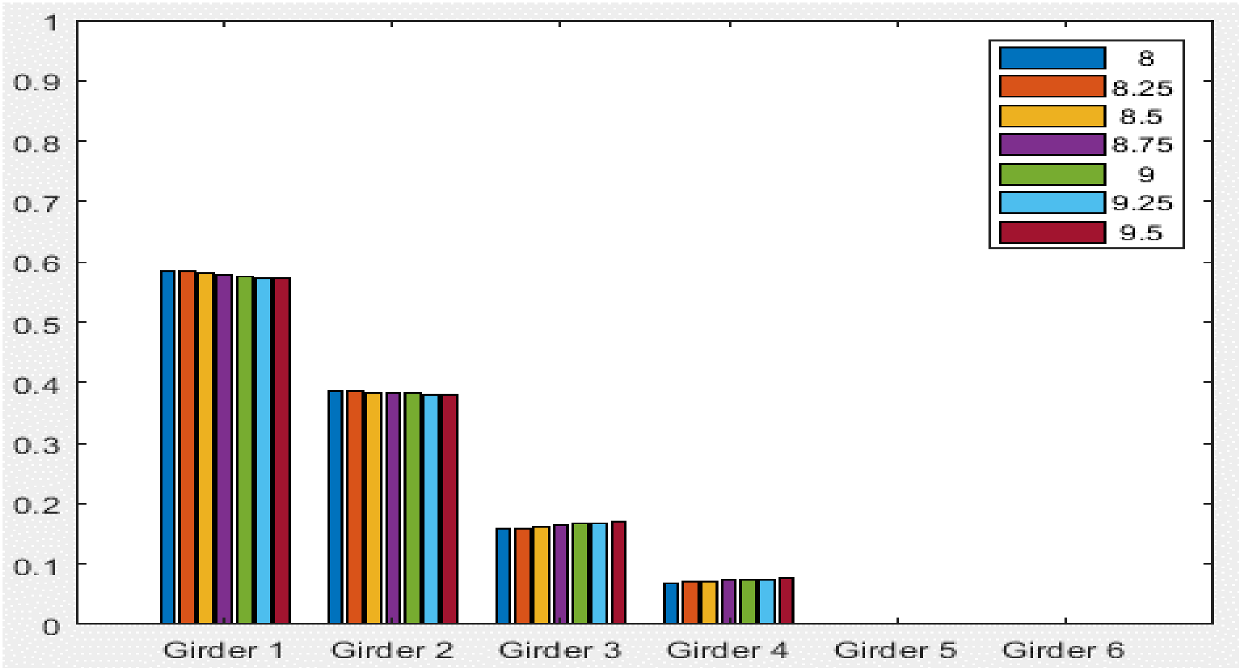

Typical Bridge #2, Stallings/Yoo Methodology, EG OLL, Variable = Deck Thickness (in)

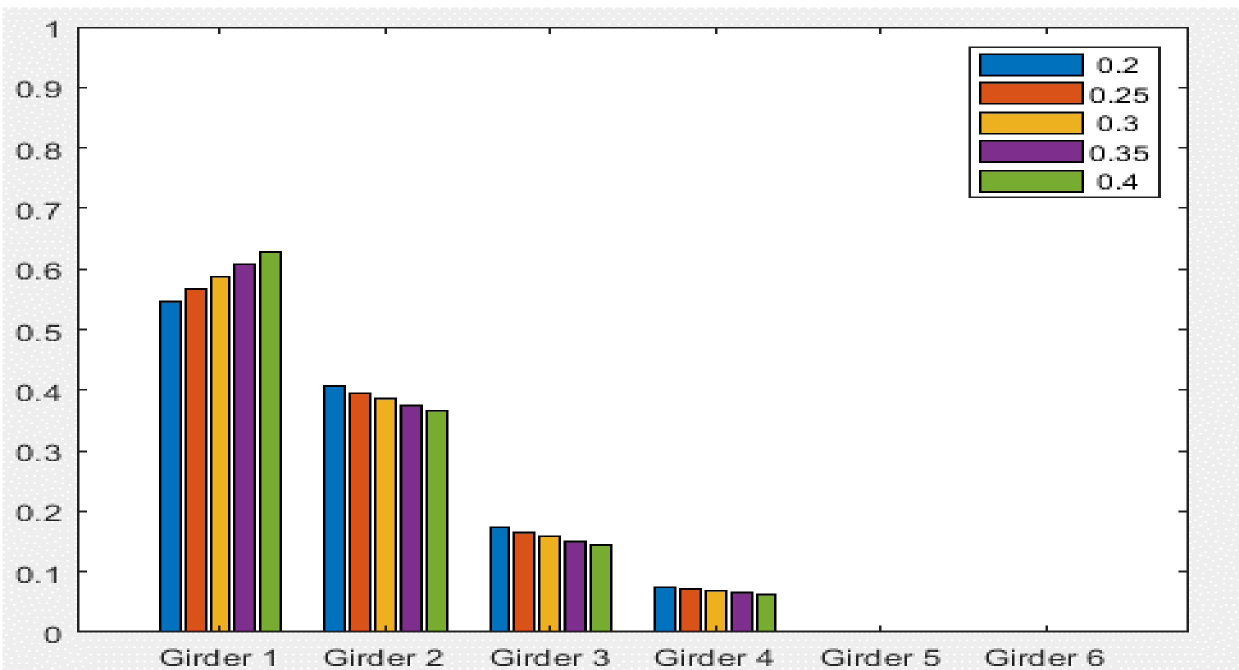

Typical Bridge #2, Stallings/Yoo Methodology, EG OLL, Variable = Overhang Ratio

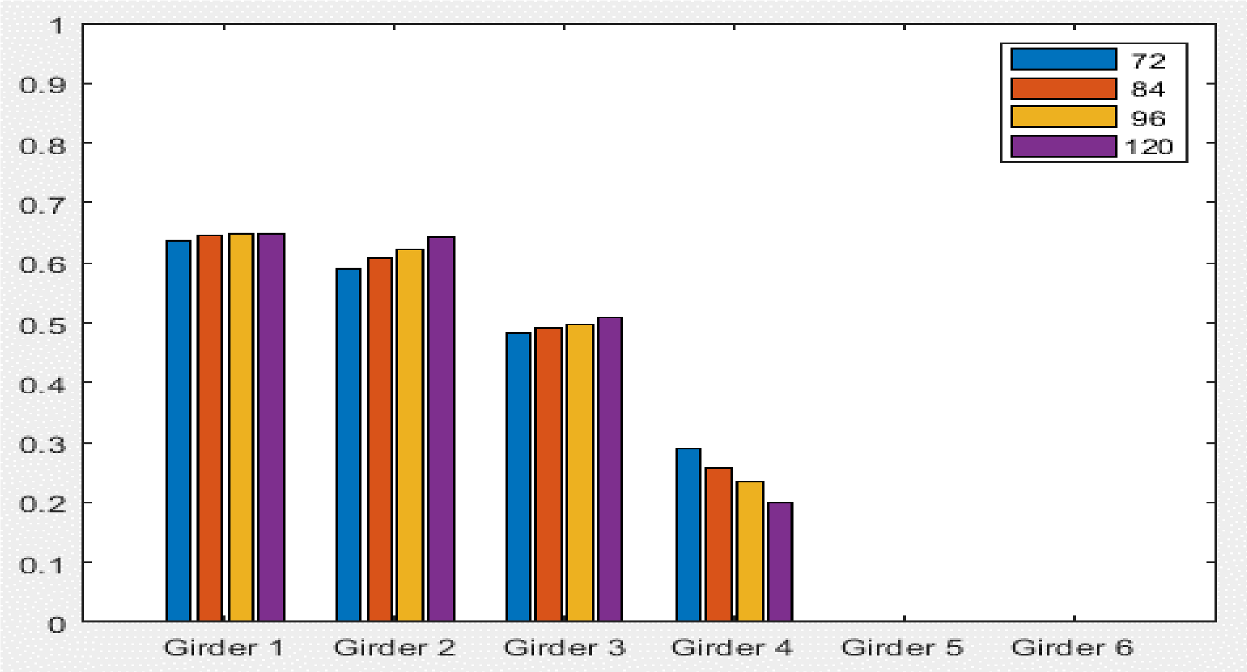

Typical Bridge #2, Stallings/Yoo Methodology, EG 2LL, Variable = PBFTG Size

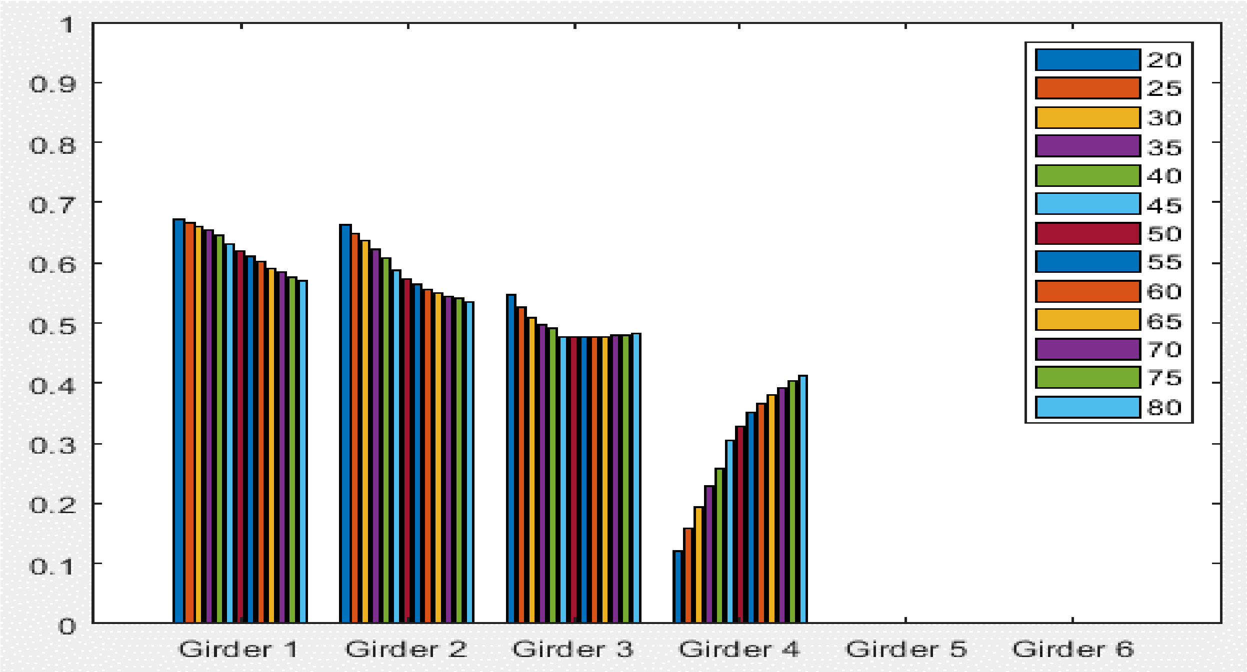

Typical Bridge #2, Stallings/Yoo Methodology, EG 2LL, Variable = Span Length (ft)

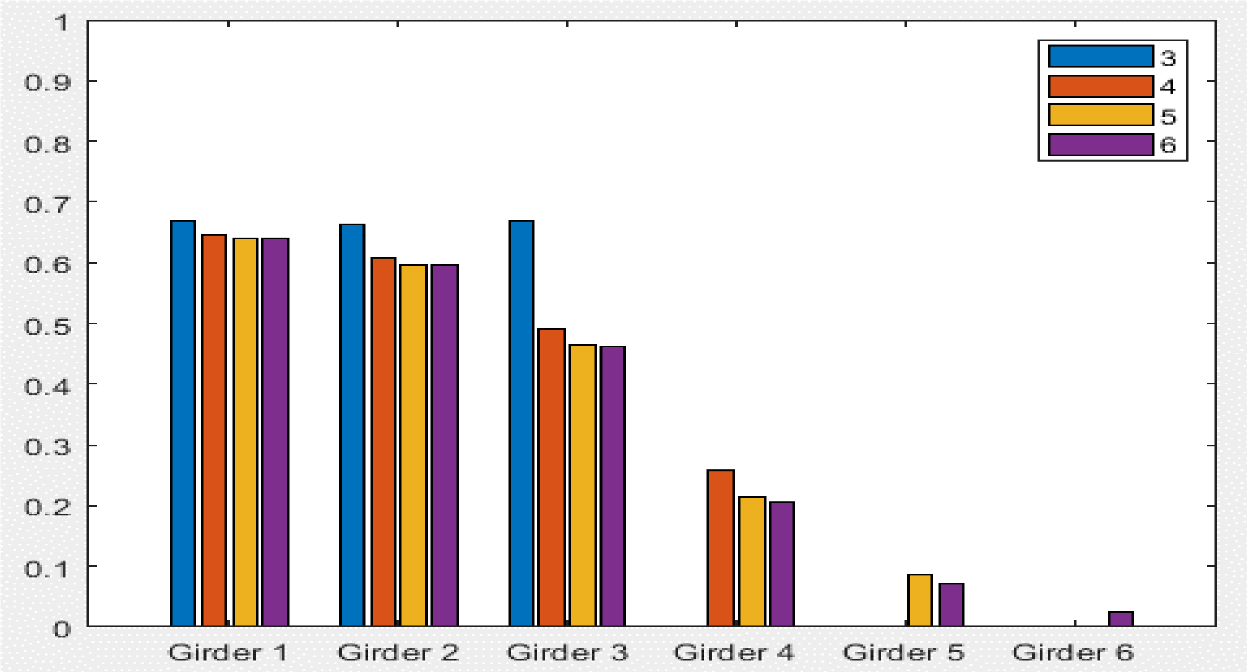

Typical Bridge #2, Stallings/Yoo Methodology, EG 2LL, Variable = Number of Girders

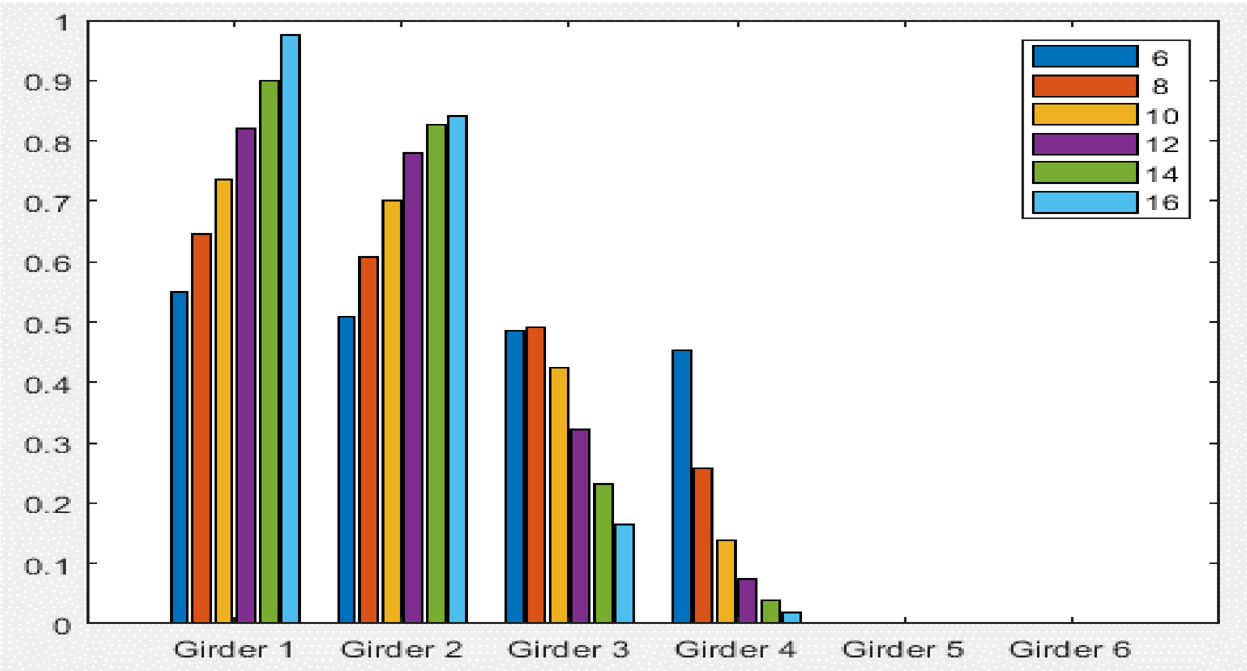

Typical Bridge #2, Stallings/Yoo Methodology, EG 2LL, Variable = Girder Spacing (ft)

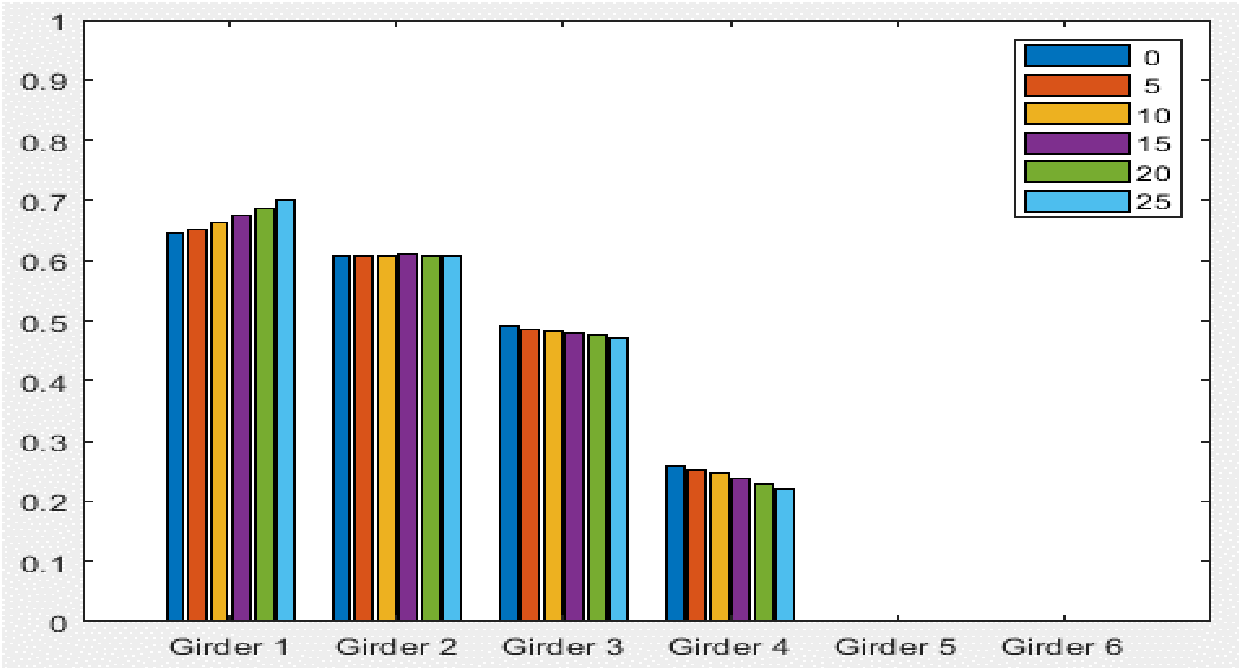

Typical Bridge #2, Stallings/Yoo Methodology, EG 2LL, Variable = Degree of Skew (deg)

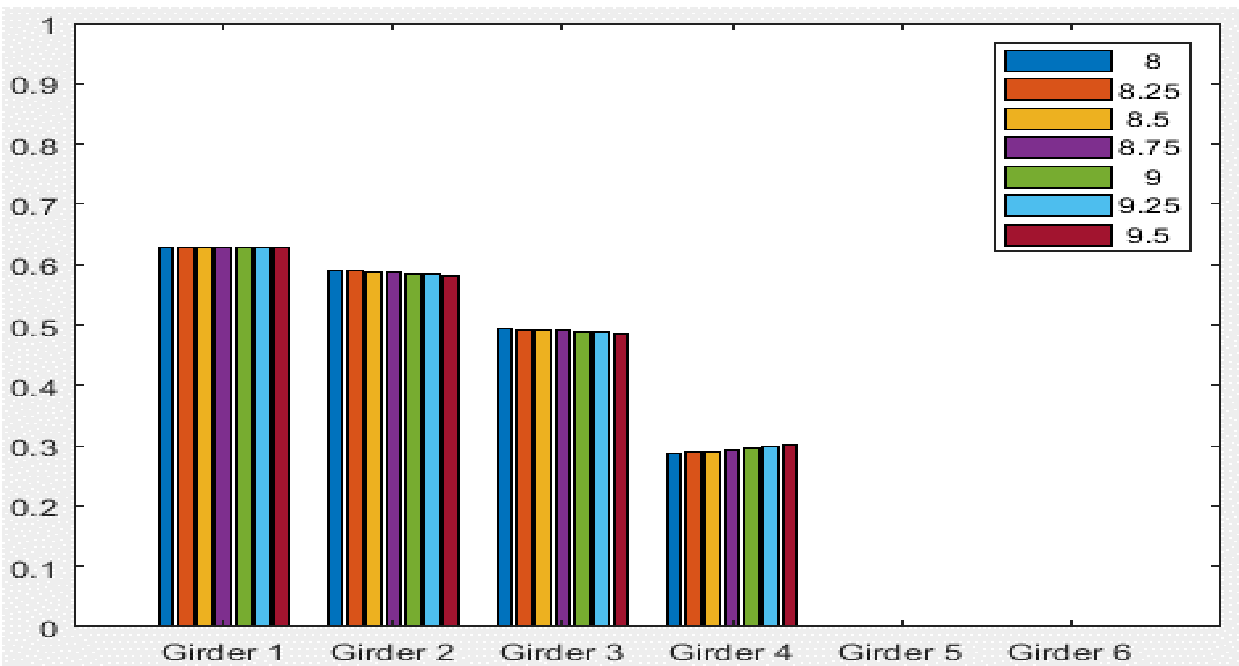

Typical Bridge #2, Stallings/Yoo Methodology, EG 2LL, Variable = Deck Thickness (in)

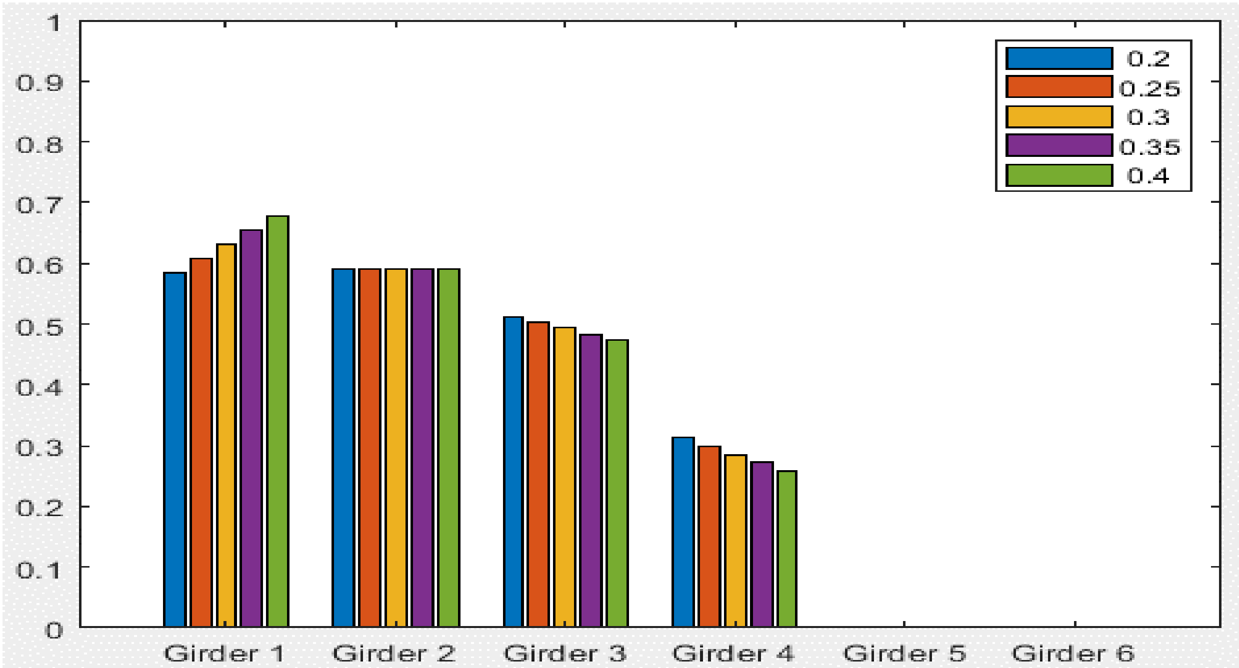

Typical Bridge #2, Stallings/Yoo Methodology, EG 2LL, Variable = Overhang Ratio

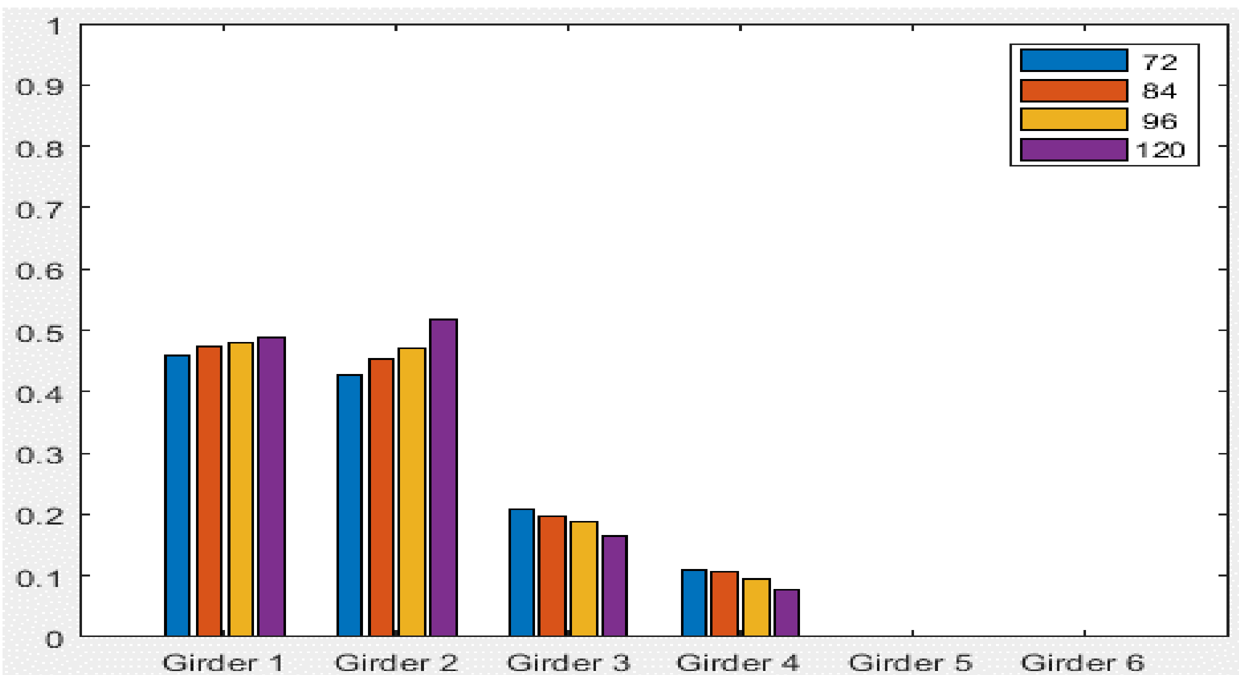

Typical Bridge #2, Tarhini/Frederick Methodology, IG OLL, Variable = PBFTG Size

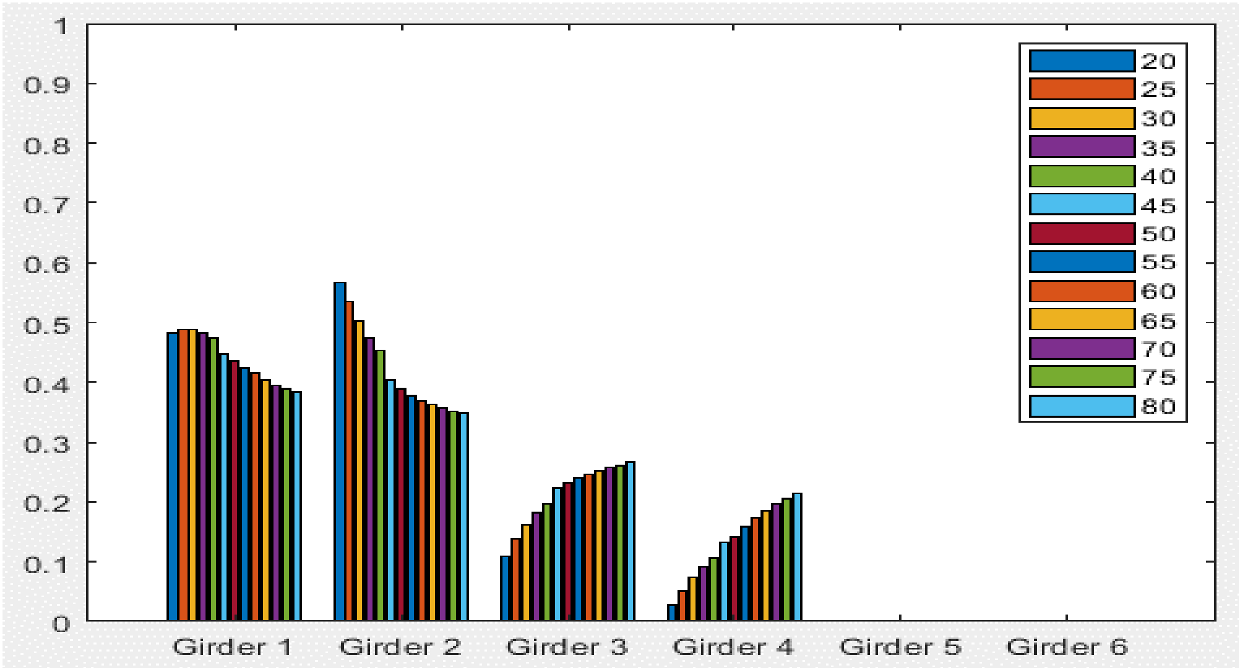

Typical Bridge #2, Tarhini/Frederick Methodology, IG OLL, Variable = Span Length (ft)

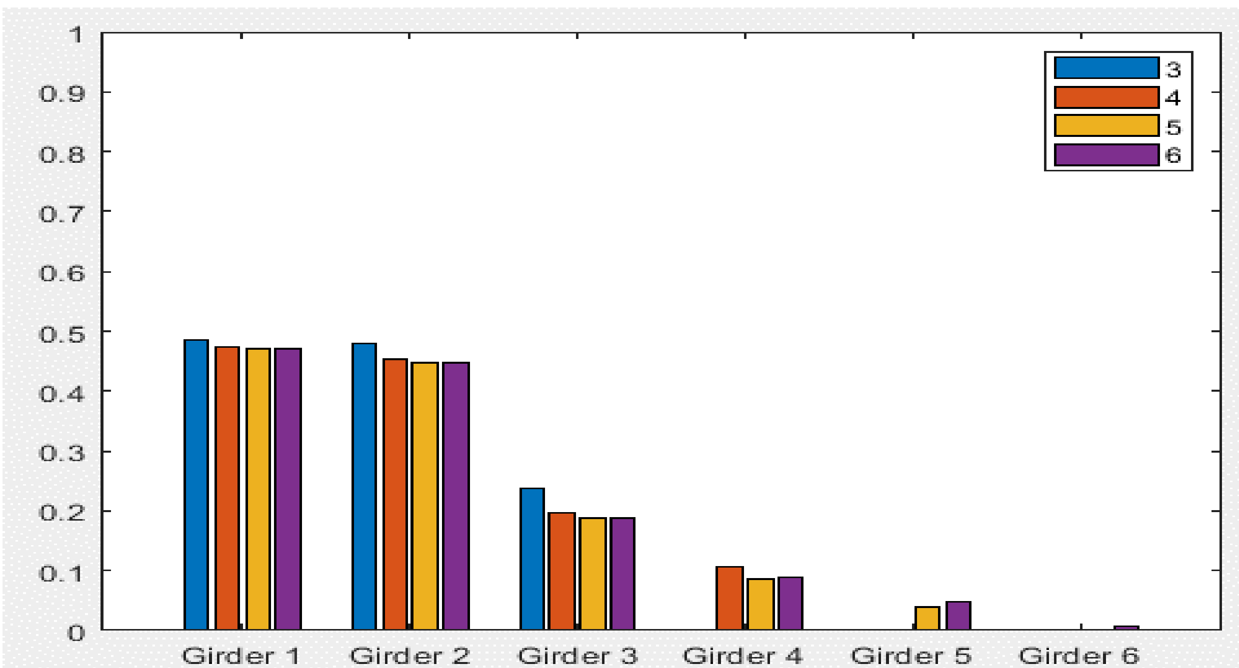

Typical Bridge #2, Tarhini/Frederick Methodology, IG OLL, Variable = Number of Girders

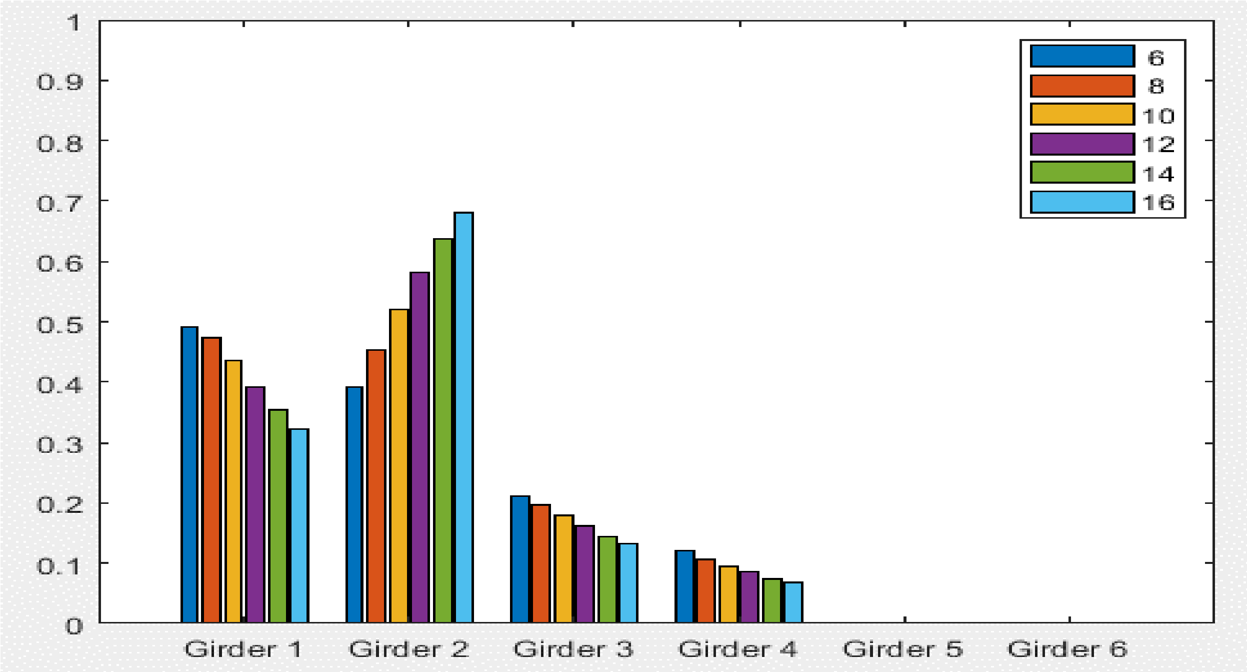

Typical Bridge #2, Tarhini/Frederick Methodology, IG OLL, Variable = Girder Spacing (ft)

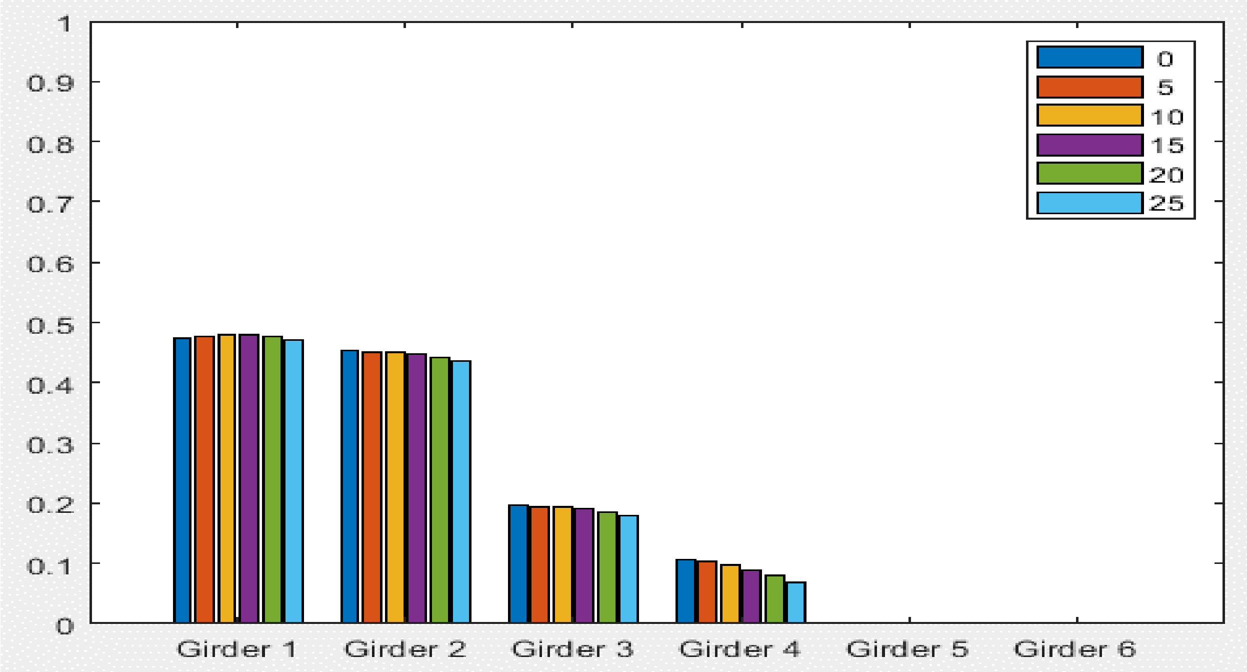

Typical Bridge #2, Tarhini/Frederick Methodology, IG OLL, Variable = Degree of Skew (deg)

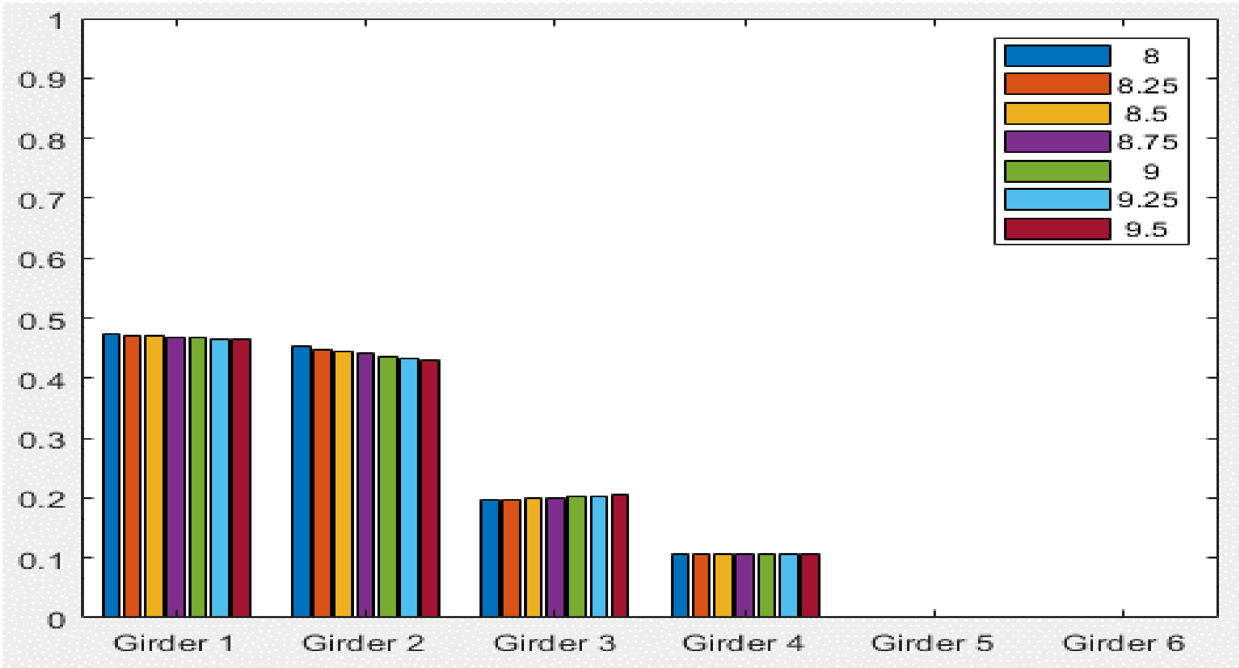

Typical Bridge #2, Tarhini/Frederick Methodology, IG OLL, Variable = Deck Thickness (in)

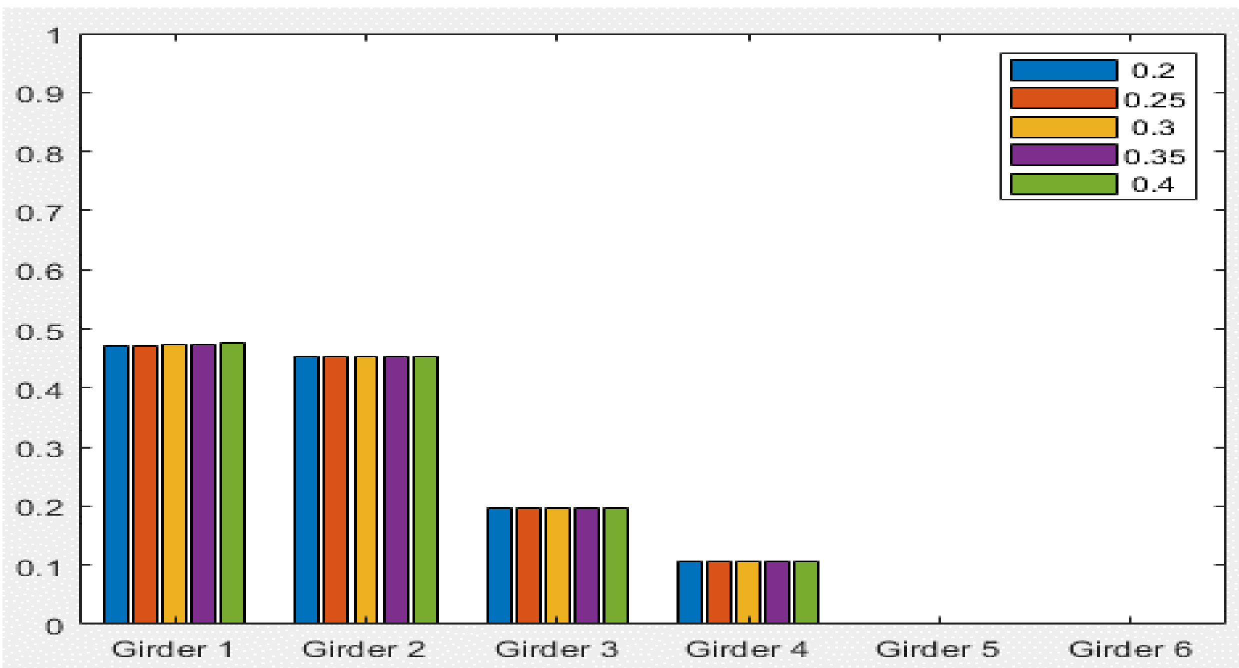

Typical Bridge #2, Tarhini/Frederick Methodology, IG OLL, Variable = Overhang Ratio

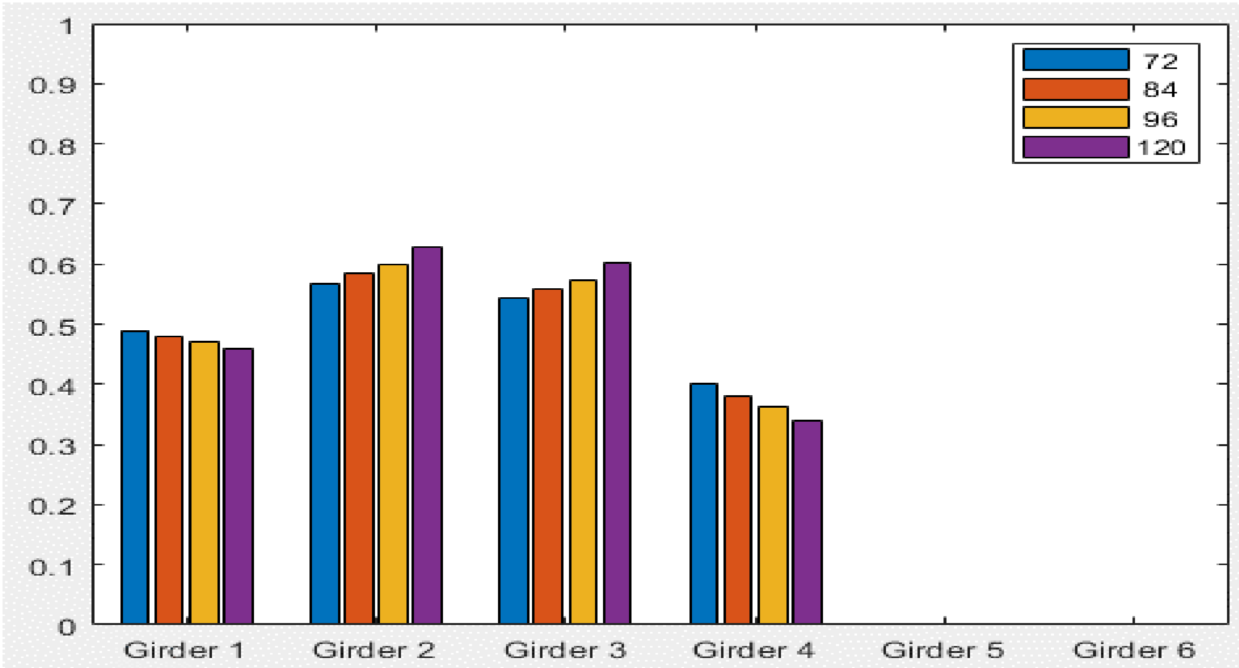

Typical Bridge #2, Tarhini/Frederick Methodology, IG 2LL, Variable = PBFTG Size

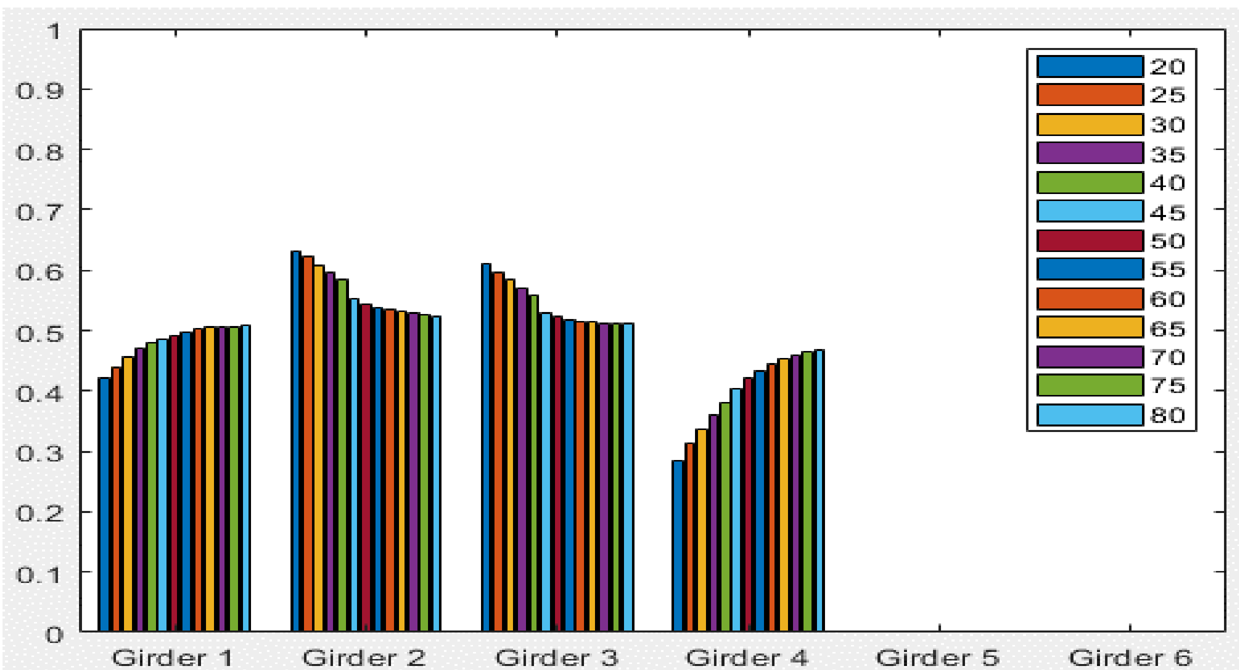

Typical Bridge #2, Tarhini/Frederick Methodology, IG 2LL, Variable = Span Length (ft)

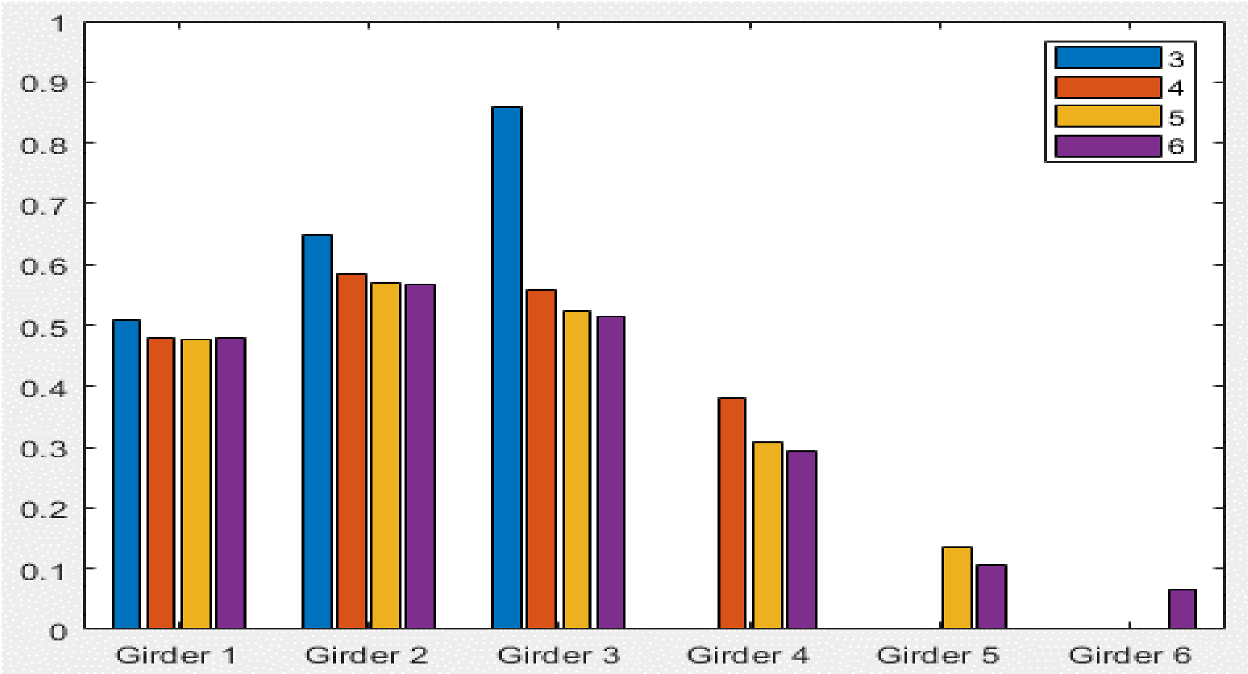

Typical Bridge #2, Tarhini/Frederick Methodology, IG 2LL, Variable = Number of Girders

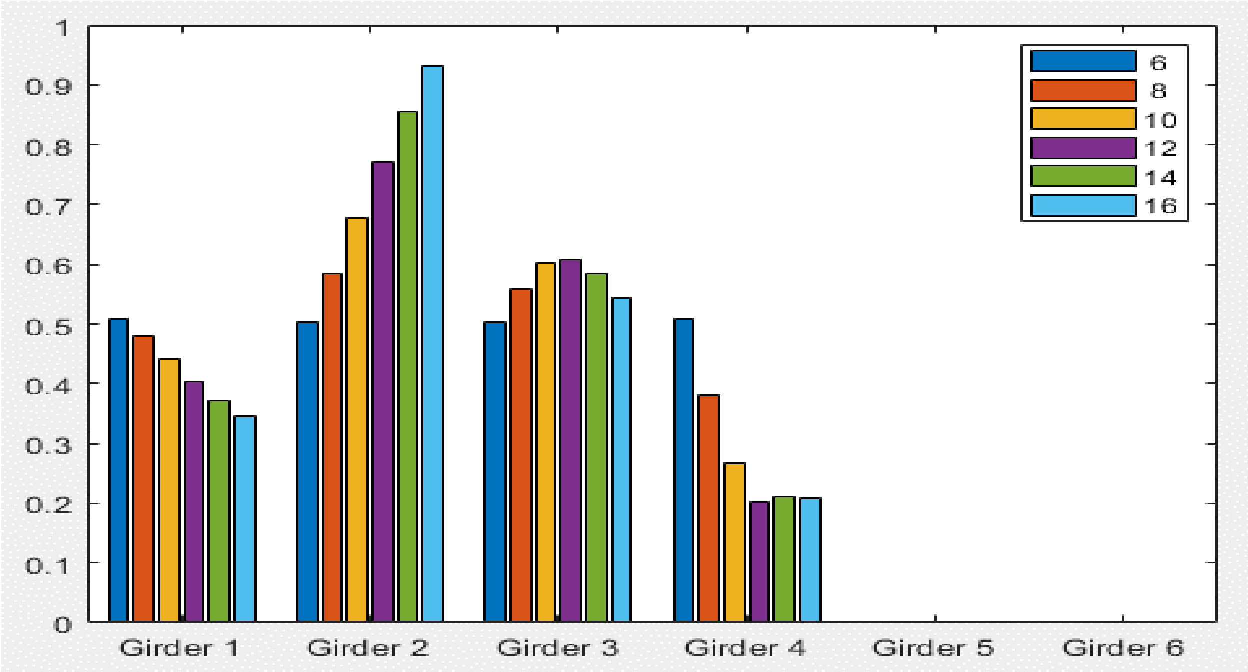

Typical Bridge #2, Tarhini/Frederick Methodology, IG 2LL, Variable = Girder Spacing (ft)

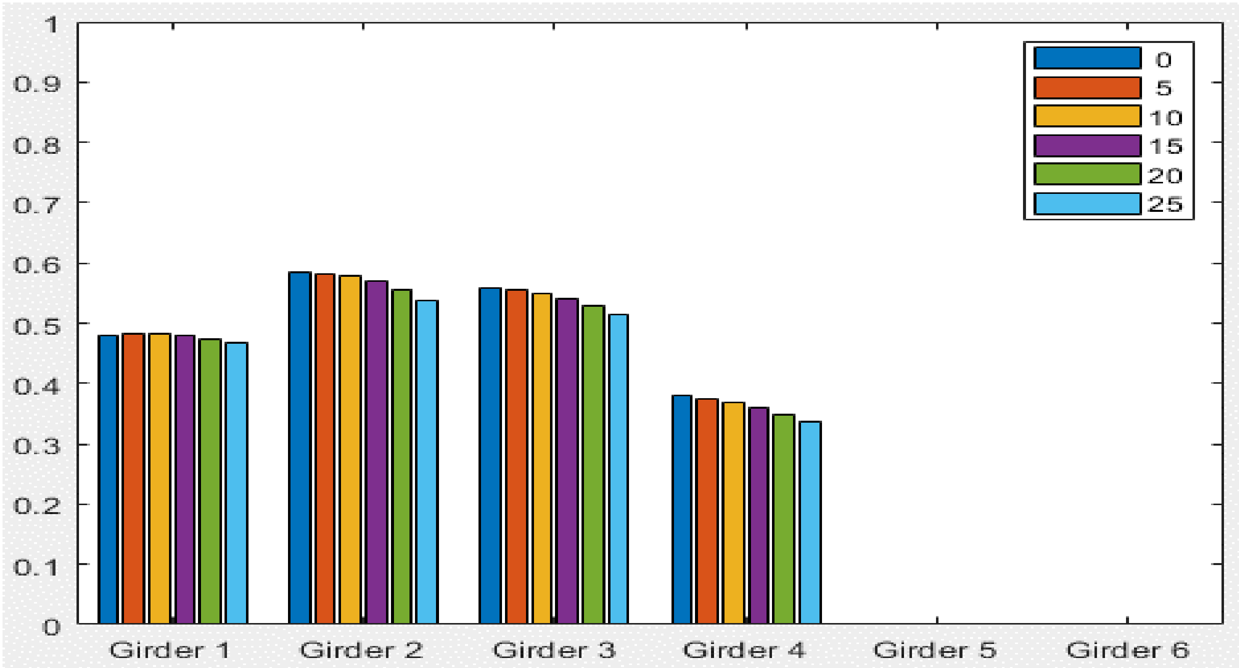

Typical Bridge #2, Tarhini/Frederick Methodology, IG 2LL, Variable = Degree of Skew (deg)

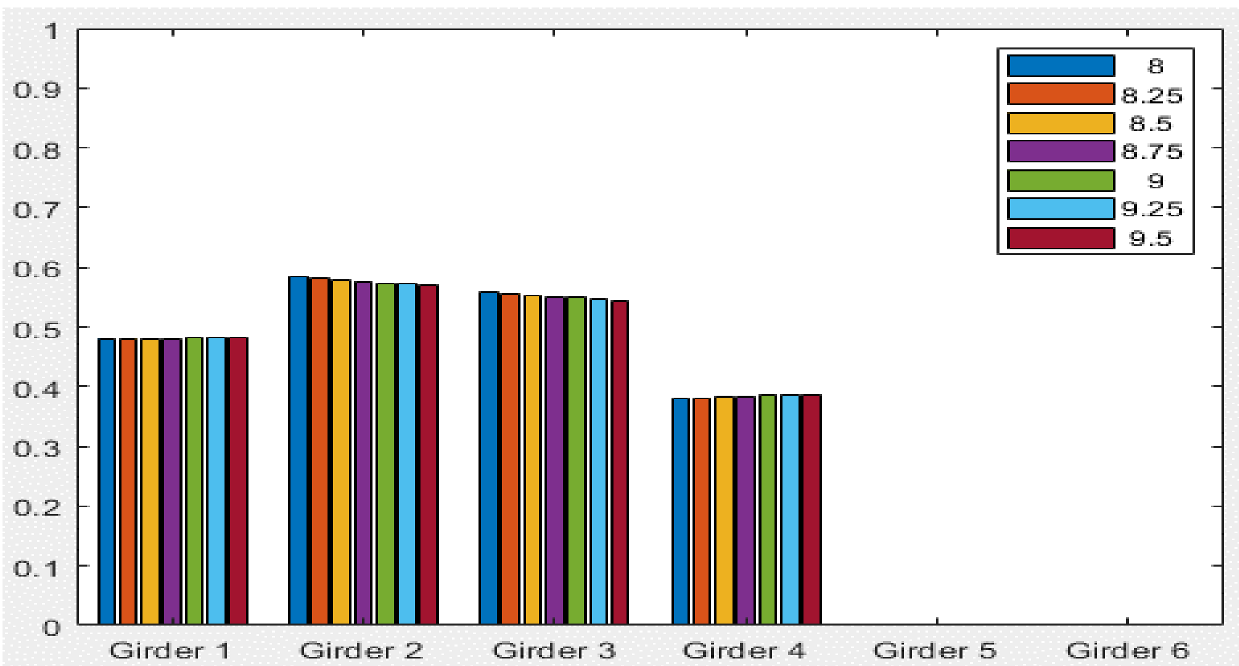

Typical Bridge #2, Tarhini/Frederick Methodology, IG 2LL, Variable = Deck Thickness (in)

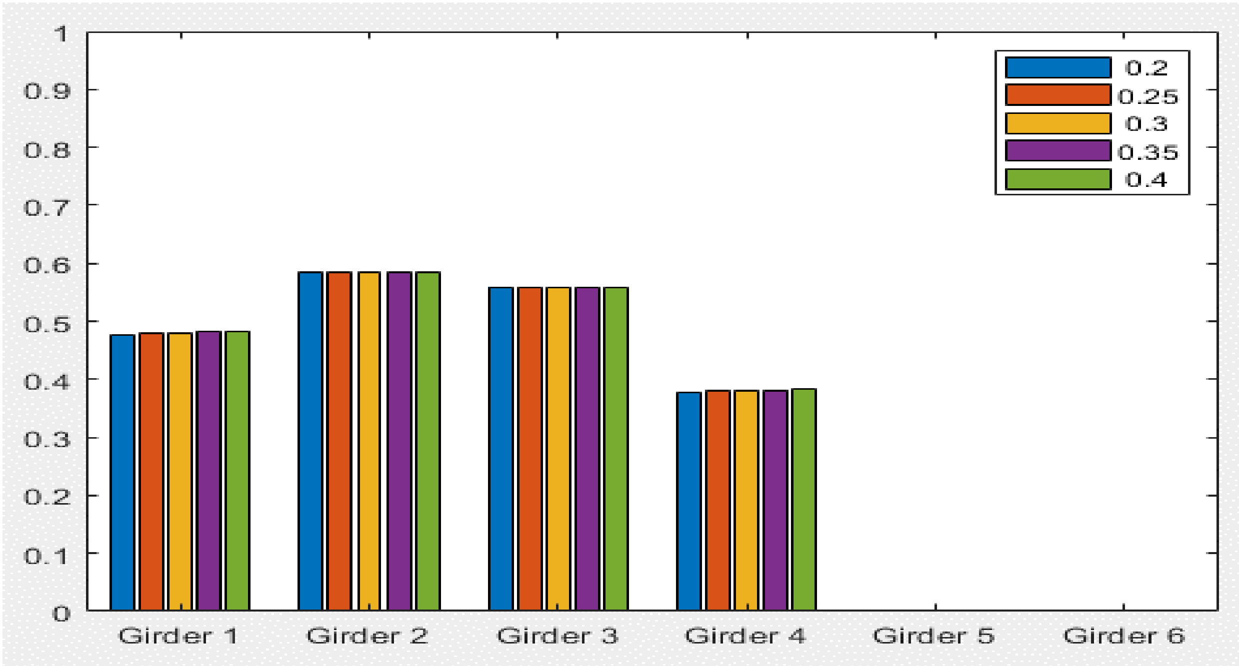

Typical Bridge #2, Tarhini/Frederick Methodology, IG 2LL, Variable = Overhang Ratio

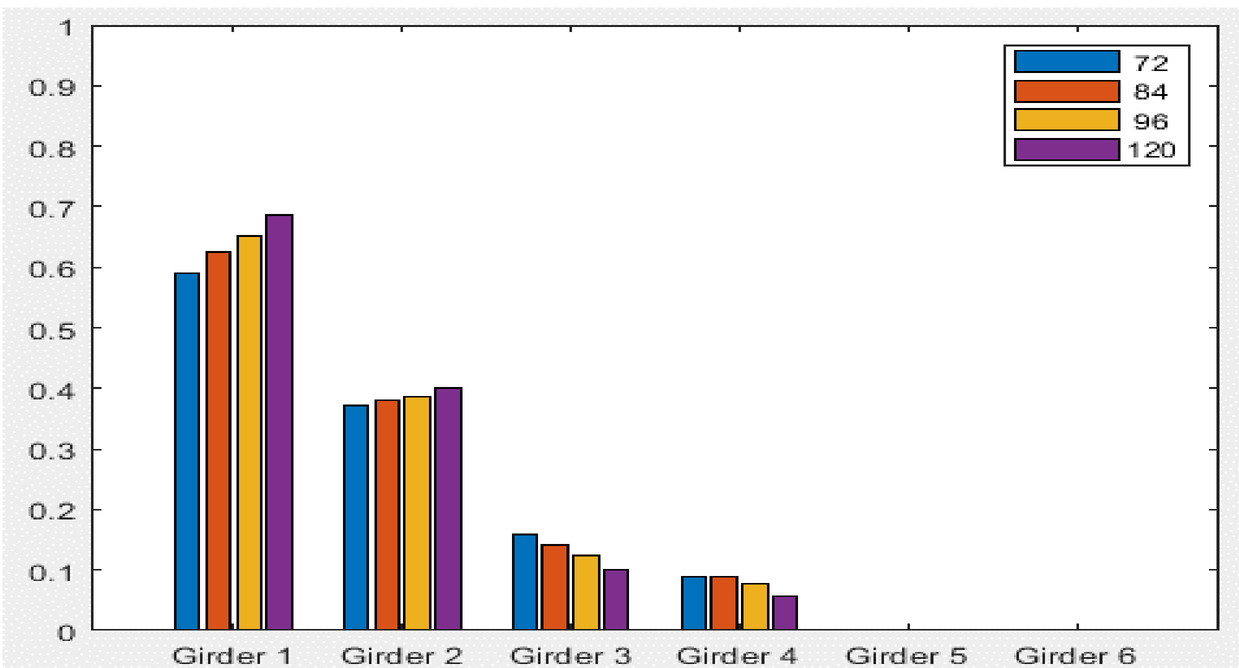

Typical Bridge #2, Tarhini/Frederick Methodology, EG OLL, Variable = PBFTG Size

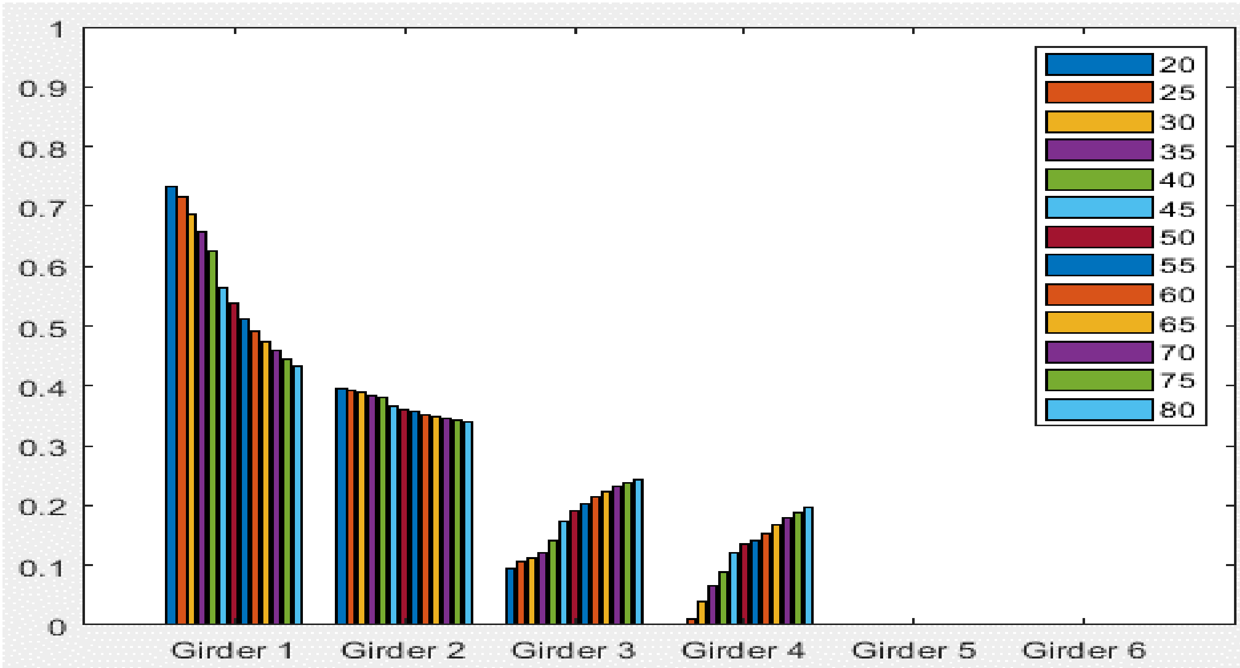

Typical Bridge #2, Tarhini/Frederick Methodology, EG OLL, Variable = Span Length (ft)

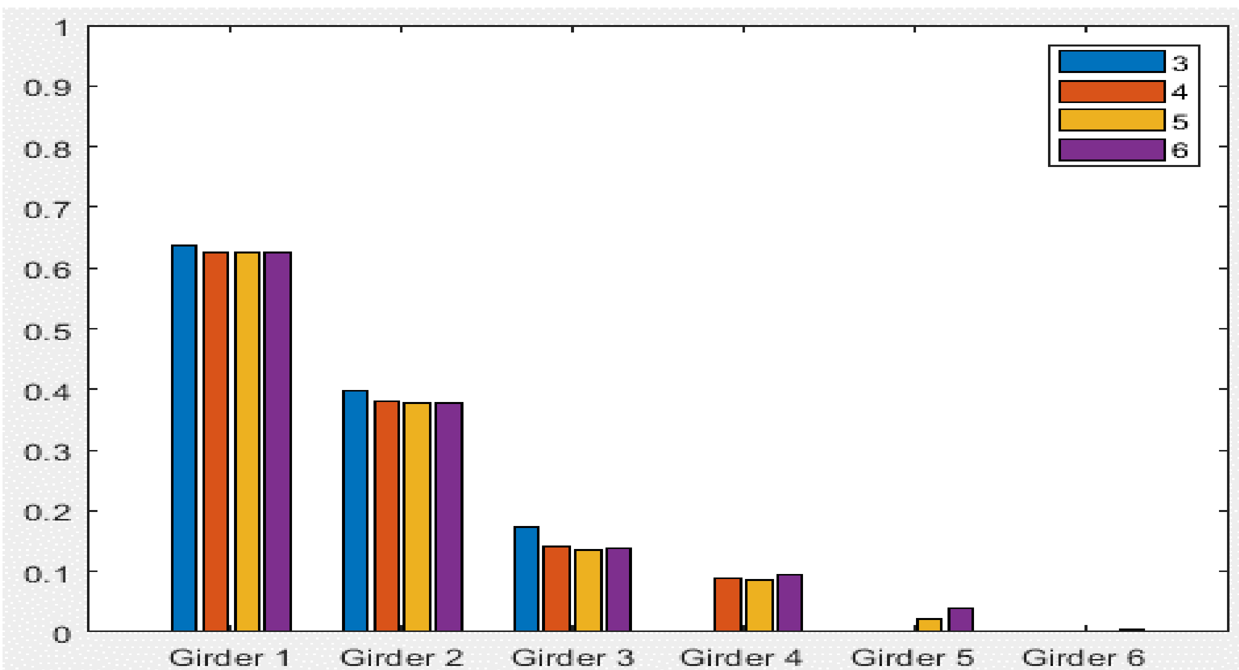

Typical Bridge #2, Tarhini/Frederick Methodology, EG OLL, Variable = Number of Girders

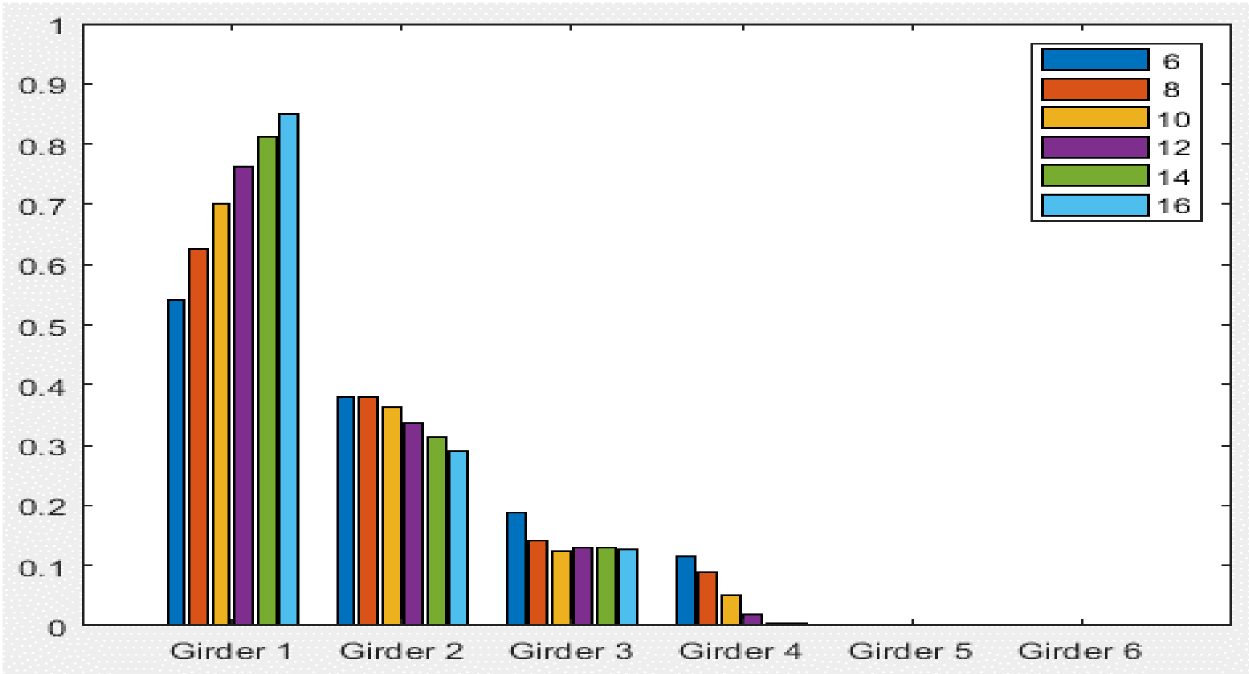

Typical Bridge #2, Tarhini/Frederick Methodology, EG OLL, Variable = Girder Spacing (ft)

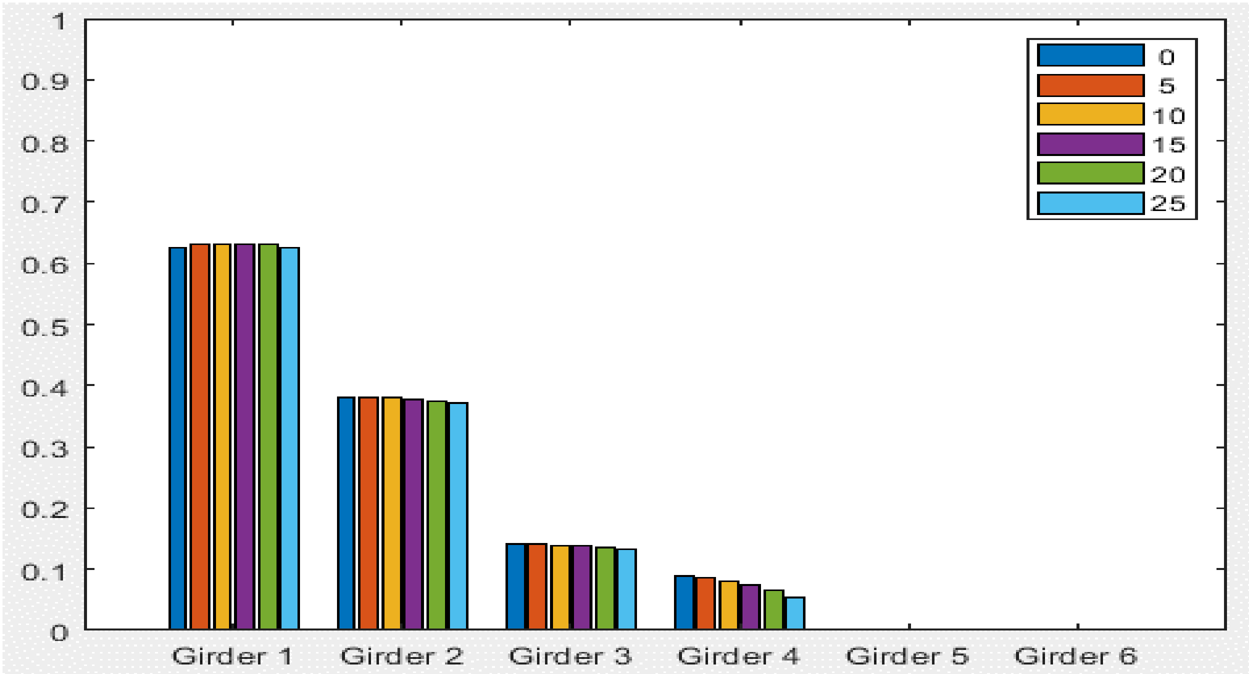

Typical Bridge #2, Tarhini/Frederick Methodology, EG OLL, Variable = Degree of Skew (deg)

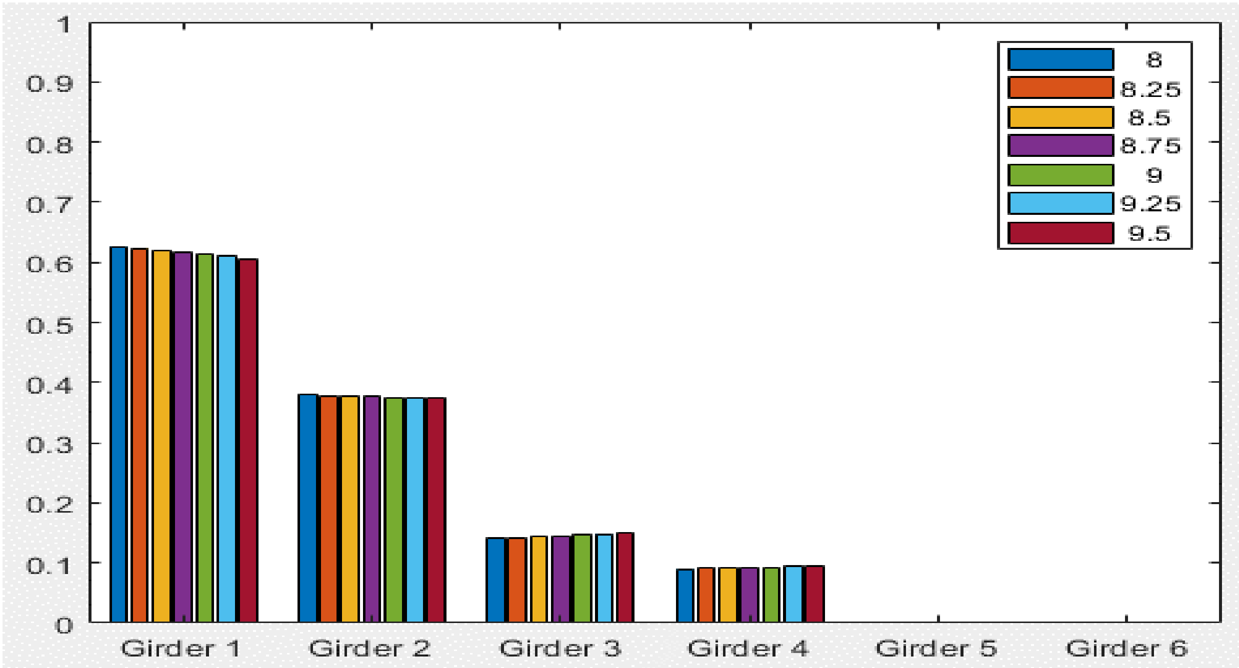

Typical Bridge #2, Tarhini/Frederick Methodology, EG OLL, Variable = Deck Thickness (in)

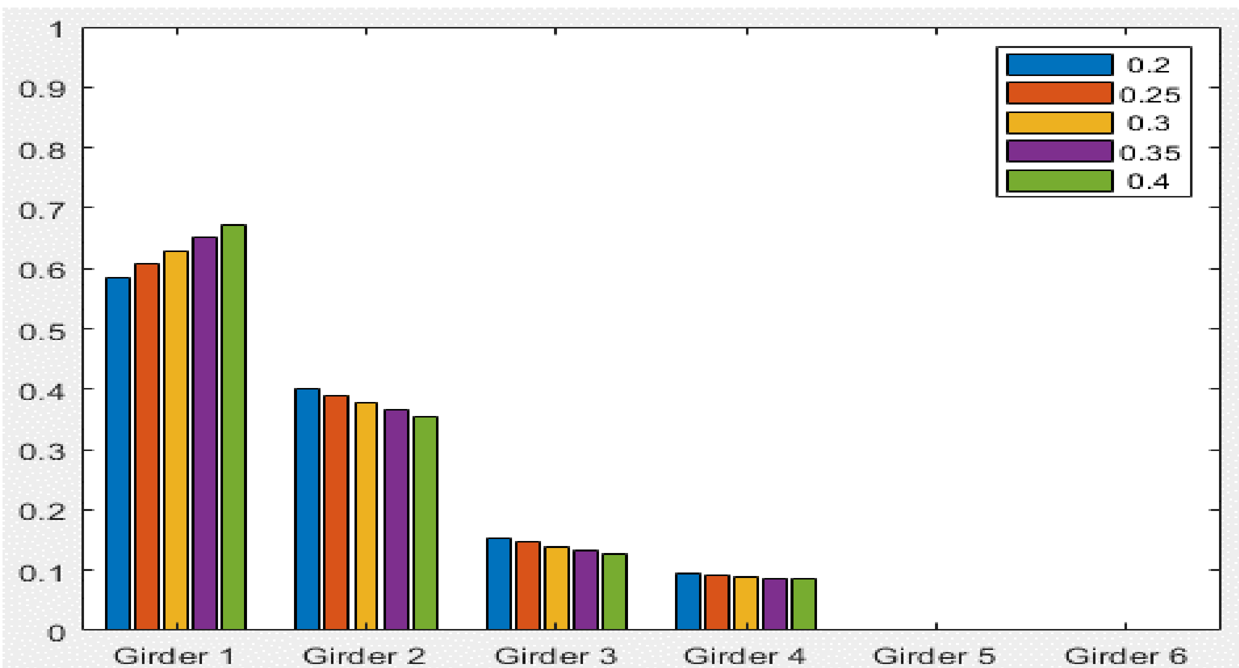

Typical Bridge #2, Tarhini/Frederick Methodology, EG OLL, Variable = Overhang Ratio

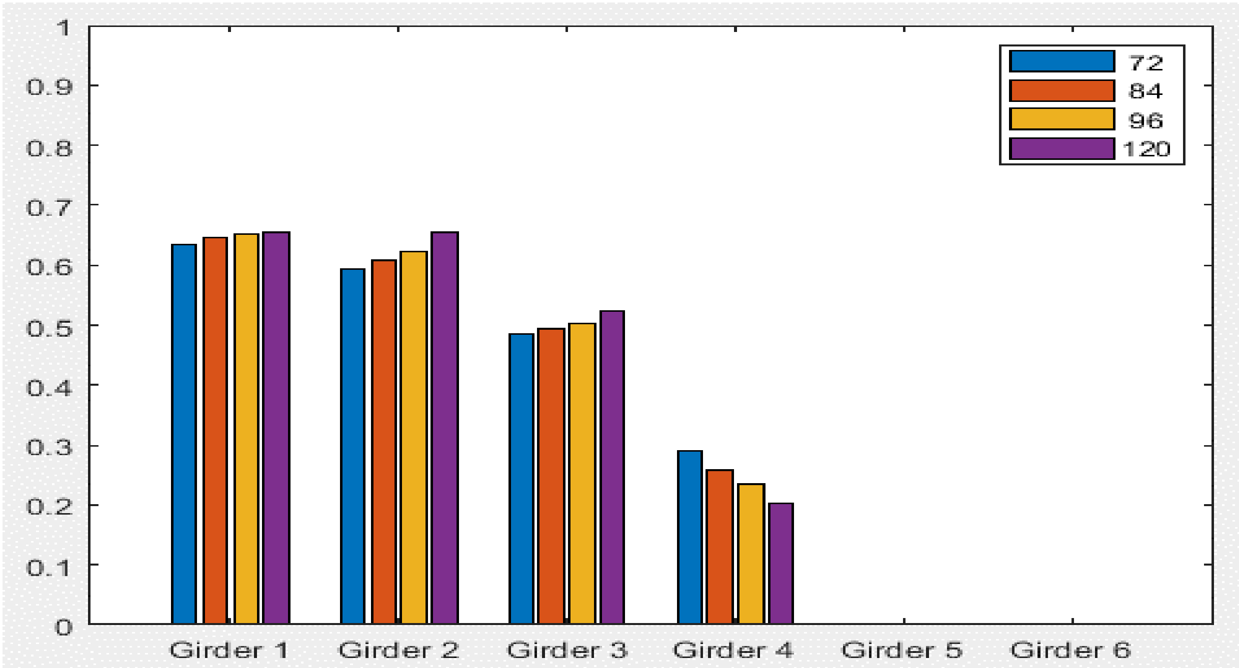

Typical Bridge #2, Tarhini/Frederick Methodology, EG 2LL, Variable = PBFTG Size

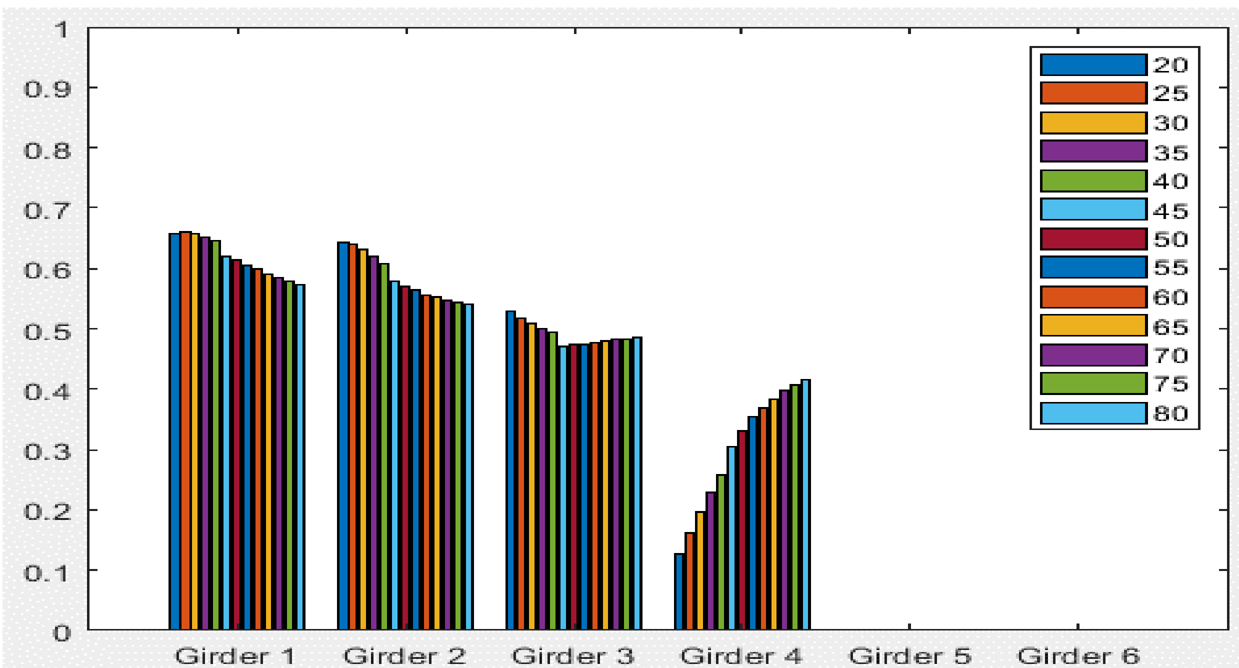

Typical Bridge #2, Tarhini/Frederick Methodology, EG 2LL, Variable = Span Length (ft)

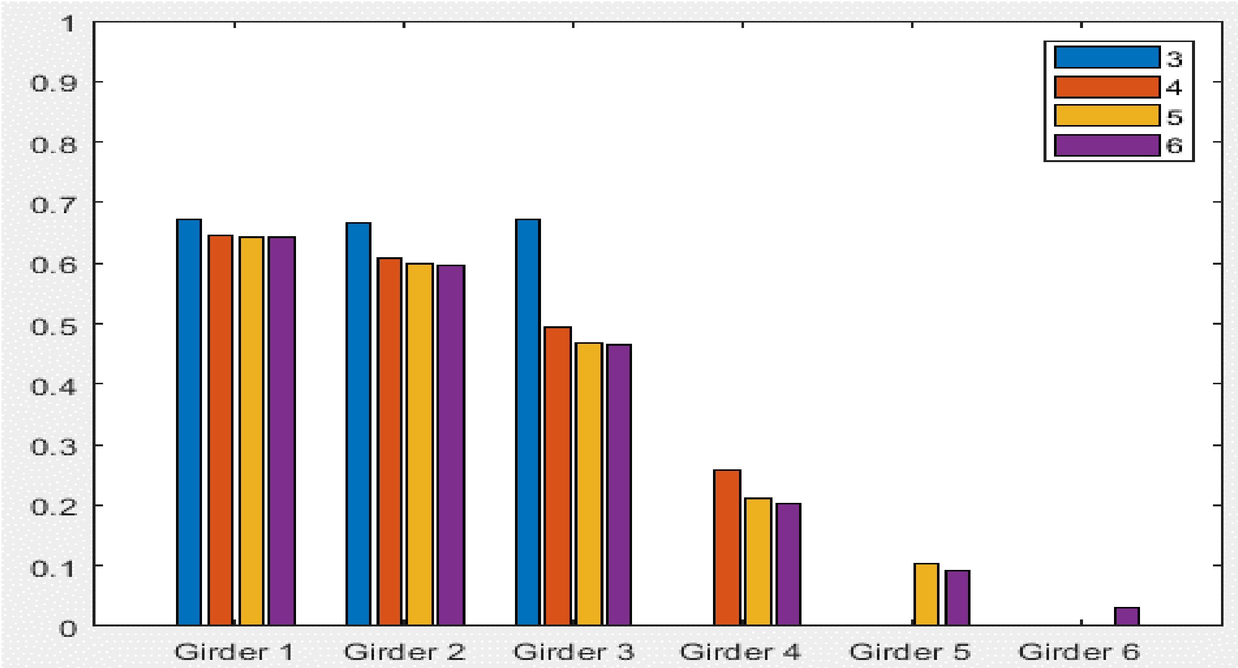

Typical Bridge #2, Tarhini/Frederick Methodology, EG 2LL, Variable = Number of Girders

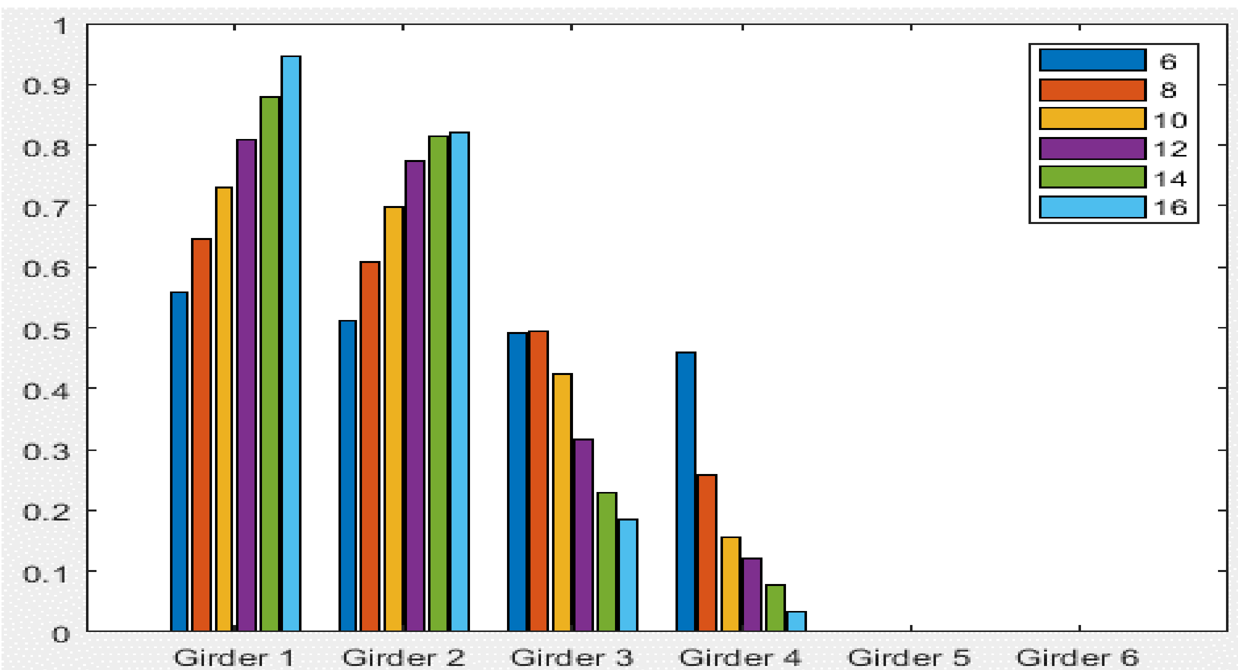

Typical Bridge #2, Tarhini/Frederick Methodology, EG 2LL, Variable = Girder Spacing (ft)

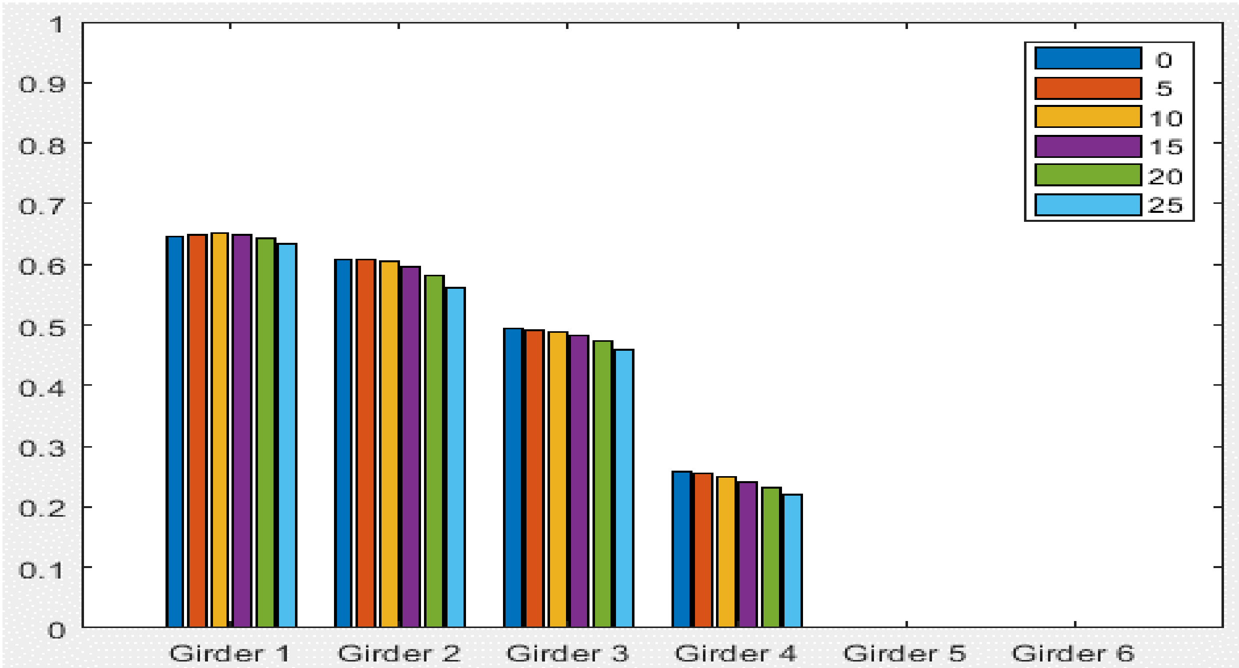

Typical Bridge #2, Tarhini/Frederick Methodology, EG 2LL, Variable = Degree of Skew (deg)

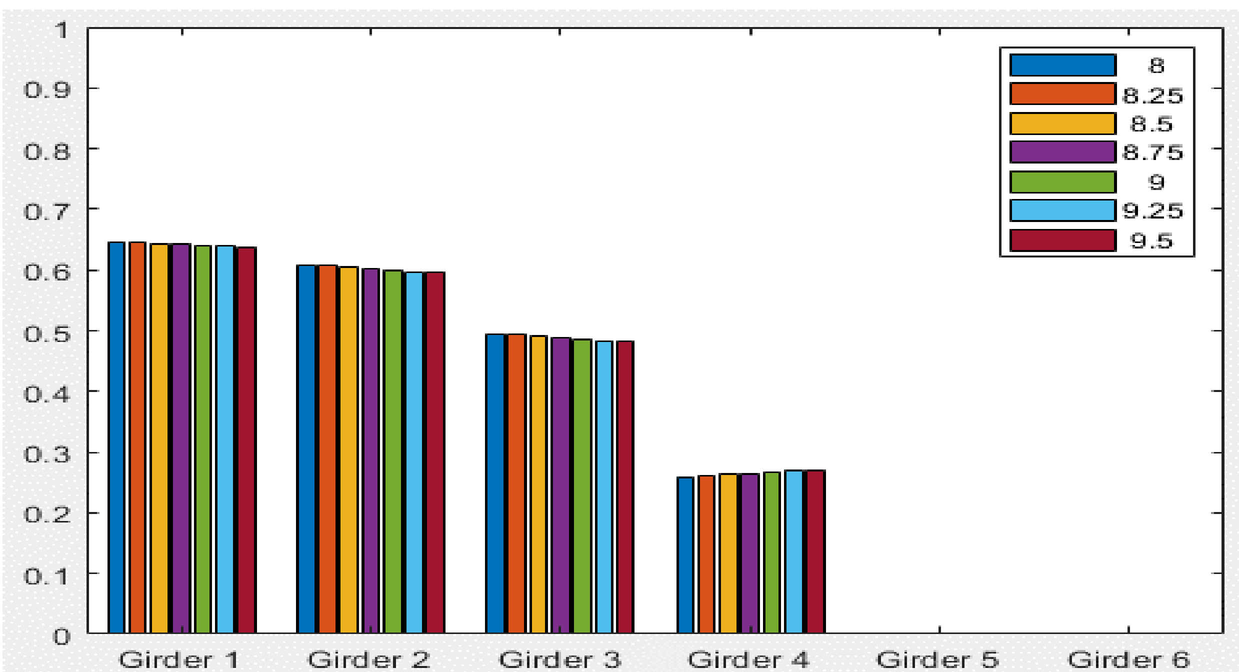

Typical Bridge #2, Tarhini/Frederick Methodology, EG 2LL, Variable = Deck Thickness (in)

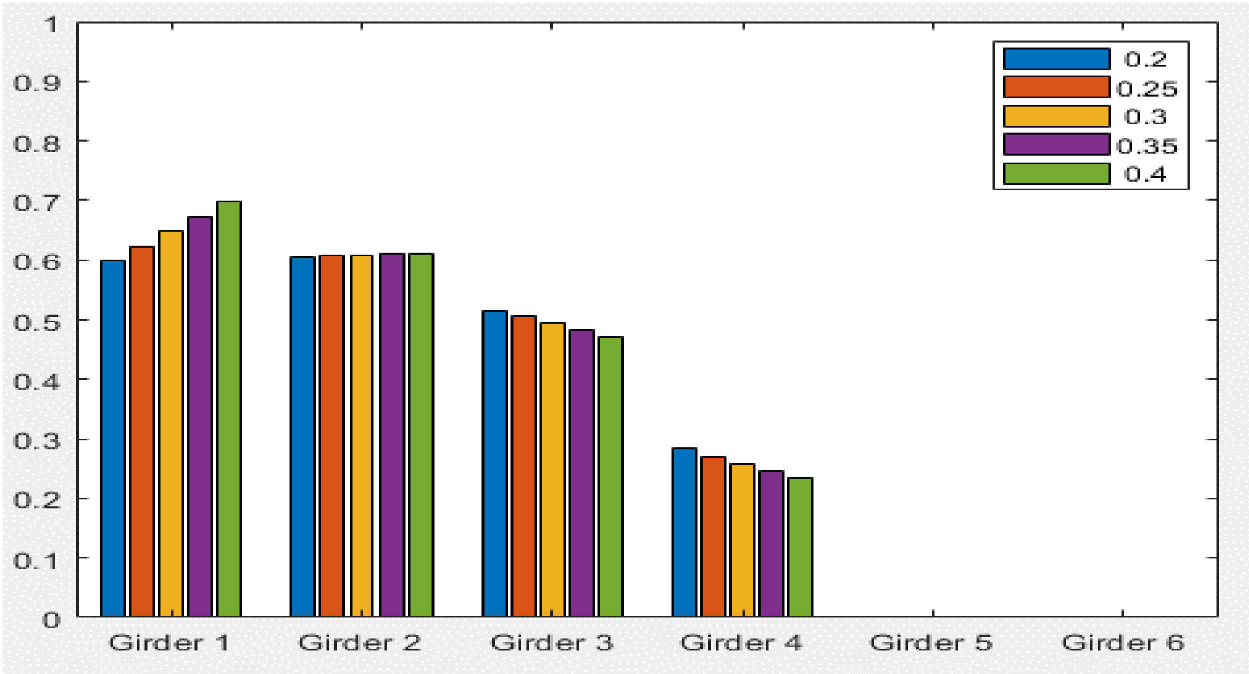

Typical Bridge #2, Tarhini/Frederick Methodology, EG 2LL, Variable = Overhang Ratio

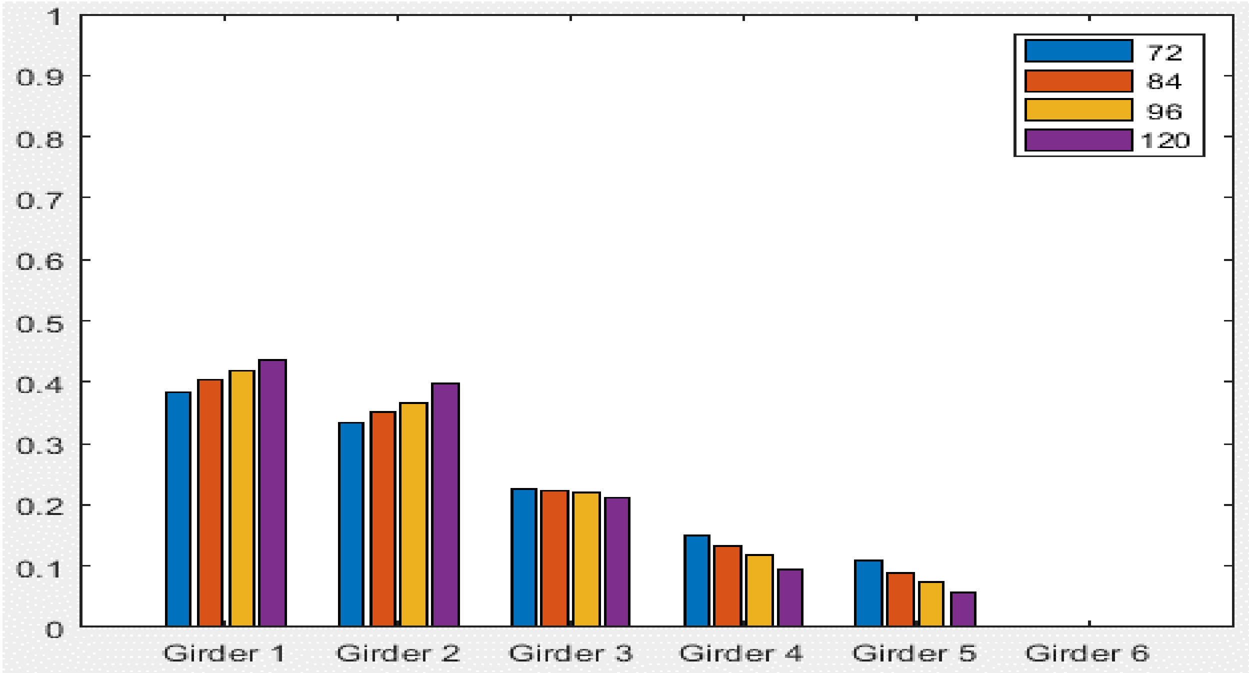

Typical Bridge #3, Stallings/Yoo Methodology, IG OLL, Variable = PBFTG Size

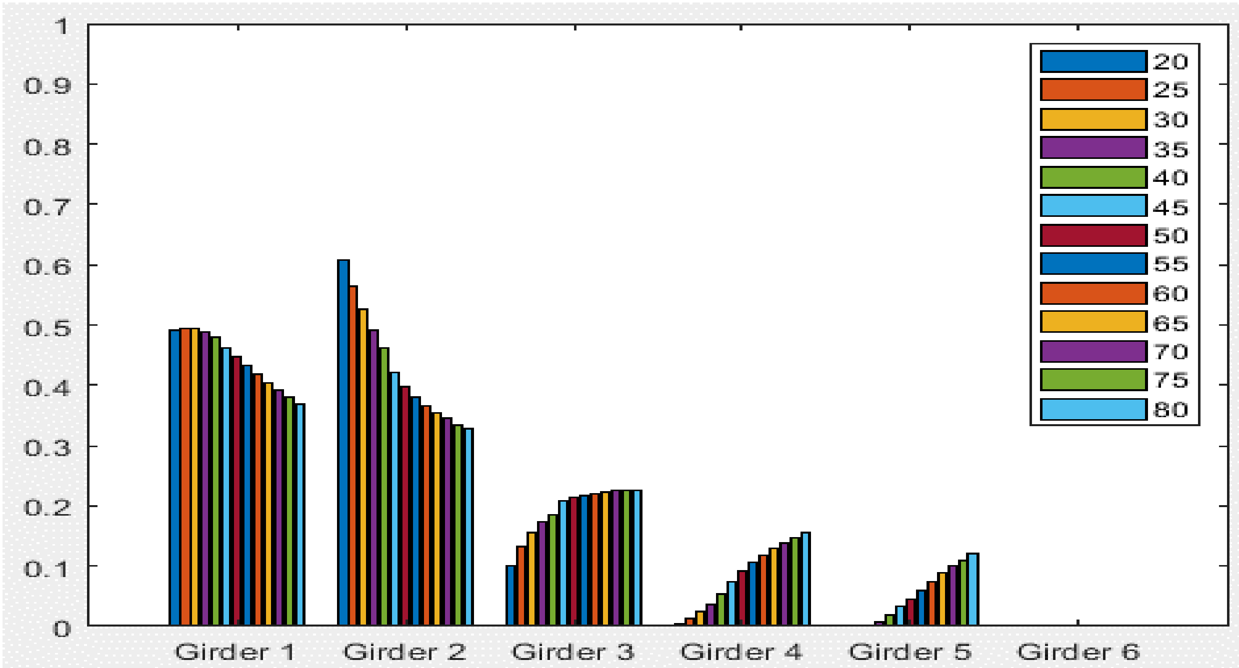

Typical Bridge #3, Stallings/Yoo Methodology, IG OLL, Variable = Span Length (ft)

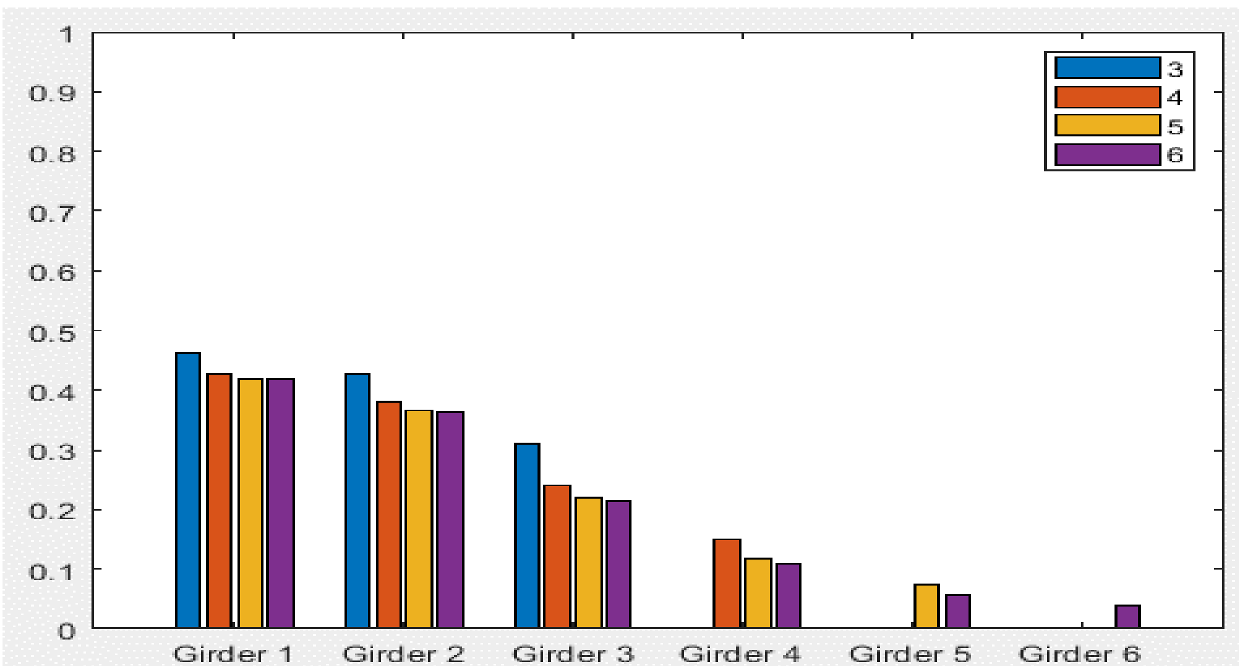

Typical Bridge #3, Stallings/Yoo Methodology, IG OLL, Variable = Number of Girders

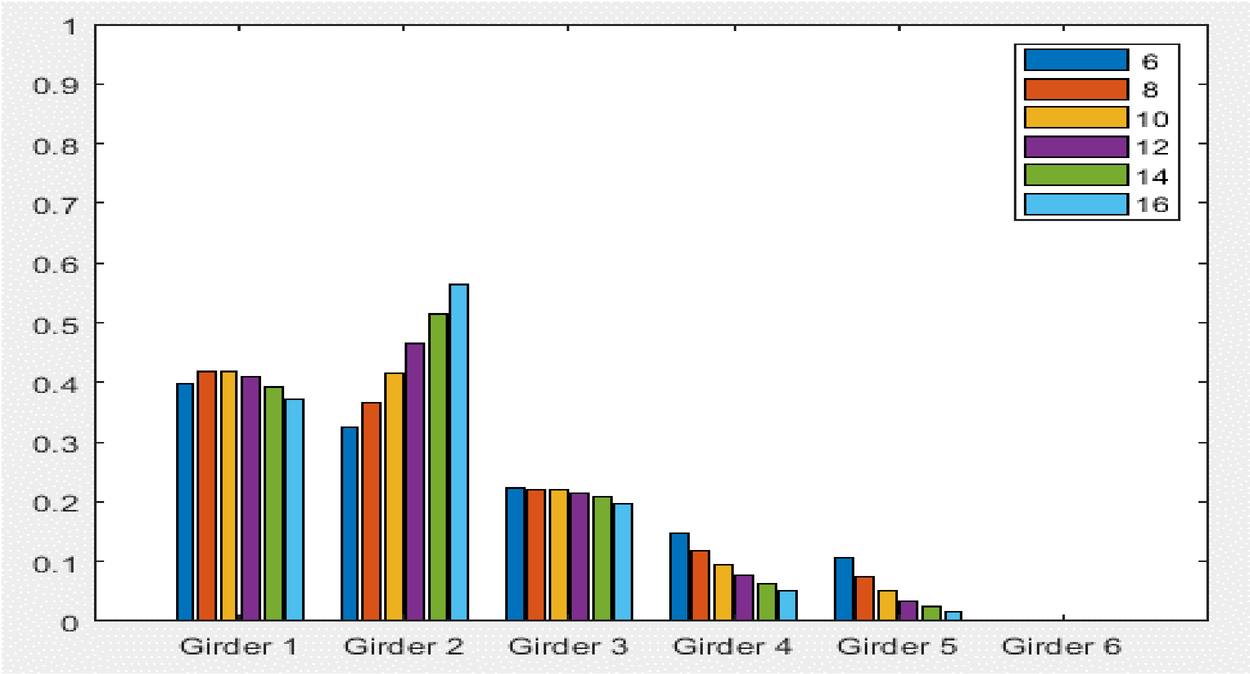

Typical Bridge #3, Stallings/Yoo Methodology, IG OLL, Variable = Girder Spacing (ft)

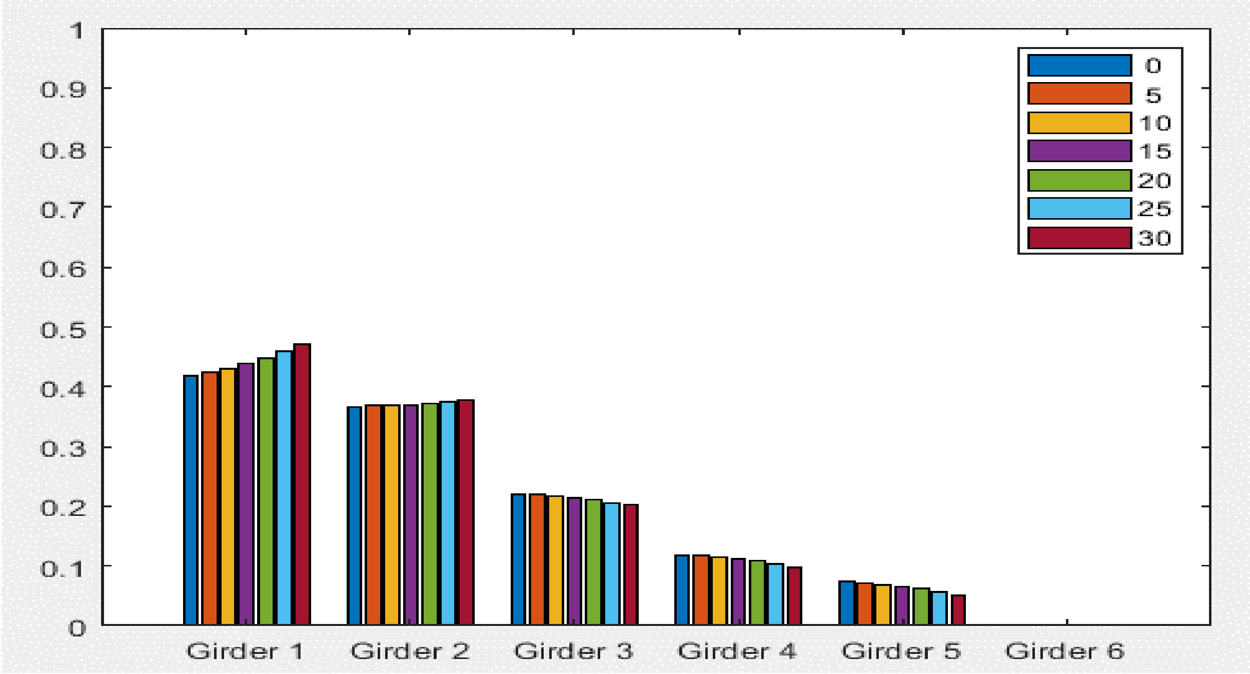

Typical Bridge #3, Stallings/Yoo Methodology, IG OLL, Variable = Degree of Skew (deg)

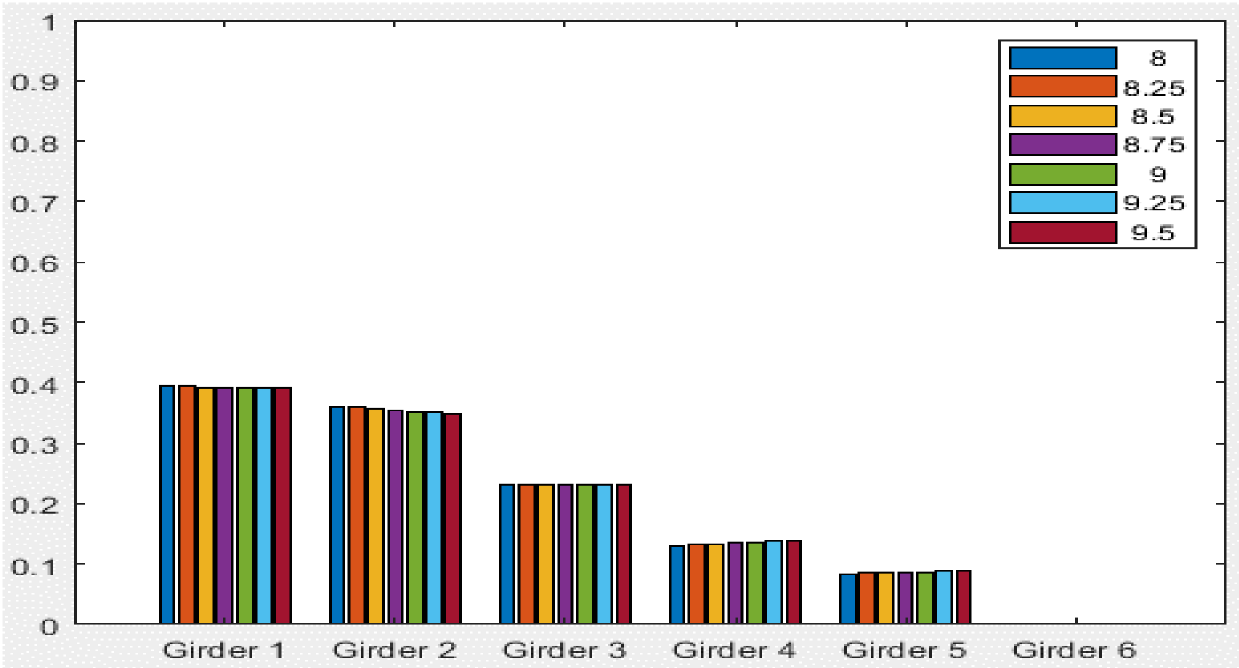

Typical Bridge #3, Stallings/Yoo Methodology, IG OLL, Variable = Deck Thickness (in)

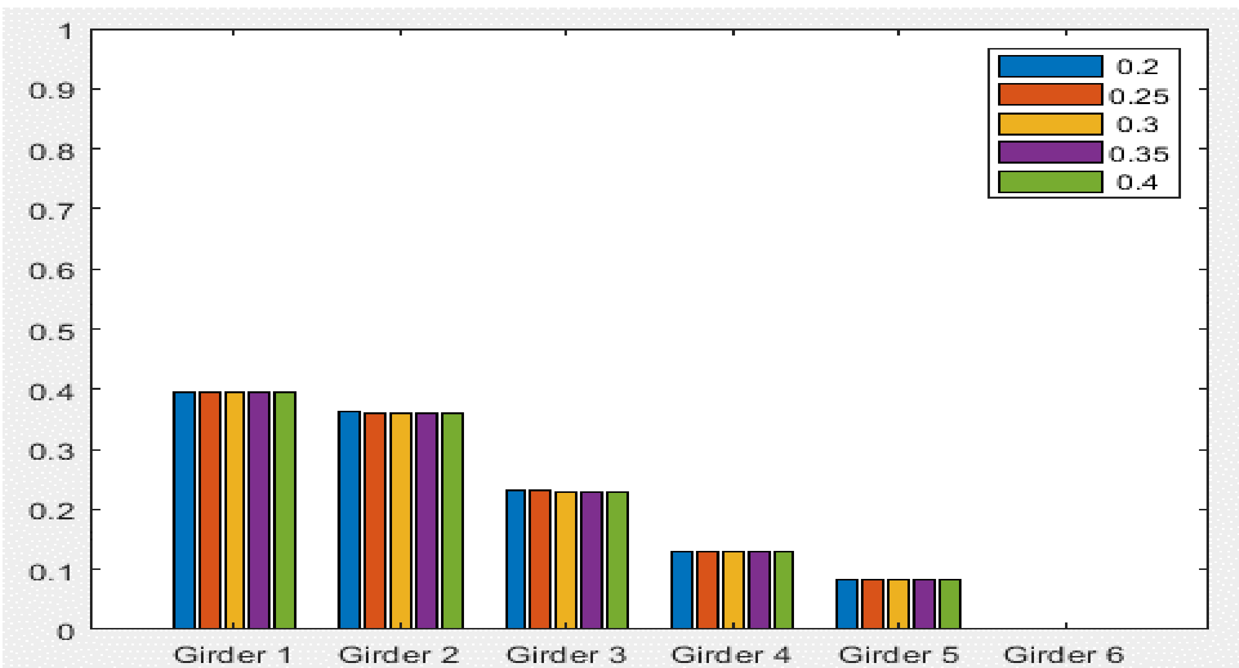

Typical Bridge #3, Stallings/Yoo Methodology, IG OLL, Variable = Overhang Ratio

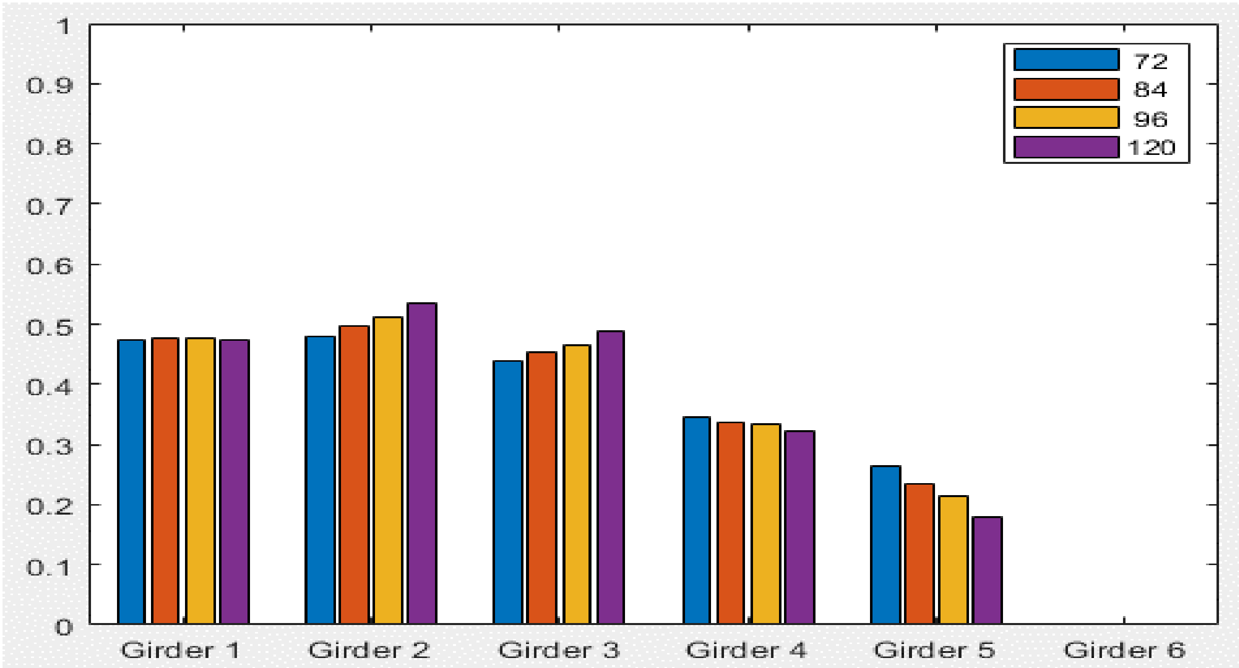

Typical Bridge #3, Stallings/Yoo Methodology, IG 2LL, Variable = PBFTG Size

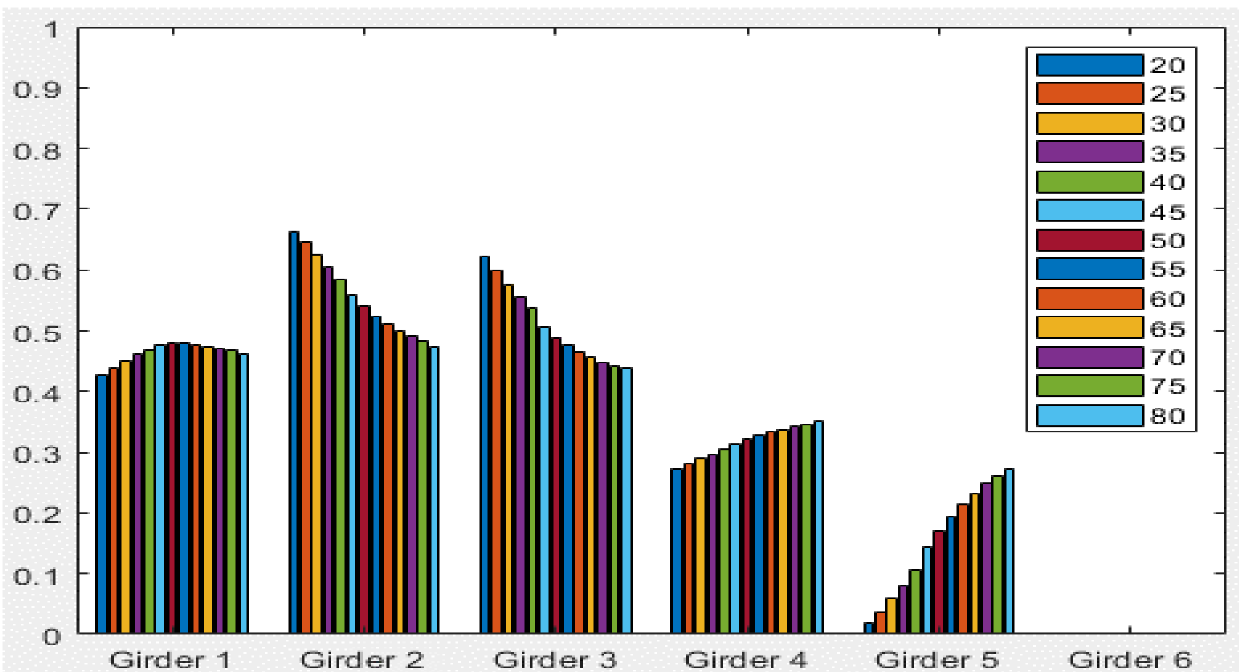

Typical Bridge #3, Stallings/Yoo Methodology, IG 2LL, Variable = Span Length (ft)

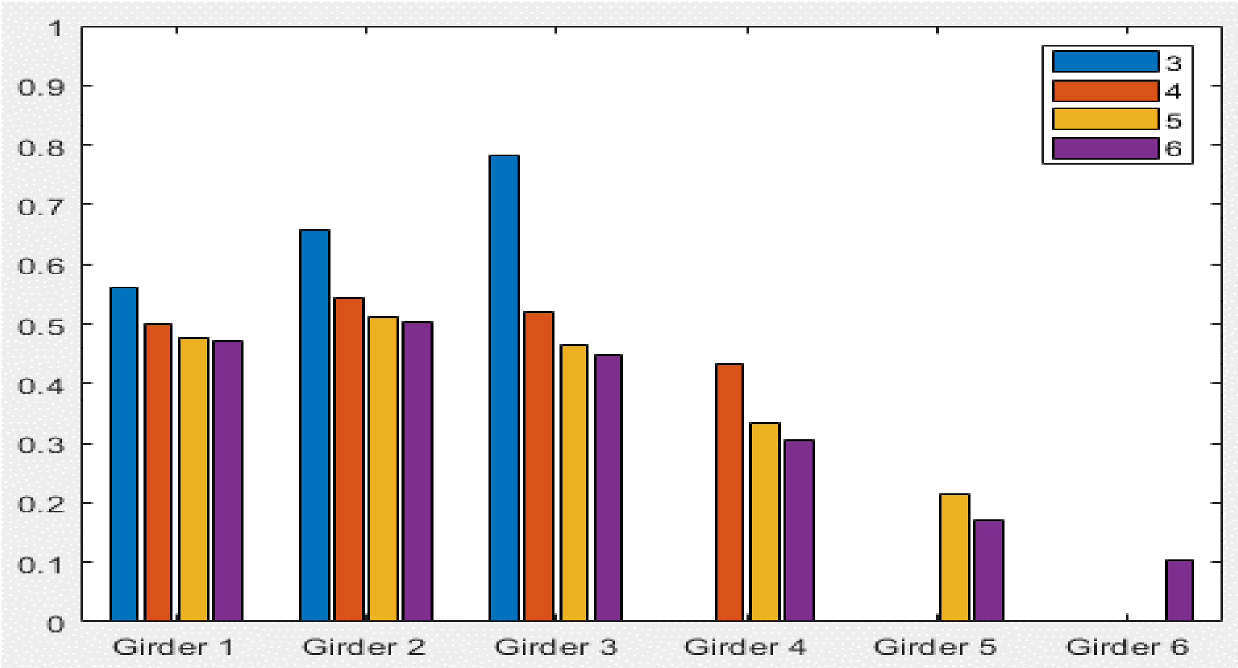

Typical Bridge #3, Stallings/Yoo Methodology, IG 2LL, Variable = Number of Girders

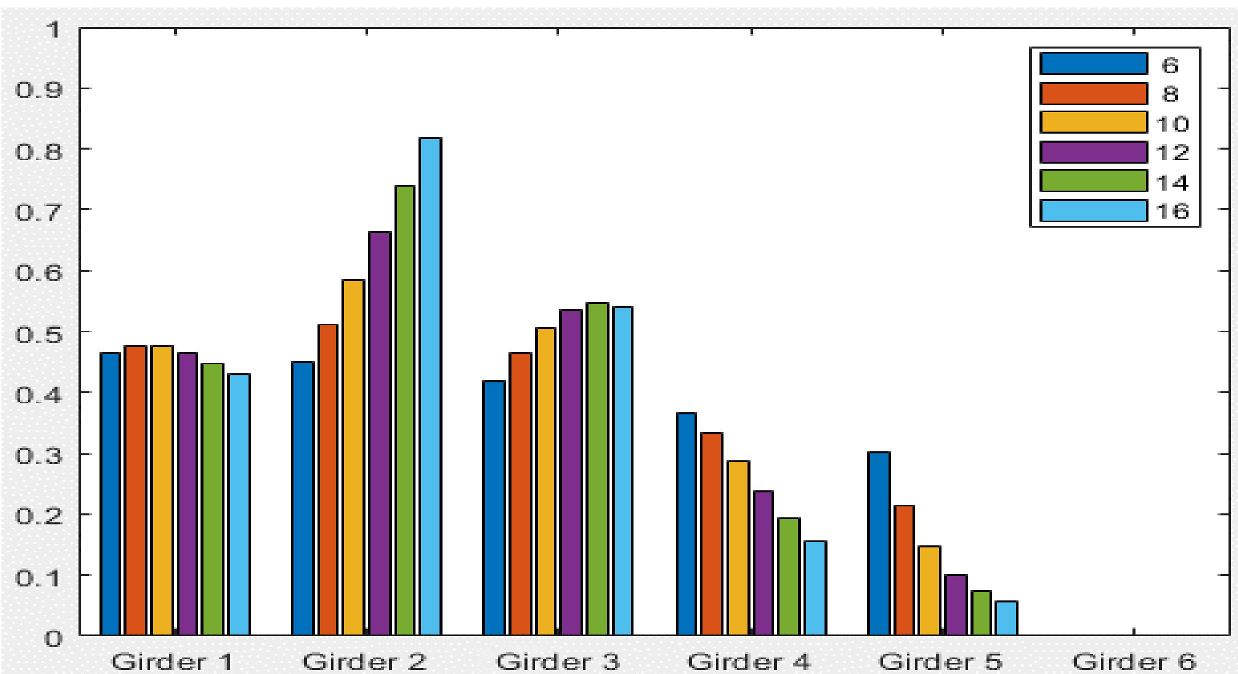

Typical Bridge #3, Stallings/Yoo Methodology, IG 2LL, Variable = Girder Spacing (ft)

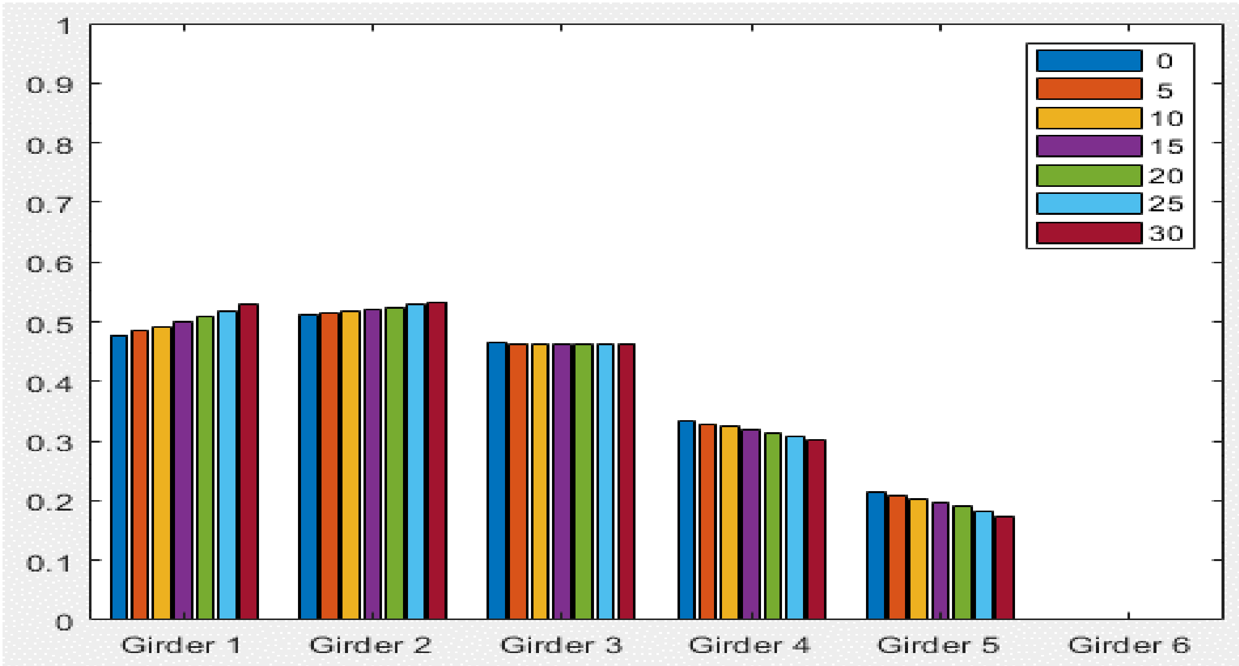

Typical Bridge #3, Stallings/Yoo Methodology, IG 2LL, Variable = Degree of Skew (deg)

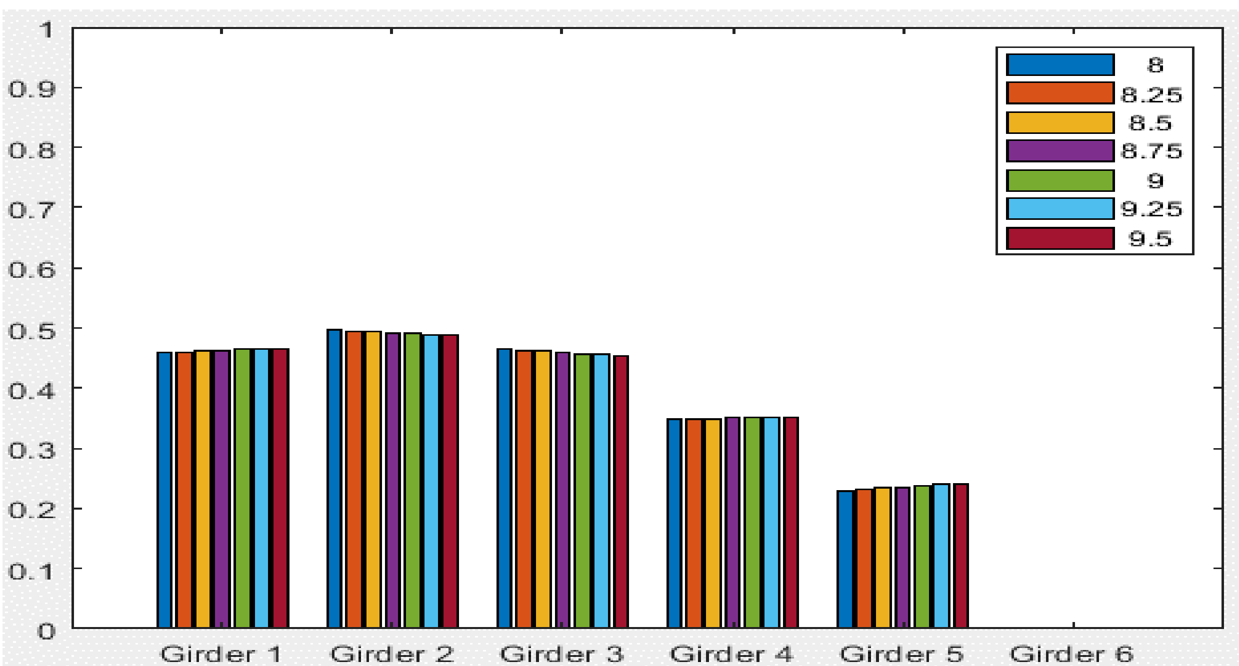

Typical Bridge #3, Stallings/Yoo Methodology, IG 2LL, Variable = Deck Thickness (in)

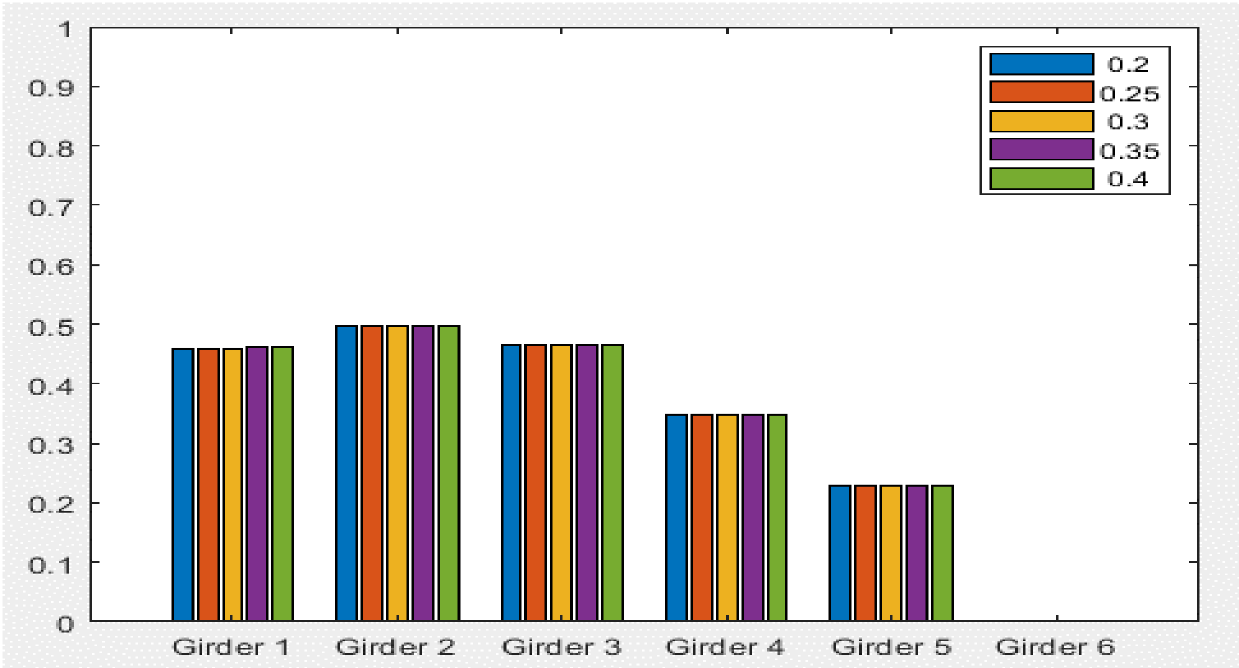

Typical Bridge #3, Stallings/Yoo Methodology, IG 2LL, Variable = Overhang Ratio

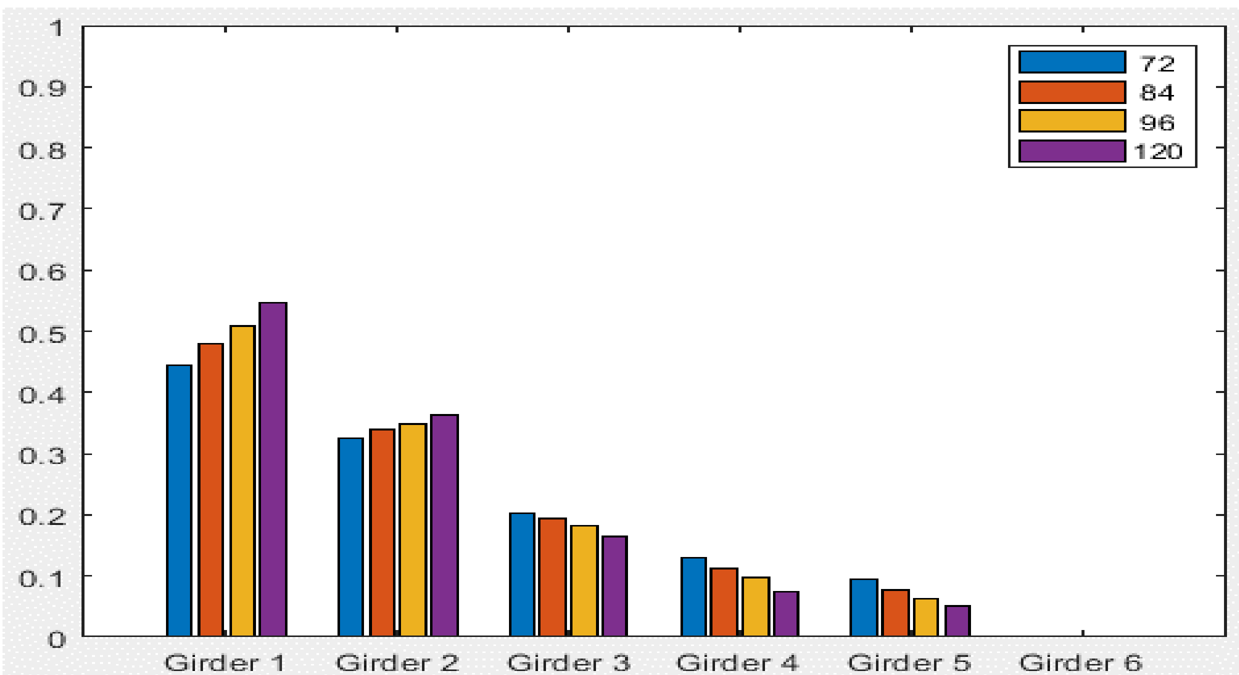

Typical Bridge #3, Stallings/Yoo Methodology, EG OLL, Variable = PBFTG Size

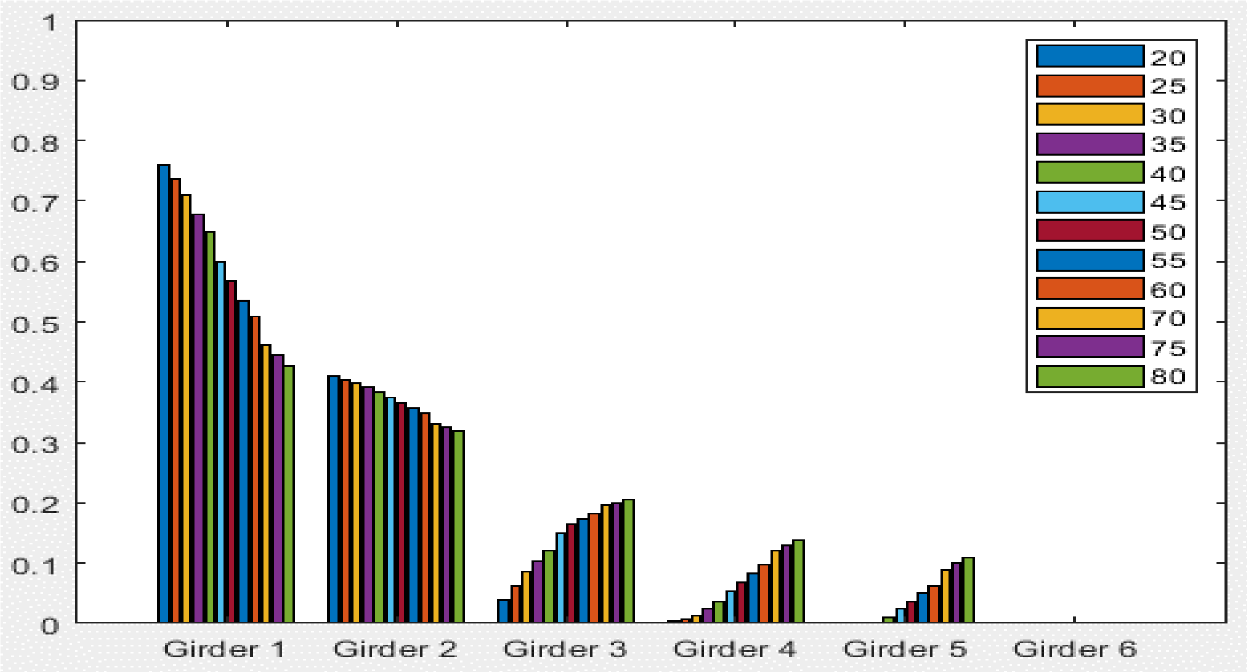

Typical Bridge #3, Stallings/Yoo Methodology, EG OLL, Variable = Span Length (ft)

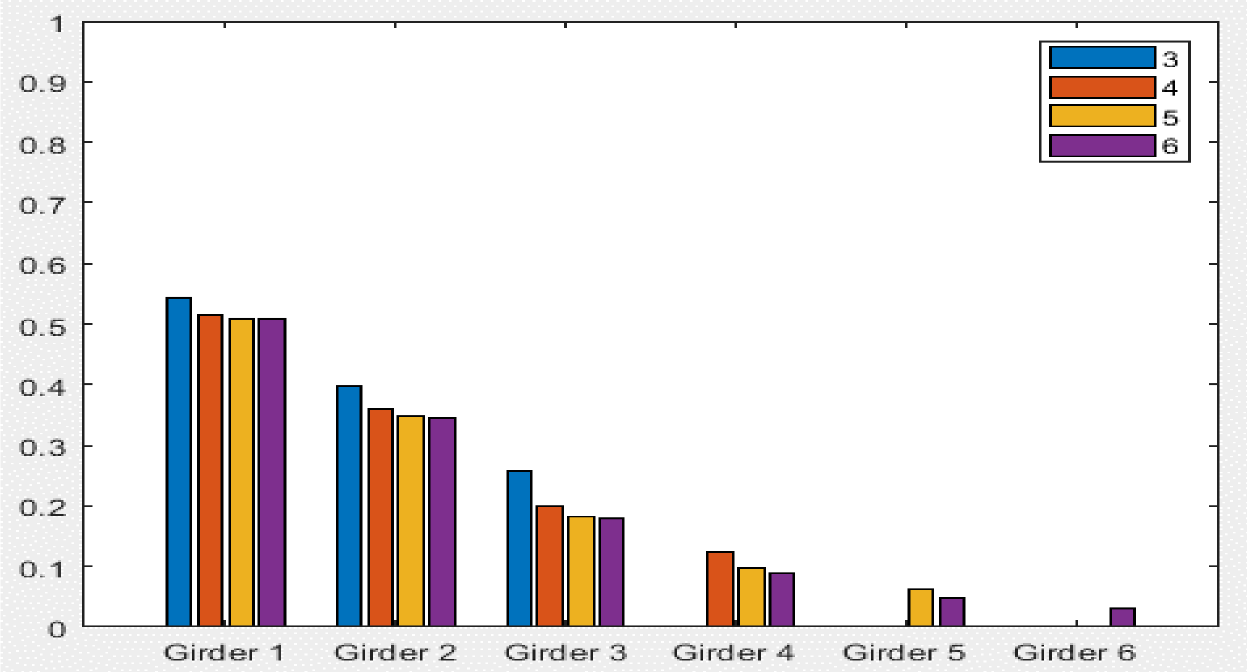

Typical Bridge #3, Stallings/Yoo Methodology, EG OLL, Variable = Number of Girders

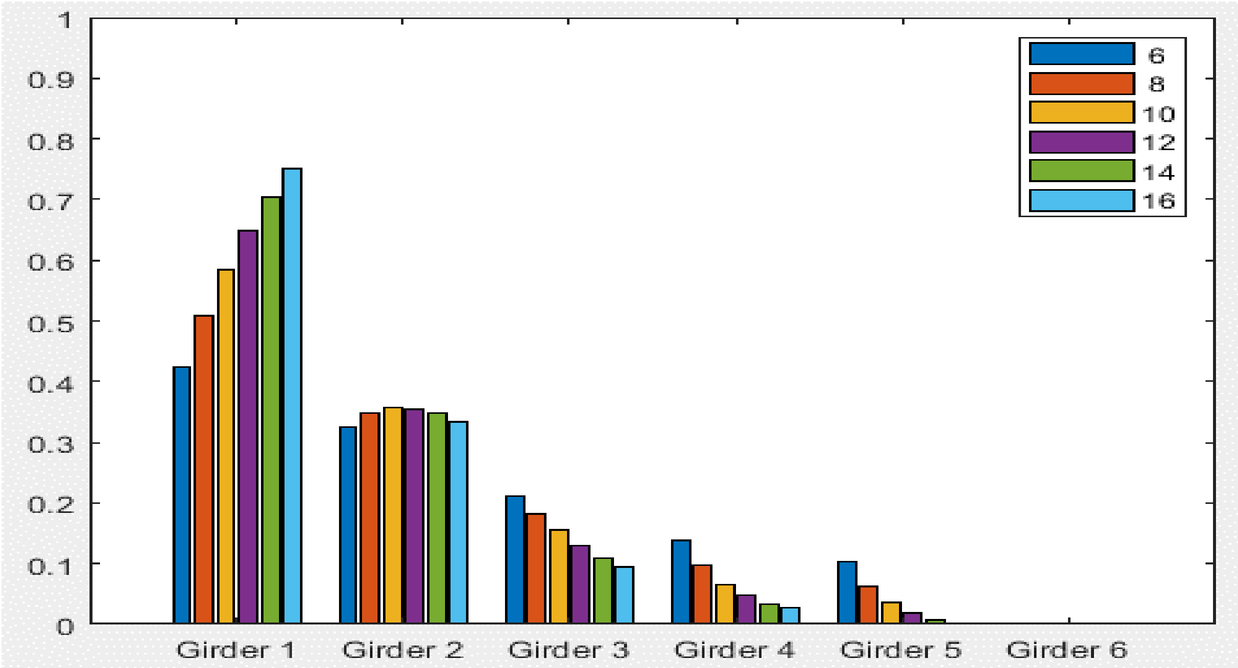

Typical Bridge #3, Stallings/Yoo Methodology, EG OLL, Variable = Girder Spacing (ft)

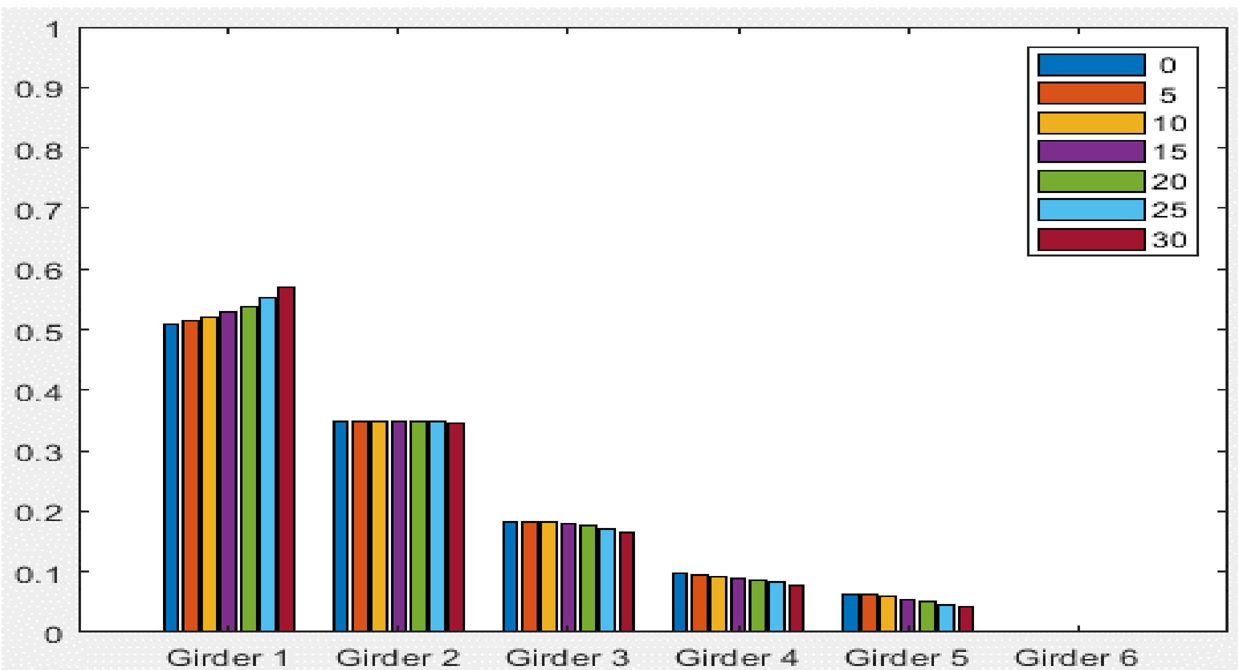

Typical Bridge #3, Stallings/Yoo Methodology, EG OLL, Variable = Degree of Skew (deg)

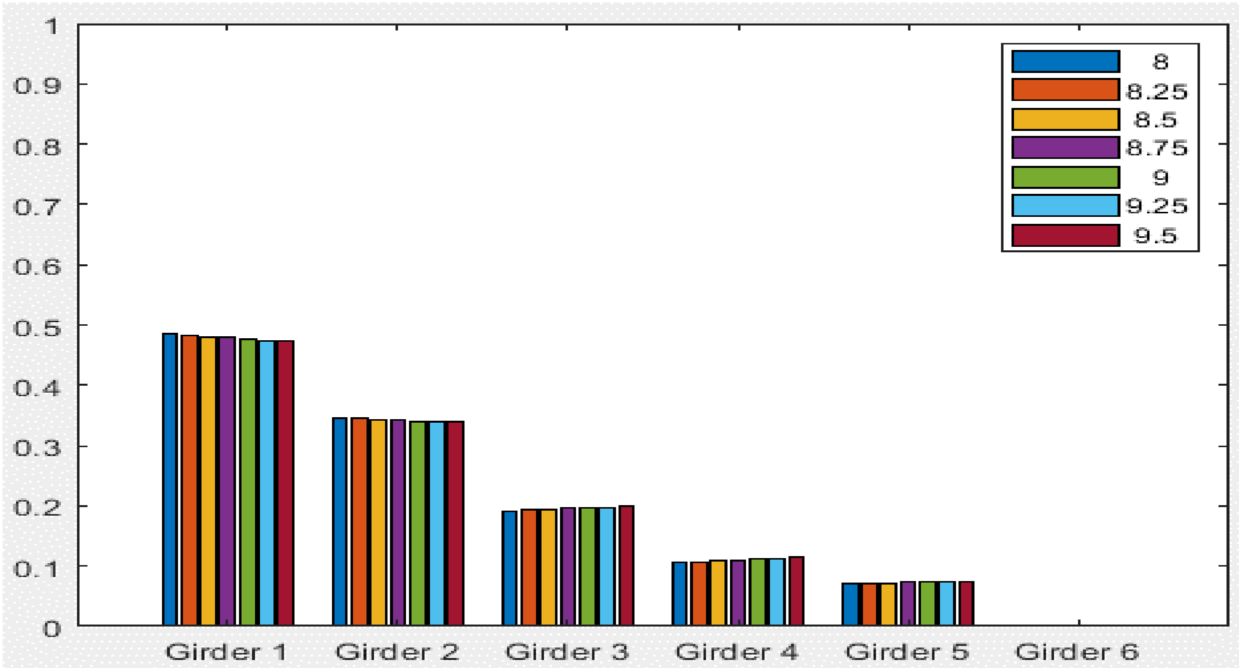

Typical Bridge #3, Stallings/Yoo Methodology, EG OLL, Variable = Deck Thickness (in)

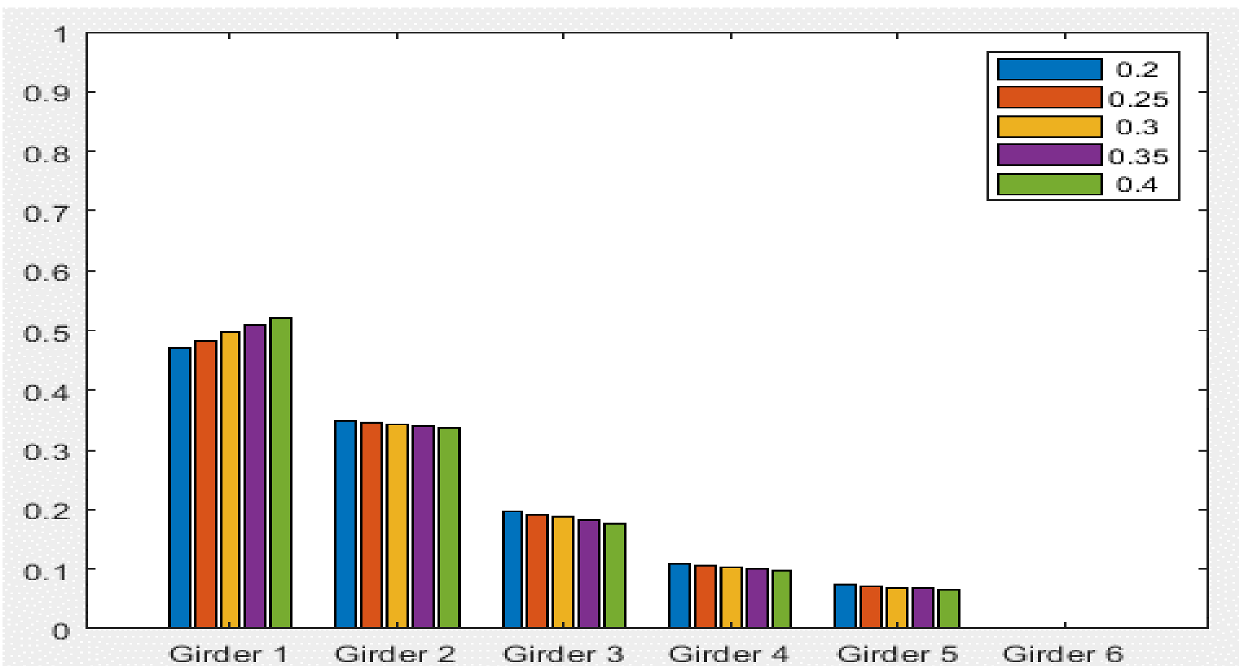

Typical Bridge #3, Stallings/Yoo Methodology, EG OLL, Variable = Overhang Ratio

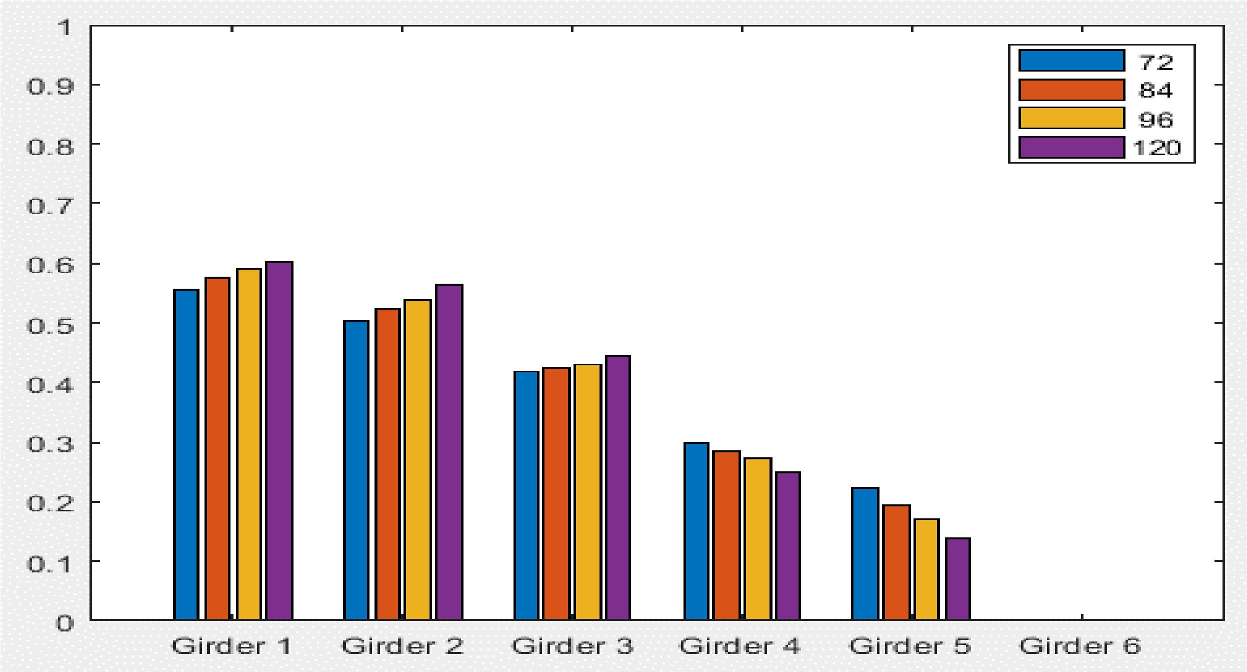

Typical Bridge #3, Stallings/Yoo Methodology, EG 2LL, Variable = PBFTG Size

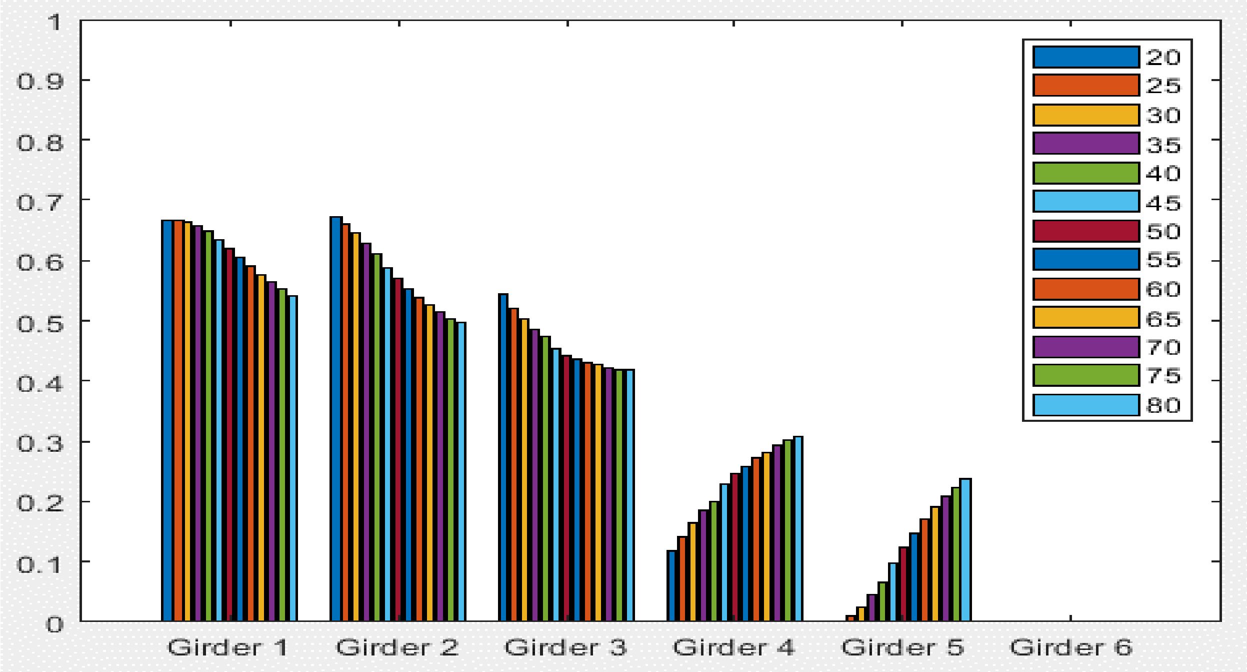

Typical Bridge #3, Stallings/Yoo Methodology, EG 2LL, Variable = Span Length (ft)

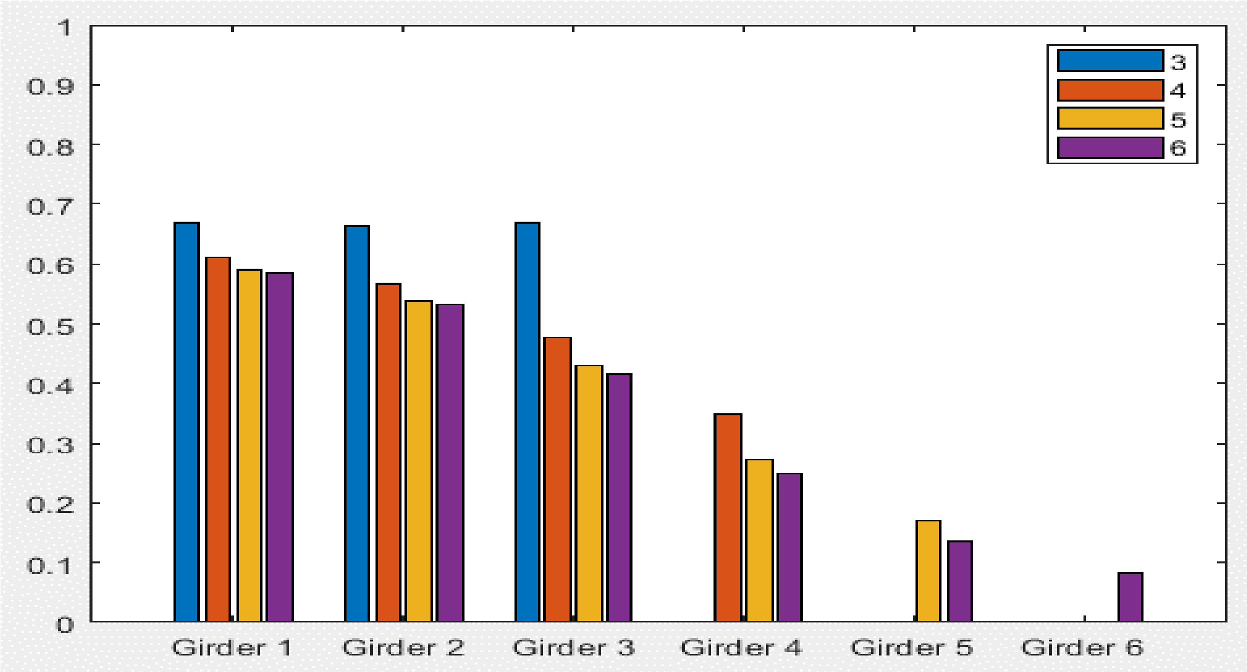

Typical Bridge #3, Stallings/Yoo Methodology, EG 2LL, Variable = Number of Girders

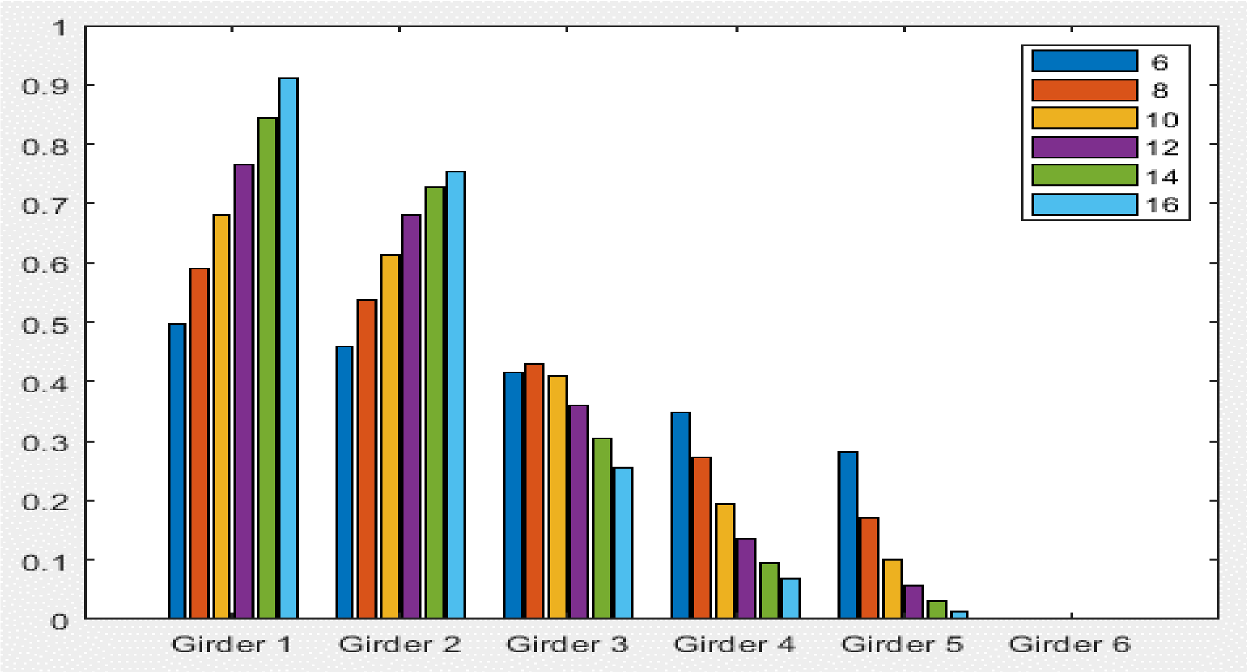

Typical Bridge #3, Stallings/Yoo Methodology, EG 2LL, Variable = Girder Spacing (ft)

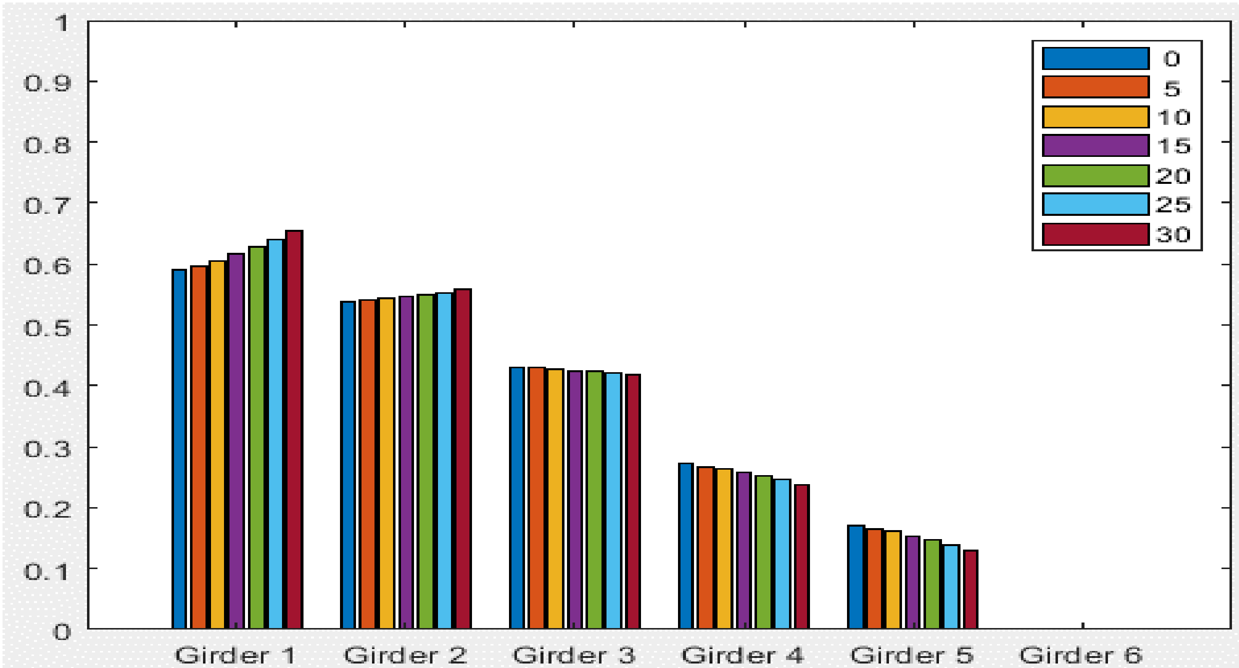

Typical Bridge #3, Stallings/Yoo Methodology, EG 2LL, Variable = Degree of Skew (deg)

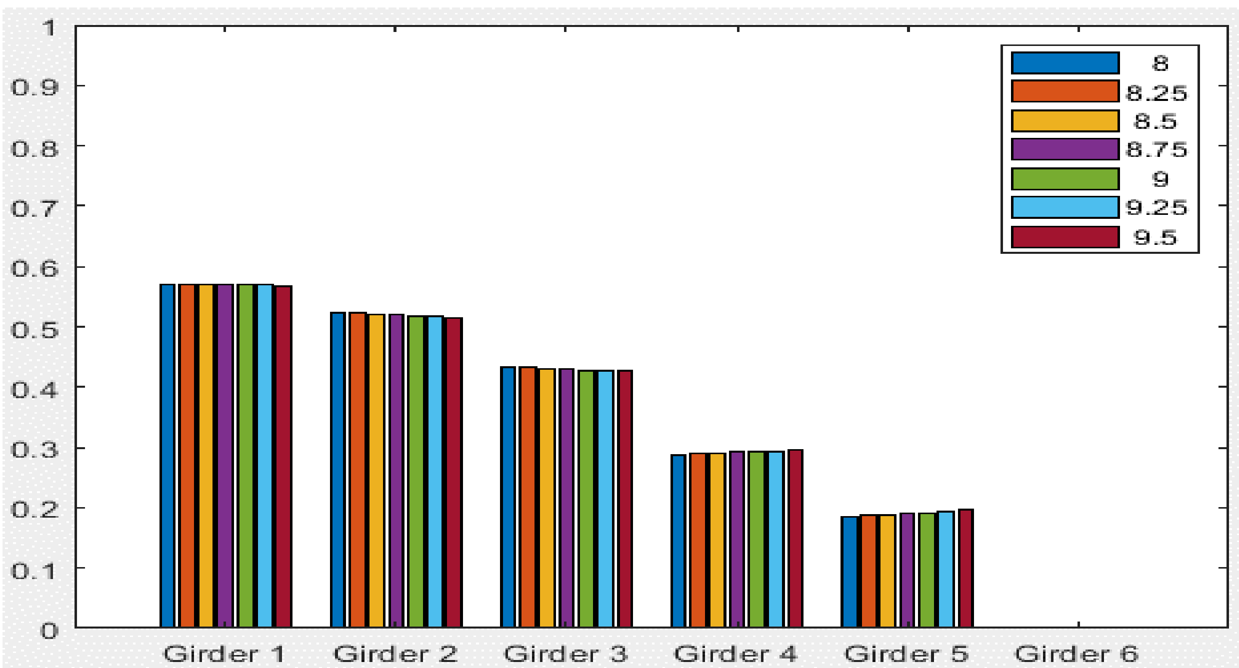

Typical Bridge #3, Stallings/Yoo Methodology, EG 2LL, Variable = Deck Thickness (in)

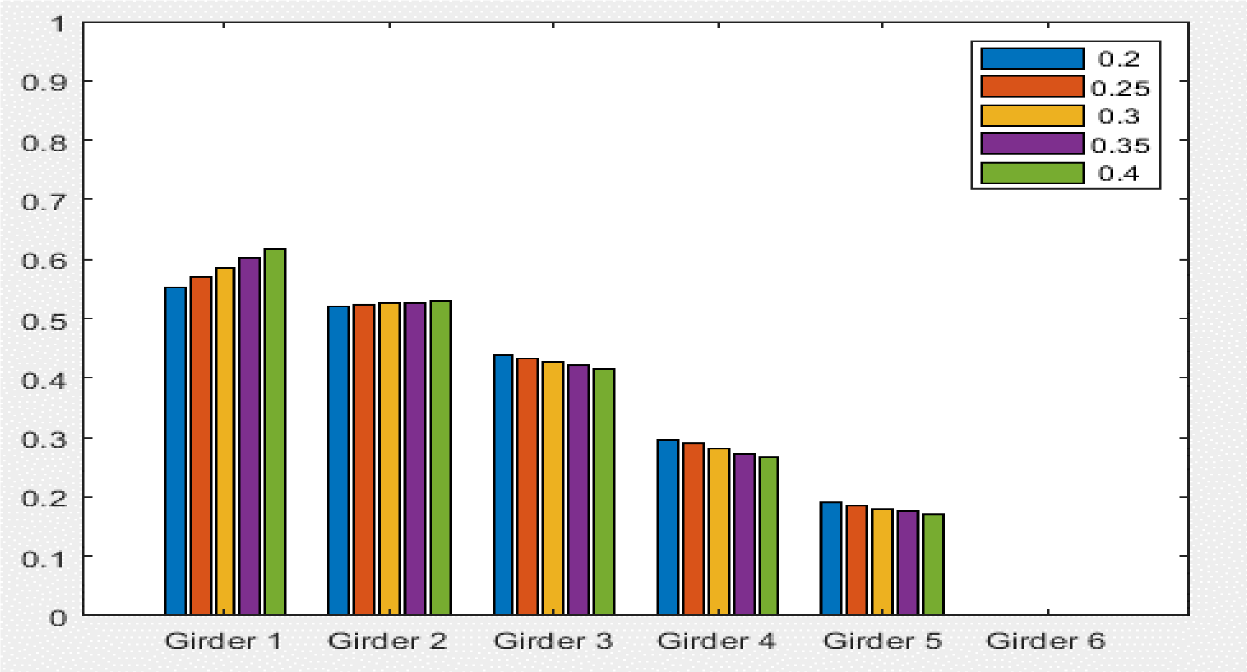

Typical Bridge #3, Stallings/Yoo Methodology, EG 2LL, Variable = Overhang Ratio

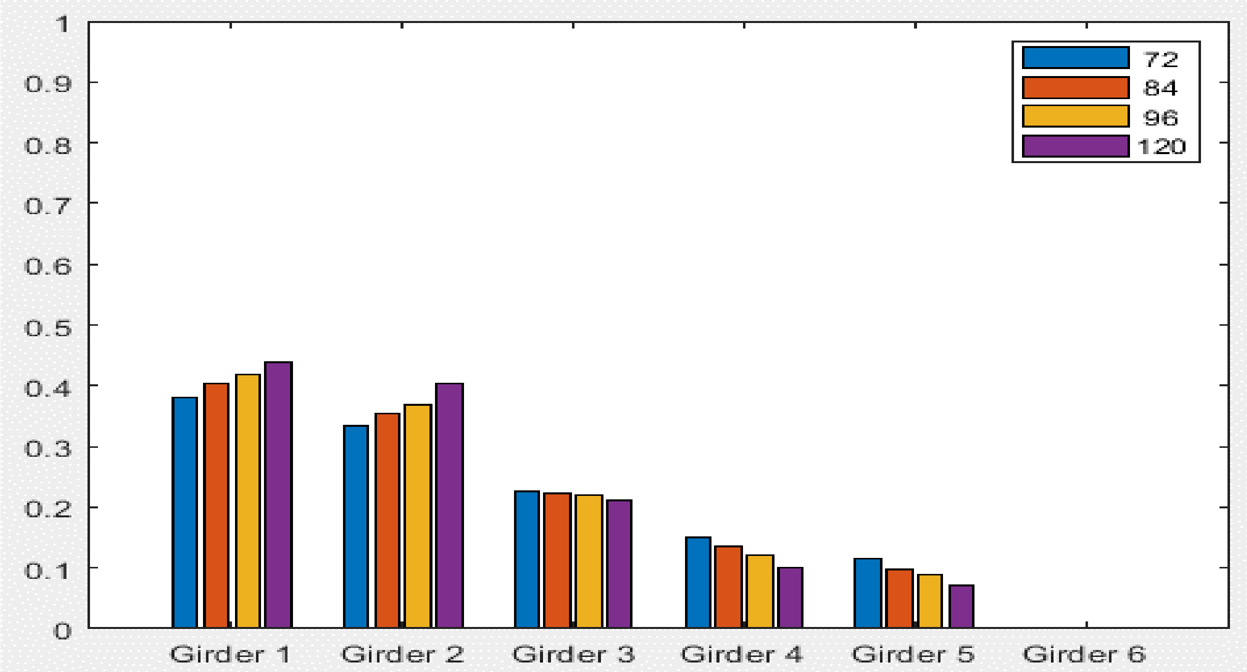

Typical Bridge #3, Tarhini/Frederick Methodology, IG OLL, Variable = PBFTG Size

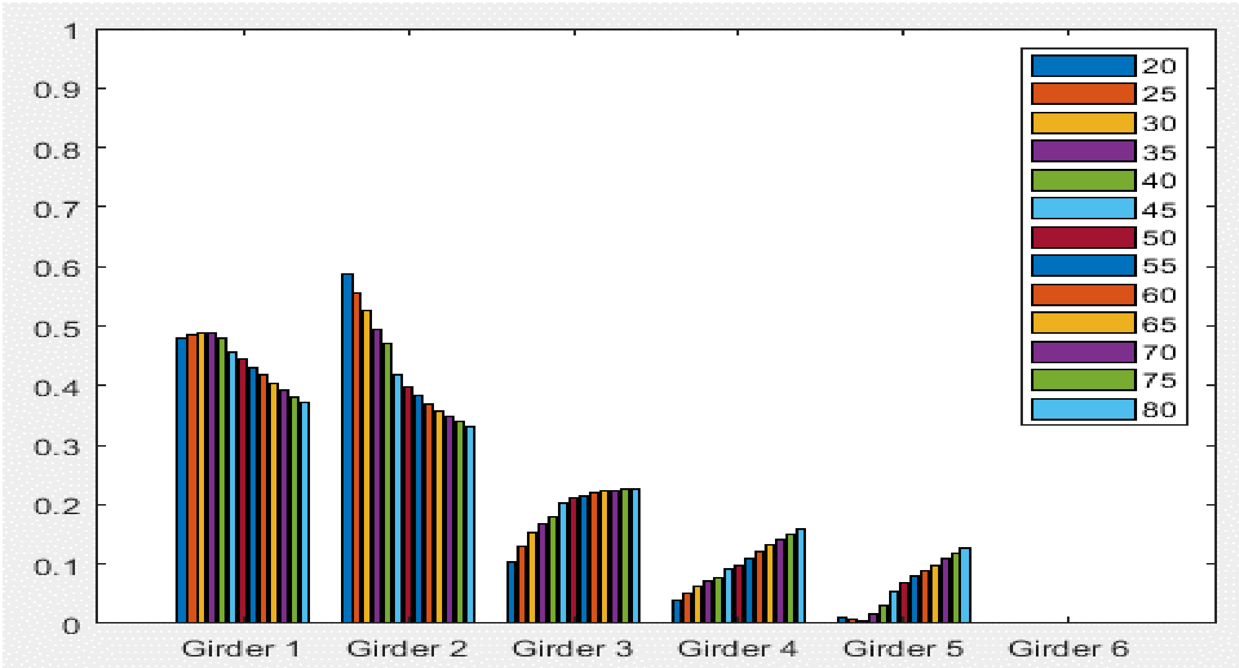

Typical Bridge #3, Tarhini/Frederick Methodology, IG OLL, Variable = Span Length (ft)

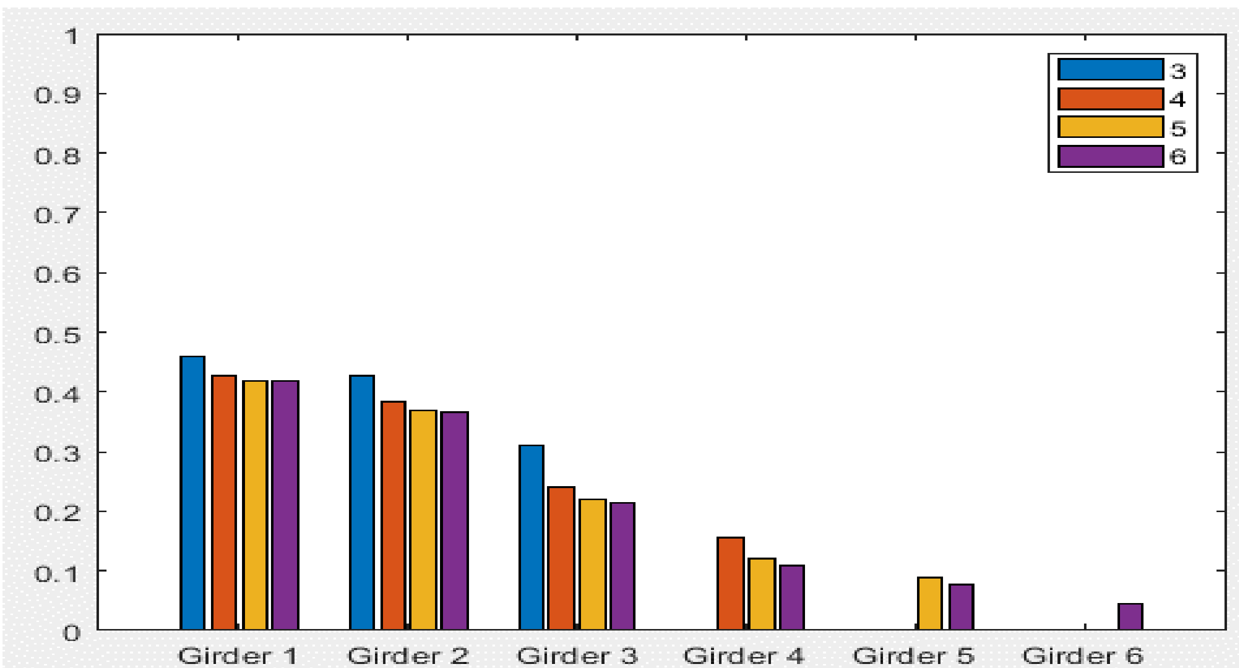

Typical Bridge #3, Tarhini/Frederick Methodology, IG OLL, Variable = Number of Girders

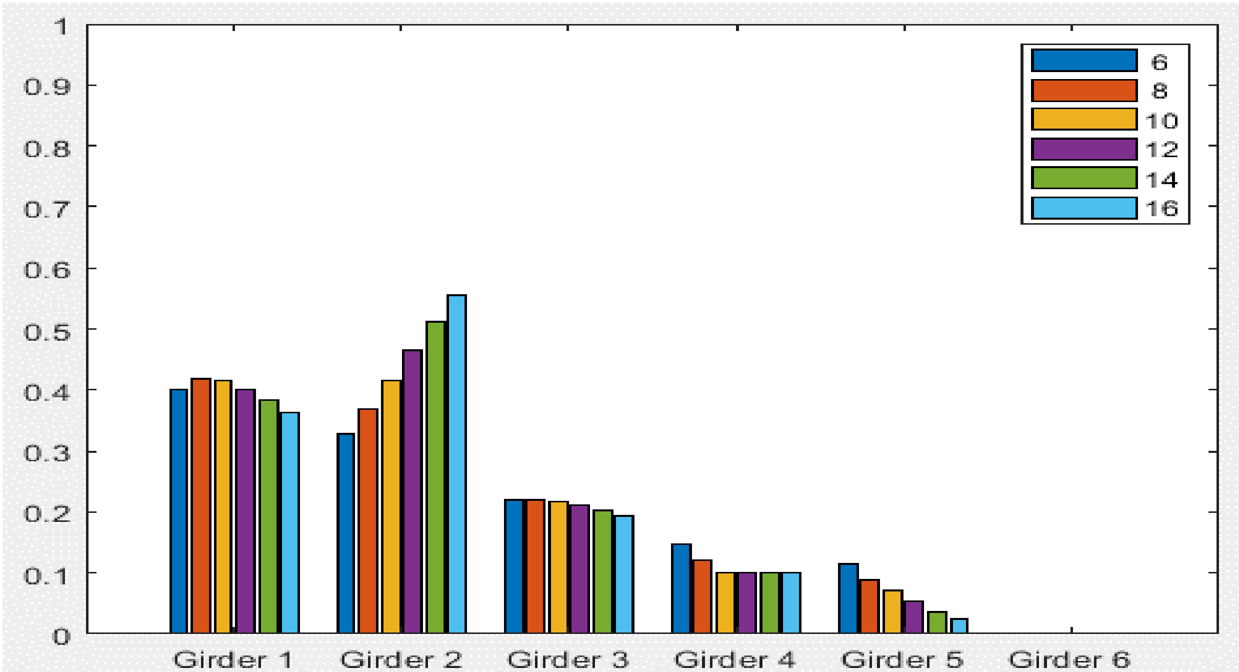

Typical Bridge #3, Tarhini/Frederick Methodology, IG OLL, Variable = Girder Spacing (ft)

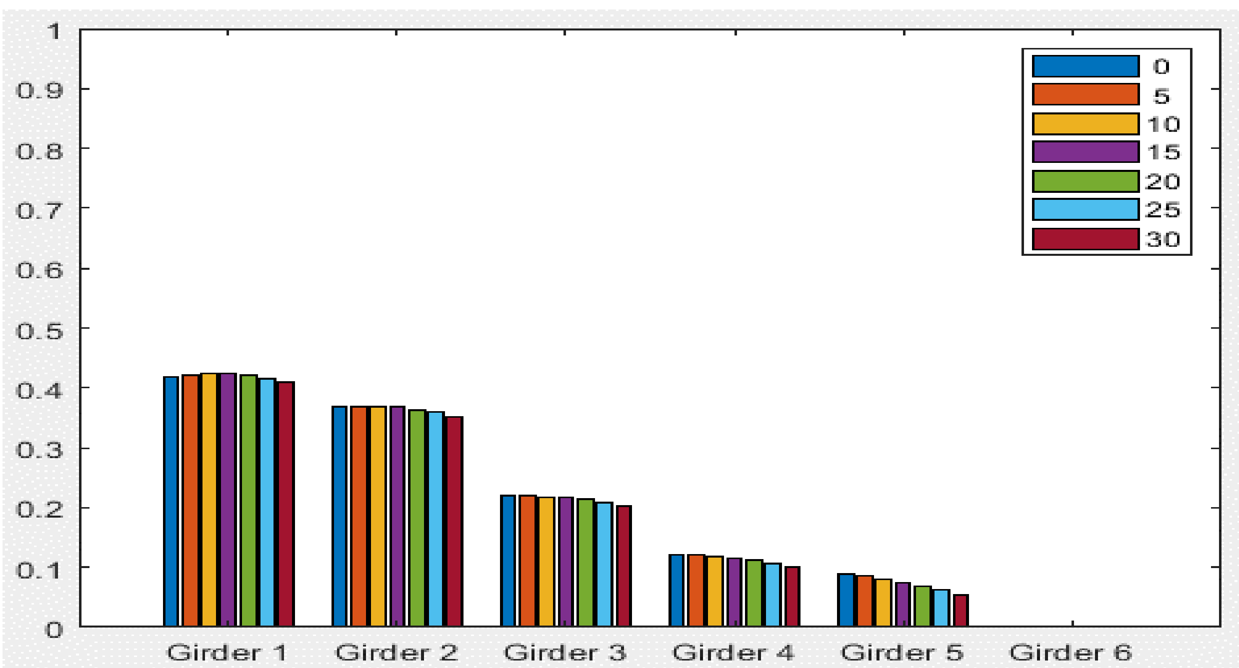

Typical Bridge #3, Tarhini/Frederick Methodology, IG OLL, Variable = Degree of Skew (deg)

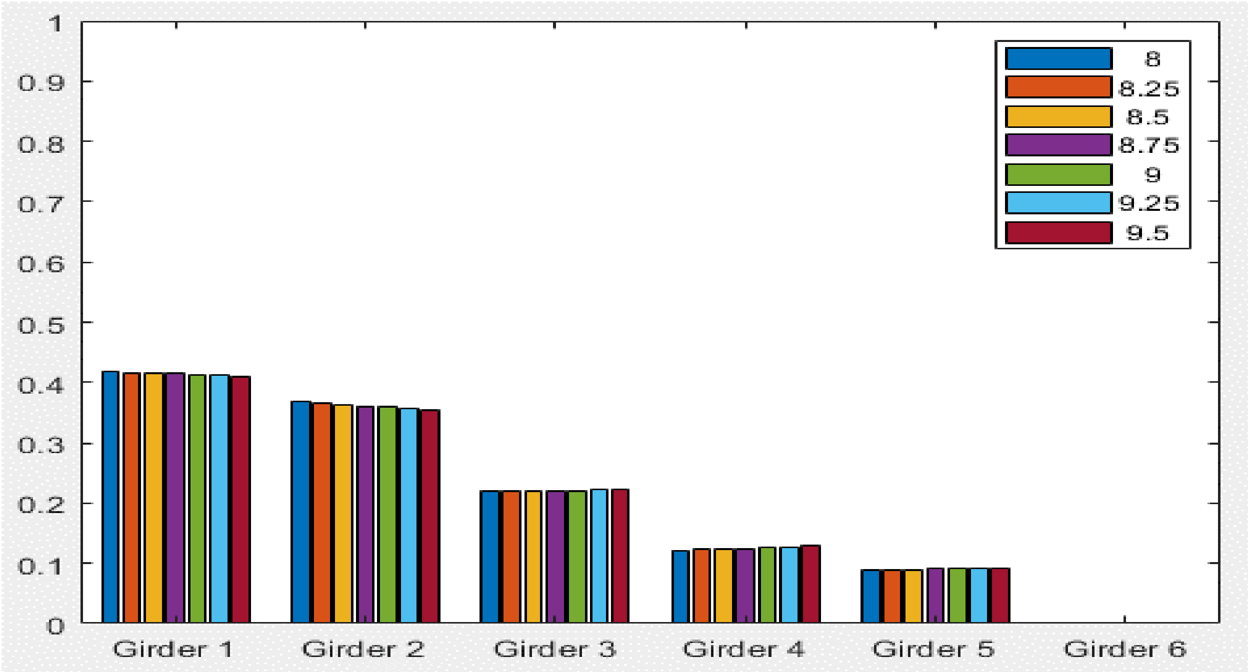

Typical Bridge #3, Tarhini/Frederick Methodology, IG OLL, Variable = Deck Thickness (in)

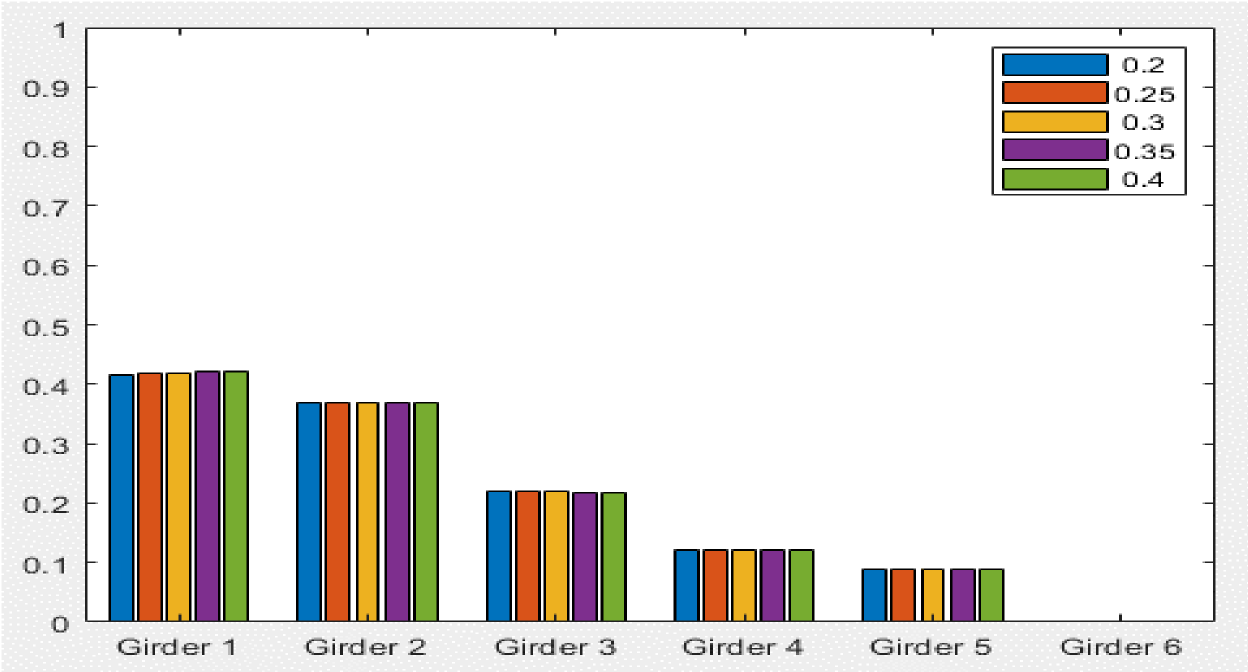

Typical Bridge #3, Tarhini/Frederick Methodology, IG OLL, Variable = Overhang Ratio

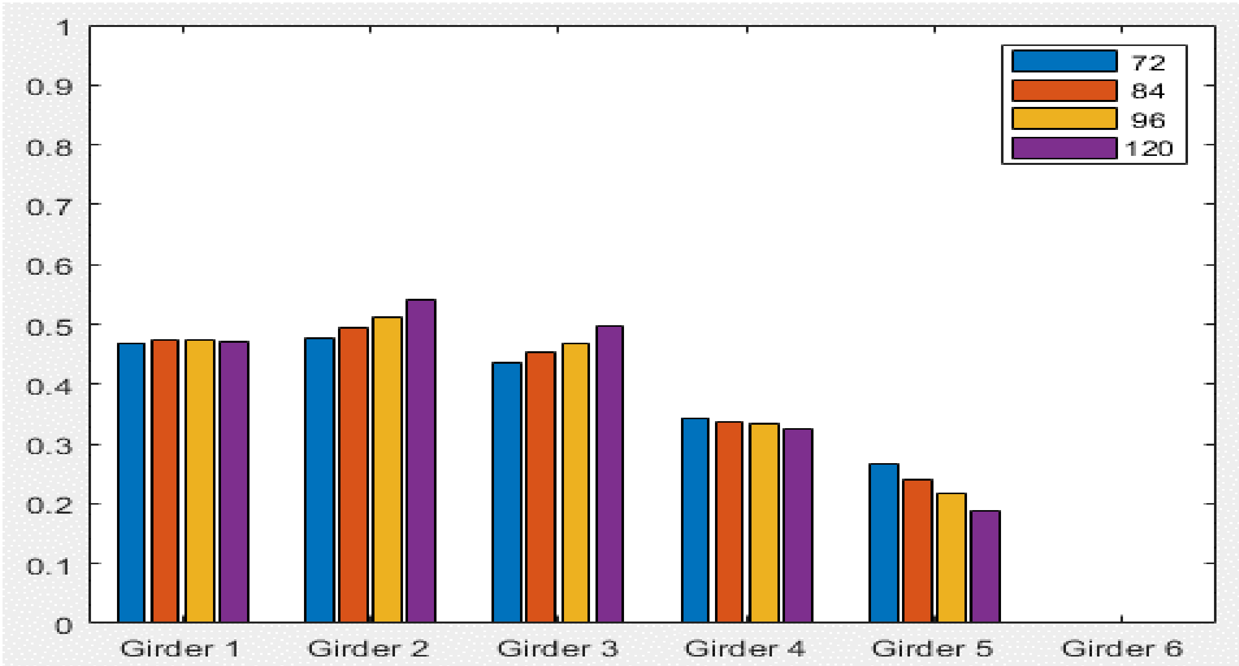

Typical Bridge #3, Tarhini/Frederick Methodology, IG 2LL, Variable = PBFTG Size

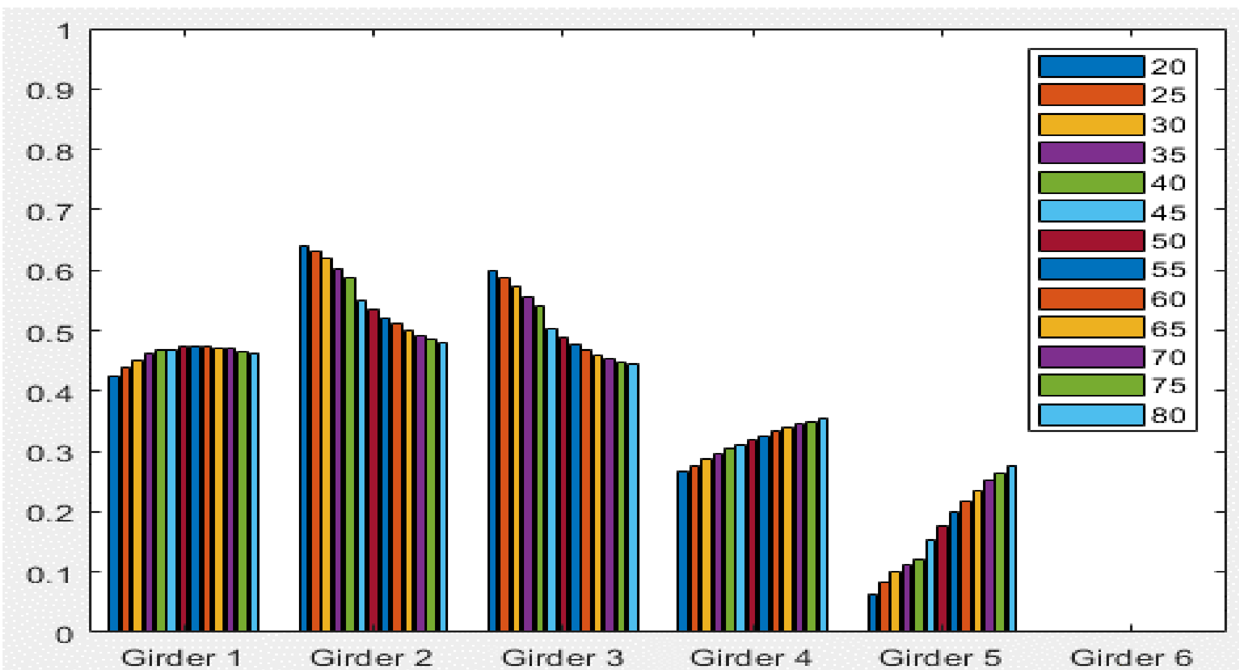

Typical Bridge #3, Tarhini/Frederick Methodology, IG 2LL, Variable = Span Length (ft)

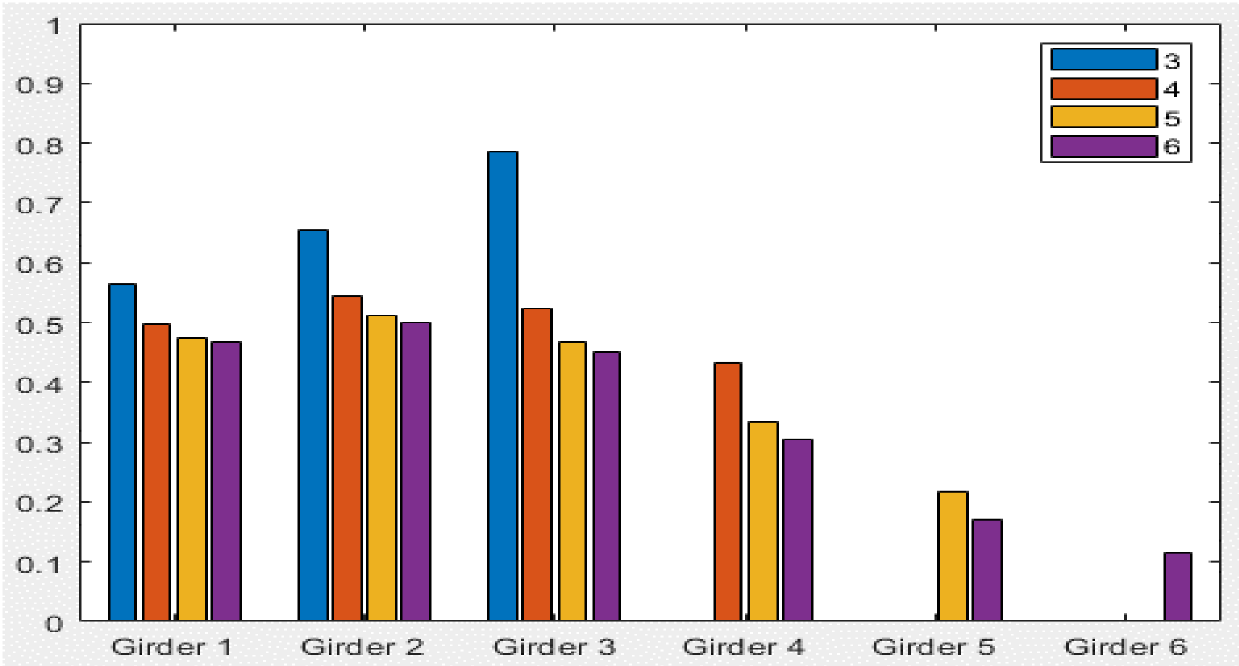

Typical Bridge #3, Tarhini/Frederick Methodology, IG 2LL, Variable = Number of Girders

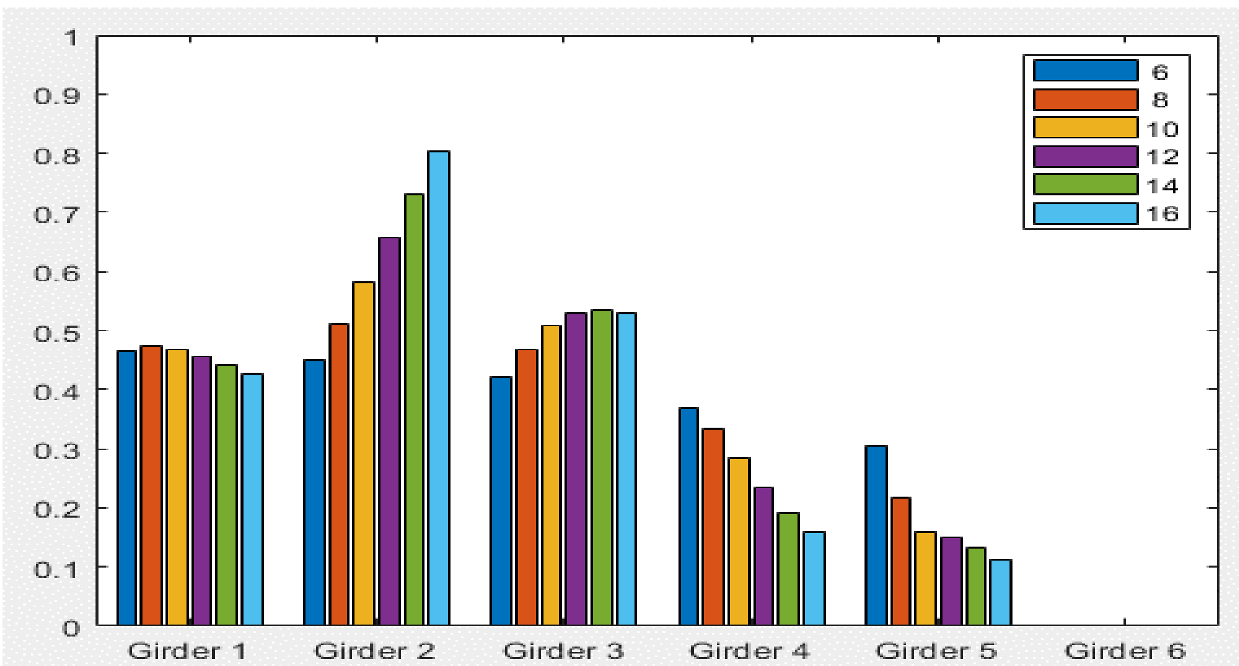

Typical Bridge #3, Tarhini/Frederick Methodology, IG 2LL, Variable = Girder Spacing (ft)

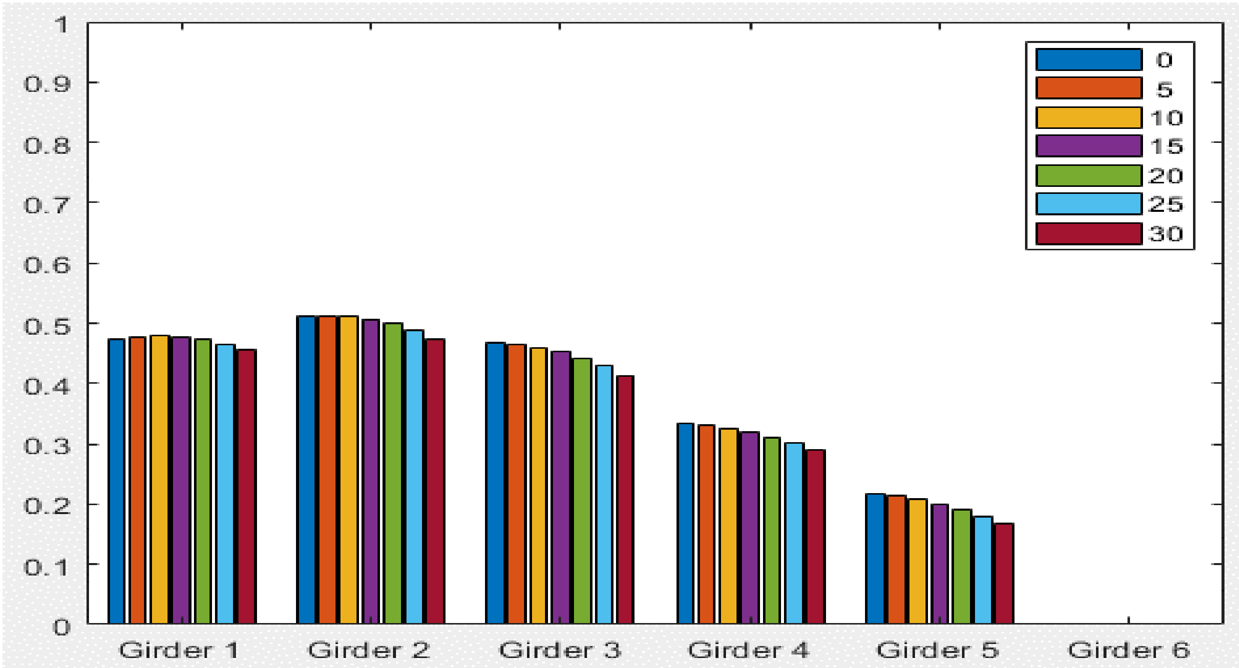

Typical Bridge #3, Tarhini/Frederick Methodology, IG 2LL, Variable = Degree of Skew (deg)

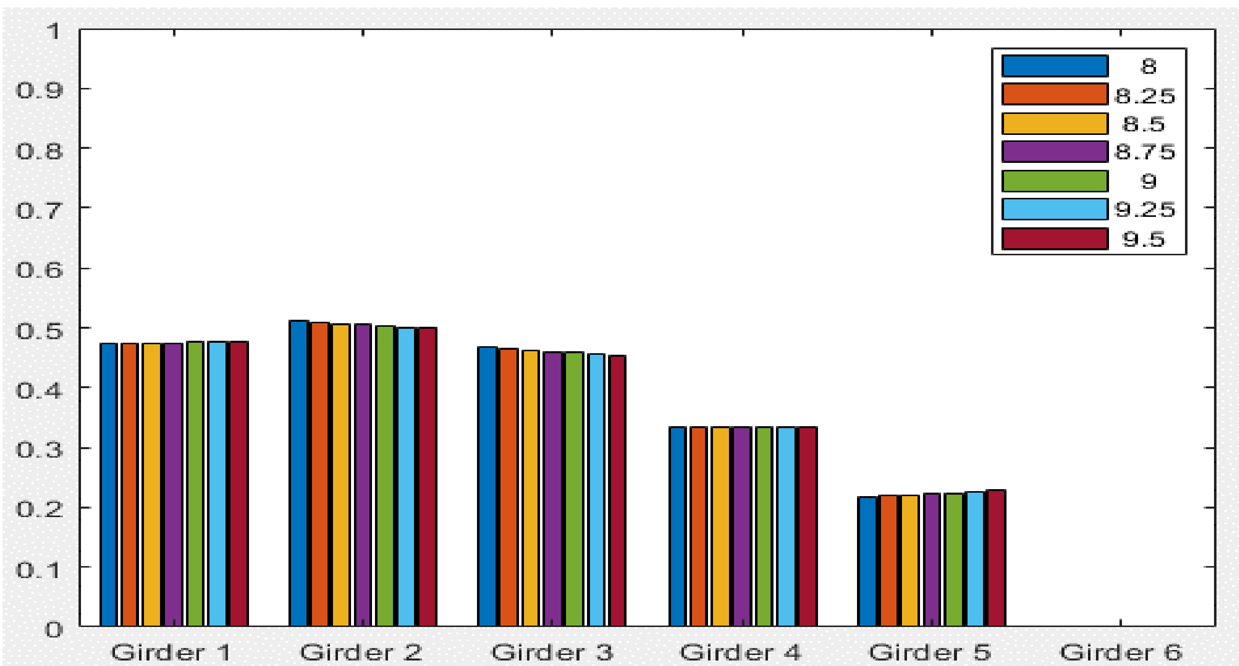

Typical Bridge #3, Tarhini/Frederick Methodology, IG 2LL, Variable = Deck Thickness (in)

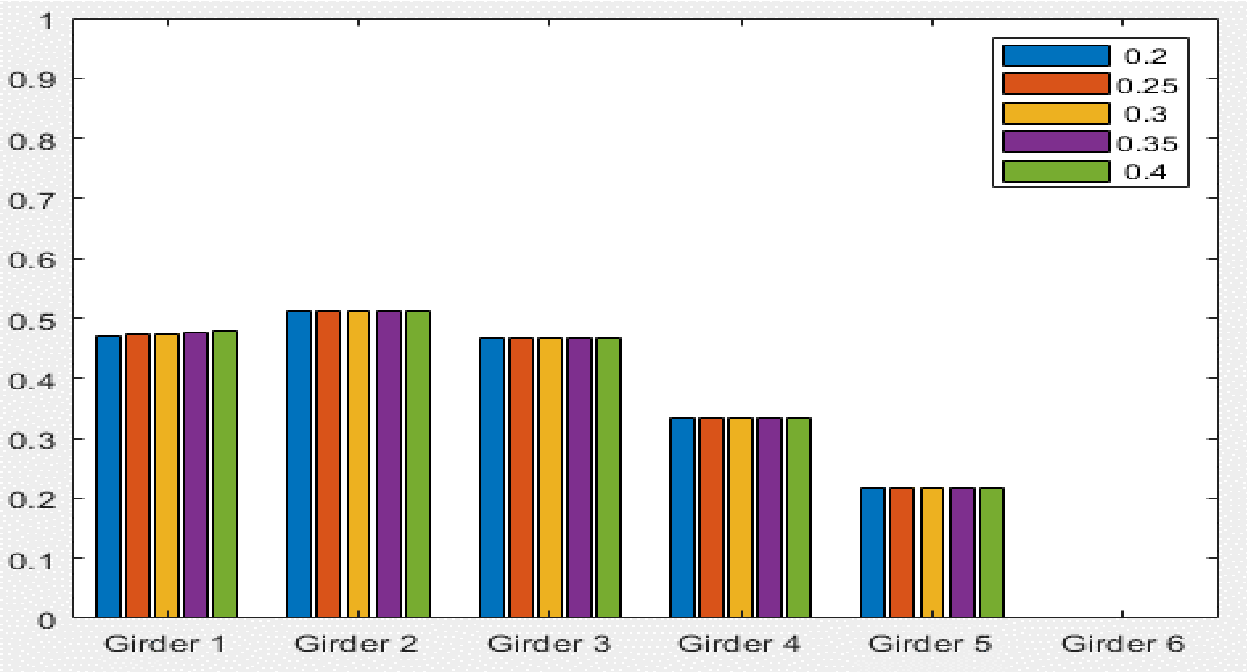

Typical Bridge #3, Tarhini/Frederick Methodology, IG 2LL, Variable = Overhang Ratio

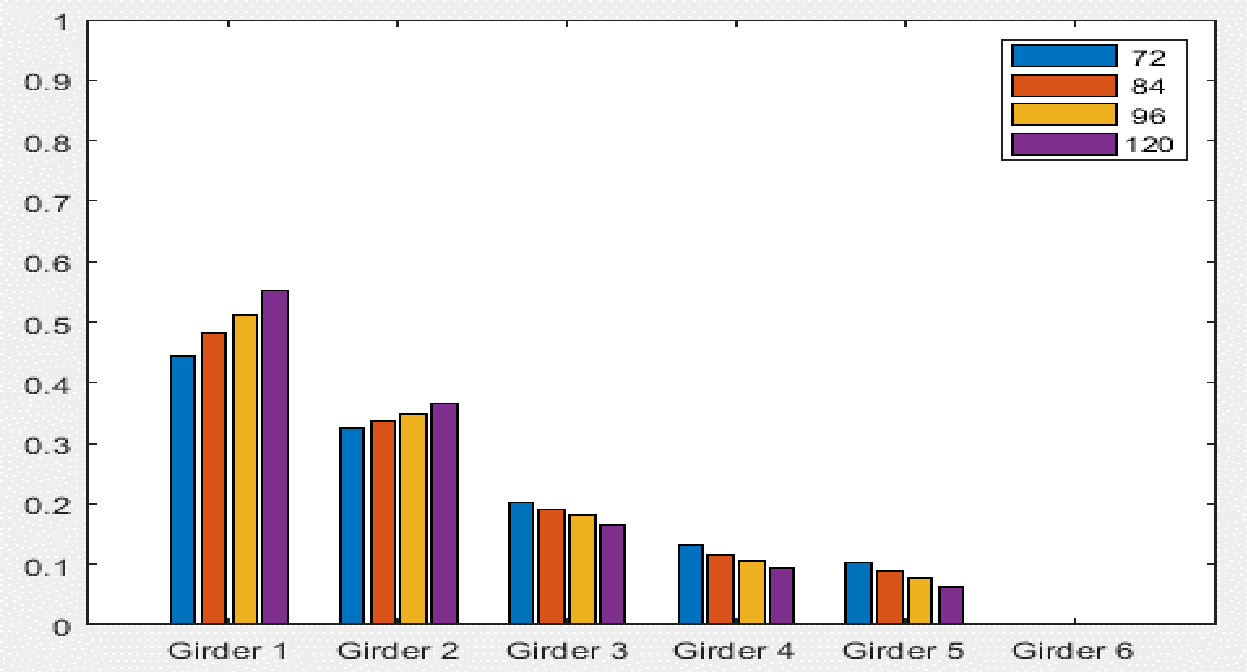

Typical Bridge #3, Tarhini/Frederick Methodology, EG OLL, Variable = PBFTG Size

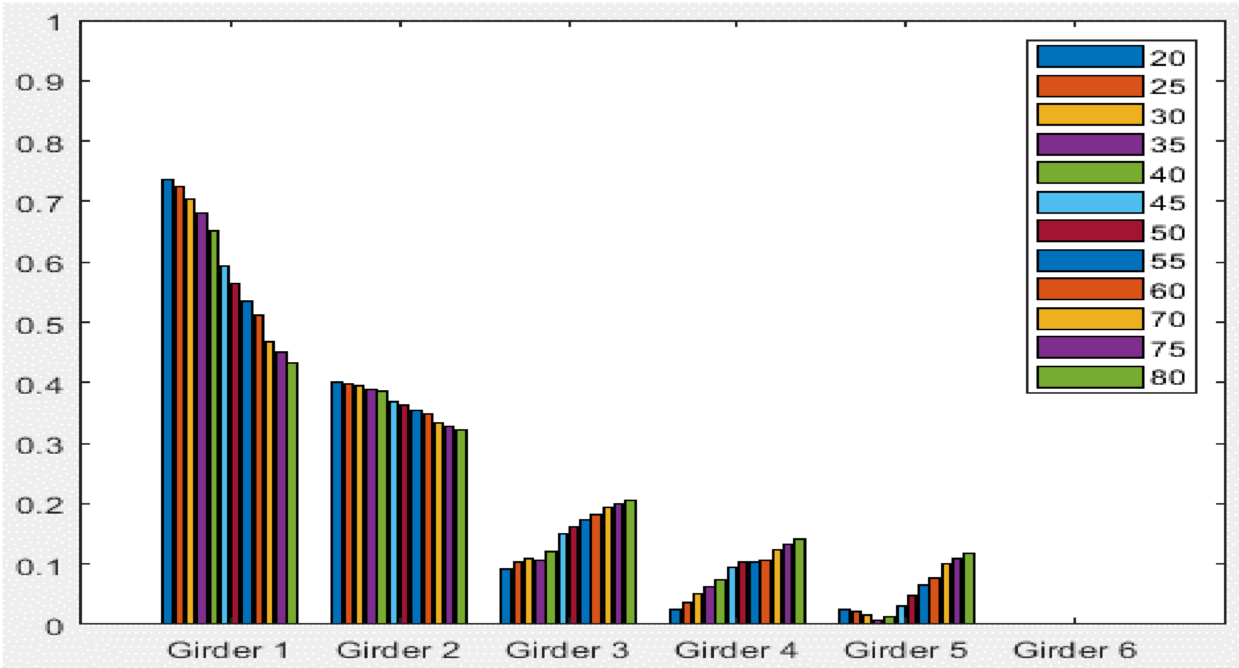

Typical Bridge #3, Tarhini/Frederick Methodology, EG OLL, Variable = Span Length (ft)

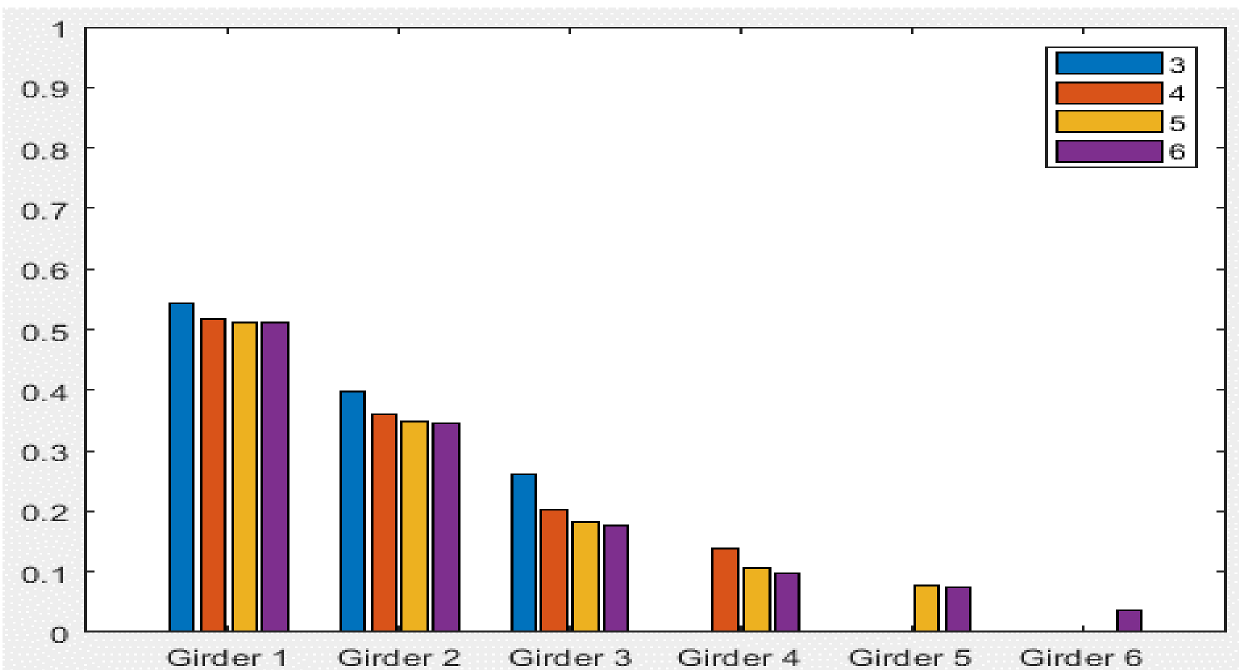

Typical Bridge #3, Tarhini/Frederick Methodology, EG OLL, Variable = Number of Girders

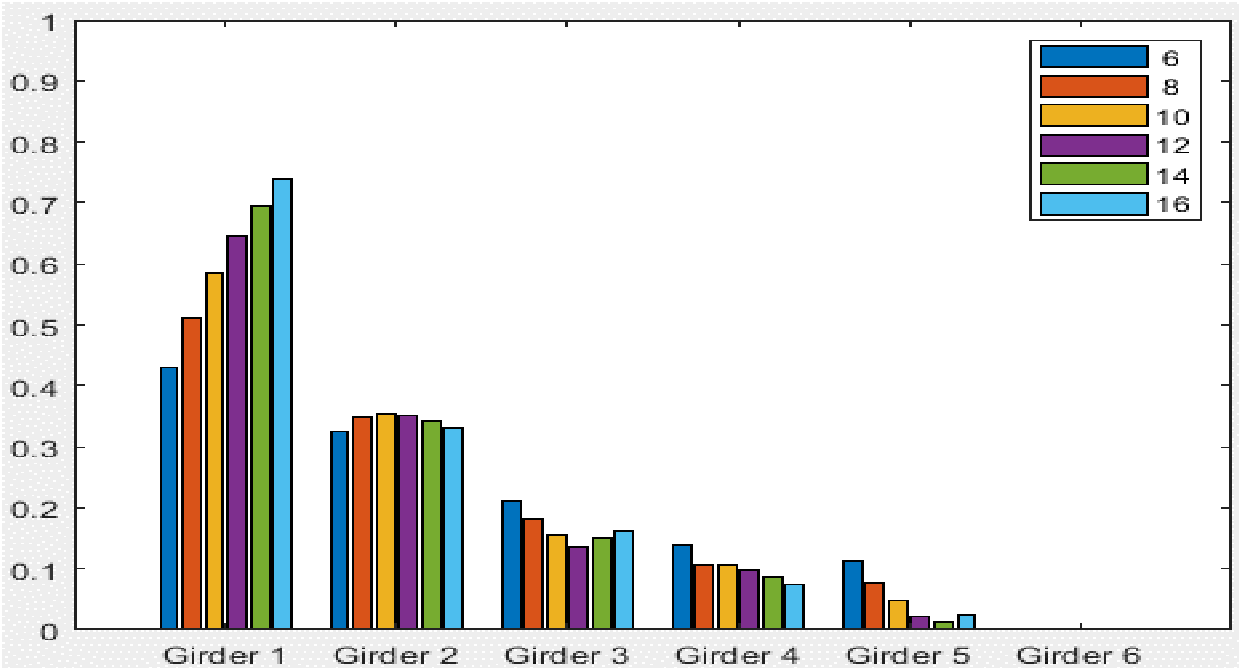

Typical Bridge #3, Tarhini/Frederick Methodology, EG OLL, Variable = Girder Spacing (ft)

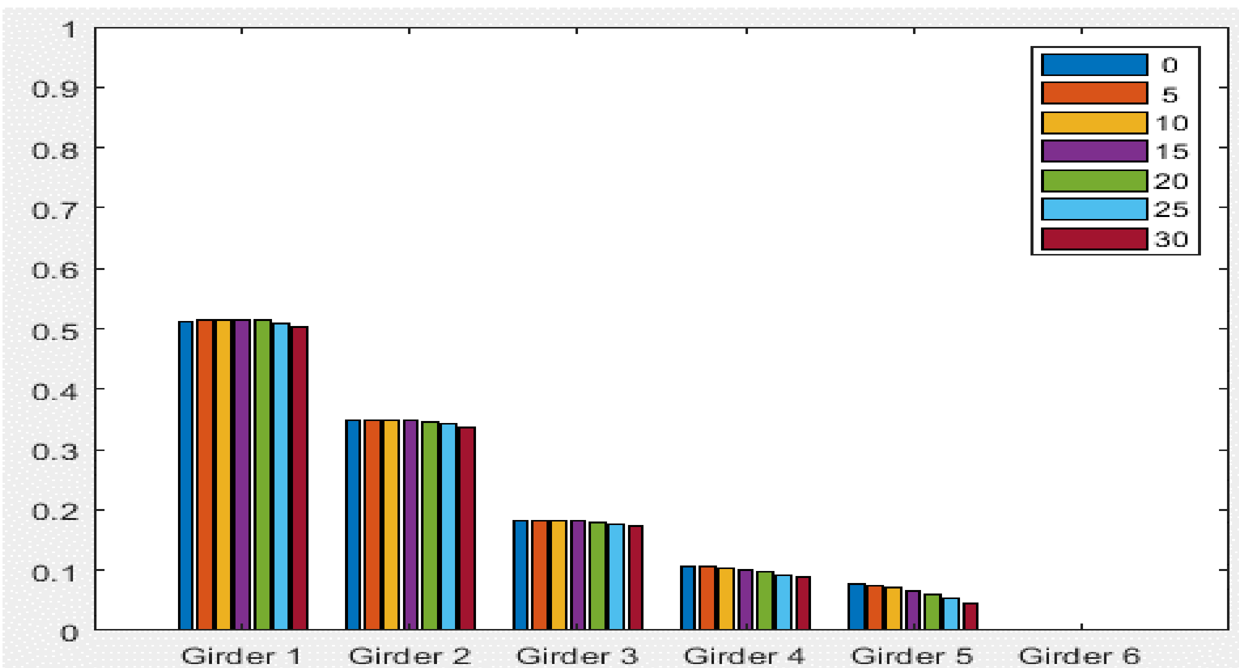

Typical Bridge #3, Tarhini/Frederick Methodology, EG OLL, Variable = Degree of Skew (deg)

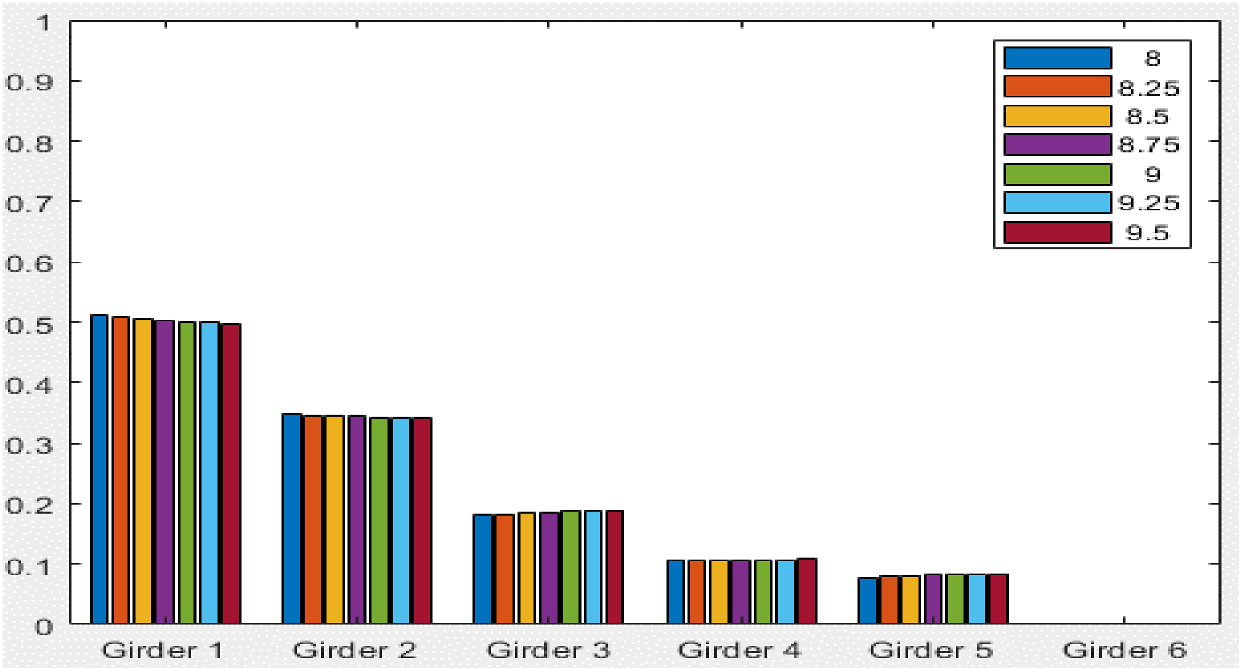

Typical Bridge #3, Tarhini/Frederick Methodology, EG OLL, Variable = Deck Thickness (in)

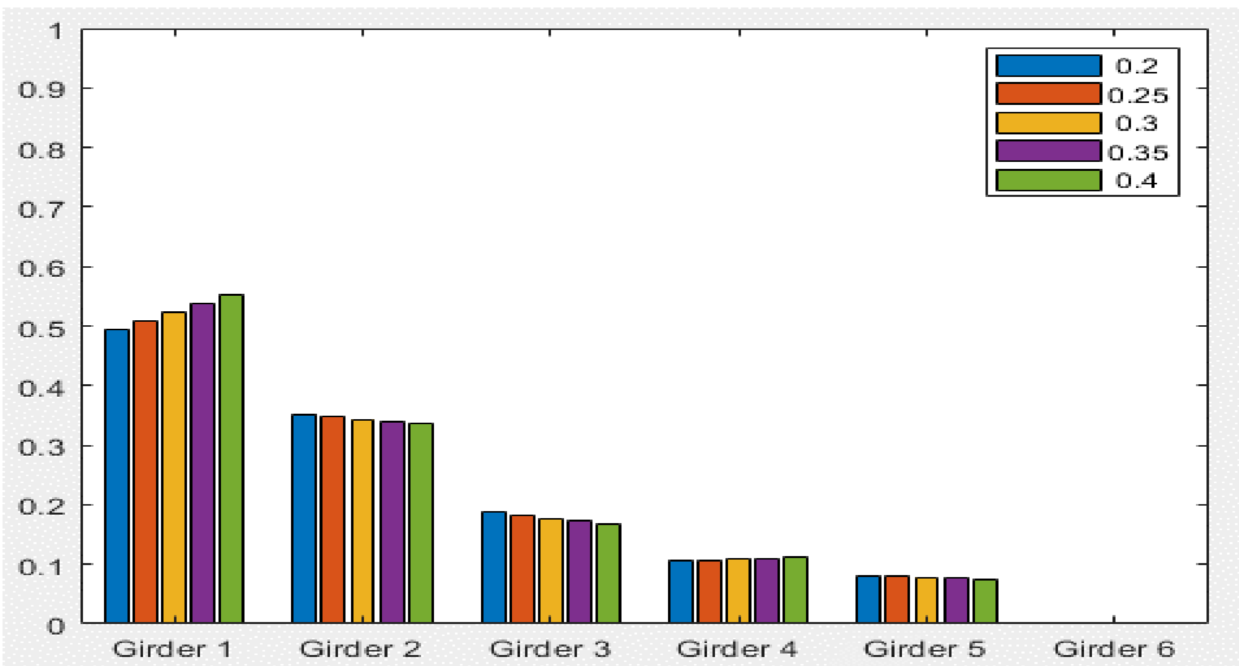

Typical Bridge #3, Tarhini/Frederick Methodology, EG OLL, Variable = Overhang Ratio

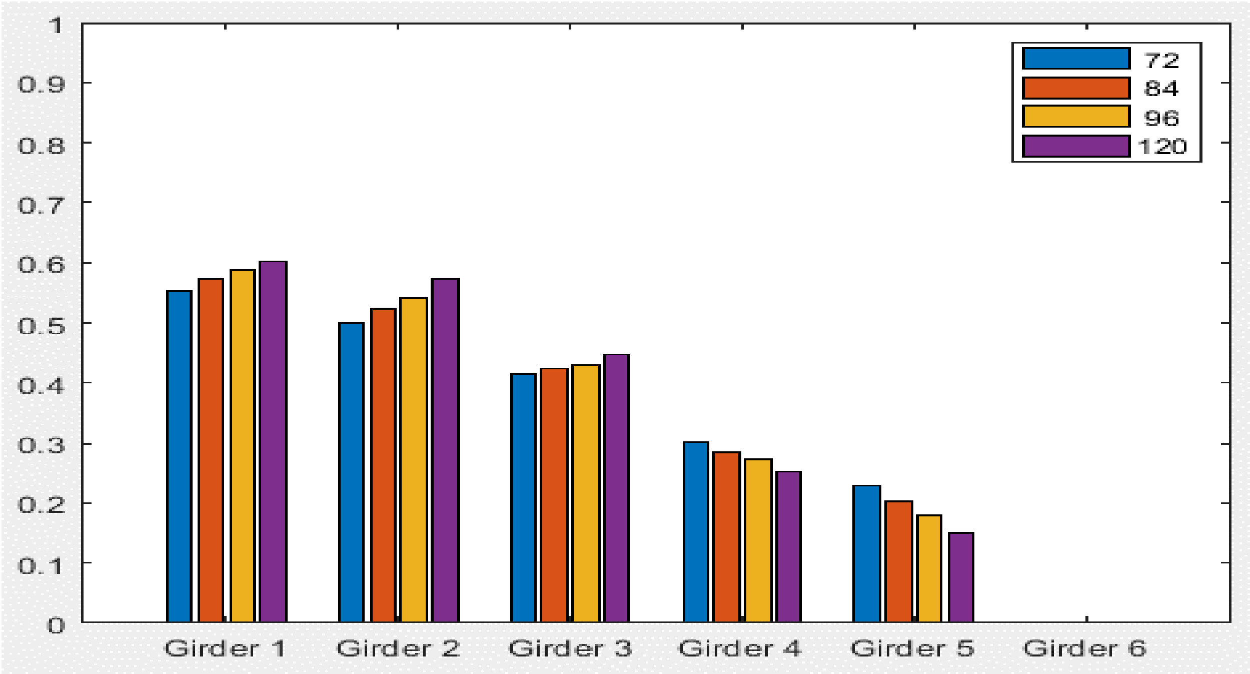

Typical Bridge #3, Tarhini/Frederick Methodology, EG 2LL, Variable = PBFTG Size

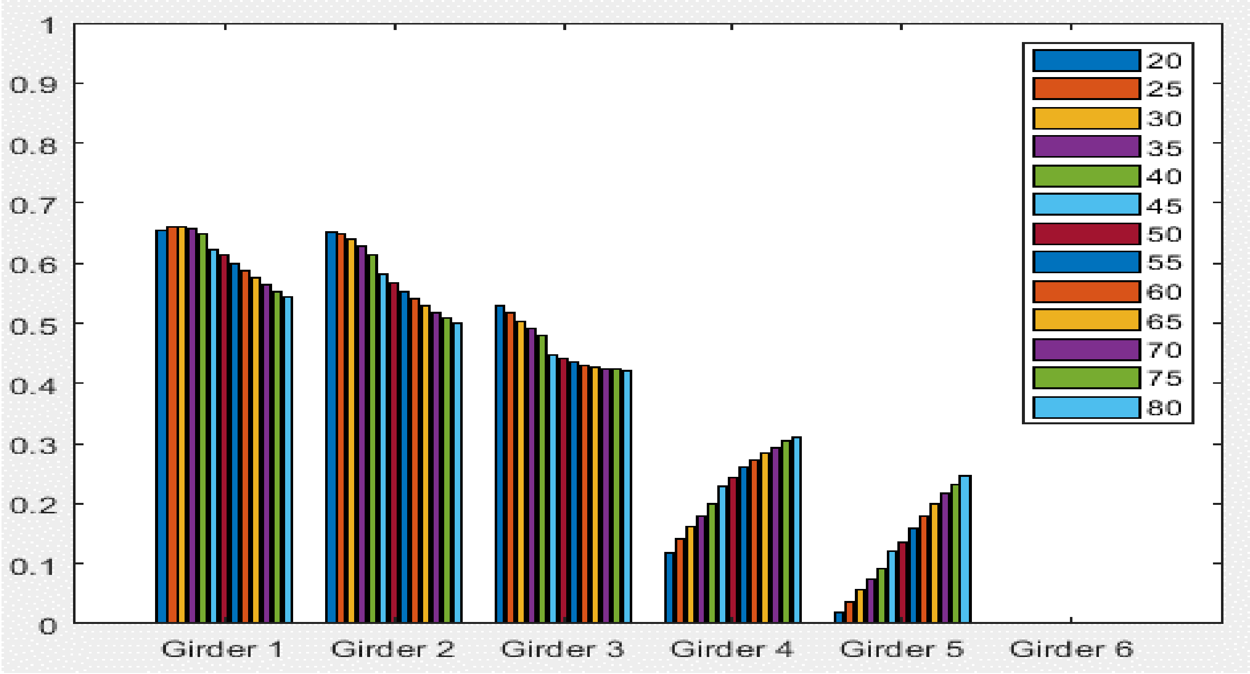

Typical Bridge #3, Tarhini/Frederick Methodology, EG 2LL, Variable = Span Length (ft)

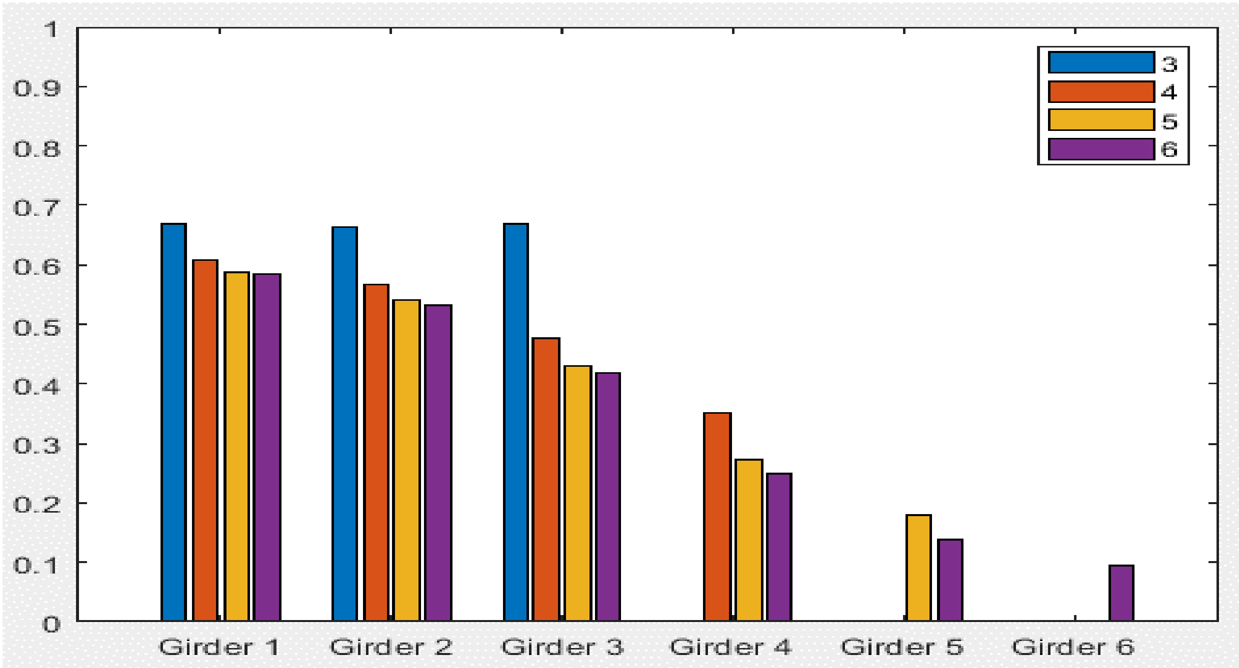

Typical Bridge #3, Tarhini/Frederick Methodology, EG 2LL, Variable = Number of Girders

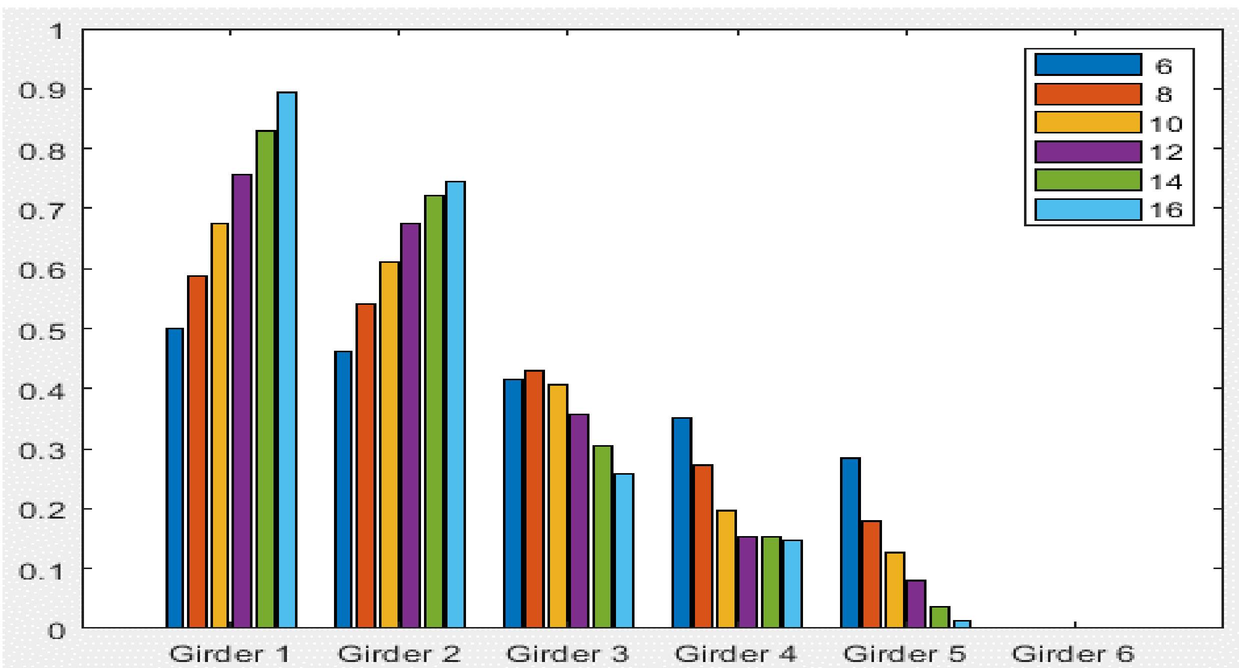

Typical Bridge #3, Tarhini/Frederick Methodology, EG 2LL, Variable = Girder Spacing (ft)

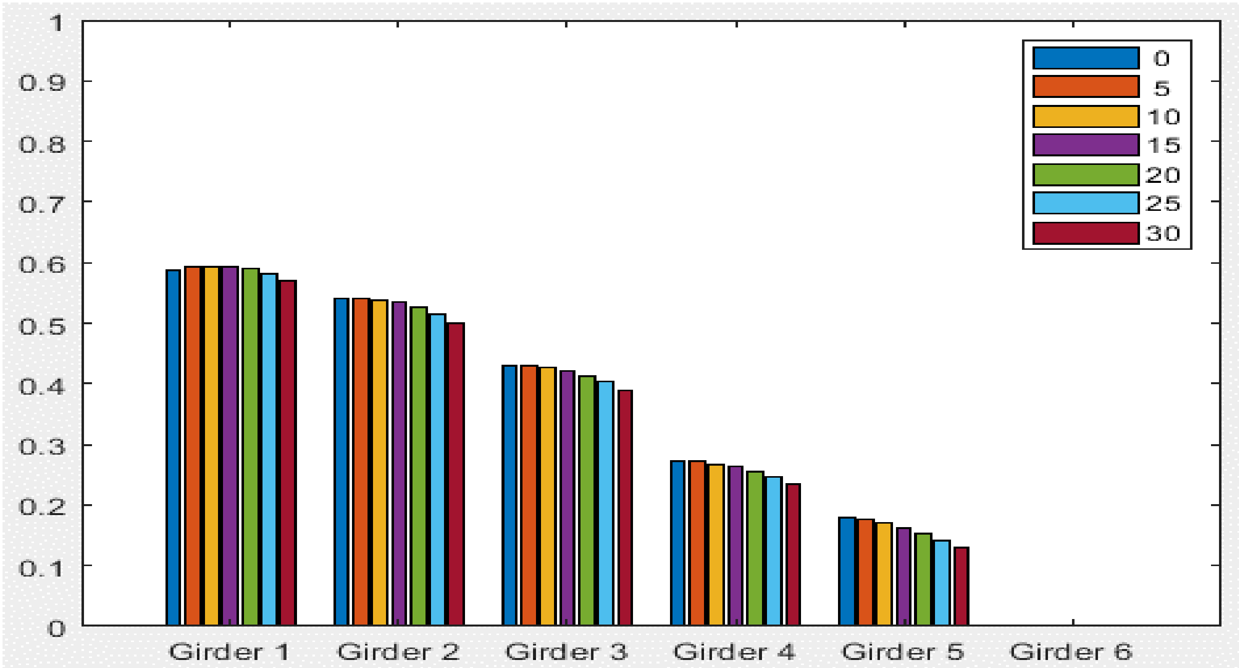

Typical Bridge #3, Tarhini/Frederick Methodology, EG 2LL, Variable = Degree of Skew (deg)

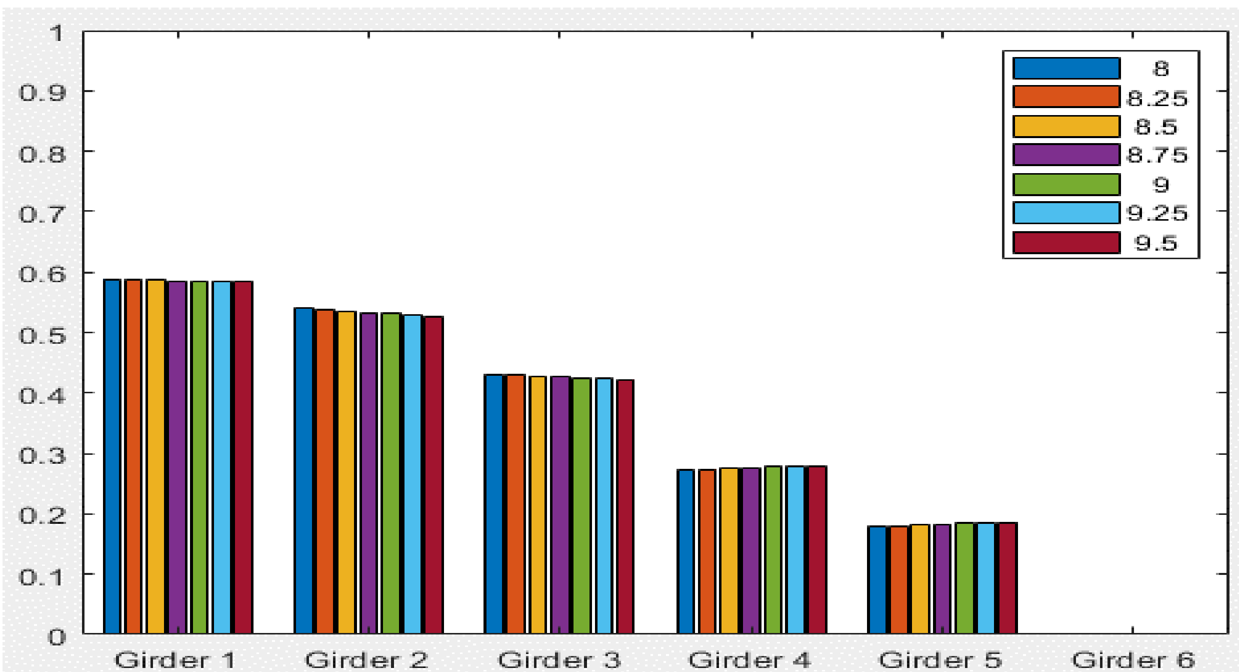

Typical Bridge #3, Tarhini/Frederick Methodology, EG 2LL, Variable = Deck Thickness (in)

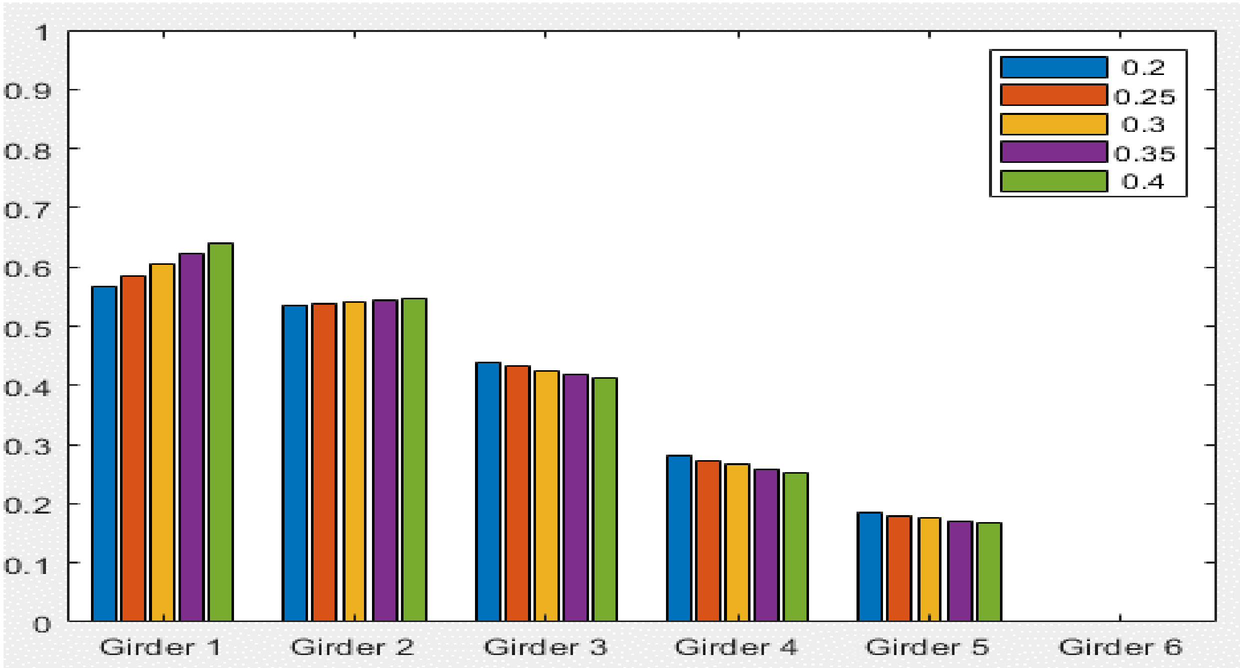

Typical Bridge #3, Tarhini/Frederick Methodology, EG 2LL, Variable = Overhang Ratio

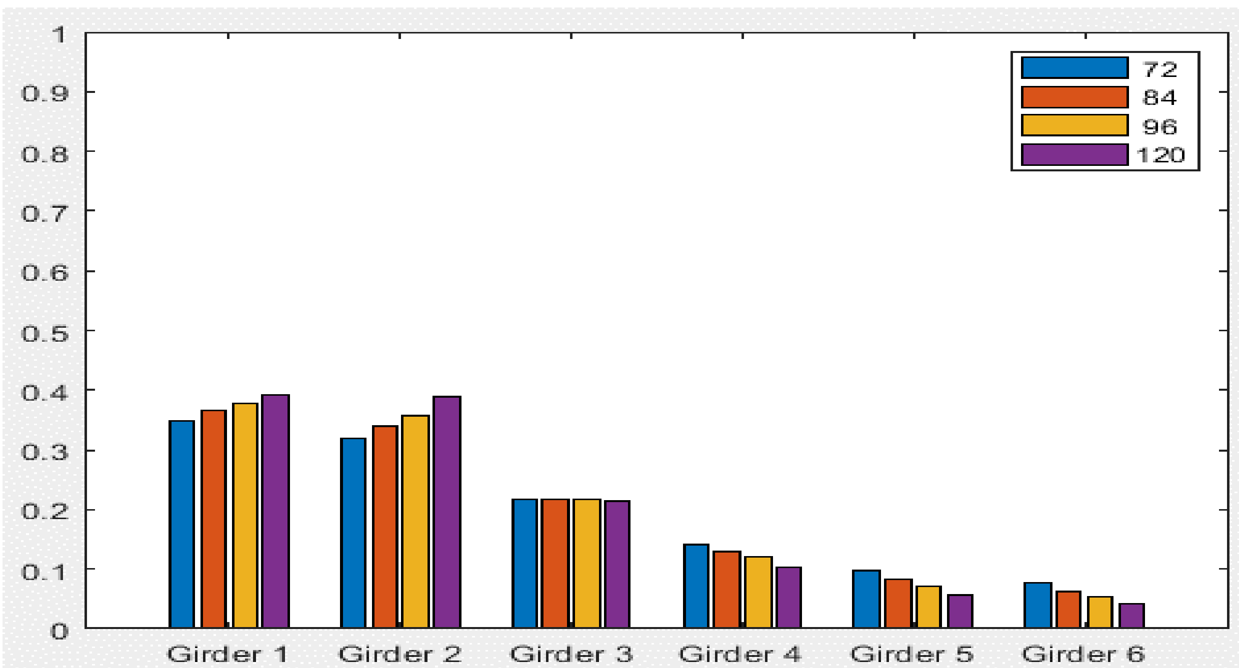

Typical Bridge #4, Stallings/Yoo Methodology, IG OLL, Variable = PBFTG Size

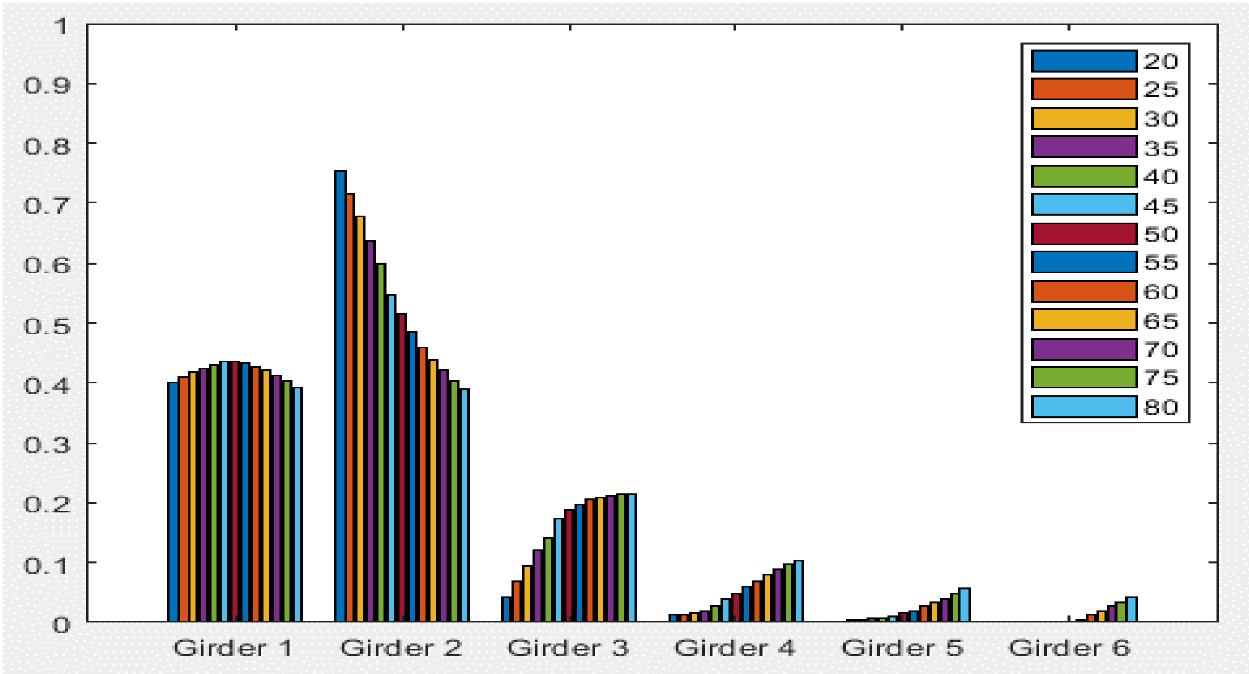

Typical Bridge #4, Stallings/Yoo Methodology, IG OLL, Variable = Span Length (ft)

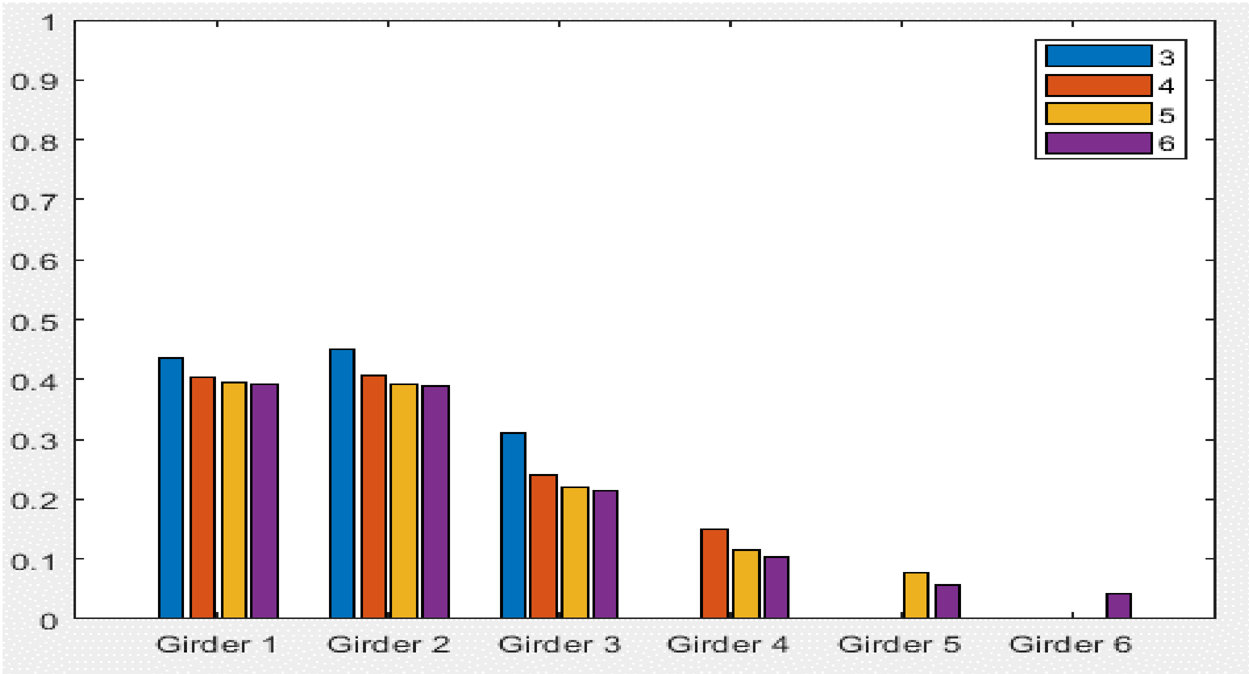

Typical Bridge #4, Stallings/Yoo Methodology, IG OLL, Variable = Number of Girders

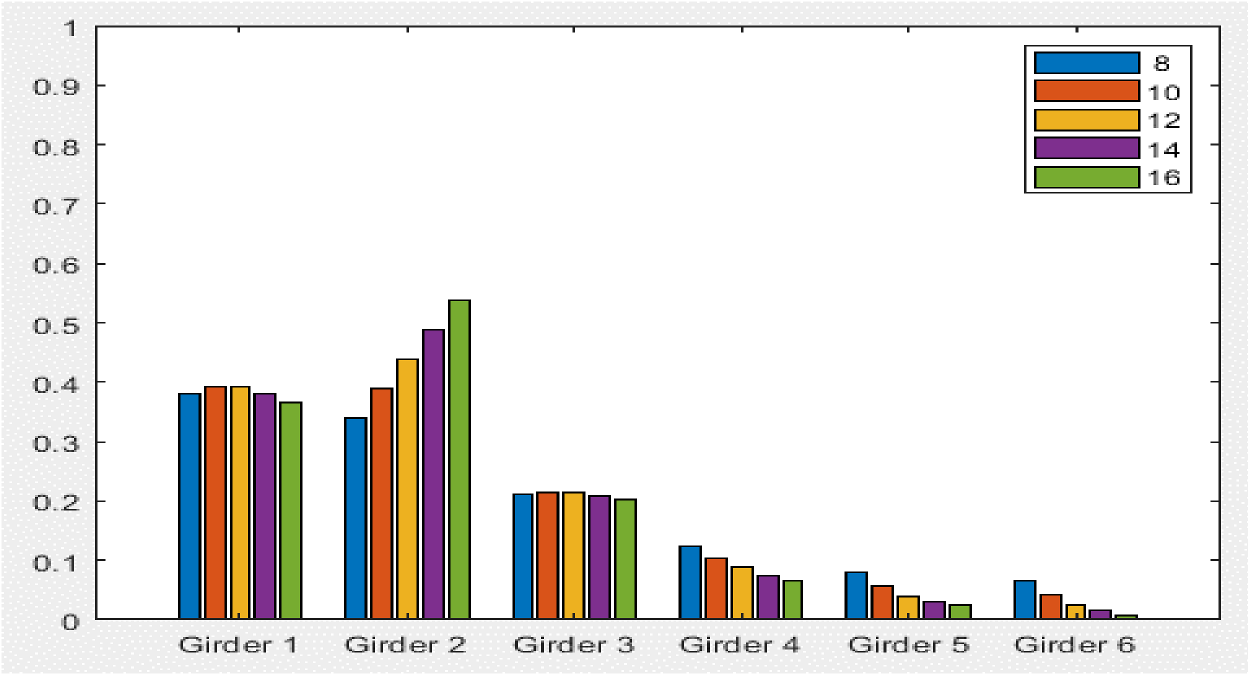

Typical Bridge #4, Stallings/Yoo Methodology, IG OLL, Variable = Girder Spacing (ft)

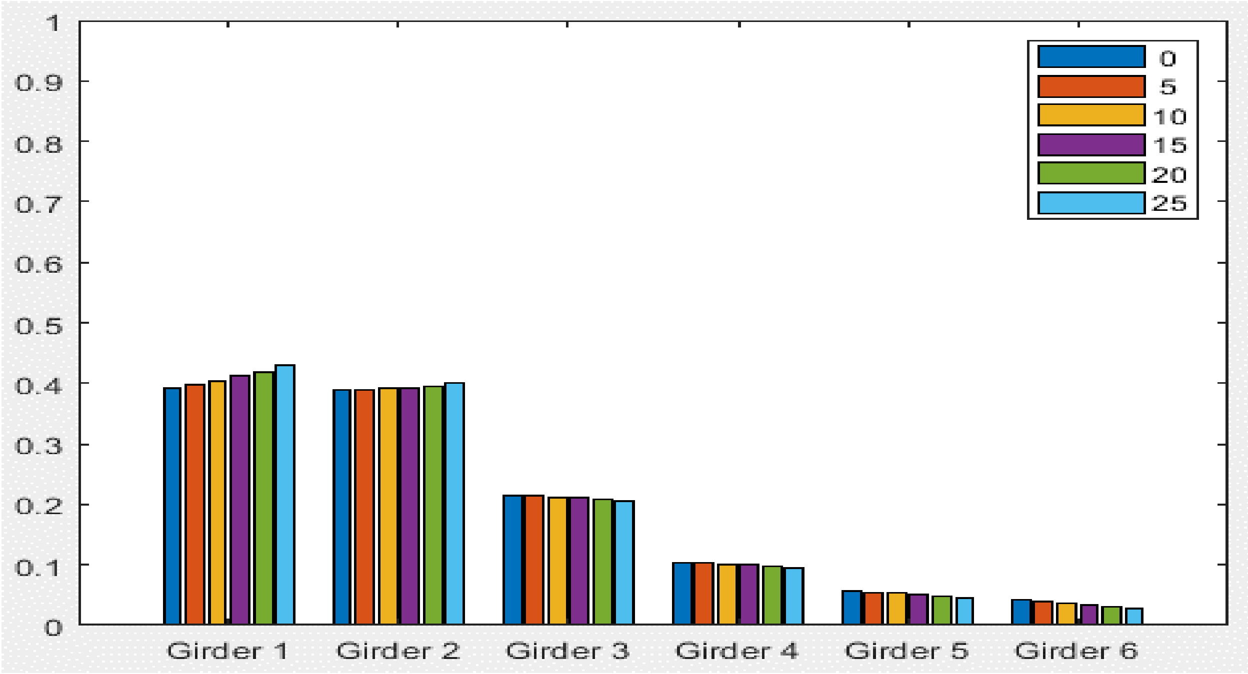

Typical Bridge #4, Stallings/Yoo Methodology, IG OLL, Variable = Degree of Skew (deg)

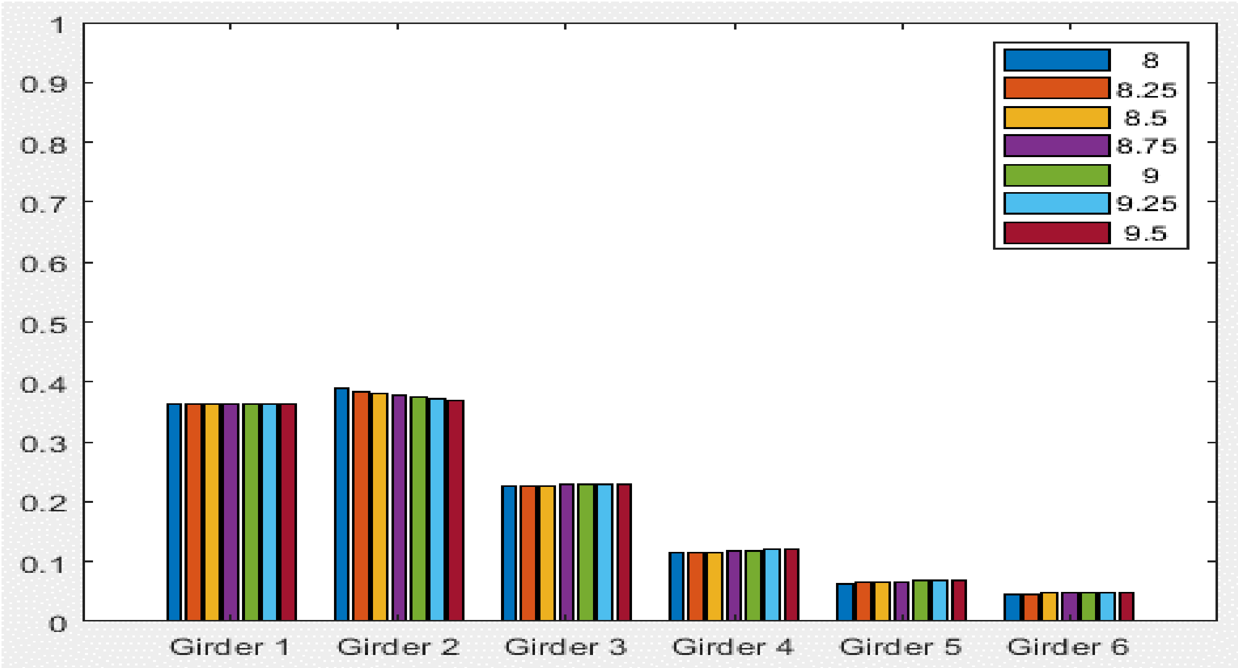

Typical Bridge #4, Stallings/Yoo Methodology, IG OLL, Variable = Deck Thickness (in)

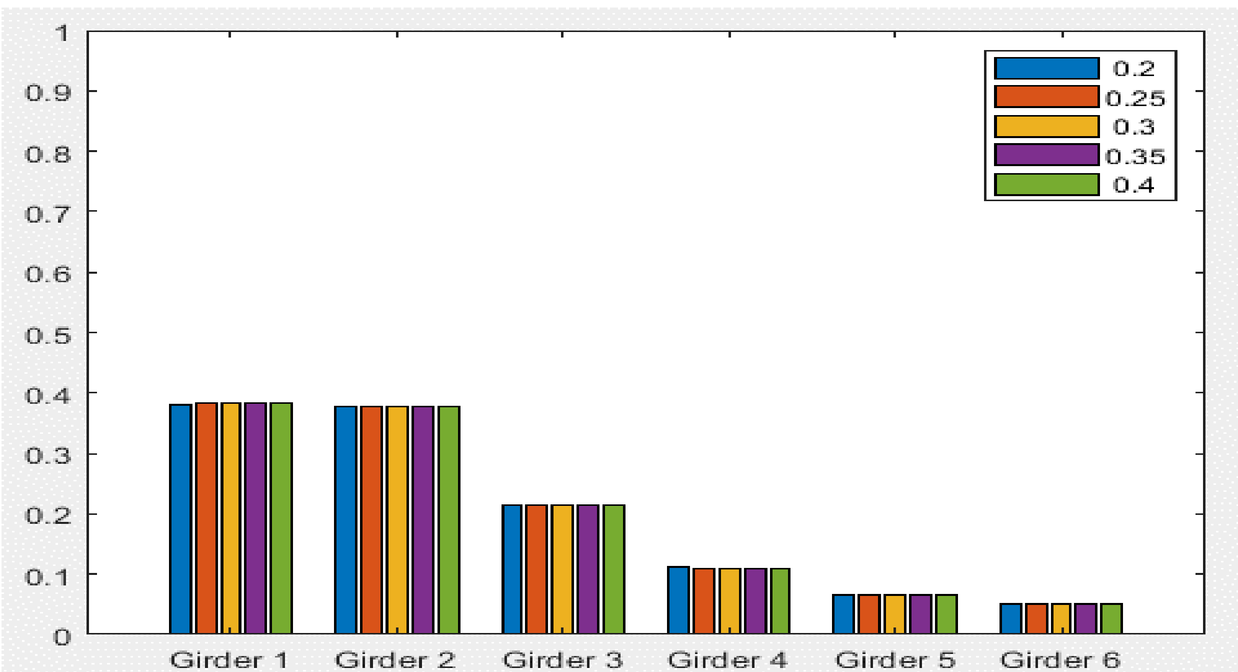

Typical Bridge #4, Stallings/Yoo Methodology, IG OLL, Variable = Overhang Ratio

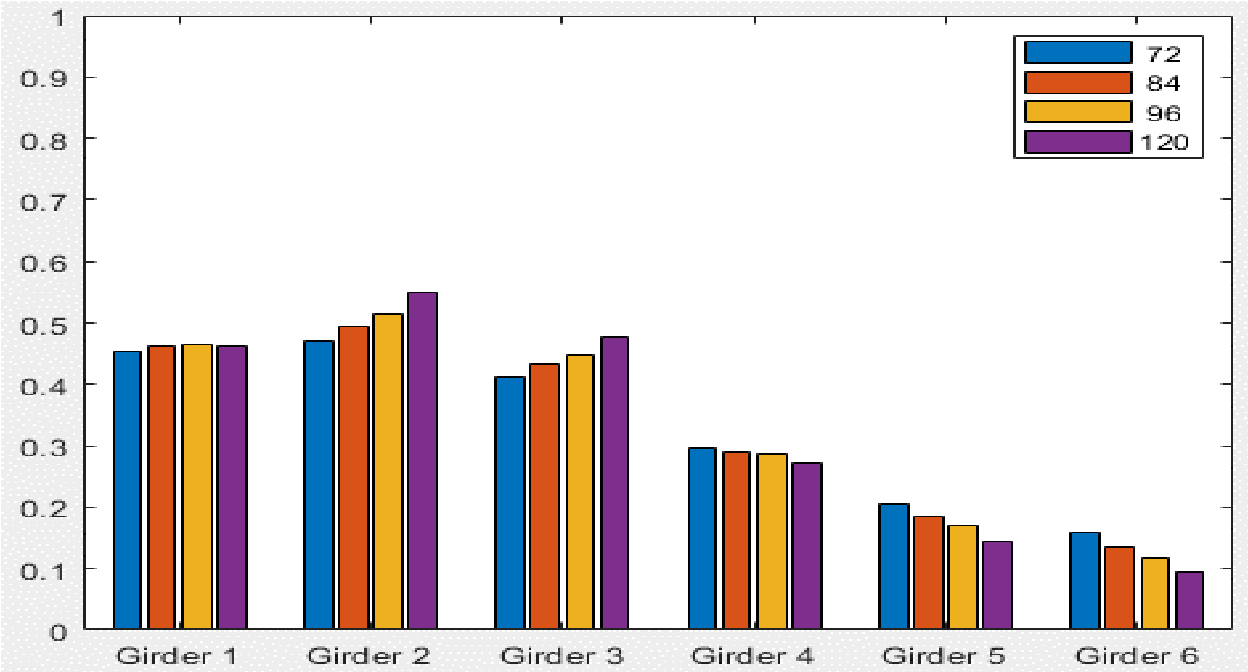

Typical Bridge #4, Stallings/Yoo Methodology, IG 2LL, Variable = PBFTG Size

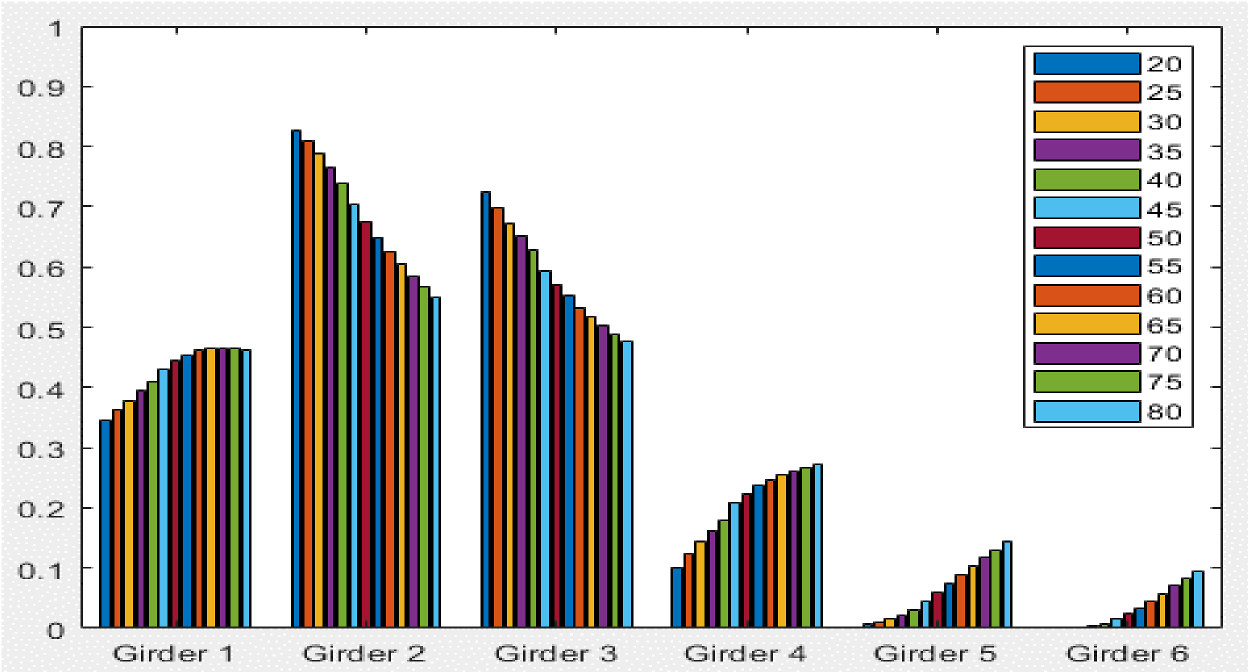

Typical Bridge #4, Stallings/Yoo Methodology, IG 2LL, Variable = Span Length (ft)

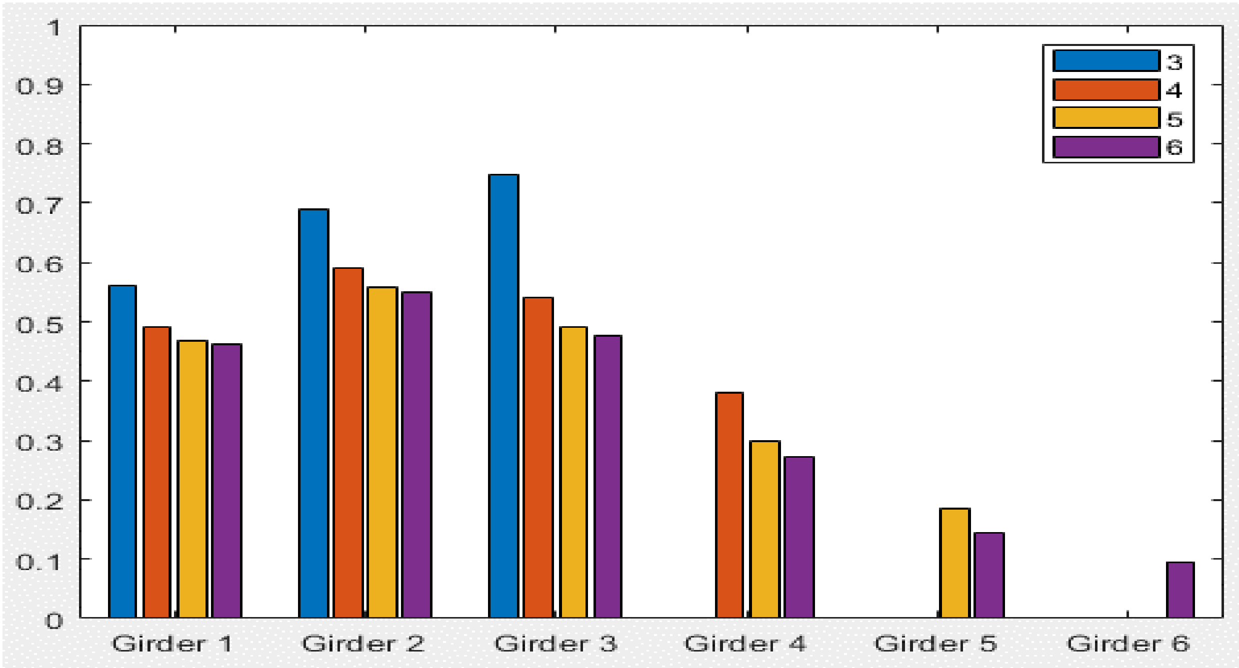

Typical Bridge #4, Stallings/Yoo Methodology, IG 2LL, Variable = Number of Girders

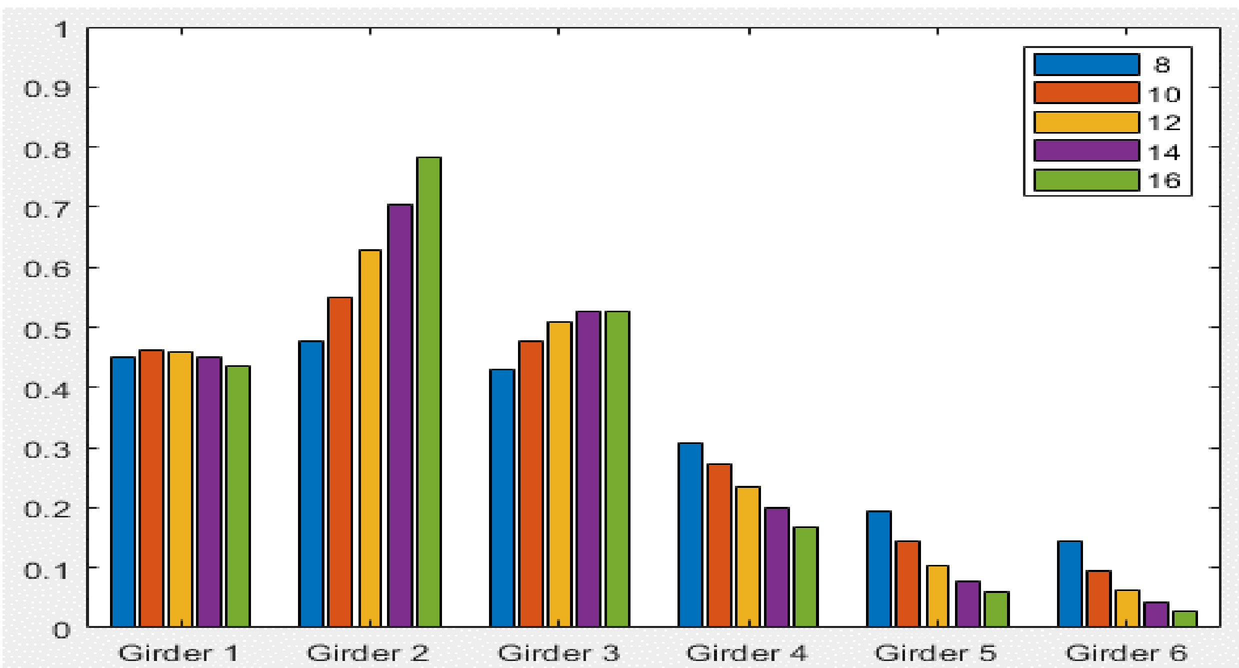

Typical Bridge #4, Stallings/Yoo Methodology, IG 2LL, Variable = Girder Spacing (ft)

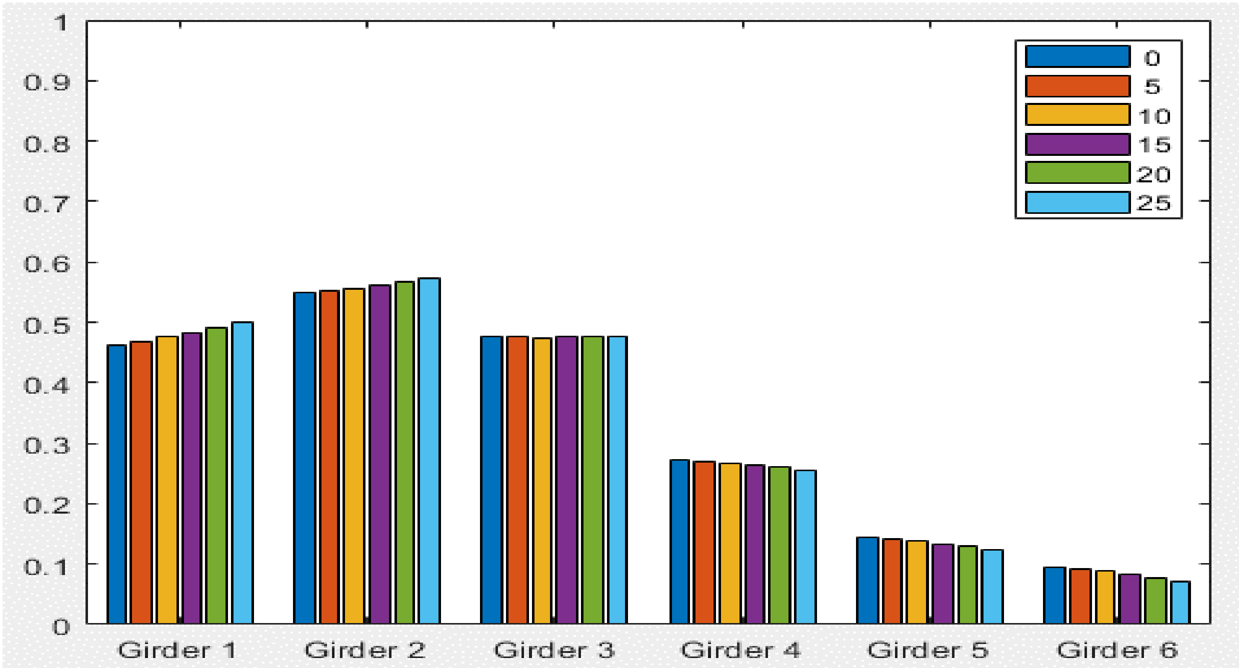

Typical Bridge #4, Stallings/Yoo Methodology, IG 2LL, Variable = Degree of Skew (deg)

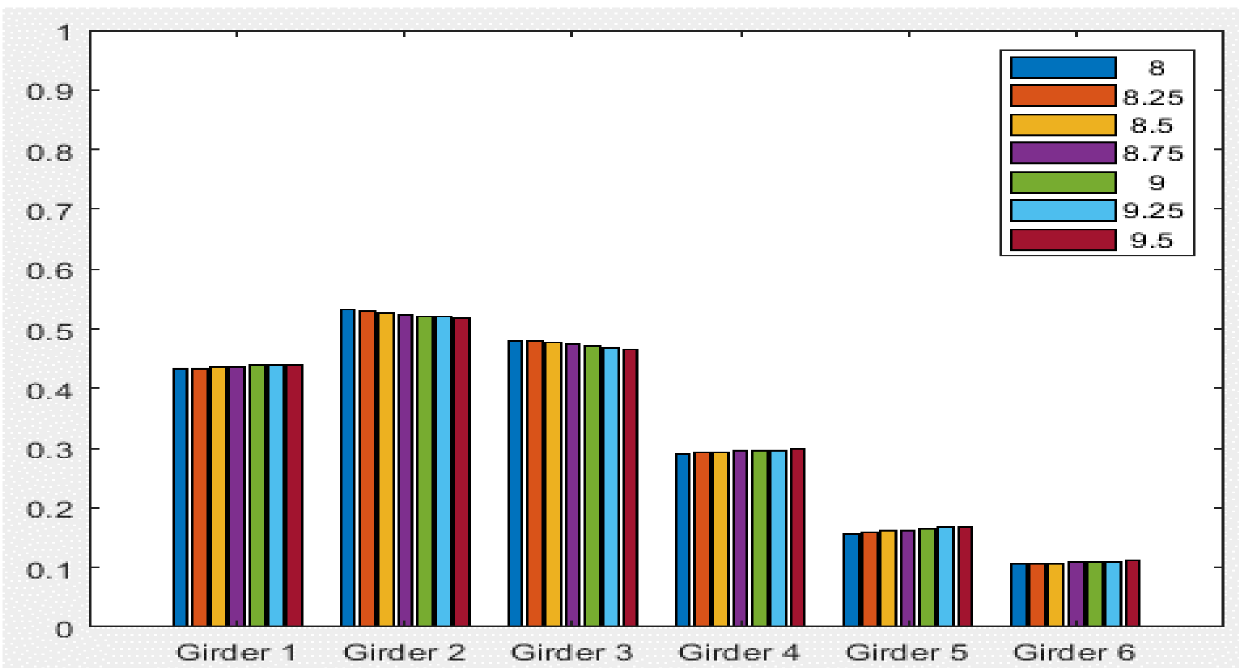

Typical Bridge #4, Stallings/Yoo Methodology, IG 2LL, Variable = Deck Thickness (in)

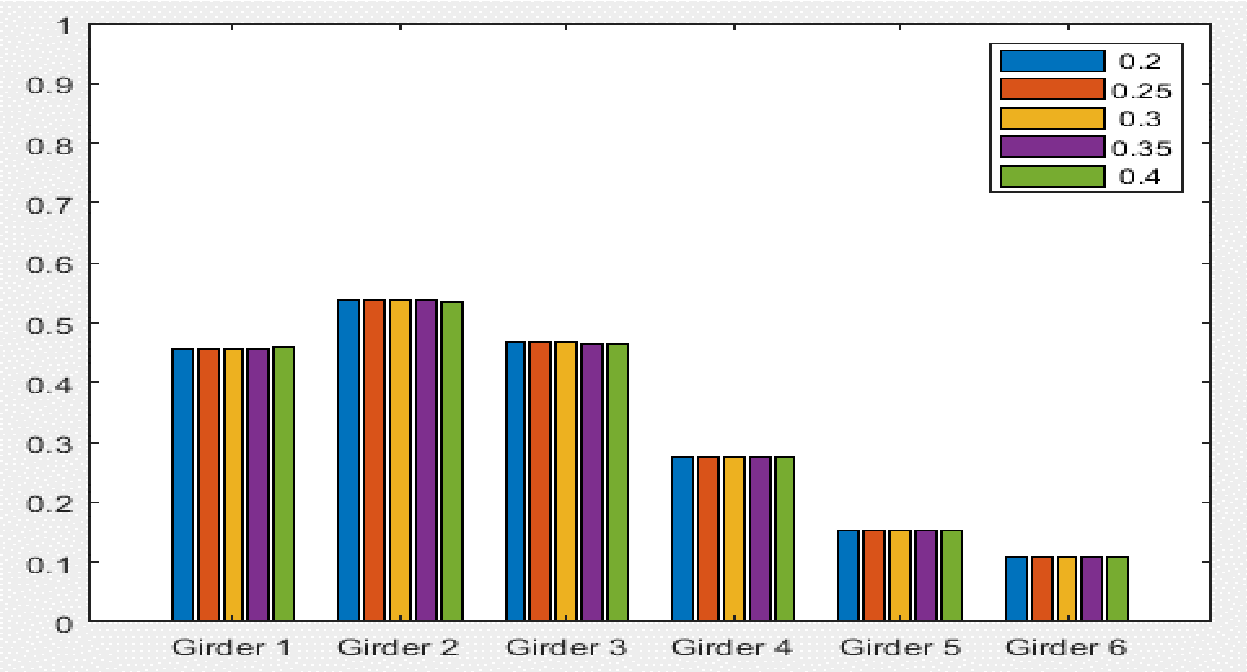

Typical Bridge #4, Stallings/Yoo Methodology, IG 2LL, Variable = Overhang Ratio

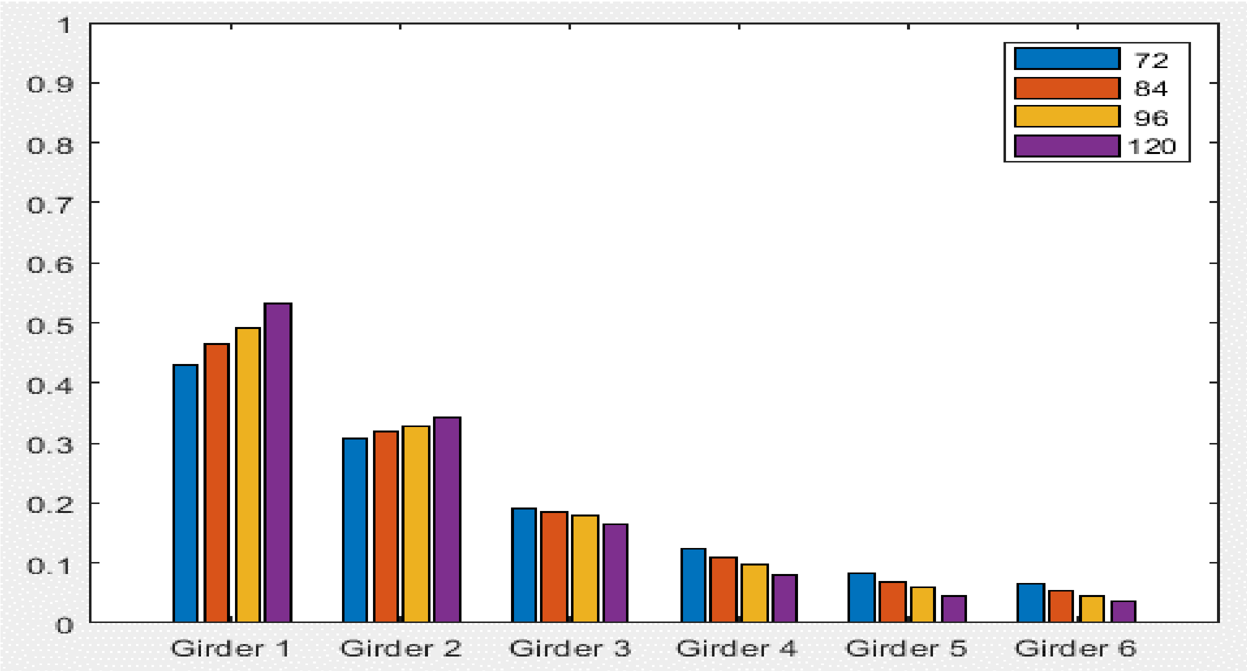

Typical Bridge #4, Stallings/Yoo Methodology, EG OLL, Variable = PBFTG Size

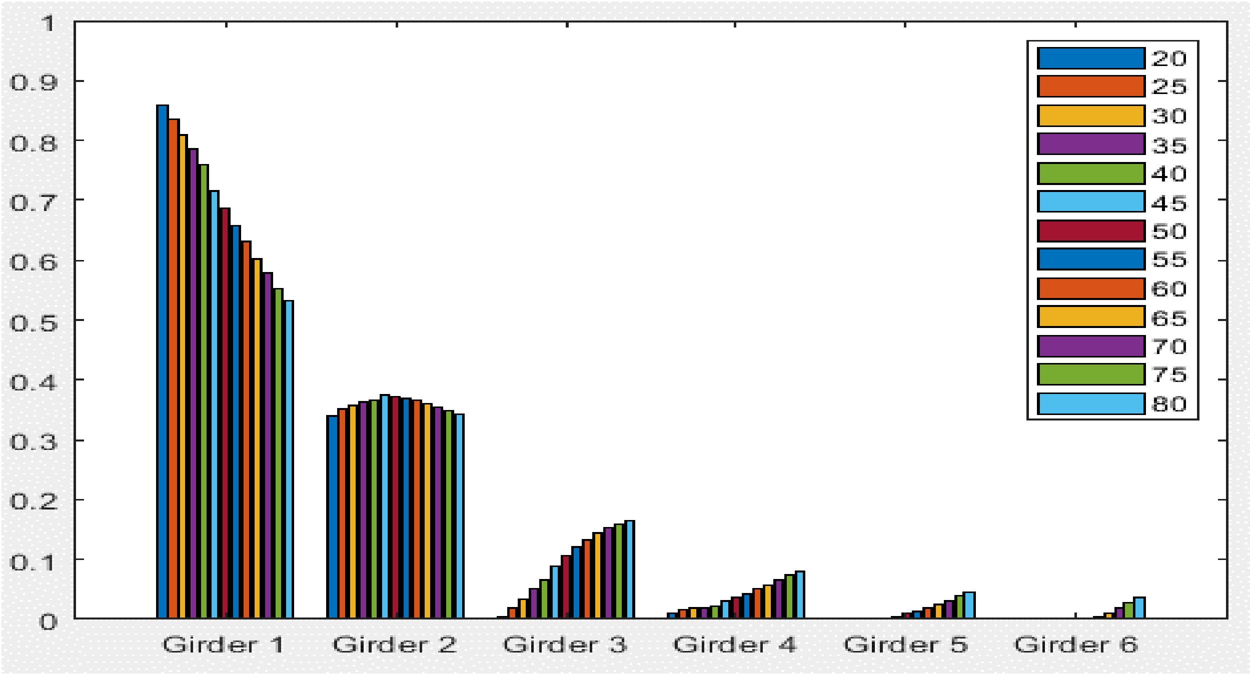

Typical Bridge #4, Stallings/Yoo Methodology, EG OLL, Variable = Span Length (ft)

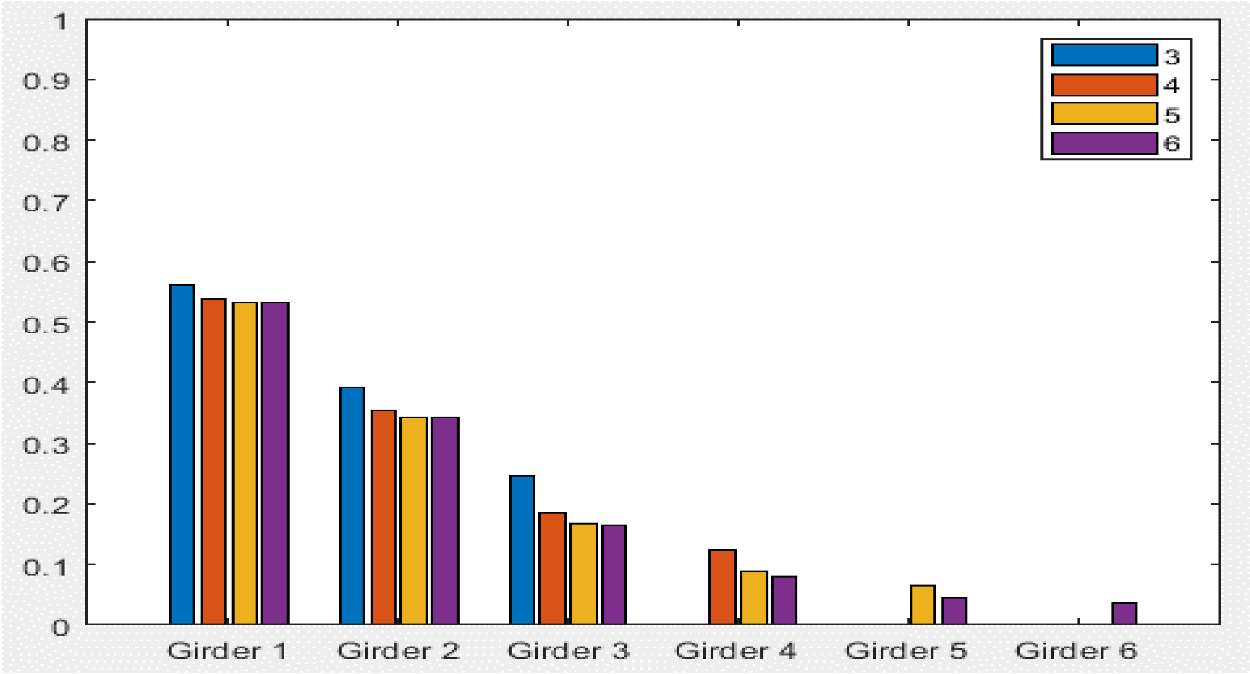

Typical Bridge #4, Stallings/Yoo Methodology, EG OLL, Variable = Number of Girders

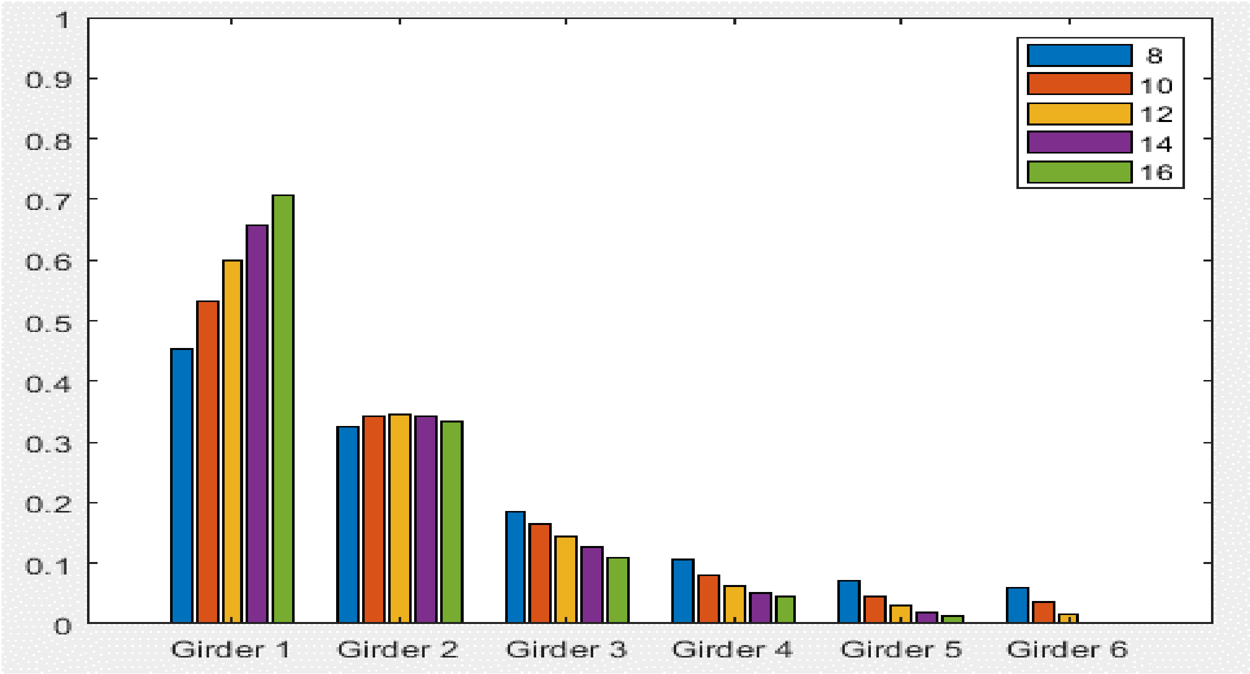

Typical Bridge #4, Stallings/Yoo Methodology, EG OLL, Variable = Girder Spacing (ft)

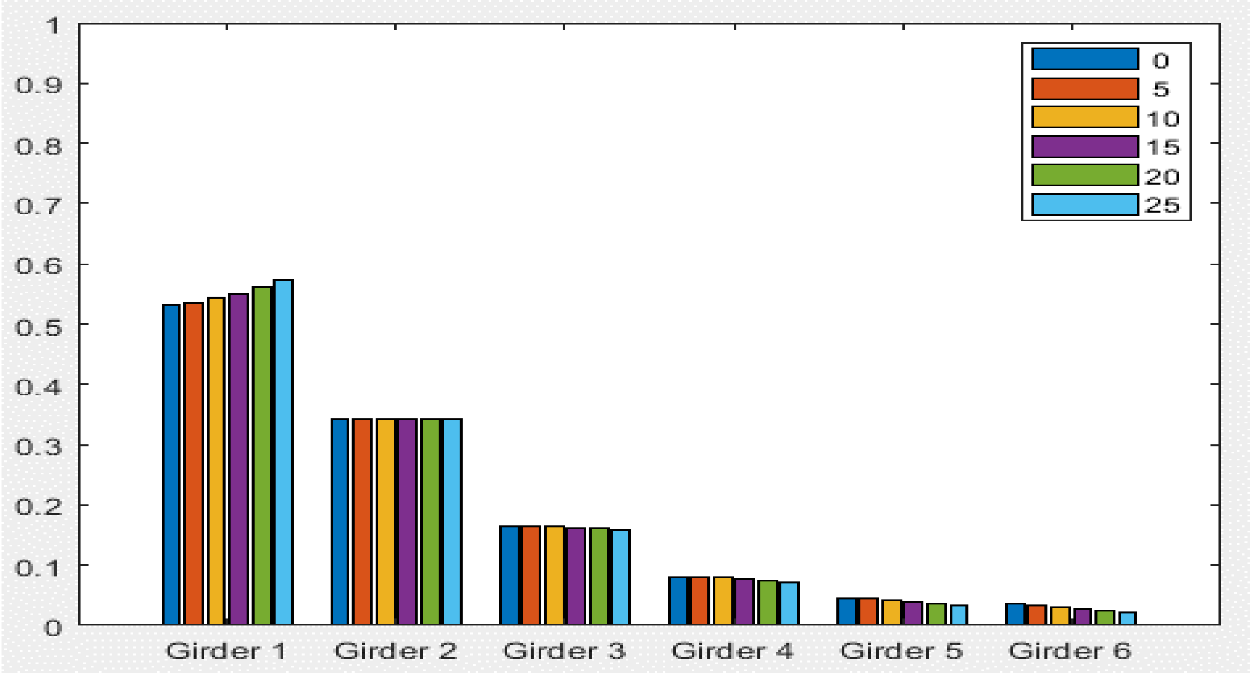

Typical Bridge #4, Stallings/Yoo Methodology, EG OLL, Variable = Degree of Skew (deg)

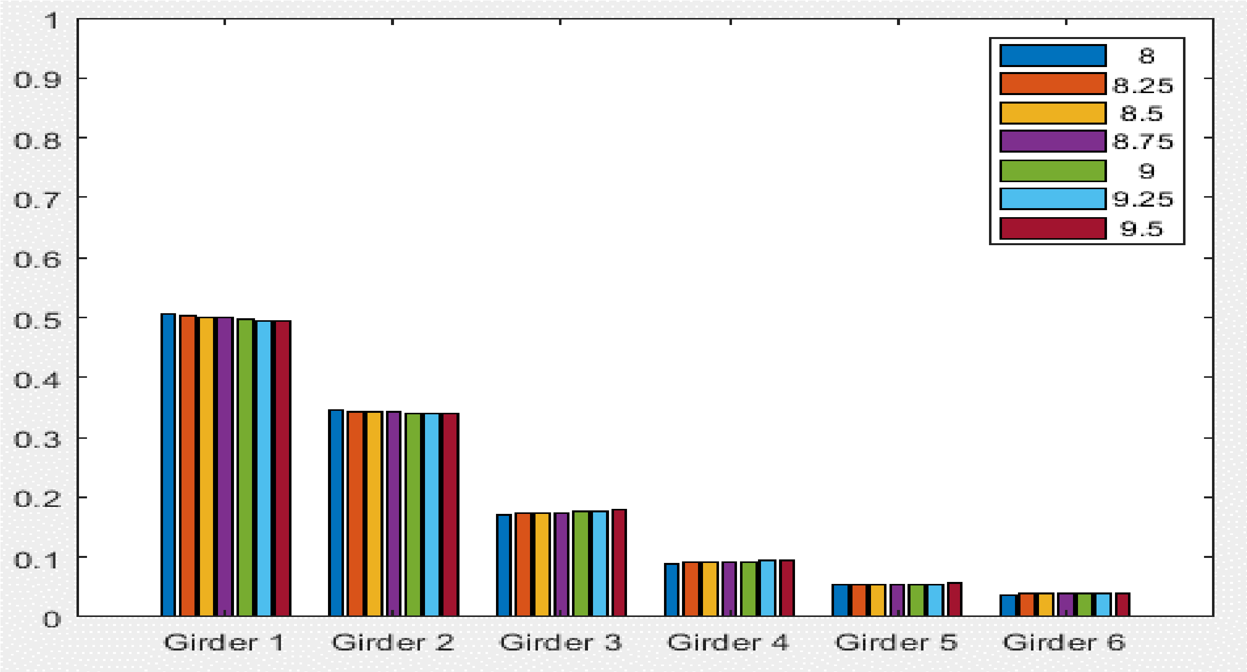

Typical Bridge #4, Stallings/Yoo Methodology, EG OLL, Variable = Deck Thickness (in)

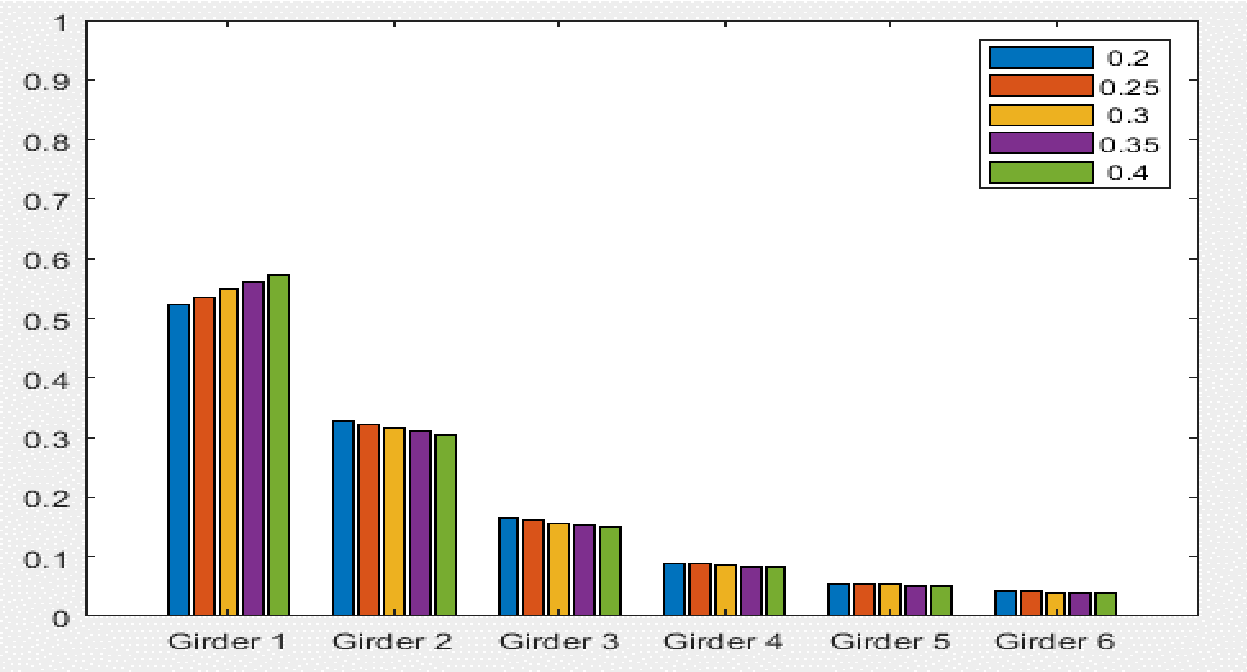

Typical Bridge #4, Stallings/Yoo Methodology, EG OLL, Variable = Overhang Ratio

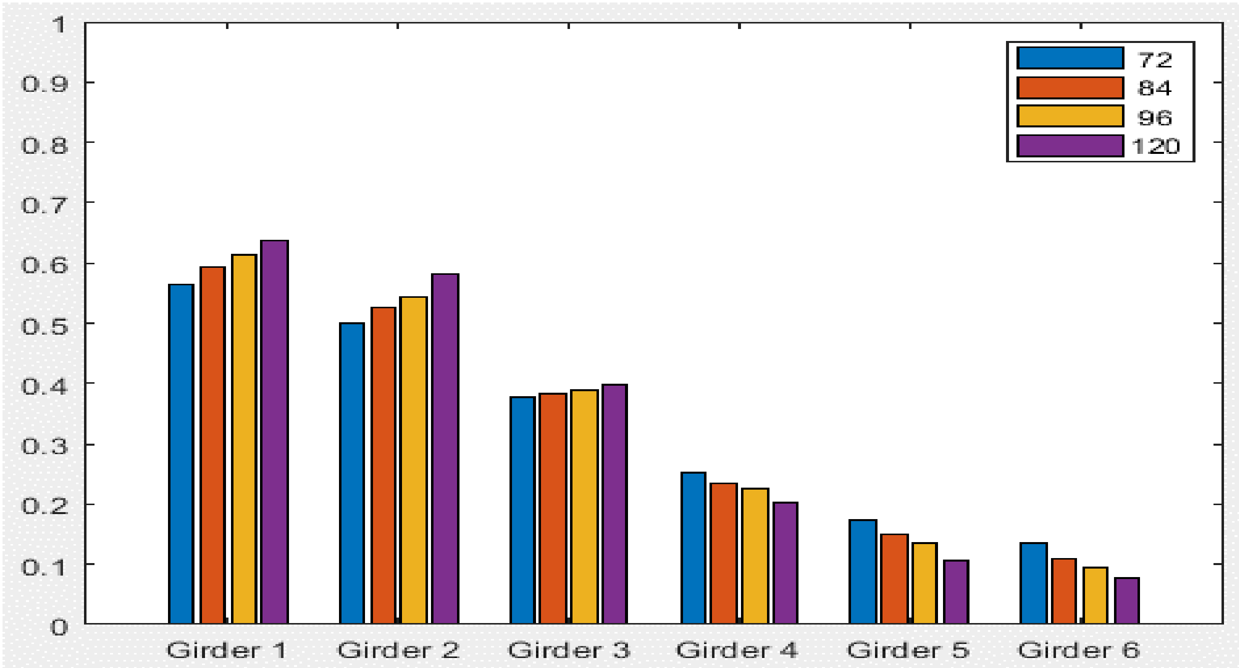

Typical Bridge #4, Stallings/Yoo Methodology, EG 2LL, Variable = PBFTG Size

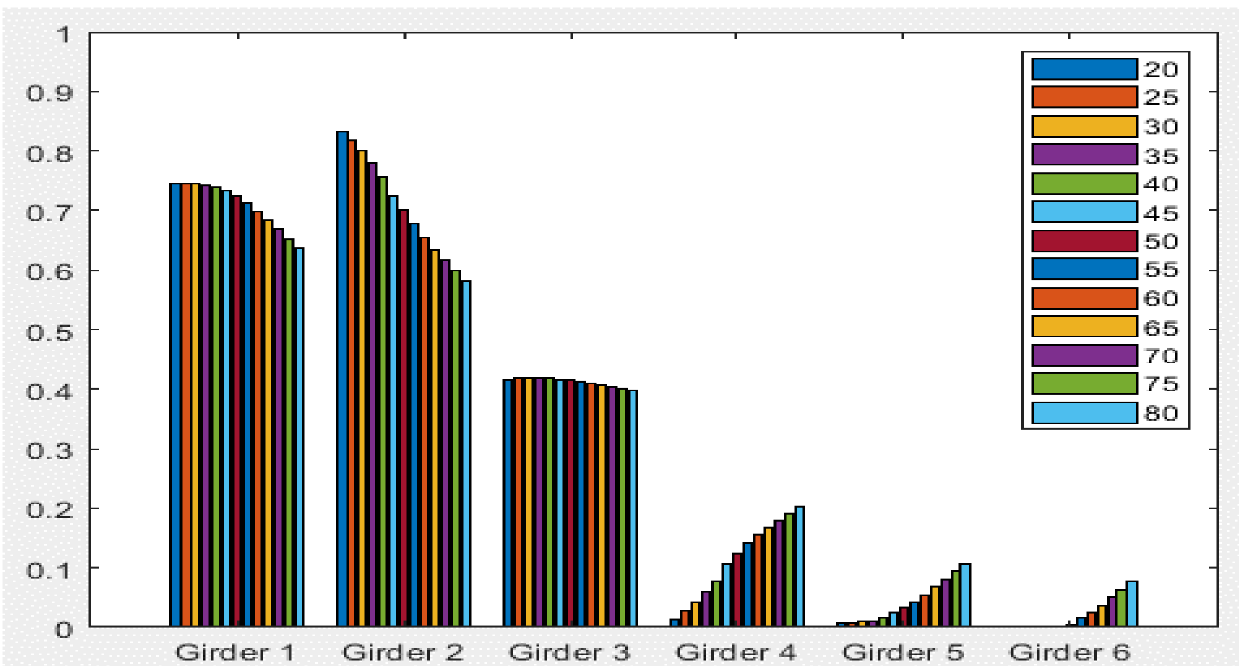

Typical Bridge #4, Stallings/Yoo Methodology, EG 2LL, Variable = Span Length (ft)

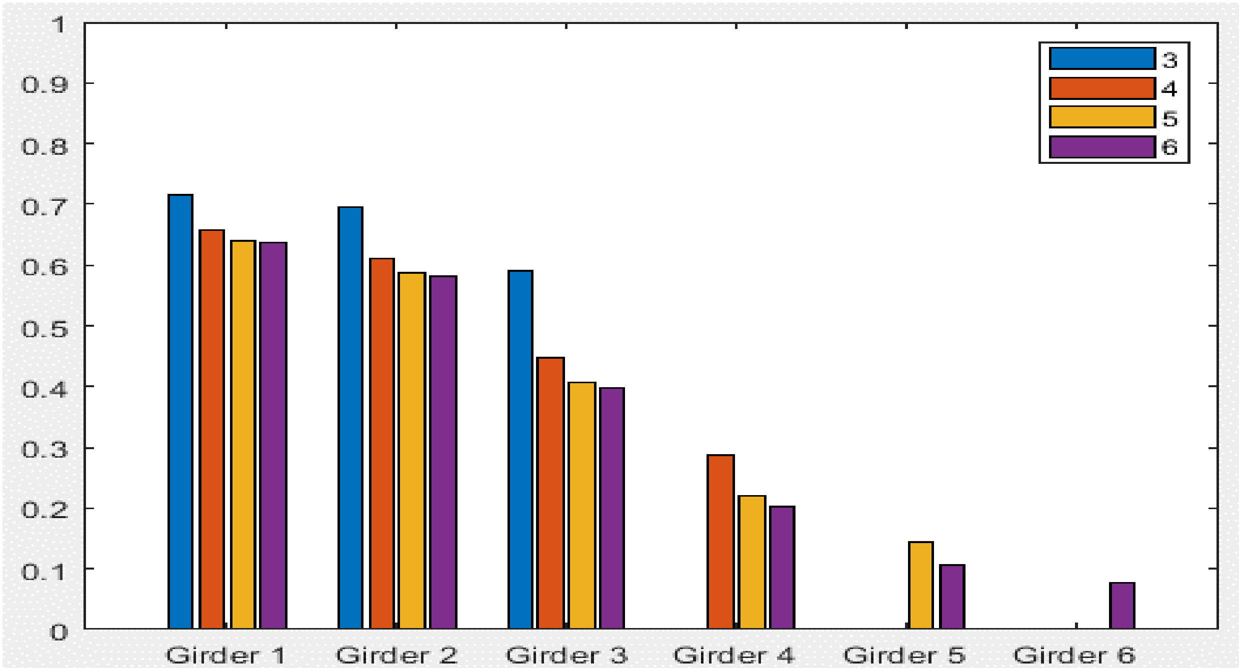

Typical Bridge #4, Stallings/Yoo Methodology, EG 2LL, Variable = Number of Girders

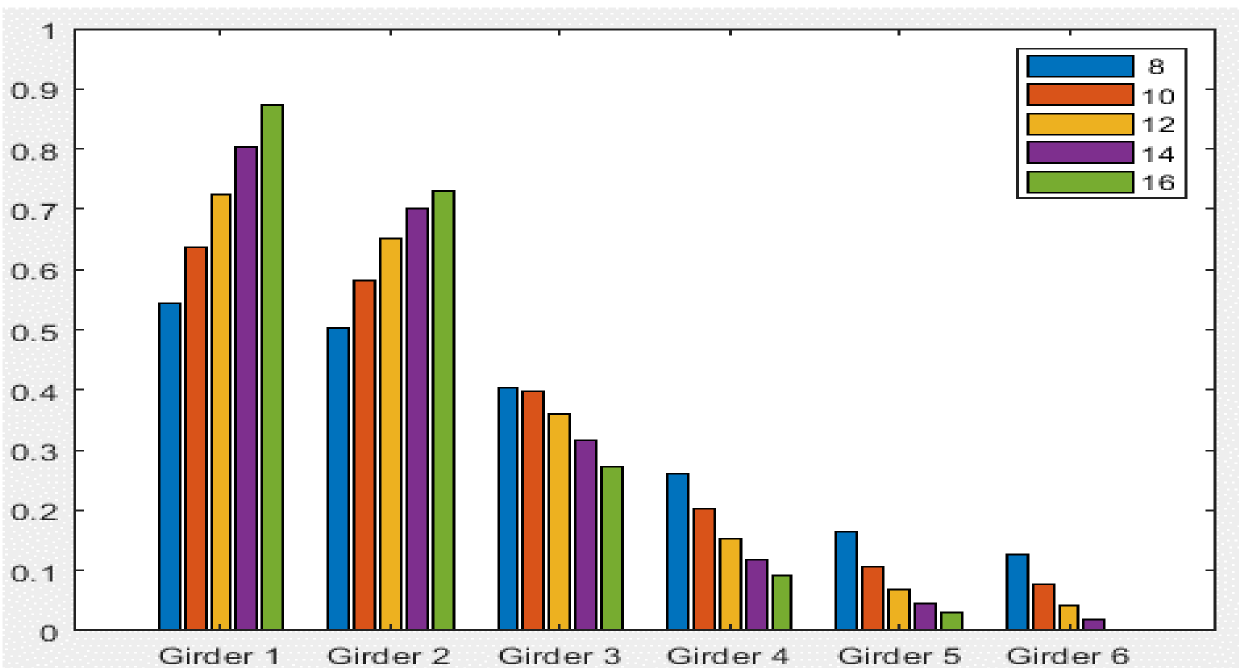

Typical Bridge #4, Stallings/Yoo Methodology, EG 2LL, Variable = Girder Spacing (ft)

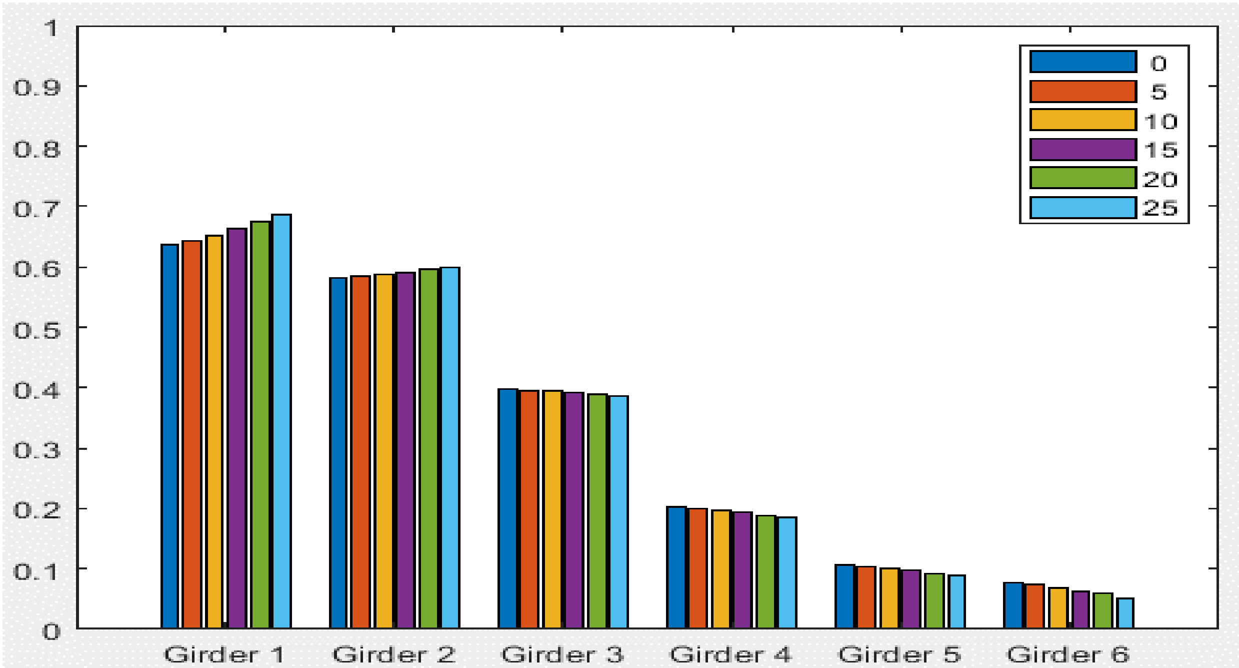

Typical Bridge #4, Stallings/Yoo Methodology, EG 2LL, Variable = Degree of Skew (deg)

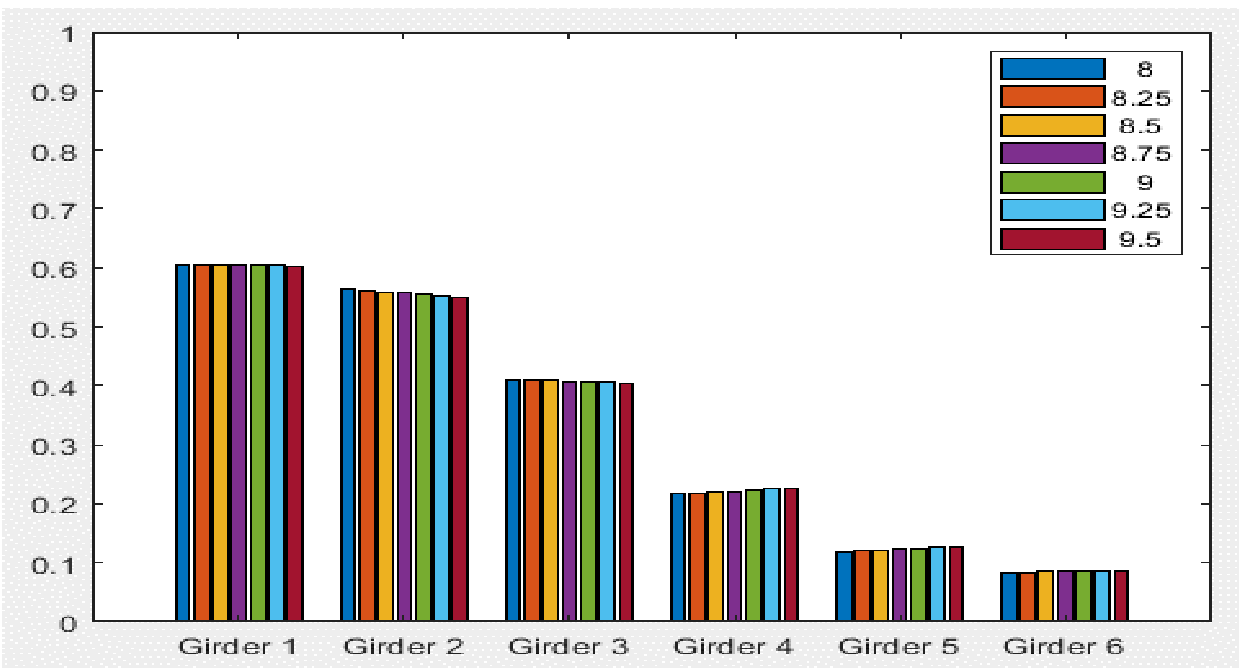

Typical Bridge #4, Stallings/Yoo Methodology, EG 2LL, Variable = Deck Thickness (in)

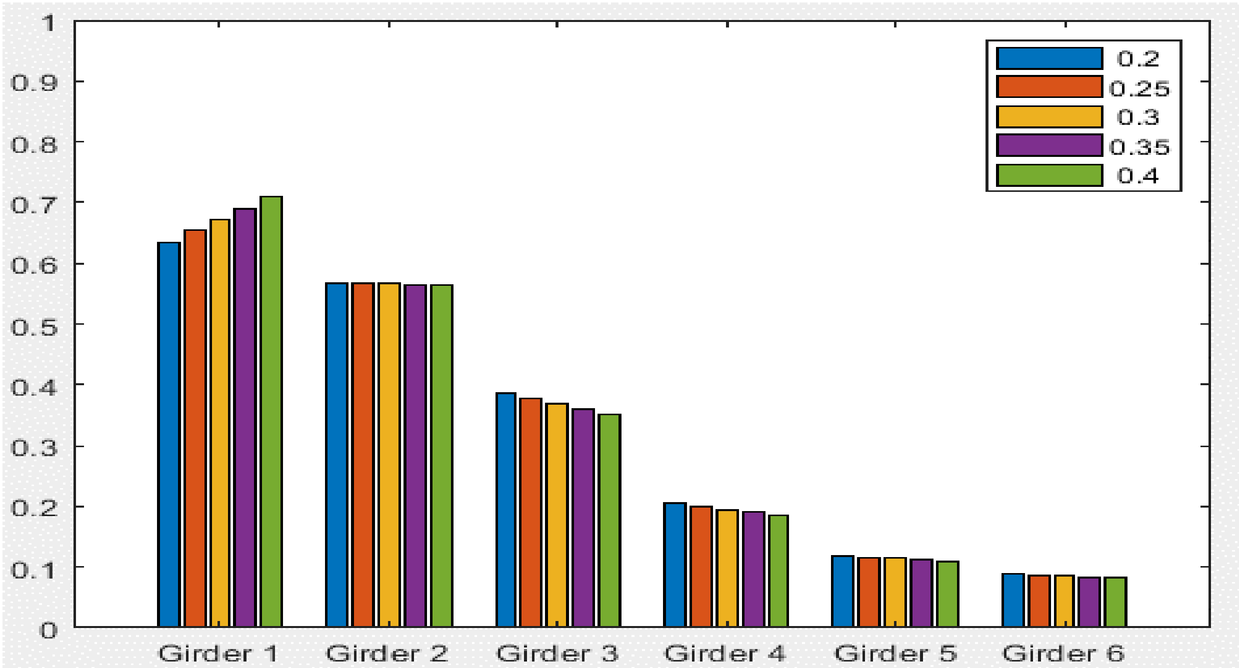

Typical Bridge #4, Stallings/Yoo Methodology, EG 2LL, Variable = Overhang Ratio

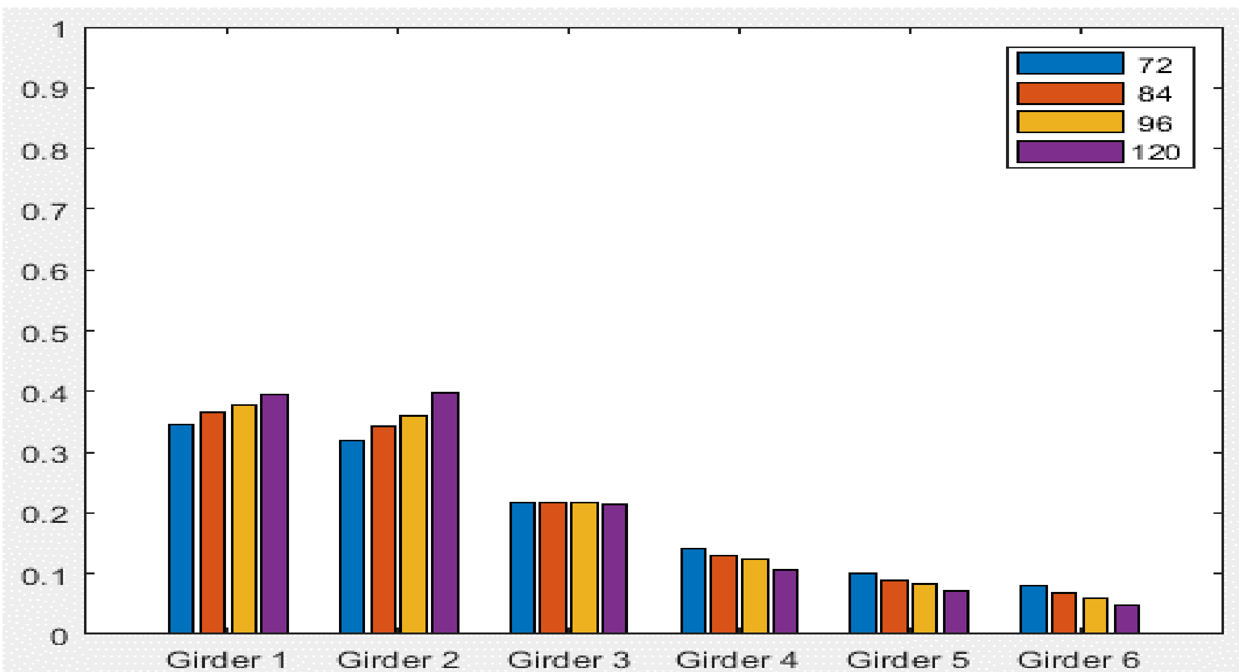

Typical Bridge #4, Tarhini/Frederick Methodology, IG OLL, Variable = PBFTG Size

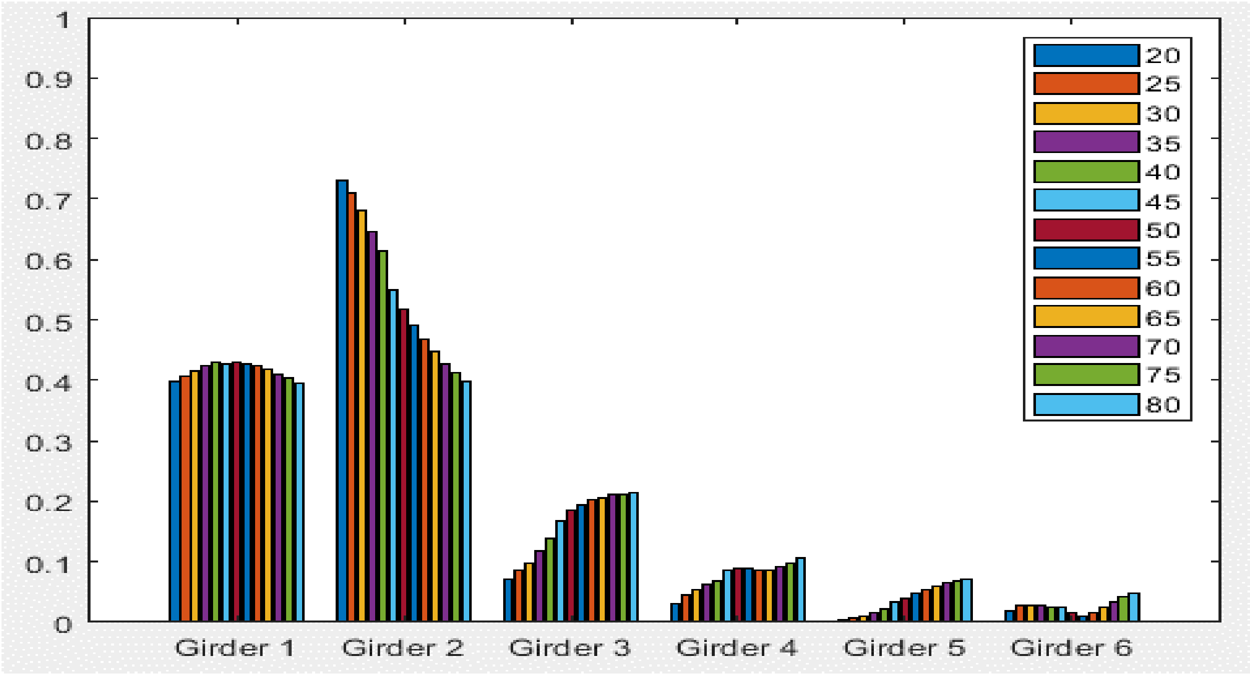

Typical Bridge #4, Tarhini/Frederick Methodology, IG OLL, Variable = Span Length (ft)

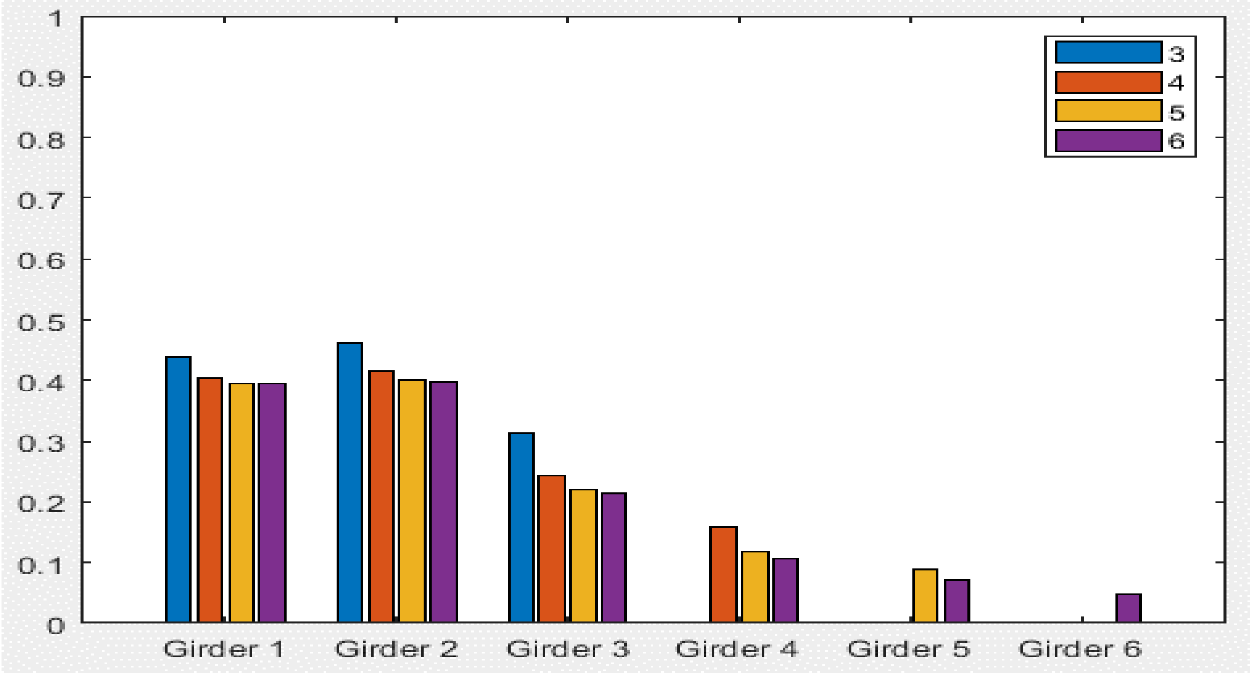

Typical Bridge #4, Tarhini/Frederick Methodology, IG OLL, Variable = Number of Girders

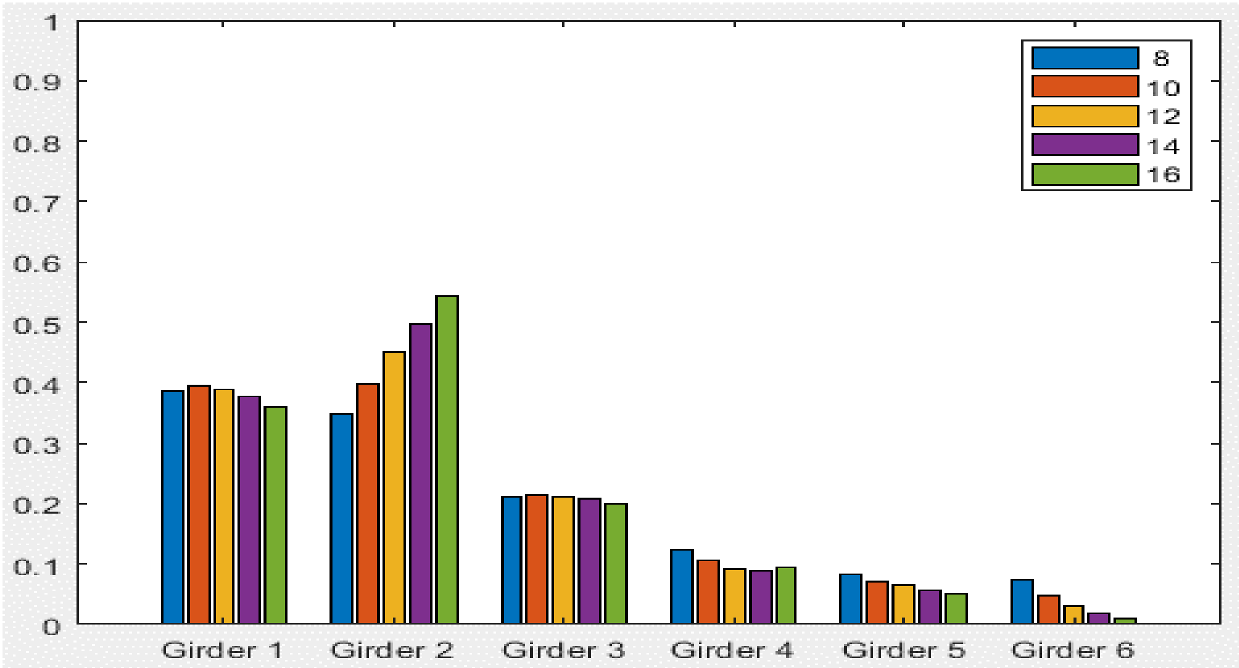

Typical Bridge #4, Tarhini/Frederick Methodology, IG OLL, Variable = Girder Spacing (ft)

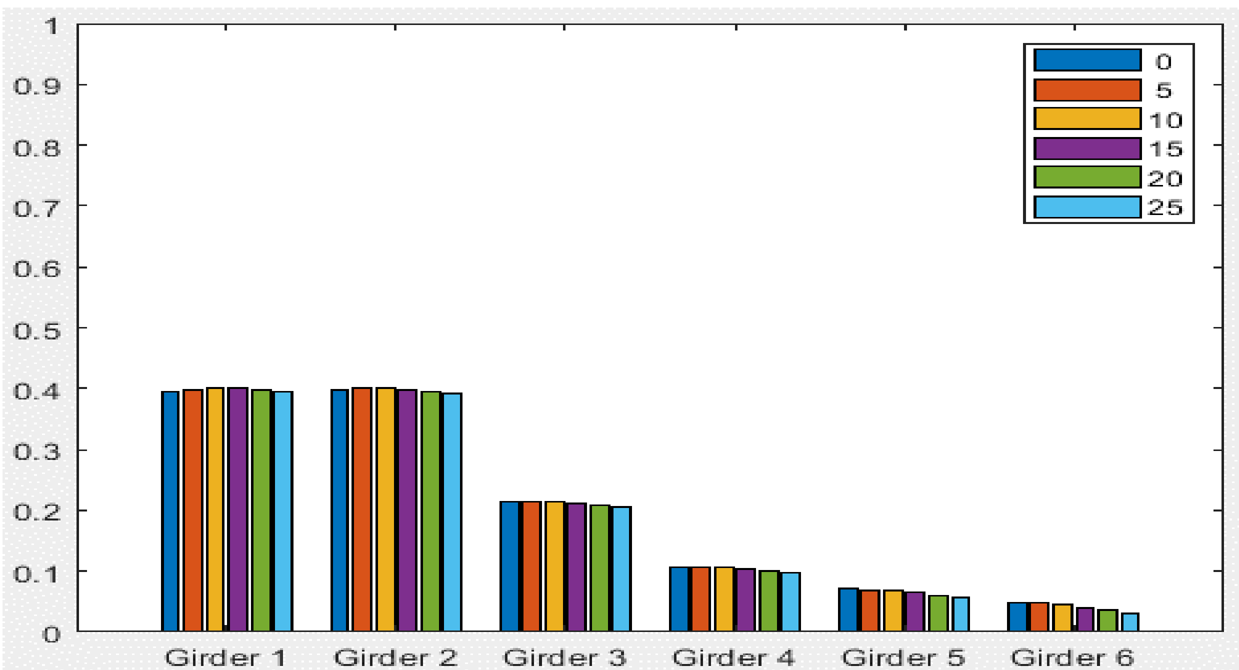

Typical Bridge #4, Tarhini/Frederick Methodology, IG OLL, Variable = Degree of Skew (deg)

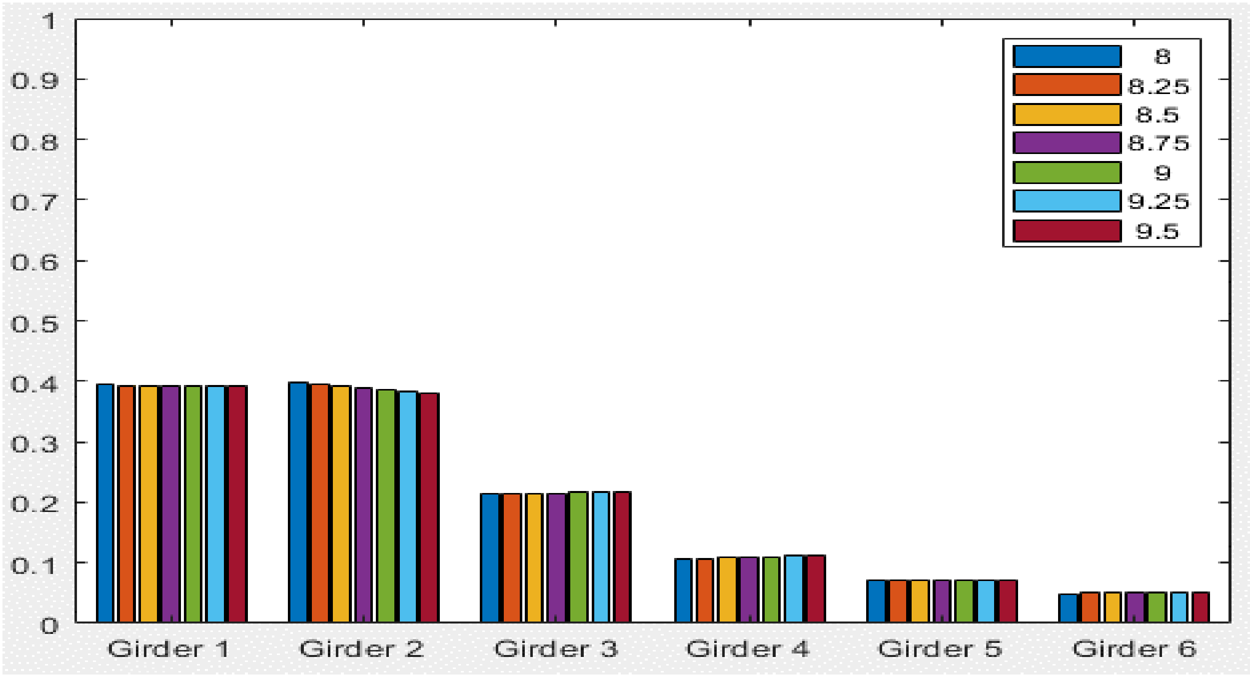

Typical Bridge #4, Tarhini/Frederick Methodology, IG OLL, Variable = Deck Thickness (in)

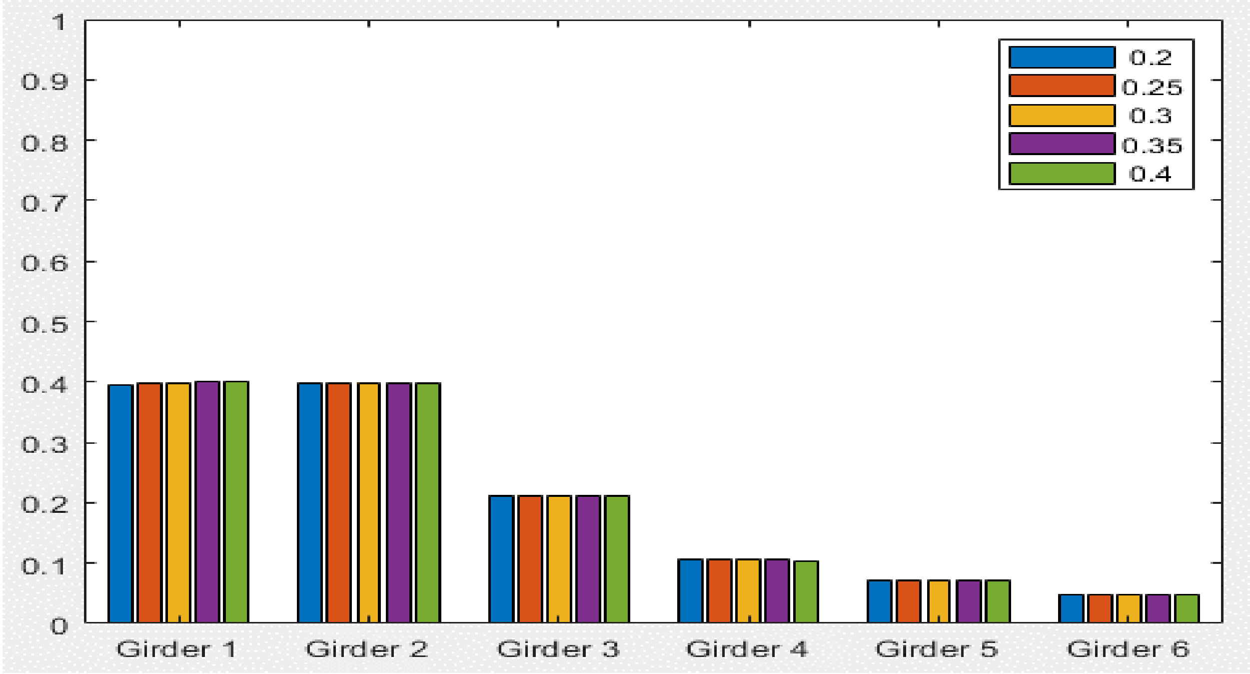

Typical Bridge #4, Tarhini/Frederick Methodology, IG OLL, Variable = Overhang Ratio

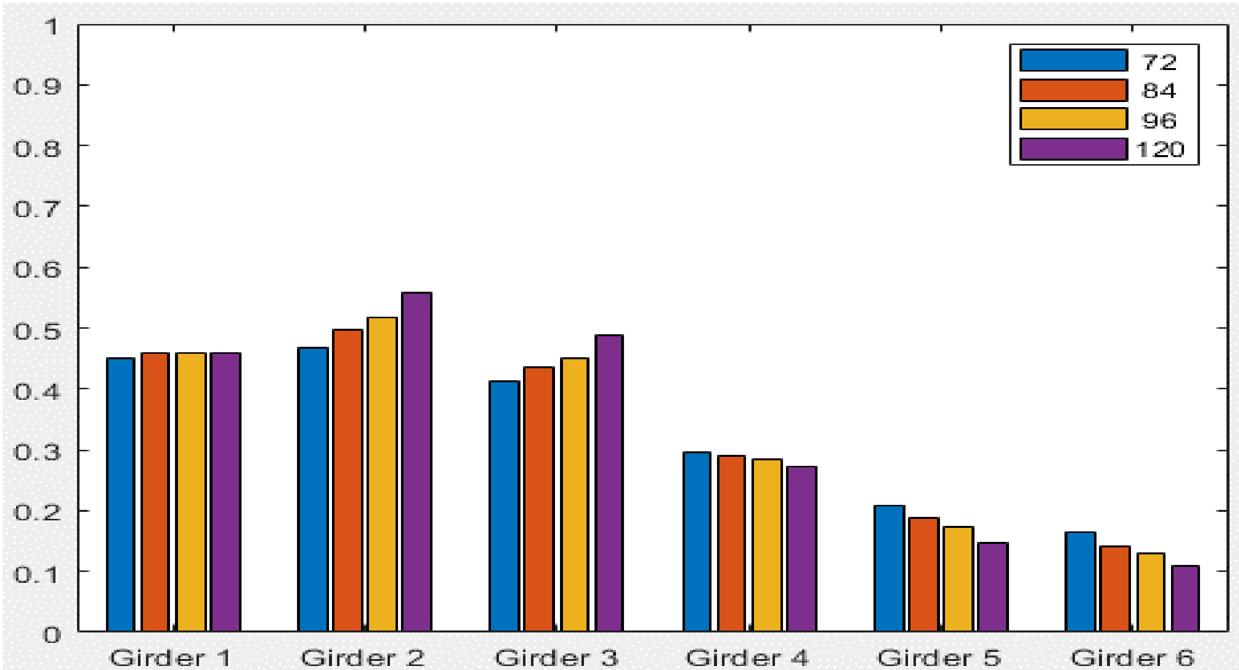

Typical Bridge #4, Tarhini/Frederick Methodology, IG 2LL, Variable = PBFTG Size

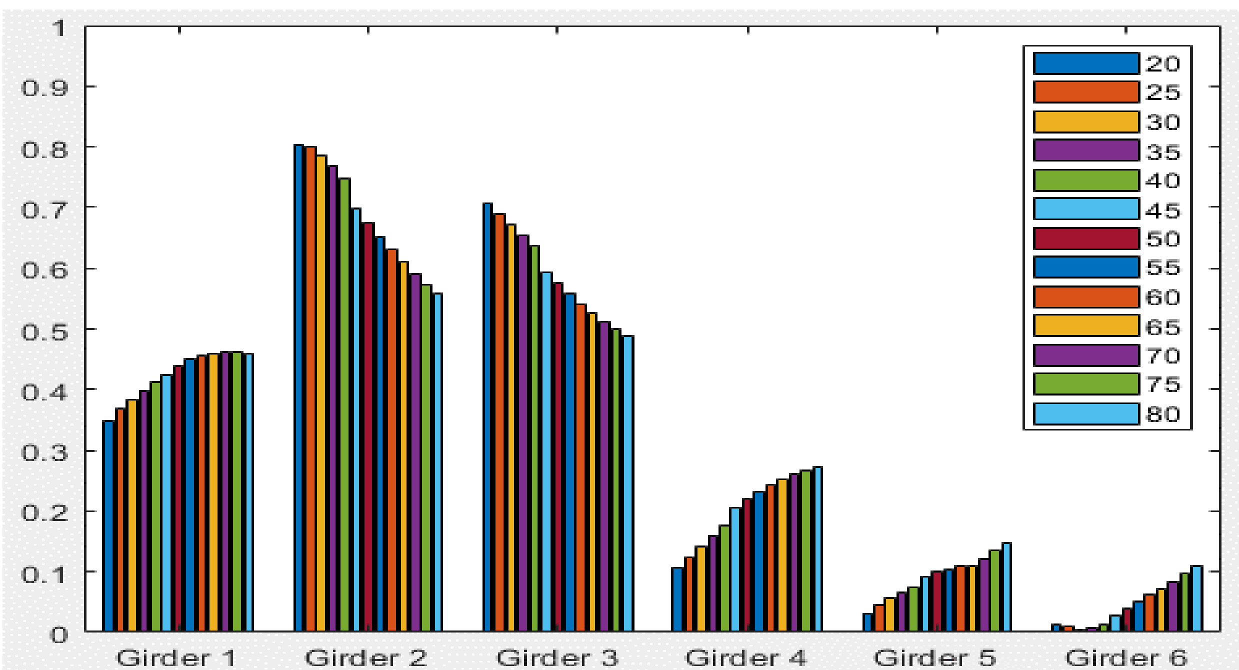

Typical Bridge #4, Tarhini/Frederick Methodology, IG 2LL, Variable = Span Length (ft)

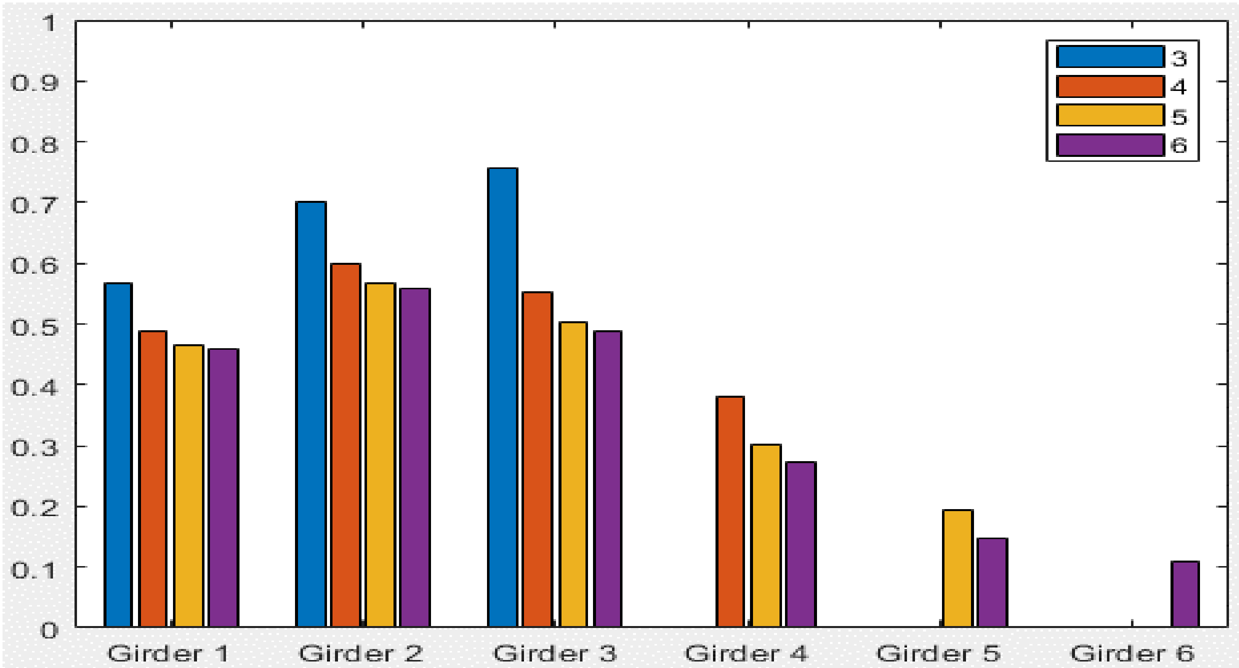

Typical Bridge #4, Tarhini/Frederick Methodology, IG 2LL, Variable = Number of Girders

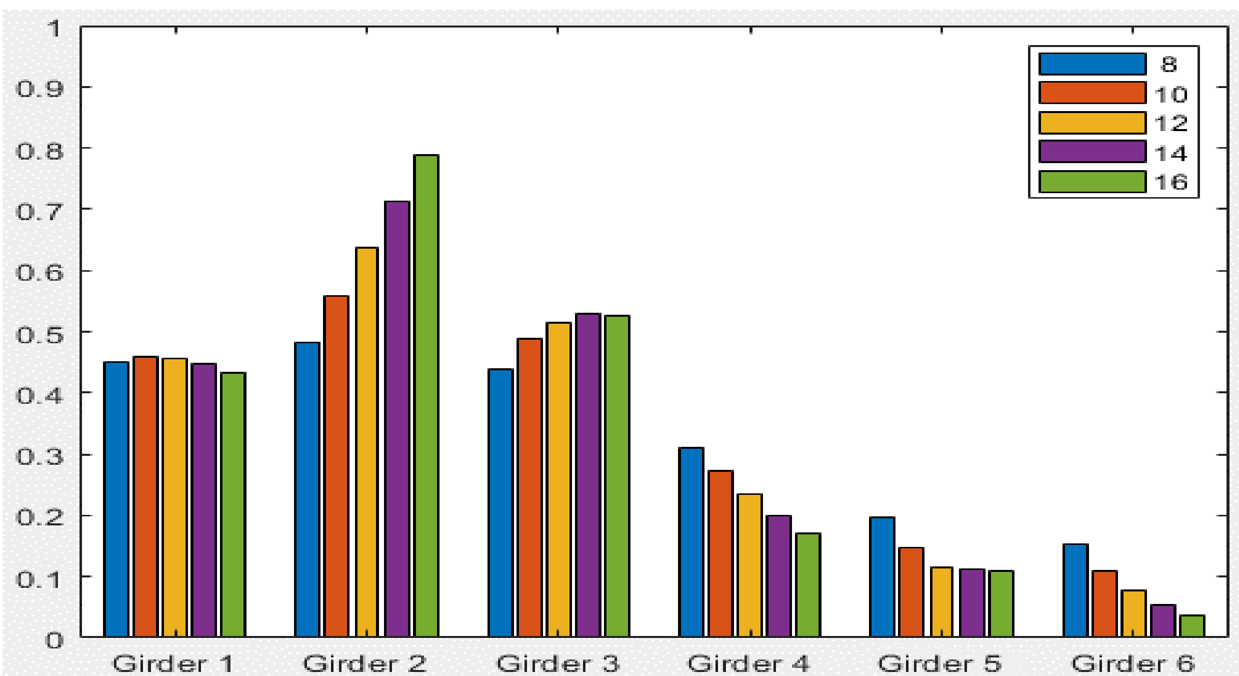

Typical Bridge #4, Tarhini/Frederick Methodology, IG 2LL, Variable = Girder Spacing (ft)

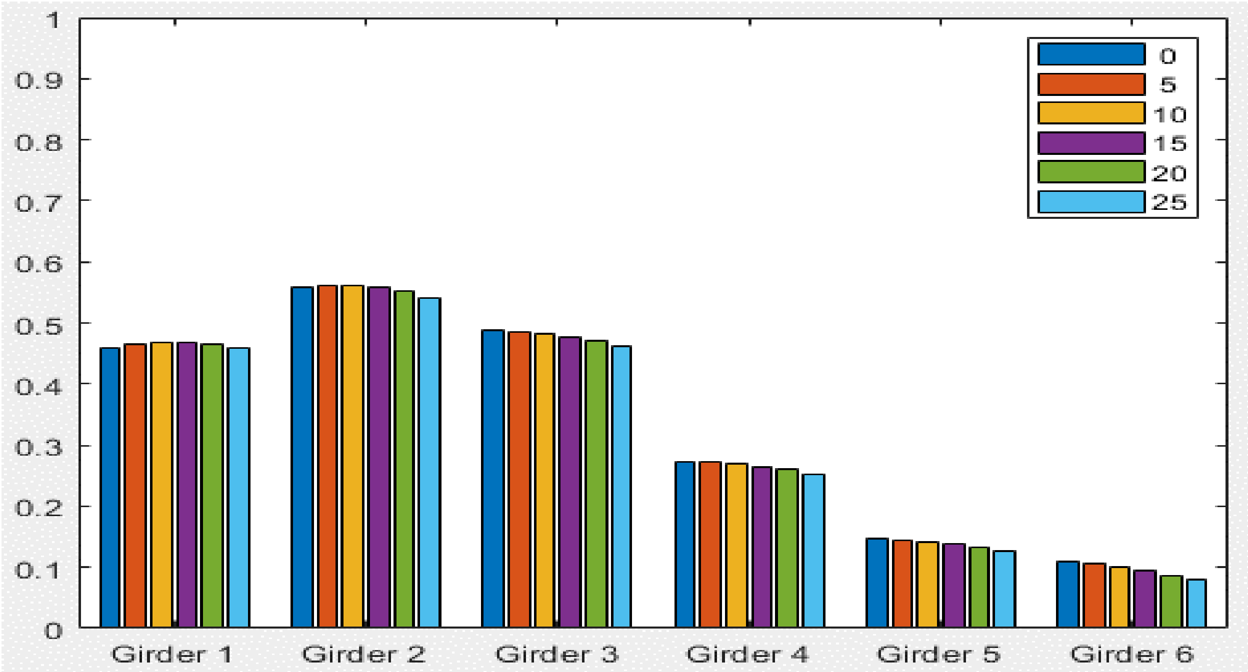

Typical Bridge #4, Tarhini/Frederick Methodology, IG 2LL, Variable = Degree of Skew (deg)

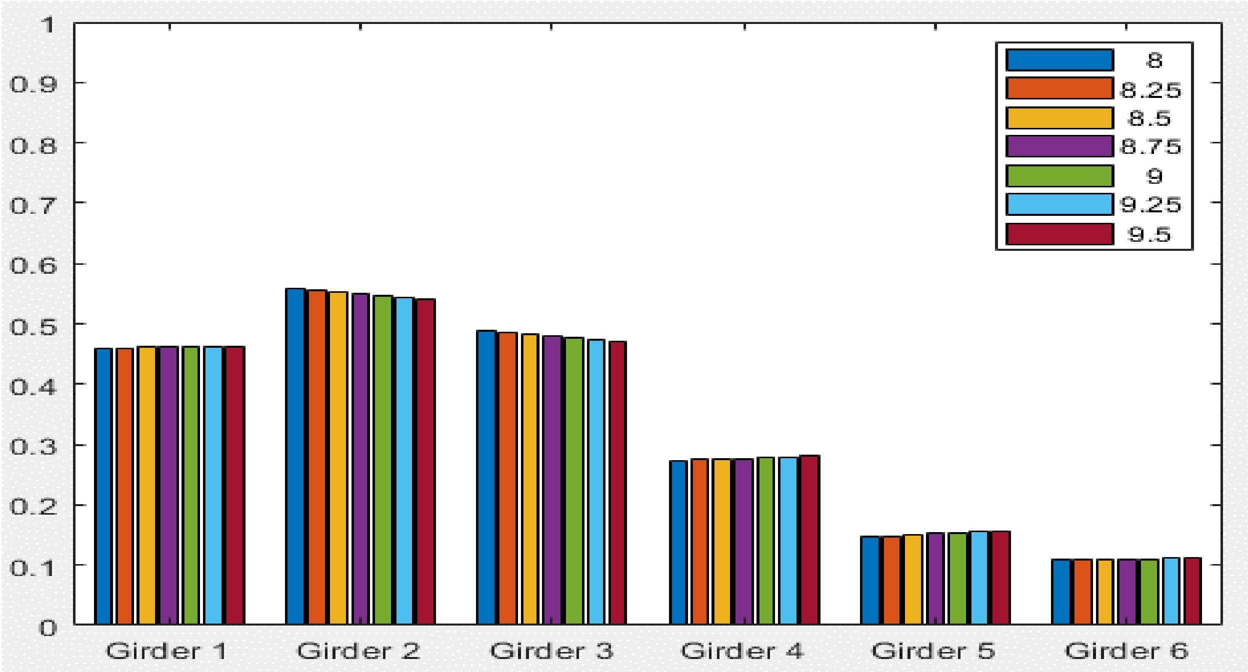

Typical Bridge #4, Tarhini/Frederick Methodology, IG 2LL, Variable = Deck Thickness (in)

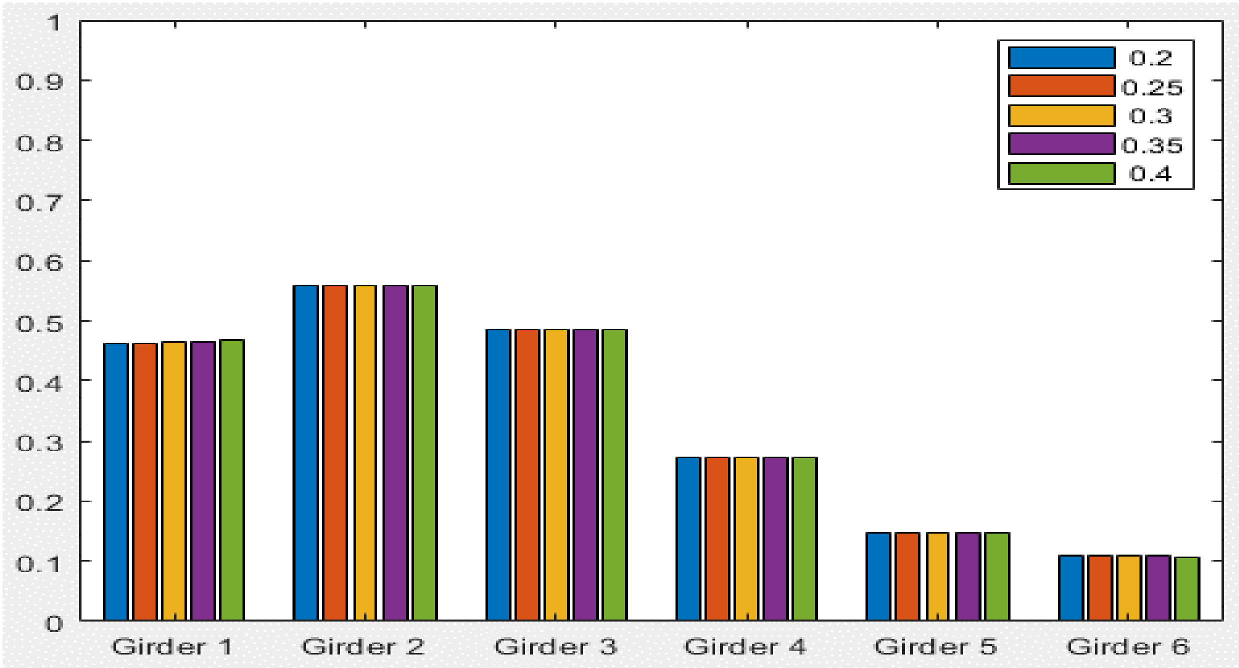

Typical Bridge #4, Tarhini/Frederick Methodology, IG 2LL, Variable = Overhang Ratio

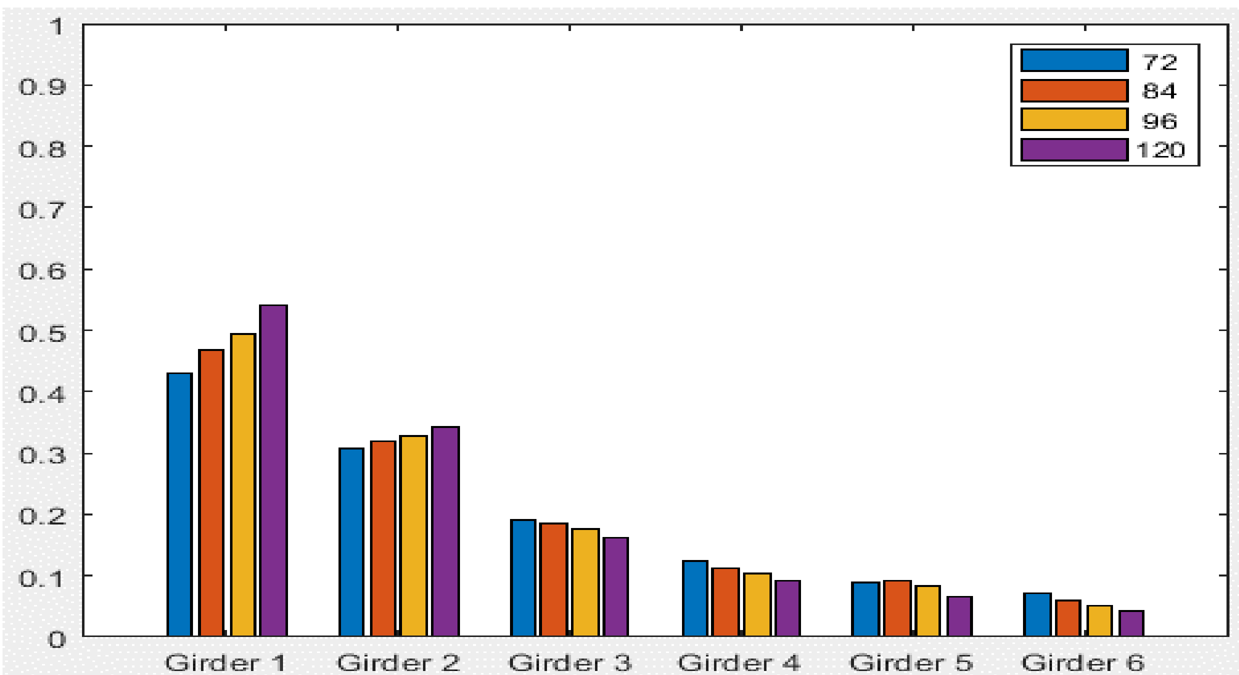

Typical Bridge #4, Tarhini/Frederick Methodology, EG OLL, Variable = PBFTG Size

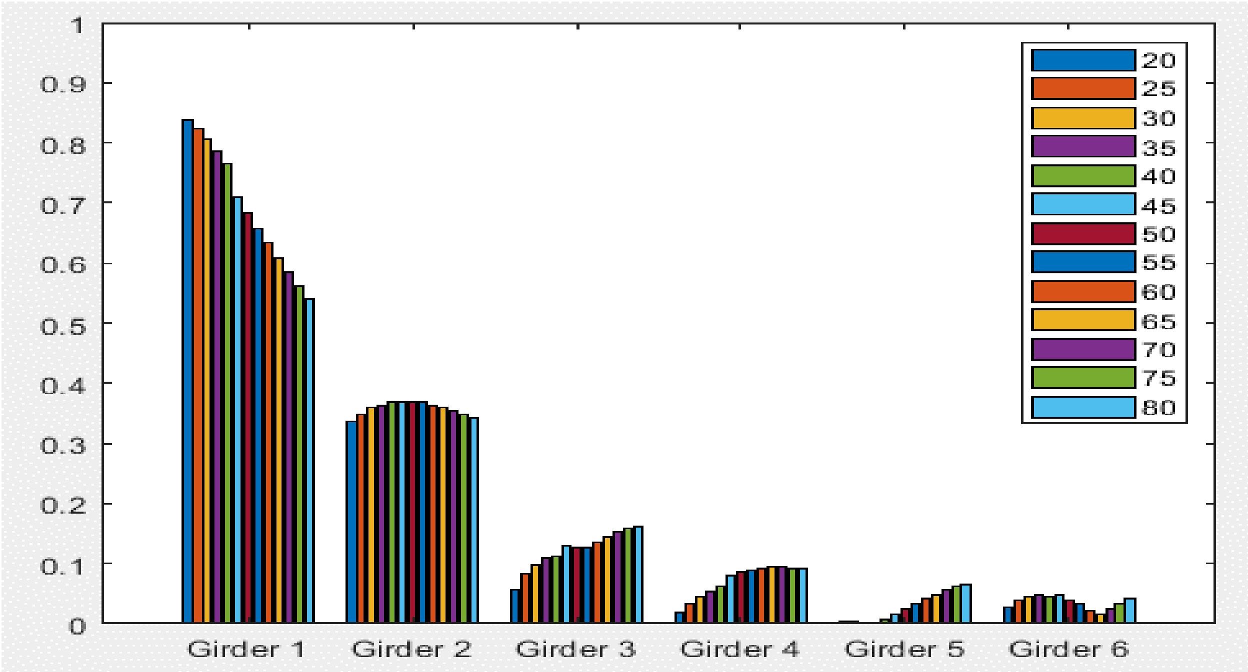

Typical Bridge #4, Tarhini/Frederick Methodology, EG OLL, Variable = Span Length (ft)

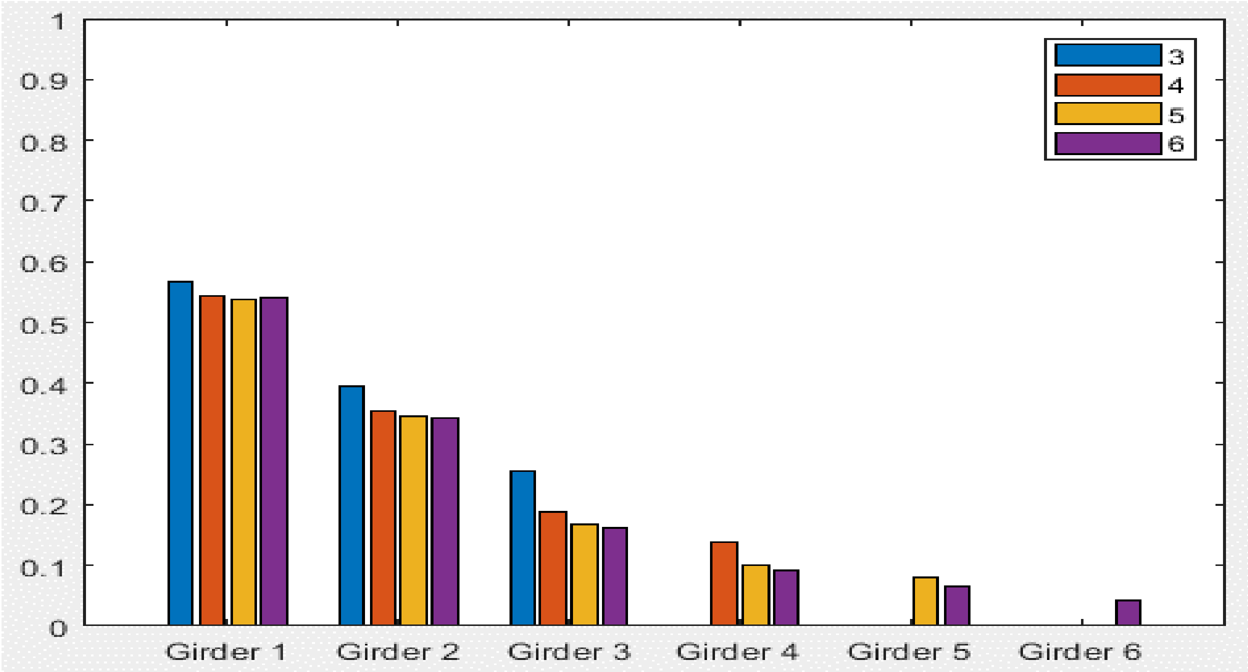

Typical Bridge #4, Tarhini/Frederick Methodology, EG OLL, Variable = Number of Girders

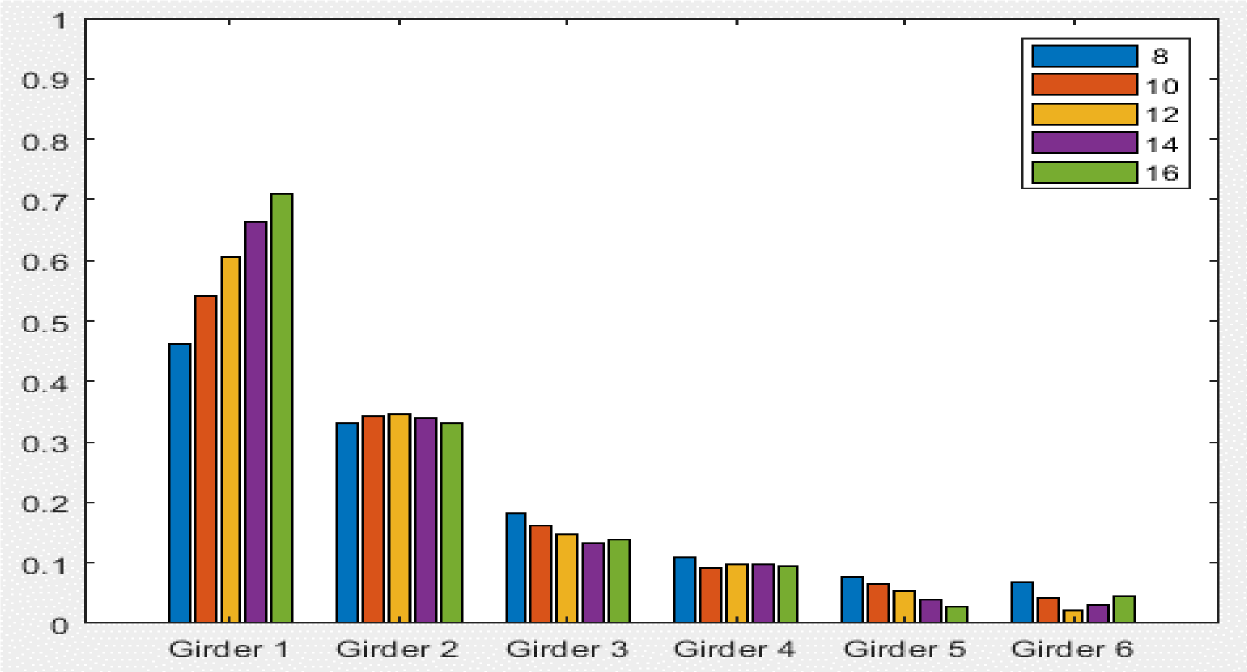

Typical Bridge #4, Tarhini/Frederick Methodology, EG OLL, Variable = Girder Spacing (ft)

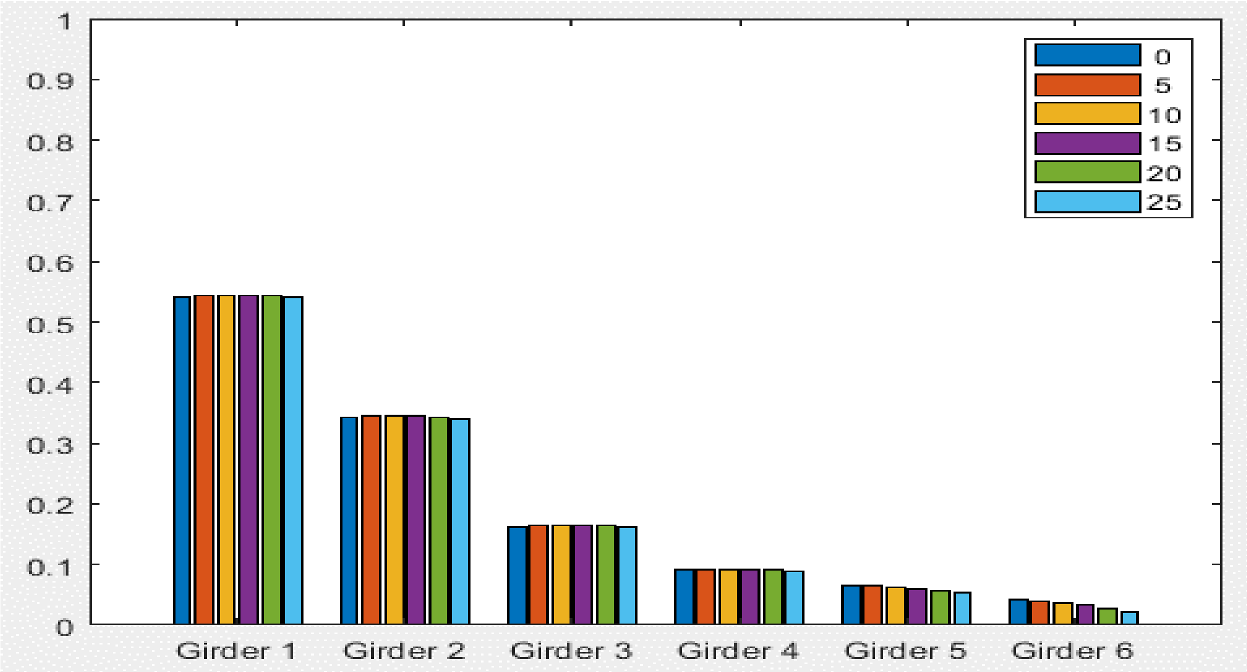

Typical Bridge #4, Tarhini/Frederick Methodology, EG OLL, Variable = Degree of Skew (deg)

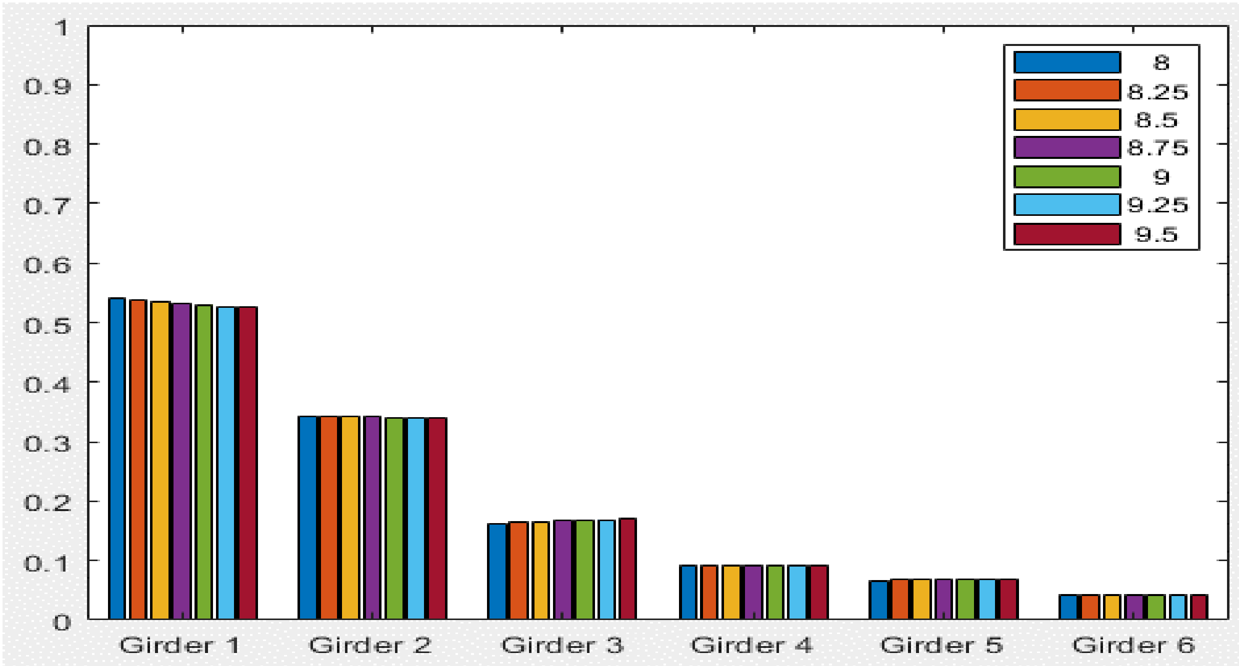

Typical Bridge #4, Tarhini/Frederick Methodology, EG OLL, Variable = Deck Thickness (in)

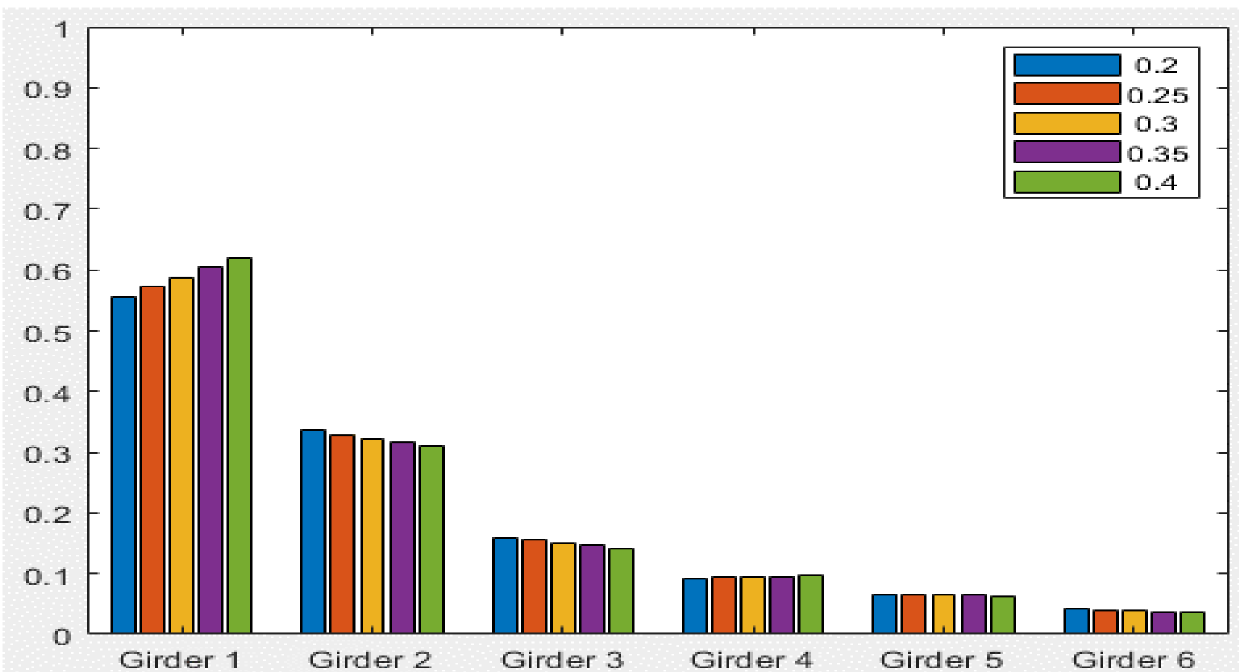

Typical Bridge #4, Tarhini/Frederick Methodology, EG OLL, Variable = Overhang Ratio

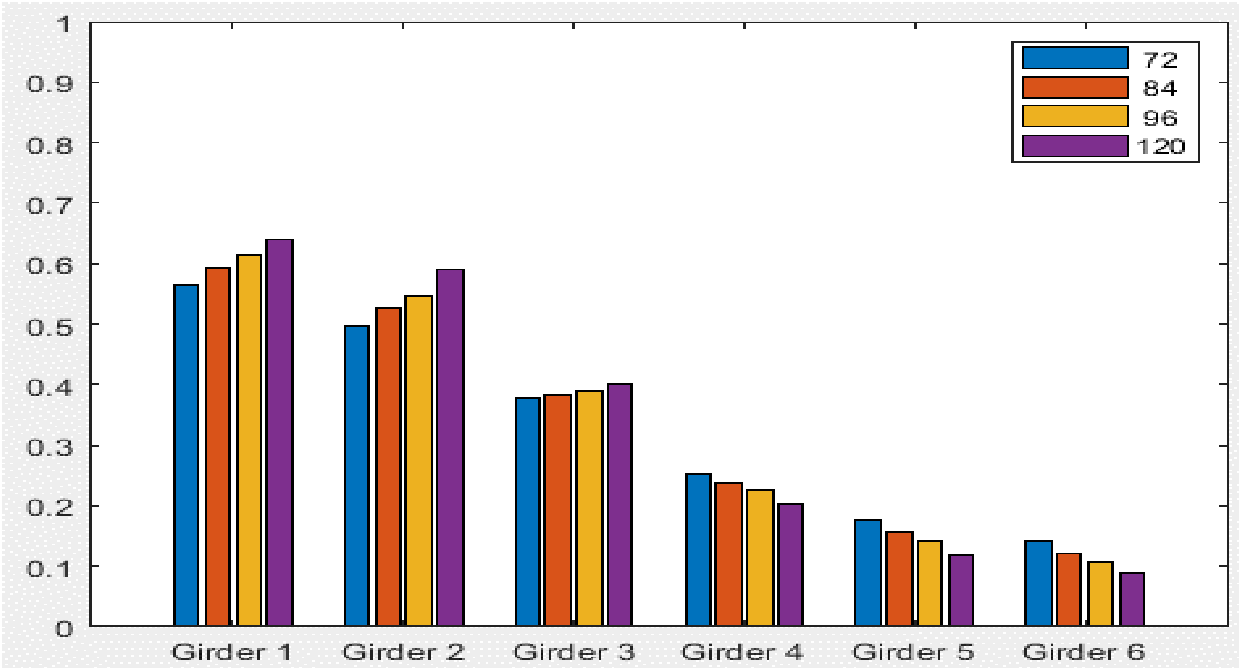

Typical Bridge #4, Tarhini/Frederick Methodology, EG 2LL, Variable = PBFTG Size

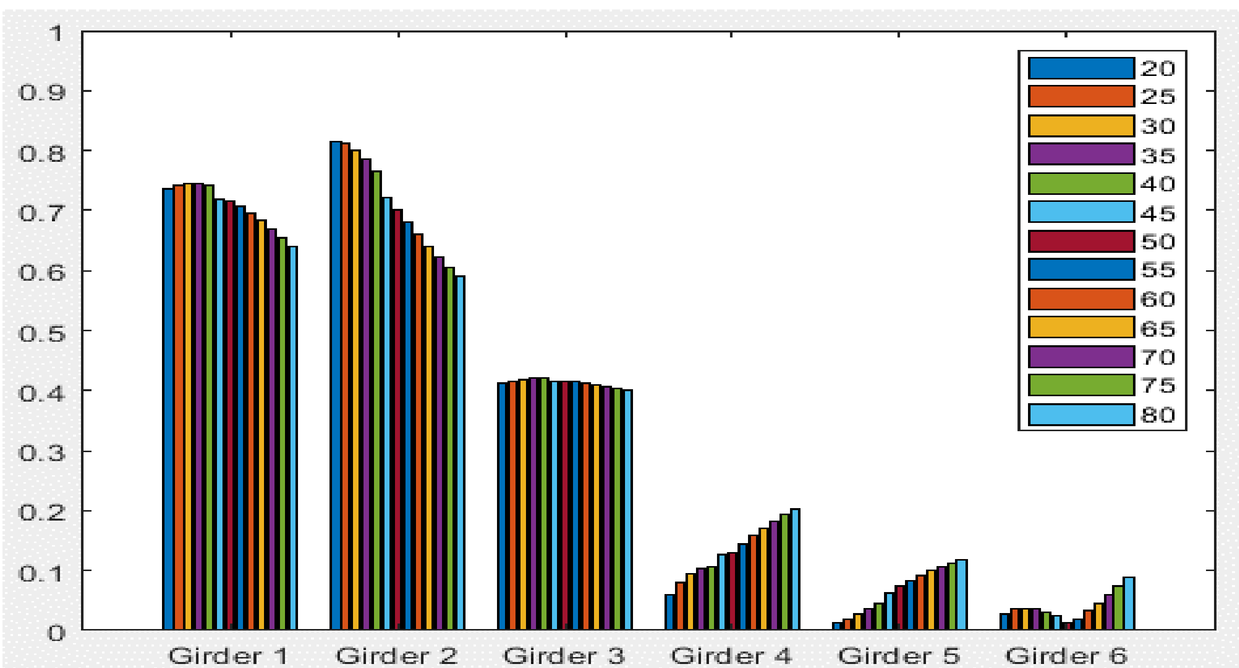

Typical Bridge #4, Tarhini/Frederick Methodology, EG 2LL, Variable = Span Length (ft)

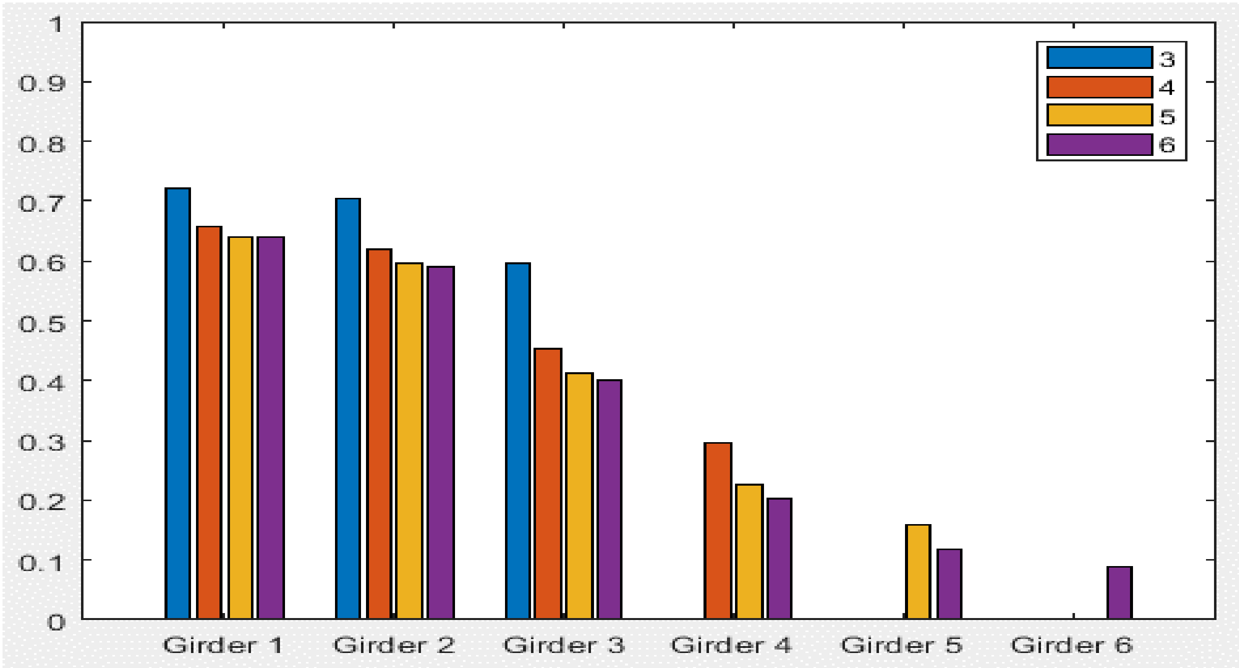

Typical Bridge #4, Tarhini/Frederick Methodology, EG 2LL, Variable = Number of Girders

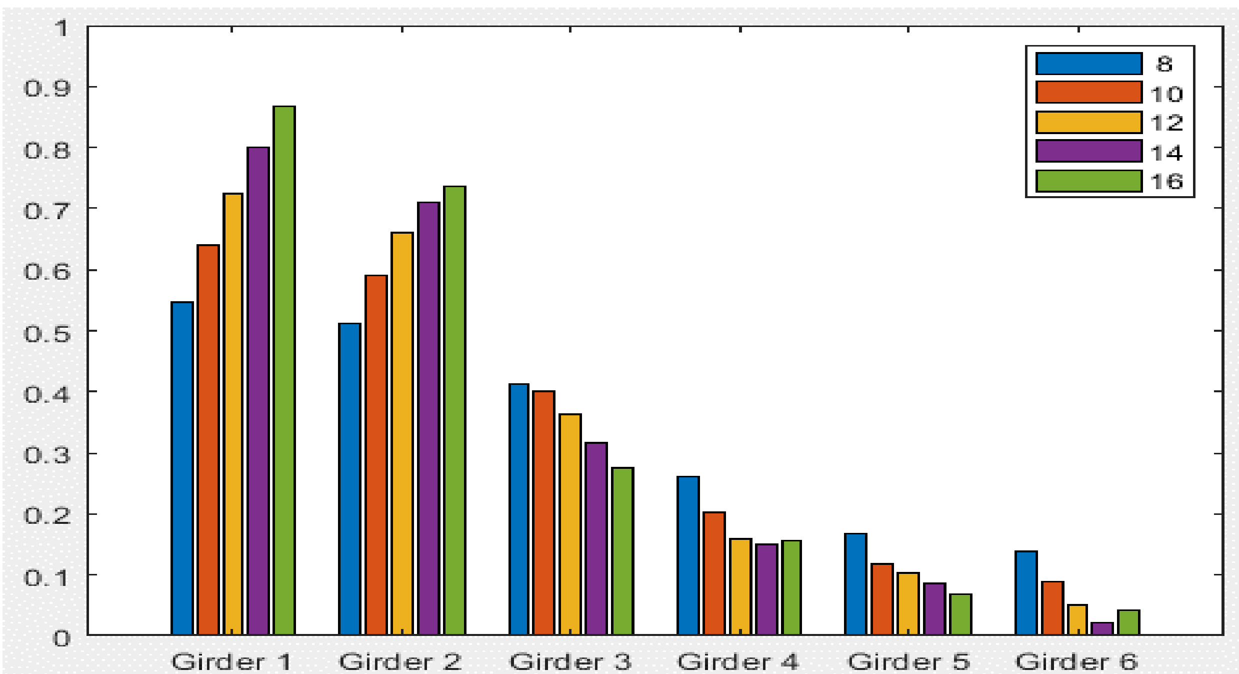

Typical Bridge #4, Tarhini/Frederick Methodology, EG 2LL, Variable = Girder Spacing (ft)

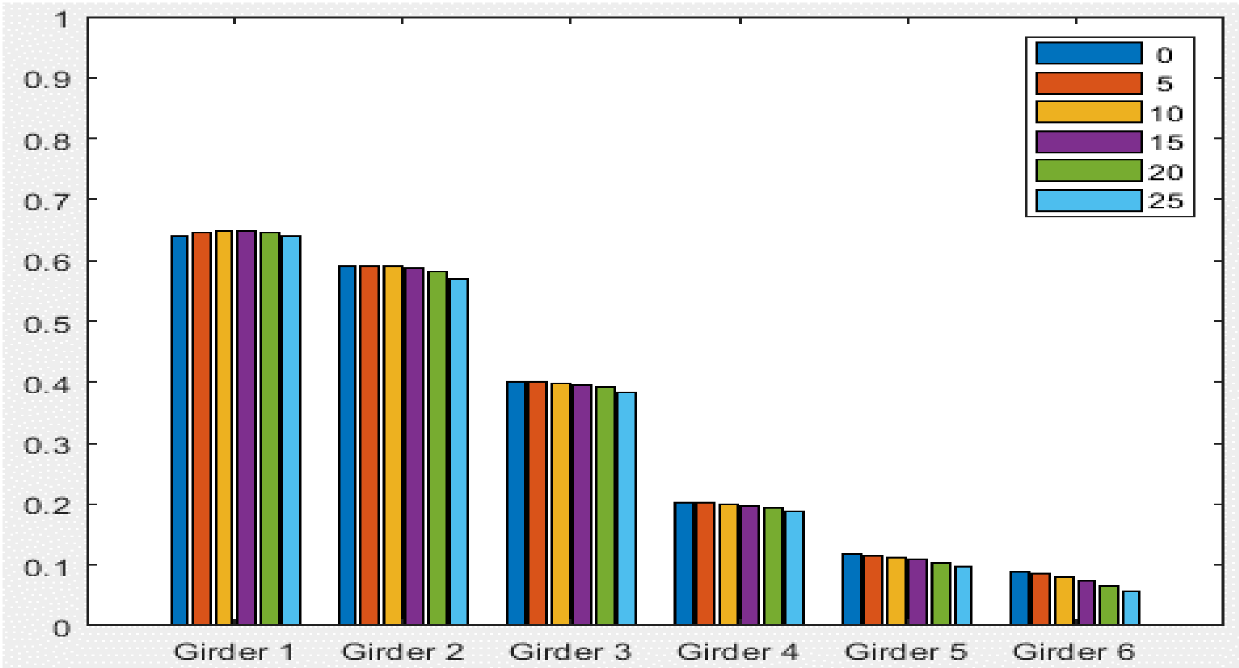

Typical Bridge #4, Tarhini/Frederick Methodology, EG 2LL, Variable = Degree of Skew (deg)

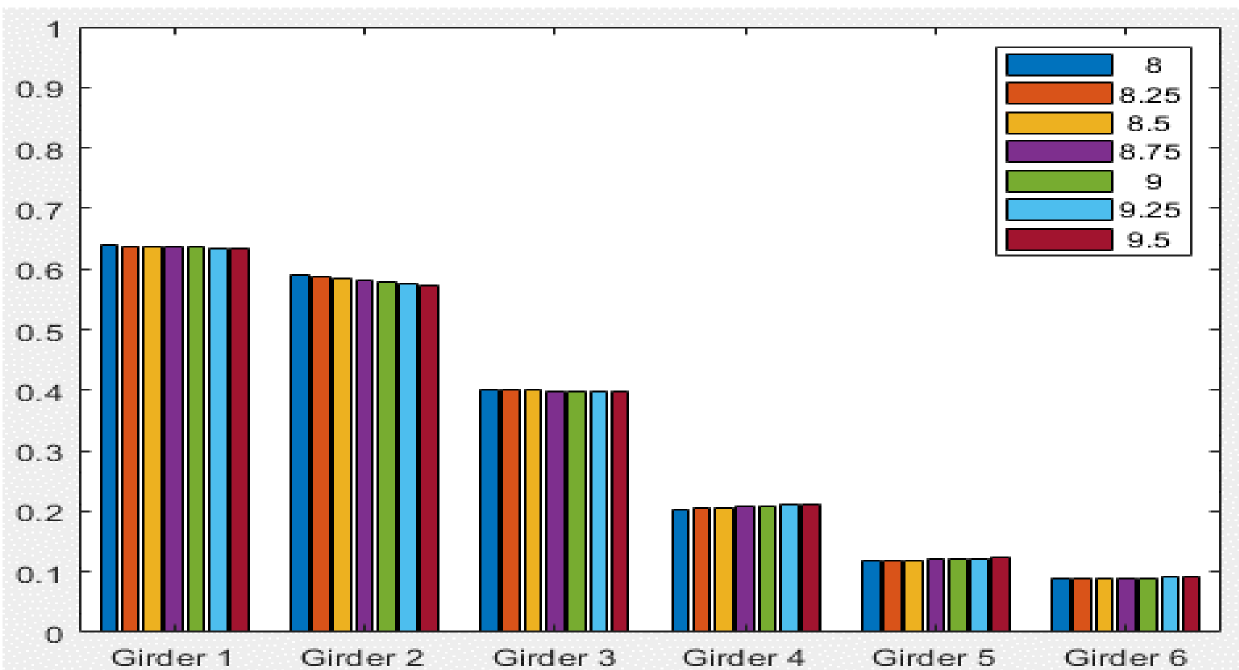

Typical Bridge #4, Tarhini/Frederick Methodology, EG 2LL, Variable = Deck Thickness (in)

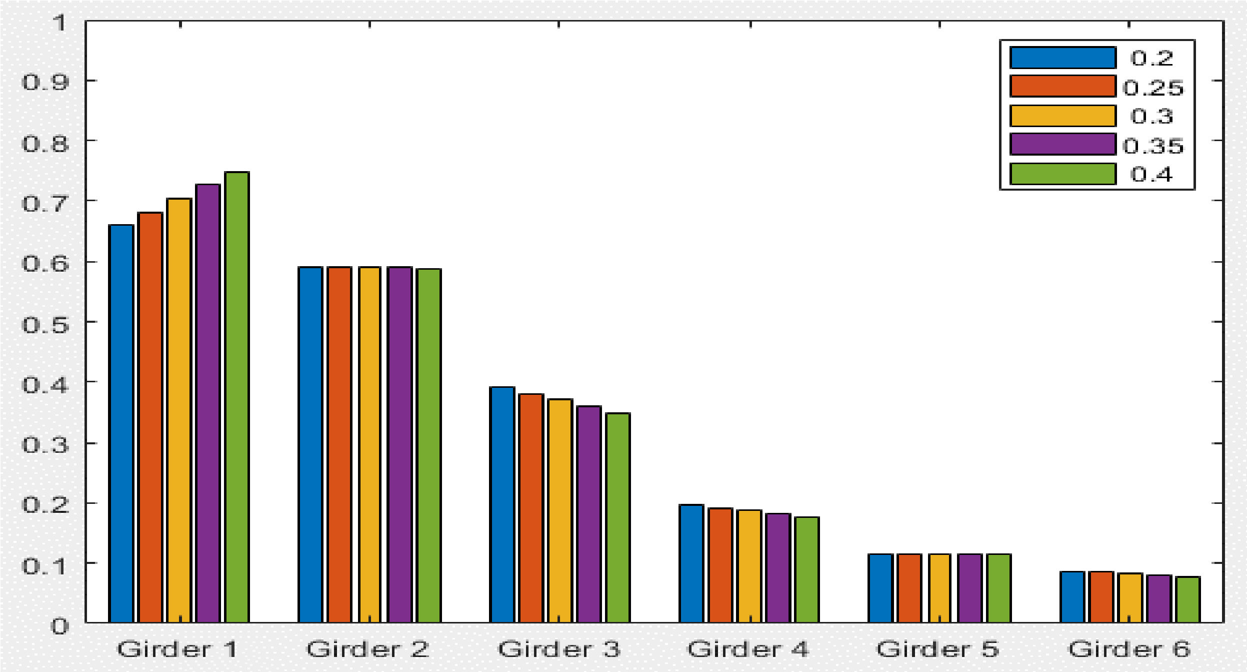

Typical Bridge #4, Tarhini/Frederick Methodology, EG 2LL, Variable = Overhang Ratio

APPENDIX B: LLDF PARAMETRIC VARIATION RESULTS

The following appendix lists in graphical form the comparison of LLDFs calculated from the finite element models of the standard bridges analyzed during the parametric study discussed in Section 8.2. For the reader's convenience, this data has been organized such that each graph is focused on the influence of a single parameter on the distribution of moment to a single girder. Note, some graphs are not available as the typical bridge may not be applicable in certain situations. These situations will be labeled 'No Data Available' in place of the typical graph. Additionally, not every parameter will be present in every graph, as some parameters are not feasible with every standard bridge. The graphs were generated using MATLAB (Mathworks, 2021).

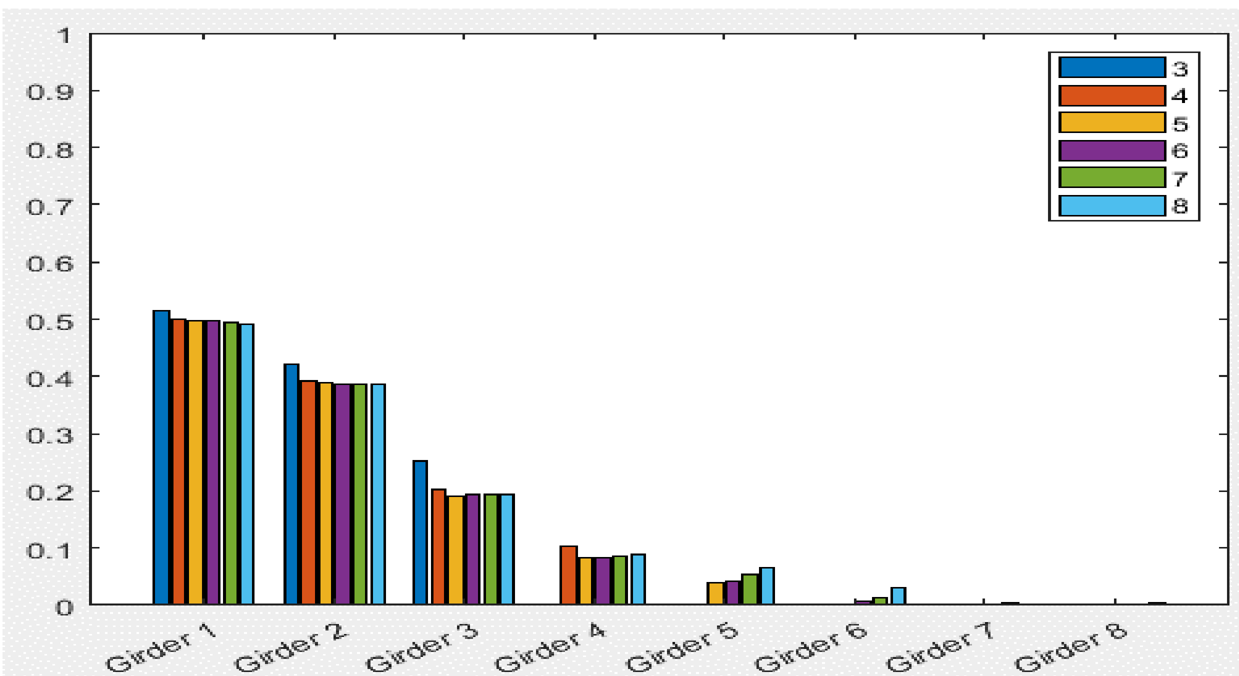

Standard Bridge #1, Tarhini/Frederick Methodology, IG OLL, Variable = Number of Beams

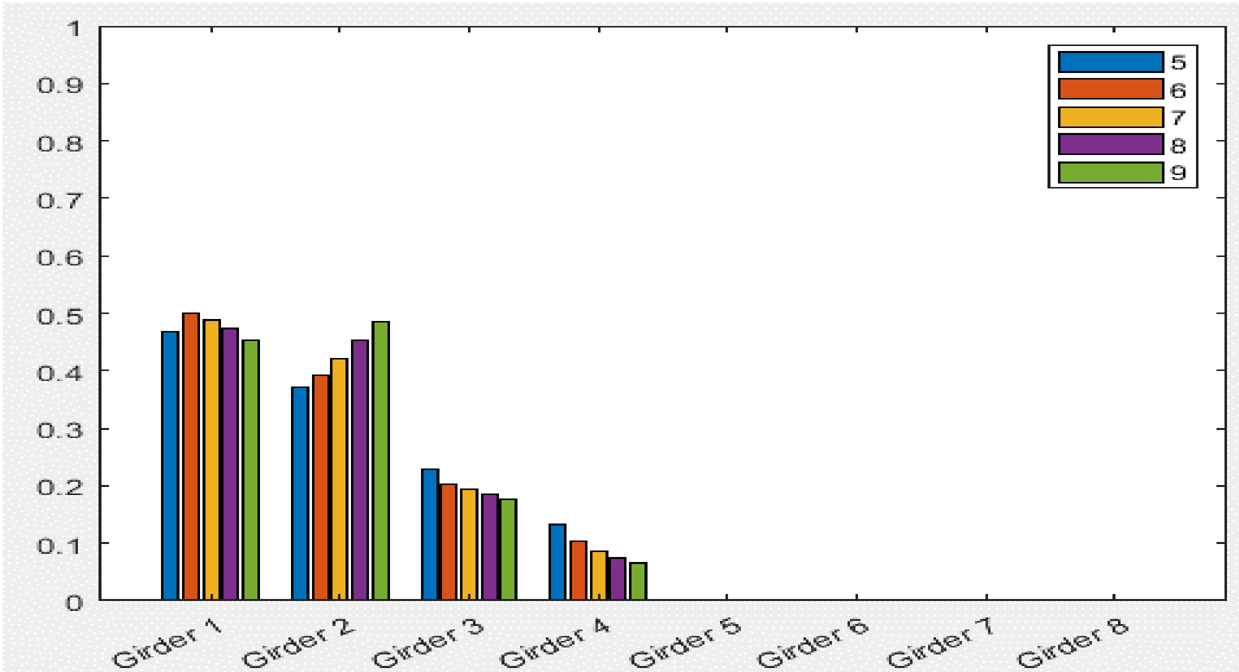

Standard Bridge #1, Tarhini/Frederick Methodology, IG OLL, Variable = Girder Spacing (ft)

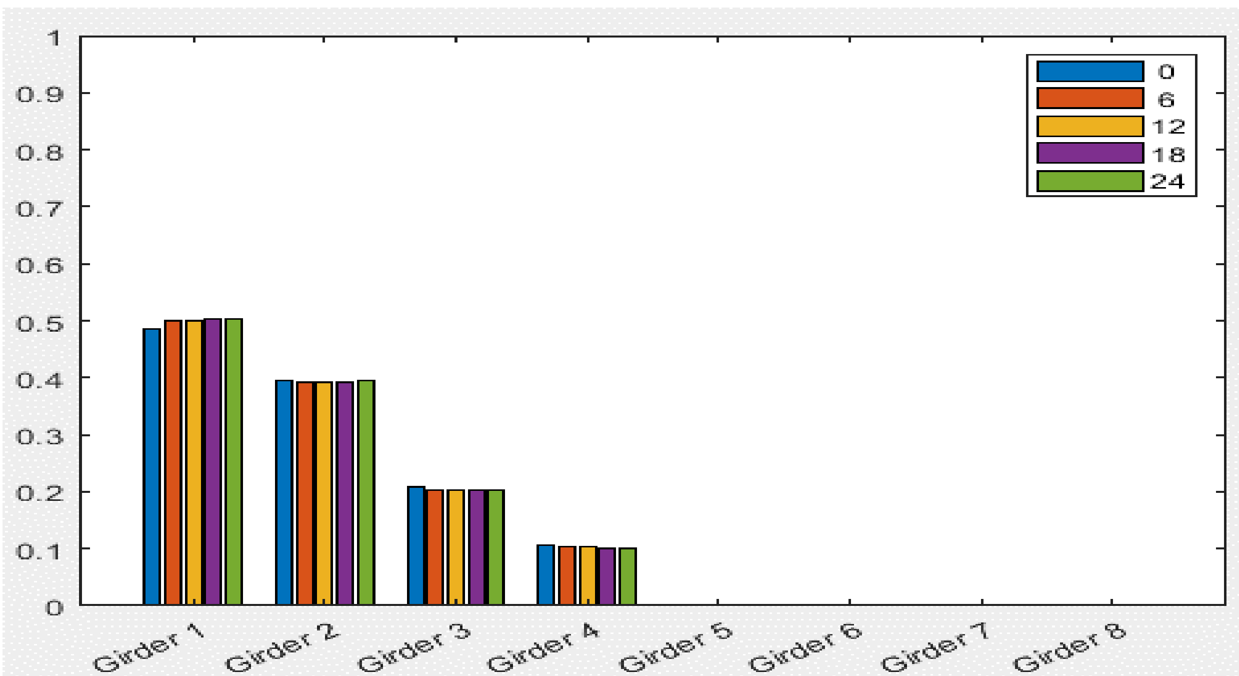

Standard Bridge #1, Tarhini/Frederick Methodology, IG OLL, Variable = Overhang Distance (in)

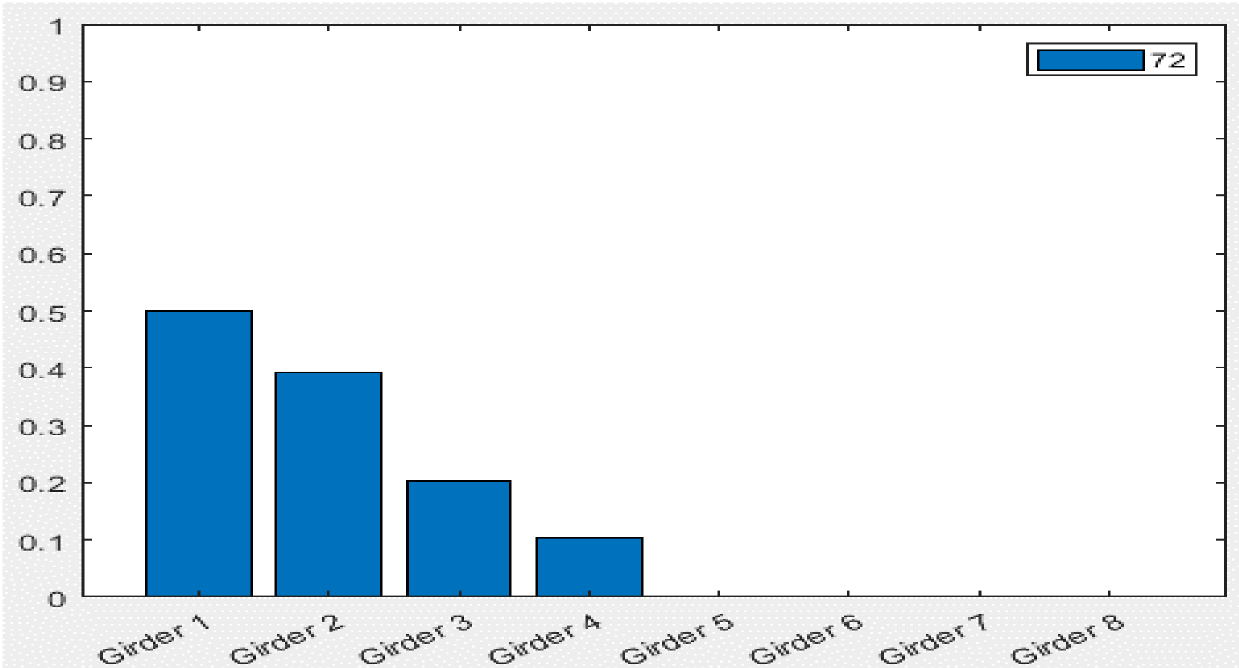

Standard Bridge #1, Tarhini/Frederick Methodology, IG OLL, Variable = Plate Size

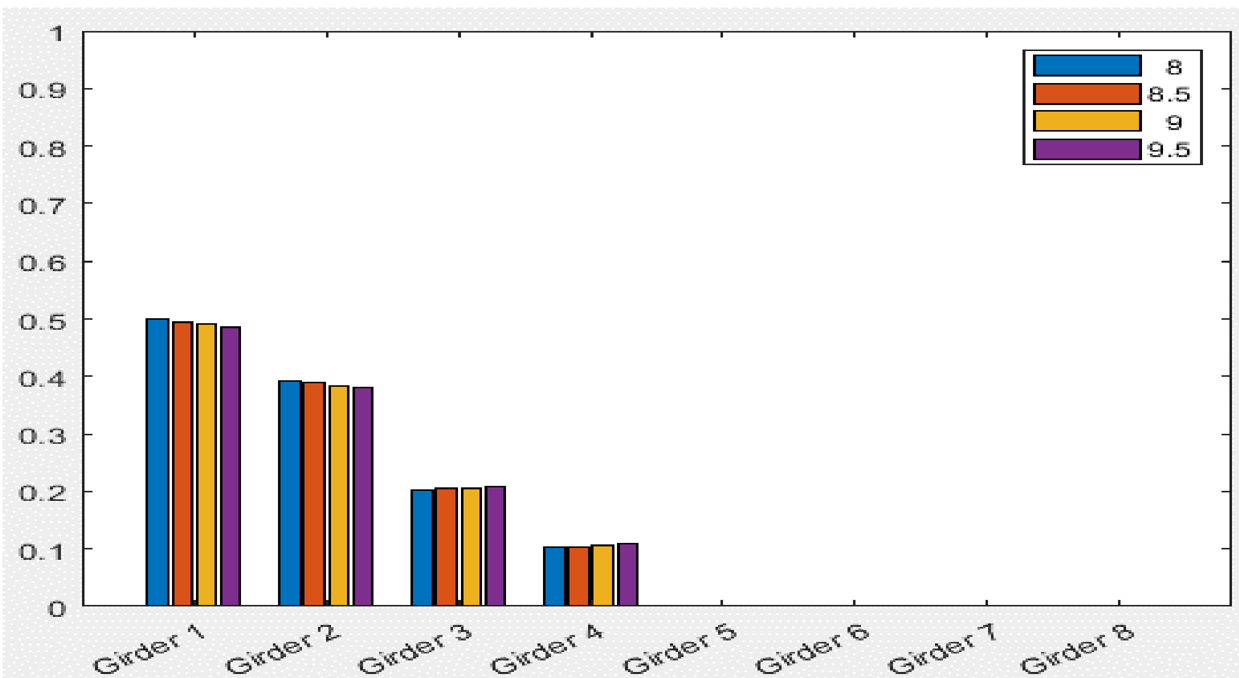

Standard Bridge #1, Tarhini/Frederick Methodology, IG OLL, Variable = Deck Thickness (in)

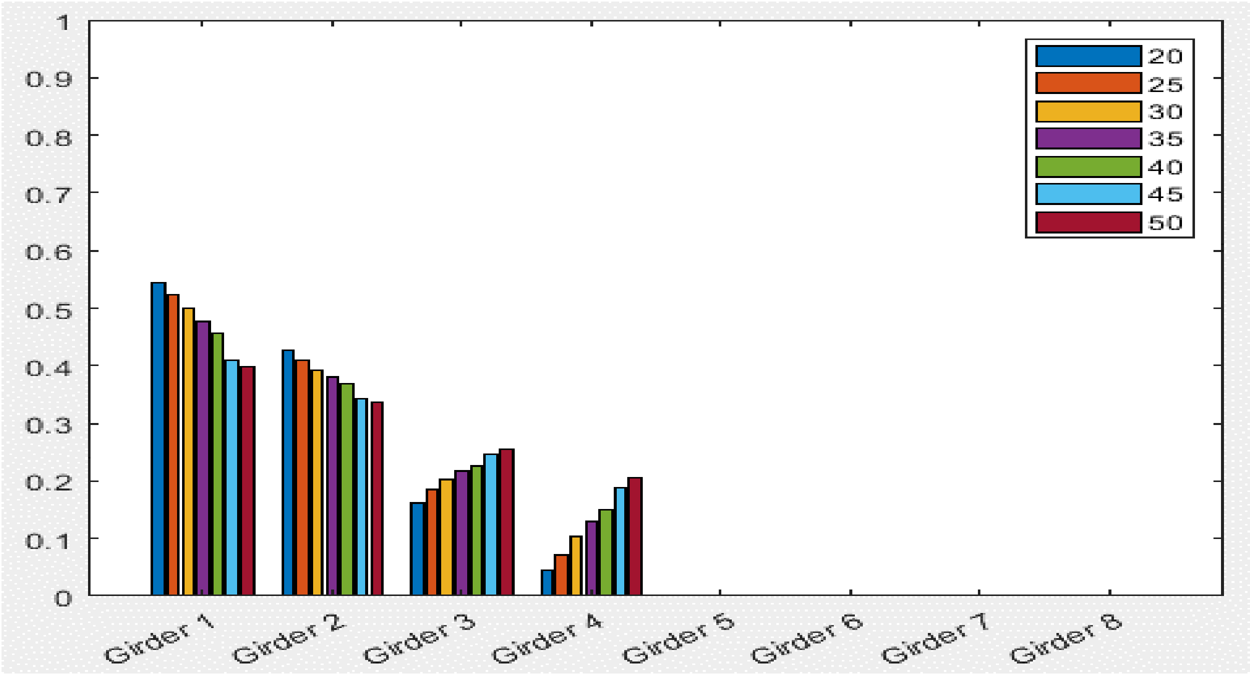

Standard Bridge #1, Tarhini/Frederick Methodology, IG OLL, Variable = Span Length (ft)

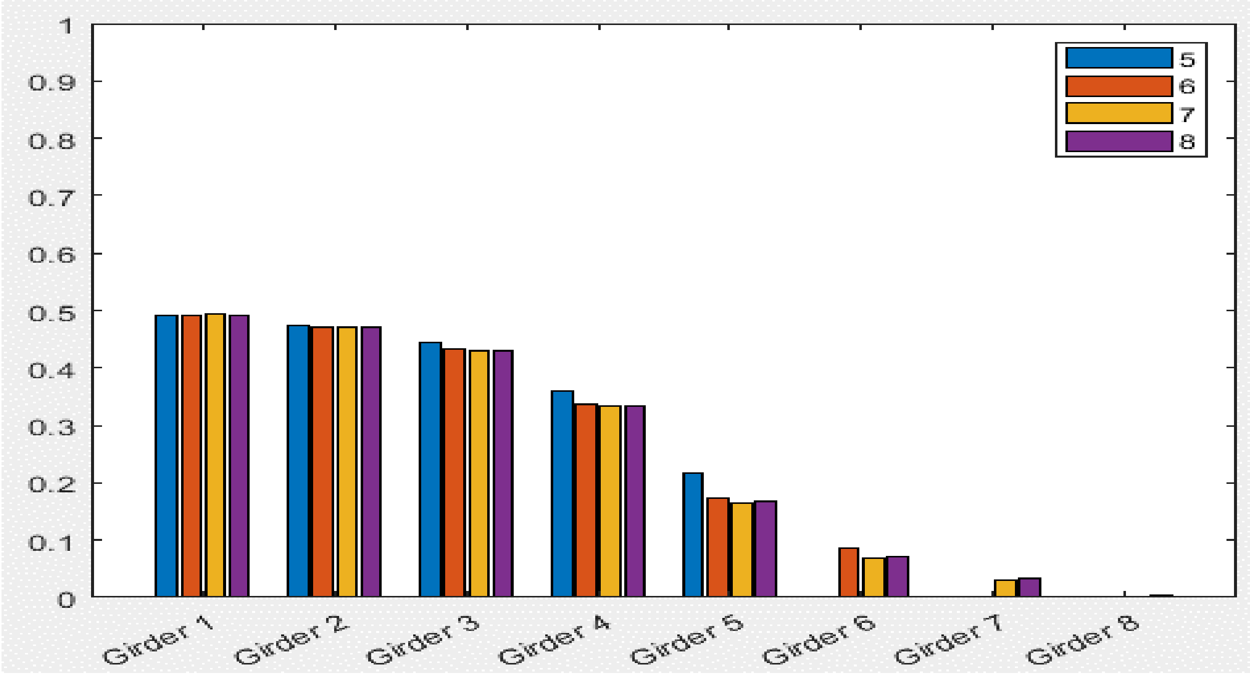

Standard Bridge #1, Tarhini/Frederick Methodology, IG 2LL, Variable = Number of Beams

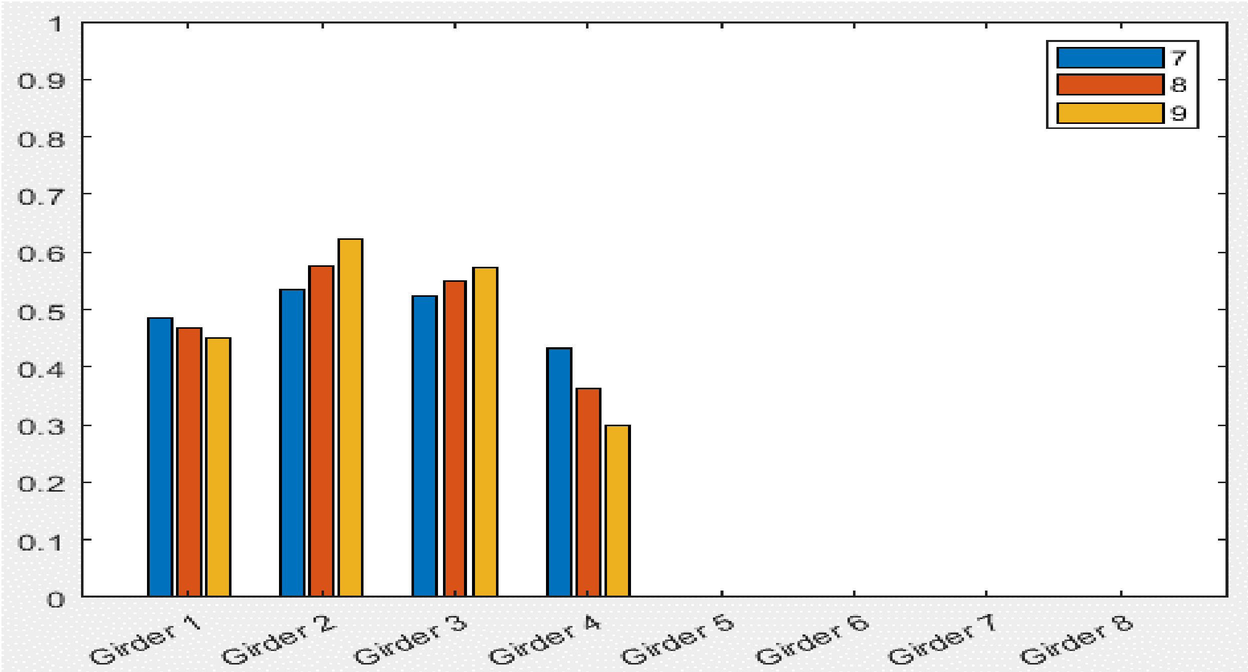

Standard Bridge #1, Tarhini/Frederick Methodology, IG 2LL, Variable = Girder Spacing (ft)

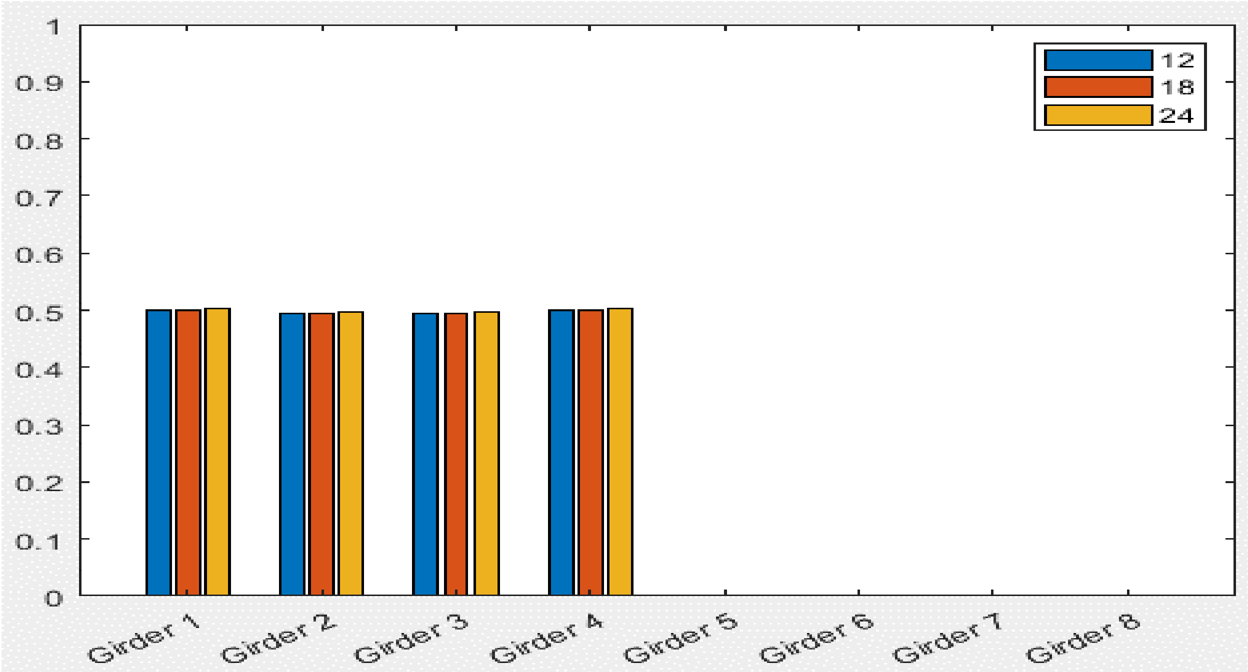

Standard Bridge #1, Tarhini/Frederick Methodology, IG 2LL, Variable = Overhang Distance (in)

NO DATA AVAILABLE

Standard Bridge #1, Tarhini/Frederick Methodology, IG 2LL, Variable = Plate Size

NO DATA AVAILABLE

Standard Bridge #1, Tarhini/Frederick Methodology, IG 2LL, Variable = Deck Thickness (in)

NO DATA AVAILABLE

Standard Bridge #1, Tarhini/Frederick Methodology, IG 2LL, Variable = Span Length (ft)

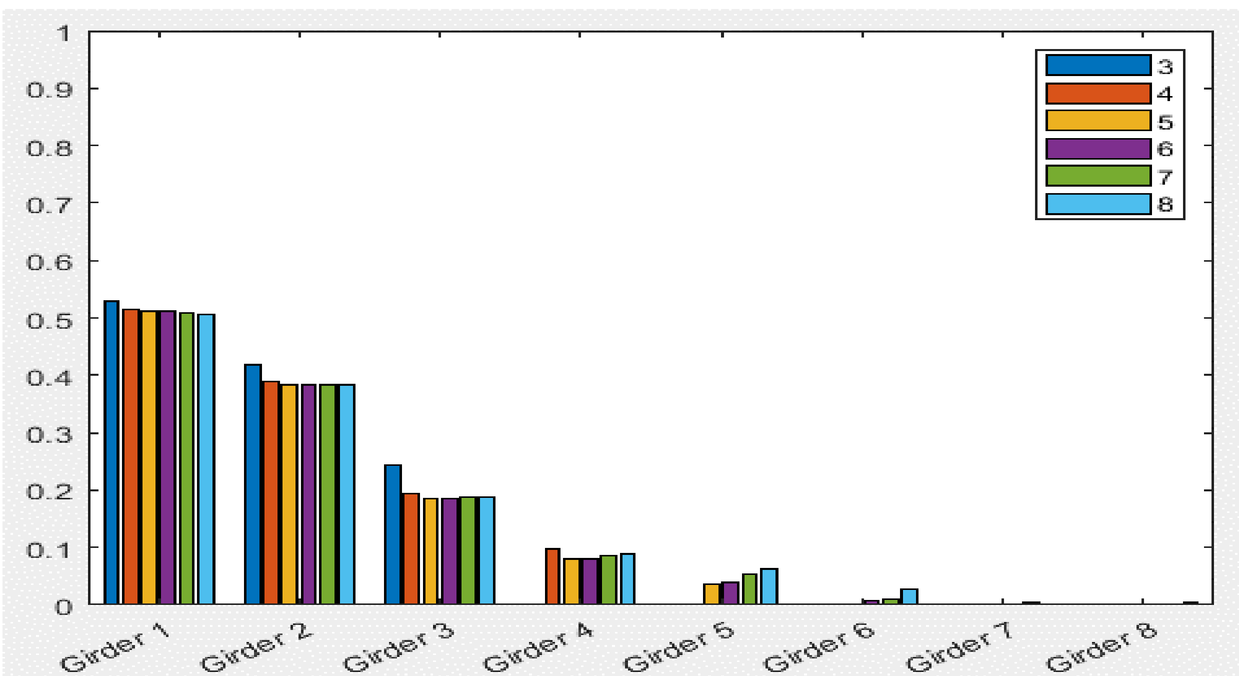

Standard Bridge #1, Tarhini/Frederick Methodology, EG OLL, Variable = Number of Beams

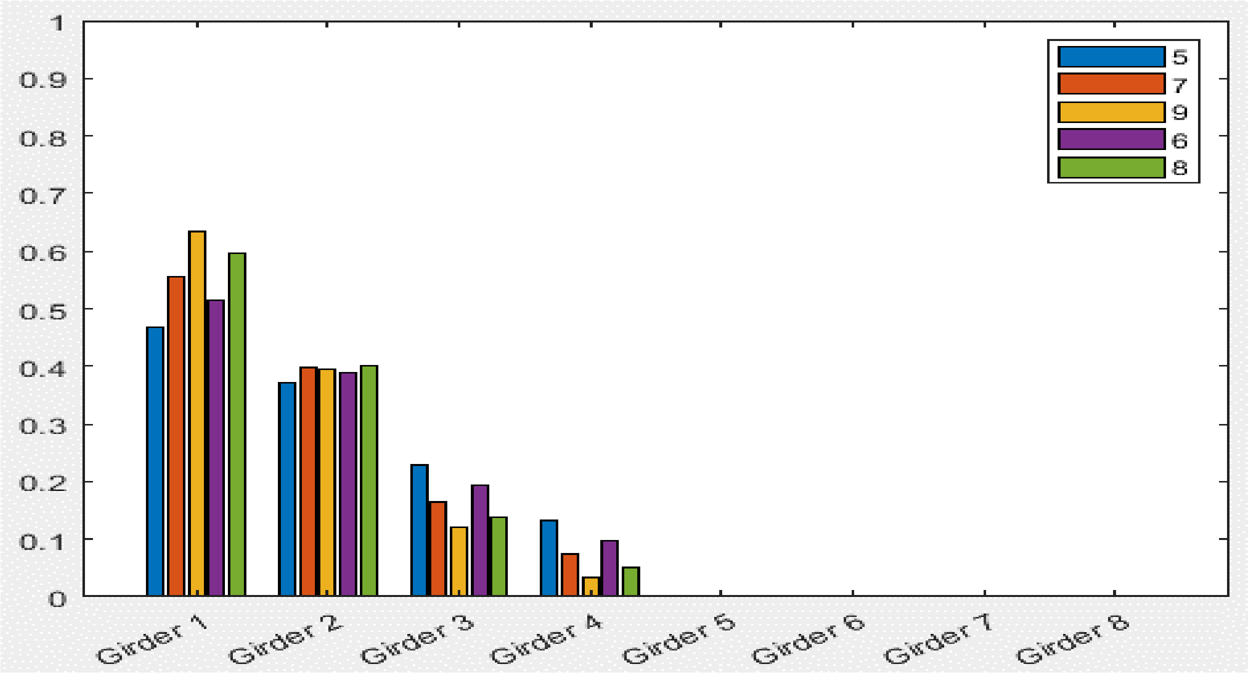

Standard Bridge #1, Tarhini/Frederick Methodology, EG OLL, Variable = Girder Spacing (ft)

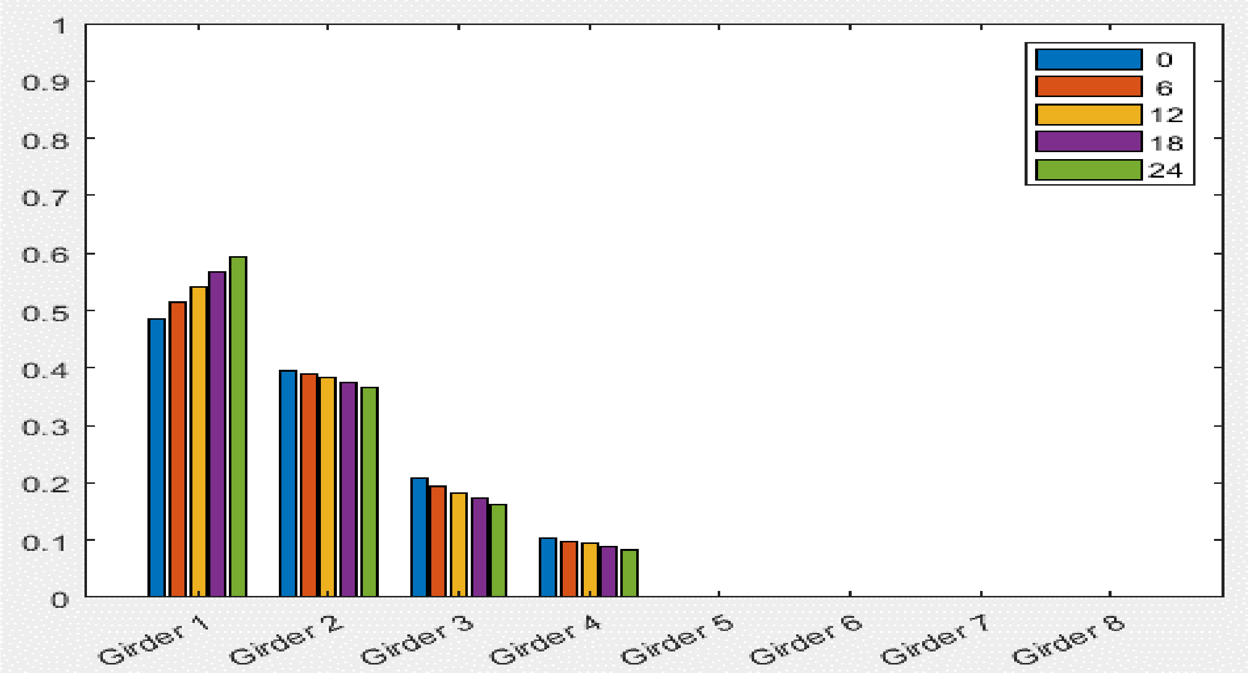

Standard Bridge #1, Tarhini/Frederick Methodology, EG OLL, Variable = Overhang Distance (in)

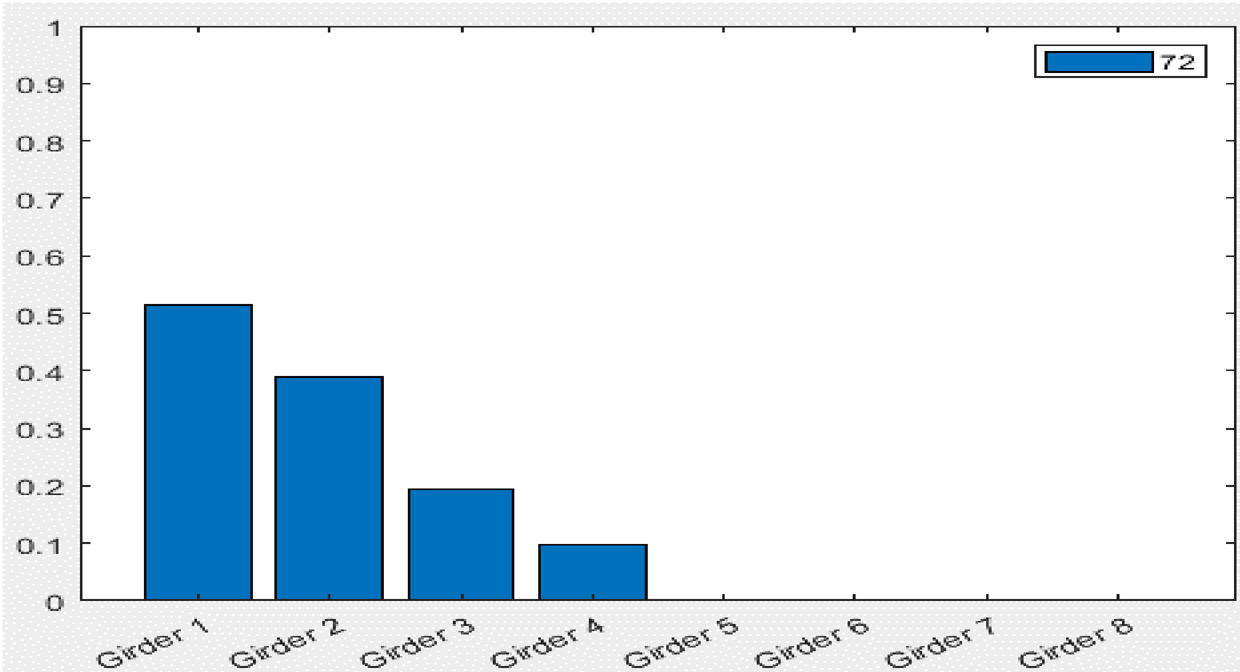

Standard Bridge #1, Tarhini/Frederick Methodology, EG OLL, Variable = Plate Size

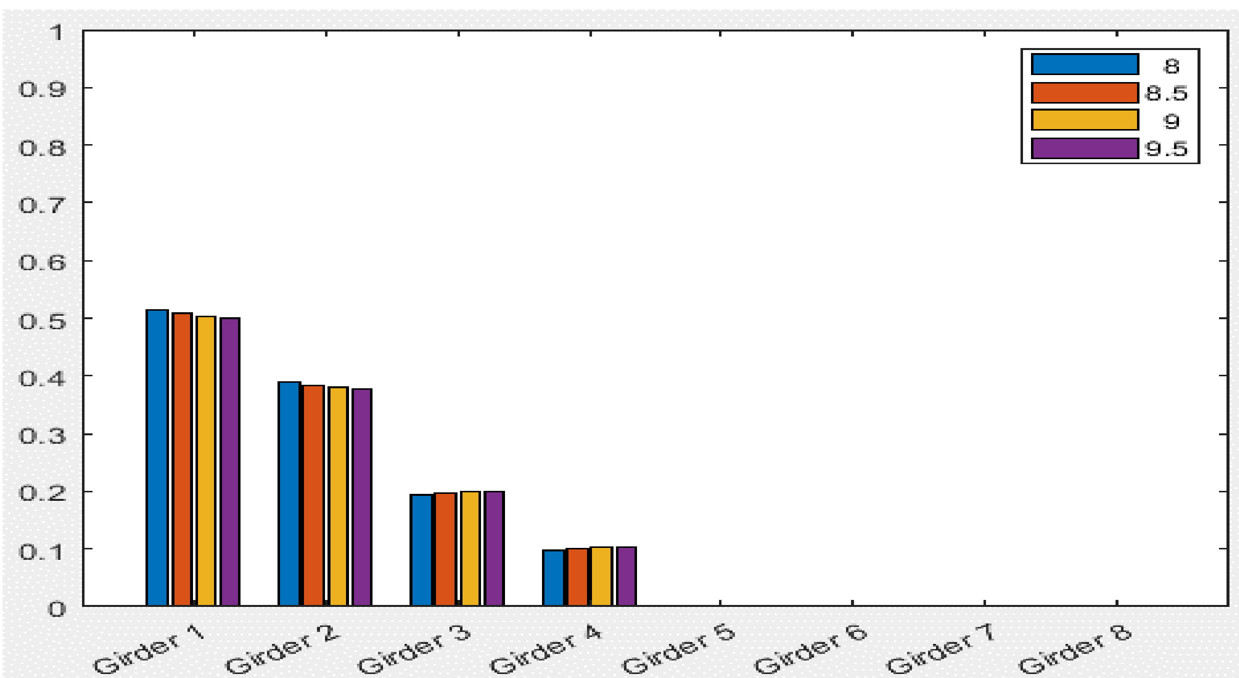

Standard Bridge #1, Tarhini/Frederick Methodology, EG OLL, Variable = Deck Thickness (in)

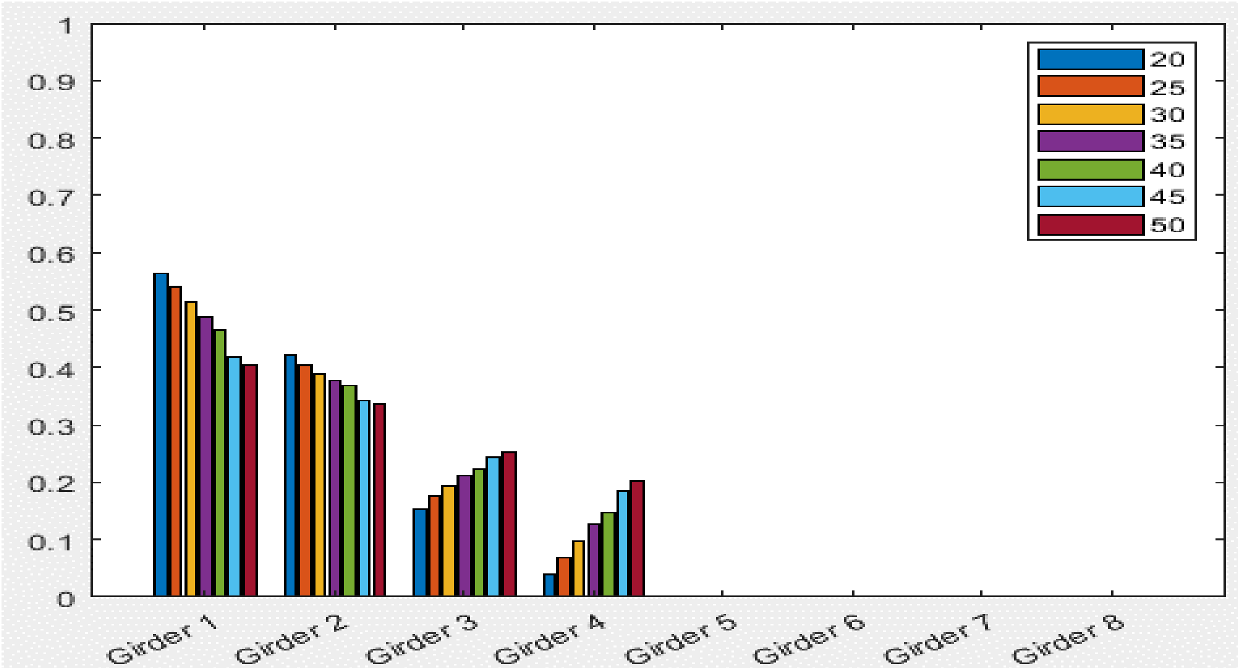

Standard Bridge #1, Tarhini/Frederick Methodology, EG OLL, Variable = Span Length (ft)

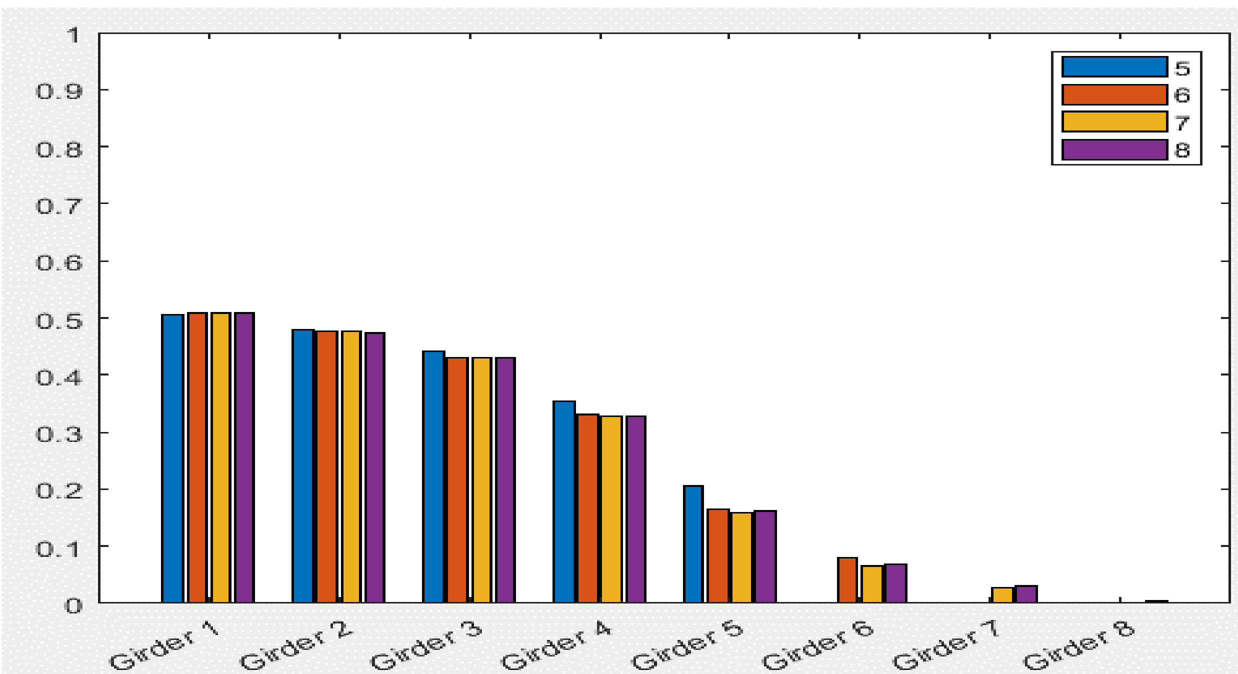

Standard Bridge #1, Tarhini/Frederick Methodology, EG 2LL, Variable = Number of Beams

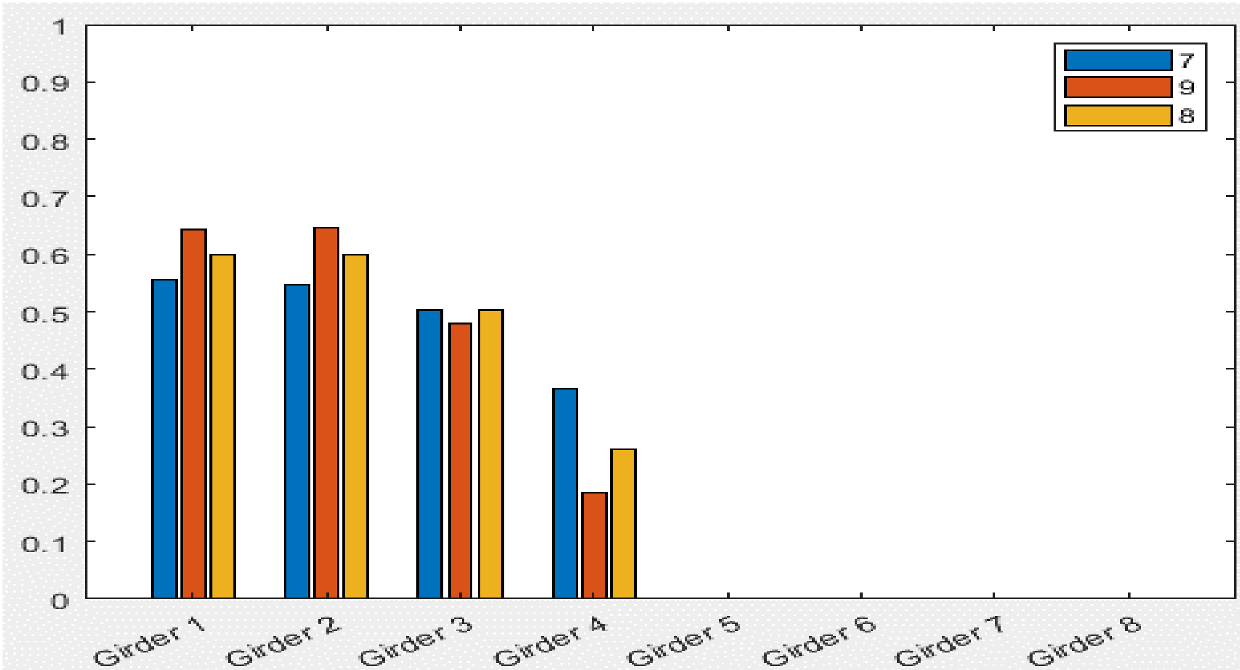

Standard Bridge #1, Tarhini/Frederick Methodology, EG 2LL, Variable = Girder Spacing (ft)

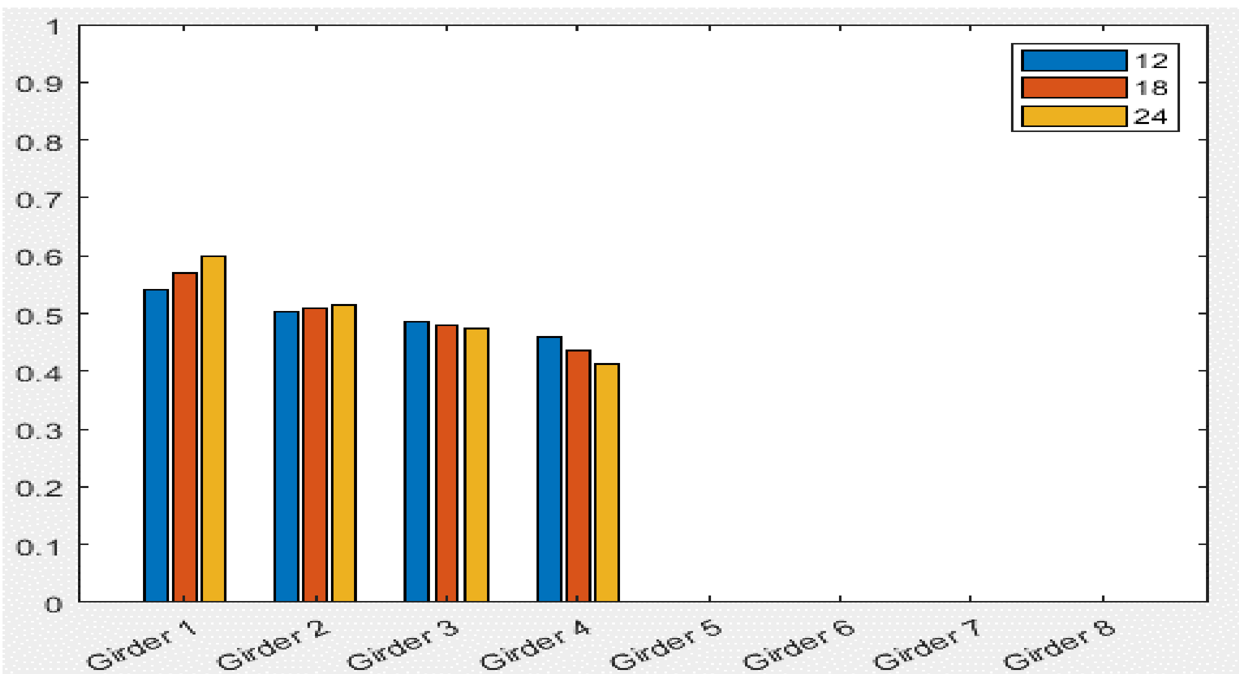

Standard Bridge #1, Tarhini/Frederick Methodology, EG 2LL, Variable = Overhang Distance (in)

NO DATA AVAILABLE

Standard Bridge #1, Tarhini/Frederick Methodology, EG 2LL, Variable = Plate Size

NO DATA AVAILABLE

Standard Bridge #1, Tarhini/Frederick Methodology, EG 2LL, Variable = Deck Thickness (in)

NO DATA AVAILABLE

Standard Bridge #1, Tarhini/Frederick Methodology, EG 2LL, Variable = Span Length (ft)

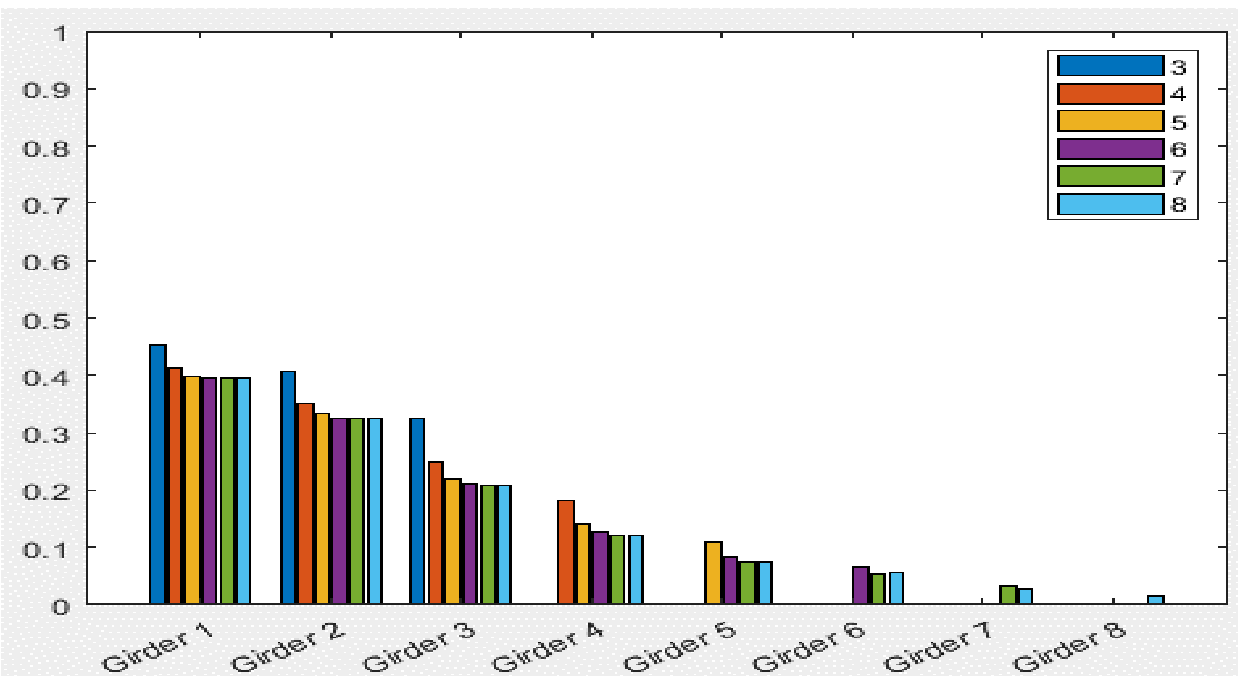

Standard Bridge #2, Tarhini/Frederick Methodology, IG OLL, Variable = Number of Beams

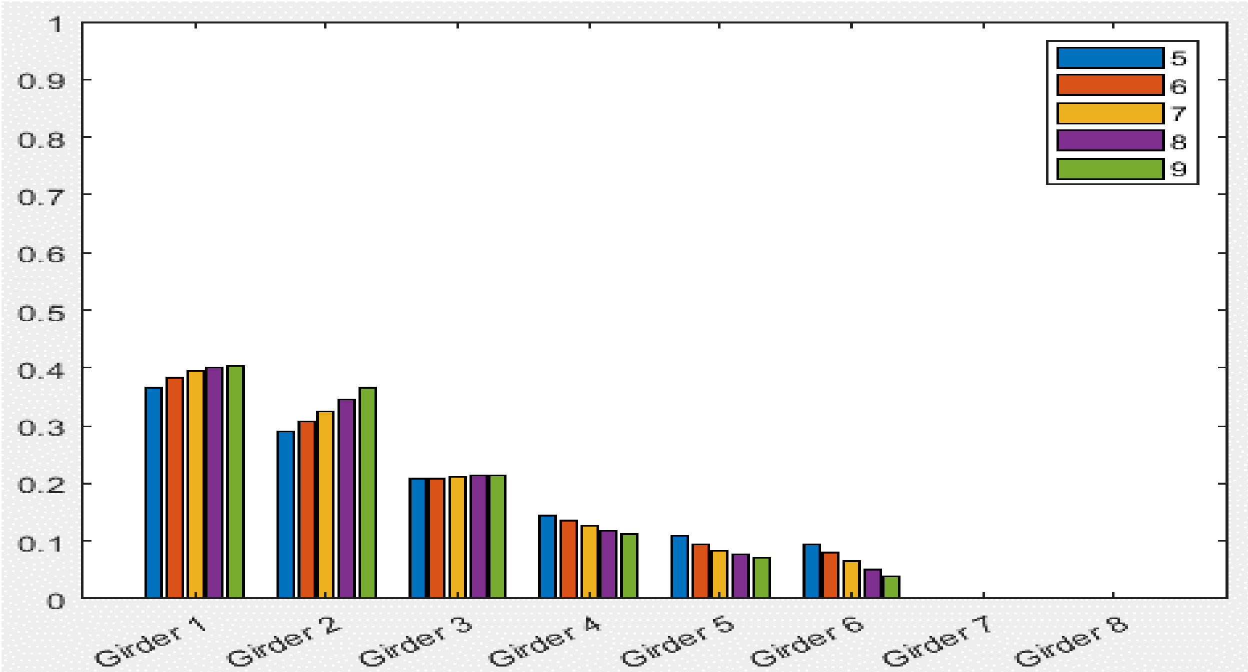

Standard Bridge #2, Tarhini/Frederick Methodology, IG OLL, Variable = Girder Spacing (ft)

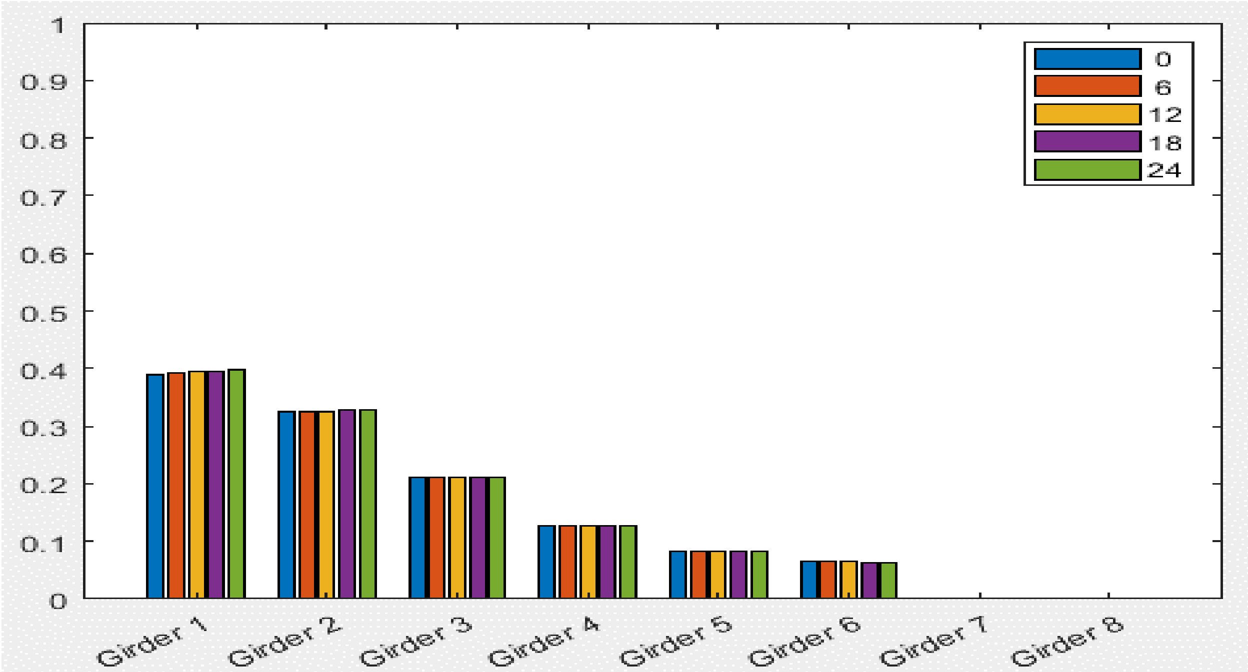

Standard Bridge #2, Tarhini/Frederick Methodology, IG OLL, Variable = Overhang Distance (in)

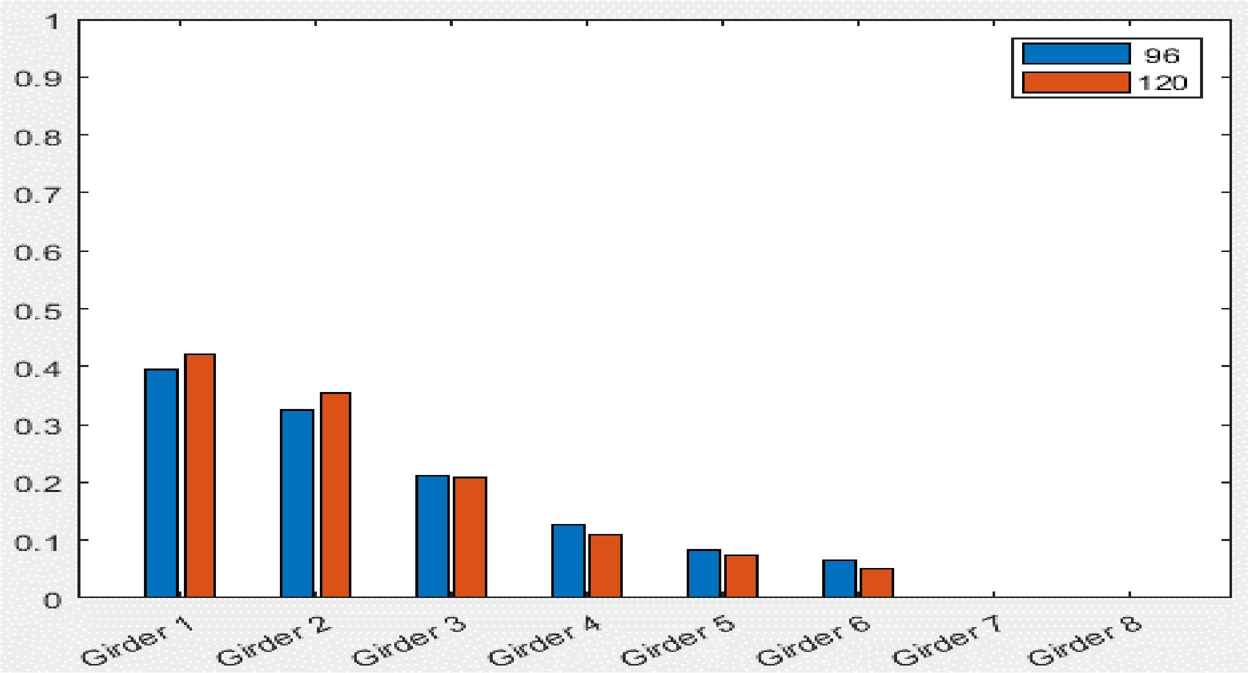

Standard Bridge #2, Tarhini/Frederick Methodology, IG OLL, Variable = Plate Size

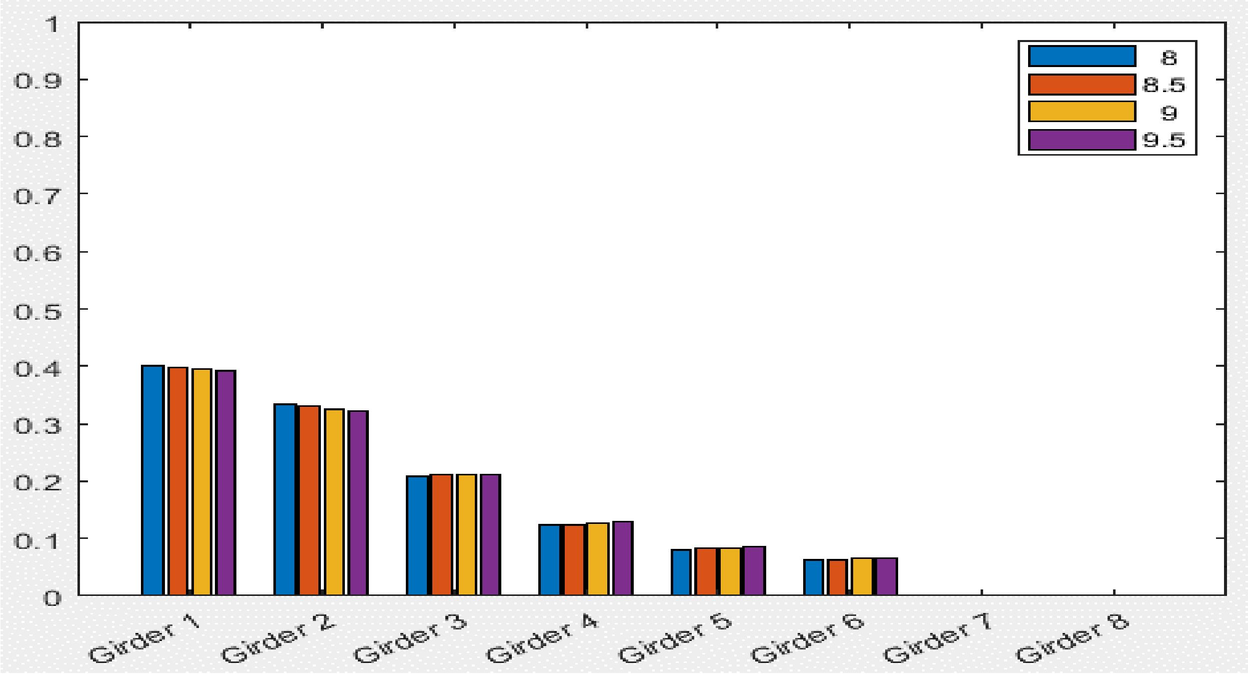

Standard Bridge #2, Tarhini/Frederick Methodology, IG OLL, Variable = Deck Thickness (in)

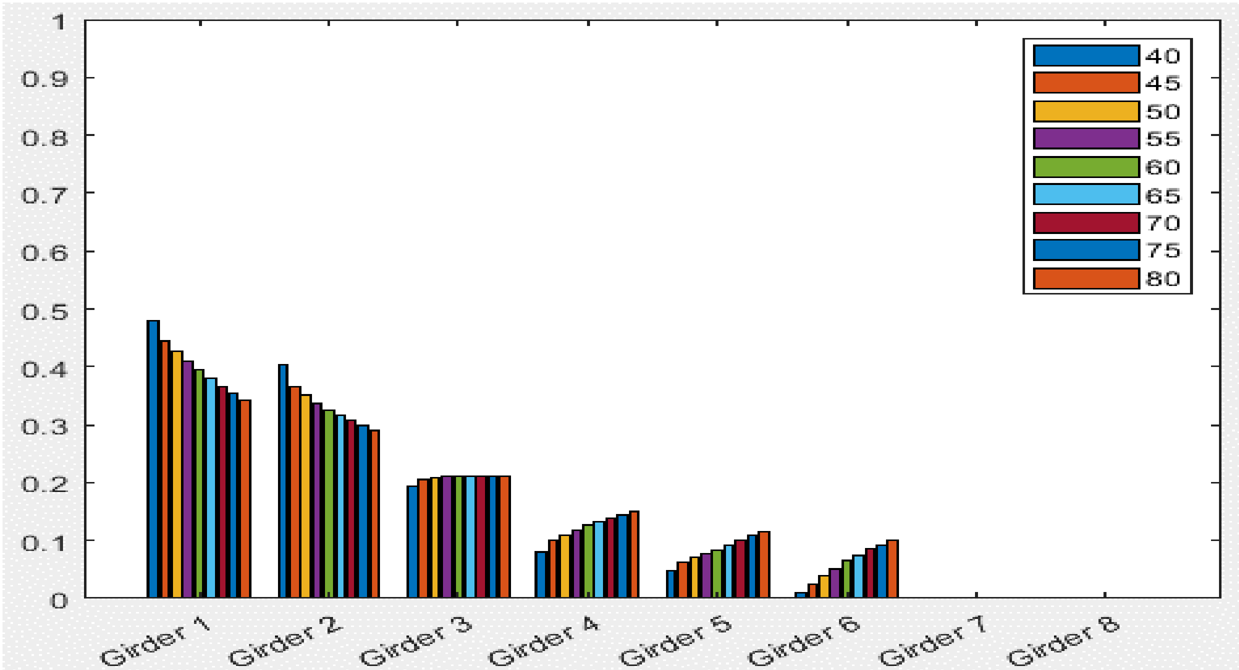

Standard Bridge #2, Tarhini/Frederick Methodology, IG OLL, Variable = Span Length (ft)

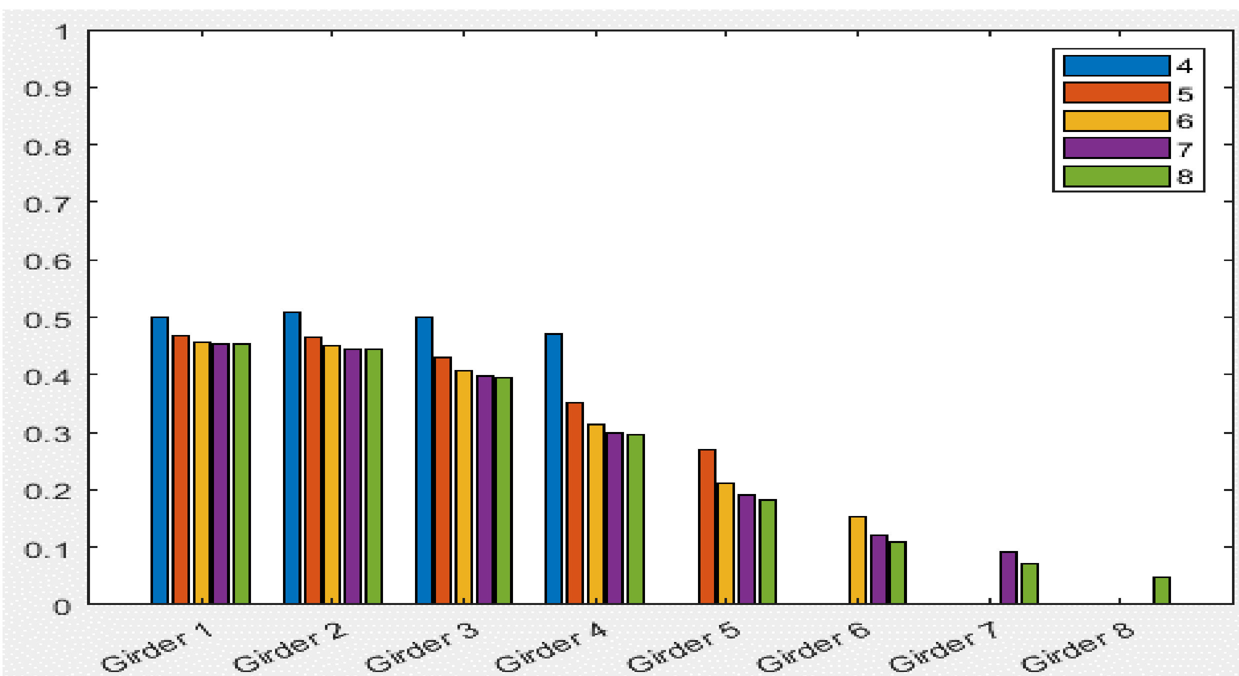

Standard Bridge #2, Tarhini/Frederick Methodology, IG 2LL, Variable = Number of Beams

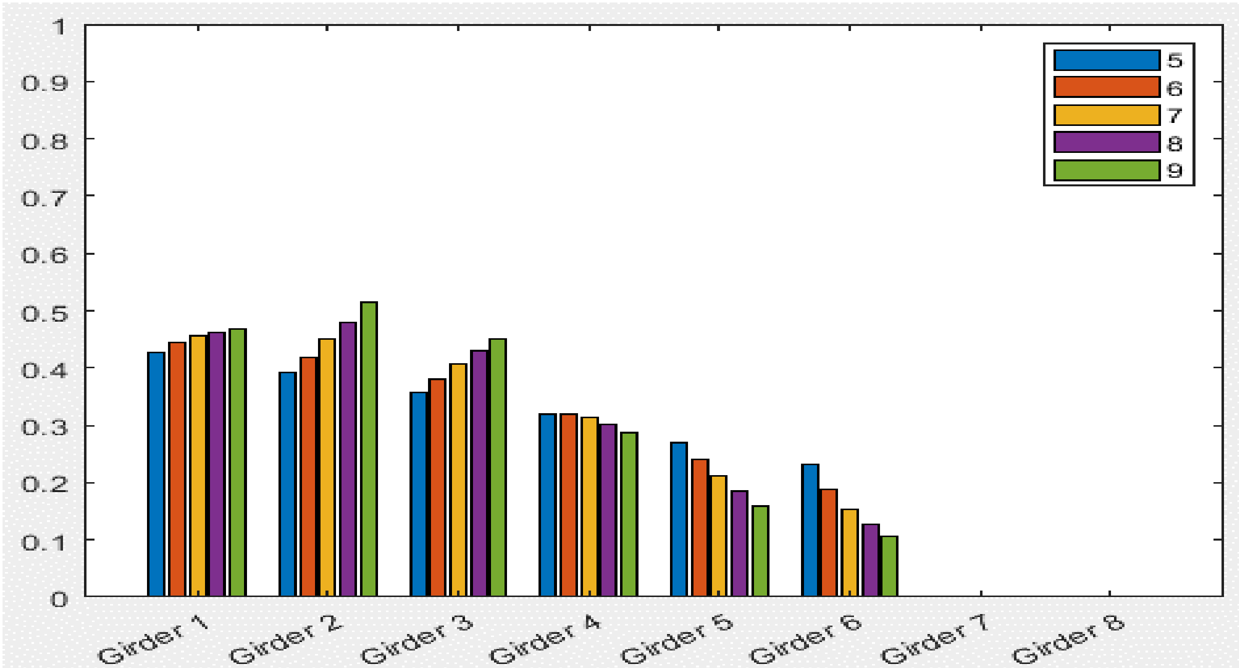

Standard Bridge #2, Tarhini/Frederick Methodology, IG 2LL, Variable = Girder Spacing (ft)

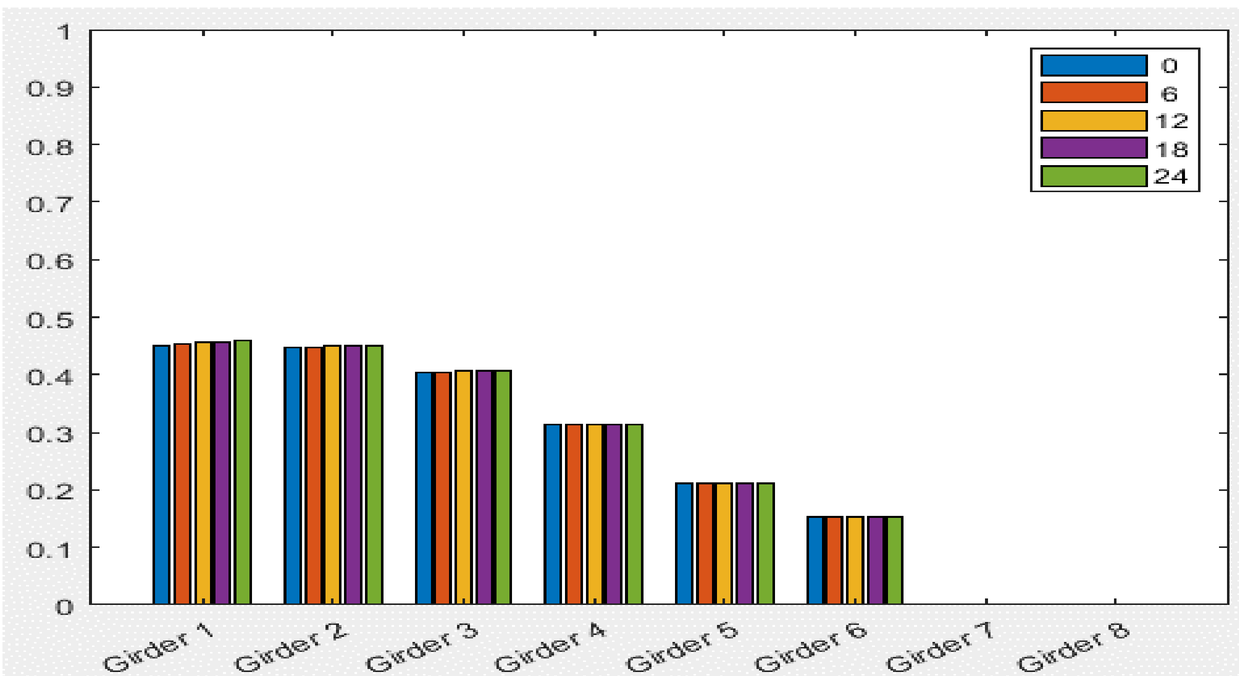

Standard Bridge #2, Tarhini/Frederick Methodology, IG 2LL, Variable = Overhang Distance (in)

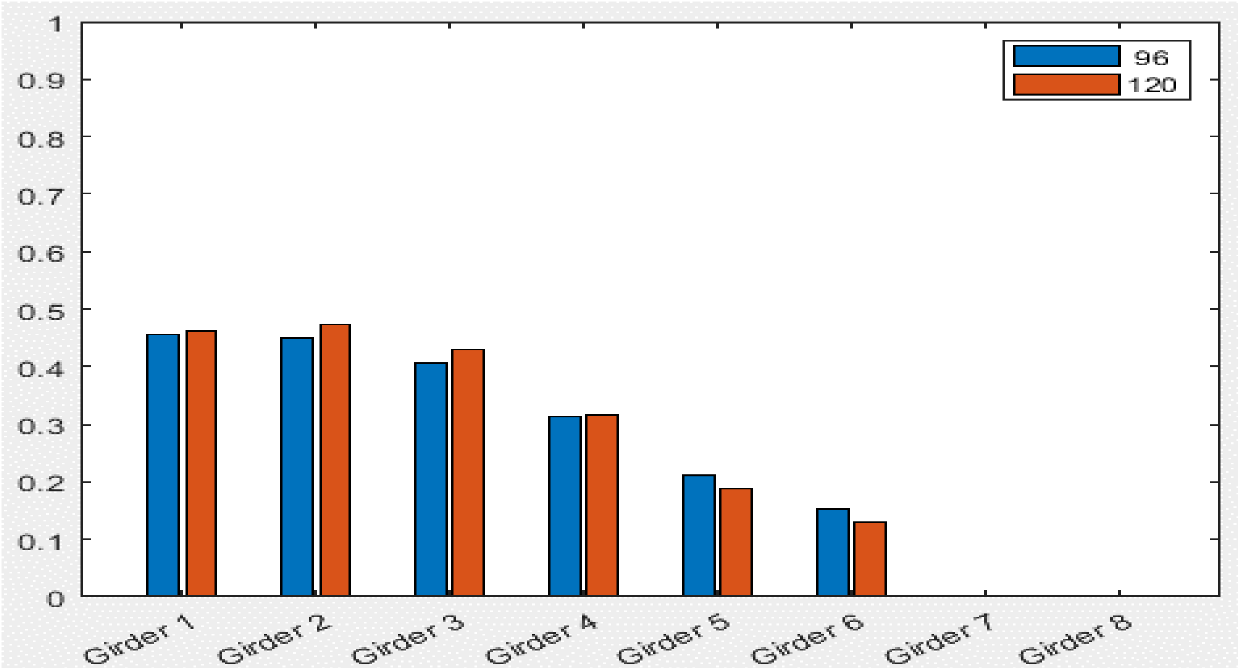

Standard Bridge #2, Tarhini/Frederick Methodology, IG 2LL, Variable = Plate Size

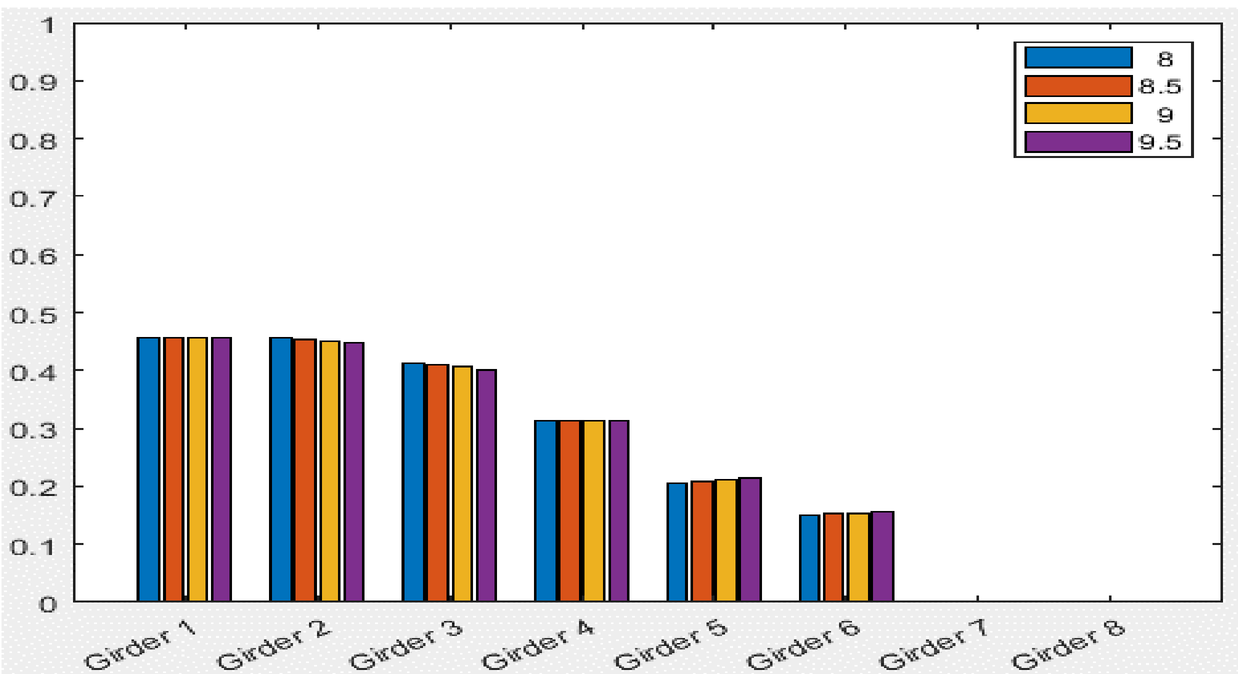

Standard Bridge #2, Tarhini/Frederick Methodology, IG 2LL, Variable = Deck Thickness (in)

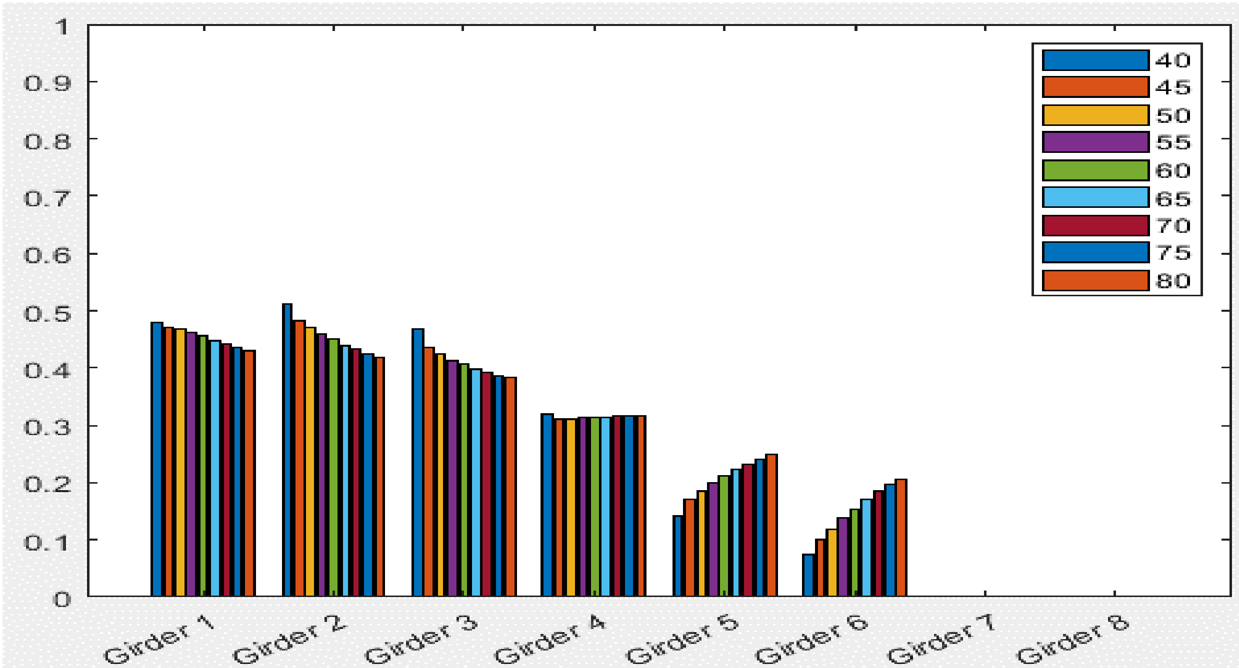

Standard Bridge #2, Tarhini/Frederick Methodology, IG 2LL, Variable = Span Length (ft)

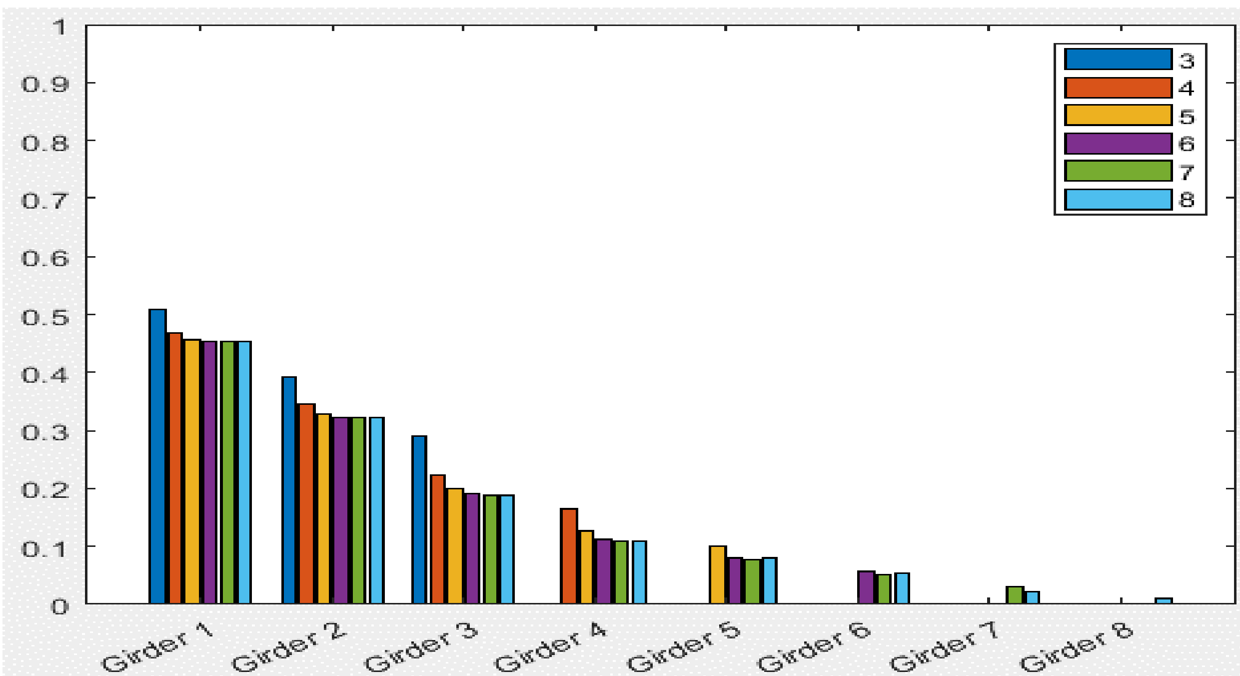

Standard Bridge #2, Tarhini/Frederick Methodology, EG OLL, Variable = Number of Beams

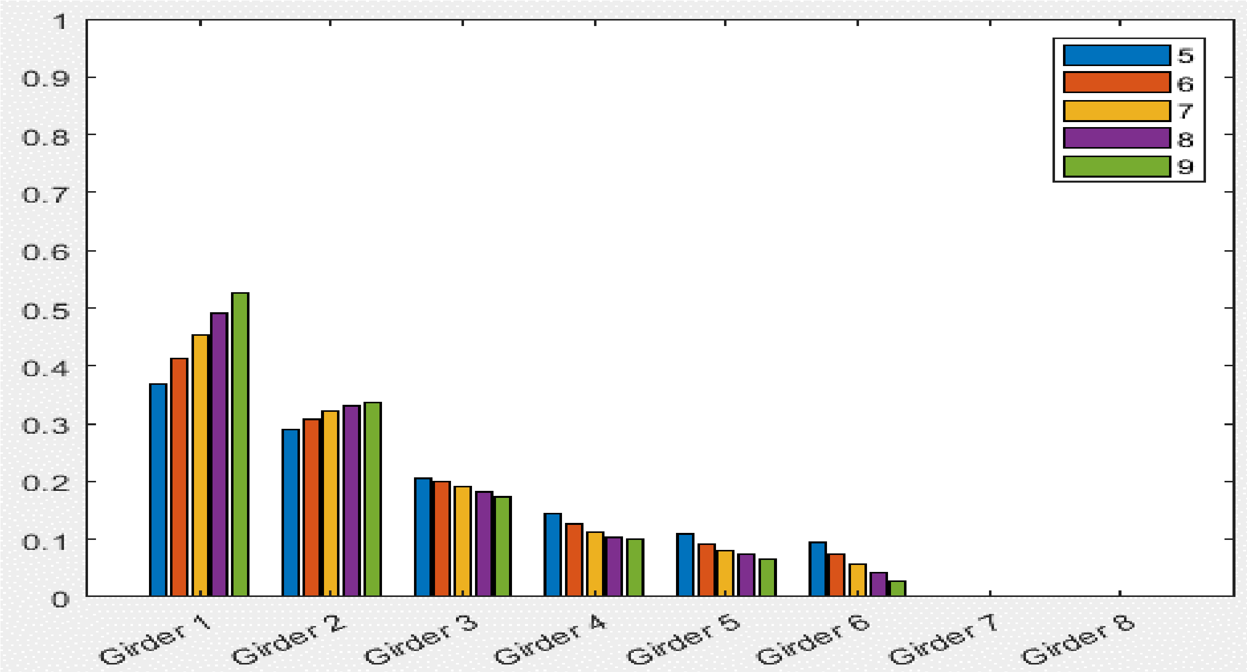

Standard Bridge #2, Tarhini/Frederick Methodology, EG OLL, Variable = Girder Spacing (ft)

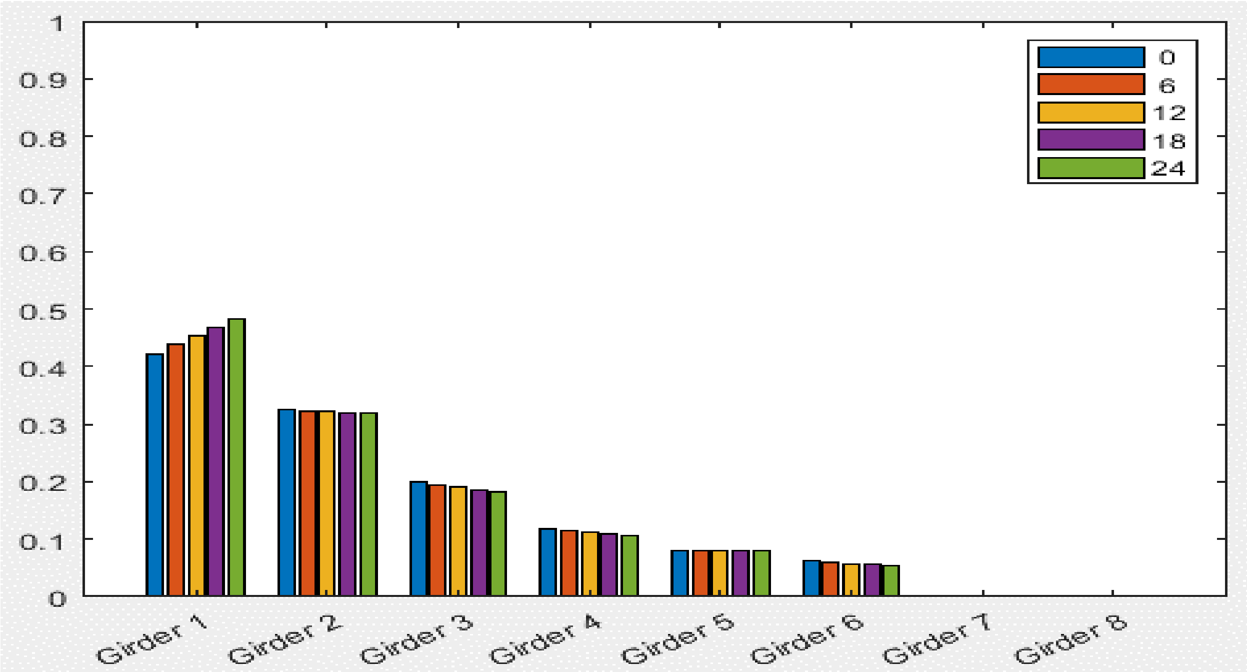

Standard Bridge #2, Tarhini/Frederick Methodology, EG OLL, Variable = Overhang Distance (in)

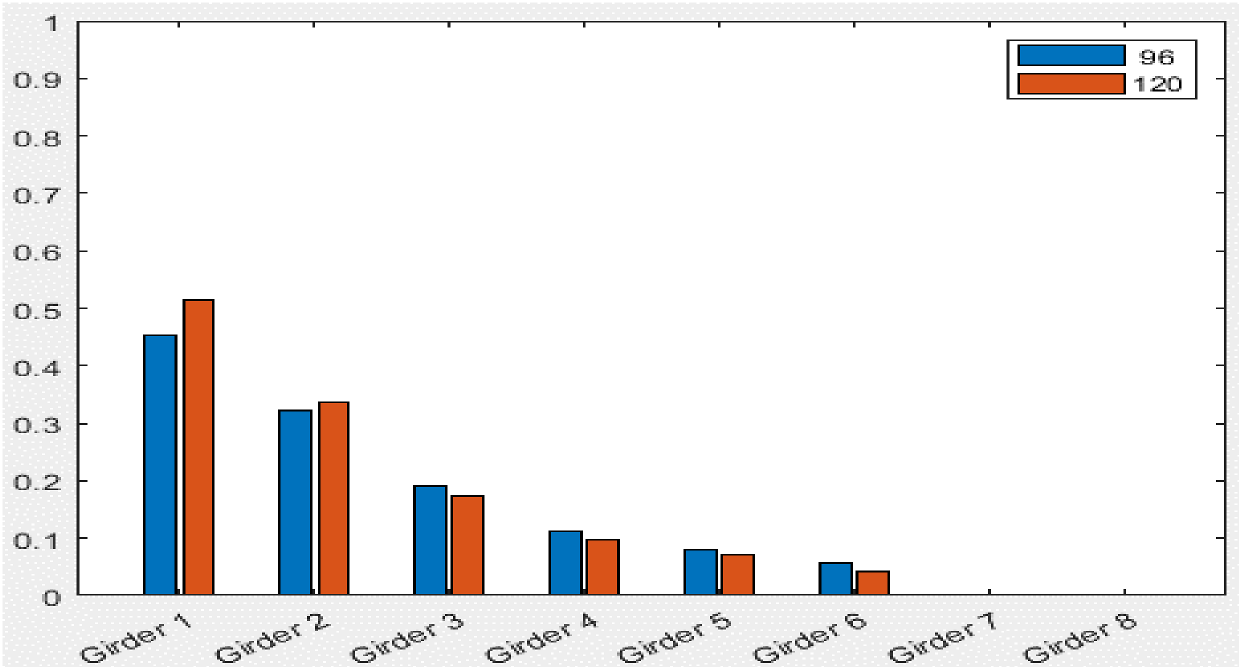

Standard Bridge #2, Tarhini/Frederick Methodology, EG OLL, Variable = Plate Size

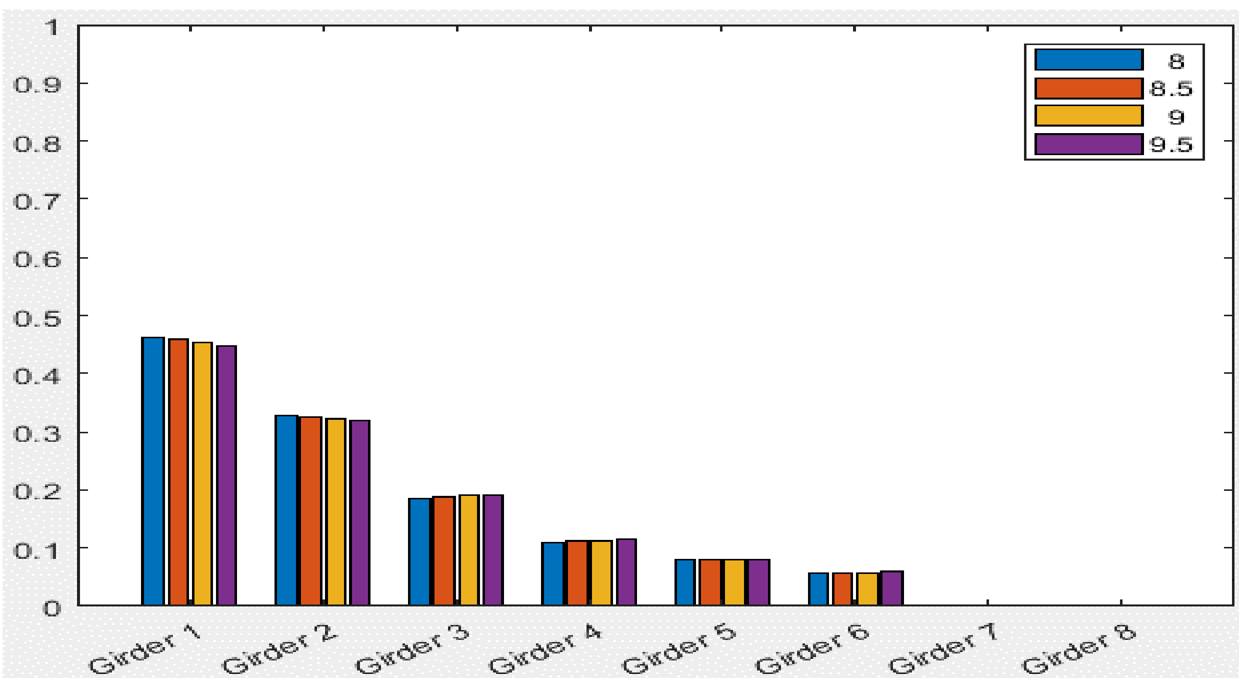

Standard Bridge #2, Tarhini/Frederick Methodology, EG OLL, Variable = Deck Thickness (in)

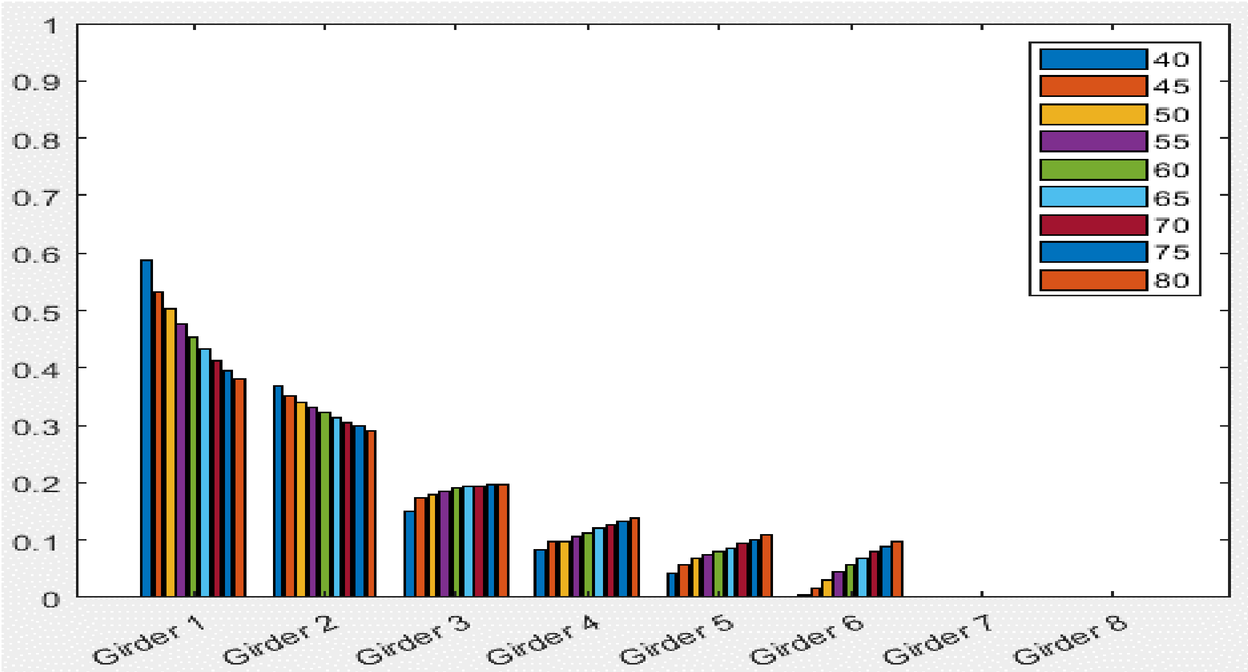

Standard Bridge #2, Tarhini/Frederick Methodology, EG OLL, Variable = Span Length (ft)

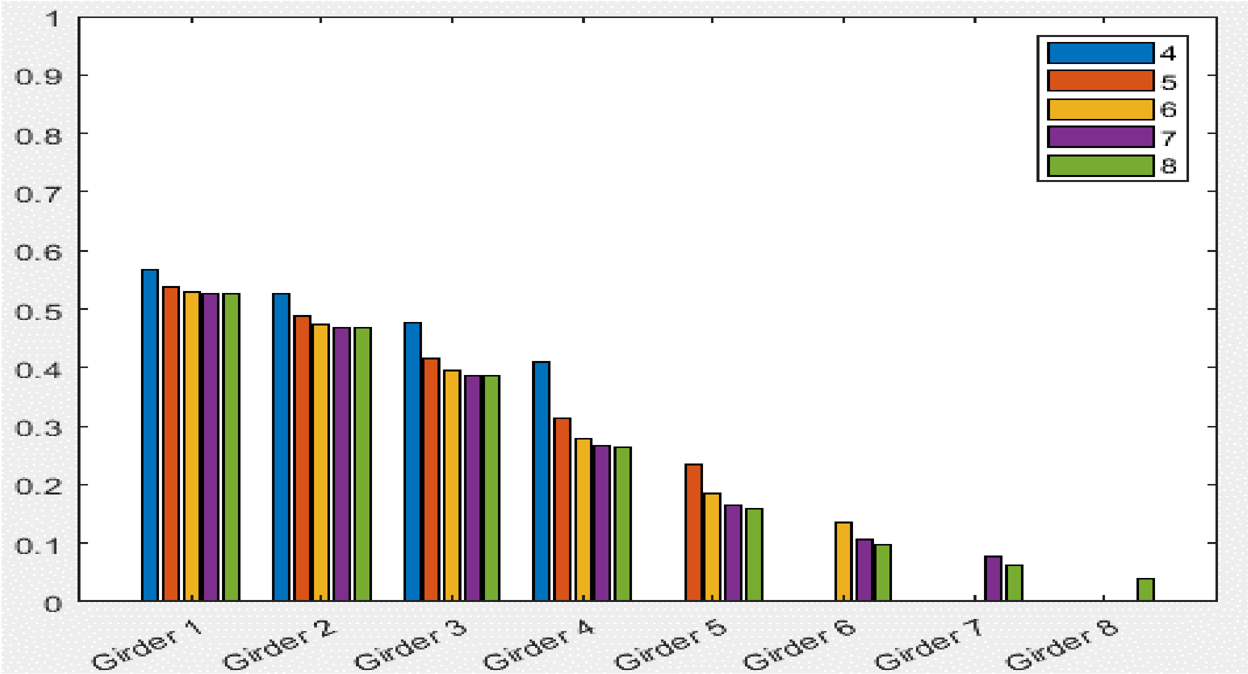

Standard Bridge #2, Tarhini/Frederick Methodology, EG 2LL, Variable = Number of Beams

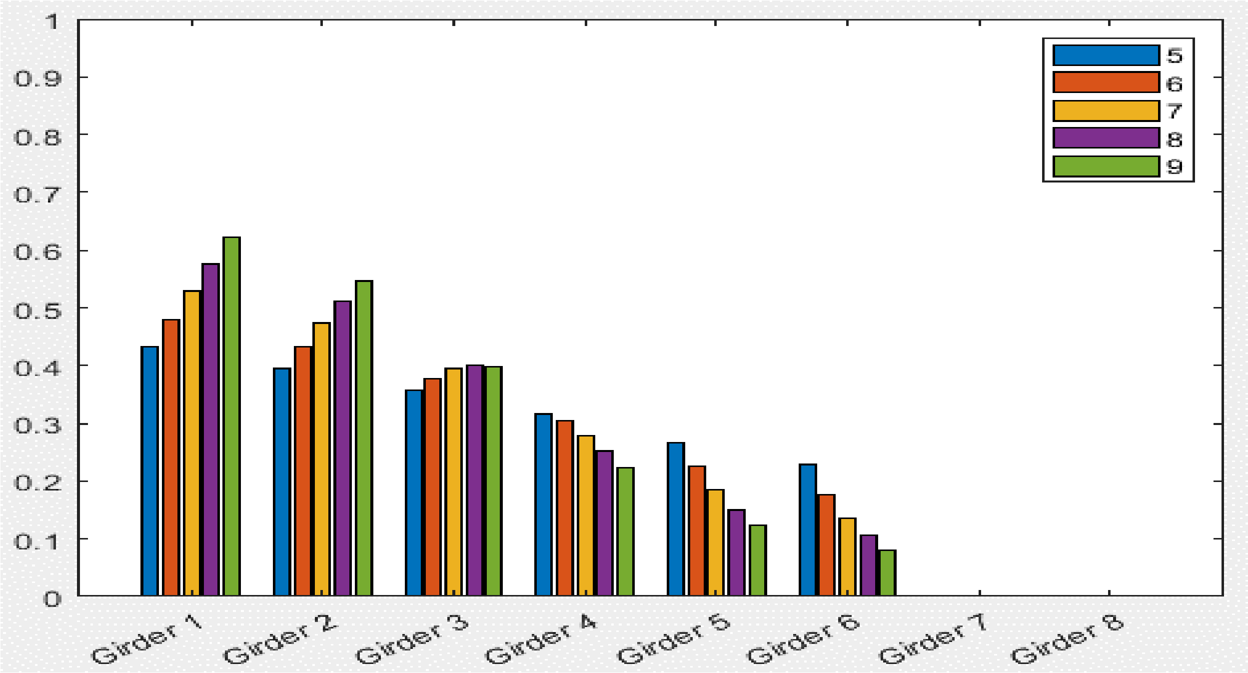

Standard Bridge #2, Tarhini/Frederick Methodology, EG 2LL, Variable = Girder Spacing (ft)

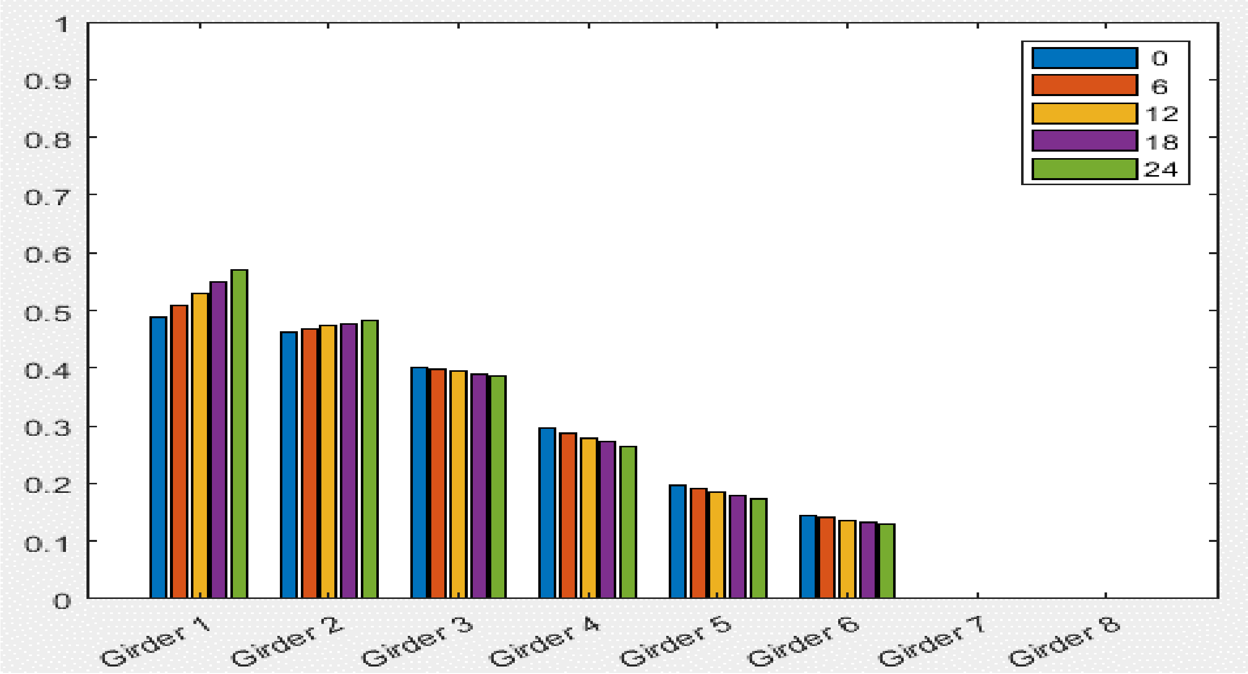

Standard Bridge #2, Tarhini/Frederick Methodology, EG 2LL, Variable = Overhang Distance (in)

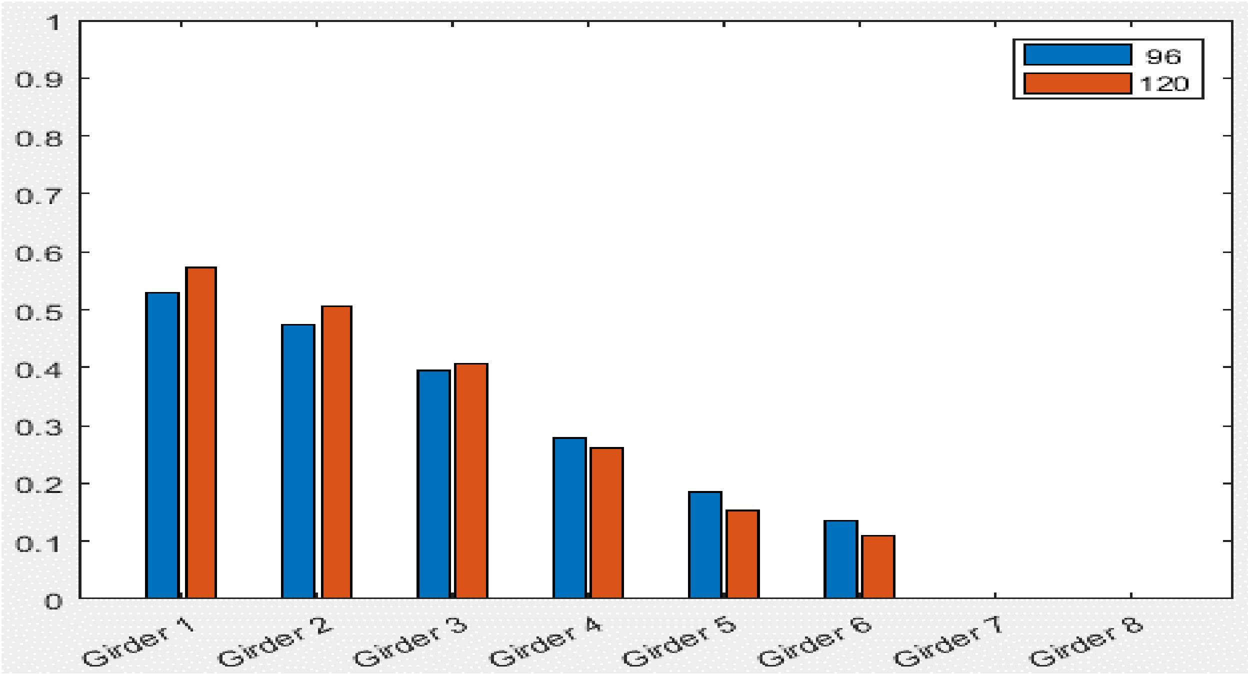

Standard Bridge #2, Tarhini/Frederick Methodology, EG 2LL, Variable = Plate Size

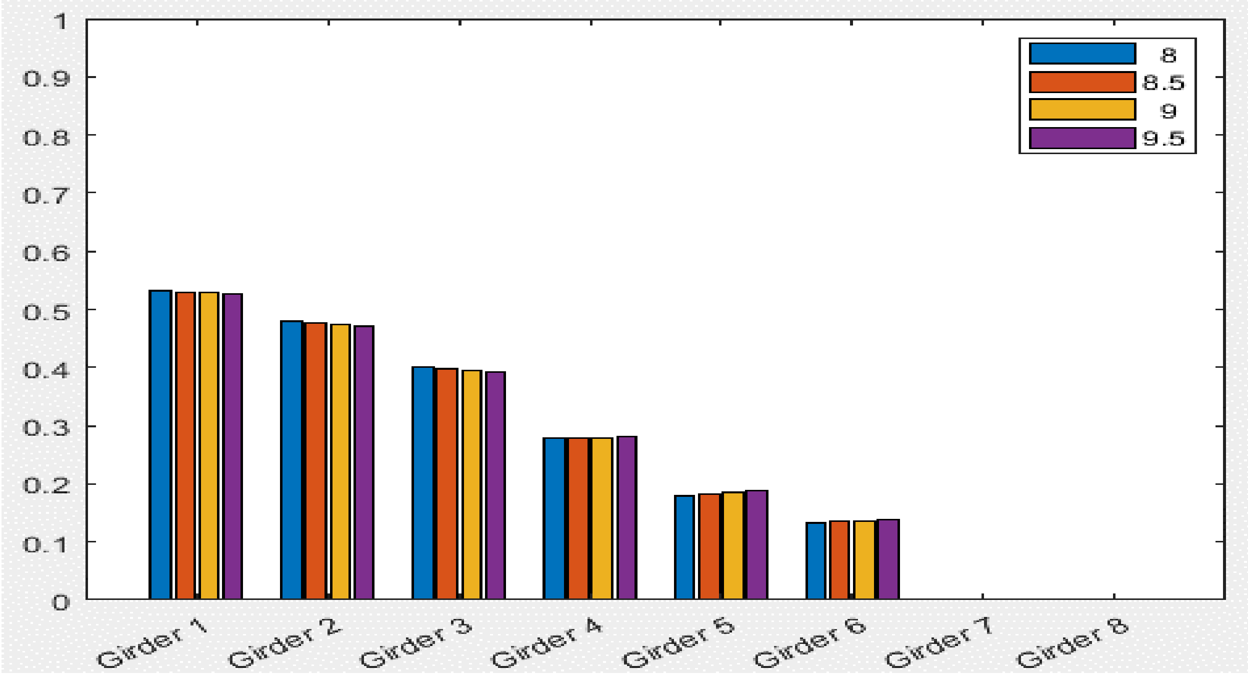

Standard Bridge #2, Tarhini/Frederick Methodology, EG 2LL, Variable = Deck Thickness (in)

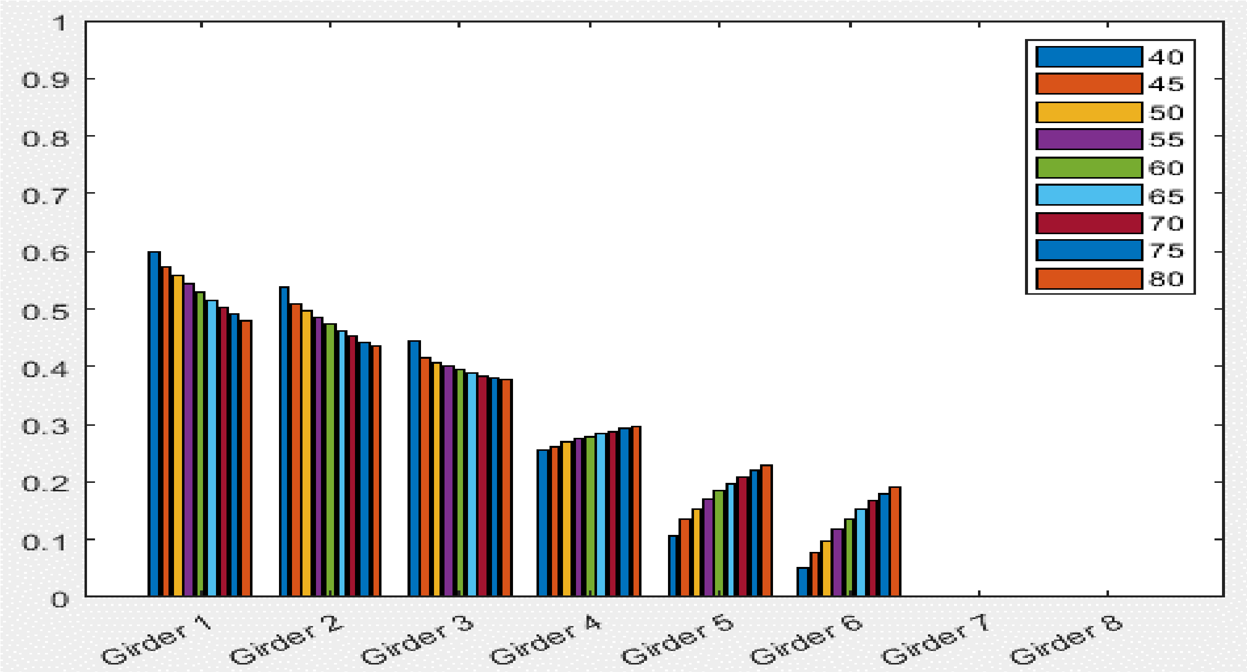

Standard Bridge #2, Tarhini/Frederick Methodology, EG 2LL, Variable = Span Length (ft)

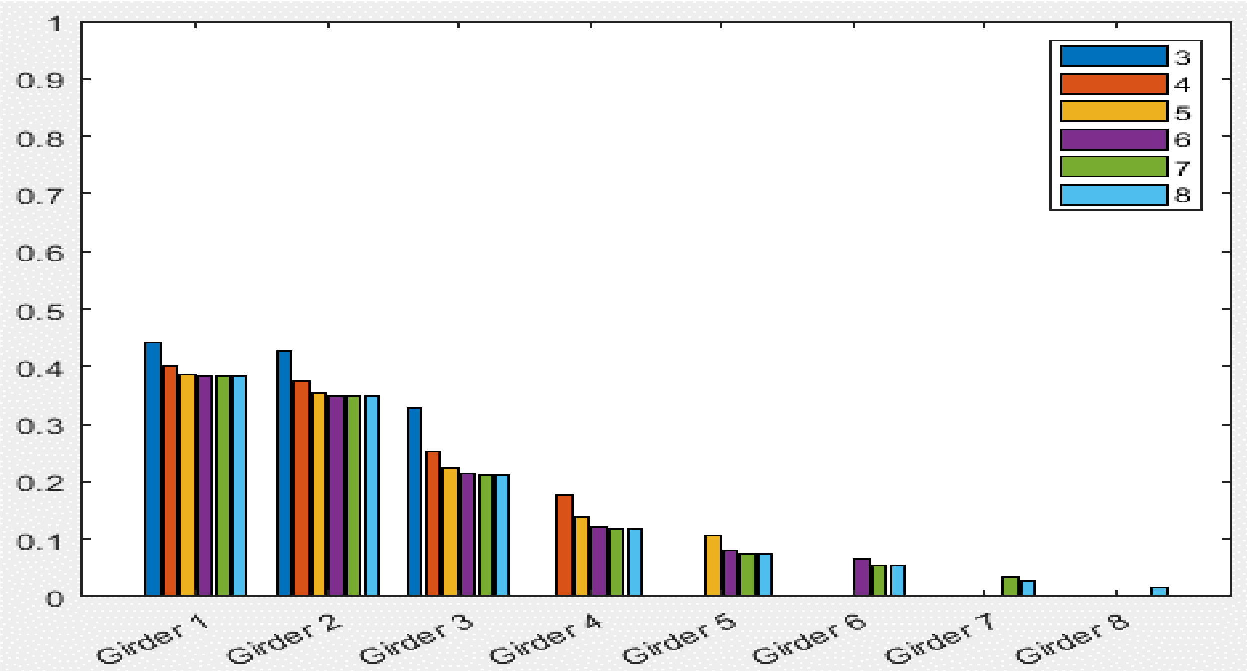

Standard Bridge #3, Tarhini/Frederick Methodology, IG OLL, Variable = Number of Beams

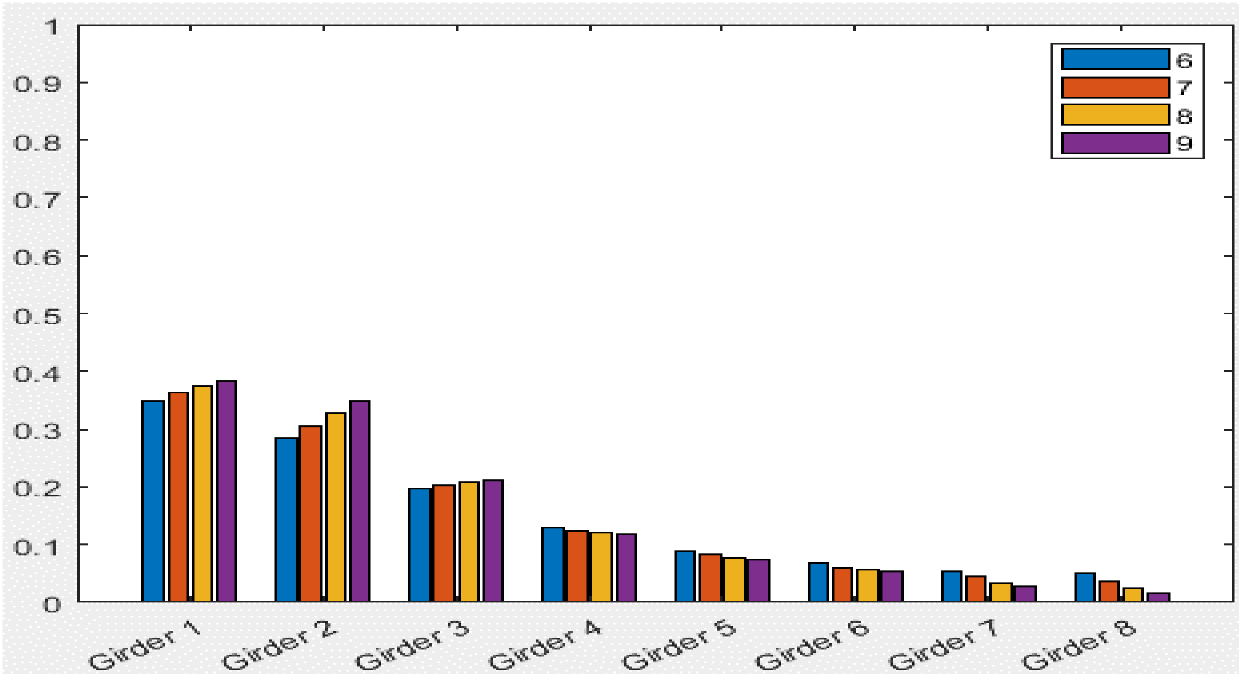

Standard Bridge #3, Tarhini/Frederick Methodology, IG OLL, Variable = Girder Spacing (ft)

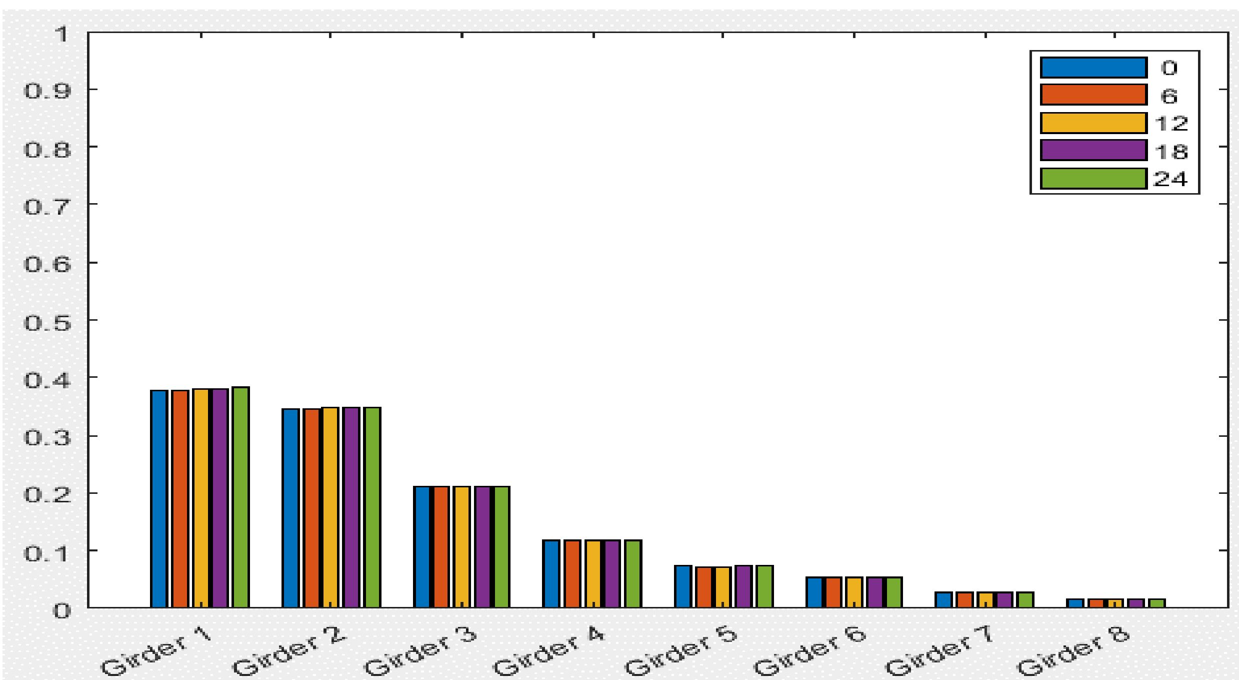

Standard Bridge #3, Tarhini/Frederick Methodology, IG OLL, Variable = Overhang Distance (in)

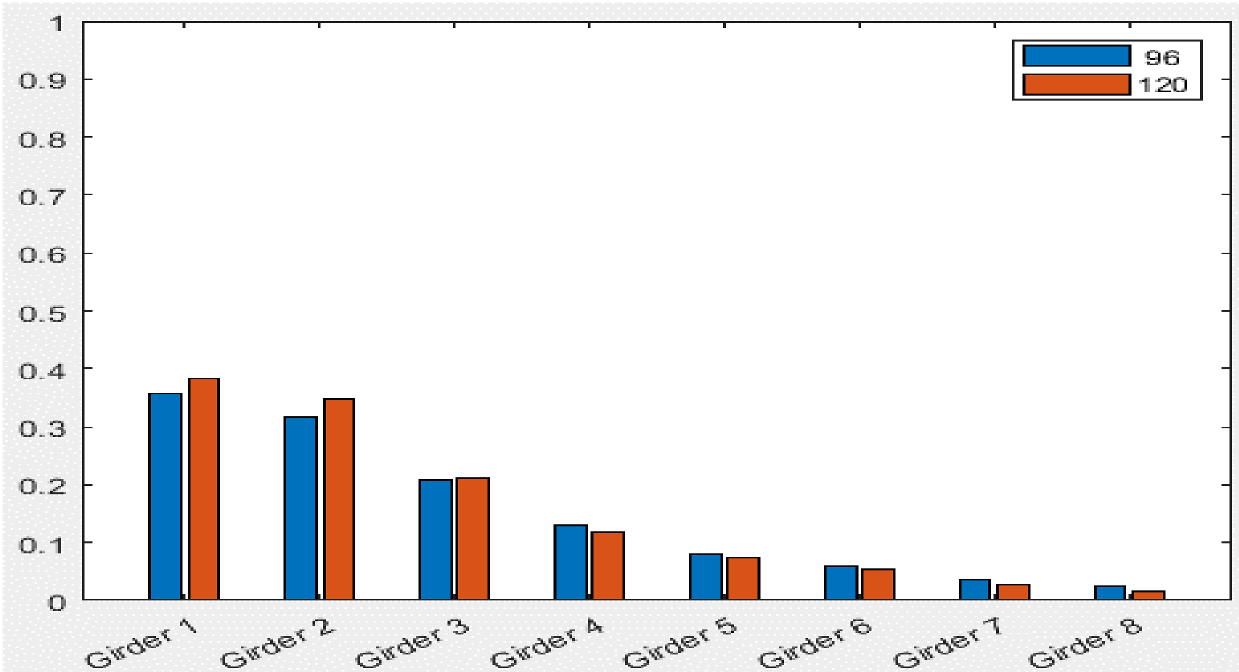

Standard Bridge #3, Tarhini/Frederick Methodology, IG OLL, Variable = Plate Size

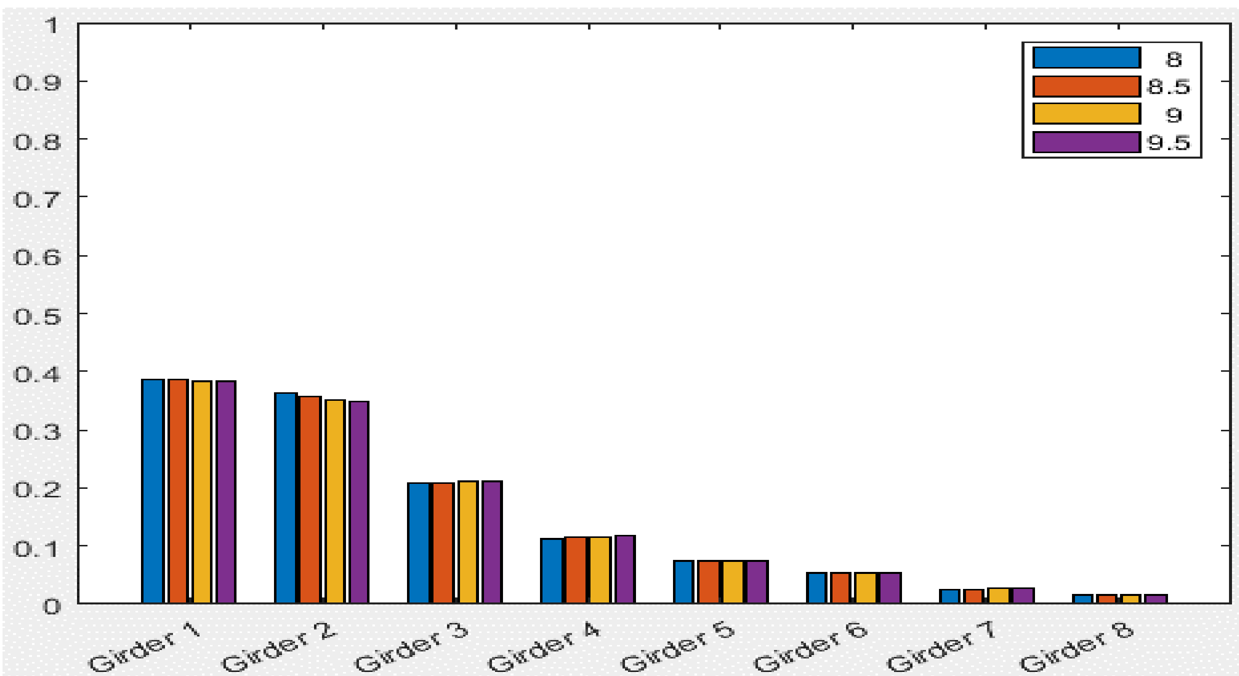

Standard Bridge #3, Tarhini/Frederick Methodology, IG OLL, Variable = Deck Thickness (in)

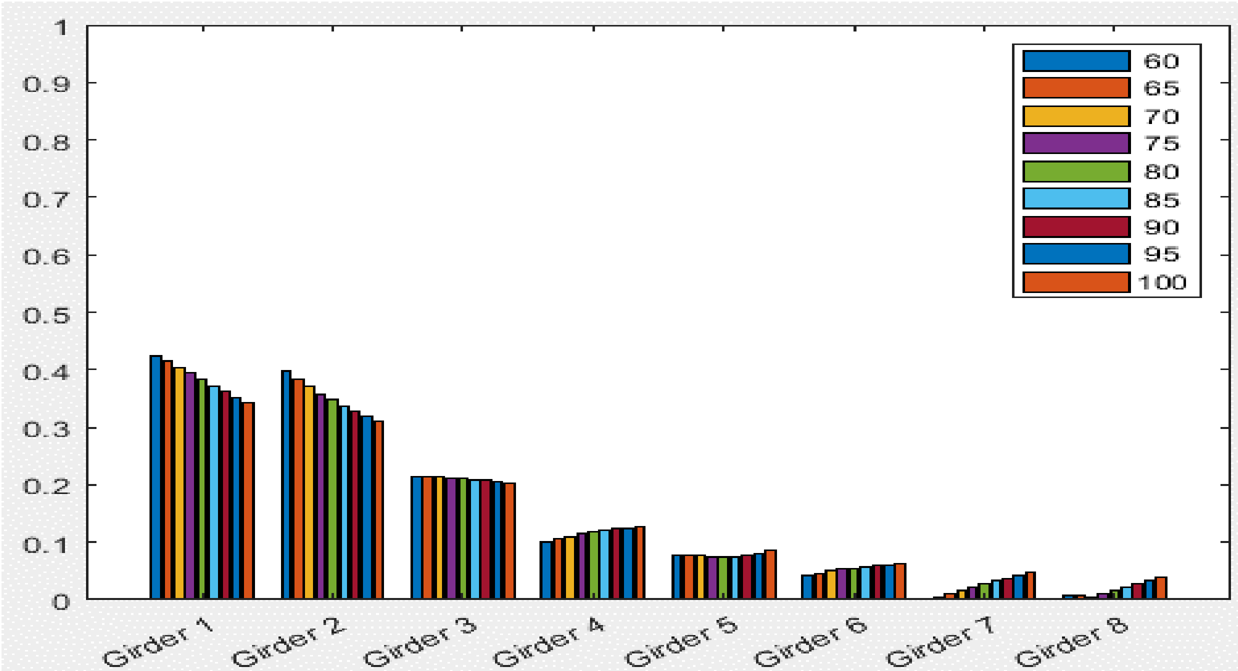

Standard Bridge #3, Tarhini/Frederick Methodology, IG OLL, Variable = Span Length (ft)

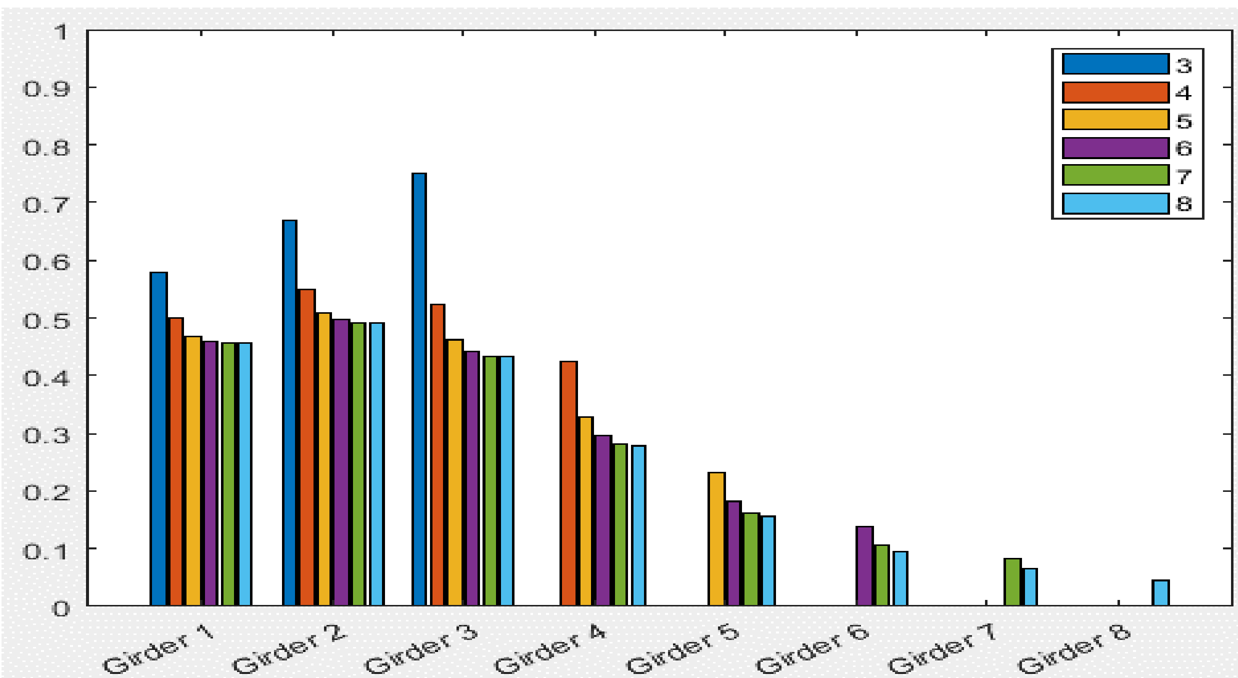

Standard Bridge #3, Tarhini/Frederick Methodology, IG 2LL, Variable = Number of Beams

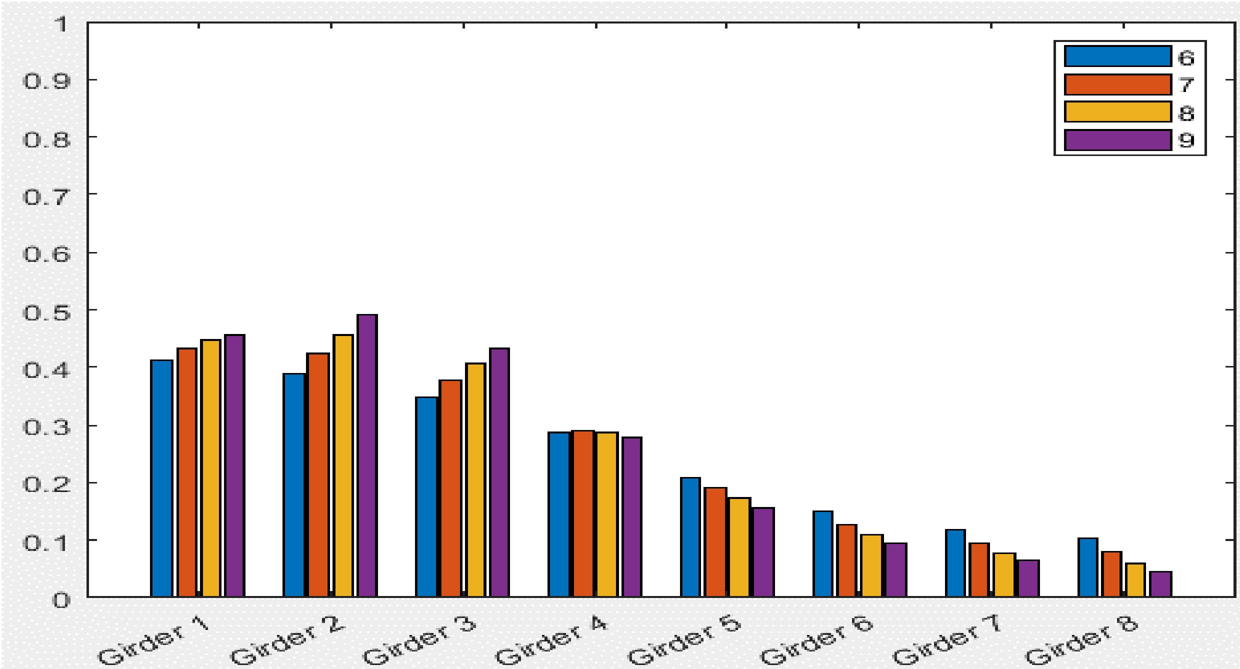

Standard Bridge #3, Tarhini/Frederick Methodology, IG 2LL, Variable = Girder Spacing (ft)

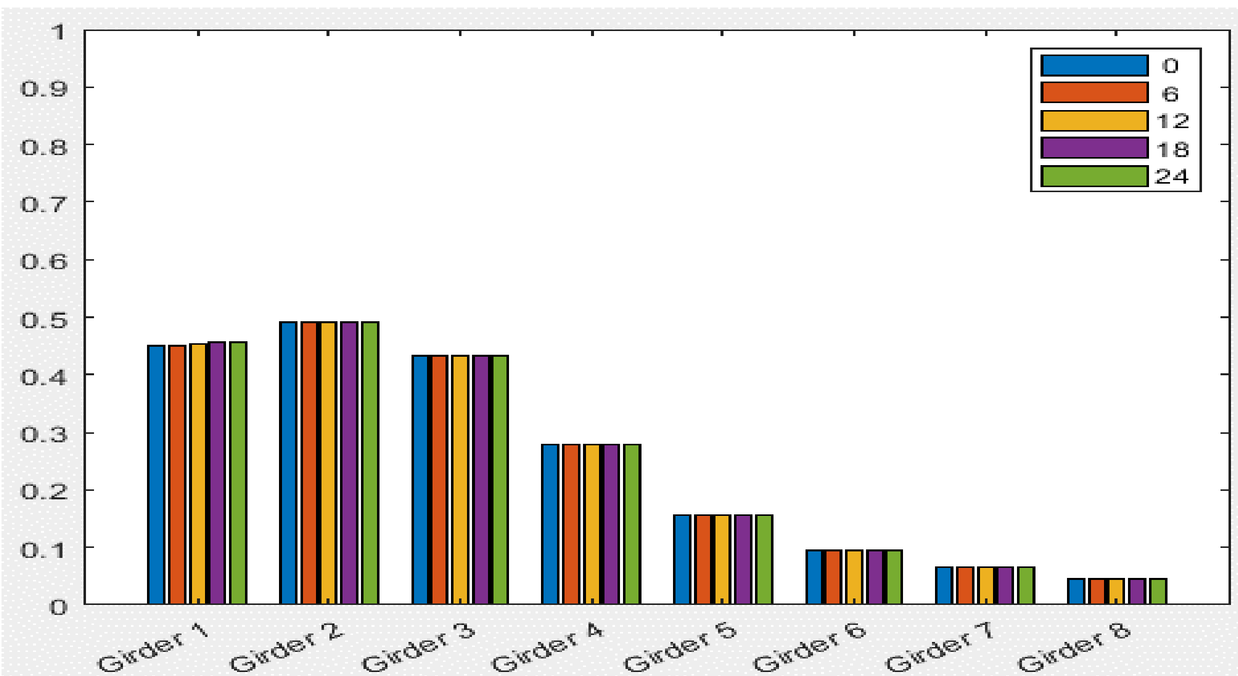

Standard Bridge #3, Tarhini/Frederick Methodology, IG 2LL, Variable = Overhang Distance (in)

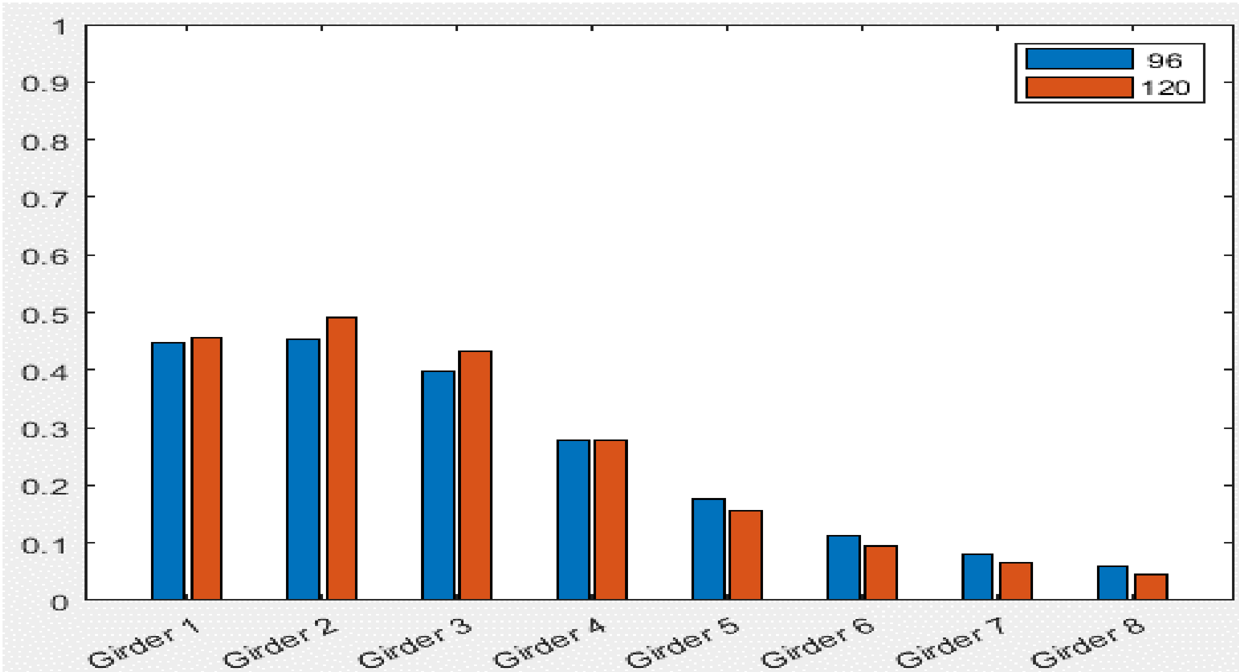

Standard Bridge #3, Tarhini/Frederick Methodology, IG 2LL, Variable = Plate Size

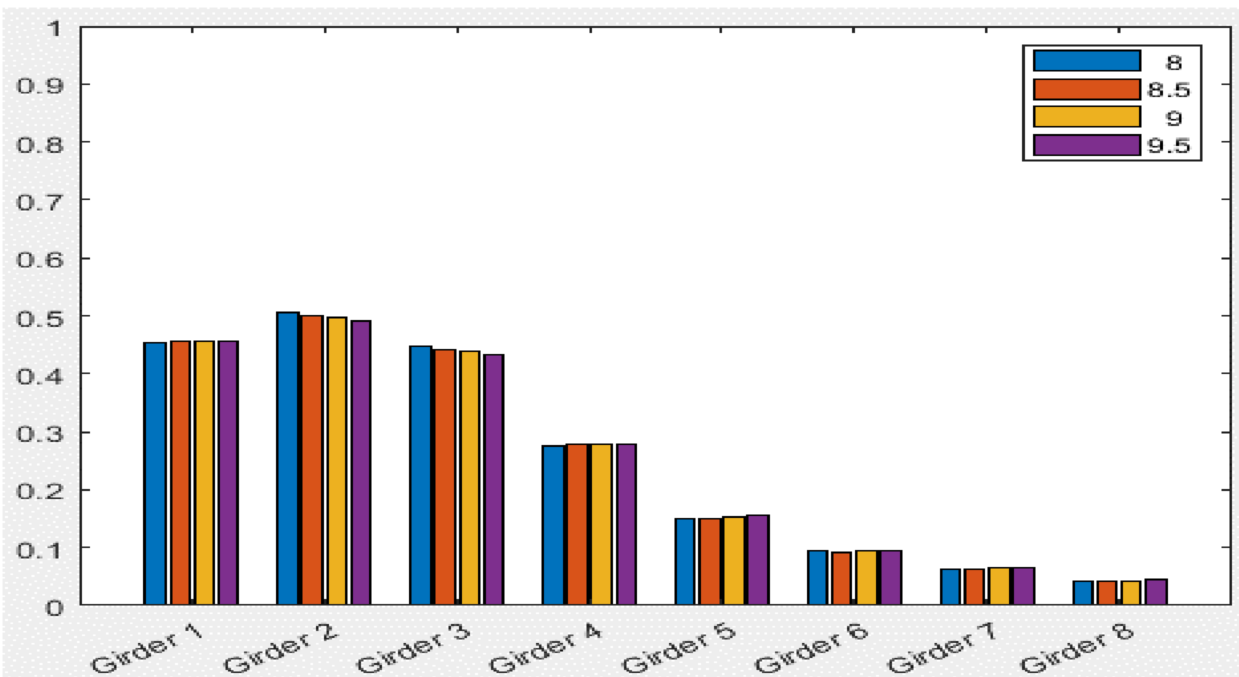

Standard Bridge #3, Tarhini/Frederick Methodology, IG 2LL, Variable = Deck Thickness (in)

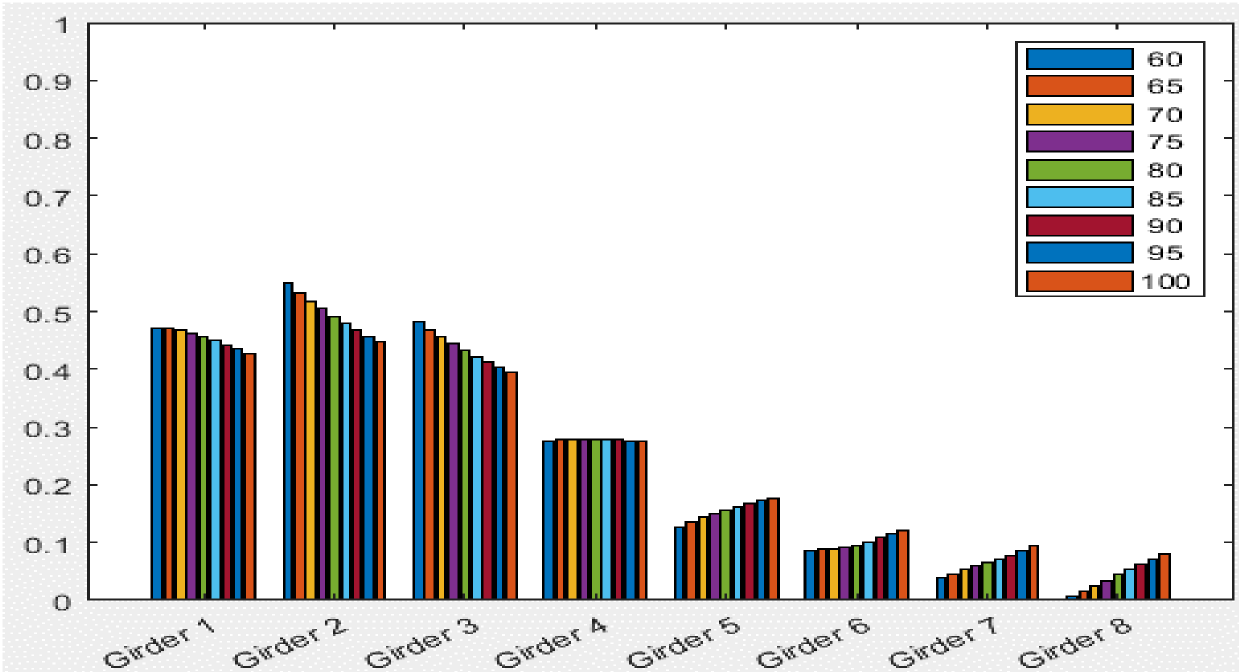

Standard Bridge #3, Tarhini/Frederick Methodology, IG 2LL, Variable = Span Length (ft)

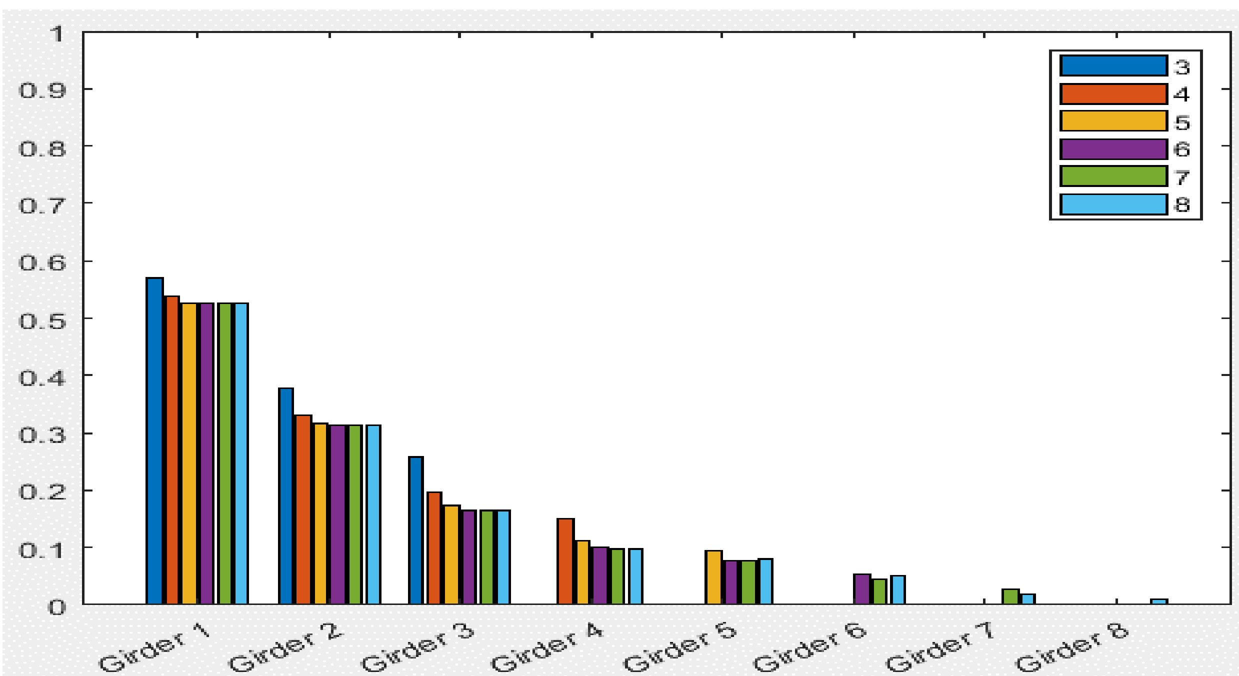

Standard Bridge #3, Tarhini/Frederick Methodology, EG OLL, Variable = Number of Beams

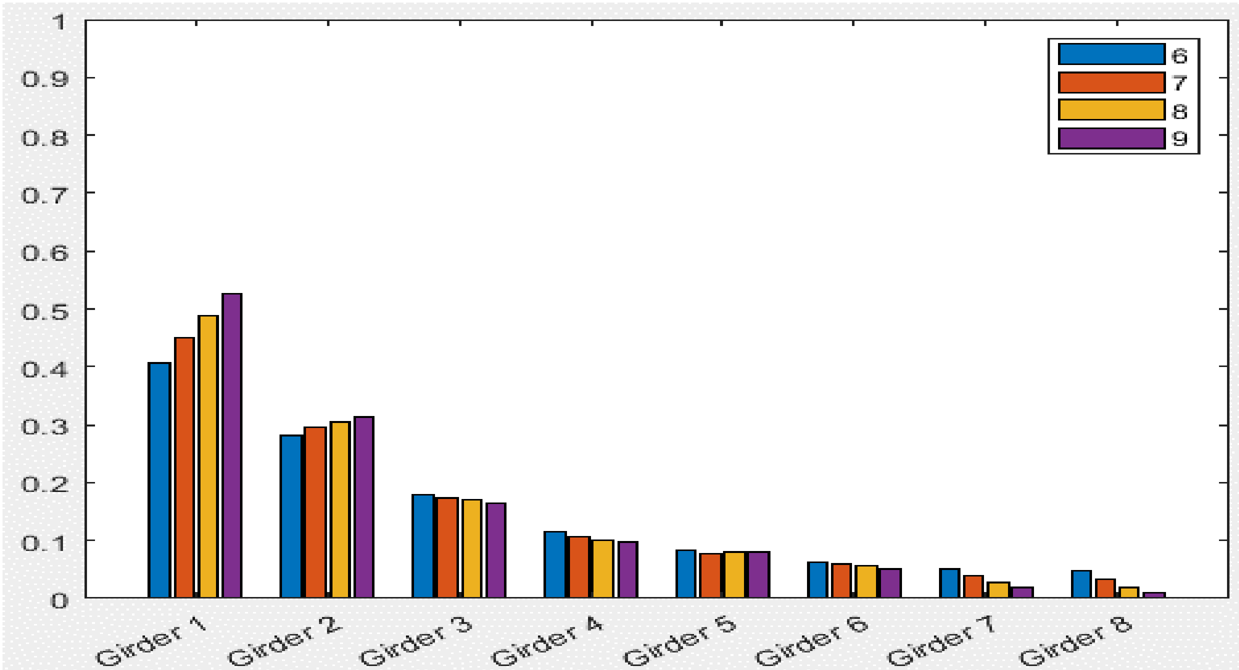

Standard Bridge #3, Tarhini/Frederick Methodology, EG OLL, Variable = Girder Spacing (ft)

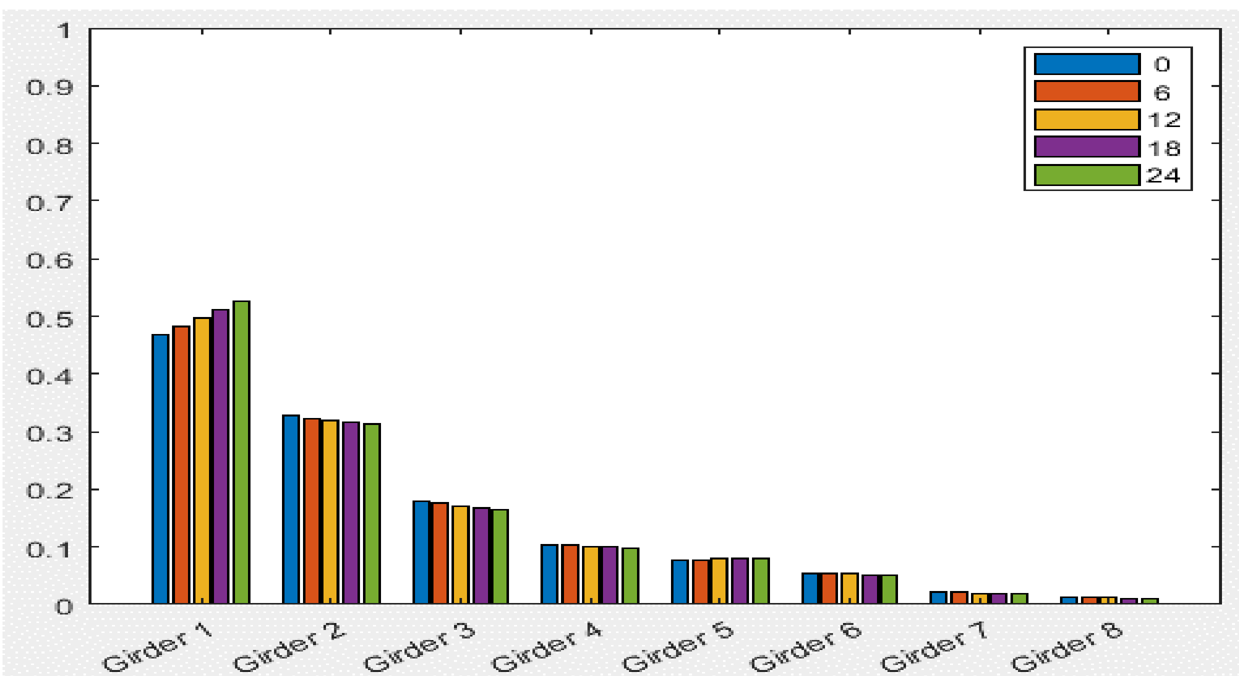

Standard Bridge #3, Tarhini/Frederick Methodology, EG OLL, Variable = Overhang Distance (in)

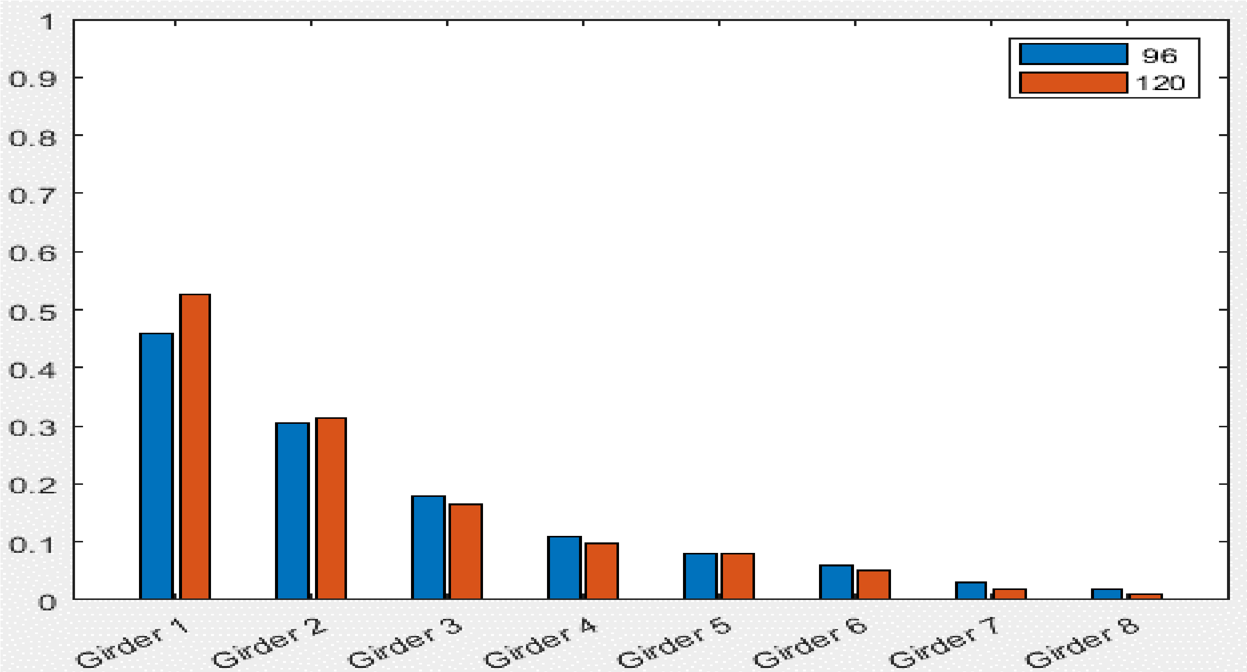

Standard Bridge #3, Tarhini/Frederick Methodology, EG OLL, Variable = Plate Size

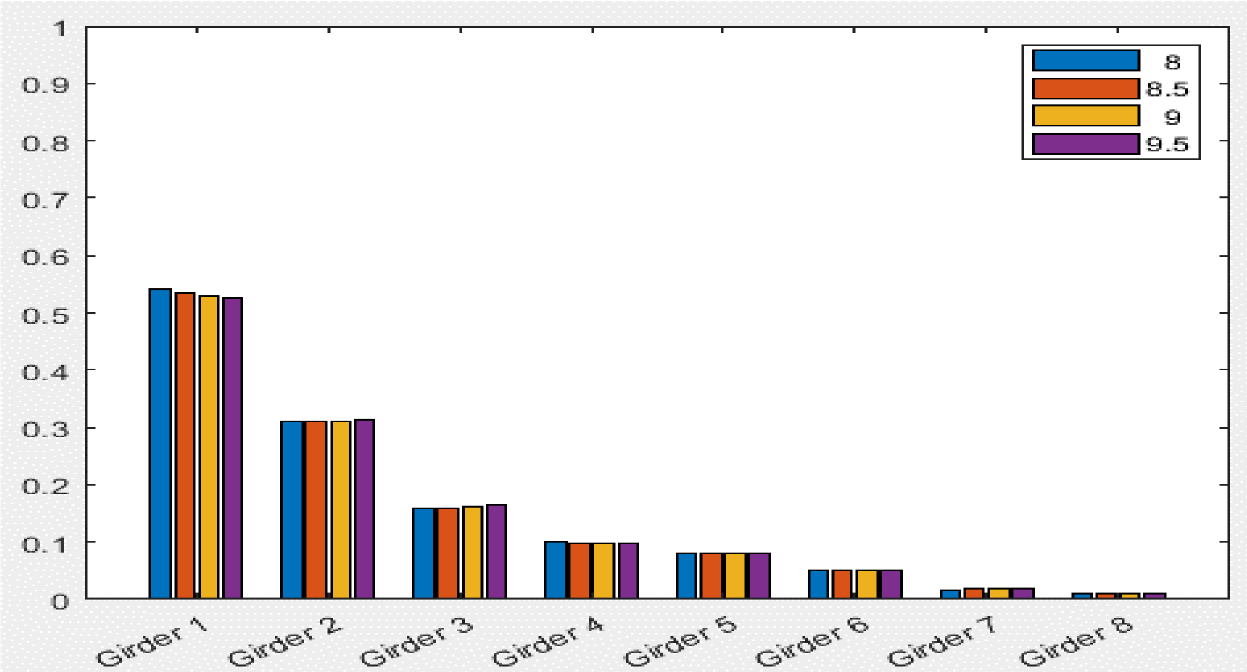

Standard Bridge #3, Tarhini/Frederick Methodology, EG OLL, Variable = Deck Thickness (in)

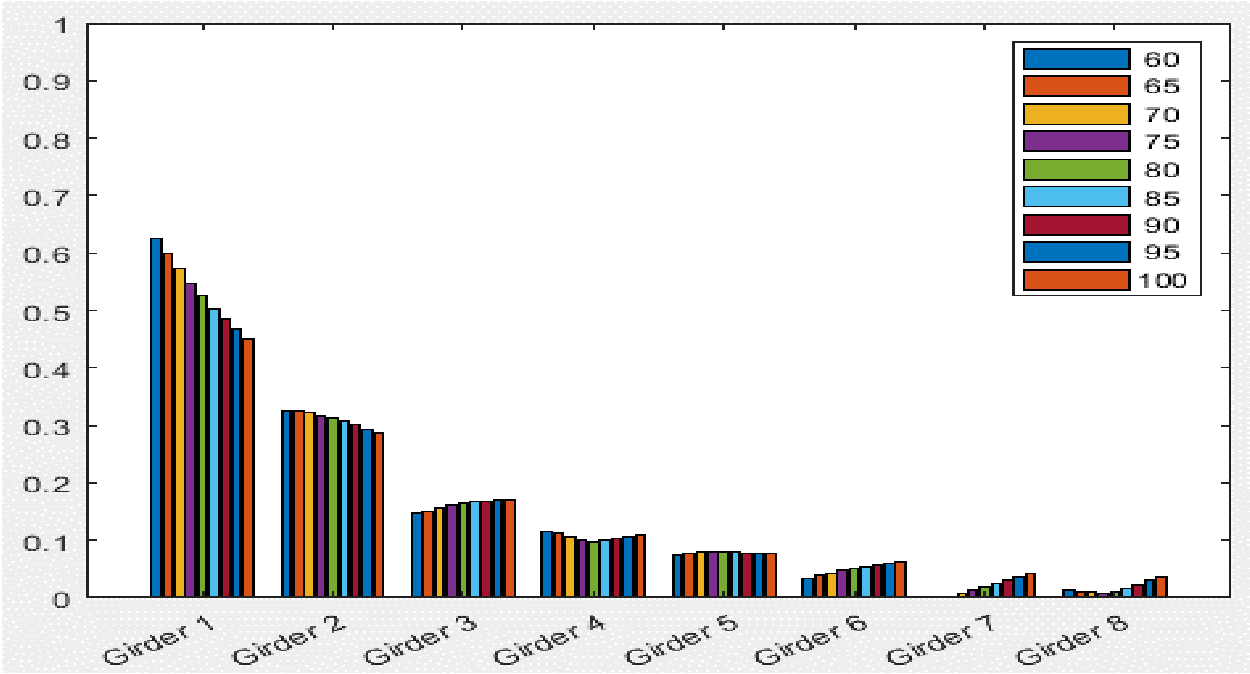

Standard Bridge #3, Tarhini/Frederick Methodology, EG OLL, Variable = Span Length (ft)

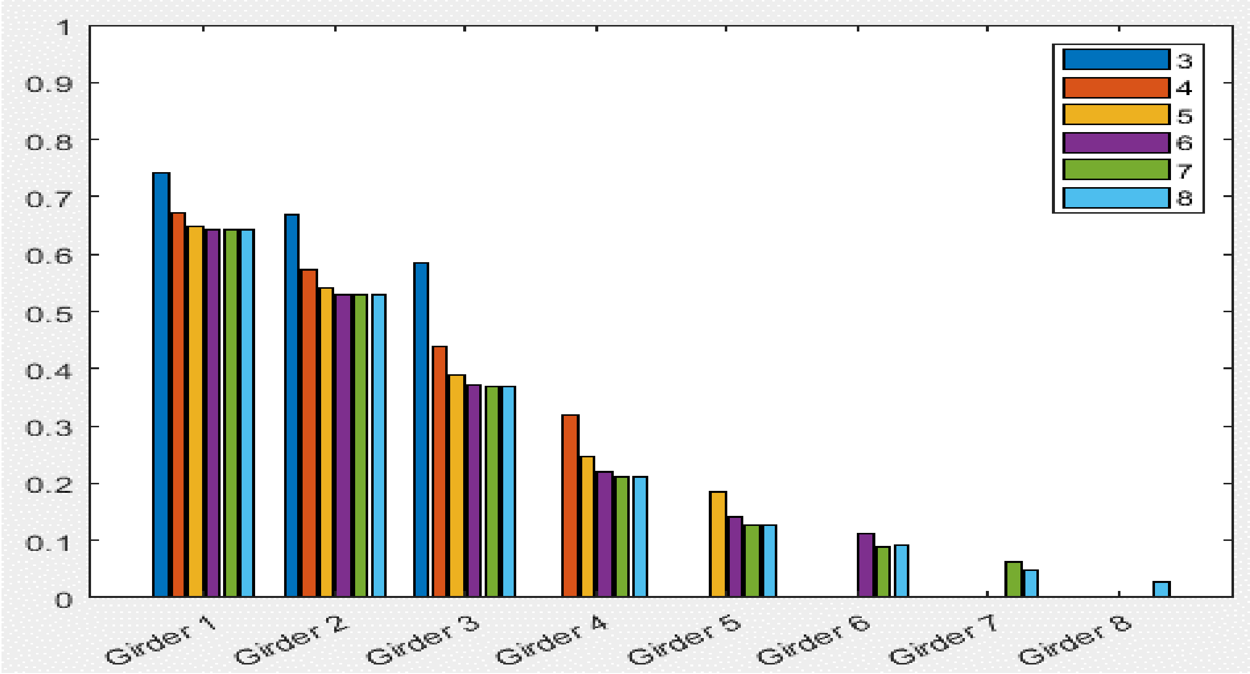

Standard Bridge #3, Tarhini/Frederick Methodology, EG 2LL, Variable = Number of Beams

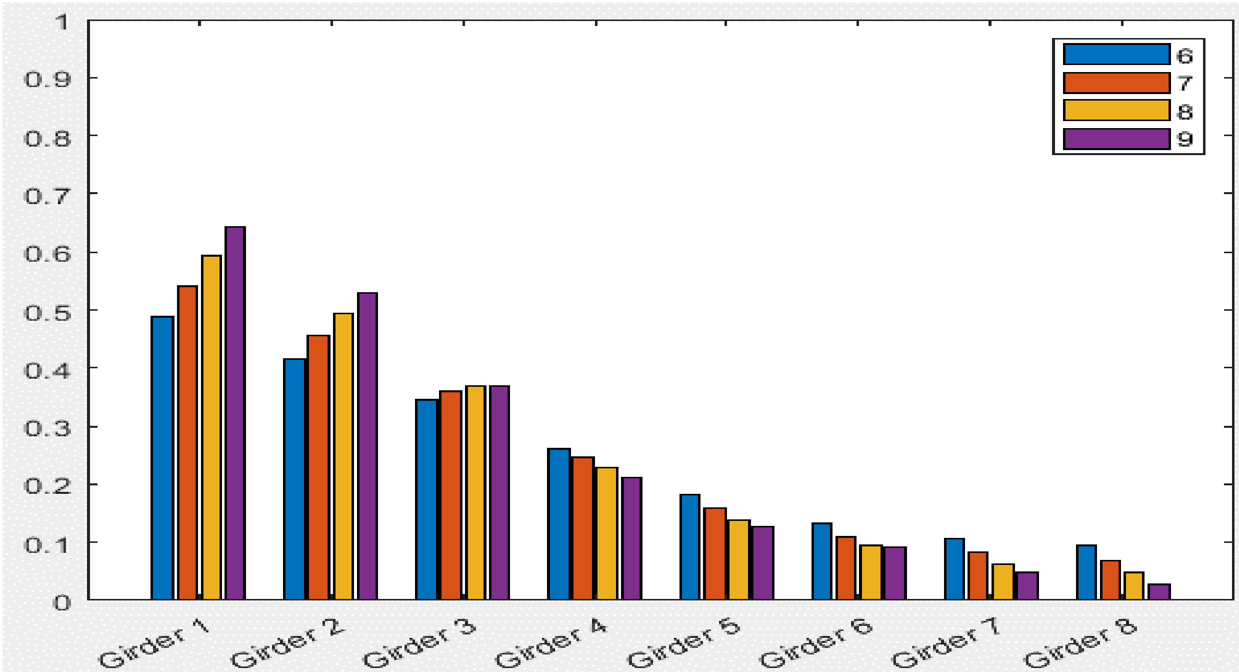

Standard Bridge #3, Tarhini/Frederick Methodology, EG 2LL, Variable = Girder Spacing (ft)

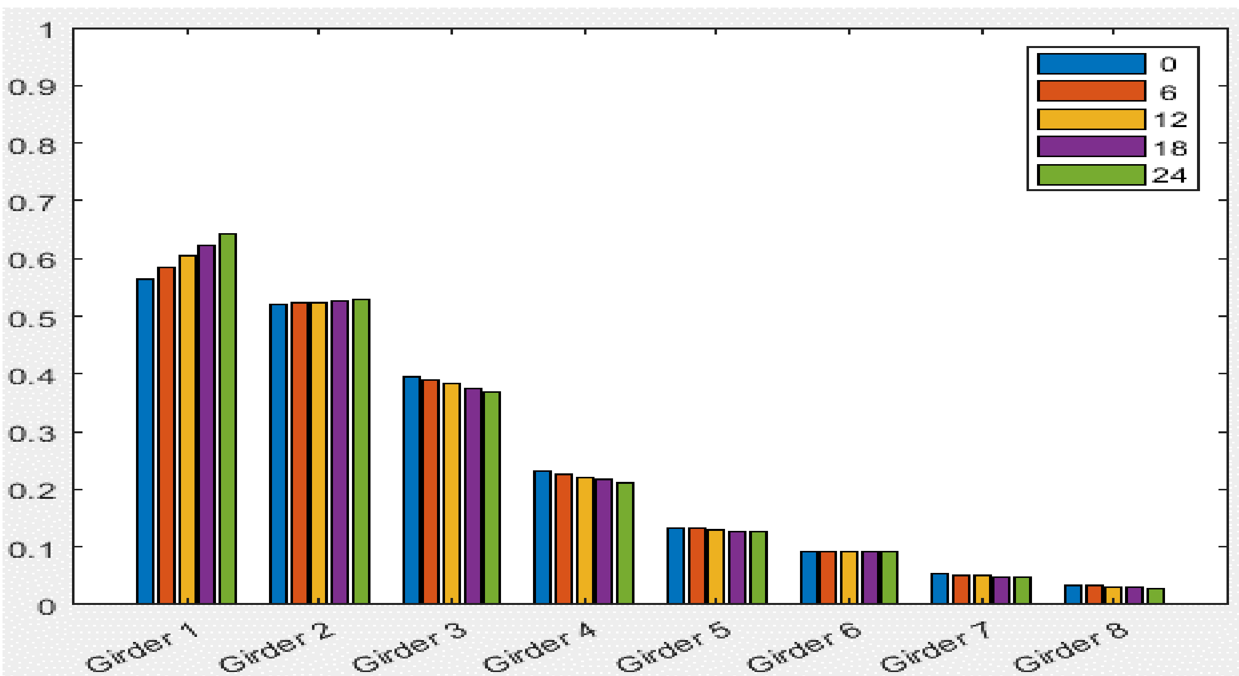

Standard Bridge #3, Tarhini/Frederick Methodology, EG 2LL, Variable = Overhang Distance (in)

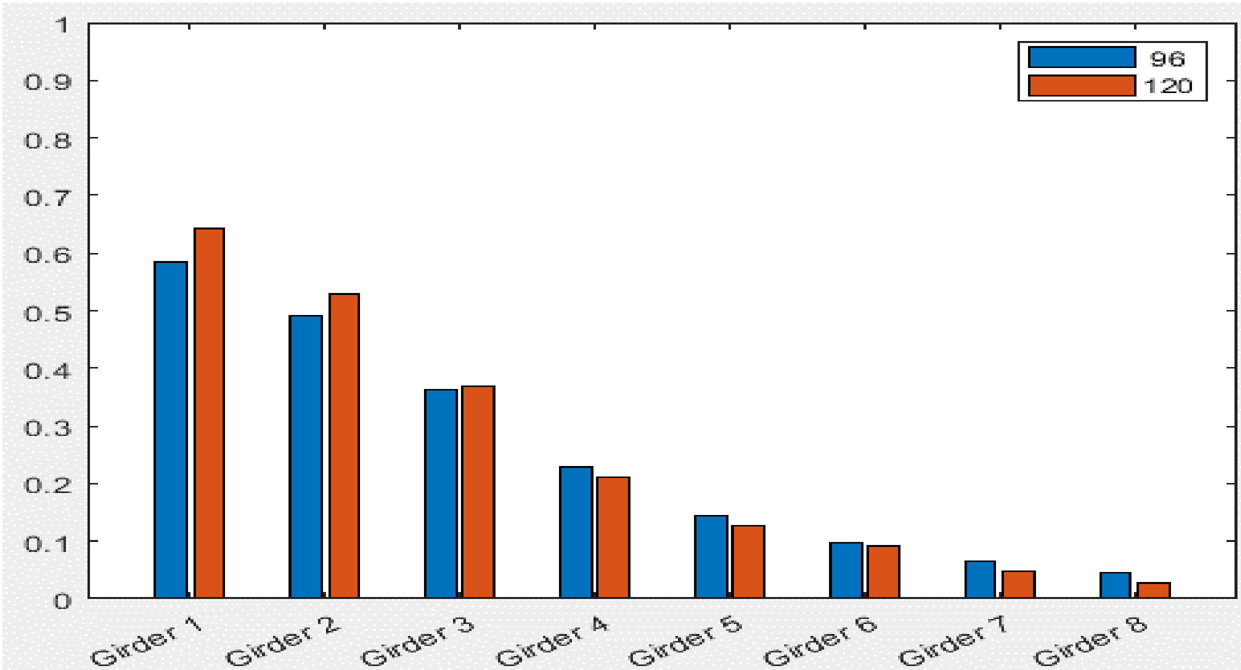

Standard Bridge #3, Tarhini/Frederick Methodology, EG 2LL, Variable = Plate Size

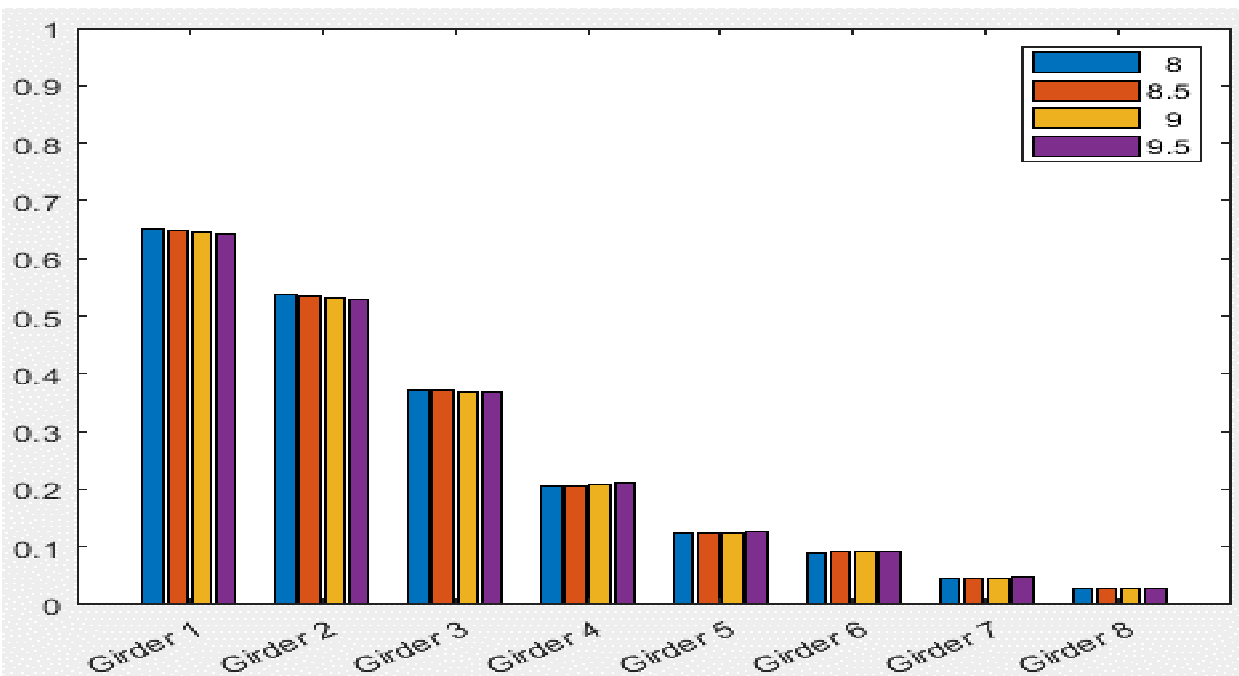

Standard Bridge #3, Tarhini/Frederick Methodology, EG 2LL, Variable = Deck Thickness (in)

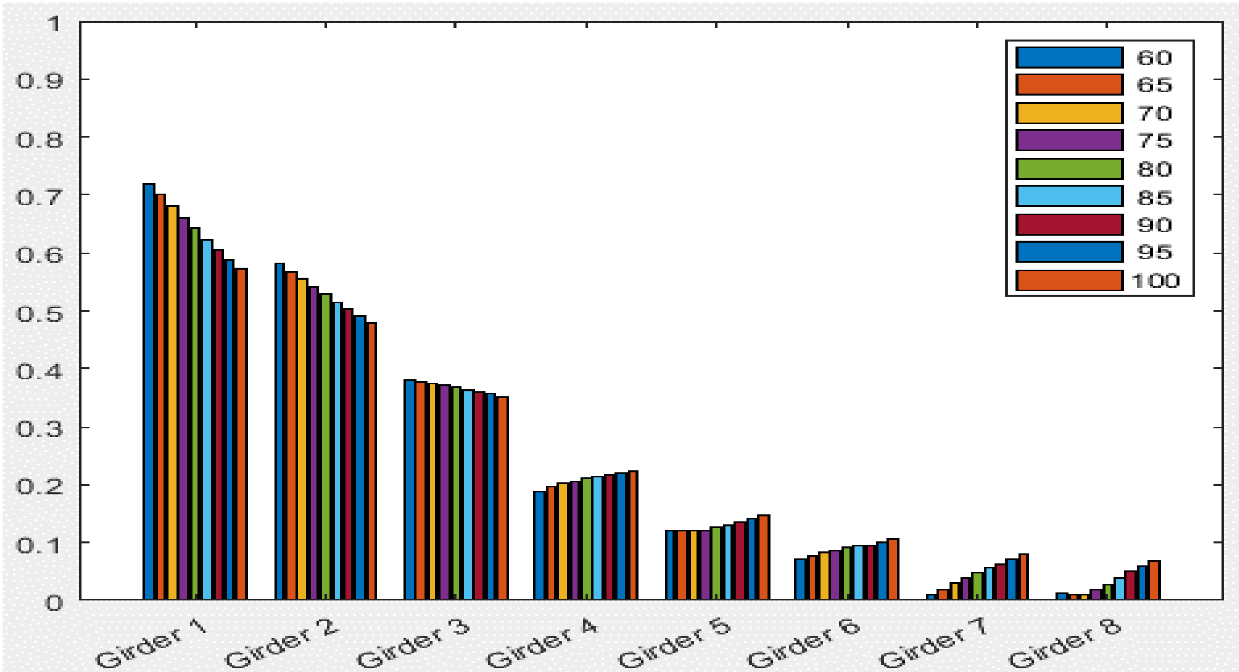

Standard Bridge #3, Tarhini/Frederick Methodology, EG 2LL, Variable = Span Length (ft)

APPENDIX C: COMPACTNESS SENSITIVITY MATRIX RESULTS

This appendix documents the results from the analytical study performed in Chapter 9. The graphs are titled according to the degrees of skew discussed in Chapter 9. In addition, for each graph, the concentrated load at midspan corresponding to the yield moment, plastic moment, and nominal capacity calculated from AASHTO LRFD BDS Article 6.11.7, assuming the section is considered noncompact, is displayed.

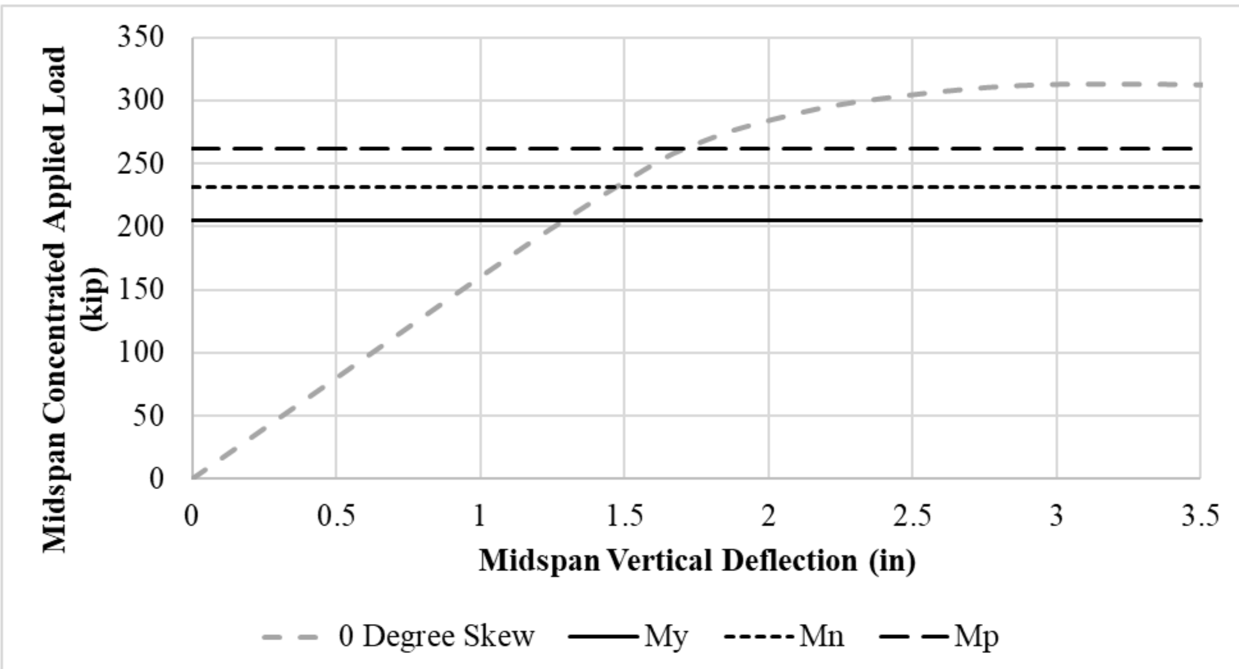

Load-Deflection Graph for the Analytical Test with 0° Skew

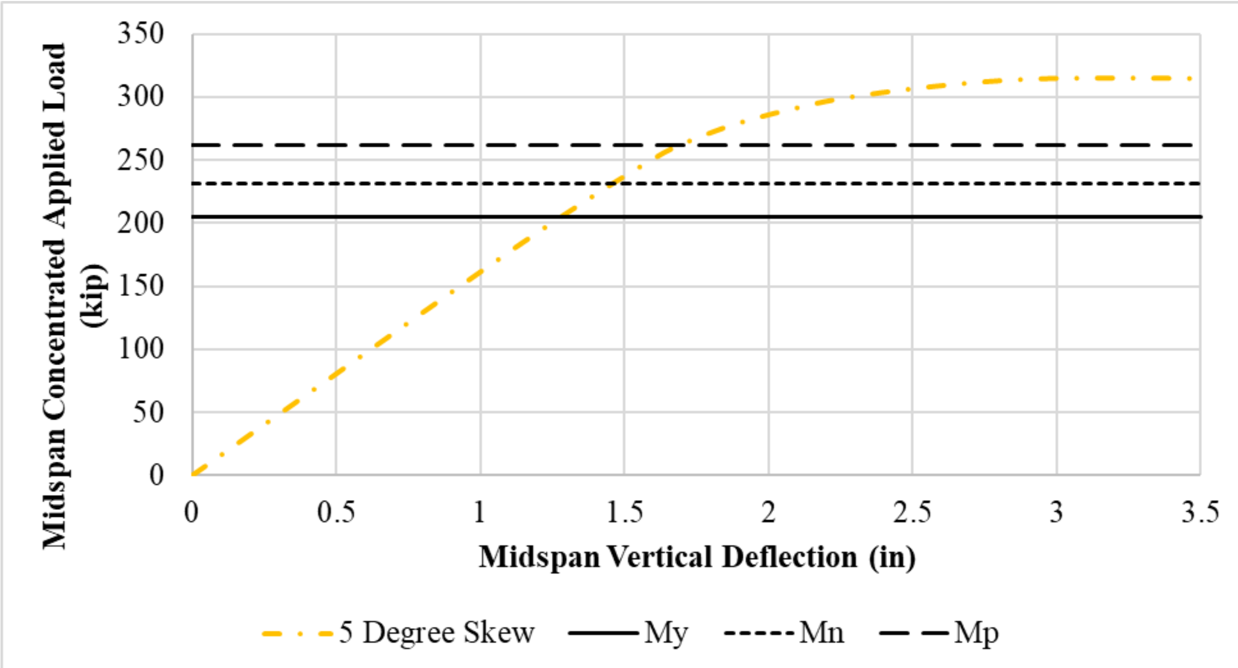

Load-Deflection Graph for the Analytical Test with 5° Skew

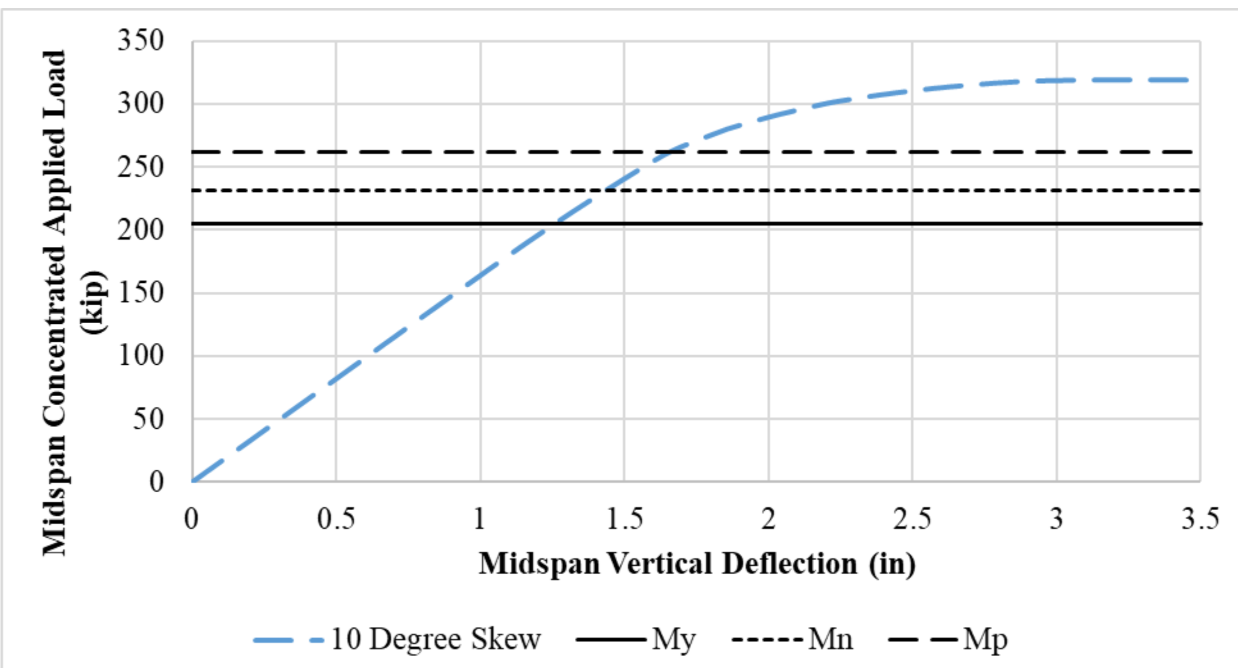

Load-Deflection Graph for the Analytical Test with 10° Skew

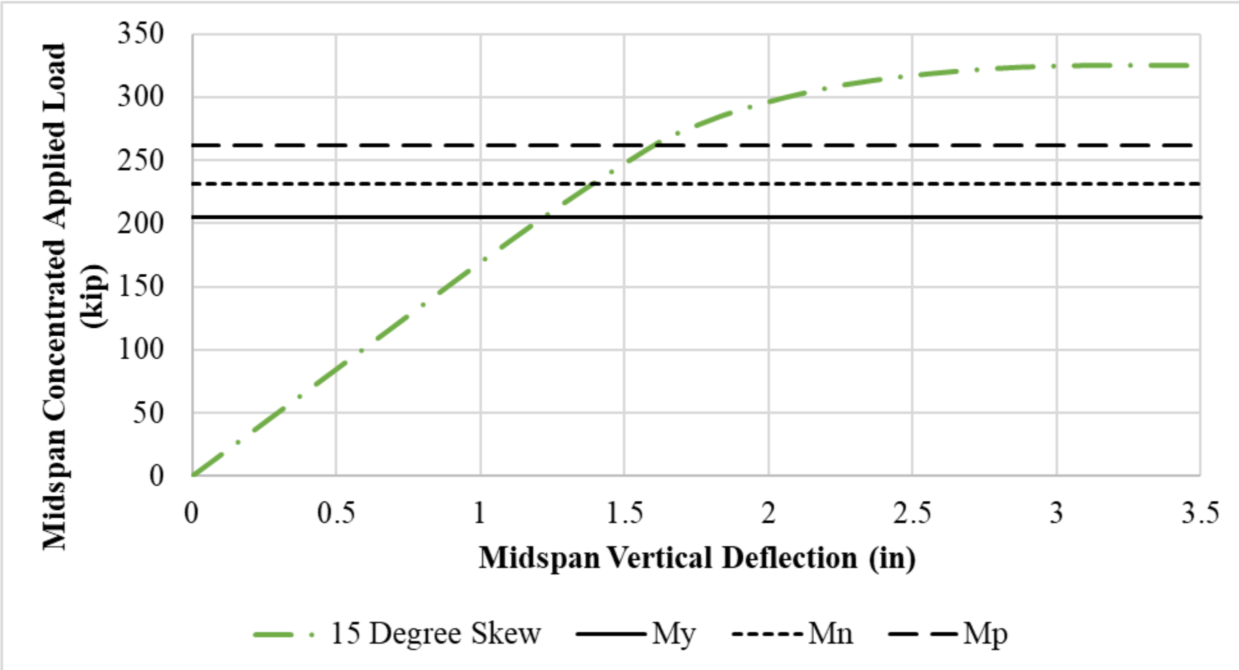

Load-Deflection Graph for the Analytical Test with 15° Skew

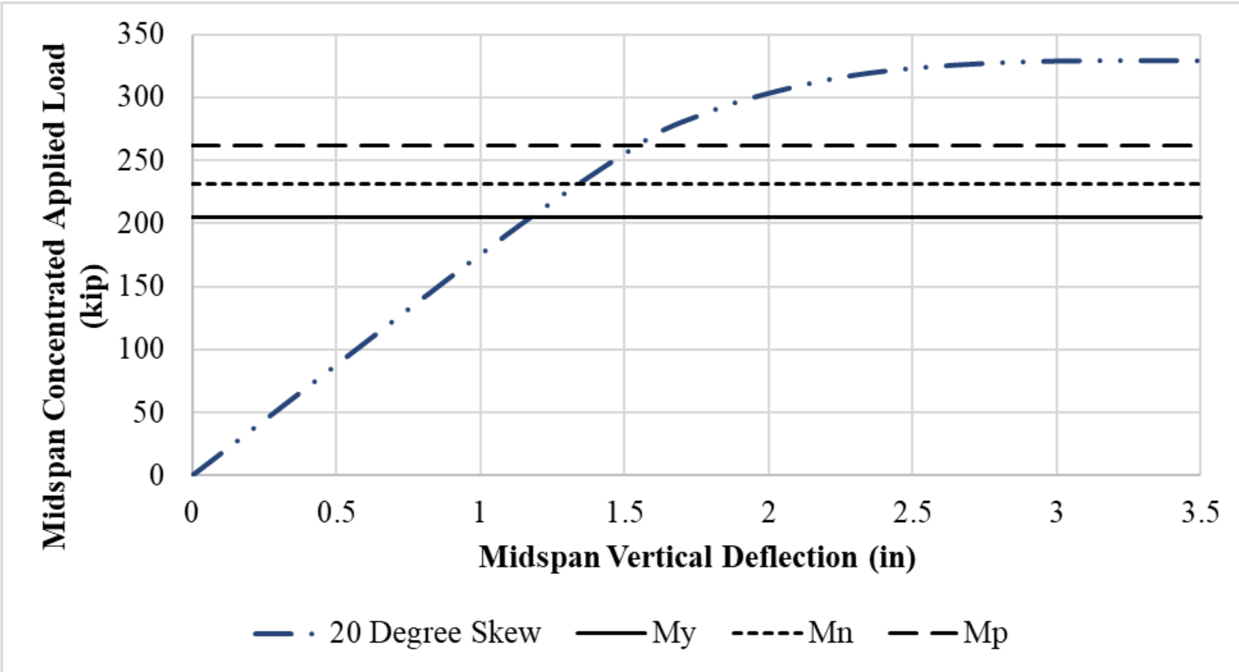

Load-Deflection Graph for the Analytical Test with 20° Skew

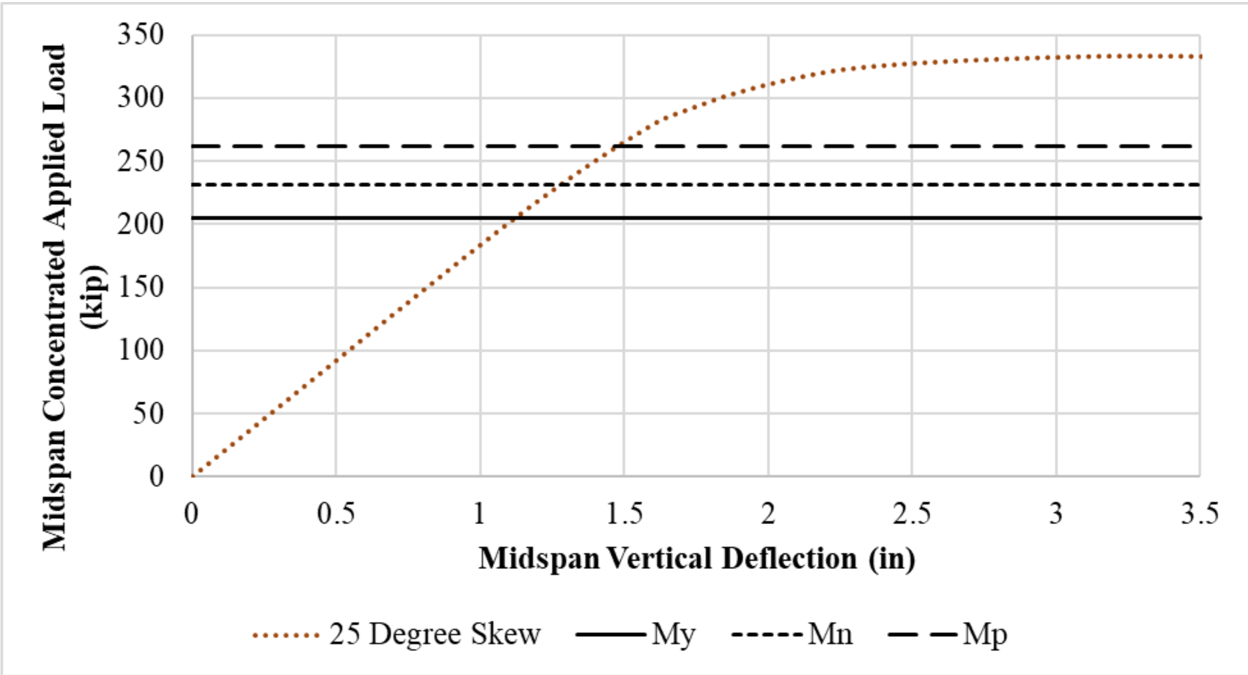

Load-Deflection Graph for the Analytical Test with 25° Skew

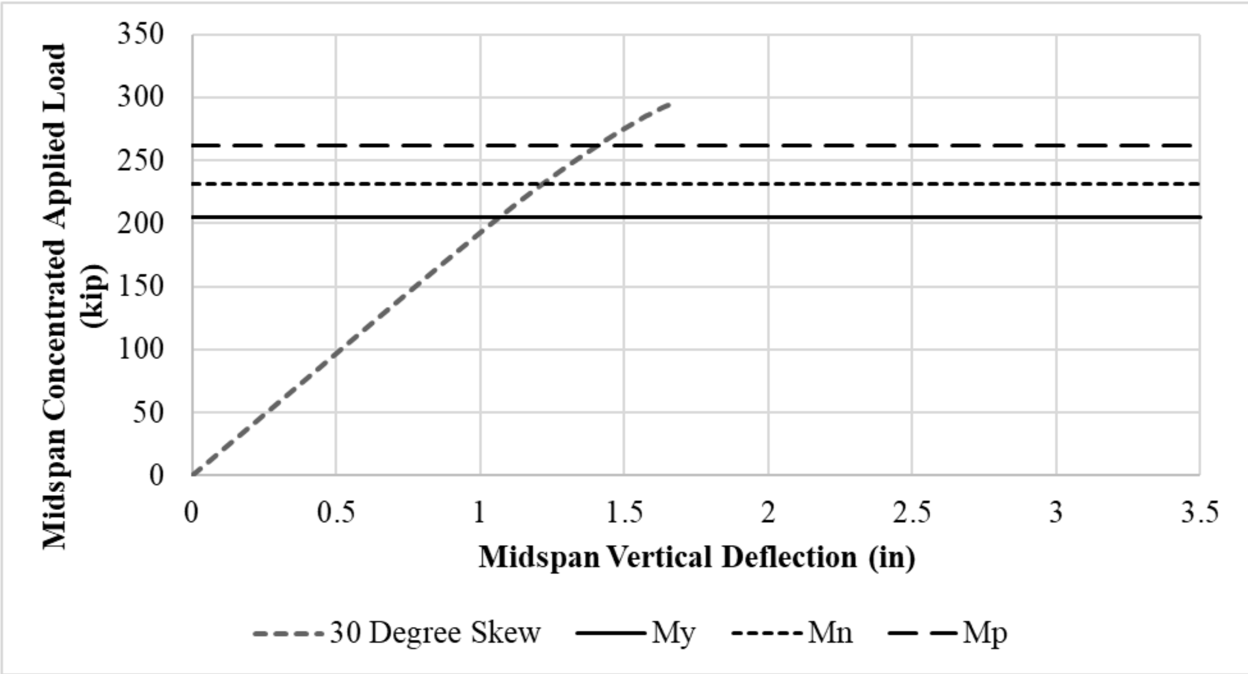

Load-Deflection Graph for the Analytical Test with 30° Skew

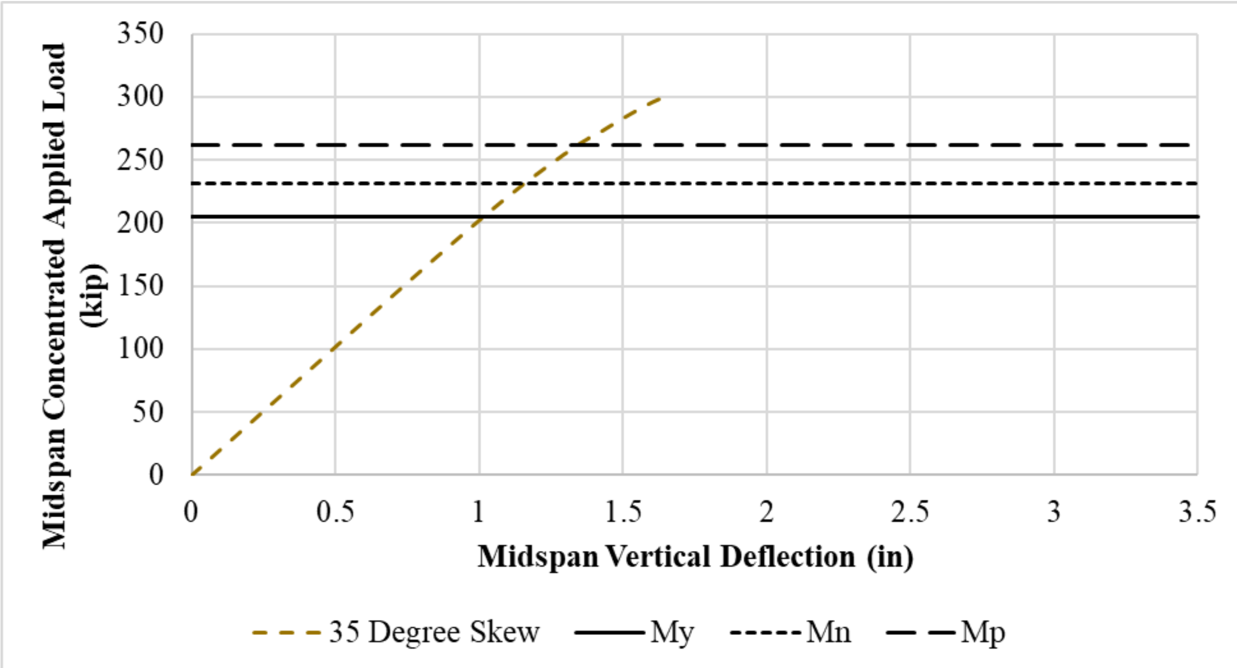

Load-Deflection Graph for the Analytical Test with 35° Skew

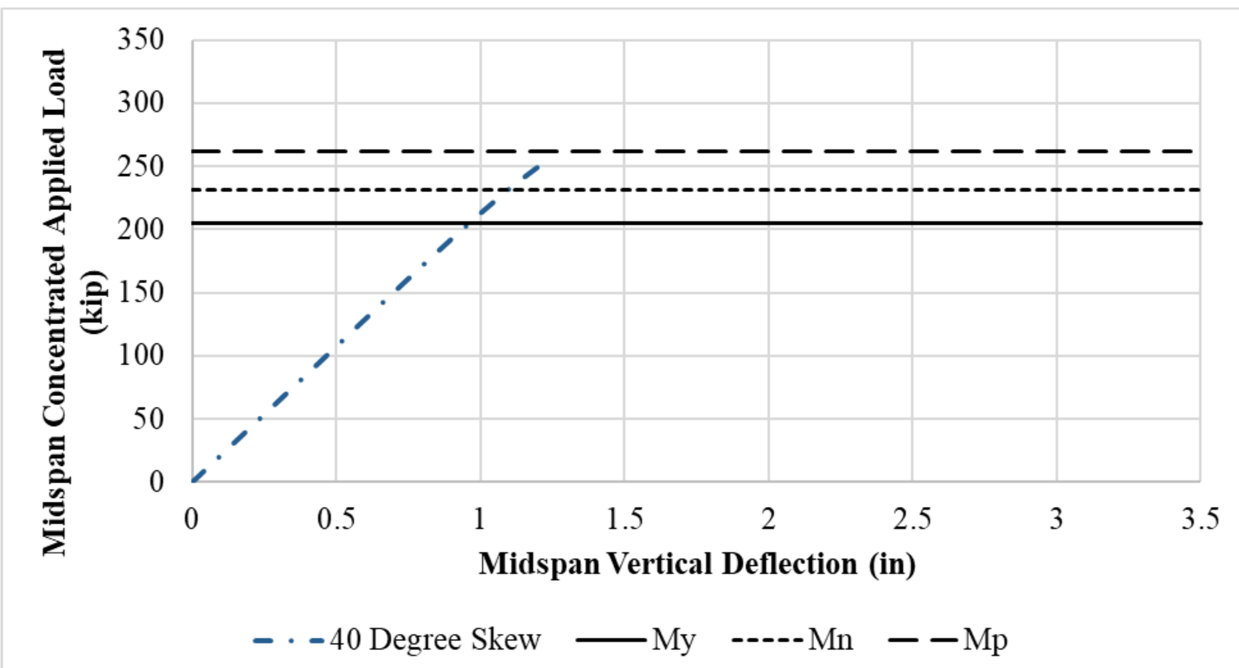

Load-Deflection Graph for the Analytical Test with 40° Skew

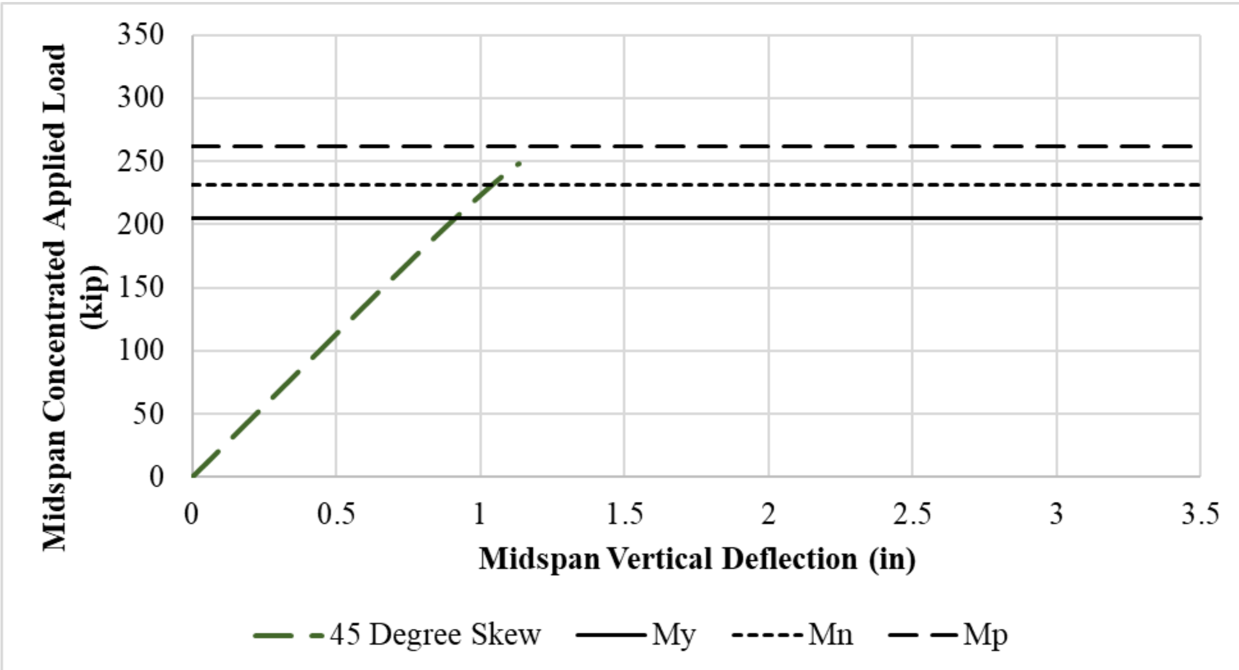

Load-Deflection Graph for the Analytical Test with 45° Skew

APPENDIX D: LOADING CALCULATIONS

D.1 Overview

According to Caner and Zia (1998), "Each span of a bridge with a jointless bridge deck [link slab] may be designed independently as a simply-supported span using standard design procedures without considering the effect of the link slab because the stiffness of the link slab is much smaller when compared to that of the composite girder." Therefore, influence line analysis was performed to determine the moments at midspan of a simply supported beam. Equation D.1 presents the set of functions for the moment at midspan:

$$f(x) = \begin{cases} x/2 & [0\,, L/2] \\ (L-x)/2 & [L/2\,, L] \end{cases} \qquad \text{Eq. D.1}$$

D.2 Simulated Link Slab

The constructed link slab was designed as if it was placed between two 80 foot spans. The 80 foot spans were chosen because modern press-brakes are limited to bending PBFTGs at 60 feet in length. A PBFTG 60 feet in length can be cut into three equal 20 foot pieces, which can be spliced onto a full 60 foot long PBFTG. Due to physical constraints in the Major Units Laboratory, two 80-foot spans could not be built, so the largest possible set up was chosen. A link slab, designed for two 80-foot spans, was placed between two 24.5 foot long PBFTG modules.

D.3 Design Loading

The first step to testing the link slab was to determine the load to induce Fatigue I moment. The Fatigue I load combination is related to infinite load-induced fatigue life and utilizes the load factors found in AASHTO LRFD BDS Table 3.4.1-1.

$$Fatigue\ I = 1.75(LL + IM) \qquad \text{Eq. D.2}$$

AASHTO LRFD BDS define the terms found in Equation D.2 as follows:

- LL = vehicular live load

- Vehicular live loading on the roadway of bridges is defined in AASHTO LRFD BDS Article 3.6.1.2 as: the combination of either the design truck and the design lane or the design tandem and the design lane, whichever yields the largest force effect.
- Note, for the fatigue limit state, the fatigue load consists of only one design truck with a fixed rear axle spacing of 30 feet (AASHTO LRFD BDS Article 3.6.1.4.1).

- IM = vehicular dynamic load allowance
  - The load allowance serves to amplify the vehicular components of the HL-93 live load (i.e., the truck and tandem)
  - For all limit states regarding deck joints, IM = 75% (AASHTO LRFD BDS Article 3.6.2).

Utilizing a load factor of 1.75, for infinite life fatigue, and an impact factor of 1.75, for limit states regarding deck joints, the Fatigue I moment was simplified from Equation D.2 into Equation D.3:

$$M_{Fatigue\ I} = 1.75(1.75M_{Fatigue\ Truck})$$

$$M_{Fatigue\ I} = 3.0625M_{Fatigue\ Truck} \qquad \text{Eq. D.3}$$

The weights and spacings of axles and wheels for the design truck are shown in Figure D.1. The fatigue load is to be taken as one design truck or axles thereof with a constant spacing of 30 feet between the 32 kip axles.

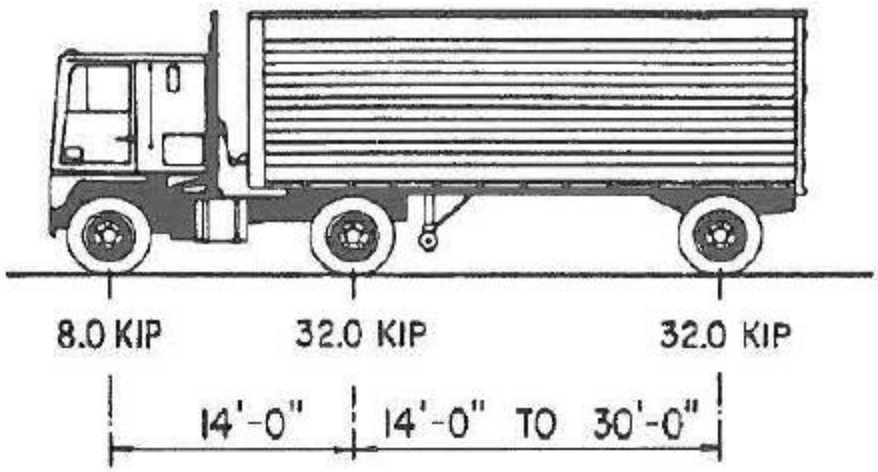

Figure D.1: Characteristics of the Design Truck

D.4 Moment Envelope

A commercially available live load generator was used to determine the maximum negative moment at the interior support. Figure D.2 shows the fatigue moment envelope, which is based on the data presented in Table D.1. For loads applied to the composite section, the envelope shown is based on the composite section properties, assuming the concrete deck to be effective over the entire span length.

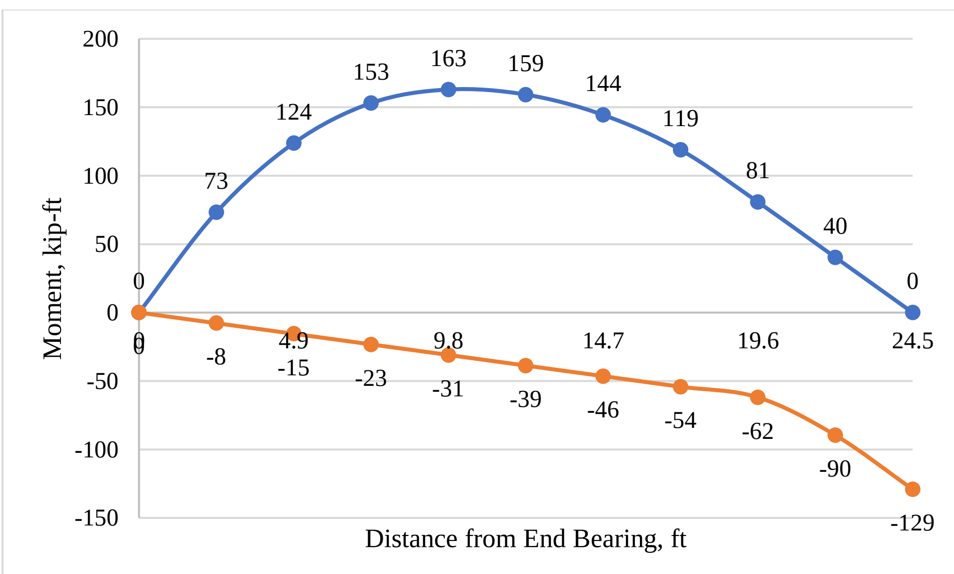

Figure D.2: Fatigue Live Load Moments

Table D.1: Unfactored and Undistributed Live Load Moments (kip-ft)

Span		Truck		Tandem		Lane		Double Truck		Double Tandem		Fatigue Truck	
x/L	x (ft)	(+)	(−)	(+)	(−)	(+)	(−)	(+)	(−)	(+)	(−)	(+)	(−)
0	0	0	0	0	0	0	0	0	0	0	0	0	0
0.1	2.45	87	-10	95	-11	15	-2	0	0	0	0	73	-8
0.2	4.9	142	-20	160	-23	26	-5	0	0	0	0	124	-15
0.3	7.35	166	-30	198	-34	33	-7	0	0	0	0	153	-23
0.4	9.8	166	-40	210	-46	36	-10	0	0	0	0	163	-31
0.5	12.25	159	-49	205	-57	36	-12	0	0	0	0	159	-39
0.6	14.7	149	-59	186	-69	32	-14	0	0	0	0	144	-46
0.7	17.15	129	-69	148	-80	24	-17	0	0	0	0	119	-54
0.8	19.6	82	-79	94	-91	12	-19	0	-79	0	-91	81	-62
0.9	22.05	40	-93	32	-103	2	-28	0	-93	0	-136	40	-90
1	24.5	0	-144	0	-114	0	-48	0	-144	0	-197	0	-129

The Fatigue I moment induced into the link slab can be calculated from the unfactored and undistributed moment caused by the Fatigue Truck, found from Table D.1 and inserted into Equation D.3:

$$M_{Fatigue\ I} = 3.0625 M_{Fatigue\ Truck}$$
$$M_{Fatigue\ I} = 3.0625(129kip - ft) = 395kip - ft$$

D.5 Load Application by Actuators

To determine the point loads which need to be applied to the spans in the lab to generate the moments which would be created by the vehicles, the applied load was considered symmetrically placed. The span length in the lab was 24.5 feet. The equation for the moment at an interior support of a continuous beam with two equal concentrated loads symmetrically placed is described by Equation D.4:

$$M = \frac{3PL}{16} \qquad \text{Eq. D.4}$$

Equation D.4 can be manipulated into Equation D.5 to determine the load required to generate the same Fatigue I Moment generated by design trucks from the AASHTO LRFD BDS:

$$P = \frac{16M}{3L} \qquad \text{Eq. D.5}$$

$$P_{Fatigue\ I} = \frac{16M_{Fatigue\ I}}{3L}$$

$$P_{Fatigue\ I} = \frac{16(395kip - ft)}{3(24.5ft)} = 86.0\ kip$$

APPENDIX E: EXPERIMENTAL DATA

The purpose of this appendix is to document the experimental data recorded from the experimental laboratory test discussed in Chapter 10. The title of each table corresponds to the number of cycles at which the static test was performed or the date of the test after retrofitting the specimens.

N = 0,000,000											
P (kip)	0	8.7	17.4	26.1	34.8	43.5	52.2	60.9	69.6	78.3	87
D1A	0	5.4095	14.1759	34.2747	64.7742	95.9287	120.3684	142.3373	164.1203	185.4382	207.4564
D1B	0	0.466	0.8388	1.7708	2.33	3.262	4.0078	5.1732	5.7328	6.6182	7.4104
D2A	0	3.3109	15.483	47.0102	93.046	141.8375	193.06	243.4477	293.5608	342.2789	390.6277
D2B	0	1.4394	3.2505	5.0147	6.872	8.5437	10.401	12.1191	13.7906	15.3694	17.0874
D3A	0	4.5536	19.7952	53.3942	99.3579	146.3017	193.4826	239.5056	284.9283	328.1231	372.2986
D3B	0	3.2708	5.9341	8.6446	11.822	14.6725	18.551	21.7757	25.1399	28.5048	32.29
D4A	0	6.1719	26.3708	61.4871	104.1347	146.1782	188.0848	229.1526	269.1953	307.0418	346.8095
D4B	0	50.7866	81.6478	92.2492	98.3467	104.1168	110.1206	114.2019	118.5646	120.7225	124.6627
G04-01	0	6.1256	9.4666	10.673	11.1834	12.3434	15.0351	17.5412	20.6964	24.0846	28.2606
G04-02	0	12.4779	23.4195	33.4302	42.6496	51.9157	62.7652	73.3354	84.0924	95.0353	106.5845
G11-03	0	23.6282	47.1173	68.9272	90.4102	111.5673	134.033	155.7058	177.3329	199.3813	220.9637
G04-04	0	34.7487	70.8508	107.5142	142.8298	177.5884	214.3062	249.7222	284.7208	319.3496	353.794
G04-05	0	143.7844	211.3537	257.6949	300.4191	336.5808	377.0909	417.6046	457.3482	501.2968	532.7884
G05-06	0	34.0515	69.0827	104.8625	140.8307	175.4039	212.263	247.3533	282.5398	317.2624	351.4747
G05-07	0	22.691	44.867	67.8417	91.3796	114.0742	138.553	161.6248	184.5579	207.9131	230.5668
G05-08	0	14.7582	28.1621	41.8939	55.9526	69.4976	83.8375	97.6637	111.4439	125.3645	139.2387
G05-09	0	8.612	14.7569	21.4138	28.6296	35.473	43.1082	50.2311	57.5403	65.362	73.1834
G05-10	0	-6.0478	-13.6773	-19.5849	-24.6091	-29.0748	-32.5173	-36.7042	-39.5418	-42.1933	-44.6586
G06-11	0	1.2578	0.3728	1.3975	3.0285	5.6837	8.3862	11.9268	15.7944	19.335	23.994
G06-12	0	16.8123	32.4707	46.5128	59.354	71.9651	84.8537	97.3726	109.1988	121.5342	133.1766
G06-13	0	30.8812	59.8112	86.6963	111.3966	135.8653	160.9399	184.9461	208.6738	232.0772	255.1557
G06-14	0	35.5816	70.8406	100.1009	126.5247	153.4156	180.7265	207.0155	232.7933	257.9681	282.9115
G06-15	0	28.5563	54.9716	80.4096	104.2181	127.422	152.0248	175.6044	199.2306	222.5321	245.4618
G07-16	0	14.5767	27.5234	40.5172	52.9989	65.5742	78.9418	91.7506	104.42	117.043	129.7129
G07-17	0	1.4908	3.4008	5.6836	8.2923	11.0409	14.3018	17.3767	21.0106	24.7838	28.185
G07-18	0	-10.729	-20.0644	-28.7958	-36.459	-43.4253	-49.3697	-55.0355	-60.6548	-65.6238	-70.6858
G07-19	0	0.9315	-2.7955	-9.6918	-14.8639	-20.3151	-21.3867	-20.9209	-19.9423	-20.0821	-18.2647
G07-20	0	11.262	19.7434	26.6955	33.9258	43.6586	53.8091	64.2382	75.1307	86.8577	98.2144
G07-21	0	20.9159	41.2734	60.9793	81.9909	103.1433	124.2029	145.0773	165.9521	187.0153	207.9387
G08-22	0	34.6276	70.1396	107.0008	143.2608	178.595	212.8634	246.577	280.3393	313.3608	345.9664
G08-23	0	33.4473	70.9914	109.4688	146.46	190.2015	225.8494	260.6617	295.1506	333.1334	367.022
G08-24	0	33.8644	70.4726	107.8735	144.5335	180.267	215.2593	249.371	283.2063	316.5323	350.1863
G08-25	0	22.336	45.3244	67.0107	88.1864	109.9677	131.7035	153.2073	174.5259	196.1711	217.5386
G09-26	0	15.2345	27.5434	37.3906	46.913	57.9682	69.2563	81.0088	92.9478	105.2584	118.127
G09-27	0	3.9636	4.5696	0.4197	-2.7042	-3.6369	-2.8443	-1.0261	0.8862	4.0101	6.7612
G09-28	0	3.4091	4.4832	3.3157	0.4202	-1.2147	-1.4482	-1.7751	-2.0086	-2.4289	-2.569
G09-29	0	0.5266	2.2038	-0.0966	-12.7946	-10.6873	-6.7588	-11.7904	-10.0181	-10.21	-13.3245
G09-30	0	16.7566	33.2344	50.877	67.0304	84.4876	102.7834	119.5903	136.3044	153.1125	169.7342
G10-31	0	25.8184	49.7262	72.5642	96.009	119.9674	142.8549	165.5569	187.4672	210.0781	231.8505
G10-32	0	22.0077	45.1332	70.0743	95.0634	120.8914	145.6968	170.131	194.2871	218.6309	242.5098
G10-33	0	18.8603	38.1417	57.6103	77.0802	96.5511	115.3215	133.9528	152.2582	170.0042	187.8436
G10-34	0	14.871	30.3021	44.8476	58.8807	72.9137	87.8337	102.0546	116.4621	130.9171	145.1391
G10-35	0	11.3896	22.5927	30.9481	38.3703	46.6324	55.2688	64.6056	73.1953	82.4852	90.9355
G11-36	0	5.5645	10.3807	11.7367	10.2403	10.6614	11.8302	13.9343	15.5242	17.0674	19.3589

N = 0,100,000											
P (kip)	0	8.7	17.4	26.1	34.8	43.5	52.2	60.9	69.6	78.3	87
D1A	0	7.8819	16.7435	36.1461	77.0999	111.2923	136.3438	159.7163	179.8711	201.7531	226.4822
D1B	0	0.7922	1.398	1.9106	2.7028	4.2406	5.3124	5.6852	3.5416	4.893	7.689
D2A	0	2.0517	10.4915	34.2265	80.4872	137.3397	194.6649	247.0519	297.5777	346.7557	397.1052
D2B	0	4.4579	6.4085	8.6375	11.5164	15.3247	17.925	19.7826	19.1324	22.1513	26.7484
D3A	0	0	0	0	0	0	0	0	0	0	0
D3B	0	4.4856	7.2423	11.588	17.3822	23.7838	29.6247	33.9237	36.0266	40.6058	46.4004
D4A	0	4.4891	12.6255	38.8127	85.766	138.5237	187.591	230.4882	269.3184	307.3098	348.1114
D4B	0	139.2539	156.6074	166.8327	174.4314	181.3736	188.1282	191.7869	202.1534	204.2175	207.3607
G04-01	0	4.5936	4.3152	-0.3712	-5.4288	-9.3264	-9.9296	-13.1776	-16.6112	-12.76	-3.1088
G04-02	0	12.5254	22.9564	30.6395	37.252	44.7027	53.3175	60.3494	64.6336	92.2972	108.83
G11-03	0	24.9338	49.4021	72.0039	93.2057	113.6146	135.3784	154.4808	170.4547	192.6415	219.3132
G04-04	0	37.9621	78.629	119.8584	159.3206	197.0621	235.1794	270.5959	305.7353	352.7637	389.214
G04-05	0	-534.354	-478.469	-562.906	-633.247	-735.352	-629.173	-577.118	-269.559	49383.85	49414.87
G05-06	0	36.7096	75.8903	116.6588	156.1716	192.939	230.7338	265.5027	295.7985	332.3426	373.3181
G05-07	0	22.8338	45.9964	70.4727	94.6222	118.1166	141.5651	161.1214	178.5218	205.4439	237.2456
G05-08	0	13.312	24.2888	35.7792	47.8775	59.9293	72.0283	81.6981	89.4063	104.262	124.9585
G05-09	0	5.2144	6.2389	7.4494	9.4979	12.6173	15.6902	17.5058	18.2973	26.2591	39.8548
G05-10	0	-6.8861	-15.7724	-23.7746	-34.0562	-41.9186	-50.3856	-58.6197	-72.1571	-59.4568	-58.6197
G06-11	0	4.9828	7.5909	9.3606	8.6153	8.1496	8.2428	8.8951	5.6815	8.8948	15.9272
G06-12	0	15.8898	29.7017	41.4354	51.1826	59.7753	69.8459	78.0233	83.4749	96.5033	111.5183
G06-13	0	30.8386	62.4697	91.4979	118.8063	142.0685	168.1234	191.0622	211.3495	238.4319	266.3528
G06-14	0	31.264	62.9494	92.4028	119.9968	144.4275	170.5354	194.0847	217.1229	224.7095	258.6411
G06-15	0	30.8304	61.9423	91.4727	118.8619	142.4791	168.5203	192.0002	212.3596	206.2104	232.6742
G07-16	0	13.1768	27.099	40.9282	52.6627	63.4191	75.7594	86.7027	95.5977	109.7551	126.3808
G07-17	0	1.9106	3.0751	4.0999	3.9602	4.9852	6.5695	8.1068	6.6623	10.7157	18.2632
G07-18	0	-10.6826	-22.8518	-34.1844	-46.5383	-55.7806	-64.5583	-72.4997	-84.1563	-87.3606	-88.986
G07-19	0	0.3262	-4.7988	-15.0964	-22.7854	-25.7207	-28.2366	-28.9351	-32.616	-30.3336	-23.7169
G07-20	0	9.9183	16.9172	21.8302	26.8831	33.6501	40.1395	48.0658	51.5885	60.1641	74.627
G07-21	0	22.0338	43.0444	63.5899	82.4122	101.6076	120.2912	139.4884	153.6077	173.7845	197.0384
G08-22	0	36.9484	75.3854	115.5427	151.6638	185.5127	219.5028	252.5199	279.1769	311.6406	345.7786
G08-23	0	34.4363	74.0413	116.1161	154.6101	191.292	219.1771	253.4891	300.9335	335.2042	371.6194
G08-24	0	37.3486	77.5338	119.3023	157.4494	193.4156	228.2689	263.2644	293.4747	327.266	362.8723
G08-25	0	23.4526	46.4875	69.0115	90.885	111.9683	133.6573	154.5562	170.8476	193.7496	220.47
G09-26	0	12.7737	22.2497	29.6356	38.4616	47.5668	58.4372	69.7723	78.7388	91.3752	107.2643
G09-27	0	2.2379	-1.9117	-11.0044	-15.4341	-17.5323	-17.6256	-17.1127	-19.4439	-15.1542	-5.9218
G09-28	0	2.0554	1.8686	-5.0917	-11.6784	-15.4154	-18.8722	-23.2168	-32.7461	-32.9796	-26.1131
G09-29	0	9.5079	18.7292	23.3636	29.0018	37.3156	44.5782	50.79	46.7285	471.8658	471.08
G09-30	0	16.9441	33.8889	49.81	65.2194	80.583	96.9714	111.2649	119.2267	137.1527	159.1768
G10-31	0	28.6104	55.4054	81.4558	106.4828	130.0656	153.4167	176.3494	191.545	214.1065	240.445
G10-32	0	24.0561	49.7422	77.5237	105.1203	130.8107	156.6882	181.8223	200.1619	224.7401	252.2515
G10-33	0	21.1478	42.4368	64.5672	85.8583	105.516	125.1275	143.1984	155.2932	173.8326	196.5298
G10-34	0	15.8513	32.0302	47.323	62.29	77.2108	92.5053	106.1217	113.4894	129.4845	149.7705
G10-35	0	11.1096	21.0527	27.9618	35.2907	43.647	51.8166	59.3795	62.0408	72.6852	87.0178
G11-36	0	5.4716	6.7811	3.1802	0.8886	0.2338	-0.7951	-2.8994	-11.5977	-9.1191	0.7949

N = 0,200,000											
P (kip)	0	8.7	17.4	26.1	34.8	43.5	52.2	60.9	69.6	78.3	87
D1A	0	6.1109	17.8193	50.2409	92.3694	124.5624	151.5316	175.8428	200.6214	222.4613	242.7618
D1B	0	1.1184	2.3766	2.9358	4.3338	6.1512	8.0152	8.621	10.3918	11.3238	12.816
D2A	0	3.3575	14.8756	46.2141	98.3097	159.1332	219.311	275.2503	329.7026	382.5274	427.0033
D2B	0	-3.9118	-8.4755	-2.5615	-10.6176	-11.9217	-12.9928	-14.1103	-12.9462	-14.2965	-12.8997
D3A	0	0	0	0	0	0	0	0	0	0	0
D3B	0	8.3164	12.3813	19.6236	25.4172	32.7998	39.4349	44.9017	50.4154	55.3221	59.901
D4A	0	-1.265	4.3516	-72.0018	-28.5208	21.1435	67.863	111.6834	154.7126	193.8583	229.5884
D4B	0	158.1744	170.7465	188.2918	194.1559	193.4521	196.2671	200.3489	205.2277	209.4971	213.2976
G04-01	0	5.6613	2.6917	-4.5478	-12.5759	-17.2628	-19.9076	-21.811	-20.511	-19.026	-14.618
G04-02	0	11.4576	19.9811	29.3899	34.2341	40.2892	48.3012	56.1265	66.5609	76.0633	87.4765
G11-03	0	25.1723	49.2238	72.0631	93.1746	114.1945	135.5414	156.8893	179.1731	200.5698	222.1075
G04-04	0	39.7412	81.4894	126.6433	168.2585	207.4071	245.6737	283.1503	320.9566	356.3875	390.6088
G04-05	0	40.4773	112.6819	177.5135	45.7826	63.7908	106.9579	96.3183	106.8581	121.471	135.3185
G05-06	0	38.7145	79.1088	121.9758	163.4488	202.2683	241.1374	278.9842	316.7878	352.6356	386.9478
G05-07	0	24.8969	47.9189	73.8031	98.0938	121.2135	144.7563	167.878	192.9705	215.2969	238.61
G05-08	0	13.8719	23.7266	33.5823	44.6522	55.6287	67.0263	78.7508	92.344	104.9102	119.2988
G05-09	0	5.3077	4.4697	2.5609	2.4678	2.8868	5.1679	7.6356	13.1765	18.81	26.0271
G05-10	0	-8.5629	-19.9173	-29.0847	-39.3218	-50.583	-60.5408	-70.1262	-77.3849	-85.6205	-90.2733
G06-11	0	16.0459	20.9296	34.2794	35.3954	35.4881	36.837	40.6979	45.5358	47.7684	54.5599
G06-12	0	14.7358	27.2088	40.4672	50.6307	59.7321	68.8797	78.9051	89.9007	100.4815	111.4312
G06-13	0	32.8865	65.7745	97.409	126.6726	154.1235	181.25	208.2847	236.0192	262.9174	287.2574
G06-14	0	39.7361	75.3335	107.2573	138.7643	167.9463	196.8037	225.8957	254.6634	282.8277	307.8278
G06-15	0	35.2562	69.0728	105.9154	137.6901	165.4188	193.6142	221.532	250.1493	271.974	299.3846
G07-16	0	14.0154	27.4723	40.7431	52.6175	62.5829	73.1073	84.7029	97.1372	108.1749	120.9822
G07-17	0	0.9315	0.1864	-0.9782	-3.0279	-6.8941	-9.316	-10.8065	-9.9216	-10.1545	-6.7077
G07-18	0	-12.4021	-26.1507	-40.2242	-55.412	-72.039	-86.3898	-99.3005	-109.982	-120.988	-126.468
G07-19	0	2.5585	-5.5365	-16.0965	-24.005	-29.0756	-32.7509	-34.1928	-33.495	-31.4946	-27.9127
G07-20	0	10.5685	17.5215	18.1705	23.2233	29.3418	36.3414	44.9639	54.8378	64.8975	75.8846
G07-21	0	23.4353	45.2872	66.0222	85.733	104.139	123.3392	142.819	163.0444	183.3184	203.1264
G08-22	0	37.6499	76.8345	116.8116	154.6092	188.3696	222.1321	255.4329	289.0143	320.9255	352.1883
G08-23	0	46.0509	99.293	138.9596	177.789	212.9812	248.1288	282.8125	317.9186	351.0662	385.7098
G08-24	0	38.1453	78.5235	119.9736	158.964	194.3322	229.6568	264.426	299.29	332.762	365.0745
G08-25	0	23.826	46.8154	68.9219	91.2617	111.2289	132.3604	153.7721	176.6282	198.0416	219.5957
G09-26	0	13.4224	22.3398	29.2605	37.2956	45.6563	55.6431	66.6052	78.9609	91.2706	104.324
G09-27	0	2.5645	-1.9584	-11.7964	-17.5779	-20.5618	-21.5876	-21.2612	-18.557	-15.1066	-10.1179
G09-28	0	2.8493	2.5225	-5.2318	-12.1454	-16.209	-19.5722	-23.5425	-24.8508	-26.8589	-25.7848
G09-29	0	36.5604	51.7424	65.8016	74.5892	79.7639	81.7169	93.922	103.3938	111.9376	130.3444
G09-30	0	18.3352	34.8094	51.2377	67.3874	83.3048	99.6415	115.56	133.015	148.3294	164.6682
G10-31	0	30.049	57.4438	82.93	108.79	132.8346	156.554	180.1812	204.089	225.6202	247.0136
G10-32	0	24.8405	49.8677	78.3395	106.6265	132.2631	158.4595	183.7729	209.2272	232.8213	255.672
G10-33	0	22.0808	43.1353	66.0118	88.0488	107.6587	127.3159	146.4609	166.3531	183.8646	201.5639
G10-34	0	16.7335	32.4422	47.3121	62.4622	76.9136	91.6452	105.7247	121.0166	134.8166	149.2236
G10-35	0	11.8578	21.475	28.3379	35.1541	42.4841	50.0943	57.7045	67.1826	75.4471	84.7852
G11-36	0	6.5483	7.8113	4.2096	0.7482	-0.8885	-2.0578	-3.7884	-2.2451	-2.0112	1.4499

N = 0,300,000											
P (kip)	0	8.7	17.4	26.1	34.8	43.5	52.2	60.9	69.6	78.3	87
D1A	0	5.469	17.155	48.9897	86.3899	118.1352	146.4694	173.4494	197.7649	221.7079	238.7772
D1B	0	0.8854	1.864	2.8892	3.5882	4.8464	7.0366	8.854	10.1588	11.184	12.7218
D2A	0	3.3109	15.1568	48.8303	94.6801	155.7884	217.9774	278.2143	333.4652	386.2949	435.0693
D2B	0	-16.4967	-14.3937	-17.8985	2.7575	-1.6356	13.2261	3.5052	3.879	3.178	2.1499
D3A	0	0	0	0	0	0	0	0	0	0	0
D3B	0	7.1483	10.8858	15.6517	20.5574	26.7251	32.7058	39.1539	44.1532	48.6858	52.9845
D4A	0	1.1712	8.338	38.4108	77.7144	125.3608	172.4963	218.4177	260.5946	300.6655	337.8334
D4B	0	157.0125	167.4677	174.2197	180.9248	186.8796	194.7099	199.0706	203.6658	207.1359	210.9338
G04-01	0	0.3717	-6.9615	-20.6055	-33.4609	-44.3195	-51.9765	-56.7103	-59.1695	-58.8911	-56.4319
G04-02	0	10.2503	17.239	19.8952	23.0631	27.723	33.1276	39.6972	48.2241	58.1964	68.8202
G11-03	0	24.4718	47.637	69.7758	91.5882	112.9813	134.002	154.8365	176.7926	198.4234	220.4286
G04-04	0	40.4134	84.7934	131.974	177.341	221.1264	262.0244	301.4797	340.4717	377.5543	413.5667
G04-05	0	71.4591	123.0366	179.9728	230.4249	274.391	321.3461	364.1356	406.1703	446.0283	483.4723
G05-06	0	39.1742	82.7312	129.7396	175.4472	219.4356	260.5378	300.5712	340.0025	377.805	414.1188
G05-07	0	23.4451	47.173	71.0894	96.4134	120.8014	143.971	167.3288	191.1099	214.8928	238.3008
G05-08	0	12.2364	20.6901	26.4342	34.561	41.8939	49.975	59.3627	70.1525	81.737	94.7693
G05-09	0	2.2347	-2.1885	-12.1521	-18.2512	-24.1176	-28.82	-30.7755	-30.3564	-27.1905	-22.0693
G05-10	0	-9.7699	-21.493	-33.2162	-43.5438	-55.2199	-66.9419	-77.7803	-86.8972	-94.6184	-100.758
G06-11	0	2.002	2.3742	2.6071	2.7001	0.9775	-1.7693	-4.1437	-4.0039	-2.8403	-0.6518
G06-12	0	14.8729	28.3608	40.7862	52.6117	63.6521	72.6139	82.0839	92.9871	103.6121	114.9311
G06-13	0	33.0698	66.1883	99.3088	130.3379	160.6247	189.0991	216.644	244.3768	270.808	295.984
G06-14	0	35.253	69.531	104.3704	136.467	168.4729	198.201	226.9072	255.3827	282.8357	309.6394
G06-15	0	32.4208	63.7264	96.7108	127.4142	155.7901	184.0743	210.6353	238.1769	263.6225	288.8367
G07-16	0	13.6886	27.1448	39.577	52.5683	63.2783	73.0107	83.2552	94.804	106.7256	118.6474
G07-17	0	0.3728	0.5126	-2.7028	-3.355	-7.1754	-11.5558	-14.2576	-14.8171	-13.8385	-11.8354
G07-18	0	-13.1904	-26.2415	-43.8899	-56.8008	-74.3551	-91.259	-106.676	-118.935	-128.501	-135.28
G07-19	0	5.8166	-2.1399	-12.6549	-28.5208	-40.0125	-42.1991	-44.5253	-44.5254	-43.083	-38.2445
G07-20	0	10.1966	16.9168	19.6978	26.3721	29.9876	37.3108	44.4491	54.8782	64.7048	75.4129
G07-21	0	23.295	44.3081	63.7839	84.8451	104.5097	122.8231	141.1845	161.1769	181.4965	201.4443
G08-22	0	37.5029	76.8659	117.0208	155.6936	191.6765	224.4112	257.0087	289.748	321.5138	352.7706
G08-23	0	31.3768	71.6616	114.7005	156.904	192.4418	215.0619	249.7638	285.6343	319.0819	374.0862
G08-24	0	38.2268	79.1045	121.1469	162.0776	199.3876	234.0978	268.5781	302.643	335.873	369.1059
G08-25	0	23.7322	46.7673	68.9191	91.7237	112.9932	133.3795	154.5579	176.4352	197.7084	219.4946
G09-26	0	12.5886	21.6468	27.918	35.9546	44.7812	53.7936	64.2465	76.1396	88.3121	101.4138
G09-27	0	2.0052	-3.4976	-14.2225	-21.0307	-24.8076	-26.813	-26.9993	-24.9011	-21.4038	-16.7874
G09-28	0	1.6813	1.0741	-7.8485	-14.9489	-19.7134	-23.7307	-27.3744	-29.0097	-29.7102	-29.5234
G09-29	0	2.1647	7.5309	9.508	11.9556	15.7214	18.828	24.1944	29.9373	36.3393	41.7061
G09-30	0	17.3533	34.6145	50.713	67.2306	84.2143	100.3609	116.6474	132.6555	148.6642	164.9525
G10-31	0	28.9281	55.9479	82.6429	109.5251	134.5458	158.1695	181.0491	204.2558	226.0647	247.2231
G10-32	0	24.0951	49.5872	78.2439	106.3906	133.9336	159.0587	184.5111	209.1273	232.9997	255.9894
G10-33	0	21.4701	43.2216	65.2539	87.8008	108.0612	127.2485	146.3431	165.5789	183.5077	200.5968
G10-34	0	15.754	31.5086	46.2382	61.4342	75.9315	90.4291	104.881	119.333	133.319	147.7252
G10-35	0	12.0456	21.1039	27.314	34.6444	41.6953	48.326	56.1239	63.5482	72.2801	81.7135
G11-36	0	5.6603	7.625	2.2918	-1.6375	-3.7892	-5.0524	-6.83	-6.3622	-4.8187	-2.6199

N = 3/16 Link Slab Restart											
P (kip)	0	8.7	17.4	26.1	34.8	43.5	52.2	60.9	69.6	78.3	87
D1A	0	5.4192	19.7163	45.5545	71.7679	100.2258	132.1435	160.8851	189.9556	215.4285	240.5292
D1B	0	2.5169	3.8226	4.8945	6.4326	7.4116	9.3226	10.7214	12.8655	14.4039	16.5014
D2A	0	8.3921	28.5797	59.3992	105.5153	157.6512	217.4423	272.7624	329.1613	379.3145	428.3999
D2B	0	16.1902	19.0293	104.7963	113.8255	121.924	122.0636	127.4632	138.4955	149.6212	233.6578
D3A	0	-838.345	-205.878	46433.07	46433.07	46433.07	46433.07	46433.07	46433.07	46433.07	46433.07
D3B	0	16.1586	26.5735	33.3919	50.813	56.371	57.0246	65.5253	82.2005	80.8453	90.8409
D4A	0	-115.214	-143.869	-130.294	-86.2397	-38.857	7.4531	51.0042	95.0746	133.0595	174.5601
D4B	0	436.5933	60.2963	1197.459	443.1239	959.8226	697.4486	159.9857	60.9232	51.0196	1030.724
G04-01	0	2.2282	-4.873	-10.5355	-15.548	-19.2141	-23.8088	-26.3153	-27.3825	-27.6145	-30.2136
G04-02	0	10.4763	18.8108	25.795	33.4313	41.2073	49.7286	58.7622	68.1684	78.3201	88.6115
G11-03	0	24.7957	49.2198	72.5708	96.2954	119.555	142.6288	166.0772	188.7327	211.5293	234.1868
G04-04	0	39.0515	81.5977	124.1008	166.6541	208.1868	249.2572	289.1663	328.753	366.7127	403.7896
G04-05	0	78.4619	120.384	256.2339	-523.929	140.4106	11419.39	3269.838	41989.73	50739.68	50653.11
G05-06	0	38.4308	80.2185	122.429	164.3636	205.4628	245.7738	285.4348	324.2135	362.296	399.216
G05-07	0	22.877	46.8341	71.2607	95.0325	118.4765	142.0627	165.5561	189.0036	212.4995	235.9495
G05-08	0	12.7968	23.5855	33.627	44.0421	54.7851	65.2937	76.9248	88.4151	100.9804	113.032
G05-09	0	3.9107	2.9797	1.2105	0.0001	0.233	0.4658	2.6073	4.7022	8.8459	13.0363
G05-10	0	-5.3024	-12.3259	-17.6279	-23.3024	-26.6044	-31.2089	-34.9299	-38.8826	-41.3014	-45.2079
G06-11	0	-10.8386	-12.4201	-9.9086	-11.8624	-10.5598	-9.5362	-8.2808	-7.5366	-4.7456	-3.9081
G06-12	0	17.5973	27.805	32.2391	46.1424	58.5215	71.4093	83.6041	95.6608	108.0876	120.191
G06-13	0	30.416	61.2995	91.1149	120.3735	146.331	173.4993	199.3665	225.6073	250.2675	276.8367
G06-14	0	57.7772	86.7198	60.769	80.5707	148.5971	201.3785	255.0449	314.7572	366.9602	420.8391
G06-15	0	31.0736	63.3591	93.8319	123.2829	149.7111	177.1185	203.1307	229.889	255.0664	281.4088
G07-16	0	12.7607	25.8943	38.7488	50.8121	63.5738	75.0785	86.9561	98.6944	110.9451	122.544
G07-17	0	0.6524	-0.3261	0.3262	0.0933	1.864	2.1434	3.5876	3.6809	5.9636	6.1031
G07-18	0	-11.1055	-24.9987	-35.732	-47.348	-54.5959	-65.2821	-72.2978	-82.7977	-89.488	-99.012
G07-19	0	-14.8806	-19.484	-33.6195	-45.4295	-57.7505	-66.3988	-69.514	-71.7455	-73.2335	-72.0245
G07-20	0	6.9054	12.3281	5.7467	10.1034	16.1749	23.0346	31.1451	40.786	49.9632	62.6175
G07-21	0	21.435	40.7284	63.0974	83.5102	103.2716	123.4068	143.4022	163.4454	184.2823	205.8655
G08-22	0	36.0652	75.1505	116.8387	155.9301	193.3069	229.2002	264.0744	297.4187	330.8583	362.9526
G08-23	0	36.8572	81.5044	123.2293	162.7863	202.1576	239.6901	274.2987	307.3983	341.7278	381.0657
G08-24	0	21.3108	-122.572	-84.1365	-44.1619	-6.0458	30.3042	66.3776	100.9177	135.2736	168.6546
G08-25	0	23.5408	46.7575	69.2307	91.5648	113.2488	135.0736	157.1315	178.3531	200.2735	223.1723
G09-26	0	12.3124	21.1872	26.4842	33.8719	42.3754	51.901	62.7746	74.1593	86.6598	99.5325
G09-27	0	1.9121	-2.1918	-14.4549	-21.9157	-27.2313	-29.003	-29.1428	-28.024	-24.9932	-20.8897
G09-28	0	3.3633	3.8773	-3.0363	-9.903	-15.088	-18.7783	-21.6747	-24.7102	-25.7382	-25.785
G09-29	0	-87.849	-115.304	-109.468	-143.13	-138.508	568.5618	931.6751	926.5476	1346.745	50000.99
G09-30	0	22.4555	46.17	-62.541	-41.7595	-22	-1.9145	17.3354	38.771	59.1845	78.9945
G10-31	0	27.3399	53.4236	79.6951	107.4587	132.4289	157.4928	182.6984	207.0196	230.3637	251.9846
G10-32	0	27.621	55.2435	81.8915	113.517	142.633	171.146	198.265	224.7806	250.9723	275.4435
G10-33	0	21.1879	42.7035	65.4802	88.7247	110.3364	131.5291	152.489	172.9366	192.8244	211.546
G10-34	0	21.6173	41.9309	62.0589	77.7609	93.6039	109.3075	125.2438	140.7621	156.327	171.1002
G10-35	0	11.2517	21.8039	29.0404	35.1571	41.9743	49.0708	56.7752	64.6665	74.0054	82.457
G11-36	0	6.0296	8.6471	6.0763	1.3086	-1.2154	-2.8981	-3.9731	-4.9079	-3.6926	-1.1687

N = 0,400,000											
P (kip)	0	8.7	17.4	26.1	34.8	43.5	52.2	60.9	69.6	78.3	87
D1A	0	6.5907	20.0526	46.6042	72.5025	96.9526	119.0666	141.6489	163.1569	180.1769	196.5429
D1B	0	0.3264	0.6526	1.5384	3.4034	5.3151	6.807	8.1125	9.8378	10.91	12.6817
D2A	0	4.5228	21.4022	54.3696	103.8014	162.7531	220.4521	280.7704	337.1765	387.243	437.1275
D2B	0	1.8153	3.3512	5.7255	9.4493	16.5712	20.2949	23.5532	27.7893	30.7685	33.7477
D3A	0	0	0	0	0	0	0	0	0	0	0
D3B	0	2.9916	5.9363	12.1531	19.5857	28.701	33.9366	43.4261	49.4566	57.0298	62.4526
D4A	0	11.2243	34.2356	77.9688	141.4937	230.8547	311.7604	388.7484	453.67	506.3814	556.0083
D4B	0	5.8701	10.1434	17.329	26.1113	33.3438	39.1675	44.8505	50.4865	55.8407	61.4296
G04-01	0	0.8326	-9.2993	-24.4279	-27.8517	-123.926	-126.608	-129.939	-131.002	-130.262	-106.583
G04-02	0	11.0372	16.4861	19.1875	23.6116	28.5949	35.7672	43.5912	53.046	63.6653	74.4709
G11-03	0	26.5174	51.2621	74.001	95.8993	117.0057	139.3263	161.6489	184.2517	206.5753	228.4339
G04-04	0	41.2448	88.6384	136.9212	181.111	222.9759	264.5652	304.6208	343.7011	381.5268	417.4454
G04-05	0	44.1124	89.413	138.6039	188.0365	234.5349	275.6337	318.2526	356.3712	395.4406	428.9652
G05-06	0	39.839	86.8584	134.3478	178.8122	220.67	262.1119	302.5316	341.742	379.3234	415.229
G05-07	0	24.4715	49.5999	75.0584	99.7205	123.3057	147.548	171.6516	195.6147	219.1573	242.0445
G05-08	0	12.3786	20.0861	26.9998	35.6421	42.6026	52.6931	63.1578	74.7902	86.8905	99.8316
G05-09	0	2.1421	-3.8647	-12.0603	-16.8559	-20.0224	-21.4658	-21.3261	-19.5566	-15.8781	-10.2907
G05-10	0	-8.7007	-18.8908	-29.685	-38.6646	-47.5976	-54.9019	-62.2525	-68.068	-72.1154	-77.3726
G06-11	0	2.0945	2.7464	1.2102	-0.0001	-0.9776	-0.0933	0.9309	3.0255	6.6099	8.984
G06-12	0	15.0602	28.7354	40.1468	51.513	60.9383	72.2121	83.1625	94.5754	105.9883	117.0783
G06-13	0	32.9385	66.8098	100.218	129.9525	157.1287	184.6329	212.9758	239.7843	264.7794	290.8926
G06-14	0	31.9196	65.284	98.6972	128.2961	156.3143	185.4976	215.1016	242.8455	268.589	296.522
G06-15	0	32.0567	65.8838	99.2011	128.5188	155.7437	183.1093	211.0821	238.0321	262.7958	288.864
G07-16	0	14.1108	27.9893	40.8432	52.4867	63.6182	75.6349	87.6517	99.6688	111.5934	123.518
G07-17	0	0.8387	-0.2793	-3.1679	-5.3571	-6.1959	-6.4288	-7.4072	-7.0813	-5.4039	-4.7052
G07-18	0	-12.2241	-27.1896	-43.689	-57.3055	-70.0395	-80.914	-93.2288	-103.638	-110.887	-119.81
G07-19	0	-0.233	-7.3613	-20.1271	-35.5017	-43.0954	-45.6111	-48.4064	-49.4312	-52.1334	-48.8258
G07-20	0	10.2869	16.9599	19.5088	19.3232	24.4208	31.9745	40.3157	48.9818	59.0848	69.3268
G07-21	0	22.0418	43.1991	63.5183	84.9106	103.4139	125.2273	144.9906	165.221	186.1511	205.8236
G08-22	0	37.3673	77.8946	119.075	158.1228	195.1771	230.5621	265.1604	299.0641	331.9486	363.3947
G08-23	0	36.6472	77.7543	121.9468	163.8669	203.514	245.915	274.564	201.6285	201.8287	202.3135
G08-24	0	37.5407	78.5693	122.3895	163.0066	200.4669	237.9761	273.5825	308.7265	342.6176	375.3021
G08-25	0	23.1775	46.7282	69.3496	90.8081	111.4293	132.8897	154.6302	176.6043	198.3466	220.1831
G09-26	0	12.402	21.7386	27.0805	33.073	40.041	48.8671	59.7374	71.2584	82.733	95.6947
G09-27	0	2.4244	-1.3988	-14.0344	-23.3592	-29.3273	-33.0104	-32.9638	-31.3787	-28.9078	-24.8047
G09-28	0	2.0091	0.0937	-9.2976	-17.4268	-23.4537	-28.92	-32.3768	-35.6938	-36.9554	-36.3483
G09-29	0	11.8424	21.2602	26.4355	31.984	37.8589	44.8531	52.9195	60.8931	69.7989	79.1715
G09-30	0	17.3476	33.952	49.9519	65.6731	81.9533	98.606	115.3991	131.9601	148.8469	164.8506
G10-31	0	28.418	56.1385	83.0222	109.1152	134.2311	159.6737	184.9319	209.2596	233.1684	254.9345
G10-32	0	25.0231	50.513	79.539	108.0552	135.2703	163.0453	189.4261	215.8546	240.563	263.7366
G10-33	0	21.3329	43.1805	66.1025	89.6795	110.3161	131.42	152.1518	172.3237	191.0489	209.0746
G10-34	0	15.8906	31.8744	47.3922	62.4451	77.2192	92.4128	107.3739	122.4282	137.2039	151.6066
G10-35	0	11.0154	21.1908	28.0522	34.3538	40.7489	48.6843	56.4798	64.2754	74.312	83.4616
G11-36	0	5.0006	7.4777	3.4585	-1.4489	-5.0003	-7.6175	-9.4403	-10.0009	-9.4868	-7.4306

N = 0,500,000											
P (kip)	0	8.7	17.4	26.1	34.8	43.5	52.2	60.9	69.6	78.3	87
D1A	0	6.2626	20.0024	47.717	70.5252	97.2147	118.1559	140.5	162.3311	187.5294	207.7258
D1B	0	0.1397	0.4197	1.8654	2.8449	3.9646	6.4363	5.83	6.5297	7.6024	8.6285
D2A	0	4.429	19.9543	54.7374	96.2839	157.3748	214.3216	270.2018	322.543	377.2224	422.4819
D2B	0	-6.5813	-8.4477	-9.7074	157.8622	77.0982	129.226	108.5452	134.1226	130.4338	191.171
D3A	0	0	0	0	0	0	0	0	0	0	0
D3B	0	-0.4672	4.7658	11.8682	19.8117	28.082	35.5586	41.1658	47.6142	54.3433	59.8573
D4A	0	10.804	34.4233	78.0642	133.1707	224.2632	307.089	385.8556	450.2642	518.5667	568.1491
D4B	0	10.7051	20.8948	27.281	38.222	44.9374	51.7935	55.2214	59.2131	63.064	66.7266
G04-01	0	0.0927	-12.0009	-26.225	-58.9349	-70.3788	-76.2162	-83.4898	-85.065	-85.8526	-82.9338
G04-02	0	9.0783	12.7099	15.5966	18.7623	21.8815	35.5234	37.6649	45.9529	54.3338	64.7636
G11-03	0	22.8413	44.6552	69.3667	91.4168	114.729	139.3973	156.5438	177.1025	197.5684	218.5023
G04-04	0	41.3025	88.9889	139.5675	183.6768	226.5784	277.637	313.6508	353.0223	389.8339	424.8779
G04-05	0	17.6995	47.3376	83.1764	2772.588	1829.752	1472.185	1302.894	1189.475	1138.198	1105.571
G05-06	0	39.6952	88.7595	141.6499	190.1181	231.5995	274.7624	316.8098	354.572	394.2952	434.5809
G05-07	0	24.0512	48.7596	76.2364	104.4173	126.6913	159.4245	177.5274	201.0702	224.0522	247.5045
G05-08	0	11.1648	17.6581	25.8331	32.5134	38.4933	48.5376	54.7977	65.9634	77.3165	90.8187
G05-09	0	-0.419	-9.4536	-17.1377	-23.4246	-29.6646	-30.8286	-33.8557	-31.6669	-28.64	-22.3069
G05-10	0	-10.6094	-22.4746	-34.6654	-43.5987	-56.0218	-64.8151	-78.5404	-85.6121	-94.0328	-99.2432
G06-11	0	1.0227	1.2082	-0.2326	-1.7662	-5.6704	-7.9942	-12.4561	-11.1546	-11.666	-8.9238
G06-12	0	16.3074	30.4038	44.2707	57.7691	67.0753	75.829	83.5233	95.4102	105.3624	116.1901
G06-13	0	32.755	66.3967	102.4138	133.2209	161.1912	184.2756	208.6182	234.4048	260.5187	284.1203
G06-14	0	32.6785	66.942	103.6289	136.0818	165.4166	195.1723	221.3902	249.1465	277.51	302.7543
G06-15	0	29.7856	59.0577	93.0158	121.6824	148.0556	169.7454	192.7009	217.3442	243.9568	266.5409
G07-16	0	13.1417	26.7965	40.5916	52.9885	63.1022	75.1736	84.1694	96.5211	107.661	119.9666
G07-17	0	-0.7467	-1.5402	-6.6736	-11.2937	-20.4871	-24.6403	-31.36	-35.5133	-39.1066	-38.1735
G07-18	0	-14.965	-30.0689	-50.191	-60.647	-79.1417	-91.9205	-111.157	-124.214	-139.129	-148.096
G07-19	0	-1.6788	-9.3264	-22.5229	-32.8749	-43.2734	-51.0605	-58.8473	-60.7589	-60.2925	-58.008
G07-20	0	9.8755	14.0479	19.5656	28.3288	36.7673	53.1815	57.9572	61.8522	70.9869	81.374
G07-21	0	21.4465	42.8471	63.8291	84.0658	101.599	121.4644	138.2057	157.4662	177.6135	197.1087
G08-22	0	38.4895	78.468	121.6538	162.7536	197.7256	232.8394	264.6116	297.268	329.4623	360.2646
G08-23	0	37.323	78.2583	123.709	168.0705	203.4585	241.129	270.6309	304.4107	338.9525	371.0262
G08-24	0	37.9184	79.5109	124.6859	167.3081	203.9379	240.7559	273.9035	308.4019	341.6004	373.5459
G08-25	0	23.5451	46.858	70.8242	92.7899	112.1503	133.4199	151.3856	172.7965	194.115	215.4814
G09-26	0	11.6595	20.2066	25.688	31.1695	36.8371	45.3379	53.3284	63.874	75.5812	88.0321
G09-27	0	0.3264	-6.0595	-18.5053	-29.5524	-38.0355	-41.2511	-45.0737	-44.561	-41.4845	-38.1749
G09-28	0	2.3359	0.6071	-8.1755	-17.9394	-25.8811	-28.5904	-36.9992	-39.5217	-40.5962	-39.5684
G09-29	0	19.9639	44.3149	49.7477	58.8967	64.4688	-189.89	-182.033	-169.7	-164.319	-145.366
G09-30	0	12.0355	9.5175	12.878	21.4157	32.6586	139.2621	149.3408	163.9461	178.3651	192.1779
G10-31	0	28.2849	54.7551	82.7637	110.4012	133.7055	158.829	179.5717	202.0868	223.7171	244.0431
G10-32	0	23.877	50.8272	80.4321	110.7839	137.2267	163.9503	187.4159	213.0246	237.8896	260.0549
G10-33	0	20.0333	41.095	63.979	86.8176	105.7336	125.8178	141.5592	159.9168	177.5277	194.1112
G10-34	0	15.5255	31.3311	48.1629	63.2701	76.2796	88.2638	99.1754	113.8179	128.554	142.3577
G10-35	0	10.8299	20.4456	27.3547	32.676	37.5313	45.2337	49.108	56.5779	65.3077	73.8976
G11-36	0	4.16	5.3754	2.1037	-5.1884	-11.4055	-13.7893	-21.1746	-22.9509	-22.6703	-21.7355

					N = 0,600,000						
P (kip)	0	8.7	17.4	26.1	34.8	43.5	52.2	60.9	69.6	78.3	87
D1A	0	5.605	19.2429	43.7649	69.9232	101.0813	134.1093	162.2813	193.4449	219.5639	247.1328
D1B	0	0.2799	0.7928	1.306	2.5656	4.5244	6.6236	7.6498	9.0025	10.4485	11.5213
D2A	0	4.8961	21.5433	53.9073	100.6846	159.9202	224.0144	278.9721	337.5757	388.1126	438.4213
D2B	0	-7.2789	-12.9244	-14.6509	-22.8155	-23.5621	-24.402	-24.2155	-21.323	-24.3555	-25.2419
D3A	0	0	0	0	0	0	0	0	0	0	0
D3B	0	4.2055	8.6908	16.2598	19.811	29.1558	38.3608	46.8186	55.65	60.4162	66.6313
D4A	0	10.9886	36.1464	83.4728	152.7866	250.2258	360.458	447.7813	538.2096	604.4025	670.4171
D4B	0	6.0574	10.7531	17.0454	18.7357	25.3101	31.227	37.6133	44.2347	46.8176	51.7015
G04-01	0	0	0	0	0	0	0	0	0	0	55650.23
G04-02	0	9.6876	12.8544	13.8327	15.0436	17.3258	21.6111	27.8983	35.7704	45.2254	55.7986
G11-03	0	25.0262	49.26	72.2339	93.621	113.8421	135.0444	157.1817	178.8995	200.6187	222.3382
G04-04	0	43.4067	93.5246	144.1134	191.5855	235.4745	278.2493	319.7689	359.7547	397.5062	434.468
G04-05	0	42.9189	94.4739	146.223	194.2027	238.7424	282.1064	324.8139	365.9196	404.7165	441.1558
G05-06	0	41.8844	91.4138	141.2276	187.551	231.5018	273.6848	314.0534	354.7518	392.1897	428.4646
G05-07	0	25.1291	50.5878	76.3758	101.4154	125.0959	148.7774	172.7413	196.3789	219.8758	243.1402
G05-08	0	11.4465	17.8939	23.9681	31.2569	38.7791	46.8628	57.3756	67.7021	80.0847	93.1688
G05-09	0	0.3726	-9.0815	-19.2809	-26.6856	-32.3208	-36.9776	-37.6296	-36.9776	-33.1122	-27.617
G05-10	0	-10.3796	-21.9695	-34.5827	-46.2183	-57.2021	-68.7904	-75.5854	-84.0087	-88.8951	-93.5022
G06-11	0	1.7193	0.3249	-0.372	-3.2063	-8.3177	-12.7779	-10.1294	-8.6427	-4.7862	-1.8125
G06-12	0	15.041	28.7025	40.9845	52.3005	61.915	71.1155	82.248	92.921	104.469	115.326
G06-13	0	33.5444	67.6033	102.0368	133.4941	161.7425	190.6436	217.8711	246.4965	272.0974	298.8175
G06-14	0	34.7236	69.2164	105.2479	139.2334	169.3102	200.9722	230.075	260.2038	287.3075	315.3905
G06-15	0	-10.9418	-0.863	14.8019	37.2369	53.7087	81.0215	102.276	129.8285	144.4574	156.2463
G07-16	0	14.5821	28.3261	41.4644	54.1375	65.1331	75.8967	88.151	99.4271	111.2165	123.0985
G07-17	0	-0.7939	-2.7553	-6.9583	-11.1613	-15.5511	-21.6211	-23.0221	-26.9449	-27.3185	-28.5794
G07-18	0	-14.8692	-31.3177	-51.3895	-70.4385	-88.0463	-109.138	-123.261	-141.053	-152.387	-165.022
G07-19	0	-0.9865	-10.0054	-24.755	-35.8404	-45.1875	-52.1392	-55.5679	-56.8358	-56.1785	-48.6162
G07-20	0	8.9088	13.3168	14.5696	16.2864	19.1178	23.897	31.1818	39.674	49.0478	84.4567
G07-21	0	21.7755	42.0128	61.5984	80.6252	98.5336	116.9084	136.5437	155.8066	175.8161	196.6197
G08-22	0	37.7509	78.1985	121.2959	161.9358	198.9094	234.0276	269.1482	302.3197	334.936	366.1142
G08-23	0	43.1403	91.1457	143.4051	197.6524	244.4451	287.2755	330.5818	368.6963	409.1281	446.1622
G08-24	0	38.405	80.0215	125.6409	168.4735	206.8448	243.1259	279.8281	314.393	347.983	380.5987
G08-25	0	24.2422	48.0663	70.9144	93.019	112.9835	133.6007	155.3822	177.1183	199.0879	199.0418
G09-26	0	11.9839	20.2514	25.0822	29.2164	34.7908	42.3622	52.3494	63.3125	75.2047	87.283
G09-27	0	0.4662	-6.2002	-20.325	-33.3773	-42.6071	-47.6414	-48.9467	-48.201	-45.9167	-42.2809
G09-28	0	1.4013	-1.5417	-12.4728	-24.1046	-32.6527	-39.1926	-44.3774	-48.0208	-49.5621	-62.3604
G09-29	0	39.9448	46.2222	53.8311	60.1563	61.8683	61.9635	68.2888	77.8481	86.171	-47.1968
G09-30	0	32.0555	68.5668	100.256	125.5906	152.1332	176.357	202.8559	228.7998	255.1622	925.4723
G10-31	0	28.896	55.4168	83.3839	111.2126	136.1992	160.3479	185.8963	209.4412	232.1948	252.7576
G10-32	0	25.2779	52.2327	81.8895	112.0134	139.3921	166.912	193.8278	219.7206	244.2177	265.4088
G10-33	0	21.5764	43.1538	65.5253	88.7864	109.4788	129.5181	150.4461	169.8799	188.1464	207.7219
G10-34	0	16.8762	32.8666	48.1583	63.031	77.345	92.2181	107.1388	122.2931	136.7949	6.9201
G10-35	0	11.0629	20.5387	27.2144	31.4156	36.5975	43.0858	50.555	58.1649	66.6143	75.7181
G11-36	0	4.2075	4.8151	-0.5139	-9.0223	-15.0529	-19.3068	-22.2988	-24.1689	-23.7481	-22.1586

N = 0,700,000											
P (kip)	0	8.7	17.4	26.1	34.8	43.5	52.2	60.9	69.6	78.3	87
D1A	0	7.3319	19.2871	43.7122	67.4845	98.6374	131.3334	165.0132	194.6309	226.9131	252.236
D1B	0	0.6064	0.8396	1.1662	2.1458	3.8719	6.064	7.5568	9.0496	10.449	11.8948
D2A	0	4.8961	20.5178	54.0942	97.1874	155.7233	218.0448	280.3742	335.1984	391.9889	438.1914
D2B	0	5.8805	11.4344	-1.4928	7.1406	13.6277	20.582	21.2354	29.9631	32.3902	35.9374
D3A	0	0	0	0	0	0	0	0	0	0	0
D3B	0	8.7838	16.0726	17.2874	28.0337	37.3788	47.7518	53.3591	62.1906	71.1622	79.4332
D4A	0	14.5837	37.956	84.7034	146.5103	247.9329	343.0147	444.9915	527.2431	606.3722	665.7162
D4B	0	15.2323	23.6687	20.2475	27.7464	35.9491	45.136	46.8233	56.4791	59.1977	65.1977
G04-01	0	-31.9305	-67.2955	-2160.58	-2369.32	-2418.94	-2584.6	-2673.3	-2661.35	-2746.94	-2807.4
G04-02	0	9.4082	13.3672	14.0191	14.9972	16.6742	20.3069	26.2223	34.1873	43.2235	54.03
G11-03	0	25.915	51.0376	74.1998	96.3823	117.3983	138.2752	160.1795	182.366	204.5068	226.4618
G04-04	0	43.2734	92.8396	143.902	191.8471	237.1879	279.7823	322.1477	362.2793	400.3162	436.4913
G04-05	0	43.5713	92.2395	144.3556	191.7128	238.5556	281.2038	323.7611	363.8681	401.9966	438.0982
G05-06	0	42.1659	90.9521	141.0937	188.5375	233.4223	275.4677	317.4701	357.0515	394.7241	430.4875
G05-07	0	24.6602	50.7745	76.2342	101.9763	126.032	149.479	173.1146	196.9388	220.4367	243.6063
G05-08	0	11.6331	18.9216	24.3411	31.7234	38.5449	46.5345	55.5991	66.7198	78.1682	91.5321
G05-09	0	-0.0002	-8.4302	-20.0739	-27.06	-34.9312	-38.9362	-41.6842	-40.7061	-38.2844	-32.5557
G05-10	0	-10.3324	-21.2225	-34.9518	-45.9351	-58.5467	-67.9004	-77.8123	-83.8154	-90.8421	-94.3785
G06-11	0	1.2078	1.115	-2.1369	-3.9487	-8.4548	-9.8947	-11.4279	-9.7555	-9.2909	-6.039
G06-12	0	14.3503	27.4132	38.545	48.895	57.956	66.282	75.989	86.707	97.15	108.007
G06-13	0	33.3096	67.1337	102.3089	133.5781	164.3837	190.9098	220.2763	246.5261	274.034	298.0058
G06-14	0	33.6536	67.8218	104.1803	136.5837	168.6636	197.1137	228.1728	256.3465	285.174	309.9512
G06-15	0	33.9649	67.1772	103.1279	135.3065	166.9215	195.3759	225.5314	253.8003	283.0627	306.6145
G07-16	0	13.6983	27.8151	40.4426	53.3955	64.3455	75.1557	86.1533	98.6421	109.8261	121.4761
G07-17	0	-0.6071	-0.9807	-6.8649	-9.2466	-15.3643	-19.3338	-24.5642	-26.152	-28.4403	-27.3195
G07-18	0	-14.8216	-29.8286	-52.1757	-68.3892	-89.9914	-107.505	-127.619	-140.996	-156.557	-165.243
G07-19	0	0.1408	-11.1133	-26.0245	-40.0441	-50.8285	-60.0184	-64.285	-65.7856	-65.3166	-63.2536
G07-20	0	10.0209	14.15	14.6604	15.7276	19.1602	23.0578	29.7848	37.7182	46.9508	56.7875
G07-21	0	22.3789	43.0338	62.0107	81.0817	99.9202	117.7802	137.0399	156.3935	176.2609	195.4762
G08-22	0	37.8376	78.557	121.4153	163.674	201.7559	237.0078	271.4721	305.3817	337.8536	370.1415
G08-23	0	38.7485	81.2947	127.1175	171.901	212.4656	249.7117	286.6762	322.4567	357.2434	390.2763
G08-24	0	38.7235	81.169	126.7805	171.094	211.0395	247.7795	283.9177	319.3141	352.6661	385.5087
G08-25	0	23.6839	47.0895	70.3103	91.8103	112.0081	132.2998	153.2903	174.7939	196.3449	217.6177
G09-26	0	12.0775	20.7169	24.8048	28.0101	32.8411	39.6233	49.1464	59.6452	71.445	83.2913
G09-27	0	0.2331	-6.2473	-21.2585	-36.549	-46.7113	-53.3306	-55.5215	-55.8011	-53.7968	-51.0465
G09-28	0	0.8876	-2.0555	-14.5749	-27.7478	-36.9974	-44.0974	-49.7028	-53.9535	-55.9616	-56.0083
G09-29	0	13.0424	18.6388	22.3855	26.1321	30.3533	34.9065	42.4477	47.0959	55.6809	65.7362
G09-30	0	17.7876	34.7843	50.0118	65.2863	80.8408	95.9767	112.2771	128.6252	144.8335	160.3903
G10-31	0	28.3338	55.8764	83.5142	111.8996	137.6291	162.2416	187.0877	210.8634	233.0082	254.408
G10-32	0	24.5289	51.6193	81.0853	111.7168	139.6964	166.6535	193.5189	219.5007	243.9475	267.0915
G10-33	0	20.6404	42.3569	64.9607	88.0793	109.3779	129.556	149.7351	169.4945	187.6194	205.0445
G10-34	0	15.7491	31.6848	46.7822	61.3214	75.4412	90.2139	105.1734	119.7608	134.3019	148.4704
G10-35	0	11.0172	20.7743	26.6097	30.4379	35.62	41.8295	48.6924	56.2558	64.9395	73.9036
G11-36	0	4.3018	5.3303	-0.7008	-10.3777	-16.9695	-21.8313	-25.0099	-27.3475	-27.0203	-25.2438

					N = 0,800,000						
P (kip)	0	8.7	17.4	26.1	34.8	43.5	52.2	60.9	69.6	78.3	87
D1A	0	-29.131	-7.6238	17.6251	36.7964	62.7955	86.8323	111.5243	132.5229	156.8903	177.4701
D1B	0	0.9332	2.2393	3.5923	4.6186	5.4116	6.9511	7.8374	9.3302	10.4497	11.9425
D2A	0	10.0743	33.9552	74.2105	116.2416	174.4191	232.5571	292.6147	347.0791	401.5493	447.1554
D2B	0	16.1086	19.5473	26.943	35.9397	40.0381	44.419	42.3463	55.6304	57.3734	63.8744
D3A	0	0	0	0	0	0	0	0	0	0	0
D3B	0	10.7624	17.7818	22.5547	32.7097	42.5836	50.5863	52.7386	55.7807	68.7906	77.1211
D4A	0	16.9879	47.6424	100.719	162.6022	259.4673	344.5967	428.1949	504.1245	577.4885	634.1355
D4B	0	46.4838	58.903	69.9165	76.9932	83.0391	90.8191	96.6781	104.6926	107.1766	112.6605
G04-01	0	-3.7597	-19.3538	-39.8671	-56.249	-71.7494	-82.0976	-90.3114	-94.1629	-95.8335	-93.745
G04-02	0	8.7112	10.9942	10.6218	11.8791	13.8826	18.2149	23.8522	31.9116	41.0892	51.712
G11-03	0	24.6966	51.0289	75.4942	98.5605	120.8339	143.2012	165.337	188.3134	211.1984	233.3362
G04-04	0	43.3288	93.2785	145.2365	193.2385	240.0795	284.7346	327.7616	368.9274	408.4648	445.6272
G04-05	0	39.8527	86.116	133.8913	178.0429	221.8213	265.509	306.3255	344.7414	383.3959	418.8
G05-06	0	42.1174	90.854	140.249	186.9918	232.7134	275.9684	318.4816	358.6671	397.4107	434.0127
G05-07	0	24.3361	49.6591	74.3724	99.3691	124.4137	148.663	172.8654	196.8353	220.6647	244.0736
G05-08	0	10.8862	16.2596	20.9318	28.5479	36.0237	44.855	53.9667	64.5735	75.9752	89.0594
G05-09	0	-1.3041	-11.5979	-23.6614	-30.6481	-37.3085	-41.1276	-43.4098	-43.0373	-41.0346	-35.7716
G05-10	0	-10.6591	-22.2024	-35.9796	-46.9175	-58.3204	-66.698	-75.8198	-81.963	-88.8044	-92.8068
G06-11	0	0.7898	-0.0467	-4.0434	-5.8093	-8.6908	-9.1555	-9.8526	-7.8544	-10.4102	-6.6459
G06-12	0	13.9933	25.8697	36.7334	47.091	57.4027	67.3467	77.2905	88.5237	99.8952	110.8985
G06-13	0	33.8851	66.562	100.6381	131.7834	163.303	192.2171	221.6916	249.2588	276.8271	302.1617
G06-14	0	33.7057	67.4604	101.7762	134.0453	167.2013	197.9378	228.9556	257.7399	286.805	313.4027
G06-15	0	33.0412	65.6192	99.8282	131.9915	165.134	195.6258	226.9573	255.6365	284.4109	310.0669
G07-16	0	12.3903	23.1507	33.7249	46.7219	59.2064	72.0645	83.4316	95.3116	107.0984	119.3983
G07-17	0	-1.4477	-1.9609	-6.4907	-8.6852	-13.3076	-15.5958	-15.7824	-17.0897	-19.9384	-18.911
G07-18	0	-17.0537	-34.4317	-57.7103	-74.3903	-94.5539	-110.489	-129.769	-143.52	-159.129	-168.281
G07-19	0	-1.0732	-11.3374	-28.2733	-44.5085	-55.2851	-63.1692	-67.8807	-71.2864	-71.053	-70.1667
G07-20	0	42.3736	-164.754	-271.161	-227.942	-364.191	-384.961	-1046.32	-701.556	-1319.76	-858.725
G07-21	0	21.907	40.925	59.1514	77.9377	97.191	116.5846	136.2124	155.934	176.0297	196.0329
G08-22	0	37.3705	77.8544	119.7809	161.7112	200.9046	238.8473	274.5172	309.4924	344.9816	375.8274
G08-23	0	38.5106	79.9428	125.3342	170.5883	212.361	253.0544	290.7835	327.8557	363.6584	398.5218
G08-24	0	38.1486	79.1355	124.4941	169.1596	210.5757	249.8099	286.5831	323.0334	357.5341	391.9896
G08-25	0	23.2654	45.2747	66.9601	88.4133	109.4953	130.7179	151.8015	173.5841	195.2284	216.9197
G09-26	0	11.567	18.9532	21.4154	23.413	28.5698	35.306	44.2258	53.982	65.1789	76.608
G09-27	0	0.466	-6.9464	-24.474	-41.1628	-52.3032	-59.7612	-63.397	-64.609	-64.0961	-61.999
G09-28	0	0.7008	-3.6438	-16.2105	-30.1316	-40.2215	-48.0694	-53.6749	-58.4393	-61.2421	-62.0362
G09-29	0	10.6882	18.5642	21.3299	23.6739	28.4089	34.2689	41.3948	48.3335	56.163	64.602
G09-30	0	15.2004	29.2823	42.0125	55.2088	69.9915	85.2407	100.7235	114.8544	129.9186	145.3564
G10-31	0	27.5421	54.7129	81.8386	110.8769	137.6323	163.2709	189.1437	213.3395	236.837	258.4707
G10-32	0	24.6674	50.4531	79.2656	110.0352	139.4101	168.088	195.0919	221.8176	246.6821	271.0359
G10-33	0	20.6464	42.0407	64.3704	87.9158	110.0139	131.5525	152.4376	172.5762	191.407	209.164
G10-34	0	15.5712	31.236	46.1087	60.7483	75.4823	90.4496	105.4639	120.8983	135.4939	149.6702
G10-35	0	10.5979	19.5622	25.4445	28.7125	33.615	39.7784	46.6884	54.2991	62.61	71.6218
G11-36	0	3.9746	4.3487	-1.6831	-11.5967	-18.7044	-24.596	-27.5419	-30.3941	-30.2541	-29.5992

N = 0,900,000											
P (kip)	0	8.7	17.4	26.1	34.8	43.5	52.2	60.9	69.6	78.3	87
D1A	0	2.9909	16.2171	37.9967	57.0664	72.6778	90.4868	108.0157	128.5372	146.4884	165.3749
D1B	0	3.4023	6.1529	8.2038	11.4204	14.5435	17.3868	19.6246	22.2817	23.9133	26.337
D2A	0	5.2679	25.0344	59.1158	110.2651	161.6525	221.5801	277.2236	336.8383	386.8495	436.1659
D2B	0	1.6756	2.2804	3.677	9.169	13.4977	18.8503	21.5966	27.0424	29.8351	33.2796
D3A	0	0	0	0	0	0	0	0	0	0	0
D3B	0	-0.9809	0.2803	2.663	4.8122	25.3687	36.7222	45.8327	57.7474	61.0179	66.3912
D4A	0	7.2541	29.9075	65.0127	139.7712	210.186	296.6738	371.4196	450.7678	510.3576	566.7208
D4B	0	11.0391	16.5825	22.9715	28.8907	37.2529	43.5955	46.2734	53.3674	58.0655	65.2068
G04-01	0	-5.0609	-21.637	-41.044	-59.9865	-74.6572	-87.0985	-94.8977	-99.9582	-102.325	-101.676
G04-02	0	5.3218	5.3688	3.5477	1.587	2.1475	1.4471	3.8746	8.6832	13.9583	19.5143
G11-03	0	19.8475	39.9762	59.7318	79.3488	98.779	119.4711	140.8189	162.774	184.0763	204.9125
G04-04	0	43.866	94.1164	143.6732	190.9989	236.2793	280.6318	322.7051	363.7101	401.0834	436.5489
G04-05	0	38.7547	89.9058	132.7834	174.42	214.8636	277.6176	323.623	365.6587	392.4239	420.819
G05-06	0	44.9987	96.1982	147.822	196.4226	242.977	287.9976	329.7131	371.4783	408.9586	444.8097
G05-07	0	26.1647	52.284	77.9353	102.5089	127.6473	151.3328	175.3943	199.4572	221.7855	243.8331
G05-08	0	11.6342	17.5211	23.175	29.4831	37.8467	45.3229	55.0421	65.3692	76.5376	87.8927
G05-09	0	1.0247	-10.1548	-20.4489	-28.5536	-34.1894	-39.4064	-41.3627	-41.8749	-39.7789	-36.0061
G05-10	0	-10.9897	-24.4936	-37.1591	-50.3365	-60.021	-71.1491	-78.4124	-86.2809	-92.0078	-98.5257
G06-11	0	1.254	-1.1148	-3.5765	-7.3852	-9.0572	-11.4725	-10.59	-10.8687	-8.4532	-8.0819
G06-12	0	19.1958	35.5314	48.3143	60.5436	71.4351	82.7881	94.2799	105.5875	116.8028	127.0492
G06-13	0	33.0269	67.3609	99.8799	132.075	160.1252	190.1802	217.5344	246.5216	271.0828	296.5304
G06-14	0	35.0882	70.9702	105.412	138.3663	168.9486	202.0471	231.097	261.6387	287.9449	314.6255
G06-15	0	32.8979	67.5201	101.3535	134.3049	165.1171	196.9086	226.5612	257.2395	283.0312	309.2897
G07-16	0	13.8943	27.7888	40.0053	50.4034	62.0605	73.8117	85.6096	97.7337	109.2525	120.3983
G07-17	0	-0.3262	-2.4228	-6.6624	-13.045	-16.4929	-22.0834	-24.3197	-27.8138	-28.7453	-30.3296
G07-18	0	-14.3638	-31.6557	-50.62	-72.4657	-89.802	-110.112	-125.309	-143.201	-154.68	-167.18
G07-19	0	-4.0695	-15.4819	-34.1439	-52.1031	-65.3853	-72.447	-77.6849	-80.9116	-81.2858	-80.6777
G07-20	0	49.6323	-7.0165	-20.7703	-75.6397	-128.701	-119.737	-68.3975	-93.0181	-81.5434	-48.4634
G07-21	0	25.5968	46.8122	65.8367	84.0226	102.3023	121.7491	141.2425	161.2033	180.6521	199.9149
G08-22	0	38.8315	79.9887	124.4948	166.8671	205.8975	243.3509	279.5524	314.0366	347.0826	378.6432
G08-23	0	43.0429	84.5784	131.9239	176.6772	218.1768	258.5938	296.6528	333.8176	368.8597	401.0232
G08-24	0	38.889	80.8985	127.4244	171.4885	212.718	251.1583	288.1121	323.4395	357.6527	389.8656
G08-25	0	23.9686	47.5661	69.8612	90.2491	110.5909	131.6786	152.2086	173.9496	194.9004	215.3861
G09-26	0	11.9363	19.7393	21.7831	22.6188	26.8458	33.0232	41.1517	51.0452	61.2641	72.5052
G09-27	0	2.3286	-2.7942	-19.1404	-35.5324	-46.2428	-51.1789	-53.8333	-53.8798	-52.6226	-49.3163
G09-28	0	0.7477	-3.7381	-17.3824	-31.3069	-41.4929	-49.5293	-55.9303	-60.6024	-62.9384	-63.4525
G09-29	0	-21.628	-30.896	-41.1467	-48.6352	-55.235	-58.4174	-58.0898	-55.8907	-53.4572	-52.5684
G09-30	0	21.1393	39.0664	54.8524	71.1045	87.1705	104.3553	121.4472	138.6791	155.0736	171.3291
G10-31	0	30.1665	58.8895	87.7073	115.6409	142.3166	168.201	193.9002	217.9214	240.4046	261.3493
G10-32	0	25.8382	53.121	83.8047	114.1637	142.4295	170.5572	197.848	224.302	248.2886	270.7392
G10-33	0	20.5651	41.7854	64.7363	86.893	108.1631	129.2002	149.2558	168.6585	186.3315	202.2752
G10-34	0	16.6012	32.8762	47.986	61.837	76.5282	91.406	106.5177	121.4899	135.3896	148.8232
G10-35	0	11.6667	20.8133	25.4802	28.7938	33.3671	39.7141	46.5277	54.6485	62.8627	71.5435
G11-36	0	4.5378	4.5381	-3.6958	-14.0347	-20.5845	-25.6369	-29.1454	-30.6424	-30.2679	-29.0518

N = 1,000,000											
P (kip)	0	8.7	17.4	26.1	34.8	43.5	52.2	60.9	69.6	78.3	87
D1A	0	5.3776	15.7588	38.2063	56.9596	76.2281	95.1235	117.2932	137.4061	159.6718	178.8506
D1B	0	0.0932	0.6062	1.5386	2.4711	3.9168	5.7817	7.1807	8.7195	10.1185	11.6573
D2A	0	5.688	21.7266	56.1838	100.8092	153.7398	210.9203	270.0202	323.5749	380.5885	427.3423
D2B	0	5.1837	1.1675	11.8151	11.3481	13.7298	19.4739	24.9851	27.0869	31.477	35.3064
D3A	0	0	0	0	0	0	0	0	0	0	0
D3B	0	7.5224	14.6244	19.624	26.3991	36.0715	45.0432	54.3418	58.7812	67.3328	74.9029
D4A	0	10.7157	30.0889	72.6281	136.2801	223.019	302.0006	392.9828	465.2462	537.8482	591.4396
D4B	0	8.6029	12.7399	22.7537	27.3608	32.7674	43.3927	48.8466	58.9549	66.5246	71.5556
G04-01	0	-4.9204	-21.3524	-42.1469	-61.5946	-78.8601	-91.0199	-100.256	-105.175	-106.474	-104.804
G04-02	0	8.3451	11.3752	11.6083	11.282	12.0743	15.3383	20.5129	27.6929	36.9241	47.5078
G11-03	0	15.5464	32.2171	58.7227	81.9047	102.7461	118.7641	139.4196	159.8419	180.499	199.8921
G04-04	0	42.85	92.0854	143.3294	191.4096	236.6527	280.1751	323.0957	363.3165	401.4433	437.7547
G04-05	0	398.7473	1422.122	2950.122	5497.938	48504.51	48504.51	48504.51	48504.51	48504.51	48504.51
G05-06	0	43.2413	93.4771	144.9761	193.8234	239.9253	283.5138	326.8727	367.438	405.8615	442.1427
G05-07	0	24.7555	50.5907	76.8487	102.2176	126.5567	151.3179	176.0811	199.7666	223.1717	246.7654
G05-08	0	11.0738	17.7085	22.8483	29.1563	36.1189	44.8569	53.9222	64.3896	76.3059	89.0167
G05-09	0	-0.233	-9.7827	-21.661	-31.0241	-38.3369	-43.088	-45.8364	-46.0228	-43.3676	-37.6852
G05-10	0	-11.3127	-22.8577	-36.2648	-48.7869	-62.2399	-72.7133	-84.3498	-92.03	-100.594	-104.923
G06-11	0	-0.0932	1.2574	-3.8199	-7.5	-12.9035	-16.8628	-19.9372	-18.1206	-17.7481	-13.5554
G06-12	0	15.706	28.9637	41.3445	52.0157	61.2095	70.8191	80.9831	91.6091	102.0041	113.4627
G06-13	0	32.5992	66.3182	100.878	133.0178	162.6912	191.7602	222.3683	249.9503	277.3473	301.9957
G06-14	0	35.7363	71.2892	108.3805	142.2164	174.4722	205.1939	237.919	266.9685	296.7181	322.1857
G06-15	0	32.618	65.9357	101.8155	134.6261	166.2752	196.2504	228.4619	256.7189	285.6288	310.5828
G07-16	0	12.5374	26.1937	38.3588	49.8253	60.4061	71.5931	83.0604	94.1548	104.7366	116.2043
G07-17	0	-1.9114	-0.5595	-6.5734	-14.2185	-20.6517	-25.2667	-29.5553	-32.5852	-35.1026	-33.6575
G07-18	0	-15.2451	-30.3041	-53.2173	-73.1083	-93.5564	-110.518	-130.082	-144.533	-160.239	-168.835
G07-19	0	2.8481	-9.5243	-28.2925	-46.1733	-60.7854	-70.4021	-76.4711	-79.9251	-80.7189	-79.5053
G07-20	0	7.2797	19.707	23.6024	29.2595	33.155	40.5746	49.8032	61.7218	66.4986	79.5305
G07-21	0	22.565	43.5461	63.0822	82.2464	100.1989	119.3179	139.0435	158.8636	178.6841	199.0652
G08-22	0	38.4867	80.273	125.2201	168.4536	207.3246	244.8983	281.4529	316.1522	349.4132	381.5623
G08-23	0	40.9048	84.9742	134.2387	180.0624	221.1234	261.3378	299.7154	337.4338	373.7863	407.7336
G08-24	0	39.0431	82.459	129.6445	175.0215	216.1245	255.045	293.1315	328.895	363.5455	397.361
G08-25	0	23.9678	47.4249	69.6733	90.9912	110.2624	131.5352	152.67	173.8519	195.7797	217.1497
G09-26	0	11.2422	18.6289	20.3014	21.2773	23.7394	29.5467	37.3054	46.3651	57.1906	68.4809
G09-27	0	0.0932	-8.3424	-26.9839	-46.4171	-61.0029	-69.7171	-74.8889	-77.4517	-77.2187	-75.3081
G09-28	0	-0.234	-4.8592	-19.0615	-33.1704	-44.6159	-51.9503	-58.5837	-63.2552	-65.077	-64.7501
G09-29	0	7.6111	13.7278	14.942	16.2029	18.7245	23.6744	29.5576	35.9088	44.1741	52.7665
G09-30	0	17.7356	34.8663	50.9737	67.1747	82.5377	100.183	117.3632	134.2644	151.3528	167.6498
G10-31	0	29.5563	57.5755	86.9485	115.9032	141.7824	168.3625	193.4049	217.1891	240.1352	261.7762
G10-32	0	25.2303	52.6503	84.215	115.2697	143.7188	172.3092	199.8768	226.0951	251.2905	274.2978
G10-33	0	20.603	42.2342	65.5953	88.9109	109.5171	130.7785	151.1528	169.9393	188.1186	205.1306
G10-34	0	16.2268	32.4077	47.703	62.2992	76.0567	91.3065	106.3704	121.0618	136.08	150.2592
G10-35	0	10.784	20.0273	24.6022	27.8235	31.6986	38.4681	45.5645	52.801	62.138	71.3827
G11-36	0	4.6778	3.6954	-4.7245	-15.2023	-23.6688	-28.1592	-31.0124	-33.0705	-31.1527	-28.8607

N = 1,200,000											
P (kip)	0	8.7	17.4	26.1	34.8	43.5	52.2	60.9	69.6	78.3	87
D1A	0	3.1793	12.2965	35.675	50.9651	68.2193	84.4925	102.4961	119.3316	140.3297	158.7098
D1B	0	0.1399	1.0734	2.1	3.0332	4.8999	6.253	7.9799	9.5198	11.153	12.7862
D2A	0	5.0804	21.208	57.2874	97.332	150.0148	206.7603	265.0972	319.4299	376.4741	423.5884
D2B	0	1.7309	9.2149	10.4779	13.8458	17.4474	25.3058	31.1533	35.0825	39.5734	43.5961
D3A	0	0	0	0	0	0	0	0	0	0	0
D3B	0	2.8503	3.6446	11.3077	14.8589	20.8868	29.8121	37.1482	41.0735	50.3729	55.6068
D4A	0	8.3303	27.6578	68.0482	122.4841	205.904	280.3009	361.2185	430.6739	499.5766	550.3576
D4B	0	16.2666	19.9342	-0.3764	-14.4799	5.5469	15.9834	15.137	17.2527	14.1498	18.193
G04-01	0	-5.1542	-20.3382	-40.8147	-60.4083	-78.5623	-92.3045	-101.125	-106.465	-108.972	-107.579
G04-02	0	8.8151	14.7853	13.7125	13.899	12.1735	13.1994	18.9832	26.5859	35.6817	45.9902
G11-03	0	26.7822	54.2214	79.9767	104.047	126.3857	148.3976	171.0664	193.7357	216.0316	238.0942
G04-04	0	44.6243	94.9829	147.3498	195.9476	243.4786	287.938	330.8165	372.7664	411.4104	447.7725
G04-05	0	40.8603	87.7879	135.4905	179.4422	224.1679	266.2012	304.3855	338.9128	374.0686	406.6261
G05-06	0	41.9826	91.9368	144.0406	192.8398	240.1991	284.2527	326.9578	367.9883	407.0636	443.7633
G05-07	0	24.4309	51.0671	77.4708	103.64	128.7797	152.9359	177.28	201.5318	225.0342	248.5845
G05-08	0	10.608	17.6647	23.0858	30.0024	36.4517	44.4901	53.5572	64.2598	75.2899	87.9563
G05-09	0	-0.8388	-9.6908	-24.2254	-31.5392	-39.6912	-45.2814	-48.7754	-48.915	-48.7286	-43.7443
G05-10	0	-11.2245	-21.7968	-34.6509	-45.7816	-58.3559	-68.8807	-79.638	-86.9958	-95.9833	-100.966
G06-11	0	1.3506	1.4436	-0.7455	-2.3756	-5.4965	-7.7322	-10.0609	-8.6173	-10.1542	-7.2199
G06-12	0	14.2798	27.6358	39.3746	50.3279	60.4036	69.3697	79.3072	89.7066	99.7829	110.3216
G06-13	0	33.0374	67.4758	103.5938	136.2192	168.1939	197.2803	228.0471	256.1581	284.6904	309.914
G06-14	0	34.4768	69.8399	107.2067	141.0393	175.3394	205.8718	238.594	268.1529	297.8995	323.7373
G06-15	0	32.7567	66.5858	103.0235	136.3451	169.809	200.3894	232.1815	260.8567	289.906	314.7202
G07-16	0	13.1137	29.5877	42.2818	54.6968	65.8513	76.8661	87.6946	98.9435	110.0059	121.9087
G07-17	0	-1.0718	-1.0718	-7.5036	-9.8346	-16.9188	-21.0672	-26.5667	-28.7106	-31.5998	-30.7144
G07-18	0	-15.527	-28.8687	-51.414	-69.8213	-91.6677	-109.748	-129.129	-143.212	-159.245	-167.889
G07-19	0	-2.4762	-13.2694	-33.5001	-50.1329	-63.2613	-72.0907	-75.5013	-78.9119	-77.6505	-75.081
G07-20	0	8.2938	19.6631	18.2186	24.1833	24.0896	28.237	35.6459	43.3344	52.6544	62.0205
G07-21	0	21.3662	42.5468	61.9552	81.3647	99.8881	118.7857	138.2436	158.1693	178.2358	197.8363
G08-22	0	39.0068	81.9646	127.3878	172.0253	212.4391	249.5115	285.7037	320.737	353.0776	386.3961
G08-23	0	39.8348	84.5352	133.4414	181.7378	225.7421	265.17	304.0817	341.8626	378.0405	412.5205
G08-24	0	39.5407	83.458	131.2879	178.005	220.8642	259.6315	297.843	334.8007	369.4804	403.045
G08-25	0	22.8505	46.1212	68.1826	89.2673	109.2828	129.2521	150.5257	171.754	193.0758	214.399
G09-26	0	10.9619	17.4651	18.812	18.7656	21.2741	26.3837	33.7229	42.4096	52.2115	63.5
G09-27	0	-1.2119	-10.861	-30.3444	-51.3188	-66.4658	-76.1606	-81.7528	-86.5068	-86.5534	-85.3418
G09-28	0	-0.5607	-6.0736	-20.3236	-36.5352	-48.7752	-57.2309	-64.0046	-70.358	-72.18	-72.9272
G09-29	0	10.7243	18.4181	20.6562	22.1948	25.7855	30.6815	37.0701	43.9248	52.738	61.6447
G09-30	0	18.0655	34.5486	48.7043	63.7447	79.3446	95.5503	112.4087	128.9882	145.9874	162.0088
G10-31	0	28.9628	57.3676	86.5201	116.7008	142.8247	169.4164	195.6827	217.9381	241.7343	263.5717
G10-32	0	24.96	52.3897	83.733	115.8701	145.7267	173.5357	201.3926	228.5991	253.1047	276.4463
G10-33	0	20.2902	41.7971	65.4556	89.1619	110.8118	131.294	151.7764	170.7633	188.9095	206.2608
G10-34	0	15.5312	31.6698	46.6426	61.4294	75.0034	89.7909	104.4857	119.3675	133.8296	148.2459
G10-35	0	10.92	19.6468	23.2866	25.8533	29.6802	35.5138	42.421	50.028	59.2222	68.9298
G11-36	0	3.929	3.1805	-6.8287	-19.2701	-27.7824	-33.4883	-37.2298	-39.9426	-38.7731	-36.014

N = 10/18 Link Slab Restart											
P (kip)	0	8.7	17.4	26.1	34.8	43.5	52.2	60.9	69.6	78.3	87
D1A	0	-1.2653	5.8089	16.444	25.6737	35.6068	46.3362	63.7197	80.8691	102.4244	120.419
D1B	0	3.8786	9.5328	14.8599	19.9067	24.4859	28.879	34.3463	39.8138	45.7486	51.45
D2A	0	11.0027	29.0923	55.9488	84.5782	113.5362	147.3915	187.9662	226.5843	271.4565	311.9474
D2B	0	16.511	41.14	68.1497	96.2336	124.5062	156.5593	194.2608	235.2785	275.4127	310.7894
D3A	0	0	0	0	0	0	0	0	0	0	0
D3B	0	2.0577	16.4167	31.6646	54.2104	72.5468	91.9131	123.4435	154.508	191.2357	228.5275
D4A	0	1.3131	21.4321	54.543	98.5378	152.9504	215.0168	297.5483	370.2853	458.8035	530.6251
D4B	0	8.0914	17.3123	27.5686	41.5418	54.1509	71.5594	91.1331	111.5074	132.2591	153.4821
G04-01	0	-3.2957	-20.7965	-33.3295	-51.0612	-65.9143	-78.6782	-88.8429	-95.7121	-102.256	-105.691
G04-02	0	5.6843	10.5698	14.2806	19.1191	22.1249	29.1697	37.3423	57.6781	70.9232	94.6447
G11-03	0	15.4668	27.7934	28.5893	29.8548	44.573	62.573	83.0107	103.8249	123.8429	141.236
G04-04	0	37.05	77.3655	120.8075	159.9181	197.4928	235.0704	272.3713	308.509	344.9757	380.0461
G04-05	0	0	0	0	0	0	0	0	0	0	0
G05-06	0	31.5321	160.1252	258.084	535.8212	623.1384	403.4362	682.1315	2044.369	1772.523	903.3965
G05-07	0	0	0	0	0	0	0	0	0	0	0
G05-08	0	9.0215	10.9849	15.1917	18.4638	21.8296	28.0468	35.947	45.2031	53.3838	62.7802
G05-09	0	-2.4222	-14.5818	-23.76	-32.8444	-41.4625	-46.1676	-48.9627	-49.1959	-49.7548	-48.4039
G05-10	0	-9.1263	-18.6717	-27.0529	-35.8064	-44.8392	-52.8474	-60.2035	-64.8594	-72.1225	-76.7781
G06-11	0	1.1146	0.4644	0.0463	-1.2075	-3.1117	-4.5051	-4.4121	-2.7867	-3.5298	-2.3686
G06-12	0	19.0502	35.2883	50.5113	64.6738	76.4844	89.633	101.3054	113.1167	123.7283	134.848
G06-13	0	26.9326	53.867	81.6865	108.3911	133.8872	159.385	185.4422	209.872	233.6518	256.2688
G06-14	0	-7.3493	-71.2062	-43.943	24.5691	21.5063	23.5279	38.8346	43.1174	45.0895	21.8147
G06-15	0	-29.7397	-46.8881	-50.1325	-42.7159	-31.0246	-20.7895	-8.6283	2.5002	14.7094	25.3216
G07-16	0	12.3608	23.1357	34.3774	44.4997	54.4359	64.9783	75.5211	87.2774	97.0742	107.8508
G07-17	0	-0.7918	-3.0735	-8.7082	-14.4355	-19.7902	-24.5864	-29.5224	-30.8726	-34.2719	-34.1785
G07-18	0	-12.4529	-26.1135	-44.931	-64.4449	-82.9821	-100.032	-117.965	-130.043	-145.001	-154.617
G07-19	0	-8.0126	-20.4969	-33.7729	-43.229	-51.7997	-61.6744	-69.7325	-76.9054	-83.7057	-88.4563
G07-20	0	0	0	0	0	0	0	0	0	0	0
G07-21	0	14.9867	30.348	44.7753	59.8573	73.5852	87.5937	101.9762	116.733	131.4435	147.1814
G08-22	0	0	0	0	0	0	0	0	0	0	0
G08-23	0	31.6794	65.0409	99.3378	134.1502	167.565	200.9353	232.6277	264.8823	296.4851	327.8101
G08-24	0	32.55	66.3128	100.5904	134.0783	167.3357	199.6168	231.2479	263.5334	294.8424	325.4546
G08-25	0	15.1984	30.1175	44.6176	59.3046	73.9923	87.5611	102.0159	116.9845	131.9535	147.0627
G09-26	0	5.0662	7.762	9.6211	11.3872	13.3393	15.7562	18.638	22.4029	25.517	29.9792
G09-27	0	0	0	0	0	0	0	0	0	0	0
G09-28	0	-14.4893	-30.4738	-48.0937	-66.0398	-84.3125	-102.024	-119.174	-135.622	-152.538	-167.583
G09-29	0	30.8304	81.211	47.057	37.4006	24.0837	26.5076	-9.9592	-5.7073	-46.9917	-89.286
G09-30	0	11.2261	21.3348	31.2101	42.9497	53.9438	66.4757	77.2839	90.0027	100.7187	111.5744
G10-31	0	27.0223	51.9422	76.3486	101.6454	125.5869	50.2027	73.3001	97.6613	120.9012	144.9841
G10-32	0	26.8167	53.9606	81.5722	109.8835	137.3115	165.4396	192.0327	219.4186	246.0144	272.7511
G10-33	0	20.9303	42.1885	62.9804	83.7268	104.5205	124.4739	144.3344	165.0374	184.9929	204.9961
G10-34	0	12.5965	24.773	36.1101	47.8673	59.2983	71.1494	82.2076	94.6656	105.6776	117.9964
G10-35	0	0.2806	-0.4204	-1.6357	-2.9909	-4.1592	-5.1873	-6.6831	-6.7298	-7.8516	-6.8701
G11-36	0	-13.1398	-28.103	-43.3459	-59.2434	-75.5143	-91.1769	-106.559	-120.631	-135.824	-148.727

N = 1,300,000											
P (kip)	0	8.7	17.4	26.1	34.8	43.5	52.2	60.9	69.6	78.3	87
D1A	0	5.5234	14.744	26.2588	40.0204	54.3911	72.5539	93.7131	117.4019	139.4056	163.4711
D1B	0	1.3086	5.093	8.504	12.8496	18.5035	24.0173	30.0451	37.1013	42.8956	48.9703
D2A	0	6.0613	20.3296	42.2916	70.4569	104.6398	145.7746	190.4575	236.3107	279.2288	324.67
D2B	0	6.0671	19.7416	38.7836	67.5349	102.7295	146.9826	192.8274	238.6293	275.0501	313.2946
D3A	0	0	0	0	0	0	0	0	0	0	0
D3B	0	4.7741	15.4926	25.9301	43.4828	69.6958	105.8346	144.9726	184.4878	219.1364	264.9796
D4A	0	18.288	71.5803	61.5971	146.5597	253.3573	443.4209	807.5434	1708.935	2468.185	1687.001
D4B	0	2.1175	7.9993	13.3635	24.5628	41.6915	65.3623	87.3869	107.3418	123.579	142.8294
G04-01	0	-47577.3	-50169.9	-48349.8	-51028.7	-97435.7	-97435.7	-97435.7	-97435.7	-48316.2	-48017.1
G04-02	0	138.7213	-146.967	-186.317	-196.75	-259.134	-317.361	-333.059	-364.974	-387.311	-384.44
G11-03	0	19.1402	40.1066	56.9551	74.7402	92.0108	108.7677	125.899	142.9845	159.8365	175.9866
G04-04	0	34.3656	70.2704	109.5308	151.7289	193.3714	230.4988	264.1345	301.3138	334.1152	364.8692
G04-05	0	-73.338	-142.957	-190.6	-280.149	-293.672	-435.95	-530.377	-1169.63	-1155.58	-1223.3
G05-06	0	34.4488	71.9258	112.6185	152.6161	191.406	228.5689	263.5457	297.6399	329.5933	361.1762
G05-07	0	0	0	0	0	0	0	0	0	0	0
G05-08	0	7.9428	11.4004	11.6807	15.1384	19.7175	25.3248	30.698	37.4735	44.4355	52.9869
G05-09	0	-1.7229	-11.6881	-25.1927	-35.3905	-43.4462	-49.4996	-54.8077	-57.9741	-60.1623	-59.5571
G05-10	0	-9.4979	-9.032	-22.3006	-30.4011	-39.5259	-49.9072	-61.6854	-69.8322	-80.213	-88.2659
G06-11	0	0.8363	0.5111	-1.208	-2.8338	-4.6917	-6.6426	-8.8722	-10.6374	-12.8672	-13.982
G06-12	0	12.4197	23.085	31.3958	40.1685	48.2949	56.1447	63.1169	70.9204	77.4311	85.3275
G06-13	0	24.6724	49.5322	72.0655	95.4845	120.1617	145.4455	167.3776	202.909	220.466	241.4699
G06-14	0	24.165	53.3425	79.2899	98.915	120.6959	150.7691	170.6311	202.7688	207.7345	226.0531
G06-15	0	22.4423	48.2853	74.0357	100.5794	126.8452	152.1809	176.6329	201.1792	223.3512	245.3844
G07-16	0	11.1713	20.9465	29.0925	39.1477	49.0165	58.0941	66.3805	75.4586	83.4195	92.2183
G07-17	0	-1.5834	-4.0055	-10.2003	-15.4171	-20.4473	-25.5704	-31.3923	-35.9102	-39.4497	-41.3595
G07-18	0	-13.5193	-27.3166	-46.3164	-64.7117	-82.8279	-100.293	-117.989	-134.663	-148.69	-161.229
G07-19	0	-13.4106	-31.0116	-51.871	-71.8451	-90.5147	-107.694	-121.846	-133.438	-142.609	-148.195
G07-20	0	0	0	0	0	0	0	0	0	0	0
G07-21	0	14.0046	26.5159	37.7202	50.6988	62.8842	75.1631	87.1156	99.8153	111.4415	125.1226
G08-22	0	0	0	0	0	0	0	0	0	0	0
G08-23	0	37.8707	76.3048	115.349	155.6571	195.6418	233.2001	268.2853	302.6252	329.725	358.6958
G08-24	0	37.8457	77.3222	114.5222	154.7022	194.2342	232.6531	267.7719	304.5212	337.8772	368.1647
G08-25	0	15.6577	30.0575	42.6404	58.2062	72.9335	86.6359	100.8514	114.6475	160.5603	170.2097
G09-26	0	-0.2321	-3.2502	-6.7792	-9.797	-12.6295	-16.0189	-17.1333	-17.5048	-16.3441	-13.001
G09-27	0	0	0	0	0	0	0	0	0	0	0
G09-28	0	-16.3551	-36.2142	-60.7451	-84.4335	-106.159	-128.444	-149.233	-168.807	-188.566	-204.869
G09-29	0	-6.7644	-13.8225	-31.2722	-42.4965	-53.3775	-61.317	-70.5803	-77.0984	-85.8713	-90.8209
G09-30	0	11.8263	22.0697	30.1246	40.1823	51.3108	61.3689	71.1943	41.5312	54.4293	64.627
G10-31	0	29.2446	55.086	78.6427	103.8803	129.6786	153.9387	177.8733	200.7828	222.1065	244.6443
G10-32	0	26.5766	54.3181	80.9907	109.9919	139.0885	166.6503	193.1425	219.4031	244.6876	269.5074
G10-33	0	20.3687	41.112	59.567	79.7043	100.3568	119.3745	137.9726	156.1504	173.4414	191.013
G10-34	0	10.8194	20.753	29.1944	39.4545	49.2954	57.4574	67.019	76.5338	86.3288	96.9636
G10-35	0	-0.6538	-3.3157	-8.1258	-11.3486	-13.1699	-16.0653	-18.5871	-19.8947	-21.8094	-21.6693
G11-36	0	-15.7503	-34.2573	-55.5674	-74.7273	-92.344	-111.035	-127.763	-144.304	-160.423	-174.206

N = 1,400,000											
P (kip)	0	8.7	17.4	26.1	34.8	43.5	52.2	60.9	69.6	78.3	87
D1A	0	7.106	16.7834	31.5568	43.8062	62.9754	81.1169	106.4599	129.9333	156.8688	182.9638
D1B	0	1.9619	5.5589	11.5381	15.6024	23.2172	29.6175	38.4472	46.1555	55.1253	62.6002
D2A	0	6.1067	17.8073	42.0959	64.0545	101.4001	140.4269	189.1568	232.9474	281.2196	325.8581
D2B	0	6.7679	15.4025	41.5416	64.7409	104.6999	146.6234	200.1763	245.4236	289.3663	324.2065
D3A	0	-698.653	45831.62	45831.62	45831.62	45831.62	45831.62	45831.62	45831.62	45831.62	45831.62
D3B	0	9.3937	12.118	34.805	52.5609	80.5582	112.973	154.7866	193.4554	234.9467	270.4261
D4A	0	13.1128	21.667	58.0929	87.3772	148.3007	212.5229	305.0625	387.0363	469.0232	536.3917
D4B	0	5.7411	5.506	19.8116	32.6587	49.4595	71.8142	96.2408	117.5623	137.3784	155.6418
G04-01	0	-4465.07	-325.076	787.6492	-1443.28	41.1463	-1846.73	-3322.9	-4510.9	-4524.87	-5650.65
G04-02	0	6.9402	11.8647	14.3504	15.945	16.6015	17.586	19.0863	22.7445	27.1531	33.3437
G11-03	0	20.7792	41.9342	62.903	82.4676	101.0975	118.5574	135.6904	152.7772	170.8012	187.702
G04-04	0	36.0917	76.4701	118.8551	160.0329	200.5615	237.7856	274.3599	309.4457	342.9967	374.0799
G04-05	0	29.0324	61.2973	96.8933	138.2798	176.9204	211.7525	243.9329	274.5231	306.2737	335.4681
G05-06	0	35.1782	74.5937	115.9669	156.2729	196.3498	232.6588	268.6446	302.9103	336.1078	367.5374
G05-07	0	0	0	0	0	0	0	0	0	0	0
G05-08	0	8.4106	12.85	15.2329	19.9994	23.9248	30.0462	36.2146	43.2243	50.935	60.4682
G05-09	0	-1.1642	-10.1987	-22.5391	-31.9455	-41.0726	-46.4275	-51.4096	-54.1571	-55.7868	-54.39
G05-10	0	-7.68	-16.3374	-25.3206	-33.326	-43.3794	-51.6174	-60.646	-68.6046	-76.7956	-83.0318
G06-11	0	1.5326	2.3686	1.8577	1.7183	-0.4644	-1.9041	-4.1803	-5.1555	-7.1066	-7.0138
G06-12	0	11.5892	22.2557	32.5528	42.1573	50.6079	58.4582	66.124	73.651	81.5477	89.2139
G06-13	0	25.7507	51.6893	79.5851	105.107	132.214	154.7114	179.0258	201.8045	225.4229	246.154
G06-14	0	27.0601	54.0748	83.1983	110.8247	140.373	164.6307	190.7632	214.8361	240.0811	262.5639
G06-15	0	26.4935	51.545	80.4161	107.9387	137.1392	161.4975	187.3475	211.8478	237.1415	258.6165
G07-16	0	11.2649	22.3898	32.1652	42.9653	53.1604	62.2847	70.2917	78.9977	87.8897	97.5267
G07-17	0	-0.8848	-1.2108	-7.1716	-9.1275	-16.2522	-19.2323	-25.7053	-29.0578	-33.6213	-33.9006
G07-18	0	-13.2395	-24.5739	-44.0373	-58.7149	-80.7318	-94.2014	-113.151	-128.338	-144.36	-154.02
G07-19	0	-9.3093	-22.389	-38.9124	-55.063	-73.6799	-90.2014	-104.303	-115.984	-125.198	-131.667
G07-20	0	0	0	0	0	0	0	0	0	0	0
G07-21	0	16.0544	31.3624	46.4377	61.8865	75.8425	89.0519	102.7285	116.6854	130.783	144.8806
G08-22	0	0	0	0	0	0	0	0	0	0	0
G08-23	0	36.6533	74.4296	114.0759	154.2405	193.8007	231.3083	267.2772	301.9876	335.392	366.8828
G08-24	0	36.398	73.8211	112.596	152.1635	191.456	228.565	264.096	298.8385	331.4905	362.7028
G08-25	0	17.9965	35.1072	51.9394	68.9584	85.2318	100.713	115.1224	130.3249	145.5276	160.6843
G09-26	0	3.9473	6.3153	5.6187	5.2011	3.5757	1.3467	-0.4178	-0.4178	0.6035	3.2507
G09-27	0	0	0	0	0	0	0	0	0	0	0
G09-28	0	-15.7475	-33.0367	-54.4367	-75.6959	-98.7764	-120.127	-139.701	-158.855	-176.606	-192.628
G09-29	0	0.9798	-3.038	-7.3986	-12.445	-18.7652	-25.5261	-29.348	-32.7281	-37.2354	-38.2645
G09-30	0	14.4602	27.2467	39.4292	51.7512	63.8417	75.9787	87.1857	98.7187	109.9732	121.1812
G10-31	0	27.9371	54.5697	80.3641	107.4193	133.7763	158.9683	183.6951	208.0028	231.099	253.8694
G10-32	0	26.853	54.4991	82.9842	112.5415	141.8213	169.6599	196.7549	223.3858	249.4596	274.8361
G10-33	0	21.8134	43.7212	65.6301	87.5863	109.2638	129.4931	149.6302	169.2075	188.1313	207.1027
G10-34	0	12.5447	24.7632	36.3761	47.4762	58.0166	67.9044	78.5387	89.0797	99.9475	111.0022
G10-35	0	0.7939	-0.3269	-2.7086	-4.6233	-7.5187	-10.274	-11.7684	-12.8892	-13.2161	-12.7024
G11-36	0	-13.8797	-30.4229	-48.9749	-66.8254	-86.4973	-104.627	-120.373	-135.791	-150.134	-163.403

N = 1,500,000											
P (kip)	0	8.7	17.4	26.1	34.8	43.5	52.2	60.9	69.6	78.3	87
D1A	0	4.5838	14.1722	24.5091	42.1435	56.3638	79.7059	101.5995	128.8734	154.6993	183.5671
D1B	0	1.2147	6.0268	9.7641	17.2863	23.36	33.3115	40.9271	49.9446	58.9153	67.9334
D2A	0	4.8481	19.5329	36.1293	68.1585	99.1635	147.5637	190.8854	237.9883	281.3644	329.3624
D2B	0	4.8595	16.4471	34.483	68.2207	100.9321	155.5656	214.5989	282.2871	303.2308	340.9605
D3A	0	0	0	0	0	0	0	0	0	0	0
D3B	0	5.2562	11.8734	24.8736	45.0549	68.5694	106.7304	60.1269	77.8856	242.6873	275.79
D4A	0	10.7519	25.6772	51.3061	98.3954	146.5201	240.8185	240.873	249.7984	508.4859	582.5521
D4B	0	4.7505	7.7607	16.8857	29.4444	46.2366	73.6609	55.5984	66.5169	147.9442	162.5766
G04-01	0	-4.4575	-14.3946	-27.4417	-43.2282	-58.3641	-73.1278	-83.6667	-93.1839	-98.4302	-101.819
G04-02	0	8.0152	13.8868	15.9838	16.5896	19.4788	19.1992	21.1564	23.8126	29.1255	35.0908
G11-03	0	20.3224	41.5821	62.2337	81.4346	99.4187	117.0753	134.2172	151.5945	169.0654	186.7716
G04-04	0	36.3186	78.0488	120.0158	161.0067	200.602	239.2207	274.9038	309.9362	342.9651	374.5031
G04-05	0	25.9674	29.9786	48.4979	26.2392	31.0831	2.1048	21.9565	49.098	44.3246	54.8233
G05-06	0	35.7195	75.5978	117.3009	157.7924	197.3537	235.7963	272.187	306.7581	340.4904	372.6363
G05-07	0	0	0	0	0	0	0	0	0	0	0
G05-08	0	8.7855	12.2435	15.9355	19.0197	24.394	29.3946	36.685	43.2747	51.8272	60.8474
G05-09	0	-1.1184	-11.4606	-22.1751	-33.1692	-40.4359	-48.0291	-51.709	-55.1098	-55.6688	-54.5972
G05-10	0	-5.3988	-13.171	-19.7796	-27.7842	-35.37	-43.3745	-49.4707	-57.5213	-63.4784	-69.9464
G06-11	0	4.2173	6.581	6.6273	-1.1129	0.6484	-1.8543	-1.5301	-1.5301	-0.9274	-0.2323
G06-12	0	88.4542	165.725	259.305	309.4935	349.9624	429.2066	437.5293	460.7807	423.3866	472.1278
G06-13	0	25.9316	53.2613	79.8477	106.7613	131.4412	156.7743	179.8732	203.5788	225.9345	248.99
G06-14	0	27.0425	54.6531	79.7125	101.8885	125.0112	145.3451	166.7205	190.3188	210.6552	233.5469
G06-15	0	19.4956	41.3709	64.8797	89.8825	111.1077	134.7132	156.0335	178.148	198.9104	220.8403
G07-16	0	11.0378	20.958	30.832	40.1009	50.1615	58.1263	67.1628	74.988	84.6768	93.7603
G07-17	0	-0.9319	-3.8199	-6.8474	-13.4155	-16.3035	-23.9429	-27.8553	-33.3982	-35.1219	-38.1491
G07-18	0	-12.7313	-27.8321	-42.8392	-63.1884	-77.5908	-98.8217	-113.176	-131.386	-143.092	-157.074
G07-19	0	-2.4299	-11.4471	-21.1185	-34.7138	-49.1033	-64.6603	-78.6752	-90.2138	-100.164	-106.984
G07-20	0	0	0	0	0	0	0	0	0	0	0
G07-21	0	16.6194	33.0056	49.7195	65.0336	79.9274	93.1876	107.1485	121.2499	135.0249	149.6876
G08-22	0	0	0	0	0	0	0	0	0	0	0
G08-23	0	31.4763	64.6363	99.7134	136.8952	172.7247	207.1087	241.4952	274.4824	307.3315	337.4721
G08-24	0	35.4745	70.9985	107.0825	144.658	180.5615	216.2815	250.5625	283.6825	316.107	346.4399
G08-25	0	17.6664	34.3071	51.4153	68.1039	84.2337	99.5717	114.9568	129.6431	145.1222	160.229
G09-26	0	5.1093	8.3139	10.9151	11.4723	12.2156	11.3796	11.3794	12.587	14.3056	17.7427
G09-27	0	0	0	0	0	0	0	0	0	0	0
G09-28	0	-14.9537	-32.3364	-50.4664	-72.1001	-92.4247	-113.029	-132.37	-150.403	-167.875	-183.478
G09-29	0	-1.0887	-3.7396	-6.1538	-10.7456	-14.4378	-18.5562	-21.7278	-25.2306	-27.8815	-29.1122
G09-30	0	12.6588	24.247	35.743	47.7971	59.4796	70.8831	81.8214	92.5736	103.4652	114.7768
G10-31	0	29.3892	54.0676	80.5673	106.6484	132.5439	157.5544	182.0996	206.0394	229.3267	252.1017
G10-32	0	26.6818	54.0635	82.2387	111.5331	139.3852	167.6115	194.8147	221.2271	247.1287	272.3799
G10-33	0	21.7796	43.1395	65.1083	86.7506	107.2249	127.6535	147.615	166.8767	185.9989	204.7473
G10-34	0	11.7029	20.4686	32.9642	44.4813	55.2058	65.8373	76.5157	86.8678	98.1997	109.3918
G10-35	0	0.6538	-1.5878	-2.9421	-5.6507	-8.0791	-11.1613	-12.6557	-14.01	-14.1501	-13.7298
G11-36	0	-14.0204	-33.0416	-49.8187	-69.7262	-87.3434	-105.427	-121.688	-137.34	-151.778	-164.44

N = 1,700,000											
P (kip)	0	8.7	17.4	26.1	34.8	43.5	52.2	60.9	69.6	78.3	87
D1A	0	7.3466	55.8742	89.5264	106.5168	115.5037	140.3596	170.6931	198.7819	226.17	255.1044
D1B	0	-0.5604	2.803	8.5491	13.1734	18.0789	29.5709	40.2689	49.052	57.5549	68.1136
D2A	0	5.1732	15.8461	37.5187	57.7009	93.1266	138.5308	187.4827	230.9374	276.6338	323.5007
D2B	0	5.5151	15.8447	37.1584	60.0624	97.5059	153.1852	218.6435	272.2318	320.9621	362.2602
D3A	0	0	0	0	0	0	0	0	0	0	0
D3B	0	2.9572	9.2481	22.4396	37.932	60.7964	98.3106	143.012	182.3641	222.9872	260.9362
D4A	0	6.4564	16.7961	43.0912	71.8208	131.7183	214.6977	319.2724	402.9376	487.7882	555.9785
D4B	0	6.8649	11.1916	19.4678	31.7883	46.2728	74.4431	102.5678	128.1073	148.568	169.9232
G04-01	0	-3.5746	-12.5802	-26.8772	-41.2202	-63.6391	-73.8504	-84.9898	-93.0196	-105.643	-103.508
G04-02	0	12.6252	18.2826	28.8477	24.2664	-101.553	-79.2025	-142.83	-141.941	-142.314	-133.105
G11-03	0	20.7951	43.2306	63.981	84.4977	98.7385	120.3341	139.1666	157.6253	169.5254	191.5456
G04-04	0	35.909	76.5312	118.2295	156.3395	182.043	224.8231	259.1151	293.7361	320.3801	356.2187
G04-05	0	25.6202	46.7322	68.5658	89.1057	3454.169	49997.49	49997.49	49997.49	49997.49	49997.49
G05-06	0	33.796	73.2665	113.7163	154.0759	1207.486	759.5659	769.8362	802.2388	1809.825	1779.342
G05-07	0	0	0	0	0	0	0	0	0	0	0
G05-08	0	9.2549	14.0697	16.3601	21.3149	20.5205	30.6172	37.3487	45.2021	44.4074	60.3019
G05-09	0	-1.3048	-9.9248	-22.9713	-31.5911	-45.9882	-47.4794	-51.952	-54.2354	-63.6462	-56.611
G05-10	0	-7.5905	-16.345	-25.7049	-33.0619	-46.6123	-49.7787	-57.7413	-65.3306	-80.9289	-81.4409
G06-11	0	0.696	-0.0464	-2.5056	-1.7632	-11.5994	-7.1451	-6.6347	-4.8254	-8.9083	-4.8256
G06-12	0	14.3	27.5394	39.6258	50.7901	57.9869	71.1811	82.1614	91.9885	97.0176	109.7515
G06-13	0	26.2145	52.384	80.7435	106.8695	128.1528	155.8644	180.3641	204.0261	222.4722	247.2078
G06-14	0	25.0719	51.7006	79.8862	109.9588	132.6322	162.5663	189.2966	214.7554	234.8405	260.8202
G06-15	0	26.1767	51.6069	79.2355	102.9853	198.0911	202.3465	212.9142	229.0471	235.1721	257.3394
G07-16	0	11.3204	21.9432	31.4476	42.7223	47.4281	60.5671	69.2803	78.4595	80.8822	94.4879
G07-17	0	-1.3519	-2.0043	-7.9691	-9.554	-21.903	-22.835	-28.3804	-31.6424	-41.0556	-38.9586
G07-18	0	-13.0593	-24.9568	-44.7537	-58.0444	-82.8123	-94.6617	-112.597	-126.769	-147.91	-154.972
G07-19	0	-6.4877	-13.7218	-24.3155	-37.896	-54.183	-62.7698	-77.1891	-87.0352	-101.314	-109.153
G07-20	0	0	0	0	0	0	0	0	0	0	0
G07-21	0	17.459	35.0582	52.3314	68.9521	76.4219	96.7315	112.0927	126.9408	137.0265	154.2565
G08-22	0	0	0	0	0	0	0	0	0	0	0
G08-23	0	35.3339	71.7441	108.8104	147.42	197.8924	241.3652	277.7907	303.429	330.0038	362.979
G08-24	0	35.6119	72.1098	108.6568	150.1353	184.1768	223.1036	258.5453	292.0358	320.7837	352.8825
G08-25	0	17.6999	34.9345	51.5173	69.9642	79.8407	101.2233	116.877	133.2766	142.5946	162.3961
G09-26	0	4.5978	7.106	8.6852	10.7286	7.431	10.7288	10.1714	12.5866	12.0758	17.8813
G09-27	0	0	0	0	0	0	0	0	0	0	0
G09-28	0	-15.7027	-32.9004	-51.9668	-71.1258	-99.3021	-114.862	-133.972	-150.511	-173.964	-183.589
G09-29	0	2.441	2.825	-0.9544	-15.5982	-35.84	-29.7601	-39.2329	-53.3008	-70.4313	-69.7611
G09-30	0	10.9285	21.1585	31.7616	42.5975	39.3425	55.712	66.7807	77.2451	81.338	96.0352
G10-31	0	28.6409	54.4376	80.3757	107.0616	139.4875	167.1098	191.2335	215.9655	233.6519	260.2991
G10-32	0	26.4923	54.0569	81.9491	111.2397	133.3141	167.1719	195.6759	222.3648	243.2326	271.5547
G10-33	0	21.254	42.6024	63.7182	86.3763	98.6168	125.9956	147.4421	167.6275	180.5709	203.7953
G10-34	0	12.0329	20.1487	31.669	44.5421	48.787	66.2783	77.7532	89.5082	92.9135	108.7274
G10-35	0	0.0463	-0.9346	-2.7571	-4.9066	-14.5794	-10.8879	-12.57	-13.0839	-19.0186	-14.1589
G11-36	0	-13.3649	-29.9537	-47.8499	-65.4657	-93.2661	-105.087	-121.86	-135.782	-157.645	-164.139

N = 1,900,000											
P (kip)	0	8.7	17.4	26.1	34.8	43.5	52.2	60.9	69.6	78.3	87
D1A	0	3.748	10.4943	22.1131	33.1698	53.457	74.6821	101.0152	126.7874	154.5294	181.4762
D1B	0	2.1021	6.3999	12.4263	16.7708	26.5809	35.9246	45.5482	54.425	63.9091	72.412
D2A	0	6.0605	16.55	37.9497	58.6042	99.6828	142.8631	190.9439	234.878	281.8948	326.8633
D2B	0	4.0673	15.6618	37.8228	61.4812	107.3516	162.3926	221.7421	277.1697	299.9512	414.9044
D3A	0	0	0	0	0	0	0	0	0	0	0
D3B	0	3.3789	9.1048	22.1992	37.9697	66.836	103.0276	141.6153	186.122	124.3524	111.4097
D4A	0	7.3927	16.1894	42.3931	71.6866	138.6099	223.6575	317.802	408.9204	409.8158	397.4247
D4B	0	1.364	3.7157	10.3942	21.4466	41.7655	67.4468	90.7308	118.2965	78.2221	77.7072
G04-01	0	-5.0143	-13.696	-27.9952	-43.2689	-59.192	-73.0721	-85.0952	-94.6577	-100.739	-103.802
G04-02	0	7.1858	12.785	16.0979	17.3579	30.9831	31.2632	34.7159	37.7958	42.5555	48.3883
G11-03	0	20.1823	42.0978	63.0778	81.9979	101.3404	118.4819	136.0931	153.751	171.4097	188.6479
G04-04	0	35.8311	76.9774	119.2447	160.1181	201.6939	239.2175	276.1845	311.6158	345.0911	376.4238
G04-05	0	41.4997	55.2706	91.8646	129.3766	165.2068	179.605	206.2384	245.493	266.7351	282.6311
G05-06	0	33.9705	73.7928	115.6778	155.6002	195.9003	233.3479	270.2837	306.0049	339.0126	370.3372
G05-07	0	0	0	0	0	0	0	0	0	0	0
G05-08	0	9.0662	14.1599	16.6835	21.497	25.9368	31.4512	37.7139	44.8642	52.529	61.7362
G05-09	0	-0.9783	-9.5489	-21.7057	-30.555	-39.9169	-46.2511	-51.2347	-54.2619	-55.8453	-54.6808
G05-10	0	-6.9364	-15.4084	-24.9978	-33.3763	-42.686	-51.7625	-61.0721	-69.1709	-77.3626	-83.553
G06-11	0	1.5312	2.1346	1.6241	0.8352	-1.4848	-3.7121	-6.2186	-7.4714	-9.049	-9.3274
G06-12	0	12.2766	23.5418	33.6119	43.4981	52.5568	60.0522	68.1452	76.8369	84.9301	91.9202
G06-13	0	32.5213	58.9876	86.899	112.2028	163.8386	186.1627	210.8656	233.705	256.5921	277.6623
G06-14	0	25.3668	52.0549	81.5267	111.6606	143.6827	170.8016	197.5918	226.4117	256.9316	282.7356
G06-15	0	26.0538	50.7994	78.6333	104.0365	101.4145	113.9523	137.7195	161.7214	184.6489	205.3309
G07-16	0	11.4602	22.6876	32.378	43.5595	53.2967	62.0096	70.0228	79.435	87.7754	97.0478
G07-17	0	-1.3048	-2.0504	-7.8298	-10.3928	-15.9858	-20.2733	-26.6582	-30.1998	-34.3015	-35.42
G07-18	0	-13.1978	-25.4192	-44.6102	-58.3639	-78.7618	-94.2804	-113.144	-128.057	-143.574	-153.516
G07-19	0	-5.4172	-12.7491	-22.9764	-37.2656	-50.2472	-65.8907	-79.9921	-93.1595	-103.852	-111.743
G07-20	0	0	0	0	0	0	0	0	0	0	0
G07-21	0	16.9419	34.2102	51.1528	67.6289	82.6123	96.2424	110.0125	124.1098	138.1613	152.1197
G08-22	0	0	0	0	0	0	0	0	0	0	0
G08-23	0	36.0402	73.7169	111.5833	150.8535	188.1186	224.7791	259.4812	294.3254	327.5838	359.0229
G08-24	0	35.7394	72.6429	109.8744	148.0853	185.2763	221.3543	255.807	290.3088	322.6739	353.4601
G08-25	0	18.068	35.0659	51.8782	69.2494	86.0163	101.3863	116.6633	132.8263	147.9648	163.3365
G09-26	0	3.2964	4.9677	5.9427	6.6854	6.9642	6.0355	6.082	7.0572	8.7282	11.8389
G09-27	0	0	0	0	0	0	0	0	0	0	0
G09-28	0	-15.2348	-32.7117	-52.0573	-73.2718	-93.4096	-114.062	-132.143	-150.596	-167.742	-183.485
G09-29	0	-1.8651	-5.2119	-9.3723	-15.3015	-20.179	-23.2869	-22.7609	-25.9169	-29.5986	-31.7981
G09-30	0	10.8907	21.7351	32.3467	42.959	52.9196	63.2061	73.8654	84.1059	93.8813	103.9826
G10-31	0	28.7318	55.4594	82.2816	109.0121	136.0239	161.4039	186.3657	210.722	234.4262	256.8716
G10-32	0	27.2349	54.7971	83.1064	112.3015	141.545	169.8122	196.9169	224.2559	250.2455	275.3515
G10-33	0	22.0951	44.0514	66.1019	88.2467	110.299	131.4176	152.1169	172.6299	191.6488	210.9486
G10-34	0	12.3577	24.6226	35.9081	47.0074	55.169	67.2012	77.8816	89.5882	100.6421	111.7428
G10-35	0	-0.0934	-1.2142	-3.2223	-5.8375	-8.4061	-11.3958	-13.1704	-14.1044	-14.945	-14.8983
G11-36	0	-15.0423	-31.9994	-49.6565	-69.5547	-88.4722	-107.435	-123.688	-140.314	-155.213	-168.989

N = 2,100,000											
P (kip)	0	8.7	17.4	26.1	34.8	43.5	52.2	60.9	69.6	78.3	87
D1A	0	4.2035	10.7892	22.6997	33.2556	52.8272	72.9132	100.0539	124.72	154.2928	183.0734
D1B	0	1.6819	6.0268	12.3805	16.585	26.5361	34.5258	44.7571	53.1672	63.2128	73.3984
D2A	0	5.2669	15.7087	36.3126	55.7992	95.0067	135.3364	183.7829	227.1975	274.1603	320.5214
D2B	0	5.0908	14.5255	36.1516	60.7684	104.5392	154.8548	212.371	396.8966	404.3673	359.4863
D3A	0	0	0	0	0	0	0	0	0	0	0
D3B	0	0.422	5.5351	16.7931	32.8354	58.5425	92.977	121.9715	65.0755	115.7415	180.7227
D4A	0	7.5746	14.3547	41.4752	69.9067	132.527	211.9475	303.1706	287.5566	373.6001	511.5031
D4B	0	-1.6447	-0.3758	7.1427	19.5017	38.111	62.5487	77.3532	65.0421	86.1443	132.3912
G04-01	0	-4.4569	-13.2311	-27.2507	-43.3594	-59.2812	-73.8107	-86.1573	-95.0693	-101.429	-104.863
G04-02	0	6.9444	12.9092	16.1256	17.1042	18.0828	19.1546	21.0652	24.8408	29.6414	35.8865
G11-03	0	20.2618	41.8789	63.2635	81.8004	100.8986	118.2224	135.6872	153.4332	171.0858	188.4592
G04-04	0	35.1013	75.6056	118.3015	159.6509	200.2117	237.7487	274.4501	309.617	343.2959	375.1595
G04-05	0	22.2631	60.4917	98.7234	134.5889	173.442	207.3697	240.4469	267.8869	299.8302	329.0744
G05-06	0	34.5489	74.7424	116.9445	157.7974	198.3272	235.9682	272.6328	307.2936	341.024	372.937
G05-07	0	0	0	0	0	0	0	0	0	0	0
G05-08	0	8.4574	13.8311	16.9616	21.6345	25.8399	31.4007	37.4283	45.092	52.5221	61.588
G05-09	0	-1.3508	-9.5479	-21.2847	-30.8317	-39.8205	-46.5735	-51.6963	-54.4904	-56.2137	-55.2356
G05-10	0	-7.2974	-15.3849	-23.937	-32.8142	-43.0389	-51.2653	-59.6775	-66.9739	-75.5715	-81.1484
G06-11	0	1.6246	2.2744	2.3206	1.0214	-1.5316	-3.899	-6.3592	-7.5662	-9.5621	-9.9335
G06-12	0	11.5027	22.5898	33.8616	43.0544	51.4628	59.4554	67.217	75.302	83.0638	91.1958
G06-13	0	26.1246	53.044	81.1311	107.3531	134.277	157.7953	182.2016	205.4424	228.451	250.4804
G06-14	0	26.9465	54.3595	84.9855	111.8432	140.9829	166.1681	192.2851	216.7738	241.4971	264.4981
G06-15	0	26.3777	52.8502	82.255	109.1956	137.8595	162.7554	188.4901	212.9698	237.4507	259.7451
G07-16	0	11.0847	22.1233	32.7429	43.5024	52.8648	62.1808	70.1927	78.9965	87.2416	96.6052
G07-17	0	-1.6303	-2.282	-7.5916	-9.9667	-16.0681	-19.8404	-25.8483	-29.2015	-33.9517	-35.1626
G07-18	0	-13.5198	-25.9241	-44.9717	-59.0014	-79.2551	-94.3989	-113.351	-127.332	-143.264	-154.69
G07-19	0	-5.4568	-13.6186	-26.3974	-42.627	-58.0631	-74.4785	-90.8459	-103.343	-114.721	-122.741
G07-20	0	0	0	0	0	0	0	0	0	0	0
G07-21	0	16.6222	34.4596	51.55	67.8004	83.118	97.1747	110.9045	124.8221	138.5529	153.0319
G08-22	0	0	0	0	0	0	0	0	0	0	0
G08-23	0	35.2193	73.1004	112.2906	152.3702	189.9802	226.9394	263.1547	297.9722	330.9722	362.2467
G08-24	0	36.6741	74.7913	113.3771	152.6163	190.4168	226.8722	262.4928	297.0468	329.3705	360.7194
G08-25	0	17.8297	34.9155	52.2813	69.1354	85.7571	101.1686	116.1154	131.6212	146.2893	161.5631
G09-26	0	2.9259	3.8549	4.18	3.9943	4.273	2.9261	1.6719	2.7866	3.9945	7.3847
G09-27	0	0	0	0	0	0	0	0	0	0	0
G09-28	0	-15.8438	-33.2291	-53.1375	-74.9615	-95.6626	-117.671	-137.156	-155.332	-173.226	-188.831
G09-29	0	-1.4929	-3.9649	-7.1833	-11.6611	-15.7659	-20.3838	-23.882	-26.9605	-29.9921	-31.1117
G09-30	0	11.314	22.5816	33.9429	44.6991	55.7347	65.8858	76.5029	86.9341	96.527	107.3313
G10-31	0	29.6246	56.8717	83.3266	110.3901	137.4081	163.1673	187.7151	212.4968	235.7398	258.4703
G10-32	0	26.7664	55.0708	84.3084	113.8265	142.2755	169.9344	197.9676	224.931	250.6384	276.2075
G10-33	0	21.95	44.4147	66.8337	88.7402	110.4605	131.715	152.363	172.4042	192.0726	211.2746
G10-34	0	12.218	24.1561	35.535	46.7742	57.7807	67.9012	78.3017	89.7752	100.1761	111.7897
G10-35	0	0.3736	-0.7472	-3.269	-6.2116	-9.2009	-12.3765	-14.8516	-16.0191	-16.6729	-16.2526
G11-36	0	-13.9764	-31.5052	-50.1083	-69.8793	-88.9016	-108.344	-126.383	-142.132	-157.647	-170.591

N = 2,300,000											
P (kip)	0	8.7	17.4	26.1	34.8	43.5	52.2	60.9	69.6	78.3	87
D1A	0	3.1296	11.0249	19.5273	34.6175	49.0069	71.4799	95.2621	122.5496	150.1663	181.2891
D1B	0	0.0465	4.0635	8.267	15.1801	21.1125	30.0809	39.563	49.0451	58.6683	69.2722
D2A	0	4.9406	16.4542	31.3703	59.0132	88.476	133.2331	177.9472	224.3906	269.393	318.7833
D2B	0	4.1565	13.8717	33.1152	64.7381	98.8855	153.7788	219.9855	276.8077	331.8137	375.6547
D3A	0	0	0	0	0	0	0	0	0	0	0
D3B	0	6.1079	11.0882	24.3851	42.334	65.3584	100.9308	143.3207	182.8467	229.9435	268.3011
D4A	0	9.9198	19.8865	41.4113	77.2567	124.4774	208.681	299.6869	389.3513	475.004	549.2421
D4B	0	12.3656	16.7854	26.1894	38.4619	57.553	84.4982	114.5958	135.3828	162.8024	181.428
G04-01	0	-3.3423	-11.9771	-25.8577	-42.7084	-57.7946	-71.906	-84.206	-93.3498	-99.291	-103.144
G04-02	0	7.3181	12.8646	15.5684	16.4538	17.7121	18.9246	20.6954	24.3778	29.7388	36.0318
G11-03	0	20.8282	42.8239	62.8602	82.5229	101.0658	118.9549	135.911	153.8015	171.506	188.6971
G04-04	0	35.4356	76.369	118.0976	160.3418	200.3066	238.9241	274.796	310.5302	344.1239	375.5302
G04-05	0	35.2655	75.9056	117.2033	159.5792	199.6221	238.313	273.829	309.628	343.2328	374.2695
G05-06	0	34.9378	75.1493	116.3902	157.9617	198.183	237.241	272.7552	307.5251	341.1769	372.591
G05-07	0	0	0	0	0	0	0	0	0	0	0
G05-08	0	9.3951	14.4902	18.4637	21.7824	27.298	32.7205	38.891	45.6692	53.943	61.703
G05-09	0	-1.0248	-9.689	-20.822	-32.141	-39.7333	-47.0927	-51.7506	-55.2904	-56.548	-56.6877
G05-10	0	-8.089	-17.2937	-26.173	-37.3297	-46.348	-56.7141	-66.5687	-75.5866	-82.8844	-91.2972
G06-11	0	1.6242	1.671	1.9494	-0.7427	-1.9959	-4.827	-7.3795	-9.7004	-10.4892	-12.2993
G06-12	0	12.1034	23.329	33.955	42.9178	51.6034	59.6422	66.9418	74.842	83.0666	90.5048
G06-13	0	25.9277	53.5855	80.5905	108.391	134.091	159.4177	182.5031	207.3651	230.1255	252.3728
G06-14	0	27.4626	55.5319	83.9287	113.6772	140.6343	167.732	191.665	217.7413	241.9563	265.1009
G06-15	0	26.9851	54.3905	82.3094	111.6723	138.1051	165.284	188.9269	215.0844	238.6831	261.5387
G07-16	0	10.8062	21.6591	31.9068	41.3628	52.5428	61.2073	69.2198	77.791	86.8293	94.9348
G07-17	0	-1.3972	-3.2139	-7.0332	-13.1349	-15.1381	-20.541	-25.4781	-30.7414	-33.1634	-36.8428
G07-18	0	-13.9877	-28.5328	-44.5643	-65.4744	-79.2743	-97.8131	-113.842	-131.404	-144.041	-158.536
G07-19	0	-6.3845	-17.01	-32.8074	-47.8592	-65.8458	-82.0611	-97.5769	-111.741	-123.669	-133.593
G07-20	0	0	0	0	0	0	0	0	0	0	0
G07-21	0	17.8496	36.0739	53.3639	69.9069	85.4692	100.7978	114.5383	127.9988	142.6746	156.5096
G08-22	0	0	0	0	0	0	0	0	0	0	0
G08-23	0	36.6977	75.4523	116.8721	156.3803	196.2184	234.051	269.6445	304.8668	338.7366	369.9926
G08-24	0	37.6535	76.891	117.247	156.211	195.4105	232.5208	268.285	303.2145	336.5185	367.173
G08-25	0	16.813	33.1611	50.0685	66.8831	83.8382	99.21	113.8374	129.024	144.2572	159.0254
G09-26	0	1.1617	0.2323	-1.3005	-1.3936	-2.1836	-4.2743	-5.668	-5.7146	-4.6461	-1.8118
G09-27	0	0	0	0	0	0	0	0	0	0	0
G09-28	0	-14.3036	-32.5804	-55.0164	-76.1429	-98.6235	-120.449	-141.245	-160.499	-178.49	-194.424
G09-29	0	-0.5133	-2.5658	-7.3709	-11.2429	-15.6745	-20.1997	-24.1648	-27.8499	-30.0422	-32.0015
G09-30	0	11.5929	22.7207	33.3828	44.3248	55.0341	65.697	75.662	85.5336	95.8711	106.1159
G10-31	0	29.3004	56.5959	83.4268	110.7721	138.3522	164.2069	189.083	213.4468	237.0182	260.2173
G10-32	0	26.1627	54.2356	84.1259	112.6209	142.7011	171.8049	199.0939	226.1051	252.373	277.6172
G10-33	0	21.485	43.0167	64.9702	86.1771	108.1329	129.2481	149.4766	168.9118	188.8618	207.551
G10-34	0	12.2668	23.368	34.3292	44.7314	55.6466	65.9557	76.2182	86.5278	97.9571	108.7336
G10-35	0	0.8875	-1.0747	-4.4388	-7.3353	-10.5123	-13.4559	-15.8388	-17.6139	-18.2213	-17.8476
G11-36	0	-12.1093	-29.6416	-50.1181	-68.7242	-88.4049	-107.243	-125.333	-141.459	-156.977	-170.438